frontiers | Research Topics

Development of novel small molecules as therapeutics for inflammatory diseases and delineating their molecular mechanisms

Edited by
Nandakumar Natarajan, Tharmarajan Ramprasath, Jacob Gopas, Ramasamy Subbiah, Peramaiyan Rajendran and Sakthivel Vaiyapuri

Published in
Frontiers in Pharmacology

ISSN 1664-8714
ISBN 978-2-83250-955-5
DOI 10.3389/978-2-83250-955-5

About Frontiers

Frontiers is more than just an open access publisher of scholarly articles: it is a pioneering approach to the world of academia, radically improving the way scholarly research is managed. The grand vision of Frontiers is a world where all people have an equal opportunity to seek, share and generate knowledge. Frontiers provides immediate and permanent online open access to all its publications, but this alone is not enough to realize our grand goals.

Frontiers journal series

The Frontiers journal series is a multi-tier and interdisciplinary set of open-access, online journals, promising a paradigm shift from the current review, selection and dissemination processes in academic publishing. All Frontiers journals are driven by researchers for researchers; therefore, they constitute a service to the scholarly community. At the same time, the *Frontiers journal series* operates on a revolutionary invention, the tiered publishing system, initially addressing specific communities of scholars, and gradually climbing up to broader public understanding, thus serving the interests of the lay society, too.

Dedication to quality

Each Frontiers article is a landmark of the highest quality, thanks to genuinely collaborative interactions between authors and review editors, who include some of the world's best academicians. Research must be certified by peers before entering a stream of knowledge that may eventually reach the public - and shape society; therefore, Frontiers only applies the most rigorous and unbiased reviews. Frontiers revolutionizes research publishing by freely delivering the most outstanding research, evaluated with no bias from both the academic and social point of view. By applying the most advanced information technologies, Frontiers is catapulting scholarly publishing into a new generation.

What are Frontiers Research Topics?

Frontiers Research Topics are very popular trademarks of the *Frontiers journals series*: they are collections of at least ten articles, all centered on a particular subject. With their unique mix of varied contributions from Original Research to Review Articles, Frontiers Research Topics unify the most influential researchers, the latest key findings and historical advances in a hot research area.

Find out more on how to host your own Frontiers Research Topic or contribute to one as an author by contacting the Frontiers editorial office: frontiersin.org/about/contact

Development of novel small molecules as therapeutics for inflammatory diseases and delineating their molecular mechanisms

Topic editors

Nandakumar Natarajan — The University of Texas Health Science Center at Tyler, United States

Tharmarajan Ramprasath — Georgia State University, United States

Jacob Gopas — Ben-Gurion University of the Negev, Israel

Ramasamy Subbiah — Madurai Kamaraj University, India

Peramaiyan Rajendran — King Faisal University, Saudi Arabia

Sakthivel Vaiyapuri — University of Reading, United Kingdom

Citation

Natarajan, N., Ramprasath, T., Gopas, J., Subbiah, R., Rajendran, P., Vaiyapuri, S., eds. (2022). *Development of novel small molecules as therapeutics for inflammatory diseases and delineating their molecular mechanisms*. Lausanne: Frontiers Media SA. doi: 10.3389/978-2-83250-955-5

Table of contents

frontiers | Frontiers in Pharmacology

TYPE Editorial
PUBLISHED 22 November 2022
DOI 10.3389/fphar.2022.1088908

OPEN ACCESS

EDITED AND REVIEWED BY
Dieter Steinhilber,
Goethe University Frankfurt, Germany

*CORRESPONDENCE
Tharmarajan Ramprasath,
rtramprasath@outlook.com
Nandakumar Natarajan,
nandakkumarn@gmail.com

SPECIALTY SECTION
This article was submitted to Inflammation Pharmacology, a section of the journal Frontiers in Pharmacology

RECEIVED 03 November 2022
ACCEPTED 15 November 2022
PUBLISHED 22 November 2022

CITATION
Ramprasath T, Natarajan N, Gopas J, Subbiah R, Rajendran P and Vaiyapuri S (2022), Editorial: Development of novel small molecules as therapeutics for inflammatory diseases and delineating their molecular mechanisms. *Front. Pharmacol.* 13:1088908. doi: 10.3389/fphar.2022.1088908

Editorial: Development of novel small molecules as therapeutics for inflammatory diseases and delineating their molecular mechanisms

Tharmarajan Ramprasath[1]*, Nandakumar Natarajan[2]*, Jacob Gopas[3], Ramasamy Subbiah[4], Peramaiyan Rajendran[5] and Sakthivel Vaiyapuri[6]

[1]Center for Molecular and Translational Medicine, Georgia State University, Atlanta, GA, United States, [2]The University of Texas Health Science Center at Tyler, Tyler, TX, United States, [3]Ben-Gurion University of the Negev, Beersheba, Israel, [4]Department of Biochemistry, School of Biological Sciences, Madurai Kamaraj University Madurai, Madurai, India, [5]Department of Biological Sciences, College of Science, King Faisal University, Al Ahsa, Saudi Arabia, [6]University of Reading, Reading, United Kingdom

KEYWORDS

NF-κB, inflammation, small molecules, NLRP3, vascular diseases

Editorial on the Research Topic
Development of novel small molecules as therapeutics for inflammatory diseases and delineating their molecular mechanisms

Introduction

Inflammation is a critical and rapid physiological response of our immune system to any infection or tissue injury which is associated with various diseases (Zhu and Hou, 2021). However, when the inflammatory response fails to resolve the cause of inflammation, it can be detrimental and lead to the development of many diseases (Hanke et al., 2016; Ramprasath et al., 2021). Though, currently many approved anti-inflammatory drugs are in clinical use (e.g., non-steroidal anti-inflammatory drugs; NSAIDs), (Kohler et al., 2016), the long-term use of anti-inflammatory drugs are associated with many side effects including, gastrointestinal reactions and damages to the cardiovascular system (Wongrakpanich et al., 2018). In medicinal chemistry, the discovery based on the small molecule approach has opened the door to a new way to develop novel therapeutics for people with severe inflammatory conditions. In recognition of the clinical value of this study, this subject featured fourteen original research and two

review articles in the field of inflammation and small molecule study with a larger perspective to generate ideas for future scientific and clinical research.

Small molecule inhibitors targeting the NLRP3 inflammasome

NF-κB is a key activator of inflammation that primes the NLR pyrin domain 3 (NLRP3)-inflammasome for its activation (Zhong et al., 2016). In this special issue, different research groups published their work focused mainly on inflammasome. Zhao et al. investigated a compound named FxUD, which suppressed the NF-κB/NLRP3 signaling pathway and lowered the serum uric acid level to alleviate renal inflammation in hyperuricemic mice. Similarly, another compound KPT-8602, was validated for its potential to inhibit the activation of the NF-κB/NLRP3 signaling. The administration of KPT-8602 attenuated both lipopolysaccharide (LPS)-induced peripheral inflammation and 1-methyl-4-phenyl-25 1,2,3,6-tetrahydropyridine (MPTP)-induced neuroinflammation *in vivo* (Liu et al.). Another study tested a compound called MCL against radiation-induced enteropathy (RIE), one of the fatal complications of treatment for abdominal and pelvic tumors. In the mouse RIE model, MCL-mediated autophagy ameliorated RIE by NLRP3 inflammasome degradation (Wu et al.). An inflammasome inhibitor 3,4-methylenedioxy-β-nitrostyrene (MNS) was shown to be more efficient in inhibiting the secretion of interleukin-1β (IL-1β) by blocking oligomerization of apoptosis-associated speck-like protein (ASC) than other inhibitors NLRP3-IN-2 and JC124. In this study, Zheng et al. demonstrated using the dextran sulfate sodium (DSS)-induced colitis model that MNS alleviated DSS-induced intestinal inflammation by inhibiting NLRP3 inflammasome activation, which may function as an effective therapeutic for IBD. Lin et al. study demonstrated the efficacy of compound 149-01 in alleviating LPS-induced systemic inflammation, monosodium urate crystals (MSU)-induced peritonitis and experimental autoimmune encephalomyelitis (EAE) by preventing the interactions between NLRP3 and NEK7.

Small molecule modulators for COVID-19

Trichomicin, a novel small-molecule compound, is isolated from the fungus *Trichoderma harzianum* (Zhu et al., 2020). Trichomicin was explored for its inhibitory effect on cytokine expression by Chen et al. This compound could inhibit the Stat3 and NF-κB phosphorylation and showed the potential to treat the patients with cytokine release syndrome, a significant cause of COVID-19 disease severity. Vascular inflammation is one of the unusual symptoms among COVID-19 survivors. Ragavan et al. showed that histamine and histamine receptor signaling is likely to be essential for SARS-CoV-2 spike protein S1 Receptor-Binding Domain (Spike) protein to induce ACE2 internalization in endothelial cells, which causes endothelial dysfunction. This effect was blocked by treating with famotidine (a histamine H2 receptor blocker), an antiviral drug (Mukherjee et al., 2021), in cultured human coronary artery endothelial cells.

Small molecule inhibitors for inflammatory diseases

ACT-1004-1239 is a compound that showed a therapeutic effect against LPS inhalation-induced lung vascular injury *in vivo*. The authors provided data to show that this compound can alleviate acute lung injury (ALI) and its more severe form, acute respiratory distress syndrome (ARDS) (Pouzol et al.). Similarly, another compound, M20 interact with the MyD88-Toll/interleukin-1 receptor domain and thereby inhibits the protein dimerization, which could serve as a potential strategy for the treatment of acute lung injury (Song et al.).

Zhou et al. demonstrated that *topical* application of an anti-inflammatory compound isolated from the Chinese herb *Sophora alopecuroides L.* suppressed epidermal proliferation, erythema and infiltration of inflammatory cells in skin lesions, thereby alleviating imiquimod (IMQ)-induced psoriasis in mice. Huang et al. showed the implication of a plant-derived compound, N-acetyldopamine dimer (NADD from *Isaria cicadae)*, for its inhibitory effects on the expression of genes in inflammation-related signaling under *in vivo* settings for ulcerative colitis.

Saikosaponin D (SSD), an active ingredient isolated from Bupleurum, could activate the Nrf2/HO-1/ROS axis, further inhibiting the production of inflammatory mediators and protecting against ECM destruction. SSD delayed the progression of osteoarthritis (OA) in DMMs model mice *in vivo*. Therefore, the authors claim SSD could have potential for the treatment of OA (Wu et al.). A Study by Lilley et al.demonstrated the role of orphan nuclear receptor 4A2 (NR4A2/Nurr1) in an animal model of RA. The study validated the hTNF-a animal model for testing small molecules and genetic strategies for targeting NR4A2. Zhao et al. study highlighted the α2M-rich serum (α2MRS) autologous joint injection to treat post-traumatic osteoarthritis. This article provided a basis for the clinical translation of α2MRS against cartilage degeneration.

Jayusman et al. provided a comprehensive review of the studies related to effects of different polyphenolic substances on periodontal inflammation. The review also explored the pharmaceutical significance of polyphenol-loaded nanoparticles in controlling periodontitis. Focusing on the effect of Dexmedetomidine (DEX) on Immune cells, Chen et al. comprehensively reviewed the published human and animal studies related to DEX, and its role in related diseases, and discussed the potential research direction.

Conclusion and future perspective

Small molecules offer numerous advantages compared to currently used biological therapies. Identifying small molecules

with shorter half-lives helps the patients stop taking their medication quickly, which could offer better medical management. Hence, employing advanced and novel approaches in the development of small molecule therapeutics is urgently needed. We hope that the scientific knowledge provided in this special issue will encourage many researchers to address the several outstanding challenges in this field to advance scientific research on inflammatory signaling events and small molecule interactions to promote better therapeutic development.

Author contributions

All the authors contributed equally to the editing and writing of this article. Furthermore, all authors approved the final version of this article.

Conflict of interest

The authors declare that the research was conducted in the absence of any commercial or financial relationships that could be construed as a potential conflict of interest.

Publisher's note

All claims expressed in this article are solely those of the authors and do not necessarily represent those of their affiliated organizations, or those of the publisher, the editors and the reviewers. Any product that may be evaluated in this article, or claim that may be made by its manufacturer, is not guaranteed or endorsed by the publisher.

References

Hanke, T., Merk, D., Steinhilber, D., Geisslinger, G., and Schubert-Zsilavecz, M. (2016). Small molecules with anti-inflammatory properties in clinical development. *Pharmacol. Ther.* 157, 163–187. doi:10.1016/j.pharmthera.2015.11.011

Kohler, O., Krogh, J., Mors, O., and Benros, M. E. (2016). Inflammation in depression and the potential for anti-inflammatory treatment. *Curr. Neuropharmacol.* 14 (7), 732–742. doi:10.2174/1570159x14666151208113700

Mukherjee, R., Bhattacharya, A., Bojkova, D., Mehdipour, A. R., Shin, D., Khan, K. S., et al. (2021). Famotidine inhibits toll-like receptor 3-mediated inflammatory signaling in SARS-CoV-2 infection. *J. Biol. Chem.* 297 (2), 100925. doi:10.1016/j.jbc.2021.100925

Ramprasath, T., Han, Y. M., Zhang, D., Yu, C. J., and Zou, M. H. (2021). Tryptophan catabolism and inflammation: A novel therapeutic target for aortic diseases. *Front. Immunol.* 12, 731701. doi:10.3389/fimmu.2021.731701

Wongrakpanich, S., Wongrakpanich, A., Melhado, K., and Rangaswami, J. (2018). A comprehensive review of non-steroidal anti-inflammatory drug use in the elderly. *Aging Dis.* 9 (1), 143–150. doi:10.14336/AD.2017.0306

Zhong, Z., Umemura, A., Sanchez-Lopez, E., Liang, S., Shalapour, S., Wong, J., et al. (2016). NF-κB restricts inflammasome activation via elimination of damaged mitochondria. *Cell* 164 (5), 896–910. doi:10.1016/j.cell.2015.12.057

Zhu, N., and Hou, J. (2021). Molecular mechanism of the anti-inflammatory effects of Sophorae Flavescentis Aiton identified by network pharmacology. *Sci. Rep.* 11 (1), 1005. doi:10.1038/s41598-020-80297-y

Zhu, F., Zhao, X., Li, J., Guo, L., Bai, L., and Qi, X. (2020). A new compound Trichomicin exerts antitumor activity through STAT3 signaling inhibition. *Biomed. Pharmacother.* 121, 109608. doi:10.1016/j.biopha.2019.109608

frontiers in Pharmacology

ORIGINAL RESEARCH
published: 05 November 2021
doi: 10.3389/fphar.2021.748740

CXCR7 Antagonism Reduces Acute Lung Injury Pathogenesis

Laetitia Pouzol[*†], *Anna Sassi*[†], *Nadège Baumlin, Mélanie Tunis, Daniel S. Strasser, François Lehembre and Marianne M. Martinic*

Idorsia Pharmaceuticals Ltd., Allschwil, Switzerland

Loss of control in the trafficking of immune cells to the inflamed lung tissue contributes to the pathogenesis of life-threatening acute lung injury (ALI) and its more severe form, acute respiratory distress syndrome (ARDS). Targeting CXCR7 has been proposed as a potential therapeutic approach to reduce pulmonary inflammation; however, its role and its crosstalk with the two chemokine receptors CXCR3 and CXCR4 via their shared ligands CXCL11 and CXCL12 is not yet completely understood. The present paper aimed to characterize the pathological role of the CXCR3/CXCR4/CXCR7 axis in a murine model of ALI. Lipopolysaccharide (LPS) inhalation in mice resulted in the development of key pathologic features of ALI/ARDS, including breathing dysfunctions, alteration in the alveolar capillary barrier, and lung inflammation. LPS inhalation induced immune cell infiltration into the bronchoalveolar space, including $CXCR3^+$ and $CXCR4^+$ cells, and enhanced the expression of the ligands of these two chemokine receptors. The first-in-class CXCR7 antagonist, ACT-1004-1239, increased levels of CXCL11 and CXCL12 in the plasma without affecting their levels in inflamed lung tissue, and consequently reduced $CXCR3^+$ and $CXCR4^+$ immune cell infiltrates into the bronchoalveolar space. In the early phase of lung inflammation, characterized by a massive influx of neutrophils, treatment with ACT-1004-1239 significantly reduced the LPS-induced breathing pattern alteration. Both preventive and therapeutic treatment with ACT-1004-1239 reduced lung vascular permeability and decreased inflammatory cell infiltrates. In conclusion, these results demonstrate a key pathological role of CXCR7 in ALI/ARDS and highlight the clinical potential of ACT-1004-1239 in ALI/ARDS pathogenesis.

Keywords: acute lung injury, acute respiratory distress syndrome, immunomodulation, CXCR7, CXCR3, CXCR4, CXCL11, CXCL12

OPEN ACCESS

Edited by:
Ramasamy Subbiah, Madurai Kamaraj University, India

Reviewed by:
Rekha Balakrishnan, City of Hope National Medical Center, United States
Ganesh Satyanarayana, Georgia State University, United States
Nandakumar Natarajan, University of California, San Francisco, United States

****Correspondence:***
Laetitia Pouzol
laetitia.pouzol@idorsia.com

[†]These authors have contributed equally to this work and share first authorship

Specialty section:
This article was submitted to Inflammation Pharmacology, a section of the journal Frontiers in Pharmacology

Received: *28 July 2021*
Accepted: *12 October 2021*
Published: *05 November 2021*

Citation:
Pouzol L, Sassi A, Baumlin N, Tunis M, Strasser DS, Lehembre F and Martinic MM (2021) CXCR7 Antagonism Reduces Acute Lung Injury Pathogenesis. Front. Pharmacol. 12:748740. doi: 10.3389/fphar.2021.748740

INTRODUCTION

Acute lung injury (ALI) and its more severe form, acute respiratory distress syndrome (ARDS), are life-threatening lung diseases that can be the result of different indirect or direct insults to the lung, such as sepsis, trauma, gastric acid aspiration, and pneumonia, including viral pneumonia, such as SARS-CoV-2-induced pneumonia (Wheeler and Bernard, 2007; Gibson et al., 2020). To date, the

Abbreviations: ALI, acute lung injury; ANOVA, analysis of variance; ARDS, acute respiratory distress syndrome; BAL, bronchoalveolar lavage; bid, twice daily; DCs, dendritic cells; LPS, lipopolysaccharide; NK cells, Natural killer cells; pDCs, plasmacytoid dendritic cells; SEM, standard error of the mean.

pathogenesis of these diseases is still not completely understood, and there is no disease-modifying therapy to reduce the high mortality incidence of ARDS (Bellani et al., 2016).

ALI and ARDS are characterized by increased lung vascular permeability, pulmonary edema, diffuse alveolar damage, and recruitment of inflammatory cells to the lungs resulting in clinical symptoms such as hypoxemia, dyspnea, and even severe acute respiratory failure (Ware and Matthay, 2000).

Many chemokines and their receptors, which are key mediators of immune cell trafficking, play a critical role in ALI pathogenesis and in its resolution (Bhatia et al., 2012; Tomankova et al., 2015). Following lung injury, chemokine gradients are established and tightly regulated via complex mechanisms to recruit inflammatory cells to the site of inflammation (Puneet et al., 2005).

CXCR3/CXCR4/CXCR7 and their ligands are overexpressed and heavily implicated in the pathology of a number of inflammatory diseases including pulmonary diseases (Saetta et al., 2002; Petty et al., 2007; Hartl et al., 2008; Costello et al., 2012; Ichikawa et al., 2013; Ngamsri et al., 2017; Liao et al., 2020).

CXCR7, also referred to as ACKR3, is an atypical chemokine receptor, which is mainly expressed on endothelial cells (Berahovich et al., 2014). CXCR7 does not couple with G proteins, but binding of its ligands leads to the recruitment of β-arrestin. CXCR7 functions predominantly as a scavenger receptor for its chemokine ligands CXCL11 and CXCL12 (Naumann et al., 2010), which bind to, and activate, the signaling chemokine receptors CXCR3 and CXCR4, respectively. While CXCR7 is not expressed on leukocytes (Berahovich et al., 2010), its scavenging activity in endothelial cells contributes to the establishment and maintenance of CXCL11 and CXCL12 concentration gradients along which $CXCR3^+$ and $CXCR4^+$ cells can migrate from the blood toward the inflamed tissue (Lewellis and Knaut, 2012; Quinn et al., 2018; Pouzol et al., 2021).

CXCR3 is a cell surface receptor expressed on subsets of adaptive and innate immune cells such as lymphocytes, natural killer (NK) cells, dendritic cells (DCs), and can be activated by three interferon-inducible chemokine ligands: CXCL9, CXCL10, and CXCL11 (Groom and Luster, 2011). CXCR3–ligand interaction results in various cellular functions including cell migration, proliferation, polarization, and tissue retention (Groom and Luster, 2011).

CXCR4 is expressed on various immune cells including lymphoid and myeloid cells, endothelial cells, and hematopoietic stem cells (Lewellis and Knaut, 2012). CXCL12–CXCR4 signaling results in pleiotropic cellular functions including cell migration, adhesion, proliferation, differentiation, and survival (Quinn et al., 2018).

Blockade of CXCR7 is expected to increase the systemic CXCL11 and CXCL12 levels and, therefore, modulate CXCR3 and CXCR4 signaling activities such as leukocyte chemotaxis and tissue retention (Berahovich et al., 2014; Pouzol et al., 2021). In line with this hypothesis, treatment with CCX771, a CXCR7 functional antagonist, which is known to increase plasma CXCL12 levels (Berahovich et al., 2014), led to reduced alveolar inflammation and lung microvascular permeability in a murine model of ALI (Konrad et al., 2017; Ngamsri et al., 2017). However, this murine model was performed in C57BL/6 mice, which do not express CXCL11 (Sierro et al., 2007). As such, the specific role of CXCR7 in ALI and its indirect effect on CXCR3 and CXCR4 via their shared ligands have not yet been evaluated in an appropriate experimental design. In addition, since so far only CCX771, which recruits β-arrestin upon binding to the receptor, has been used in the ALI model (Zabel et al., 2009), it remains unclear whether the observed efficacy is due to its agonistic activity or its functional antagonism induced by receptor desensitization (Menhaji-Klotz et al., 2020).

To elucidate the role of CXCR7 on pulmonary inflammation, an ALI/ARDS experimental model was established through inhalation of nebulized lipopolysaccharide (LPS) in DBA/1 mice, a strain susceptible to LPS-induced ALI (Alm et al., 2010) and known to express both CXCL11 and CXCL12 (Richard-Bildstein et al., 2020). Since the pathological mechanisms of LPS-induced ALI/ARDS can vary between the early and late phases of the inflammatory response (Domscheit et al., 2020), this model was characterized over time for the main features of ALI/ARDS, namely, lung dysfunction, vascular permeability, inflammatory cell recruitment, and CXCR3/CXCR4/CXCR7 chemokine ligands release. Furthermore, the mechanistic and functional roles of CXCR7 were evaluated over time using the selective and first-in-class CXCR7 antagonist ACT-1004-1239, which blocks CXCL11- and CXCL12-induced β-arrestin recruitment (Richard-Bildstein et al., 2020).

MATERIALS AND METHODS

Mice and Treatment Administration

Male DBA/1 mice were purchased from Janvier Laboratories (Le Genest-Saint-Isle, France) and allowed to acclimatize for at least 7 days before use. The gender of mice was chosen based on previous studies showing that ARDS occurs more commonly in males than in females (Lemos-Filho et al., 2013). Mice had free access to food and drinking water *ad libitum* and were group housed in a light-controlled environment.

The CXCR7 antagonist ACT-1004-1239 was synthetized as previously described (Richard-Bildstein et al., 2020). The compound was formulated in 0.5% methylcellulose (Sigma-Aldrich, Schnelldorf, Germany) and 0.5% Tween 80 (Sigma-Aldrich) in water. ACT-1004-1239 and vehicle (0.5% methylcellulose, 0.5% Tween 80 in water) were administered orally (p.o.), twice a day (b.i.d.) at a volume of 5 ml/kg/administration (10 ml/kg/day) at doses and times indicated in the figure legends. The twice-daily oral administration regimen was based on the pharmacokinetic properties of this compound, which has been shown to be a high-clearance drug in rodents (Richard-Bildstein et al., 2020).

Murine Model of Lipopolysaccharide-Induced Acute Lung Injury

LPS challenge was performed as previously described (de Souza Xavier Costa et al., 2017). Briefly, mice were exposed to nebulized

LPS (*Escherichia coli* O111:B4, purified by phenol extraction; Sigma-Aldrich) at 0.8 mg/ml diluted in NaCl 0.9% (B Braun Medical, Sempach, Switzerland) in a plexiglas chamber connected to a nebulizer (System Assistance Medicale, Ledat, France) for 30 min. Control mice inhaled NaCl 0.9% only. Vehicle or ACT-1004-1239 was given p.o., 1 h prior (preventive setting) or 3 h post inhalation (therapeutic setting).

At different time points indicated in the figure legends (5, 24, 48, 72 h) following LPS or NaCl challenge, mice were euthanized with an overdose (150 mg/kg, intraperitoneally) of pentobarbital (Esconarkon, Streuli Pharma SA, Uznach, Switzerland), and samples were collected.

In Vivo Lung Function

Lung function was measured in unrestrained, conscious, and spontaneously breathing mice by whole-body plethysmography (Emka Technologies, Paris, France) as previously described (Piali et al., 2017). Briefly, each mouse was placed alone in a calibrated plethysmography chamber, and lung function parameters were recorded for 1 h for baseline assessment. Right after the baseline, ACT-1004-1239 or vehicle was given orally 1 h prior to nebulized LPS or NaCl inhalation. Respiration parameters were measured for 6 h just after the challenge in the plethysmograph. Enhanced pause, Penh, [(Te/RT)-1)*PEF/PIF, where Te is the expiratory time, RT is the relaxation time, PEF is the peak expiratory flow, and PIF is the peak inspiratory flow) was used as an index of alterations in respiration (Hamelmann et al., 1997; Prada-Dacasa et al., 2020). Data were analyzed using the IOX2 software (Emka) and expressed as area under the curve (AUC), recorded for 30 min and averaged at 5-min intervals. The time indicated in the figure refers to the starting time of the analyzed period (e.g., 60 min refers to the AUC calculated for the 60- to 90-min time interval). The mean Penh AUC baseline measurement was set to 100% for each mouse, and calculated Penh AUC data were expressed as percentage of this mean baseline measurement.

Bronchoalveolar Lavage Collection

BAL fluid was collected at different time points indicated in the figure legends following LPS or NaCl challenge. BAL was performed by injection of a total volume of 2.25 ml of phosphate-buffered saline (PBS, Bioconcept, Allschwil, Switzerland) supplemented with EDTA (0.5 mM, Gibco, Thermo Fisher Scientific, Waltham, MA, United States) through the mouse incised trachea. After centrifugation, BAL supernatant was collected and kept at −20°C until use. BAL cells were analyzed by flow cytometry.

Flow Cytometry of the Bronchoalveolar Lavage Cells

BAL cells were stained with the following surface fluorochrome-conjugated monoclonal anti-mouse antibodies: APC-Cy7 anti-mouse CD19 (Clone 6D5; BioLegend, San Diego, CA, United States), APC anti-mouse CXCR3 (Clone CXCR3-173; BioLegend), BV510 anti-mouse CD11b (Clone M1/70; BioLegend), BV605 anti-mouse CD4 (Clone GK1.5; BioLegend), FITC anti-mouse B220 (Clone Ra3-6B2; BD), PB anti-mouse CD45 (Clone 30-F11; BioLegend), PECy7 anti-mouse βTCR (Clone H57-597; BioLegend), PE anti-mouse CXCR4 (Clone 2B11; Invitrogen, Thermo Fisher Scientific), BV650 anti-mouse CD8 (Clone 53-6.7; BioLegend), APC-Cy7 anti-mouse Gr-1 (Clone RB6-8C5; BioLegend), AF700 anti-mouse CD3 (Clone 17A2; BioLegend), FITC anti-mouse CD49b (Clone DX5; BioLegend), BV-605 anti-mouse B220 (Clone RA3-6B2; BioLegend), and PECy7 anti-mouse CD11c (Clone N418; BioLegend). Staining was performed on ice, in the dark, during 45 min after preincubation with Fc receptor blocker (CD16/CD32; BD Biosciences). Dead cells were excluded based on their positive staining with propidium iodide (PI; CAS 25535-16-4; Sigma-Aldrich). Samples were acquired on a CytoFLEX Flow cytometer (Beckman Coulter Life Sciences, Nyon, Switzerland), and data were analyzed using the Kaluza analysis software version 2.1 (Beckman Coulter). Cells were first gated in forward scatter versus side scatter, and doublets were excluded based on forward scatter area–height. From the single cells, dead cells were excluded based on their positive staining with PI. Cell subsets were quantified among viable/$CD45^+$ cells (PI^-, $CD45^+$ cells): neutrophils ($CD11b^+$, Gr-1^{high} cells), monocytes/macrophages ($CD11b^+$, Gr-1^{low} cells), alveolar macrophages ($CD11b^{int}$, SSC^{high}), B cells ($CD11b^-$, Gr-1^-, $CD49^-$, $CD3^-$, $B220^+$ cells), plasmacytoid dendritic cells (pDCs) ($CD11b^-$, Gr-1^{int}, $B220^+$, $CD11c^+$ cells), T cells ($CD11b^-$, $B220^-$, $CD49b^-$, $CD3^+$ cells), natural killer (NK) cells ($CD11b^-$, $CD3^-$, $CD49b^+$), and dendritic cells (DCs) ($CD11b^-$, $B220^-$, $CD49b^-$, $CD3^-$, $CD11c^+$ cells). The $CXCR4^+$ and $CXCR3^+$ leukocytes were identified based on the fluorescence minus one control for CXCR4 and CXCR3, respectively. The gating strategies are illustrated in **Supplementary Figures S1, S3**.

CXCL12 and CXCL11 Measurement

Whole blood was collected in EDTA-coated tubes (BD Microtainer, Becton Dickinson, Franklin Lakes, NJ, United States) and centrifuged to prepare plasma. After blood and BAL collection, mice were transcardially perfused with PBS/EDTA. Lungs were collected as a whole and kept at −20°C until use. Frozen mouse lungs were homogenized (FastPrep, MP Biomedicals, Illkirch, France) in RIPA buffer supplemented with 1% protease inhibitor (Sigma-Aldrich, P8340) and phosphatase inhibitor (PhosSTOP Tablets, Sigma-Aldrich). Plasma samples and lung homogenates were assayed for CXCL12 concentration using the mouse CXCL12/SDF1α Quantikine ELISA (catalog no. MCX120; R&D Systems, Minneapolis, MN, United States) according to the instruction of the manufacturer. The method was monitored using quality control samples provided in the assay kit. Mouse CXCL12 levels in BAL supernatant were determined using a commercially available electrochemiluminescence sandwich immunoassay (K152VBK-1; U-plex mouse CXCL12; Meso Scale Discovery). Recombinant human CXCL12 standard DuoSet kit (DY350; RnD Systems) was used for the standard curve. The assay was performed according to the instruction for use.

Mouse CXCL11 was quantified using an ultrasensitive immunoassay built on the Single Molecule Counting (SMC™) technology (Erenna® Immunoassay System, Merck Millipore, Billerica, MA, United States). Paramagnetic microparticles

(beads) coated with anti-mouse CXCL11 monoclonal antibody (MAB572; R&D Systems) was used as the capturing antibody. Recombinant murine CXCL11 (250-29; Peprotech, Cranbury, NJ, United States) was used as a standard, and Fluor-labeled anti-mouse CXCL11 polyclonal antibody (AF572; R&D Systems) was used as the detection antibody. The number of fluorescently labeled detection antibodies counted with the Erenna® System is directly proportional to the amount of mouse CXCL11 present in the EDTA Plasma.

CXCL9 and CXCL10 Measurement

Concentrations of the chemokines CXCL9 and CXCL10 in BAL supernatant were measured using a commercial mouse cytokine magnetic bead multiplex immunoassay kit (#MCYTOMAG-70K, Merck Millipore) according to the instruction of the manufacturer. Samples were acquired on a Luminex 200 instrument system (Thermo Fischer Scientific), and data were analyzed using SoftMaxPro software (Molecular Device, San Jose, CA, USA).

Bronchoalveolar Lavage Supernatant Proteins

Protein concentrations in the BAL supernatant were determined using the BCA Protein assay kit (Pierce #23225, Thermo Fisher Scientific) according to the instruction of the manufacturer.

Statistical Analysis

All data were expressed as mean ± standard error of the mean (SEM). Statistical analysis was performed using Prism version 8.1.1 (GraphPad software, San Diego, CA, United States) using the tests specified in the figure legends. Briefly, data were evaluated using two-tailed unpaired Student *t*-test, one-way or two-ways analysis of variance (ANOVA) with a *post-hoc* multiple comparison tests as appropriate. Differences were considered significant at p values <0.05.

RESULTS

Lipopolysaccharide-Induced Acute Lung Injury/Acute Respiratory Distress Syndrome Model in DBA/1 Mice

Characterization of the consequences of LPS inhalation in DBA/1 mice was conducted to confirm in this experimental animal model (Matute-Bello et al., 2008) the presence of key features defining human ALI/ARDS, namely, breathing dysfunction, increased alveolar capillary barrier permeability, and immune cell infiltrates into the airspaces and the lung tissue.

Whole-body plethysmography on conscious, unrestrained mice was performed to monitor the physiological lung dysfunction caused by LPS. Inhalation of nebulized LPS caused a significant increase in enhanced pause (Penh), an index used as a marker of breathing pattern alteration (Hamelmann et al., 1997; Prada-Dacasa et al., 2020), compared with control mice receiving NaCl nebulization (**Figure 1A**). The increase in Penh peaked between 1.5 and 2 h after LPS challenge and remained elevated throughout the 6-h evaluation period.

To assess the effect of LPS on alveolar capillary barrier permeability, total protein concentration was measured in the BAL supernatant up to 72 h after LPS challenge. Total BAL protein concentration was significantly increased from 24 h up to 72 h after LPS challenge, compared with control mice (**Figure 1B**). To determine the effect of LPS on inflammatory cell recruitment to the alveolar space, BAL immune cell phenotyping was performed using flow cytometry. LPS inhalation led to a time-dependent infiltration of $CD45^+$ immune cells into the BAL compared with control mice, peaking 24 h after LPS challenge (**Figure 1C** and **Supplementary Figure S1**). In control mice, the main BAL immune cell population was represented by tissue resident alveolar macrophages (**Figure 1D** and **Supplementary Figure S1**). In contrast, in LPS-exposed mice, 5 h after LPS challenge, neutrophils represented the majority of BAL immune infiltrates (**Figure 1D**). This early massive influx of neutrophils peaked 24 h after the LPS challenge before strongly decreasing 48 and 72 h post-LPS challenge (**Table 1**). Other BAL immune cells such as NK cells, B cells, pDCs, and classical $CD11b^-$ DCs also peaked 24 h after LPS challenge (**Table 1**) but altogether represented less than 9% of the overall BAL population at any given time point (**Figure 1D**). In contrast, infiltration of inflammatory macrophages and T cells peaked later, at 48 h after LPS challenge (**Table 1**), and together represented more than 20% of the BAL immune cells (**Figure 1D**). At 72 h post-LPS challenge, BAL immune cell numbers were still significantly increased compared with control mice (**Figure 1C** and **Table 1**). Infiltration of neutrophils was also confirmed in the lung tissue by histology, 24 h after LPS challenge (**Supplementary Figure S2**).

Taken together, these results demonstrate that inhalation of nebulized LPS in DBA/1 mice induced an acute and time-dependent increase in breathing dysfunction, vascular permeability, and infiltration of immune cells into the alveolar space and the lung tissue, and confirm this model as suitable to evaluate these pathogenic features of human ALI/ARDS in DBA/1 mice.

The Increase of CXCR3 and CXCR4 Ligands in the Bronchoalveolar Lavage is Associated With an Increase of $CXCR3^+$ and $CXCR4^+$ Bronchoalveolar Lavage Immune Cell Infiltrates

To confirm that in this strain of mice both the CXCR3/CXCL9/10/11 and CXCR4/CXCL12 axes played a role in the recruitment of immune infiltrates into the BAL, the expression of CXCR3 and CXCR4 on infiltrating immune cells and the release of their ligands were characterized in the alveolar space following LPS challenge.

In the BAL supernatant, LPS challenge led to a significant increase in the three CXCR3 ligands CXCL9, CXCL10, and CXCL11, compared with control mice (**Figure 2A**), reaching

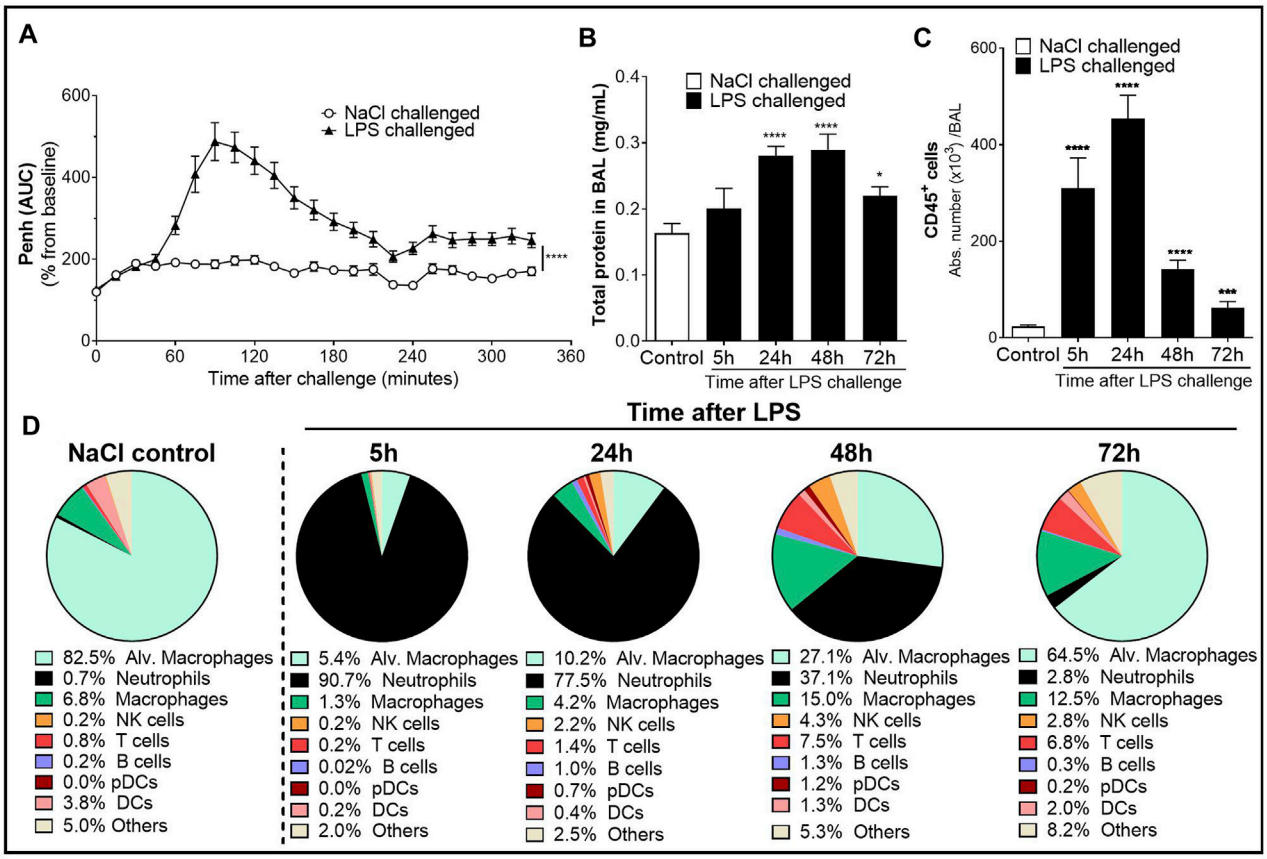

FIGURE 1 | Characterization of the lipopolysaccharide (LPS)-induced acute lung injury (ALI)/acute respiratory distress syndrome (ARDS) model in male DBA/1 mice. LPS inhalation was associated with a significant breathing pattern alteration **(A)**, an increase in alveolar–capillary barrier permeability **(B)**, and increased immune cell infiltrates in the bronchoalveolar space **(C, D)** compared with NaCl-exposed mice (control mice). **(A)** Breathing pattern alteration was measured by the change in the calculated enhanced pause (Penh) using whole-body plethysmography in conscious unrestrained mice over a period of 6 h following LPS (black triangles) or NaCl inhalation (white circles). Results are expressed as the mean percentage Penh area under the curve (AUC) normalized to the baseline ± SEM (n = 16 mice per group). ****$p < 0.0001$ paired Student t-test. **(B)** Alveolar–capillary barrier permeability was assessed by measuring the total protein concentration in the bronchoalveolar lavage (BAL) supernatant at 5, 24, 48, and 72 h after LPS challenge (black bars, n = 7–16 mice per time point) or NaCl challenge (control mice, white bar, n = 20; all time points were pooled). Results are expressed as mean ± SEM. *$p < 0.05$, ****$p < 0.0001$ paired Student t-test. **(C)** Time course of $CD45^+$ immune cells in the BAL measured by flow cytometry in samples collected at 5, 24, 48, and 72 h after LPS challenge (black bars, n = 7–16 mice per time point) or NaCl challenge (control mice, white bar, n = 20; all time points were pooled). Results are expressed as mean ± SEM. ***$p < 0.001$, ****$p < 0.0001$ paired Student t-test. **(D)** Frequencies of BAL immune cell populations over time. Results are expressed as proportions among total $CD45^+$ cells for each time point.

the highest increase 24 h post-LPS challenge. Seventy-two hours after LPS challenge, CXCL11 returned to control levels, while CXCL9 and CXCL10 were still significantly elevated compared with control mice (**Figure 2A**). CXCR3 expression was mainly detected on $CD11b^-$ BAL lymphoid cells compared with $CD11b^+$ BAL myeloid cells; in the latter population, CXCR3 was only detected at low levels 48 and 72 h post LPS challenge (**Figures 2B, C** and **Supplementary Figure S3**). Interestingly, the expression of CXCR3 (**Figure 2C**) and proportion of $CXCR3^+$ BAL lymphoid and myeloid cells (**Figure 2D**) increased over time following LPS nebulization. At 72 h post LPS challenge, almost 60% of BAL lymphoid cells expressed CXCR3 (**Figure 2D**); in absolute counts, $CXCR3^+$ BAL lymphoid cells were only slightly reduced compared with earlier time points but were still significantly increased compared with control mice (**Figure 2E**).

LPS inhalation also led to a significant increase in BAL CXCL12 levels compared with control mice, which peaked at 24 h and returned to control levels 72 h post-LPS challenge (**Figure 2F**). In the BAL from LPS-challenged mice, CXCR4 expression was detected on the cell surface of most infiltrating leukocytes, with the highest surface expression detected on myeloid cells (**Figure 2G** and **Supplementary Figure S3**). While the expression of CXCR4 on lymphoid cells and the proportion of $CXCR4^+$ BAL lymphoid infiltrates remained stable following LPS nebulization, the expression of CXCR4 on myeloid cells and the proportion of $CXCR4^+$ BAL myeloid infiltrates increased over time, reaching over 80% at the last time point investigated (**Figures 2H, I**). In absolute counts, the highest number of $CXCR4^+$ BAL myeloid cells was reached 24 h post-LPS challenge but still remained significantly elevated 72 h post-LPS challenge, compared with control mice (**Figure 2J**).

TABLE 1 | Time course of immune cells present in the bronchoalveolar lavage (BAL) following LPS or NaCl challenge in DBA/1 mice.

Challenge:		NaCl (control)	Lipopolysaccharide (LPS)			
Time points post challenge		Pool (*n* = 20)	5 h (*n* = 8)	24 h (*n* = 16)	48 h (*n* = 16)	72 h (*n* = 7–8)
			Abs number (×10^3 cells/BAL)			
$CD11b^{low}$ FSC^{high}	Alveolar macrophages	19.4 ± 2.9	16.6 ± 2.7	46.3 ± 13.1*	38.7 ± 10.2	40.5 ± 9.6*
$CD11b^+$ cells (Myeloid cells)	Neutrophils	0.2 ± 0.0	281.0 ± 61.4****	352.3 ± 29.2****	53.0 ± 8.3****	1.7 ± 0.3****
	Inflammatory macrophages	1.6 ± 0.3	4.1 ± 0.5***	19.1 ± 3.6****	21.4 ± 3.1****	7.8 ± 1.4****
$CD11b^-$ cells (Lymphoid cells)	NK cells	0.1 ± 0.0	0.6 ± 0.1****	9.9 ± 1.6****	6.1 ± 1.1****	1.7 ± 0.4****
	T cells	0.2 ± 0.0	0.6 ± 0.1***	6.2 ± 0.8****	10.7 ± 2.1****	4.3 ± 0.9****
	B cells	0.0 ± 0.0	0.1 ± 0.0	4.6 ± 1.6**	1.8 ± 0.4****	0.2 ± 0.0*
	pDCs	0.0 ± 0.0	0.0 ± 0.0	3.4 ± 0.9***	1.7 ± 0.6**	0.1 ± 0.0****
	DCs	0.9 ± 0.2	0.7 ± 0.0	1.8 ± 0.4*	1.8 ± 0.2**	1.3 ± 0.2

Note. Acute lung injury (ALI) was induced by LPS nebulization in male DBA/1 mice, and flow cytometry analysis of BAL immune infiltrates was performed 5, 24, 48, and 72 h after LPS challenge (n = 7–16 mice per time point). Control mice received a nebulization of NaCl 0.9% (n = 20 mice; all time points were pooled). The gating strategy for all immune populations is illustrated in ***Supplementary Figure S1A****. Results are expressed as mean ± SEM.*
**p < 0.05, **p < 0.01, ***p < 0.001, ****p < 0.0001 versus control mice using Student t-test.*

In conclusion, LPS challenge of DBA/1 mice resulted in a significant increase in CXCR3/CXCR4 ligand levels, including the CXCR7 ligands CXCL11 and CXCL12, in the BAL supernatant. This increase was associated with a significant increase in predominantly $CXCR3^+$ lymphoid and $CXCR4^+$ myeloid cells in the BAL.

CXCR7 Antagonism Increases Plasma CXCL11 and CXCL12 Levels and is Associated With a Reduction in $CXCR3^+$ and $CXCR4^+$ Bronchoalveolar Lavage Immune Cell Infiltrates After Lipopolysaccharide Challenge

The scavenging activity of CXCR7 expressed on endothelial cells has been proposed to generate CXCL11 and CXCL12 chemokine gradients, thus, enabling a directional migration of $CXCR3^+$ and $CXCR4^+$ cells, respectively, from the circulation toward sites of inflammation (Berahovich et al., 2014; Tobia et al., 2019; Pouzol et al., 2021). To evaluate this hypothesis, the impact of CXCR7 antagonism on plasma and lung tissue CXCL11 and CXCL12 levels and BAL immune cell infiltrates was investigated in the ALI/ARDS DBA/1 mouse model following treatment with ACT-1004-1239.

CXCR7 antagonism further increased the LPS-induced elevation of CXCL11 plasma levels at all time points investigated compared with vehicle-treated, LPS-challenged mice (**Figure 3A**), confirming the proposed scavenging activity of CXCR7. In contrast, in the lung tissue, treatment with ACT-1004-1239 did not further increase CXCL11 concentrations but rather tended to normalize CXCL11 levels from LPS-challenged mice throughout the study period (**Figure 3B**). In the BAL from LPS-challenged mice, treatment with ACT-1004-1239 significantly reduced LPS-induced $CXCR3^+$ lymphoid cell recruitment (**Figure 3C**) and showed a trend to decrease the late recruitment of the few $CXCR3^+$ myeloid cells induced by LPS, although this did not reach statistical significance (**Figure 3D**).

Treatment with ACT-1004-1239 led to a robust and significant increase in plasma CXCL12 concentrations at all time points tested compared with vehicle-treated, LPS-challenged mice (**Figure 3E**). In contrast to the effect seen in plasma, in the lung tissue, CXCR7 antagonism did not further increase the LPS-induced elevation in CXCL12 levels and even resulted in a slight reduction in CXCL12 levels at 24 h post LPS challenge compared with vehicle-treated LPS-challenged mice (**Figure 3F**). In the BAL from LPS-challenged mice, at all time points investigated, treatment with ACT-1004-1239 significantly reduced BAL $CXCR4^+$ lymphoid (**Figure 3G**) and $CXCR4^+$ myeloid cell infiltrates (**Figure 3H**) compared with vehicle-treated LPS-challenged mice.

To investigate the dose-dependent effect of CXCR7 antagonism on plasma CXCL11 and CXCL12 levels and on immune cell recruitment to the alveolar space, mice were treated with three different doses of ACT-1004-1239 (10, 30, and 100 mg/kg, p.o., twice daily) or vehicle for 3 days, starting 1 h prior to LPS challenge. Treatment with ACT-1004-1239 dose-dependently increased plasma CXCL11 and CXCL12 concentrations (**Figures 4A, B**); this was accompanied by a dose-dependent decrease in the major immune cell infiltrates present in the BAL after 72 h (**Figure 4D**), namely, T cells (**Figure 4C**) and macrophages (**Figure 4D**).

Taken together, these data demonstrate that CXCR7 antagonism with ACT-1004-1239 significantly increased plasma CXCL11 and CXCL12 levels in a dose-dependent manner and was associated with a reduction in $CXCR3^+$ and $CXCR4^+$ BAL immune infiltrates.

CXCR7 Antagonism Reduces Lipopolysaccharide -Induced Acute Lung Injury/Acute Respiratory Distress Syndrome

To monitor whether the CXCR7 antagonist ACT-1004-1239 would affect LPS-induced breathing dysfunction, whole-body plethysmography on conscious, unrestrained DBA/1 mice was performed. As previously reported (Lefort et al., 2001), LPS nebulization caused a significant increase in enhanced pause

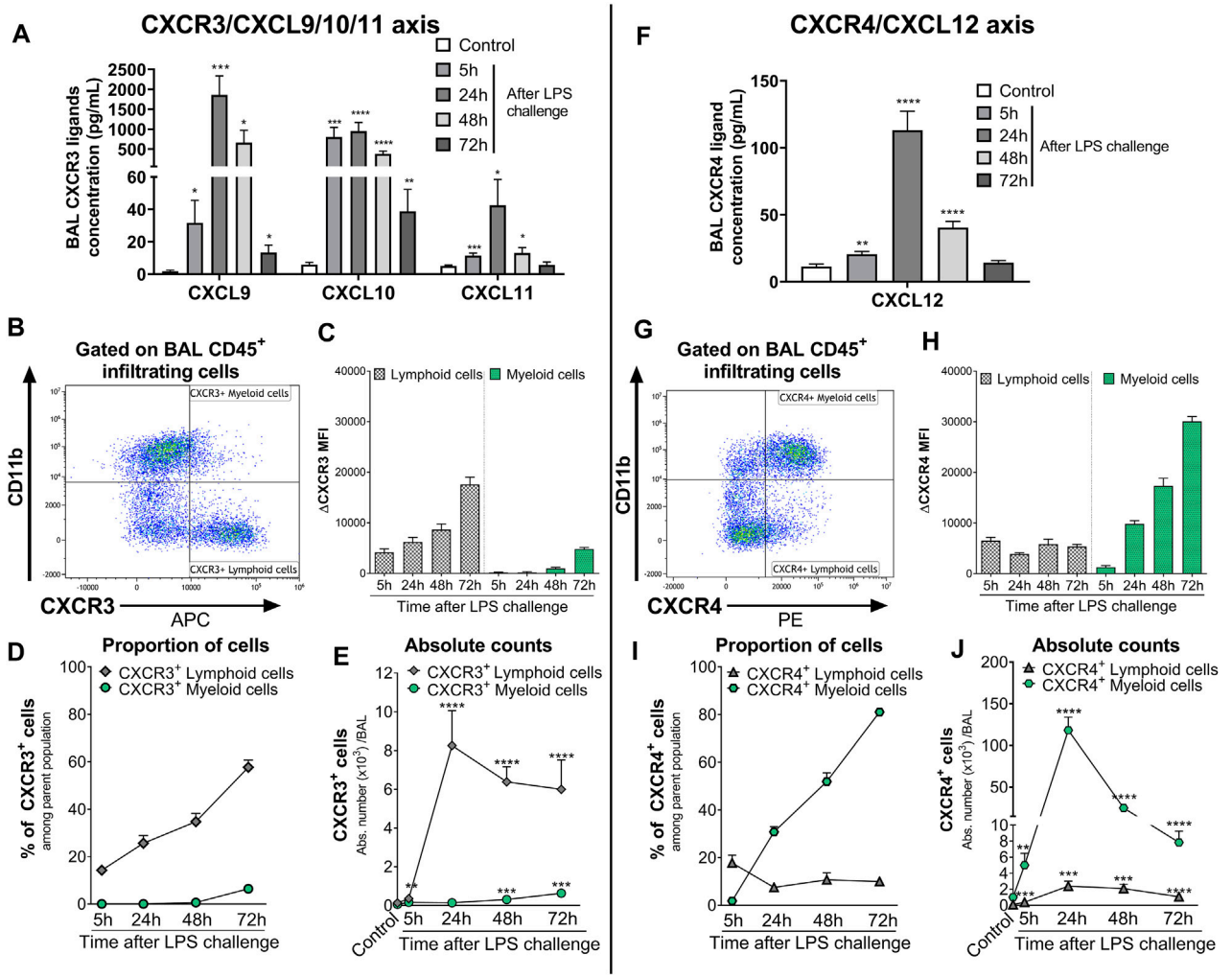

FIGURE 2 | Kinetics of the expression of CXCR3/CXCR4 and its ligands in the BAL of LPS-challenged DBA/1 mice. ALI was induced by nebulized LPS inhalation in male DBA/1 mice. Control mice inhaled NaCl 0.9% (n = 12 mice; all time points were pooled). **(A)** LPS inhalation increased protein concentrations of the CXCR3 ligands CXCL9, CXCL10, and CXCL11, measured in the BAL 5, 24, 48, and 72 h following LPS challenge, compared with control mice. Results are expressed as mean ± SEM (n = 8 mice per time point). *p < 0.05, **p < 0.01, ***p < 0.001, ****p < 0.0001 versus control mice using Student t-test. **(B)** Representative gating strategy for $CXCR3^+$ myeloid and lymphoid cells. **(C)** CXCR3 expression on BAL lymphoid and myeloid-infiltrating cells. Results are expressed as mean ± SEM of the mean fluorescence intensity (MFI) of CXCR3 obtained for each LPS-challenged mouse (n = 7–8 mice per time point) corrected by the MFI obtained in the fluorescence minus one (FMO) controls for CXCR3. Negative MFI values were set to 0. The complete gating strategy for lymphoid and myeloid cells is illustrated in **Supplementary Figure S3**. **(D)** Proportion of $CXCR3^+$ lymphoid and myeloid cells expressed as percentages (mean ± SEM) of the $CD45^+CD11b^-$ and $CD45^+CD11b^+$ parent population, respectively, in the BAL (see gating strategy in **Supplementary Figure S3**) (n = 7–8 mice per time point). **(E)** Time course of BAL $CXCR3^+$ lymphoid and myeloid cell infiltrates. Results are expressed as absolute counts in the BAL (mean ± SEM). **p < 0.01, ***p < 0.001, ****p < 0.0001 using Student t-test versus control mice. **(F)** LPS inhalation increased protein concentrations of the CXCR4 ligand CXCL12, measured in the BAL 5, 24, 48, and 72 h following LPS nebulization compared with control mice. Results are expressed as mean ± SEM (n = 7–8 mice per time point). **p < 0.01, ****p < 0.0001 versus control mice using Student t-test. **(G)** Representative gating strategy for $CXCR4^+$ myeloid and lymphoid cells. **(H)** CXCR4 expression on BAL lymphoid and myeloid-infiltrating cells. Results are expressed as mean ± SEM of the MFI of CXCR4 obtained for each LPS-challenged mouse (n = 7–8 mice per time point) corrected by the MFI obtained in the FMO controls for CXCR4. Negative MFI values were set to 0. The gating strategy for lymphoid and myeloid cells is illustrated in **Supplementary Figure S3**. **(I)** Proportion of $CXCR4^+$ lymphoid and myeloid cells expressed as percentages (mean ± SEM) of the $CD45^+CD11b^-$ and $CD45^+CD11b^+$ parent population, respectively, in the BAL (see gating strategy in **Supplementary Figure S3**) (n = 7–8 mice per time point). **(H)** Time course of BAL $CXCR4^+$ lymphoid and myeloid cell infiltrates. Results are expressed as absolute counts in the BAL (mean ± SEM) (n = 7–8 mice per time point). **p < 0.01, ***p < 0.001, ****p < 0.0001 using Student t-test versus control mice.

(Penh) AUC versus vehicle-treated mice challenged with NaCl (**Figure 5A**). A single oral administration of ACT-1004-1239 (100 mg/kg, p.o.), given 1-h prior to LPS challenge, significantly reduced the LPS-induced elevated Penh AUC, reaching values from control mice at the end of the evaluation period (**Figure 5A**), indicating a normalization of the breathing pattern. In addition, the effect of CXCR7 antagonism on LPS-induced alveolar capillary barrier permeability increase was assessed 48 h post-LPS challenge, at the peak of the LPS effect (**Figure 1B**). Treatment with ACT-1004-1239 (100 mg/kg, p.o., twice daily) was initiated either 1-h

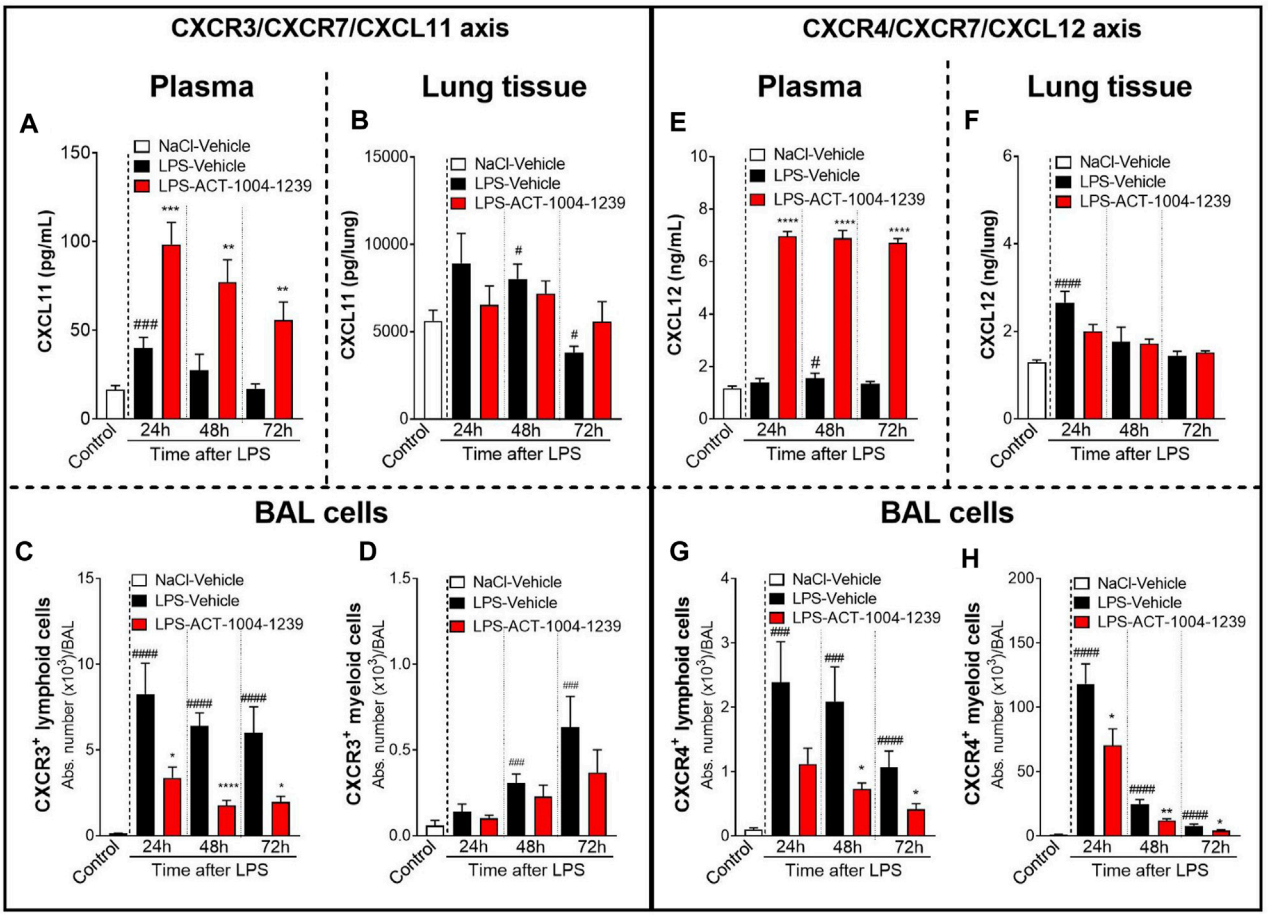

FIGURE 3 | Antagonism of CXCR7 increases plasma CXCL11 and CXCL12 levels and decreases CXCR3$^+$ and CXCR4$^+$ BAL infiltrates post LPS challenge. ALI was induced by nebulized LPS inhalation, and DBA/1 mice were treated with vehicle (LPS-vehicle, black bars) or ACT-1004-1239 (LPS-ACT-1004-1239, 100 mg/kg, red bars) orally, twice daily, 1 h prior to LPS challenge. Control mice received vehicle 1 h prior to NaCl 0.9% inhalation (NaCl-vehicle, white bars; n = 12 mice, pool of all time points). Protein concentrations of CXCL11 and CXCL12 in the plasma and lung tissue and BAL flow cytometry of immune infiltrates were performed 24, 48, and 72 h after challenge (n = 6–8 mice per time point). Time course of CXCL11 protein concentration in the plasma **(A)** and lung tissue **(B)**. Chemokine concentrations are expressed in pg/ml (plasma) or pg/lung homogenate (mean ± SEM). $^{**}p < 0.01$, $^{***}p < 0.001$ versus LPS-vehicle-treated animals or $^{\#}p < 0.05$, $^{\#\#\#}p < 0.001$ versus NaCl-vehicle-treated control mice using Student t-tests. Time course of BAL CXCR3$^+$ lymphoid **(C)** and myeloid **(D)** infiltrates. Results are expressed as absolute cell counts in the BAL (mean ± SEM). $^{*}p < 0.05$, $^{****}p < 0.0001$ versus LPS-vehicle-treated animals or $^{\#\#\#}p < 0.001$, $^{\#\#\#\#}p < 0.0001$ versus NaCl-vehicle-treated control mice using Student t-tests. Time course of CXCL12 concentration in the plasma **(E)** and lung tissue **(F)**. Chemokine concentrations are expressed in ng/ml (plasma) or ng/lung homogenate (mean ± SEM). $^{****}p < 0.0001$ versus LPS-vehicle-treated animals or $^{\#}p < 0.05$, $^{\#\#\#}p < 0.001$ versus NaCl-vehicle-treated control mice using Student t-tests. Time course of BAL CXCR4$^+$ lymphoid **(G)** and BAL CXCR4$^+$ myeloid **(H)** infiltrates. Results are expressed as absolute counts in the BAL (mean ± SEM). $^{*}p < 0.05$, $^{**}p < 0.01$, using Student t-test versus LPS-vehicle-treated animals or $^{\#\#\#}p < 0.001$, $^{\#\#\#\#}p < 0.0001$ versus NaCl-vehicle-treated control mice using Student t-tests.

prior to LPS challenge (preventive setting) or 3 h after LPS challenge (therapeutic setting), when neutrophil infiltration was already apparent (data not shown). In both settings, treatment with the CXCR7 antagonist significantly reduced the overall protein content in the BAL, compared with vehicle-treated, LPS-challenged mice (**Figure 5B**). Moreover, treatment with ACT-1004-1239 reduced LPS-induced leukocyte recruitment to the BAL 48 h post-LPS challenge. Preventive ACT-1004-1239 treatment significantly reduced all evaluated immune cell subsets present in the BAL (**Figure 5C**), whereas therapeutic administration of ACT-1004-1239 significantly reduced macrophages and lymphocytes, and showed a trend to reduce all other evaluated cell subtypes without reaching statistical significance (**Figure 5C**).

In summary, blockade of the CXCR7 axis improved clinical signs of nebulized LPS inhalation as shown by an improvement in the breathing pattern, a reduction in the vascular barrier dysfunction, and a reduction in immune cell infiltrates into the BAL, thus, confirming the importance of the CXCR3/CXCR4/CXCR7 axis in ALI/ARDS.

DISCUSSION

Acute lung injury and its more severe form, ARDS, represent lung disease conditions of multifactorial etiology, associated with diffuse alveolar damage and hypoxemia. Despite better

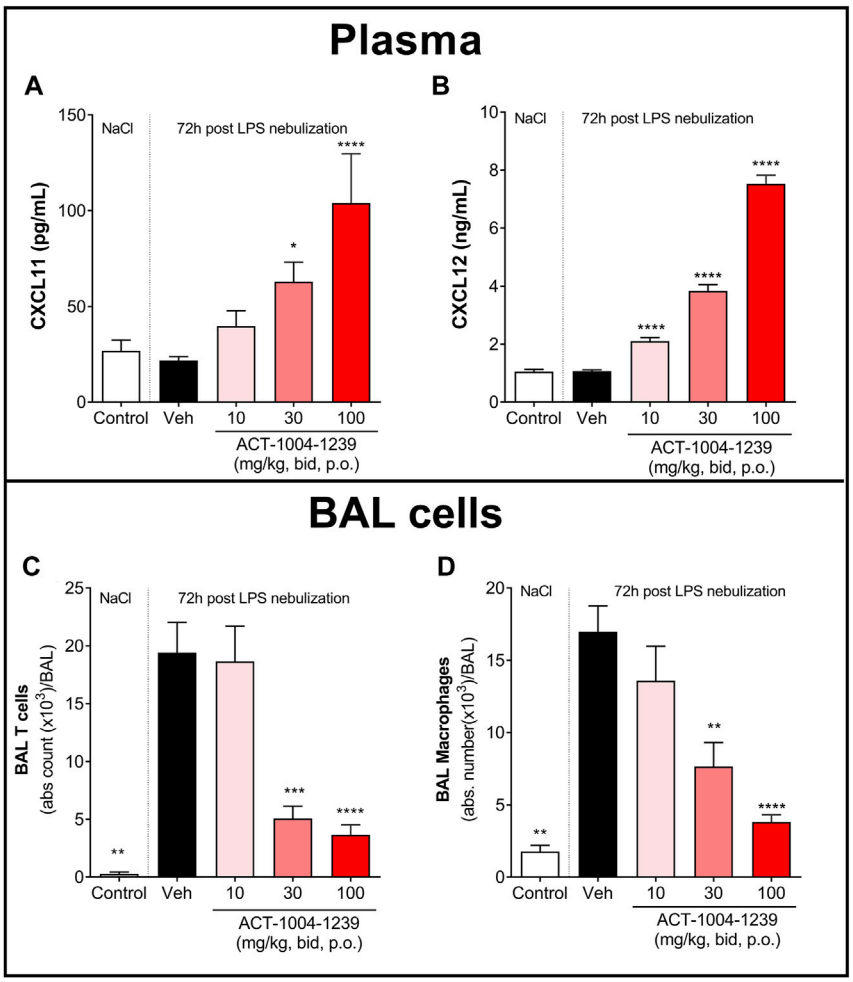

FIGURE 4 | Treatment with ACT-1004-1239 dose-dependently increases plasma CXCL11 and CXCL12 levels and reduces BAL T cell and inflammatory macrophage infiltrates in the LPS-induced ALI/ARDS model. Vehicle (Veh; black bars) or ACT-1004-1239 (10, 30, or 100 mg/kg; bars with different shades of red) was given orally, twice daily, starting 1 h prior to LPS nebulization, for a total of six administrations. Control mice (white bars) were challenged by NaCl nebulization and received vehicle administrations. Plasma CXCL11 **(A)** and plasma CXCL12 levels **(B)** 72 h after LPS or NaCl challenge. Results are expressed as mean + SEM (n = 10–25 mice per treatment-LPS groups and n = 4–5 mice for control group). *$p < 0.05$, ****$p < 0.0001$ versus vehicle-treated LPS-challenged mice, using one-way ANOVA test followed by Dunnett's multiple comparisons test. Total BAL T cell **(C)** and BAL inflammatory macrophage counts **(D)** 72 h after LPS challenge. Results are expressed as mean ± SEM with n = 11–23 mice per treatment-LPS groups and n = 3 for controls. **$p < 0.01$, ***$p < 0.001$, ****$p < 0.0001$ versus vehicle-treated LPS-challenged mice, using one-way ANOVA test followed by Dunnett's multiple comparisons test.

knowledge regarding the pathogenesis of ALI/ARDS, mortality remains high (40%), and current treatment is restricted to supportive care with mechanical ventilation, emphasizing the need to develop and test new therapies for this life-threatening condition (Dushianthan et al., 2011; Bellani et al., 2016). The lack of effective therapy has been recently underlined by the coronavirus disease 19 (COVID-19) pandemic, which causes ARDS in 3%–5% of the patients infected with SARS-CoV-2 (Horie et al., 2020).

The preclinical ALI/ARDS model, induced by LPS inhalation in rodents, is a commonly used model, which manifests key features of human ALI/ARDS (Menezes et al., 2005; Matute-Bello et al., 2008). In the current study, the consequences of LPS inhalation were characterized over time in DBA/1 mice, a strain of mice expressing both CXCR7 ligands (CXCL11 and CXCL12). In line with previous reports in similar models but not expressing CXCL11 (Lefort et al., 2001; Lax et al., 2014), inhalation of nebulized LPS in DBA/1 mice induced key parameters recommended by the American Thoracic Society to detect the presence of ARDS in laboratory animals: LPS inhalation caused a rapid and significant recruitment of inflammatory cells to the alveolar space, especially neutrophils at early time points after LPS challenge followed by macrophages and T cells at later time points. Furthermore, LPS inhalation increased alveolar capillary barrier permeability. The LPS-induced breathing pattern alteration was also observed, which has been shown to be associated with altered lung function (Håkansson et al., 2012).

The duration of the pulmonary inflammatory contributes to the pathogenesis of ALI/ARDS and may determine the severity

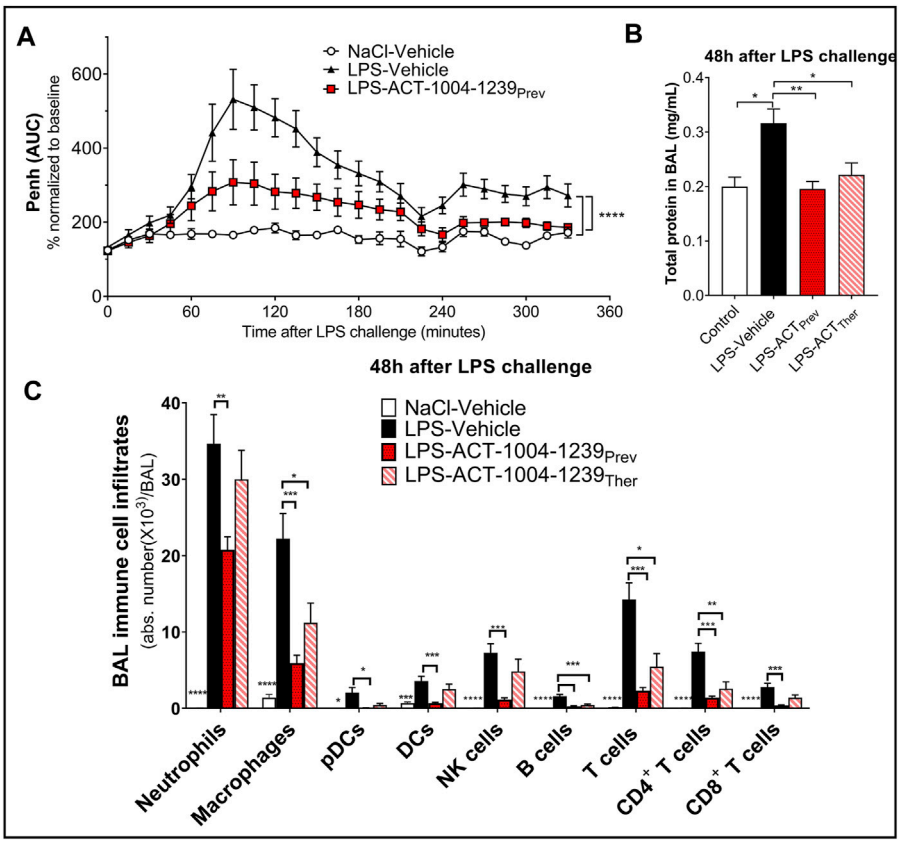

FIGURE 5 | Antagonism of CXCR7 reduces LPS-induced ALI/ARDS. Treatment with the CXCR7 antagonist ACT-1004-1239 significantly reduced LPS-induced breathing pattern alteration **(A)**, alveolar–capillary barrier permeability **(B)**, and immune cell infiltrates in the bronchoalveolar space **(C)** compared with vehicle-treated-LPS exposed mice. Mice were treated with vehicle (LPS-vehicle; black) or ACT-1004-1239 (100 mg/kg, LPS-ACT-1004-1239) orally, twice daily, starting 1 h prior to LPS challenge (preventive setting; LPS-ACT_{Prev}; red) or 3 h after LPS challenge (therapeutic setting; LPS-ACT_{Ther}; hatched bar). Control mice were treated with vehicle and inhaled NaCl 0.9% (NaCl-vehicle; white). **(A)** Preventive treatment with ACT-1004-1239 reduced the LPS-induced breathing pattern alteration, measured by the calculated enhanced pause (Penh) using whole-body plethysmography in conscious unrestrained mice over a period of 6 h following LPS inhalation. Results are expressed as the mean percentage Penh area under the curve (AUC) normalized to the baseline ± SEM (n = 8 mice per group). ****$p < 0.0001$ using two-way ANOVA, followed by Dunnett's multiple comparisons test versus LPS-vehicle-treated mice. **(B)** Preventive and therapeutic treatment with ACT-1004-1239 reduced alveolar–capillary barrier permeability, measured by a reduction in total protein concentration in BAL supernatant 48 h after LPS challenge (n = 7–16 mice per LPS-challenged groups; n = 6 NaCl-vehicle control mice). Results are expressed as mean + SEM. *$p < 0.05$, **$p < 0.01$ versus LPS-vehicle-treated mice using one-way ANOVA followed by Dunnett's multiple comparisons test. **(C)** Preventive and therapeutic treatment with ACT-1004-1239 reduced immune cell infiltrates in the BAL, measured by flow cytometry 48 h after LPS challenge (n = 7–16 mice per LPS-challenged groups; n = 6 NaCl-vehicle control mice). Results are expressed as mean ± SEM. *$p < 0.05$, **$p < 0.01$, ***$p < 0.001$, ****$p < 0.0001$ versus LPS-vehicle-treated mice using two-way ANOVA followed by Dunnett's multiple comparisons test. The gating strategy for all immune populations is illustrated in **Supplementary Figures S1A,B**.

and subsequent mortality in patients (Meduri et al., 1995; Yang et al., 2003); however, the mechanisms leading to a persistent inflammation remain unclear. Previous reports have suggested that both the CXCR3 and CXCR4 axis play a pivotal role in the prolonged recruitment and/or retention of immune cells in ALI/ARDS, exerting a damaging effect in the lung (Petty et al., 2007; Nie et al., 2008; Kelsen et al., 2009).

Consistent with findings from human patients and mouse models of ALI (Saetta et al., 2002; Petty et al., 2007; Hartl et al., 2008; Costello et al., 2012; Ichikawa et al., 2013; Ngamsri et al., 2017; Liao et al., 2020), in this study using LPS-challenged DBA/1 mice, CXCR3 and CXCR4 ligands were elevated in the BAL, which was associated with increased BAL $CXCR3^+$ and $CXCR4^+$ cell infiltrates. In line with previously reported data (Petty et al., 2007), the expression of CXCR4 on BAL myeloid cells steadily increased over time following LPS-induced lung injury. Importantly, the same observation was made regarding the expression of CXCR3, especially on lymphoid cells, suggesting a distinct role for CXCR3 and CXCR4 in the recruitment and persistence/retention of BAL infiltrates during ALI/ARDS. Interestingly, a similar observation was made in the BAL from patients with COVID-19, where most BAL infiltrates expressed CXCR3 and/or CXCR4 (Liao et al., 2020), and the increased presence of activated lung-homing $CXCR4^+$ T cells was associated with fatal COVID-19 (Neidleman et al., 2021).

CXCR7 has been reported to scavenge both CXCL11 and CXCL12. Even though CXCL11 was found at lower levels than CXCL9 and CXCL10 in the BAL from LPS challenged mice, this

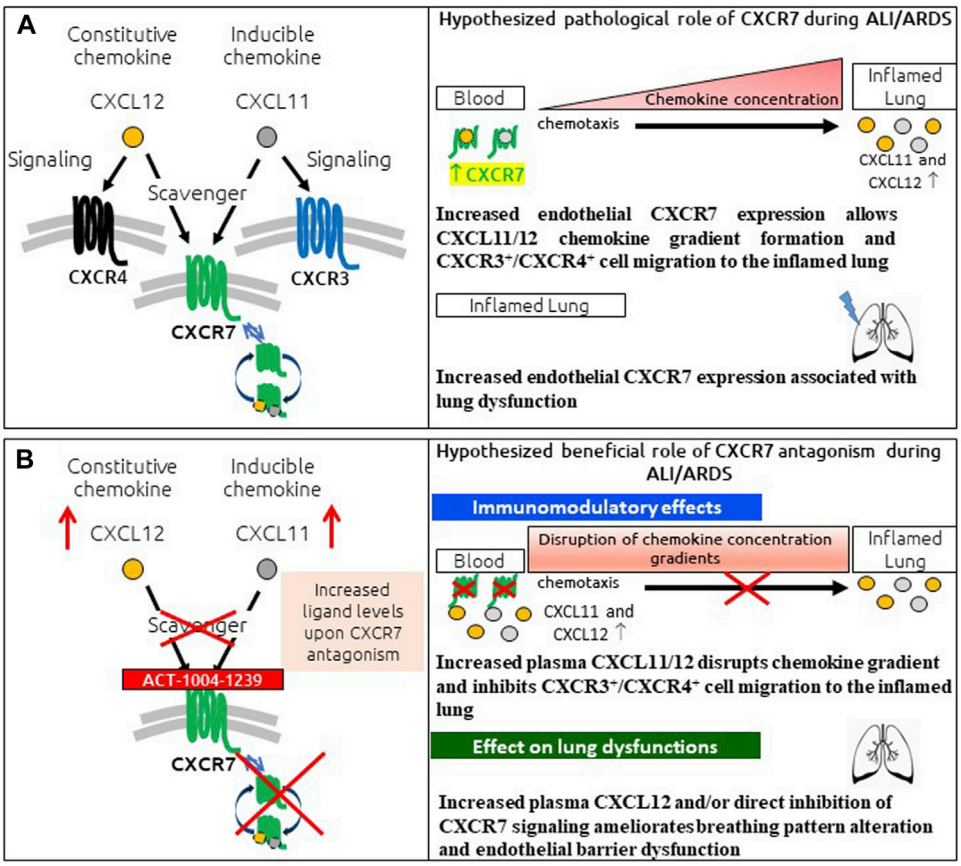

FIGURE 6 | Summary of pathological role of CXCR7 and potential benefit of CXCR7 antagonism during ALI/ARDS. **(A)** CXCR7 functions predominantly as a scavenger receptor for its two ligands: the interferon-inducible chemokine CXCL11 and the constitutive chemokine CXCL12. Binding of its ligands leads to internalization of the CXCR7–ligand complex and ligand degradation. CXCL11 and CXCL12 also bind and activate the signaling chemokine receptors CXCR3 and CXCR4, respectively. The CXCR3/CXCR4/CXCR7 axes play an important role in lung inflammation. CXCR7 scavenging activity tightly regulates the extracellular levels of its ligands, facilitating the establishment and maintenance of CXCL11/12 chemokine concentration gradients and $CXCR3^+/CXCR4^+$ cell migration from the blood to the inflamed lung. In addition, increased CXCR7 expression in the inflamed lung has been reported to be associated with breathing pattern alteration and endothelial barrier dysfunction. **(B)** CXCR7 antagonism with the CXCR7 antagonist ACT-1004-1239 exhibits immunomodulatory effects: by blocking the scavenging activity of the receptor and consequently increasing CXCL11 and CXCL12 plasma concentrations, chemokine gradients are disrupted, inhibiting $CXCR3^+$ and $CXCR4^+$ cell migration to the inflamed lung. In addition, treatment with ACT-1004-1239, by increasing plasma CXCL12 and/or by direct inhibition of CXCR7 signaling, ameliorates ALI-induced breathing pattern alteration and endothelial barrier dysfunction.

chemokine represents the most potent CXCR3 ligand (Sauty et al., 2001). To date, the role of the CXCR3/CXCR7/CXCL11 axis in preclinical ALI models has not been investigated as previous studies were conducted in C57BL/6 mice, a mouse strain lacking CXCL11 (Sierro et al., 2007). We show here that antagonizing CXCR7 with ACT-1004-1239 not only led to the elevation of CXCL12 in the plasma, confirming previous data (Richard-Bildstein et al., 2020; Pouzol et al., 2021) but also of the inducible chemokine CXCL11, in a dose-dependent manner, confirming the inhibition of the scavenging activity of CXCR7 *in vivo*. In contrast, CXCR7 antagonism did not further increase the LPS-induced elevation of CXCL11 and CXCL12 concentrations in the inflamed lung tissue, but rather tended to normalize them, likely leading to a disruption in the chemokine concentration gradient from the blood to the injured lung tissue. Consequently, a significant reduction in $CXCR3^+$ lymphoid and $CXCR4^+$ myeloid and lymphoid cells in the BAL was observed upon treatment with the CXCR7 antagonist, suggesting an inhibition of directional migration of these cells from the blood to the inflamed tissue and/or a reduction in their retention in the tissue. The immunomodulatory effect of CXCR7 antagonism was consistently shown both in a preventive and therapeutic setting, highlighting its potential clinical impact on acute pulmonary inflammation.

Besides the pivotal role of CXCR7 on immune cell infiltration to the BAL, expression of CXCR7 in the vasculature has been associated with a disruption of the endothelial barrier function (Totonchy et al., 2014). CXCR7 antagonism with ACT-1004-1239, both in a preventive and therapeutic setting, successfully reduced alterations in the alveolar capillary barrier function as shown by a reduction in the overall protein content in the BAL following LPS challenge. Furthermore, CXCL12 has been shown to promote endothelial barrier integrity *in vivo* via CXCR4 (Kobayashi et al., 2014) and to enhance barrier function in

human pulmonary artery endothelial cells following thrombin activation *in vitro* (Cheng et al., 2017). These data suggest that the reduced vascular permeability seen in the ALI/ARDS model following CXCR7 antagonism could be a result of a direct effect on endothelial cells and/or indirect effect via increased CXCL12 concentration.

An additional interesting finding of this study was the effect of ACT-1004-1239 on breathing pattern alteration following LPS challenge. Endotoxins have been related to pulmonary functional disturbances both in humans (Leaker et al., 2013) and mice (Lefort et al., 2001) and have been shown to exacerbate established emphysema in several experimental models (Kobayashi et al., 2013; de Oliveira et al., 2019). Therefore, this aspect may be relevant to the pathogenesis of ARDS, especially at the late stages where emphysema-like lesions are present (Terzi et al., 2014). In the present study, treatment with ACT-1004-1239 reduced the Penh increase observed within 2 h following LPS inhalation. Published data in similar models reported that LPS-induced Penh increase was dependent on TNFα release (Schnyder-Candrian et al., 2005). However, the effect observed with ACT-1004-1239 on this early breathing pattern change could not be explained by a reduction in LPS-induced BAL TNFα elevation (data not shown). More studies are needed to unravel the mechanisms that account for this effect.

So far, only CCX771, which recruits β-arrestin upon binding to the CXCR7 receptor, has been evaluated in the context of ALI (Zabel et al., 2009; Ngamsri et al., 2017). Our study using ACT-1004-1239, a CXCR7 antagonist of the β-arrestin pathway, provides evidence that the observed efficacy obtained with CCX771 in ALI was likely due to its functional antagonistic effect and not to its agonistic effect.

In conclusion, the presented data provide a characterization of the LPS-induced ALI/ARDS model in DBA/1 mice, demonstrating a key role for CXCR7 on pathological hallmarks of human disease (**Figure 6A**). The scavenging activity of CXCR7 contributed to the establishment and maintenance of CXCL11 and CXCL12 concentration gradients, thereby allowing the recruitment of $CXCR3^+$ and $CXCR4^+$ leukocytes to the BAL (**Figure 6A**). Antagonizing CXCR7 with ACT-1004-1239 increased plasma CXCL11 and CXCL12 levels and reduced infiltration of $CXCR3^+$ and $CXCR4^+$ leukocytes to the BAL (**Figure 6B**). Furthermore, CXCR7 antagonism reduced vascular permeability and breathing dysfunction (**Figure 6B**). This broad mechanism of action positions ACT-1004-1239 as a potential new therapy to target main pathological features of human ALI/ARDS.

DATA AVAILABILITY STATEMENT

The datasets presented in this study can be found in online repositories. The names of the repository/repositories and accession number(s) can be found in the article/ **Supplementary Material**.

ETHICS STATEMENT

The animal study was reviewed and approved by the Basel Cantonal Veterinary Office.

AUTHOR CONTRIBUTIONS

LP was responsible for the conception, design and execution of the studies, data interpretation, and manuscript drafting. AS was responsible for the execution of the studies, data interpretation, and manuscript drafting. NB, MT, and DS carried out the experiments and analyzed the data. FL was involved in the study concept and design. MM was involved in the data interpretation and manuscript drafting. All authors helped to critically revise the intellectual content of the manuscript and approved the final submission.

ACKNOWLEDGMENTS

We thank Idorsia's immunology, translational biomarker, DMPK, and formulation and preclinical galenics groups for their continuous support with *in vivo* experiments. We thank J. Scherer for supporting the evaluation of the lung function. We thank E. Gerossier and A. Zurbach for constant *in vivo* support. We thank J. Hoerner and H. Farine for the measurement of CXCL11. We thank E. Vezzali for histology. We thank the core team members of the project, especially P. Guerry, C. Gnerre, E. Lindenberg, M. Holdener, P. Coloma, C. Huynh, and S. Schuldes for their careful review of the manuscript.

SUPPLEMENTARY MATERIAL

The Supplementary Material for this article can be found online at: https://www.frontiersin.org/articles/10.3389/fphar.2021.748740/full#supplementary-material

REFERENCES

Alm, A. S., Li, K., Chen, H., Wang, D., Andersson, R., and Wang, X. (2010). Variation of Lipopolysaccharide-Induced Acute Lung Injury in Eight Strains of Mice. *Respir. Physiol. Neurobiol.* 171 (2), 157–164. doi:10.1016/j.resp.2010.02.009

Bellani, G., Laffey, J. G., Pham, T., Fan, E., Brochard, L., Esteban, A., et al. (2016). Epidemiology, Patterns of Care, and Mortality for Patients With Acute Respiratory Distress Syndrome in Intensive Care Units in 50 Countries. *JAMA* 315 (8), 788–800. doi:10.1001/jama.2016.0291

Berahovich, R. D., Zabel, B. A., Lewén, S., Walters, M. J., Ebsworth, K., Wang, Y., et al. (2014). Endothelial Expression of CXCR7 and the Regulation of Systemic CXCL12 Levels. *Immunology* 141 (1), 111–122. doi:10.1111/imm.12176

Berahovich, R. D., Zabel, B. A., Penfold, M. E., Lewén, S., Wang, Y., Miao, Z., et al. (2010). CXCR7 Protein is not Expressed on Human or Mouse Leukocytes. *J. Immunol.* 185 (9), 5130–5139. doi:10.4049/jimmunol.1001660

Bhatia, M., Zemans, R. L., and Jeyaseelan, S. (2012). Role of Chemokines in the Pathogenesis of Acute Lung Injury. *Am. J. Respir. Cell Mol. Biol.* 46 (5), 566–572. doi:10.1165/rcmb.2011-0392TR

Cheng, Y. H., Eby, J. M., LaPorte, H. M., Volkman, B. F., and Majetschak, M. (2017). Effects of Cognate, Non-Cognate and Synthetic CXCR4 and ACKR3

Ligands on Human Lung Endothelial Cell Barrier Function. *PLoS One* 12 (11), e0187949. doi:10.1371/journal.pone.0187949

Costello, C. M., McCullagh, B., Howell, K., Sands, M., Belperio, J. A., Keane, M. P., et al. (2012). A Role for the CXCL12 Receptor, CXCR7, in the Pathogenesis of Human Pulmonary Vascular Disease. *Eur. Respir. J.* 39 (6), 1415–1424. doi:10.1183/09031936.00044911

de Oliveira, M. V., Rocha, N. N., Santos, R. S., Rocco, M. R. M., de Magalhães, R. F., Silva, J. D., et al. (2019). Endotoxin-Induced Emphysema Exacerbation: A Novel Model of Chronic Obstructive Pulmonary Disease Exacerbations Causing Cardiopulmonary Impairment and Diaphragm Dysfunction. *Front. Physiol.* 10, 664. doi:10.3389/fphys.2019.00664

de Souza Xavier Costa, N., Ribeiro Júnior, G., Dos Santos Alemany, A. A., Belotti, L., Zati, D. H., Frota Cavalcante, M., et al. (2017). Early and Late Pulmonary Effects of Nebulized LPS in Mice: An Acute Lung Injury Model. *PLoS One* 12 (9), e0185474. doi:10.1371/journal.pone.0185474

Domscheit, H., Hegeman, M. A., Carvalho, N., and Spieth, P. M. (2020). Molecular Dynamics of Lipopolysaccharide-Induced Lung Injury in Rodents. *Front. Physiol.* 11, 36. doi:10.3389/fphys.2020.00036

Dushianthan, A., Grocott, M. P., Postle, A. D., and Cusack, R. (2011). Acute Respiratory Distress Syndrome and Acute Lung Injury. *Postgrad. Med. J.* 87 (1031), 612–622. doi:10.1136/pgmj.2011.118398

Gibson, P. G., Qin, L., and Puah, S. H. (2020). COVID-19 Acute Respiratory Distress Syndrome (ARDS): Clinical Features and Differences from Typical Pre-COVID-19 ARDS. *Med. J. Aust.* 213 (2), 54–56.e1. doi:10.5694/mja2.50674

Groom, J. R., and Luster, A. D. (2011). CXCR3 in T Cell Function. *Exp. Cell Res.* 317 (5), 620–631. doi:10.1016/j.yexcr.2010.12.017S0014-4827(10)00575-6

Håkansson, H. F., Smailagic, A., Brunmark, C., Miller-Larsson, A., and Lal, H. (2012). Altered Lung Function Relates to Inflammation in an Acute LPS Mouse Model. *Pulm. Pharmacol. Ther.* 25 (5), 399–406. doi:10.1016/j.pupt.2012.08.001

Hamelmann, E., Schwarze, J., Takeda, K., Oshiba, A., Larsen, G. L., Irvin, C. G., et al. (1997). Noninvasive Measurement of Airway responsiveness in Allergic Mice Using Barometric Plethysmography. *Am. J. Respir. Crit. Care Med.* 156 (3 pt 1), 766–775. doi:10.1164/ajrccm.156.3.9606031

Hartl, D., Krauss-Etschmann, S., Koller, B., Hordijk, P. L., Kuijpers, T. W., Hoffmann, F., et al. (2008). Infiltrated Neutrophils Acquire Novel Chemokine Receptor Expression and Chemokine Responsiveness in Chronic Inflammatory Lung Diseases. *J. Immunol.* 181 (11), 8053–8067. doi:10.4049/jimmunol.181.11.8053

Horie, S., McNicholas, B., Rezoagli, E., Pham, T., Curley, G., McAuley, D., et al. (2020). Emerging Pharmacological Therapies for ARDS: COVID-19 and Beyond. *Intensive Care Med.* 46 (12), 2265–2283. doi:10.1007/s00134-020-06141-z

Ichikawa, A., Kuba, K., Morita, M., Chida, S., Tezuka, H., Hara, H., et al. (2013). CXCL10-CXCR3 Enhances the Development of Neutrophil-Mediated Fulminant Lung Injury of Viral and Nonviral Origin. *Am. J. Respir. Crit. Care Med.* 187 (1), 65–77. doi:10.1164/rccm.201203-0508OC

Kelsen, S. G., Aksoy, M. O., Georgy, M., Hershman, R., Ji, R., Li, X., et al. (2009). Lymphoid Follicle Cells in Chronic Obstructive Pulmonary Disease Overexpress the Chemokine Receptor CXCR3. *Am. J. Respir. Crit. Care Med.* 179 (9), 799–805. doi:10.1164/rccm.200807-1089OC

Kobayashi, K., Sato, K., Kida, T., Omori, K., Hori, M., Ozaki, H., et al. (2014). Stromal Cell-Derived Factor-1α/c-x-c Chemokine Receptor Type 4 Axis Promotes Endothelial Cell Barrier Integrity via Phosphoinositide 3-Kinase and Rac1 Activation. *Arterioscler Thromb. Vasc. Biol.* 34 (8), 1716–1722. doi:10.1161/ATVBAHA.114.303890

Kobayashi, S., Fujinawa, R., Ota, F., Kobayashi, S., Angata, T., Ueno, M., et al. (2013). A Single Dose of Lipopolysaccharide Into Mice With Emphysema Mimics Human Chronic Obstructive Pulmonary Disease Exacerbation as Assessed by Micro-Computed Tomography. *Am. J. Respir. Cell Mol. Biol.* 49 (6), 971–977. doi:10.1165/rcmb.2013-0074OC

Konrad, F. M., Meichssner, N., Bury, A., Ngamsri, K. C., and Reutershan, J. (2017). Inhibition of SDF-1 Receptors CXCR4 and CXCR7 Attenuates Acute Pulmonary Inflammation via the Adenosine A2B-Receptor on Blood Cells. *Cell Death Dis* 8 (5), e2832. doi:10.1038/cddis.2016.482

Lax, S., Wilson, M. R., Takata, M., and Thickett, D. R. (2014). Using a Non-Invasive Assessment of Lung Injury in a Murine Model of Acute Lung Injury. *BMJ Open Respir. Res.* 1 (1), e000014. doi:10.1136/bmjresp-2013-000014

Leaker, B. R., Barnes, P. J., and O'Connor, B. (2013). Inhibition of LPS-Induced Airway Neutrophilic Inflammation in Healthy Volunteers with an Oral CXCR2 Antagonist. *Respir. Res.* 14, 137. doi:10.1186/1465-9921-14-137

Lefort, J., Motreff, L., and Vargaftig, B. B. (2001). Airway Administration of *Escherichia coli* Endotoxin to Mice Induces Glucocorticosteroid-Resistant Bronchoconstriction and Vasopermeation. *Am. J. Respir. Cell Mol. Biol.* 24 (3), 345–351. doi:10.1165/ajrcmb.24.3.4289

Lemos-Filho, L. B., Mikkelsen, M. E., Martin, G. S., Dabbagh, O., Adesanya, A., Gentile, N., et al. (2013). Sex, Race, and the Development of Acute Lung Injury. *Chest* 143 (4), 901–909. doi:10.1378/chest.12-1118

Lewellis, S. W., and Knaut, H. (2012). Attractive Guidance: How The Chemokine SDF1/CXCL12 Guides Different Cells to Different Locations. *Semin. Cell Dev. Biol.* 23 (3), 333–340. doi:10.1016/j.semcdb.2012.03.009

Liao, M., Liu, Y., Yuan, J., Wen, Y., Xu, G., Zhao, J., et al. (2020). Single-Cell Landscape of Bronchoalveolar Immune Cells in Patients with COVID-19. *Nat. Med.* 26 (6), 842–844. doi:10.1038/s41591-020-0901-9

Matute-Bello, G., Frevert, C. W., and Martin, T. R. (2008). Animal Models of Acute Lung Injury. *Am. J. Physiol. Lung Cell Mol. Physiol.* 295 (3), L379–L399. doi:10.1152/ajplung.0001010.2008

Meduri, G. U., Headley, S., Kohler, G., Stentz, F., Tolley, E., Umberger, R., et al. (1995). Persistent Elevation of Inflammatory Cytokines Predicts a Poor Outcome in ARDS. Plasma IL-1 Beta and IL-6 Levels are Consistent and Efficient Predictors of Outcome Over Time. *Chest* 107 (4), 1062–1073. doi:10.1378/chest.107.4.1062

Menezes, S. L., Bozza, P. T., Neto, H. C., Laranjeira, A. P., Negri, E. M., Capelozzi, V. L., et al. (2005). Pulmonary and Extrapulmonary Acute Lung Injury: Inflammatory and Ultrastructural Analyses. *J. Appl. Physiol.* 98 (5), 1777–1783. doi:10.1152/japplphysiol.01182.2004

Menhaji-Klotz, E., Ward, J., Brown, J. A., Loria, P. M., Tan, C., Hesp, K. D., et al. (2020). Discovery of Diphenylacetamides as CXCR7 Inhibitors with Novel β-Arrestin Antagonist Activity. *ACS Med. Chem. Lett.* 11, 1330–1334. doi:10.1021/acsmedchemlett.0c00163

Naumann, U., Cameroni, E., Pruenster, M., Mahabaleshwar, H., Raz, E., Zerwes, H. G., et al. (2010). CXCR7 Functions as a Scavenger for CXCL12 and CXCL11. *PLoS One* 5 (2), e9175. doi:10.1371/journal.pone.0009175

Neidleman, J., Luo, X., George, A. F., McGregor, M., Yang, J., Yun, C., et al. (2021). Distinctive Features of SARS-CoV-2-Specific T Cells Predict recovery from Severe COVID-19. *Cell Rep.*36 (3), 109414. doi:10.1016/j.celrep.2021.10941

Ngamsri, K. C., Müller, A., Bösmüller, H., Gamper-Tsigaras, J., Reutershan, J., and Konrad, F. M. (2017). The Pivotal Role of CXCR7 in Stabilization of the Pulmonary Epithelial Barrier in Acute Pulmonary Inflammation. *J. Immunol.* 198 (6), 2403–2413. doi:10.4049/jimmunol.1601682

Nie, L., Xiang, R., Zhou, W., Lu, B., Cheng, D., and Gao, J. (2008). Attenuation of Acute Lung Inflammation Induced by Cigarette Smoke in CXCR3 Knockout Mice. *Respir. Res.* 9, 82. doi:10.1186/1465-9921-9-82

Petty, J. M., Sueblinvong, V., Lenox, C. C., Jones, C. C., Cosgrove, G. P., Cool, C. D., et al. (2007). Pulmonary Stromal-Derived Factor-1 Expression and Effect on Neutrophil Recruitment During Acute Lung Injury. *J. Immunol.* 178 (12), 8148–8157. doi:10.4049/jimmunol.178.12.8148

Piali, L., Birker-Robaczewska, M., Lescop, C., Froidevaux, S., Schmitz, N., Morrison, K., et al. (2017). Cenerimod, a Novel Selective S1P1 Receptor Modulator With Unique Signaling Properties. *Pharmacol. Res. Perspect.* 5 (6), 5723703. doi:10.1002/prp2.370

Pouzol, L., Baumlin, N., Sassi, A., Tunis, M., Marrie, J., Vezzali, E., et al. (2021). ACT-1004-1239, a First-in-Class CXCR7 Antagonist With Both Immunomodulatory and Promyelinating Effects for the Treatment of Inflammatory Demyelinating Diseases. *FASEB J.* 35 (3), e21431. doi:10.1096/fj.202002465R

Prada-Dacasa, P., Urpi, A., Sánchez-Benito, L., bianchi, p., and Quintana, A. (2020). Measuring Breathing Patterns in Mice Using Whole-Body Plethysmography. *Bio Protoc.* 10 (17), e3741. doi:10.21769/BioProtoc.3741

Puneet, P., Moochhala, S., and Bhatia, M. (2005). Chemokines in Acute Respiratory Distress Syndrome. *Am. J. Physiol. Lung Cell Mol. Physiol.* 288 (1), L3–L15. doi:10.1152/ajplung.00405.2003

Quinn, K. E., Mackie, D. I., and Caron, K. M. (2018). Emerging Roles of Atypical Chemokine Receptor 3 (ACKR3) in Normal Development and Physiology. *Cytokine* 109, 17–23. doi:10.1016/j.cyto.2018.02.024

Richard-Bildstein, S., Aissaoui, H., Pothier, J., Schäfer, G., Gnerre, C., Lindenberg, E., et al. (2020). Discovery of the Potent, Selective, Orally Available CXCR7 Antagonist ACT-1004-1239. *J. Med. Chem.* 63 (24), 15864–15882. doi:10.1021/acs.jmedchem.0c01588

Saetta, M., Mariani, M., Panina-Bordignon, P., Turato, G., Buonsanti, C., Baraldo, S., et al. (2002). Increased Expression of the Chemokine Receptor CXCR3 and its Ligand CXCL10 in Peripheral Airways of Smokers With Chronic Obstructive Pulmonary Disease. *Am. J. Respir. Crit. Care Med.* 165 (10), 1404–1409. doi:10.1164/rccm.2107139

Sauty, A., Colvin, R. A., Wagner, L., Rochat, S., Spertini, F., and Luster, A. D. (2001). CXCR3 Internalization Following T Cell-Endothelial Cell Contact: Preferential Role of IFN-Inducible T Cell Alpha Chemoattractant (CXCL11). *J. Immunol.* 167 (12), 7084–7093. doi:10.4049/jimmunol.167.12.7084

Schnyder-Candrian, S., Quesniaux, V. F., Di Padova, F., Maillet, I., Noulin, N., Couillin, I., et al. (2005). Dual Effects of p38 MAPK on TNF-Dependent Bronchoconstriction and TNF-Independent Neutrophil Recruitment in Lipopolysaccharide-Induced Acute Respiratory Distress Syndrome. *J. Immunol.* 175 (1), 262–269. doi:10.4049/jimmunol.175.1.262

Sierro, F., Biben, C., Martínez-Muñoz, L., Mellado, M., Ransohoff, R. M., Li, M., et al. (2007). Disrupted Cardiac Development but Normal Hematopoiesis in Mice Deficient in the Second CXCL12/SDF-1 Receptor, CXCR7. *Proc. Natl. Acad. Sci. U S A.* 104 (37), 14759–14764. doi:10.1073/pnas.0702229104

Terzi, E., Zarogoulidis, K., Kougioumtzi, I., Dryllis, G., Kioumis, I., Pitsiou, G., et al. (2014). Acute Respiratory Distress Syndrome and Pneumothorax. *J. Thorac. Dis.* 6 (Suppl. 4), S435–S442. doi:10.3978/j.issn.2072-1439.2014.08.34

Tobia, C., Chiodelli, P., Barbieri, A., Buraschi, S., Ferrari, E., Mitola, S., et al. (2019). Atypical Chemokine Receptor 3 Generates Guidance Cues for CXCL12-Mediated Endothelial Cell Migration. *Front. Immunol.* 10, 1092. doi:10.3389/fimmu.2019.01092

Tomankova, T., Kriegova, E., and Liu, M. (2015). Chemokine Receptors and Their Therapeutic Opportunities in Diseased Lung: Far Beyond Leukocyte Trafficking. *Am. J. Physiol. Lung Cell Mol. Physiol.* 308 (7), L603–L618. doi:10.1152/ajplung.00203.2014

Totonchy, J. E., Clepper, L., Phillips, K. G., McCarty, O. J., and Moses, A. V. (2014). CXCR7 Expression Disrupts Endothelial Cell Homeostasis and Causes Ligand-Dependent Invasion. *Cell Adh Migr* 8 (2), 165–176. doi:10.4161/cam.28495

Ware, L. B., and Matthay, M. A. (2000). The Acute Respiratory Distress Syndrome. *N. Engl. J. Med.* 342 (18), 1334–1349. doi:10.1056/NEJM200005043421806

Wheeler, A. P., and Bernard, G. R. (2007). Acute Lung Injury and the Acute Respiratory Distress Syndrome: A Clinical Review. *Lancet* 369 (9572), 1553–1564. doi:10.1016/S0140-6736(07)60604-7

Yang, K. Y., Arcaroli, J. J., and Abraham, E. (2003). Early Alterations in Neutrophil Activation are Associated With Outcome in Acute Lung Injury. *Am. J. Respir. Crit. Care Med.* 167 (11), 1567–1574. doi:10.1164/rccm.200207-664OC

Zabel, B. A., Wang, Y., Lewén, S., Berahovich, R. D., Penfold, M. E., Zhang, P., et al. (2009). Elucidation of CXCR7-Mediated Signaling Events and Inhibition of CXCR4-Mediated Tumor Cell Transendothelial Migration by CXCR7 Ligands. *J. Immunol.* 183 (5), 3204–3211. doi:10.4049/jimmunol.0900269

Conflict of Interest: Authors LP, AS, NB, MT, DS, FL, and MM were employed by the company Idorsia Pharmaceuticals Ltd.

Publisher's Note: All claims expressed in this article are solely those of the authors and do not necessarily represent those of their affiliated organizations, or those of the publisher, the editors, and the reviewers. Any product that may be evaluated in this article, or claim that may be made by its manufacturer, is not guaranteed or endorsed by the publisher.

frontiers in Pharmacology

ORIGINAL RESEARCH
published: 08 November 2021
doi: 10.3389/fphar.2021.772504

Pharmacological Basis for Use of a Novel Compound in Hyperuricemia: Anti-Hyperuricemic and Anti-Inflammatory Effects

Lei Zhao[1], Yihang Li[2,3], Dahong Yao[1,4], Ran Sun[1], Shifang Liu[2], Xi Chen[2,3], Congcong Lin[1], Jian Huang[1], Jinhui Wang[1] and Guang Li[2,3]**

[1]Department of Medicinal Chemistry and Natural Medicine Chemistry, College of Pharmacy, Harbin Medical University, Harbin, China, [2]Yunnan Branch, Institute of Medicinal Plant, Chinese Academy of Medical Sciences, Peking Union Medical College, Jinghong, China, [3]Yunnan Key Laboratory of Southern Medicinal Utilization, Jinghong, China, [4]School of Pharmaceutical Sciences, Shenzhen Technology University, Shenzhen, China

OPEN ACCESS

Edited by:
Nandakumar Natarajan, University of California, San Francisco, United States

Reviewed by:
Awadhesh K. Arya, University of Maryland, Baltimore, United States
Rekha Balakrishnan, City of Hope National Medical Center, United States

***Correspondence:**
Jinhui Wang
wangjinhui@hrbmu.edu.cn
Guang Li
lhbg311@hotmail.com

Specialty section:
This article was submitted to Inflammation Pharmacology, a section of the journal Frontiers in Pharmacology

Received: *08 September 2021*
Accepted: *21 October 2021*
Published: *08 November 2021*

Citation:
Zhao L, Li Y, Yao D, Sun R, Liu S, Chen X, Lin C, Huang J, Wang J and Li G (2021) Pharmacological Basis for Use of a Novel Compound in Hyperuricemia: Anti-Hyperuricemic and Anti-Inflammatory Effects. Front. Pharmacol. 12:772504. doi: 10.3389/fphar.2021.772504

Background: The prevalence of hyperuricemia is considered high worldwide. Hyperuricemia occurs due to decreased excretion of uric acid, increased synthesis of uric acid, or a combination of both mechanisms. There is growing evidence that hyperuricemia is associated with a decline of renal function.

Purpose: This study is aimed at investigating the effects of the novel compound on lowering the serum uric acid level and alleviating renal inflammation induced by high uric acid in hyperuricemic mice.

Methods: Hyperuricemic mice model was induced by potassium oxonate and used to evaluate the effects of the novel compound named FxUD. Enzyme-linked immunosorbent assay was used to detect the related biochemical markers. Hematoxylin-eosin (HE) staining was applied to observe pathological changes. The mRNA expression levels were tested by qRT-PCR. The protein levels were determined by Western blot. In parallel, human proximal renal tubular epithelial cells (HK-2) derived from normal kidney was used to further validate the anti-inflammatory effects *in vitro*.

Results: FxUD administration significantly decreased serum uric acid levels, restored the kidney function parameters, and improved the renal pathological injury. Meanwhile, treatment with FxUD effectively inhibited serum and liver xanthine oxidase (XOD) levels. Reversed expression alterations of renal inflammatory cytokines, urate transporter 1 (URAT1) and glucose transporter 9 (GLUT9) were observed in hyperuricemic mice. Western blot results illustrated FxUD down-regulated protein levels of inflammasome components. Further studies showed that FxUD inhibited the activation of NF-κB signaling pathway in the kidney of hyperuricemic mice. In parallel, the anti-inflammatory effect of FxUD was also confirmed in HK-2.

Conclusion: Our study reveals that FxUD exhibits the anti-hyperuricemic and anti-inflammatory effects through regulating hepatic XOD and renal urate reabsorption transporters, and suppressing NF-κB/NLRP3 pathway in hyperuricemia. The results

provide the evidence that FxUD may be potential for the treatment of hyperuricemia with kidney inflammation.

Keywords: hyperuricemia, xanthine oxidase, NF-κB, NLRP3 inflammasome, urate reabsorption transporter

INTRODUCTION

Hyperuricemia is a metabolic disorder characterized by an excessively increased serum urate concentration, which may occur due to overproduction and/or insufficient intestinal excretion and/or urate underexcretion of kidney (Lu et al., 2019). Uric acid is the ultimate oxidation product of purine catabolism, which induces the formation and deposition of monosodium urate crystals and eventually leads to gout. Therefore, hyperuricemia is the main risk factor for gout (Dalbeth et al., 2018). Hyperuricemia is common and its prevalence has been increasing globally (Dehlin et al., 2020). Hyperuricemia occurs primarily in higher primates, including human, as a result of the inactivation of uricase genes during human evolution. Serum uric acid concentration is an important indicator for human health (Chen et al., 2016). When the uric acid level surpasses its solubility point of 6.8 mg/dl, hyperuricemia is believed to have developed (Terkeltaub, 2010). Alteration of serum uric acid homeostasis has been related to multiple diseases. For instance, an abnormally high serum uric acid is the root cause of gout and has been intimately associated with cardiovascular disease and renal disease (Galassi and Borghi, 2015).

Uric acid crystals formed or deposited in the kidney can induce kidney injury (Waisman et al., 1975). In the process of hyperuricemia-induced kidney damage, the deposition of uric acid crystals has an association with a common pathway that triggers kidney inflammation and injury (Herlitz et al., 2012). Innate immune pathways are also increasingly considered to play an important role in the pathogenesis of hyperuricemia (Kielstein et al., 2020), and particularly lead to activation of the NLRP3 inflammasome which contributes to the release of IL-1β and other pro-inflammatory cytokines (So and Martinon, 2017). Additionally, increased cellular urate, oxidative stress induced directly or indirectly by xanthine oxidase can be related to inflammasomes (Isaka et al., 2016). The processing of uric acid in the kidney mainly encompasses glomerular filtration, tubular reabsorption, tubular secretion, and reabsorption after secretion (Mendez Landa, 2018). Uric acid transporters are necessary for the kidney to handle uric acid, and can be grossly classified into reabsorption-related and secretion-related proteins (Su et al., 2020). Reabsorption-related proteins primarily consist of urate anion transporter 1 (URAT1), glucose transporter 9 (GLUT9), and organic anion transporter 4 (OAT4) (Hagos et al., 2007). For example, the clearly defined function of URAT1 is to promote reabsorption of uric acid at the apical membrane of proximal tubule epithelial cells (TECs) (Enomoto et al., 2002). GLUT9 functions as a transporter that reabsorbs both uric acid and glucose into tubular cells (Chiba et al., 2020). Accordingly, the regulation of cellular uric acid transporters would be able to result in alteration in urate excretion in the kidney (Nakayama et al., 2011). The mechanisms and pathways through which elevated uric acid could impact renal function and eventually lead to kidney damage, have been investigated previously.

Not all patients with gout are able to tolerate allopurinol therapy, and febuxostat still has certain side effects during clinical application. Therefore, the discovery of a promising treatment option for hyperuricemia and gout is urgently needed, and it is of major importance to search for new drugs to ameliorate hyperuricemia. Although the symptoms of kidney injury caused by hyperuricemia have long been known, the underlying molecular mechanisms have not been fully understood. Inflammation is an important physiological response to defense against noxious stimuli, such as pressure on tissues, infection or injury (Rock et al., 2013). Uric acid has been well-known for a long time, but there are few new experimental researches and discoveries around it (Medzhitov, 2008). In our study, we synthesized a novel compound named FxUD and its specific role in those pathological states accompanied by an underlying inflammatory process deserved further investigations. To be specific, we aimed to investigate the protective role of FxUD on high uric acid-induced renal injury, and in the meantime, understanding the specific underlying molecular mechanism was another important task.

MATERIALS AND METHODS

Reagents and Kits

FxUD is a pale yellow-white crystalline powder. Its chemical structure and synthetic routes are shown in **Figure 1**. Unless otherwise noted, reagents used in the experiment were purchased from Aladdin and used without further purification. The uric acid assay kit was purchased from Elabscience. Blood urea nitrogen (BUN) assay kit and creatinine (Cr) assay kit were purchased from Jiangsu Meibiao Biotechnology (Mbbiology). Xanthine oxidase (XOD) detection kit was purchased from Jianglai Biotechnology. LDH assay kit was purchased from Nanjing Jian Cheng Bioengineering Institute. The enhanced chemiluminescence detection kit was purchased from Kangwei Century. The bicinchoninic acid (BCA) and Cell Counting Kit-8 (CCK-8) assay kit were purchased from Beyotime Biotechnology. The hematoxylin-eosin (HE) staining kit was purchased from Solarbio Life Sciences.

Animals

Healthy ICR male mice weighing 20–25 g of SPF grade were used. They were allowed to acclimatize to their living environment for

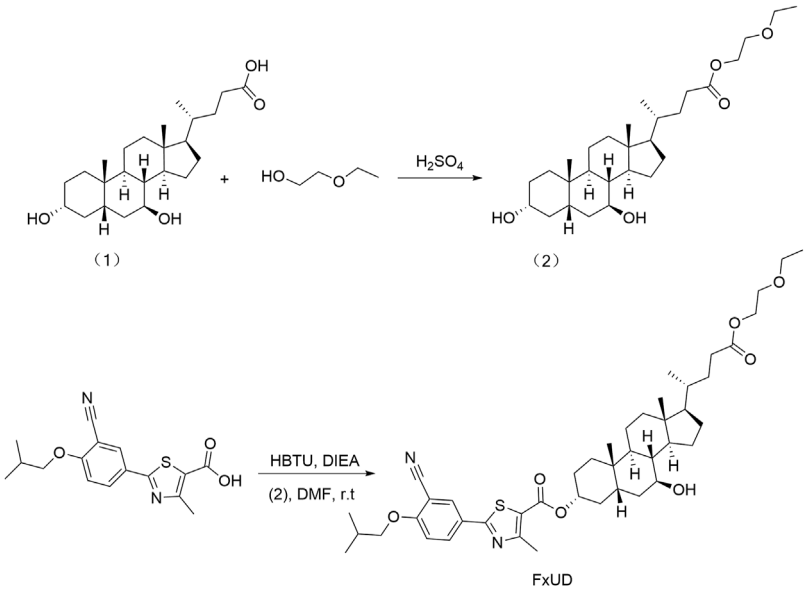

FIGURE 1 | The synthetic route of the novel compound named FxUD.

at least 7 days before the formal experiments. The animals were housed in air-conditioned room at 25 ± 2°C with relative humidity (60 ± 5%) in a regular 12 h light/dark cycle with free access to a standard mouse chow and water during the experimental period. All procedures were in line with the Experimental Animal Ethics Committee of Harbin Medical University.

Animal Treatment, Drug Administration and Samples Collection

According to the previous studies, hyperuricemia was induced in mice by uricase inhibitor potassium oxonate (PO) (Wang et al., 2016; Wang et al., 2018). In briefly, the mice were allocated into six groups (n = 10/group) randomly. An hour after the food was withdrawn, PO (250 mg/kg/day) was administered by gavage for seven consecutive days. FxUD (6, 12, 24 mg/kg/day) and febuxostat (FEB) (5 mg/kg/day), dissolved in 0.5% carboxymethyl cellulose sodium (CMC-Na), were administered 1 h after PO administration, respectively. Blood samples were obtained by extracting the eyeball after final administration on the 7 th day, allowed to clot for approximately 1 h at room temperature, and then centrifuged at 10,000×g at 4°C for 5 min (Qin et al., 2018) in order to collect the serum. Following this, mice were euthanized by decapitation. Meanwhile, liver tissues were taken and kidneys were dissected on an ice plate quickly and some parts were immediately fixed for HE staining, other parts were conserved at −80°C for further qRT-PCR and Western blot analysis.

Biochemical Assays

Serum and hepatic XOD levels were detected by XOD detection kits according to the manufacturer's instructions. Serum Cr, BUN, ALT, AST and LDH levels were determined in accordance with the manufacturer's protocols.

RNA Isolation and Quantitative Reverse Transcription-PCR Analysis

Total RNA was extracted using the using Foregene RNA isolation kit (Foregene Co. Ltd., China) according to the manufacturer's instructions. Reverse transcription was performed using the TOYOBO ReverTra Ace® qPCR RT Master Mix (Osaka, Japan) after RNA quantification. Real-time PCR was performed using the PowerUP™ SYBR™ Green Master Mix (Thermo Fisher Scientific). The comparative Ct ($2^{-\Delta\Delta Ct}$) method was used to determine the relative mRNA expression, normalized to GAPDH. The used primers were listed as below: XOD, 5′-TCAGAAGCCAAGAAGGTG-3′ and 5′-ATGTTCTGG GGTGTCAGC-3′; IL-1β, 5′-CTCACAAGCAGAGCACAAGC-3′ and 5′-CAGTCCAGCCCATACTTTAGG-3′; TNF-α, 5′-CCTGGAGGAGAAGAGGAAAGAGA-3′ and 5′-TTGAGG ACCTCTGTGTATTTGTCAA-3′; IL-6, 5′-CCATCCAGTTGC CTTCTTGG-3′ and 5′-TGCAAGTGCATCATCGTTGT-3′; MCP-1, 5′-TAAAAACCTGGATCGGAACCAAA-3′ and 5′-GCATTAGCTTCAGATTTACGGGT-3′; URAT1, 5′-AGCTCT TGGACCCCAATGC-3′ and 5′-CTTCAGAGCGTGAGAGTC ACACA-3′; GLUT9, 5′-TCTCAGTTGCTTGGGAGCAG-3′ and 5′-AGCTAAAGCAAGCTCCCTGG-3′; GAPDH, 5′-GCT GAGTATGTGGAGT-3′ and 5′-GTTCACACCCATCACAA AC-3′.

Western Blot Analysis

Western blot analysis was performed as previous study with some modifications (Faqihi et al., 2020). In briefly, tissues or cells protein extracts were prepared by using

radioimmunoprecipitation (RIPA) lysis buffer (Beyotime) and then centrifuged at 12,000×*g* at 4°C for 20 min. The protein concentration was determined by BCA protein assay kit. Nuclear and cytoplasmic protein extraction was performed using a Nuclear and Cytoplasmic Protein Extraction Kit (Beyotime). After electrophoresis, separated proteins were transferred from the SDS-polyacrylamide gels to a nitrocellulose membrane. Then, the membranes were blocked with 5% skim milk for 2 h at room temperature and incubated with the indicated primary antibodies at 4°C overnight for IL-1β, TNF-α, IL-6, MCP-1, URAT1, GLUT9, NLRP3, ASC, c-caspase-1, NF-κB, p-NF-κB, IκBα, p-IκBα, β-actin and Histone H3. Next day, the membranes were washed three times, and then they were incubated with secondary antibodies corresponding to the respective species of primary antibodies for 1 h at room temperature. The bands were scanned by a gel imaging system using enhanced chemiluminescence detection kit. The grayscale values were analyzed by Image J software.

Histopathological Examination

Tissues were fixed with 4% paraformaldehyde for 24 h, and then embedded in paraffin and sectioned transversely at 4 μm for HE staining. The stained sections were visualized under light microscopy at 200× magnifications.

Cell Culture and Treatments

Human renal proximal tubule epithelial cell line (HK-2) was maintained in RPMI-1640 medium with 10% fetal bovine serum, 100 U/ml penicillin and 100 μg/ml streptomycin (Hou et al., 2019) in a humidified incubator under an atmosphere of 95% air and 5% CO_2 for further study. The medium was changed every other day. After 12 h starvation in serum-free cell culture medium, HK-2 cells were subsequently incubated with 0.1% DMSO (control group), uric acid (4 mg/dl) and uric acid combined with 200 μM FxUD for 24 h, respectively. In addition, to further explore the role on pathway, HK-2 cells were pre-treated with NF-κB inhibitor SN50 (20 μM) or NLRP3 inhibitor MCC950 (10 μM) (MCE) for 1 h and then were stimulated with uric acid for 24 h.

Cell Viability Analysis

Cell viability was measured by CCK-8 assay kit. HK-2 cells were seeded into 96-well plates at a density of 2×10^5 cells/well and allowed to adhere overnight. After treatment with various concentrations of chemicals for 24 and 48 h, or treated with various concentration of uric acid for 24 h, 10 μL CCK-8 regent was added to each well of 96-well plates, and the plate was incubated at 37°C for 2–4 h following the manufacturer's protocols. Absorbance was measured at 450 nm using a SpectraMax M3 microplate reader.

Statistical Analysis

Statistical analysis was performed with the GraphPad Prism 8.0 software package. All data were presented as the mean ± standard deviation (SD). Comparison among and between groups was analyzed with one-way analysis of variance (ANOVA) and Student's t-test, respectively. And statistical significance was concluded at $^*p < 0.05$.

RESULTS

FxUD Decreases Serum Uric Acid Levels and Ameliorates Renal Function in Hyperuricemic Mice

We firstly assessed uric acid levels in the serum of mice. As shown in **Figure 2A**, after 7 days of potassium oxonate (PO) administration, the PO group exhibited higher serum uric acid levels compared to control group, indicating that hyperuricemia was successfully established. Uric acid levels in the serum were significantly reduced in the FxUD and febuxostat (FEB) group in comparison to the PO group, and the inhibitory effect of FxUD appeared to be dose dependent. Uric acid is mainly excreted by the kidney, and a small amount is excreted by the gastrointestinal tract. Insufficient excretion of uric acid can cause kidney damage (Pilemann-Lyberg et al., 2019). As the creatinine (Cr) and blood urea nitrogen (BUN) levels in serum are effective indicators of renal function, the levels of Cr and BUN in the serum of each group were detected by detection kit. As expected, in comparison with the control group, Cr (**Figure 2B**) and BUN (**Figure 2C**) levels in the PO group were significantly increased. After treatment with FxUD and FEB, the serum Cr and BUN levels were significantly decreased to approximately the normal values. The inflammatory state and some changes in tissue structure were observed as obvious pathological features of hyperuricemia in clinical trials (Gupta and Singh, 2019). Histopathological examination for renal tissues of the mice was shown in **Figure 2D**. Kidney sections isolated from control group mice maintained a normal kidney structure, without obvious inflammatory responses. The normal appearance of renal glomerulus, tubules and interstitium stayed with a compact arrangement of cells was seen. However, the kidneys in PO group mice displayed histological alterations consist of inconspicuous boundaries between adjacent proximal tubule cells and swelling. The kidneys of mice treated with high-dose FxUD and FEB showed restoration of normal tubular histology to some extent. The above results indicated that FxUD could ameliorate the kidney damage induced by hyperuricemia.

FxUD Exerts Ameliorative Effects on Changes of Liver Biomarkers and Hepatic XOD in Hyperuricemic Mice

Uric acid is the end product of the catabolism of purine compounds in the liver. We tested alanine aminotransferase (ALT) and aspartate aminotransferase (AST) levels in mice serum as indicators for liver function (**Figures 3A,B**). Administration of PO increased the levels of serum ALT and AST in hyperuricemic mice compared to control mice. FxUD treated hyperuricemic mice exhibited decreased altered parameters. In the process of purine metabolism, xanthine oxidoreductase is a key enzyme that catalyzes the oxidation of

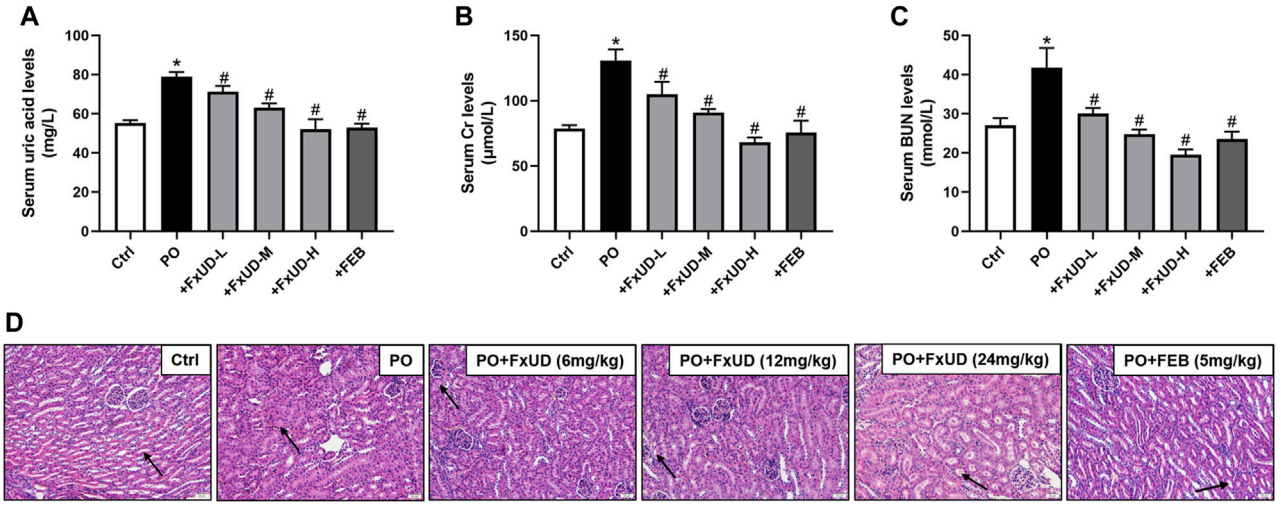

FIGURE 2 | FxUD reduces serum uric acid levels and restores renal function in hyperuricemic mice. **(A)** Uric acid, **(B)** Cr and **(C)** BUN levels in serum from the mice ($n = 8$). **(D)** The representative pictures of renal histopathology in each group ($n = 4$). Kidneys in control group maintained a normal renal tubular structure (arrow) with no evidence of inflammation, kidneys in PO group exhibited inconspicuous boundaries between adjacent tubule cells and swelling, while regulated tubule cells and the cytoplasm were relatively clear in kidneys of high-dose FxUD or FEB treatment group. Magnification 200×, scale bar 20 μm. Values are expressed as the means ± SD. $^{*}p < 0.05$ vs. Ctrl, $^{\#}p < 0.05$ vs. PO. Ctrl, control; PO, potassium oxonate; FEB, febuxostat; Cr, creatinine; BUN, urea nitrogen.

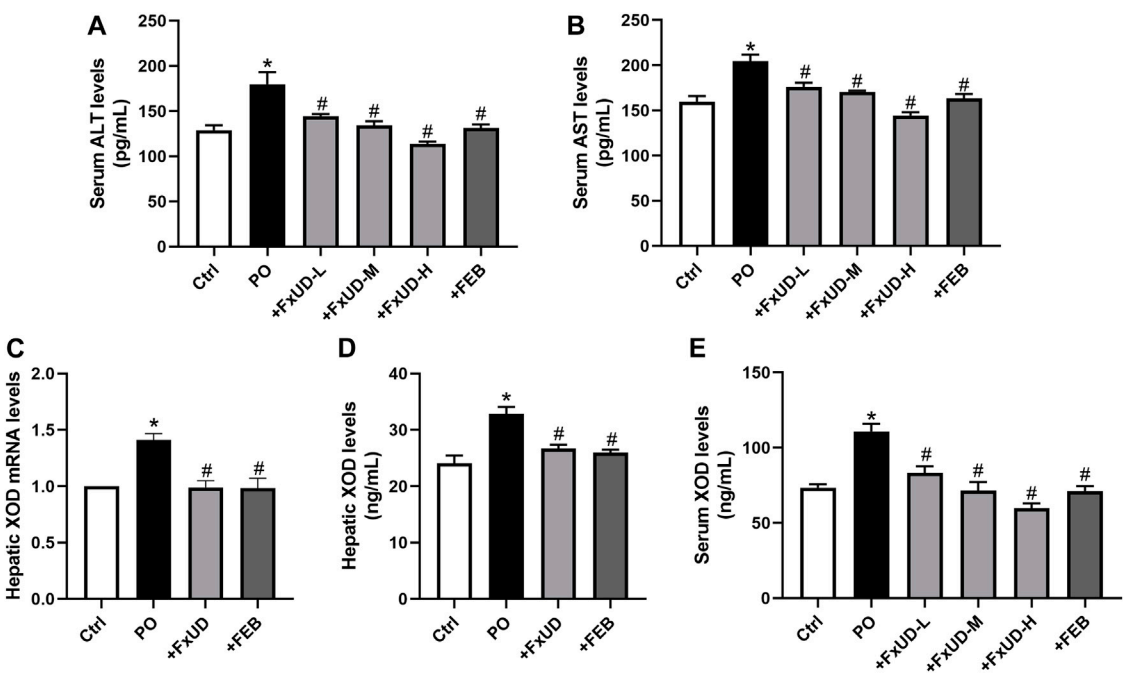

FIGURE 3 | Ameliorative effects of FxUD on changes of liver biomarkers and hepatic XOD in hyperuricemic mice. **(A)** ALT and **(B)** AST levels in mice serum as indicators of liver function ($n = 8$). **(C)** XOD mRNA expression ($n = 5$). **(D)** XOD protein levels in the liver were detected by ELISA kit ($n = 8$). **(E)** XOD in serum of mice ($n = 8$). Values are expressed as the means ± SD. $^{*}p < 0.05$ vs. Ctrl, $^{\#}p < 0.05$ vs. PO. ALT, alanine aminotransferase; AST, aspartate aminotransferase; XOD, xanthine oxidase.

hypoxanthine and xanthine to form the final product uric acid. Therefore, xanthine oxidoreductase is currently considered to be the most promising target for preventing the accumulation of uric acid in the treatment of hyperuricemia (Smelcerovic et al., 2017). As shown in **Figures 3C,D**, qRT-PCR and ELISA were performed to measure xanthine oxidase (XOD) mRNA and protein levels, hyperuricemic mice showed up-regulation of XOD mRNA and protein expression in the liver, however, FxUD remarkably down-regulated XOD mRNA and protein expression of hyperuricemic mice. Consistent changes were observed at both the mRNA and

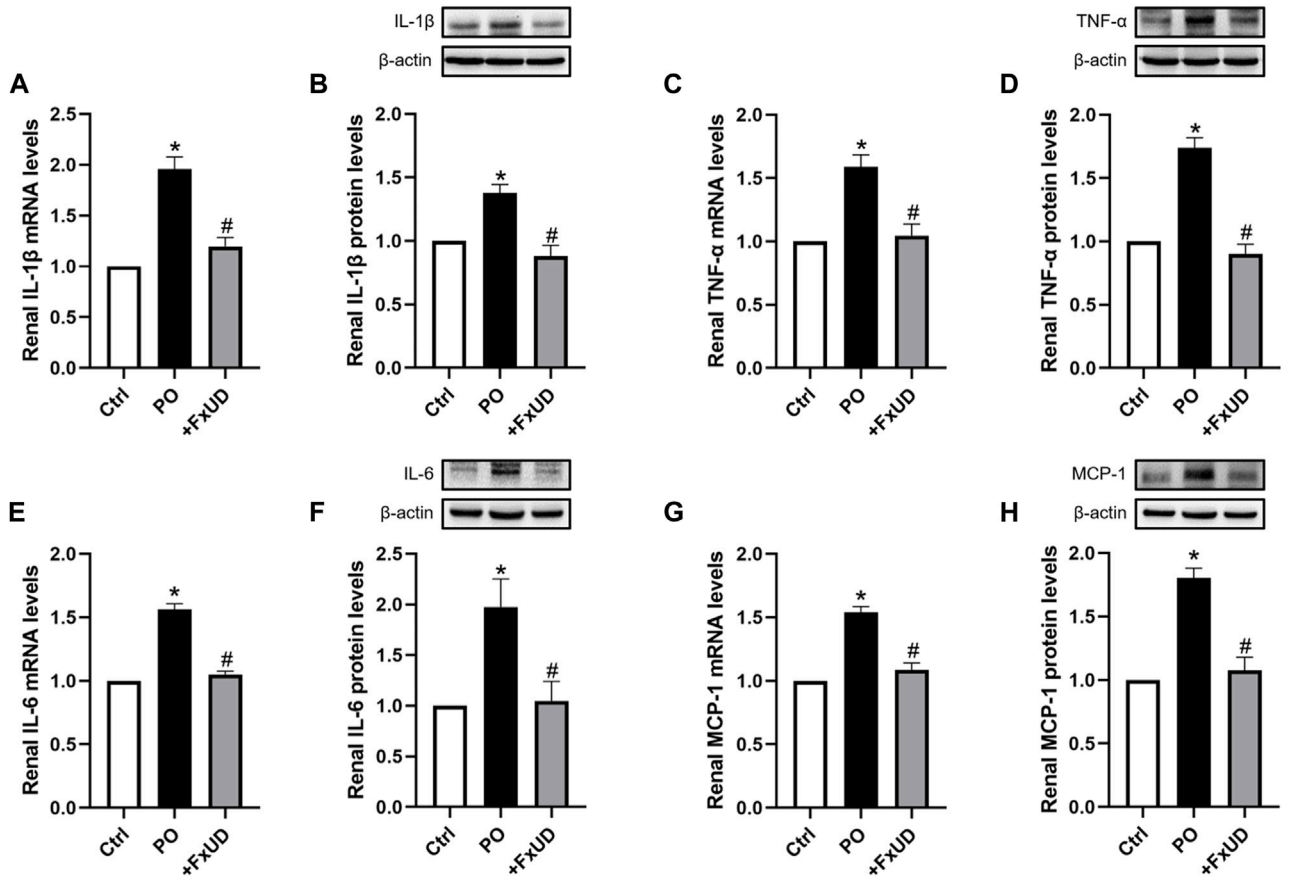

FIGURE 4 | FxUD decreases the expression of renal inflammatory cytokines in hyperuricemic mice. **(A)** qRT-PCR assay and **(B)** Western blot analysis of IL-1β. **(C)** qRT-PCR and **(D)** Western blot results of TNF-α. **(E)** qRT-PCR and **(F)** Western blot results of IL-6. **(G)** MCP-1 mRNA and **(H)** protein expression in the kidney. Values are expressed as the means ± SD (n = 4–5). $^{*}p < 0.05$ vs. Ctrl, $^{\#}p < 0.05$ vs. PO.

protein levels in FEB group. Simultaneously, XOD in serum (**Figure 3E**) was increased in hyperuricemic mice and was normalized significantly by FxUD. Thus, the results demonstrated a potential mechanism of uric acid-lowering property of FxUD partly was the inhibition of hepatic XOD in hyperuricemic mice.

FxUD Reduces the Expression of Inflammatory Cytokines in the Kidneys of Hyperuricemic Mice

Inflammation can cause persistent malfunction of tissue (Dkhil et al., 2018). Thus, qRT-PCR and Western blot analysis of inflammatory factors such as cytokines IL-1β (interleukin-1β), TNF-α (tumor necrosis factor-α) and IL-6 (interleukin-6) in kidney were performed to explore the possible mechanisms. As shown in **Figure 4**, potassium oxonate significantly increased the mRNA levels of renal inflammatory cytokines including IL-1β, TNF-α, IL-6, and MCP-1 (monocyte chemoattractant protein-1) in hyperuricemic mice. Surprisingly, after treatment with a high dosage of FxUD, the mRNA levels of the above four inflammatory cytokines were all significantly decreased. The protein results were consistent with those of mRNA expression. These results illustrated that FxUD could suppress the expression of renal inflammatory cytokines to protect against the kidney damage induced by PO, and we therefore hypothesized that FxUD might inhibit the activation of NF-κB p65. Of course, further experiments would be needed to validate this hypothesis.

Effects of FxUD on Uric Acid Reabsorption Transporters in the Kidneys of Hyperuricemic Mice

Under-excretion of uric acid has been implicated to lead to hyperuricemia (Liote, 2003). Therefore, the renal urate transporter has become a significant physiologic target for drugs to treat hyperuricemia. Human urate transporter 1 (hURAT1) is located on the brush-border membrane of proximal tubules in the kidney. As the homolog of hURAT1, mURAT1, which has the same tissue distribution as hURAT1, participates in renal urate reabsorption and plays an important role in regulating serum uric acid alteration (Takiue et al., 2011). And mGLUT9 in mouse encoded by SLC2A9 is considered to be

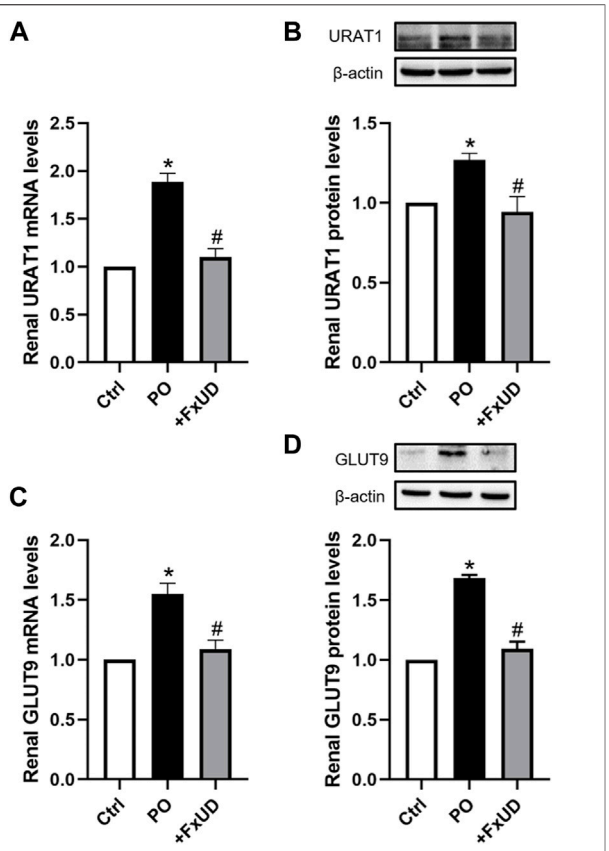

FIGURE 5 | FxUD reduces renal reabsorption of uric acid in hyperuricemic mice. **(A)** mRNA and **(B)** protein levels of URAT1 in the kidney. **(C)** mRNA and **(D)** protein levels of GLUT9 in the kidney of mice. Values are expressed as the means ± SD (n = 4–5). $^{*}p < 0.05$ vs. Ctrl, $^{\#}p < 0.05$ vs. PO.

expressed in the apical and basolateral membrane of distal convoluted tubules and could be associated with renal urate reabsorption (Vitart et al., 2008). Therefore, we investigated whether FxUD affected renal urate transport-related proteins in PO-induced hyperuricemic mice. The changes of renal urate transporters including URAT1 and GLUT9 were analyzed (**Figure 5**). Our results showed that compared to the control group, the mRNA and protein expression levels of URAT1 and GLUT9 were significantly increased in hyperuricemic mice, and FxUD resulted in a significant decrease in both mRNA and protein levels of URAT1 and GLUT9 compared to PO group. The results suggested that FxUD could be a useful alternative for prevention or treatment on hyperuricemia via reducing renal reabsorption of uric acid.

FxUD Inhibits the Activation of NLRP3 Inflammasome in the Kidneys of Hyperuricemic Mice

NLRP3 (NOD-like receptor family pyrin domain containing 3) inflammasome, suggesting inflammation may be present, plays a vital role in the pathogenesis of kidney inflammation (Chen et al., 2019). The soluble urate and urate crystals have been proved to promote activation of NLRP3 inflammasome, and then trigger congenital immune against danger signals (Braga et al., 2017). In our results described above, FxUD could reduce the expression levels of inflammatory cytokine IL-1β in mice with hyperuricemia, which is downstream product of NLRP3 inflammasome pathway (Ruiz et al., 2017). On this basis, we surveyed the effects of FxUD on regulating the protein expressions of NLRP3 inflammasome signaling pathway (**Figure 6**). We found that the protein expression levels of NLRP3 and its downstream signaling molecules were significantly increased in the kidney tissues after treatment with PO when compared to the control group, whereas FxUD reduced these inflammatory factors in kidneys of mice with hyperuricemia suggesting that FxUD could reduce kidney inflammation through inhibiting the activation of NLRP3 inflammasome.

FxUD Attenuates Inflammation by Suppressing NF-κB Signaling Pathway in the Kidneys of Hyperuricemic Mice

Once xanthine oxidase produces too much uric acid, which exceeds the excretion capacity of the kidney, the uric acid that cannot be promptly excreted will deposit in the kidney, directly leading to renal injury (Zhang et al., 2019). Uric acid crystals deposited in the kidney will induce the release of inflammatory cytokines via regulating the nuclear factor-κB (NF-κB) signaling pathway, thereby exacerbate renal injury (Li et al., 2014). To explore the molecular basis of FxUD on alleviating inflammation, 9 transcriptomes including 3 controls, 3 models, and 3 treatments, respectively, were sequenced using RNA-Seq technology. Gene ontology (GO) terms were depicted in **Figure 7A**. The analysis showed enrichment in pathways encompassing metabolism, innate immunity, transporter, and protein binding, as well as pathways that may indicate underlying mechanism in uric acid-induced inflammatory status. Accordingly, pathway enrichment analysis of differentially genes expressions regulated by FxUD treatment compared with the model group based on the KEGG database was performed, and a bubble plot for KEGG enrichment results was generated (**Figure 7B**). As expected, we found that NF-κB pathway signaling was involved in the KEGG enrichment results between the model and treat group. This suggested that NF-κB was involved in general inflammatory processes. In order to clarify the intracellular signal transduction associated with uric acid-induced inflammation, we intended to verify the targets revealed by transcriptomic analysis. The involvement of NF-κB in the priming effects of uric acid was evaluated by Western blot (**Figures 7C–E**). The level of phosphorylated NF-κB p65 was increased by PO treatment, and this effect was reversed by FxUD. Moreover, the phosphorylation of IκBα induced by PO was reduced by the treatment with FxUD. Together, these data suggested that FxUD might exert the inhibitory effect by suppressing the activation of NF-κB signaling pathway.

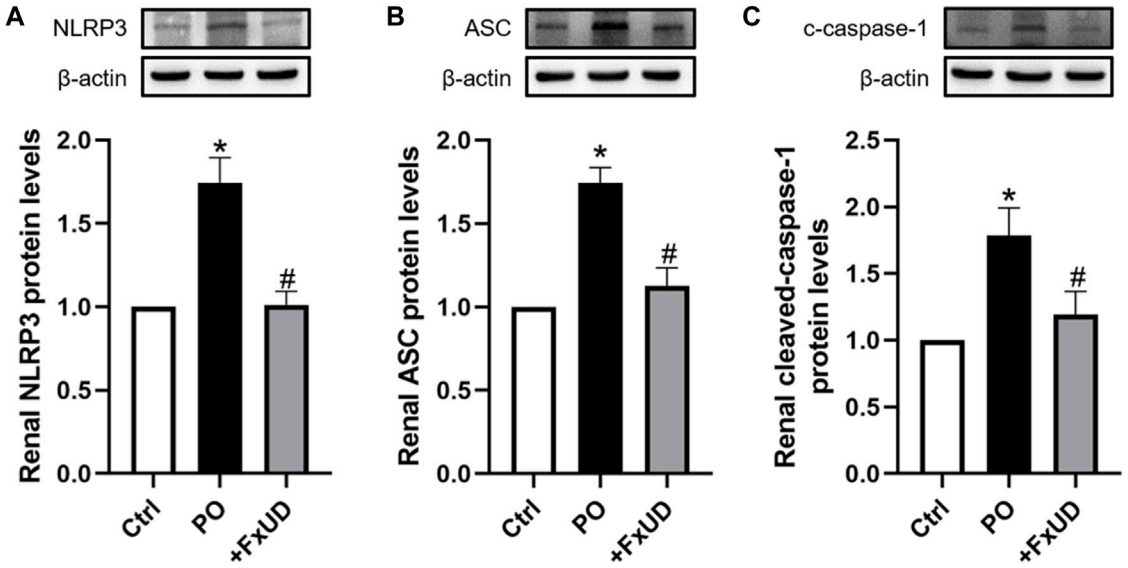

FIGURE 6 | FxUD inhibits the activation of NLRP3 inflammasome in the kidney of mice with hyperuricemia. Graphic representations of the ratios **(A)** NLRP3/β-actin, **(B)** ASC/β-actin and **(C)** c-caspase-1/β-actin. β-actin was used as loading control. Values are expressed as the means ± SD ($n = 5$). $^{*}p < 0.05$ vs. Ctrl, $^{\#}p < 0.05$ vs. PO.

Effects of FxUD on Inflammatory Cytokines and Uric Acid Reabsorption Transporters in HK-2 Cells

A proximal tubular cell line derived from normal kidney, HK-2, was used as an *in vitro* cell model to further study the anti-inflammatory effects of FxUD. Here, we attempted to identify whether FxUD could influence cell survival rate. The effects of FxUD on cell viability were analyzed by CCK-8 assay. HK-2 cells were incubated with FxUD of various concentrations as indicated for 24 or 48 h, respectively. And the presence of FxUD had no obvious effect on cell survival (**Figure 8A**). Then followed, various concentrations of uric acid (UA) were incubated to HK-2 cells for 24 h. And CCK-8 analysis illustrated that uric acid dose-dependently reduced the cell viability (**Figure 8B**). The subsequent parts were focused on further confirming our hypothesis that FxUD could relieve renal dysfunction through inflammation inhibition and regulating urate transport-related proteins *in vitro*. As shown in **Figures 8C–H**. In consistent with the results from animal experiments, uric acid exposure led to higher expression of inflammatory cytokines and uric acid reabsorption transporters compared to the control group. However, FxUD administration could down-regulate those proteins expressed levels in cells. The data above indicated that FxUD could suppress inflammation-associated proteins and urate reabsorption-related proteins expressions in UA-treated HK-2 cells *in vitro*.

Effects of FxUD on NLRP3 Inflammasome and NF-κB Signaling Pathway in HK-2 Cells

As shown in **Figures 9A–C**, to further reveal the specific role of FxUD in NLRP3 pathway, NLRP3, ASC, cleaved-caspase-1 proteins expressions induced by uric acid treatment were also examined. Our results showed that FxUD displayed inhibitory role in NLRP3 expression under uric acid stimulation. Subsequently, the protein level of ASC was reduced, leading to cleaved-caspase-1 down-regulation. To investigate the importance of NF-κB/NLRP3 signaling in inflammation reduction in tubular cells, we treated HK-2 cells with uric acid in the absence or presence of specific NF-kB inhibitor (NF-κB SN50) and NLRP3 inhibitor (MCC950), Western blot analysis was performed to detect the changes in the levels of key proteins. As shown in **Figures 9D,E**, SN50 and MCC950 reduced the levels of p-NF-κB and NLRP3 in HK-2 cells exposed to uric acid. More importantly, the protein levels were also restored significantly by FxUD treatment. These results collectively demonstrated that FxUD had a potential role in alleviating inflammation response by NF-κB/NLRP3 inhibition in UA-induced HK-2 cells.

The Assessment of FxUD on Cardiovascular Safety

Currently, drug-induced toxicity concluding nephrotoxicity, hepatotoxicity and cardiotoxicity is widespread. A major concern in drug development is toxicity to organs (Russell et al., 2017). Therefore, it is necessary to evaluate cardiotoxicity of the novel compound FxUD. Lactate dehydrogenase (LDH) is the commonly used indicator to assess the heart toxicity (Zhou et al., 2016). As shown in **Figure 10A**, serum LDH level indicated that FxUD did not exhibit cardiac toxicity compared with the control group. Meanwhile, we performed HE staining to determine the effect of FxUD on the hearts of mice (**Figure 10B**). Results revealed that the structure of myocardial cells was also normal, the muscle fibers were intact, and there was no inflammatory infiltration,

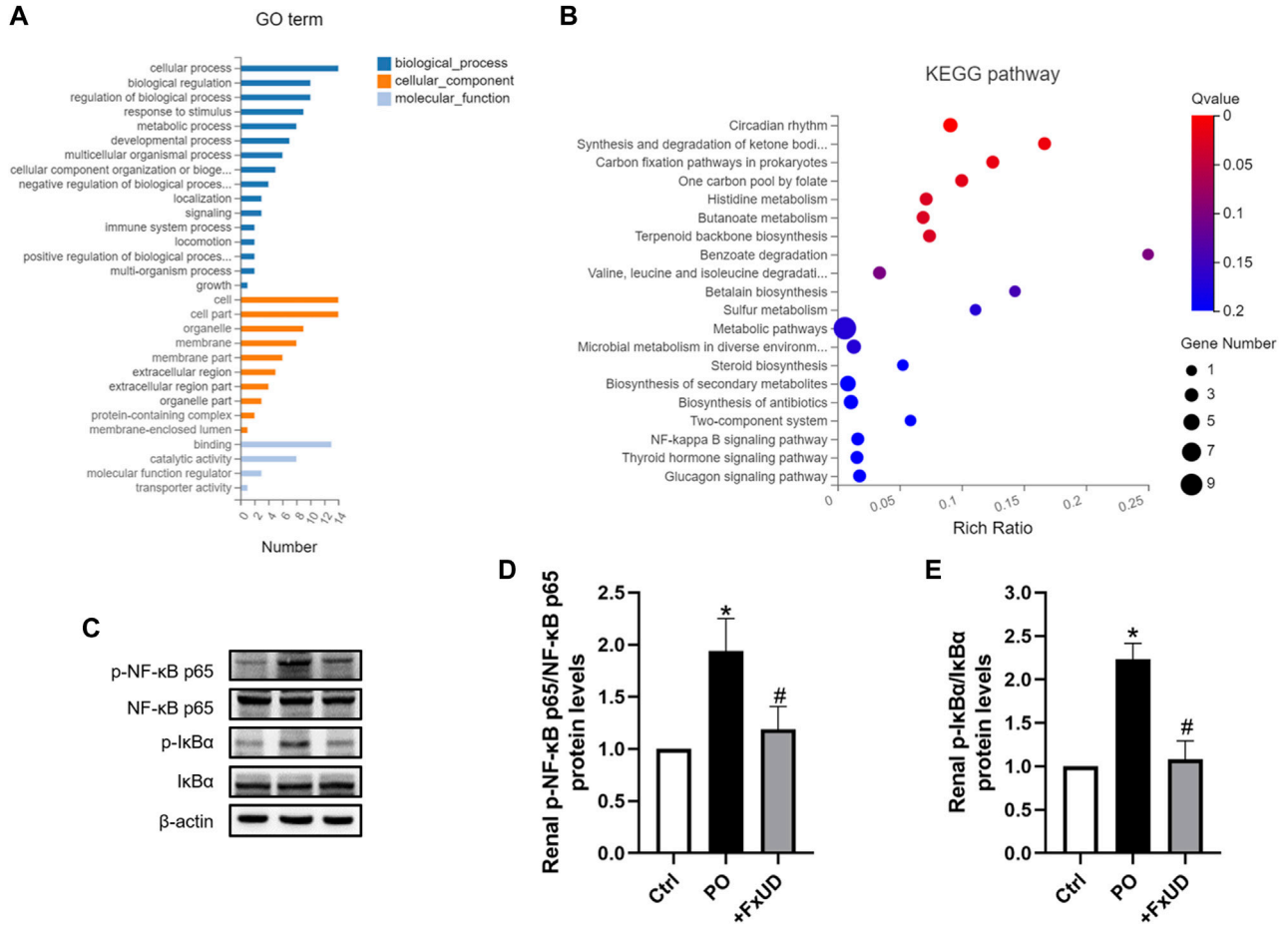

FIGURE 7 | FxUD attenuates uric acid induced inflammation by suppressing NF-κB signaling pathway in the kidney of mice with hyperuricemia. **(A)** Gene ontology analysis. **(B)** The scatter plot for KEGG enrichment results. **(C)** Representative Western blot bands were shown. **(D)** Graphic presentation of relative p-NF-κB p65 and normalized to NF-κB p65 ($n = 5$). **(E)** Graphic presentation of relative p-IκBα and normalized to IκBα ($n = 5$). Values are expressed as the means ± SD. $^{*}p < 0.05$ vs. Ctrl, $^{\#}p < 0.05$ vs. PO.

myocardial fibrosis or myocardial necrosis. Therefore, only tentative conclusions could be drawn that FxUD was not cytotoxic on the heart and may serve as candidate drug for further investigation.

DISCUSSION

In recent years, the prevalence of hyperuricemia has increased, and more and more young people are suffering from this disease (Yong et al., 2018). Febuxostat is more effective and safer than allopurinol, although this drug has not been on the market for a long time. However, concerns about the cardiovascular safety of febuxostat cause reconsideration of the application of febuxostat (Bardin and Richette, 2019). Therefore, the search for natural products or compounds of high efficacy and safety has important significance. In our study, targeting of the therapy of hyperuricemia, we had synthesized a new compound named FxUD on the basis of febuxostat. Nephropathy induced by hyperuricemia is a common complication of hyperuricemia. Although the pathogenesis of renal complications caused by hyperuricemia is unclear, hyperuricemia has been considered as an independent risk factor for renal disease (Balakumar et al., 2020) and has been put forward to be usually recognized as a marker of renal abnormalities (Kang et al., 2002). Recent evidences clearly suggest that the pathogenic role of high uric acid in renal dysfunction involves a variety of pathological and molecular mechanisms (Kang, 2018). Thus, this study is meaningful in that it investigates the uric acid-lowering effects of the new compound and delineates the possible molecular mechanisms by which it ameliorates renal damage induced by hyperuricemia.

Serum urate level is the representative hallmark of hyperuricemia (Ichida et al., 2012). Urate is mainly synthesized in the liver, and nearly two-thirds of urate is excreted through the kidney daily (Vitart et al., 2008). Therefore, underexcretion of uric acid can cause kidneys damage. Cr and BUN levels are the most important biochemical makers to detect abnormal renal function (Wang et al., 2018). The present study showed that FxUD

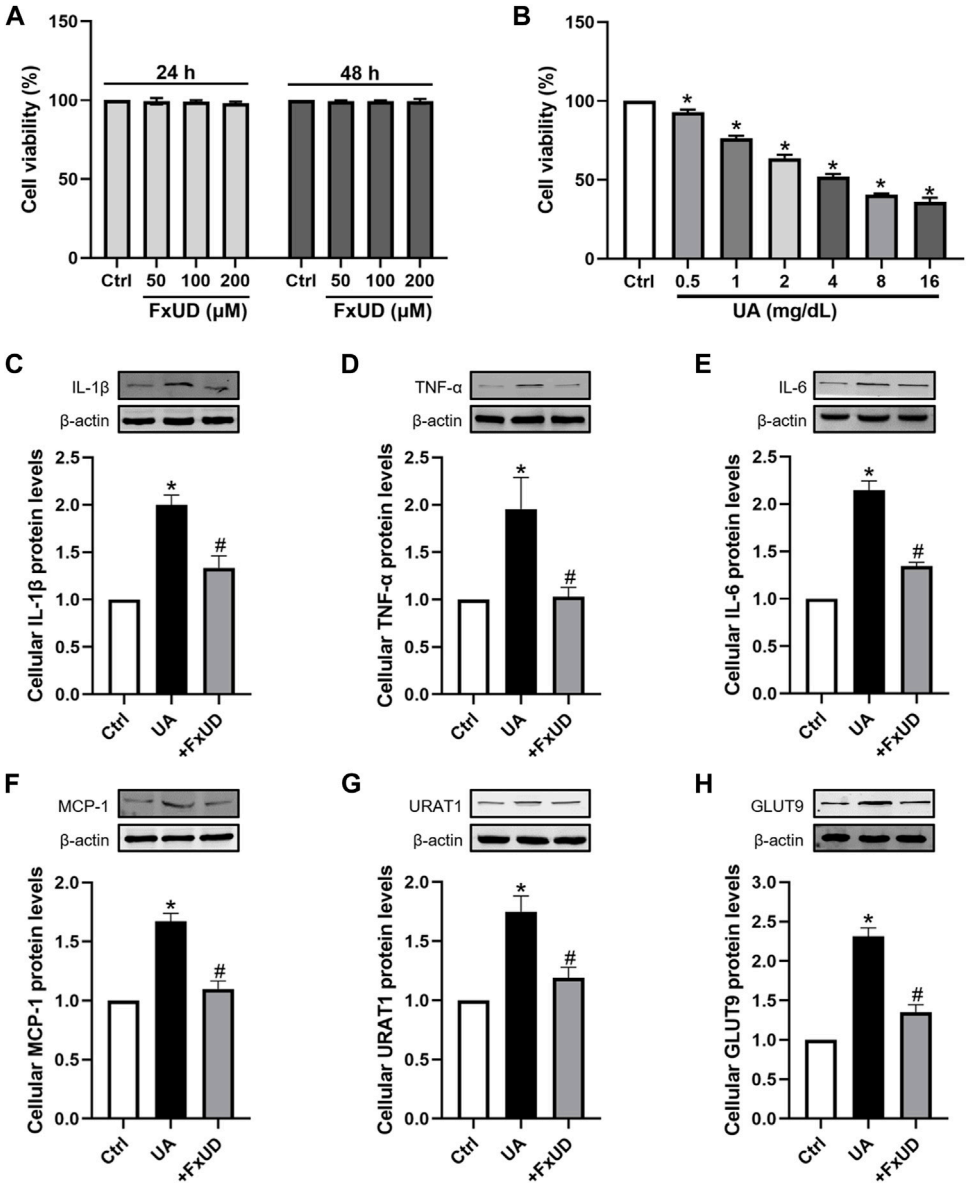

FIGURE 8 | FxUD regulates the expression of inflammatory cytokines and uric acid reabsorption transporters in uric acid-exposed HK-2 cells. **(A)** Changes in the viability of HK-2 cells following 24 or 48 h of treatment with chemicals at different concentrations, measured using CCK-8 assay ($n = 3$). **(B)** Cell viability after treated with various concentrations of UA for 24 h, and the following studies were performed ($n = 4$). **(C–H)** Representative Western blot bands and protein levels of IL-1β, TNF-α, IL-6, MCP-1, URAT1 and GLUT9 in HK-2 cells, respectively ($n = 4$). Values are expressed as the means ± SD. $^{*}p < 0.05$ vs. Ctrl, $^{\#}p < 0.05$ vs. UA. UA, uric acid.

dose-dependently reduced the levels of uric acid, Cr and BUN in serum, and alleviated potassium oxonate induced hyperuricemia. Simultaneously, renal histological examinations also indicated that potassium oxonate induced lesions in kidney tissues to some extent, which could be obviously reversed by FxUD treatment, which further exhibited the involvement of hyperuricemia associated with inflammatory mechanisms. In fact, increasing evidence supports the conclusion that inflammation is the major mechanism for renal injury in rodents and patients with hyperuricemia (Malik et al., 2016).

In general, the levels of uric acid in the serum are regulated by a balance between uric acid production and excretion. The higher xanthine oxidase (XOD) activity can lead to excessive synthesis of uric acid (Zhao et al., 2006). XOD is a critical enzyme involved in uric acid production, and as a result, inhibiting the activity of XOD may be a feasible and effective way of controlling hyperuricemia. Our results showed that treatment with FxUD could significantly suppress XOD levels in serum and the liver, indicating that one of the potential mechanisms of FxUD on lowering uric acid may be because of the inhibitory effect on XOD levels.

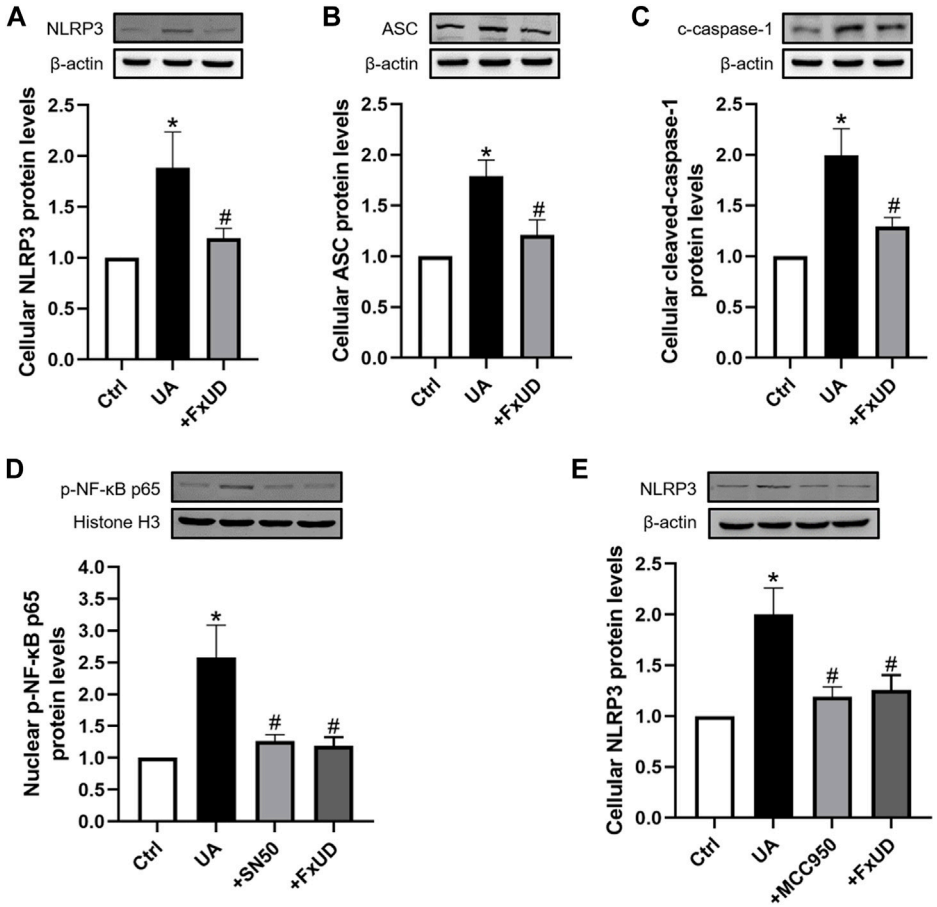

FIGURE 9 | FxUD inhibits the activation of NLRP3 inflammasome and NF-κB signaling pathway in uric acid-exposed HK-2 cells. **(A)** NLRP3, **(B)** ASC, **(C)** c-caspase-1 protein levels in HK-2 cells were measured using Western blot analysis. The protein levels of **(D)** p-NF-κB and **(E)** NLRP3 in HK-2 cells exposed to UA after treatment with SN50 or MCC950. Values are expressed as the means ± SD (n = 4). $^{*}p < 0.05$ vs. Ctrl, $^{\#}p < 0.05$ vs. UA.

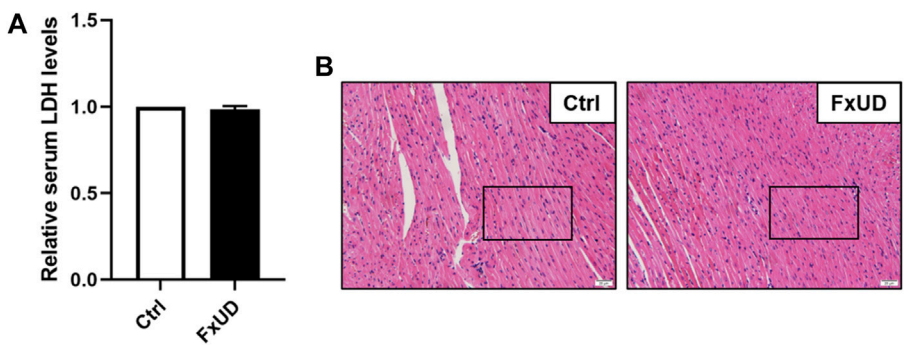

FIGURE 10 | The effect of FxUD on cardiovascular safety. **(A)** The serum LDH levels. **(B)** Cardiotoxicity was assessed by HE staining to determine the effect on heart, no significant histological changes were noted. Magnification 200×, scale bar 20 μm. Values are expressed as the means ± SD (n = 4). $^{*}p < 0.05$ vs. Ctrl.

Inflammation is a vital mechanism in the occurrence and maintenance of kidney injury (You et al., 2019). We further examined the changes in the expression levels of common inflammatory cytokines in kidney tissues. The results confirmed that FxUD significant reversed the elevation of inflammatory cytokines in kidney, indicating that the nephroprotective effects of FxUD might be attributed to its anti-inflammatory effect.

The clearance of uric acid is achieved through the interaction between the reabsorption and secretion of uric acid in the kidney,

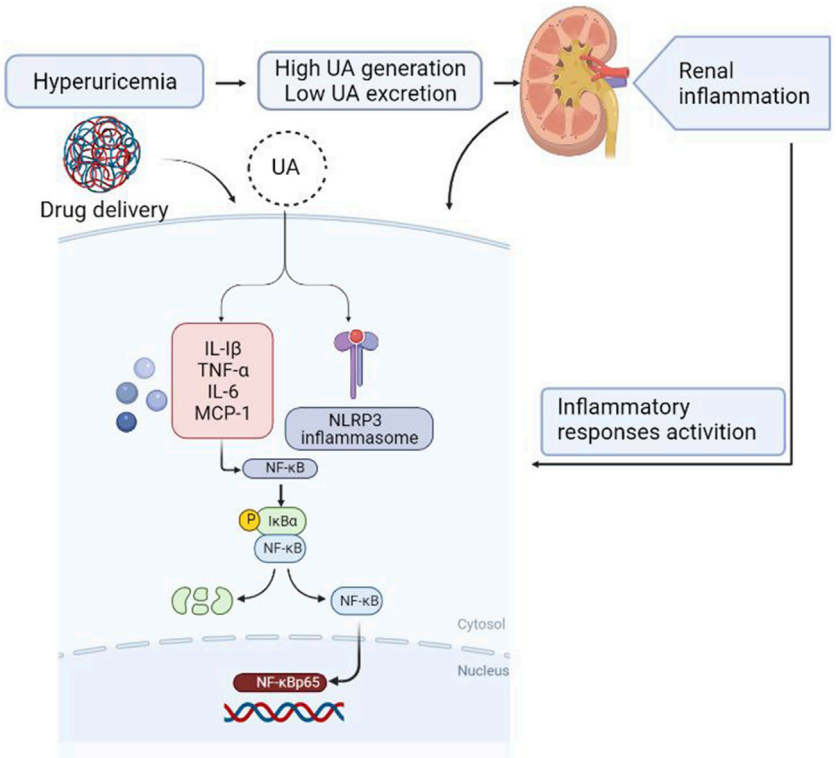

FIGURE 11 | Diagram of the speculative mechanism how the drug affects inflammation induced by hyperuricemia in the kidney generated using BioRender.

and is related to a variety of transporters present in the kidney (Lee et al., 2019). Among them, URAT1 and GLUT9 are important transporters that mediate the reabsorption of uric acid and the primary targets in the development of novel anti-hyperuricemic drugs. The results revealed that oral administration of FxUD significantly decreased mRNA and protein levels of renal URAT1 and GLUT9. In addition, genome-wide association studies of serum uric acid showed that several transporters such as ABCG2 (Nakayama et al., 2011) and organic anion transporter 1 (OAT1) (Hediger et al., 2005) also play a significant role in uric acid excretion. Thus, the effects of FxUD on uric acid excretion via the kidney are worthy of further research.

It has been reported that the increase in IL-1β and IL-18 expressions is closely related to activation of the NLRP3 inflammasome pathway. Our above results also found that uric acid could induce release of IL-1β consistently with the previous studies (Nicholas et al., 2011). In addition, increasing evidence have demonstrated that oxidative stress can increase the production of oxidative enzyme and then induce an increase in ROS, thereby activate NLRP3 inflammasome signal pathway and up-regulate the expressions of pro-inflammatory cytokines (Sharma et al., 2018). The NLRP3 inflammasome complex embraces NLRP3, ASC adaptor and caspase-1. Our results showed that potassium oxonate could resulted in increased expression of NLRP3, ASC adaptor and cleaved-caspase-1 in experimental mice, and these alterations could be remarkably reversed by FxUD treatment suggesting that FxUD might alleviate kidney injury via regulating NLRP3 inflammasome signal pathway in hyperuricemic mice.

High uric acid level can stimulate NF-κB activation in primary renal proximal tubule cells (Han et al., 2007). NF-κB has long been regarded as a typical pro-inflammatory signaling pathway, mainly based on the activation of NF-κB induced by pro-inflammatory cytokines, and NF-κB acts as a master regulator of pro-inflammatory responses to modulate expressions of pro-inflammatory genes including cytokines, chemokines, and adhesion molecules, which has been fully researched elsewhere (Lawrence, 2009). During inflammatory reaction activation, increased AMPK phosphorylation enhances SIRT1 expression, and ultimately decreases NF-κB p65 acetylation and nuclear translocation. Less inflammatory cytokines release further attenuates NF-κB p65 acetylation and transport through lower NF-κB p65 inhibitory factor IκBα phosphorylation and degradation (Zhang et al., 2016). What's more, NF-κB pathway signaling was involved in the KEGG enrichment analysis between the model and FxUD treat group. In order to clarify the specific involvement of this signal transduction mechanisms, we performed further experimental validation. In our study, the results showed that NF-κB p65 and IκBα were significantly activated in hyperuricemic mice induced by potassium oxonate, and FxUD was found to suppress renal NF-κB signaling and exerted its functions on reducing inflammation in kidney of hyperuricemic mice.

Moreover, the disturbance on NF-κB signaling and NLRP3 inflammasome was detected in uric acid-exposed HK-2 cells *in vitro*. Results showed that FxUD treatment was associated with

reduced expressions of inflammatory cytokines and uric acid reabsorption transporters, and also demonstrated that FxUD had a potential role in suppressing inflammation response via NF-κB/NLRP3 activation in uric acid-induced cells. Finally, to assess the underlying influence of FxUD on cardiovascular and safety, we selected two common indications which were linked to cardiotoxicity, the results indicated that FxUD had no noticeable toxicity on the heart.

In summary, this study shows that the anti-hyperuricemic and anti-inflammatory effects of FxUD in potassium oxonate-induced hyperuricemic mice and HK-2 cells exposed to uric acid. The mechanisms of its anti-hyperuricemic effect may be due to its significant inhibition against XOD, down-regulation of URAT1 and GLUT9. The molecular mechanisms involved in inflammatory response in the kidney under high serum uric acid level attribute to suppression of NF-κB signaling and NLRP3 inflammasome activation (**Figure 11**). Results from our research provide further insights for the development of effective and safe therapeutic candidates to combat hyperuricemia.

DATA AVAILABILITY STATEMENT

The datasets analyzed in this article are publicly available. The RNA-seq data presented in the study are deposited in the public repository with GEO accession number GSE186871 or SRA accession number SRP343909. Requests to access further datasets should be directed to JW, wangjinhui@hrbmu.edu.cn.

ETHICS STATEMENT

The animal study was reviewed and approved by the Experimental Animal Ethics Committee of Harbin Medical University.

AUTHOR CONTRIBUTIONS

LZ designed the study. LZ, YL, DY, RS, and SL performed experiments. LZ and DY prepared figures. LZ analyzed the data and wrote the manuscript. JH, XC, and CL supervised the experiments. JW and GL discussed all sections of the manuscript. All authors reviewed and approved the final manuscript.

FUNDING

This project was supported by National Science and Technology Major Project of the Ministry of Science and Technology of China (Grant no. 2018ZX09735005), National Natural Science Foundation of China (Grant no. 82003580), Foundation Committee of Basic and Applied Basic Research of Guangdong Province (Grant no. 2019A1515110482) and Shenzhen Natural Science Foundation (Grant no. JCYJ20190808171803553).

REFERENCES

Balakumar, P., Alqahtani, A., Khan, N. A., Mahadevan, N., and Dhanaraj, S. A. (2020). Mechanistic Insights into Hyperuricemia-Associated Renal Abnormalities with Special Emphasis on Epithelial-To-Mesenchymal Transition: Pathologic Implications and Putative Pharmacologic Targets. *Pharmacol. Res.* 161, 105209. doi:10.1016/j.phrs.2020.105209

Bardin, T., and Richette, P. (2019). The Role of Febuxostat in Gout. *Curr. Opin. Rheumatol.* 31 (2), 152–158. doi:10.1097/BOR.0000000000000573

Braga, T. T., Forni, M. F., Correa-Costa, M., Ramos, R. N., Barbuto, J. A., Branco, P., et al. (2017). Soluble Uric Acid Activates the NLRP3 Inflammasome. *Sci. Rep.* 7, 39884. doi:10.1038/srep39884

Chen, C., Lü, J. M., and Yao, Q. (2016). Hyperuricemia-Related Diseases and Xanthine Oxidoreductase (XOR) Inhibitors: An Overview. *Med. Sci. Monit.* 22, 2501–2512. doi:10.12659/msm.899852

Chen, Y., Li, C., Duan, S., Yuan, X., Liang, J., and Hou, S. (2019). Curcumin Attenuates Potassium Oxonate-Induced Hyperuricemia and Kidney Inflammation in Mice. *Biomed. Pharmacother.* 118, 109195. doi:10.1016/j.biopha.2019.109195

Chiba, Y., Murakami, R., Matsumoto, K., Wakamatsu, K., Nonaka, W., Uemura, N., et al. (2020). Glucose, Fructose, and Urate Transporters in the Choroid Plexus Epithelium. *Int. J. Mol. Sci.* 21 (19), 7230. doi:10.3390/ijms21197230

Dalbeth, N., Phipps-Green, A., Frampton, C., Neogi, T., Taylor, W. J., and Merriman, T. R. (2018). Relationship between Serum Urate Concentration and Clinically Evident Incident Gout: an Individual Participant Data Analysis. *Ann. Rheum. Dis.* 77 (7), 1048–1052. doi:10.1136/annrheumdis-2017-212288

Dehlin, M., Jacobsson, L., and Roddy, E. (2020). Global Epidemiology of Gout: Prevalence, Incidence, Treatment Patterns and Risk Factors. *Nat. Rev. Rheumatol.* 16 (7), 380–390. doi:10.1038/s41584-020-0441-1

Dkhil, M. A., Al-Quraishy, S., and Moneim, A. E. A. (2018). Ziziphus Spina-Christi Leaf Extract Pretreatment Inhibits Liver and Spleen Injury in a Mouse Model of Sepsis via Anti-oxidant and Anti-inflammatory Effects. *Inflammopharmacology* 26 (3), 779–791. doi:10.1007/s10787-017-0439-8

Enomoto, A., Kimura, H., Chairoungdua, A., Shigeta, Y., Jutabha, P., Cha, S. H., et al. (2002). Molecular Identification of a Renal Urate Anion Exchanger that Regulates Blood Urate Levels. *Nature* 417 (6887), 447–452. doi:10.1038/nature742

Faqihi, F., Alharthy, A., Alodat, M., Asad, D., Aletreby, W., Kutsogiannis, D. J., et al. (2020). A Pilot Study of Therapeutic Plasma Exchange for Serious SARS CoV-2 Disease (COVID-19): A Structured Summary of a Randomized Controlled Trial Study Protocol. *Trials* 21 (1), 506. doi:10.1186/s13063-020-04454-4

Galassi, F. M., and Borghi, C. (2015). A Brief History of Uric Acid: From Gout to Cardiovascular Risk Factor. *Eur. J. Intern. Med.* 26 (5), 373. doi:10.1016/j.ejim.2015.04.005

Gupta, M. K., and Singh, J. A. (2019). Cardiovascular Disease in Gout and the Protective Effect of Treatments Including Urate-Lowering Therapy. *Drugs* 79 (5), 531–541. doi:10.1007/s40265-019-01081-5

Hagos, Y., Stein, D., Ugele, B., Burckhardt, G., and Bahn, A. (2007). Human Renal Organic Anion Transporter 4 Operates as an Asymmetric Urate Transporter. *J. Am. Soc. Nephrol.* 18 (2), 430–439. doi:10.1681/ASN.2006040415

Han, H. J., Lim, M. J., Lee, Y. J., Lee, J. H., Yang, I. S., and Taub, M. (2007). Uric Acid Inhibits Renal Proximal Tubule Cell Proliferation via at Least Two Signaling Pathways Involving PKC, MAPK, cPLA2, and NF-kappaB. *Am. J. Physiol. Ren. Physiol.* 292 (1), F373–F381. doi:10.1152/ajprenal.00104.2006

Hediger, M. A., Johnson, R. J., Miyazaki, H., and Endou, H. (2005). Molecular Physiology of Urate Transport. *Physiology (Bethesda)* 20, 125–133. doi:10.1152/physiol.00039.2004

Herlitz, L. C., D'Agati, V. D., and Markowitz, G. S. (2012). Crystalline Nephropathies. *Arch. Pathol. Lab. Med.* 136 (7), 713–720. doi:10.5858/arpa.2011-0565-RA

Hou, C., Liu, D., Wang, M., Gong, C., Li, Y., Yang, L., et al. (2019). Novel Xanthine Oxidase-Based Cell Model Using HK-2 cell for Screening Antihyperuricemic Functional Compounds. *Free Radic. Biol. Med.* 136, 135–145. doi:10.1016/j.freeradbiomed.2019.04.007

Ichida, K., Matsuo, H., Takada, T., Nakayama, A., Murakami, K., Shimizu, T., et al. (2012). Decreased Extra-renal Urate Excretion Is a Common Cause of Hyperuricemia. *Nat. Commun.* 3, 764. doi:10.1038/ncomms1756

Isaka, Y., Takabatake, Y., Takahashi, A., Saitoh, T., and Yoshimori, T. (2016). Hyperuricemia-induced Inflammasome and Kidney Diseases. *Nephrol. Dial. Transpl.* 31 (6), 890–896. doi:10.1093/ndt/gfv024

Kang, D. H., Nakagawa, T., Feng, L., Watanabe, S., Han, L., Mazzali, M., et al. (2002). A Role for Uric Acid in the Progression of Renal Disease. *J. Am. Soc. Nephrol.* 13 (12), 2888–2897. doi:10.1097/01.asn.0000034910.58454.fd

Kang, D. H. (2018). Hyperuricemia and Progression of Chronic Kidney Disease: Role of Phenotype Transition of Renal Tubular and Endothelial Cells. *Contrib. Nephrol.* 192, 48–55. doi:10.1159/000484278

Kielstein, J. T., Pontremoli, R., and Burnier, M. (2020). Management of Hyperuricemia in Patients with Chronic Kidney Disease: a Focus on Renal Protection. *Curr. Hypertens. Rep.* 22 (12), 102. doi:10.1007/s11906-020-01116-3

Lawrence, T. (2009). The Nuclear Factor NF-kappaB Pathway in Inflammation. *Cold Spring Harb Perspect. Biol.* 1 (6), a001651. doi:10.1101/cshperspect.a001651

Lee, Y. S., Sung, Y. Y., Yuk, H. J., Son, E., Lee, S., Kim, J. S., et al. (2019). Anti-hyperuricemic Effect of Alpinia Oxyphylla Seed Extract by Enhancing Uric Acid Excretion in the Kidney. *Phytomedicine* 62, 152975. doi:10.1016/j.phymed.2019.152975

Li, Y. W., Zhang, Y., Zhang, L., Li, X., Yu, J. B., Zhang, H. T., et al. (2014). Protective Effect of tea Polyphenols on Renal Ischemia/reperfusion Injury via Suppressing the Activation of TLR4/NF-κB P65 Signal Pathway. *Gene* 542 (1), 46–51. doi:10.1016/j.gene.2014.03.021

Lioté, F. (2003). Hyperuricemia and Gout. *Curr. Rheumatol. Rep.* 5 (3), 227–234. doi:10.1007/s11926-003-0072-y

Lu, J., Dalbeth, N., Yin, H., Li, C., Merriman, T. R., and Wei, W. H. (2019). Mouse Models for Human Hyperuricaemia: a Critical Review. *Nat. Rev. Rheumatol.* 15 (7), 413–426. doi:10.1038/s41584-019-0222-x

Malik, R., Aneni, E. C., Shahrayar, S., Freitas, W. M., Ali, S. S., Veledar, E., et al. (2016). Elevated Serum Uric Acid Is Associated with Vascular Inflammation but Not Coronary Artery Calcification in the Healthy Octogenarians: the Brazilian Study on Healthy Aging. *Aging Clin. Exp. Res.* 28 (2), 359–362. doi:10.1007/s40520-015-0395-3

Medzhitov, R. (2008). Origin and Physiological Roles of Inflammation. *Nature* 454 (7203), 428–435. doi:10.1038/nature07201

Méndez Landa, C. E. (2018). Renal Effects of Hyperuricemia. *Contrib. Nephrol.* 192, 8–16. doi:10.1159/000484273

Nakayama, A., Matsuo, H., Takada, T., Ichida, K., Nakamura, T., Ikebuchi, Y., et al. (2011). ABCG2 Is a High-Capacity Urate Transporter and its Genetic Impairment Increases Serum Uric Acid Levels in Humans. *Nucleosides Nucleotides Nucleic Acids* 30 (12), 1091–1097. doi:10.1080/15257770.2011.633953

Nicholas, S. A., Bubnov, V. V., Yasinska, I. M., and Sumbayev, V. V. (2011). Involvement of Xanthine Oxidase and Hypoxia-Inducible Factor 1 in Toll-like Receptor 7/8-mediated Activation of Caspase 1 and Interleukin-1β. *Cell Mol. Life Sci.* 68 (1), 151–158. doi:10.1007/s00018-010-0450-3

Pilemann-Lyberg, S., Hansen, T. W., Rossing, P., Winther, S. A., Theilade, S., Ahluwalia, T. S., et al. (2019). Response to Comment on Pilemann-Lyberg et al. Uric Acid Is an Independent Risk Factor for Decline in Kidney Function, Cardiovascular Events, and Mortality in Patients With Type 1 Diabetes. Diabetes Care 2019;42:1088-1094. *Diabetes Care* 42 (6), e188. doi:10.2337/dci19-0037

Qin, Z., Wang, S., Lin, Y., Zhao, Y., Yang, S., Song, J., et al. (2018). Antihyperuricemic Effect of Mangiferin Aglycon Derivative J99745 by Inhibiting Xanthine Oxidase Activity and Urate Transporter 1 Expression in Mice. *Acta Pharm. Sin B* 8 (2), 306–315. doi:10.1016/j.apsb.2017.05.004

Rock, K. L., Kataoka, H., and Lai, J. J. (2013). Uric Acid as a Danger Signal in Gout and its Comorbidities. *Nat. Rev. Rheumatol.* 9 (1), 13–23. doi:10.1038/nrrheum.2012.143

Ruiz, P. A., Morón, B., Becker, H. M., Lang, S., Atrott, K., Spalinger, M. R., et al. (2017). Titanium Dioxide Nanoparticles Exacerbate DSS-Induced Colitis: Role of the NLRP3 Inflammasome. *Gut* 66 (7), 1216–1224. doi:10.1136/gutjnl-2015-310297

Russell, S., Wojtkowiak, J., Neilson, A., and Gillies, R. J. (2017). Metabolic Profiling of Healthy and Cancerous Tissues in 2D and 3D. *Sci. Rep.* 7 (1), 15285. doi:10.1038/s41598-017-15325-5

Sharma, A., Tate, M., Mathew, G., Vince, J. E., Ritchie, R. H., and de Haan, J. B. (2018). Oxidative Stress and NLRP3-Inflammasome Activity as Significant Drivers of Diabetic Cardiovascular Complications: Therapeutic Implications. *Front. Physiol.* 9, 114. doi:10.3389/fphys.2018.00114

Šmelcerović, A., Tomović, K., Šmelcerović, Ž., Petronijević, Ž., Kocić, G., Tomašič, T., et al. (2017). Xanthine Oxidase Inhibitors beyond Allopurinol and Febuxostat; an Overview and Selection of Potential Leads Based on In Silico Calculated Physico-Chemical Properties, Predicted Pharmacokinetics and Toxicity. *Eur. J. Med. Chem.* 135, 491–516. doi:10.1016/j.ejmech.2017.04.031

So, A. K., and Martinon, F. (2017). Inflammation in Gout: Mechanisms and Therapeutic Targets. *Nat. Rev. Rheumatol.* 13 (11), 639–647. doi:10.1038/nrrheum.2017.155

Su, H. Y., Yang, C., Liang, D., and Liu, H. F. (2020). Research Advances in the Mechanisms of Hyperuricemia-Induced Renal Injury. *Biomed. Res. Int.* 2020, 5817348. doi:10.1155/2020/5817348

Takiue, Y., Hosoyamada, M., Kimura, M., and Saito, H. (2011). Enhancement of Androgen Action in the Kidneys of Transgenic Mice Harboring the Mutant Human UMOD Gene. *J. Pharmacol. Sci.* 115 (3), 383–389. doi:10.1254/jphs.10240fp

Terkeltaub, R. (2010). Update on Gout: New Therapeutic Strategies and Options. *Nat. Rev. Rheumatol.* 6 (1), 30–38. doi:10.1038/nrrheum.2009.236

Vitart, V., Rudan, I., Hayward, C., Gray, N. K., Floyd, J., Palmer, C. N., et al. (2008). SLC2A9 Is a Newly Identified Urate Transporter Influencing Serum Urate Concentration, Urate Excretion and Gout. *Nat. Genet.* 40 (4), 437–442. doi:10.1038/ng.106

Waisman, J., Mwasi, L. M., Bluestone, R., and Klinenberg, J. R. (1975). Acute Hyperuricemic Nephropathy in Rats. An Electron Microscopic Study. *Am. J. Pathol.* 81 (2), 367–378.

Wang, M., Zhao, J., Zhang, N., and Chen, J. (2016). Astilbin Improves Potassium Oxonate-Induced Hyperuricemia and Kidney Injury through Regulating Oxidative Stress and Inflammation Response in Mice. *Biomed. Pharmacother.* 83, 975–988. doi:10.1016/j.biopha.2016.07.025

Wang, K., Hu, L., and Chen, J. K. (2018a). RIP3-deficience Attenuates Potassium Oxonate-Induced Hyperuricemia and Kidney Injury. *Biomed. Pharmacother.* 101, 617–626. doi:10.1016/j.biopha.2018.02.010

Wang, N., Li, P., Pan, J., Wang, M., Long, M., Zang, J., et al. (2018b). Bacillus Velezensis A2 Fermentation Exerts a Protective Effect on Renal Injury Induced by Zearalenone in Mice. *Sci. Rep.* 8 (1), 13646. doi:10.1038/s41598-018-32006-z

Yong, T., Li, D., Li, M., Liang, D., Diao, X., Deng, C., et al. (2018). Anti-Hyperuricemic Effect of 2-Hydroxy-4-Methoxy-Benzophenone-5-Sulfonic Acid in Hyperuricemic Mice through XOD. *Molecules* 23 (10), 2671. doi:10.3390/molecules23102671

You, Y. K., Luo, Q., Wu, W. F., Zhang, J. J., Zhu, H. J., Lao, L., et al. (2019). Petchiether A Attenuates Obstructive Nephropathy by Suppressing TGF-β/Smad3 and NF-κB Signalling. *J. Cel Mol Med* 23 (8), 5576–5587. doi:10.1111/jcmm.14454

Zhang, J., Zhang, Y., Xiao, F., Liu, Y., Wang, J., Gao, H., et al. (2016). The Peroxisome Proliferator-Activated Receptor γ Agonist Pioglitazone Prevents NF-κB Activation in Cisplatin Nephrotoxicity through the Reduction of P65 Acetylation via the AMPK-SIRT1/p300 Pathway. *Biochem. Pharmacol.* 101, 100–111. doi:10.1016/j.bcp.2015.11.027

Zhang, Z. C., Zhou, Q., Yang, Y., Wang, Y., and Zhang, J. L. (2019). Highly Acylated Anthocyanins from Purple Sweet Potato (Ipomoea Batatas L.) Alleviate Hyperuricemia and Kidney Inflammation in Hyperuricemic Mice: Possible Attenuation Effects on Allopurinol. *J. Agric. Food Chem.* 67 (22), 6202–6211. doi:10.1021/acs.jafc.9b01810

Zhao, X., Zhu, J. X., Mo, S. F., Pan, Y., and Kong, L. D. (2006). Effects of cassia Oil on Serum and Hepatic Uric Acid Levels in Oxonate-Induced Mice and Xanthine Dehydrogenase and Xanthine Oxidase Activities in Mouse Liver. *J. Ethnopharmacol.* 103 (3), 357–365. doi:10.1016/j.jep.2005.08.040

Zhou, H., Zhang, P., Hou, Z., Xie, J., Wang, Y., Yang, B., et al. (2016). Research on the Relationships between Endogenous Biomarkers and Exogenous Toxic Substances of Acute Toxicity in Radix Aconiti. *Molecules* 21 (12), 1623. doi:10.3390/molecules21121623

Conflict of Interest: The authors declare that the research was conducted in the absence of any commercial or financial relationships that could be construed as a potential conflict of interest.

Publisher's Note: All claims expressed in this article are solely those of the authors and do not necessarily represent those of their affiliated organizations, or those of the publisher, the editors and the reviewers. Any product that may be evaluated in this article, or claim that may be made by its manufacturer, is not guaranteed or endorsed by the publisher.

frontiers in Pharmacology

ORIGINAL RESEARCH
published: 29 November 2021
doi: 10.3389/fphar.2021.775117

Discovery of a Novel MyD88 Inhibitor M20 and Its Protection Against Sepsis-Mediated Acute Lung Injury

Jiali Song[1†], Daoxing Chen[1†], Yingqiao Pan[1], Xueqin Shi[1], Qian Liu[1], Xiaoyao Lu[1], Ximing Xu[2,3,4], Gaozhi Chen[1] and Yuepiao Cai[1*]*

[1]School of Pharmaceutical Sciences, Wenzhou Medical University, Wenzhou, China, [2]Key Laboratory of Marine Drugs of Ministry of Education, School of Medicine and Pharmacy, Ocean University of China, Qingdao, China, [3]Center for Innovation Marine Drug Screening & Evaluation, Pilot National Laboratory for Marine Science and Technology (Qingdao), Qingdao, China, [4]Marine Biomedical Research Institute of Qingdao, Qingdao, China

OPEN ACCESS

Edited by:
Nandakumar Natarajan, University of California, San Francisco, United States

Reviewed by:
Badrinath Narayanasamy, Pusan National University, South Korea
Stalinraja Maruthamuthu, University of California, San Francisco, United States
Madan Kumar Arumugam, University of Nebraska Medical Center, United States

***Correspondence:**
Gaozhi Chen
cgztc@163.com
Yuepiao Cai
ypcai@wmu.edu.cn

[†]These authors contributed equally to this work

Specialty section:
This article was submitted to Inflammation Pharmacology, a section of the journal Frontiers in Pharmacology

Received: 13 September 2021
Accepted: 04 November 2021
Published: 29 November 2021

Citation:
Song J, Chen D, Pan Y, Shi X, Liu Q, Lu X, Xu X, Chen G and Cai Y (2021) Discovery of a Novel MyD88 Inhibitor M20 and Its Protection Against Sepsis-Mediated Acute Lung Injury. Front. Pharmacol. 12:775117. doi: 10.3389/fphar.2021.775117

Myeloid differentiation factor 88 (MyD88) is a hub protein in the Toll-like receptor signaling pathway, which acts as a master switch for numerous inflammatory diseases, including acute lung injury (ALI). Although this protein is considered as a crucial therapeutic target, there are currently no clinically approved MyD88-targeting drugs. Based on previous literature, here we report the discovery via computer-aided drug design (CADD) of a small molecule, M20, which functions as a novel MyD88 inhibitor to efficiently relieve lipopolysaccharide-induced inflammation both *in vitro* and *in vivo*. Computational chemistry, surface plasmon resonance detection (SPR) and biological experiments demonstrated that M20 forms an important interaction with the MyD88-Toll/interleukin-1 receptor domain and thereby inhibits the protein dimerization. Taken together, this study found a MyD88 inhibitor, M20, with a novel skeleton, which provides a crucial understanding in the development and modification of MyD88 inhibitors. Meanwhile, the favorable bioactivity of the hit compound is also conducive to the treatment of acute lung injury or other more inflammatory diseases.

Keywords: myeloid differentiation factor 88, computer-aided drug design, virtual screening, cryptic pocket, anti-inflammatory inhibitor, acute lung injury

INTRODUCTION

Acute lung injury (ALI) is a serious lung disease that is clinically defined as moderate or mild acute respiratory distress syndrome (ARDS). It is caused by various direct or indirect injuries of the lung parenchyma and has an approximately 40% fatality rate (Ding et al., 2020). Sepsis, the leading cause (6–42%) of ALI (Kumar, 2020), is classically activated by lipopolysaccharide (LPS) from Gram-negative pathogens (Dickson and Lehmann, 2019). It is widely known that LPS triggers inflammatory responses by activating Toll-like receptors (TLRs) (Chen et al., 2019). In the TLR signaling pathway, most of the inflammatory responses are mediated by a vital switch molecule called

Abbreviations: DMEM, Dulbecco's Modified Eagle's Medium; ELISA, enzyme-linked immune sorbent assay; ERK, extracellular regulated protein kinases; FBS, fetal bovine serum; HA, influenza hemagglutinin epitope; IL-6, interleukin-6; ip, intraperitoneally; iv, intravenous injection; JNK, c-Jun N-terminal kinase; MAPK, mitogen-activated protein kinase; qPCR, quantitative PCR; SDS-PAGE, sodium dodecyl sulfate-polyacrylamide gel electrophoresis; PBS, phosphate buffer saline; P38, P38MAPK; TNF-α, tumor necrosis factor-α.

Myeloid differentiation factor 88 (MyD88). Currently, the main clinical treatment methods to combat lung injury diseases include drug therapy and mechanical ventilation. Although the use of protective mechanical ventilation therapy alone plays a certain role in lung protection, this treatment fails to effectively reduce the mortality of patients. Currently, anti-inflammatory drug therapy nowadays is a comprehensive treatment method for ALI/ARDS patients, which has obtained good theoretical support and preliminary research foundation. Additionally, previous studies have reported that the design of inhibitors to prevent MyD88 from self-polymerization is also a good anti-inflammatory treatment strategy (Di Padova et al., 2018).

MyD88 is a 33-kDa protein containing an N-terminal death domain and a C-terminal Toll/interleukin-1 receptor (TIR) domain, which are separated by a short intermediate domain (Chen et al., 2020). Meantime, it is also the hub protein of the TLR signaling pathway. There is emerging evidence that MyD88 can be recruited to TLR complexes as a dimer, thus affecting the signal transduction and mediating inflammation (Di Padova et al., 2018). Therefore, the use of inhibitors targeting MyD88 is considered an advanced anti-inflammatory treatment strategy. Of note, the majority of inhibitors are peptidomimetic compounds derived from BB-loop and their further modified compounds. In 2003, Loiarro et al. (2005) first developed a peptide with anti-inflammatory activity. After this, Fantò et al. (2008) designed and synthesized a series of peptidomimetic compounds using heptapeptide as a template. Then, Xie et al. (2016) reported a new skeleton of MyD88 inhibitor. Until now, no more new skeletons of MyD88 inhibitors had been reported. Currently, protein–protein interaction (PPI) is widely regarded as one of the key processes involved in the regulation of cellular mechanisms. Thus, targeting PPIs has gradually become an alternative strategy to interfere with protein activity and modify biological processes involved in the pathology of many diseases (Thabault et al., 2021). Furthermore, the strategy of inhibiting MyD88 homodimerization has also been considered to be one of the preferred directions in the development of new inhibitors (Zhang et al., 2016; Liu et al., 2018). Unfortunately, the discovery of novel MyD88 inhibitors has been progressing slowly. Hence, developing MyD88 homodimerization inhibitors for therapeutic intervention has become an urgent and challenging need.

In recent years, computer-aided drug design (CADD) has played essential roles in modern drug discovery and development (Drayman et al., 2021; Singh et al., 2021). Meanwhile, structure-based virtual screening (SBVS) is widely adopted to design and identify more bioactive compounds based on pockets in protein structures. Nevertheless, the pockets adopted in SBVS are always acquired from protein crystallization structure directly, leading to the ignorance of the dynamic properties of the target proteins. Employing molecular dynamics simulation may contribute to better understanding of the dynamic property of the protein properties and incentivize the discovery of potential cryptic pockets. This approach encourages us to go beyond the inherent limitations of screening based solely on crystallization structure to discover newer bioactive molecules.

In this study, based on the concept of inhibiting the homodimerization of the MyD88-TIR domain, 20 potential candidate compounds with novel structures were selected from a commercial library containing more than 40,000 compounds. Finally, we are very pleased to find that all of these compounds exhibit a certain anti-inflammatory activity. Of note, we preliminarily discovered a novel small-molecule inhibitor of MyD88, M20, which provides support for our predicted patterns. We conducted a deeper exploration of this compound, which will be discussed in the following sections.

MATERIALS AND METHODS

Molecular Dynamics Simulation

All molecular dynamics (MD) simulations were conducted using the AMBER16 software package (Salomon-Ferrer et al., 2013). Before simulation, systems were prepared using the LEaP module of the AMBER16 package. The ff14SB (Maier et al., 2015) was applied to describe proteins, and the GAFF2 (Wang et al., 2004) was applied to describe small molecules. Next, each system was soaked into a rectangular box with periodic boundary conditions of TIP3P water molecules with at least 10 Å distance around the proteins or complexes. Finally, appropriate chloride or sodium ions were added to maintain the electroneutrality of the simulation system. The MD simulation was completed by the *pmemd* module in the AMBER16 software package. The entire calculation process was divided into the following seven steps: 1) imposing a restriction force of 5.0 kcal mol^{-1} $Å^{-2}$ on the complex or the protein, and minimizing the energy of solvent molecules; 2) A restriction force of 4.0 kcal mol^{-1} $Å^{-2}$ was applied to the main chain of the complex or protein. Minimizing the energy of the solvent molecules and the complex or protein side chains; 3) optimizing the energy of the entire system without any restraint force; 4) heating the system gradually at constant volume from 0 K to target temperature (300, 330, and 370 K) over a coupling time of 100 ps; 5) performing 100 ps simulation to accommodate solvent density; 6) removing all restrictions, and then performing another 100 ps simulation on the entire system to relax the pressure; 7) producing the simulation with the target time in the trajectory generation stage. The dynamic trajectory obtained from the simulation will be used for further studies.

The cutoff distance of the non-bond was set to 10 Å, and the particle mesh Ewald (PME) method (Sagui and Darden, 1999) was used to manage the long-range electrostatic interaction. All covalent bonds including hydrogen atoms were restricted by the SHAKE algorithm (Kräutler et al., 2001), and the integration step length of the simulation process was 2 fs. The protein structures used here were based on the X-ray structure of the MyD88-TIR domain from the Protein Data Bank (PDB code: 4DOM, https://www.rcsb.org).

Virtual Screening Flow

The database containing the structural information of approximately 40,640 chemicals (https://enamine.net) was used for virtual screening, and the Glide module of Schrödinger suit

was employed (https://www.schrodinger.com). The X-ray structure of the MyD88-TIR domain was downloaded from the Protein Data Bank (PDB code: 4DOM) for docking. The Protein Preparation module was used to preprocess the protein crystal structure. In the grid preparation process, the grid center was defined by the CA atom of residue Leu252. Then, default settings were adopted for the other settings of the binding pocket. During the docking process, the ligand was allowed to be flexible, whereas the receptor was kept as a rigid structure. The SP mode of Glide was performed to explore the appropriate binding poses in the first round of screening, and 10,000 compounds with the highest scores were selected. In the second-round screening via the XP mode of Glide, approximately 600 molecules were selected. Eventually, according to the diversity of molecules and the potential interactive mode between small molecules and the MyD88-TIR domain, 20 top-ranking molecules were selected and purchased for bioactivity assay by clustering.

Chemicals and Reagents

Compounds were obtained from Enamine with a purity over 90% (**Supplementary Table S1**). We used LPS (Solarbio, Beijing, China; L8880); CCK8 assay kit (Beyotime, Shanghai, China; C0038); TNF-α and IL-6 ELISA kits (Invitrogen, Carlsbad, CA, United States); ERK (9102S), P-ERK (9101S), P38 (8690T), P-P38 (4631S), JNK (9252T), P-JNK (4668T), MyD88 (D80F5), GAPDH (2118S), rabbit IgG (7074P2), and mouse IgG (7076P2) antibodies (CST, Shanghai, China); HA antibody (Santa Cruz, CA, United States ; sc-7392); FLAG antibody (Proteintech, Wuhan, China; 20543-1-AP); Ly6G antibody (Servicebio, Wuhan, China; GB11229); F4/80 antibody (Servicebio, Wuhan, China; GB11027); and Prime Script™ RT reagent kit (Takara, Shiga, Japan; RR047A).

Preparation of the Compounds

The 20 selected compounds, including M20, were dissolved in dimethyl sulfoxide to prepare 10-mM stock solutions and then frozen at −20°C for further study. M20 had a purity of 98.14%. M20 was dissolved in 10% dimethyl sulfoxide and 90% corn oil for *in vivo* assay. The control group and the ALI group were given the same solvent (10% dimethyl sulfoxide and 90% corn oil).

Cell Culture and Treatment

The extraction and cultivation methods of mouse peritoneal primary macrophages (MPMs) were as described previously (Liu et al., 2021). HEK293T cells were purchased from American Type Culture Collection (ATCC, Manassas, VA, United States), and were cultured in DMEM (Gibco, Eggenstein, Germany) accompanied with 10% (v/v) FBS, 100 mg/ml streptomycin, and 100 U/mL penicillin G.

ELISA

After incubation with the compounds for 45 min, MPMs were then incubated with LPS (500 ng/ml). Compounds and LPS were incubated with cells in the next twenty-four hours. After that, the sample supernatants were collected and centrifuged at 24,000*g* for 10 min at 4°C. Following the manufacturer's instructions, the TNF-α and IL-6 ELISA kits were used to detect the secretion of pro-inflammatory cytokines in the supernatant.

Quantitative Real-Time PCR

Total RNA from MPMs or lung tissues was extracted by TRIzol reagent (Invitrogen, Carlsbad, CA, United States). The RNA concentration was measured at a ratio of 260/280 nm, and the samples with A260/A280 in the range of 1.8–2.0 were allowed for further study. Then, reverse transcription was carried out using the Prime Script™ RT reagent kit. Next, SYBR Green Super mix (Bio-Rad, Hercules, CA, United States) was used for amplification. The primer sequences of the genes used are shown in **Supplementary Table S2**.

Western Blot Analysis

Proteins were extracted from cells or lung tissue using lysis buffers (Boster, Wuhan, China) with pre-added protein phosphatase inhibitors (Applygen, Beijing, China) according to the manufacturer's instructions. The tissues were homogenized into small pieces before lysis so that the protein could be extracted fully in the lysis solution. After the lysis was completed, protein levels were determined by the BCA assay kit (Beyotime, Shanghai, China). Next, the prepared samples were separated by 10% SDS-PAGE and electro-transferred to polyvinylidene difluoride membranes. After this, the membranes were blocked with 10% milk (BD, Franklin Lakes, NJ, United States) and then exposed to primary antibodies at 4°C overnight. The next day, the membranes were incubated with the corresponding secondary antibody. The immune complexes were visualized by enhanced chemiluminescence reagent (Bio-Rad, Hercules, CA, United States).

Animals

Eight-week-old male C57BL/6J mice with a weight of 18–22 g were obtained from the Animal Center of Wenzhou Medical University and were given access to a chow diet and water *ad libitum*. Before the experiment, the mice were housed in a pathogen-free animal facility with the temperature maintained at 22–24°C under a 12-h light/dark cycle. All animal experiments were approved by the Wenzhou Medical College Animal Policy and Welfare Committee and were performed in accordance with the Code of Ethics of the World Medical Association.

These mice were randomly allotted to four groups: control group (n = 6); ALI group (n = 6); 20 mg/kg M20 pre-treated group (n = 6); and 40 mg/kg M20 pre-treated group (n = 6).

The mice were injected, intravenously (iv) through the tail vein, with LPS (15 mg/kg, 0.9% saline) or an equal volume of 0.9% saline. Mice were pre-administered with M20 intraperitoneally (ip) 6 h and 30 min before LPS injection. Six hours later, the mice were sacrificed. Finally, bronchoalveolar lavage fluid (BALF), blood samples and lung tissues were collected from the mice and stored in a refrigerator at −80°C.

Histological Assay

The lung tissues were fixed in 4% paraformaldehyde for paraffin embedding and histopathological analysis. These tissue specimens were sectioned to 4-μm-thick slices and they underwent hematoxylin and eosin staining (H&E detection kit) and immunohistochemistry (IHC) staining in accordance with the kit instructions. Images were obtained with a Nikon microscope.

BALF Analysis

We inserted a sterilized pipette tip into the trachea and then injected ice-cold PBS into the lungs. A 1-ml sample of BALF was obtained and centrifuged at 24,000 *g* for 15 min at 4°C. The supernatant was then taken to detect the level of inflammatory factors and the protein concentration of the lung tissue, while the lower sediment was resuspended in 30 μl PBS to determine the total number of cells in BALF (Liu et al., 2021).

Surface Plasmon Resonance Detection

A protein interaction array system (SPR Instrument, Biacore T200, GE, Connecticut, United States) was used to detect the binding between the protein and the molecule. We used 1 × PBS (5% DMSO, 0.5% Tween 20) for sample dilution and analysis. Both 0.4 M N-ethyl-N-[3-dimethylaminopropyl]-carbodiimide and 0.1 M N-hydroxysuccinimide were used to activate the CM7 protein chip. The recombinant MyD88 protein was dissolved in 10 mM sodium acetate buffer without Tris and other amino-containing compounds. The acid salt was cured to allow for the excess N-hydroxy succinimide ester to block unreacted active sites. To detect the binding between MyD88 protein and M20, the compound M20 with different concentrations (0 μM, 1.95 μM, 3.91 μM, 7.81 μM, 15.6 μM, 31.3 μM, 62.5 μM, 125 Mm, and 250 μM), were dissolved in 1 × PBS (5% DMSO, 0.5% Tween 20) buffer and passed through the sensor chip at a flow rate of 60 μl/min. The response curves of the samples with different concentrations were all displayed after subtracting the reference flow cell. The Biacore T200 instrument analysis software was used to subtract the control value and to perform the kinetic fitting mathematical model analysis.

Co-Immunoprecipitation Assay

After protein quantification, HA antibody was added and incubated with the samples at 4°C overnight. The next day, protein A+ G agarose beads were added and incubated for 4 h before collecting protein. The agarose beads were washed with PBS and then boiled in the sample buffer. The sample was used to detect FLAG epitopes of the dimerization of MyD88 and the density of immune reaction bands was analyzed using ImageJ software.

Statistical Analysis

All experiments followed the principle of randomization and blindness. Data were expressed as the mean ± standard error of mean (SEM) as indicated. Different groups were compared with Student's *t* test. Statistical analysis was performed with GraphPad Prism software (GraphPad Prism Software, San Diego, CA, United States). p values <0.05 were considered statistically significant.

RESULTS

Study of MyD88-TIR Stability

Many of the previous MyD88 inhibitors were designed based on BB-loop peptidomimetics. However, we wanted to explore potential druggable regions in MyD88-TIR domain other than the BB-loop. On the basis of previous studies and the protein itself, it is possible that we may be able to find new inhibitors of MyD88. Therefore, here we conducted an in-depth analysis of the MyD88 protein structure (PDB code: 4DOM).

Proteins are in an irregular state of motion in most organisms. They often have highly flexible regions that can directly or indirectly determine the PPIs (Yu and Huang, 2014). As for the MyD88-TIR domain, identifying its flexible region is beneficial to understand the dynamic characteristics and polymerization mode. To capture the MyD88-TIR flexible region, in MD simulations, the protein was placed at the temperatures of 300, 330, and 370 K for 50 ns each. MD simulations were performed at higher temperatures in order to reveal more information related to protein unfolding (Yu et al., 2017). As shown in **Figures 1A,B**, the BB-loop (193–204 aa), αC' (231–246 aa), and αD (262–270 aa) domains were more flexible than other regions. This indicated that the BB-loop, αC′ and αD have abnormal dynamic properties.

There has been a large amount of research on the effect of BB-loop motif on the polymerization of the TIR domain (Loiarro et al., 2005; Jiang et al., 2006; Ohnishi et al., 2009; Olson et al., 2015; Clabbers et al., 2021). Many of them have made successive efforts, but mostly focused on the realm of peptides derived from BB-loop and their derivatives. Hence, here we mainly focused on the αC′ and αD motifs. As shown in **Figure 1C**, the protein is colored by residue hydrophobicity. Motifs αC′ and αD are adjacent, and αC′ touches αD with a hydrophobic interaction. It is worth noting that αC′, αD, and βD can form a hydrophobic core here. **Figure 1C** shows that the residue Leu252 of βD further connects αC′ and αD via hydrophobic interaction. This finding is consistent with the previously reported L252P mutation (Zhan et al., 2016), which also affects the dynamic status of TIR. Combined with the standpoint reported by previous studies, it was found that L252P mutation can promote MyD88 polymerization (Ngo et al., 2011; Loiarro et al., 2013; Vyncke et al., 2016). A possible mechanism for the L252P mutation involves its effect on the αC′–βD–αD hydrophobic core.

Identification of a Potential Druggable Site

To verify the above hypothesis, long-time MD simulations were used to explore changes in the αC′–βD–αD hydrophobic core. Wild-type TIR, polymerization-inhibitable mutant K238A (Vyncke et al., 2016; Ve et al., 2017), and polymerization-promotable mutant L252P were subjected to 300 ns MD simulation. The stability of the αC′–βD–αD hydrophobic core was reflected by the changes in the distance between the CA atoms on the residue Ala240 and the CA atoms on residue Ile267 ($d_{Ala240@CA\_Ile267@CA}$) during the MD simulation (**Figure 1D**). After this calculation, we observed that the hydrophobic core was destroyed, and a hydrophobic pocket was formed when $d_{Ala240@CA\_Ile267@CA}$ was greater than 8.5 Å (**Figure 1E**). All the results of MD systems are shown in **Figure 1F**. The $d_{Ala240@CA\_Ile267@CA}$ of WT and the K238A mutant were likely to be less than 8.5 Å during the long-

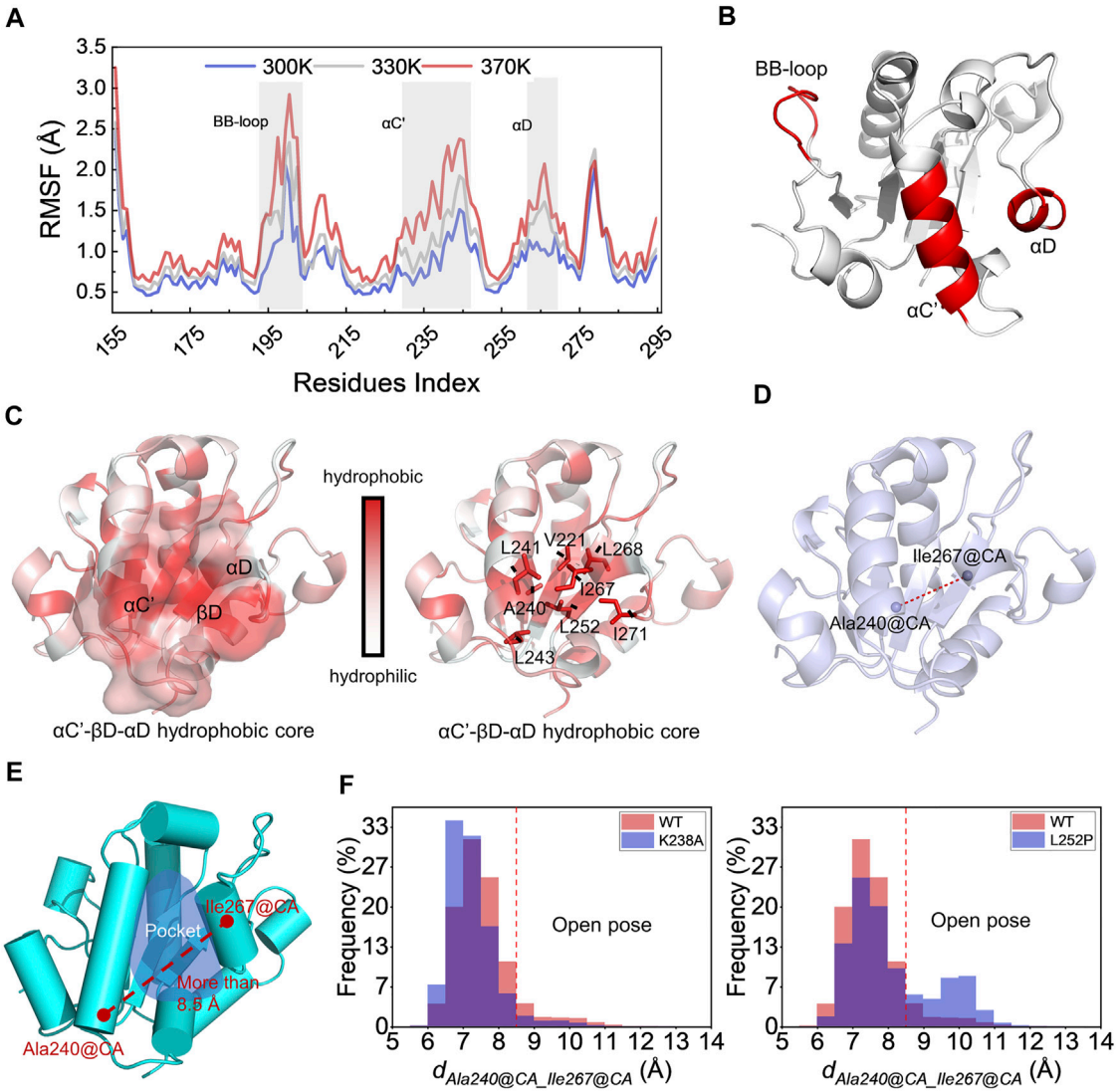

FIGURE 1 | Study of MyD88-TIR stability and identification of potential druggable site. **(A)** Root mean square fluctuations of the CA atoms for the wild-type MyD88-TIR monomer MD simulation at the temperatures of 300, 330, and 370 K. **(B)** The three-dimensional locations of BB-loop, αC′, and αD motif. **(C)** The hydrophobicity analysis, red represented hydrophobicity and white represented hydrophilicity. **(D)** Schematic diagram of the distance between Ala240@CA and Ile267@CA ($d_{Ala240@CA\_Ile267@CA}$) on the MyD88-TIR domain. **(E)** The "Open pose" which was found in MD simulation. **(F)** Statistical results of $d_{Ala240@CA\_Ile267@CA}$ changes during MD simulation.

time MD simulation. Especially for K238A, there was almost no conformation with $d_{Ala240@CA\_Ile267@CA}$ greater than 8.5 Å. In contrast, the L252P mutant had a relatively high probability of sampling conformation with $d_{Ala240@CA\_Ile267@CA}$ greater than 8.5 Å. This means that L252P could destroy the hydrophobic core, i.e., promote the separation of αC′ and αD. This preferred conformation brought about by the L252P mutation is very likely to be the polymer conformation, which we called "Open pose" here. The surface of αC′ and αD in the "Open pose" might directly participate in the MyD88-TIR aggregation.

In summary, based on the in-depth analysis of the MyD88 protein structure, we identified flexible regions other than the BB-loop and further discovered the hydrophobic core. The destruction of the hydrophobic core can form a hydrophobic pocket, which is a potential druggable site to discover inhibitors that block the polymerization of MyD88-TIR domain. Next, we carried out the following virtual screening.

Preliminary Discovery of a Small Molecular Inhibitor M20, Which Targets the MyD88-TIR Domain

The employment of structure-based drug design is a distinctive approach in discovering new inhibitors or drug molecules in a time-saving and cost-effective manner (Singh et al., 2021). Therefore, virtual screening was employed to sift the database

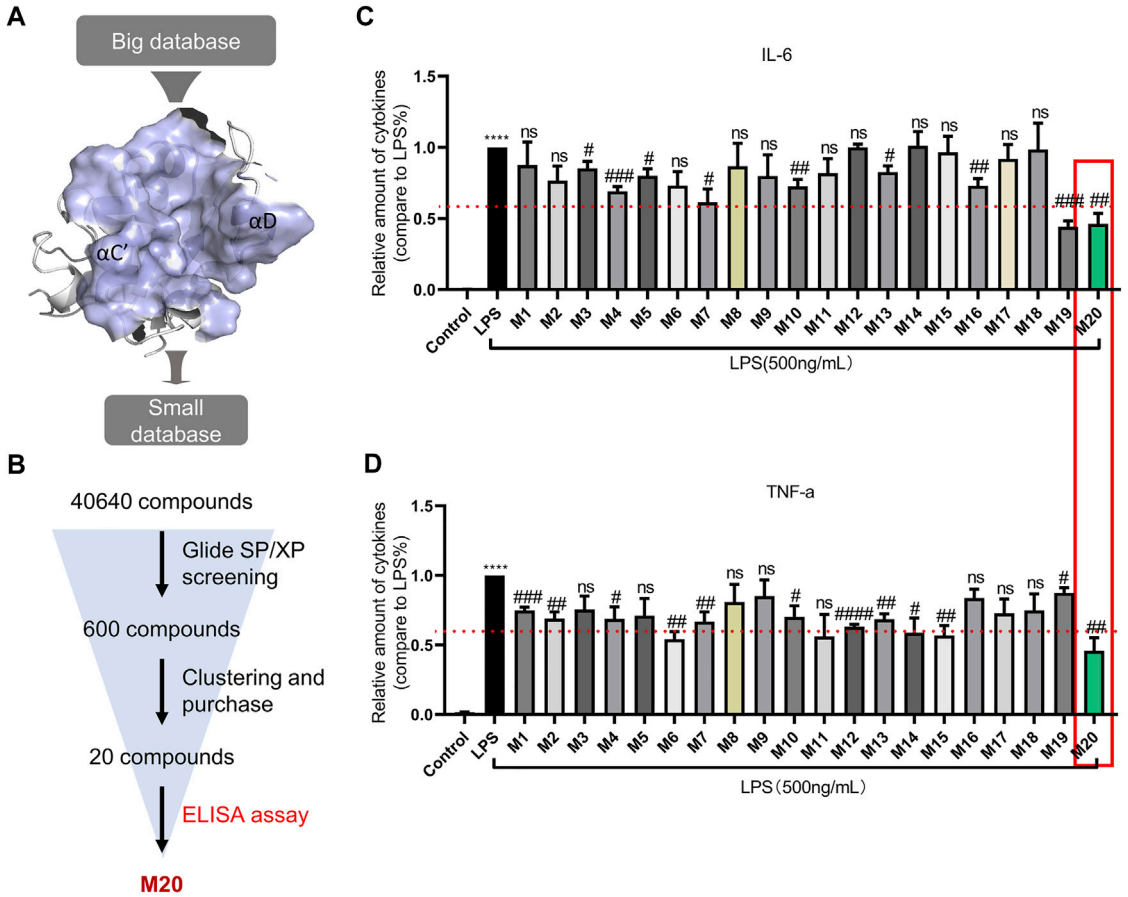

FIGURE 2 | Preliminary discovery of a small molecular inhibitor M20, which targets the MyD88-TIR domain. **(A)** The druggable pocket of "Open pose" for structure-based virtual screening. **(B)** Workflow of screening for new MyD88 inhibitors. The concentrations of IL-6 **(C)** and TNF-α **(D)** in supernatants from MPMs that were pre-treated with 10-μM dose of compounds, followed by stimulation with 500 ng/ml LPS for 24 h and were detected by ELISA. The data were expressed as the mean ± SEM as indicated. Different groups were compared with Student's *t* test. It was utilized for the statistical analysis, and significant differences were indicated as * or #. ****$p < 0.0001$ vs the control group; #$p < 0.05$, ##$p < 0.01$, ###$p < 0.005$, and ####$p < 0.0001$ vs the LPS alone group.

of 40,640 small molecules from the Enamine library and discover those potentially inhibiting MyD88-TIR homodimerization. As shown in **Figure 2A**, the "Open pose" was used for structure-based virtual screening. After docking via the Glide SP/XP methods, 600 binding poses of compounds were produced with MyD88-TIR domain. All the compounds with a docking score greater than the cutoff score of −5 kcal/mol were selected for scaffold clustering through the Canvas module.

Twenty top-ranking molecules, each of a different scaffold, were selected for purchase and assay (**Supplementary Table S1**; **Figure 2A,B**). Compounds that exhibited pro-inflammatory cytokine inhibition rate greater than 40% at 10 μM were selected for further biological activity assay. In this round of screening, the compound M20 stood out with approximately 50% inhibition rates both for TNF-α and IL-6, whereas M4, M7, M10, M13, and M19 failed to achieve more effective inhibition rates on the two indexes (**Figure 2C,D**).

Thus, M20 was selected as a compound with great potential for further biological activity evaluation. To provide a potential treatment for MyD88-driven inflammation, we conducted a deeper activity study on pyrazolo[3,4-b] pyridine analog M20. The chemical structure of M20 is shown in **Figure 3A**.

M20 Is a Potent Compound that Inhibits LPS-Induced Inflammation in Vitro

Previous studies have confirmed that LPS mainly activates the Toll-like receptor 4 (TLR4) signaling pathway (Lim and Staudt, 2013; Chen et al., 2020). Then, the intracellular TIR domain recruits MyD88, induces a signal cascade, promotes inflammation, and produces pro-inflammatory cytokines such as TNF-α, IL-6, and IL-1β. To avoid toxic effects, we first evaluated the effect of the candidate compound M20 on cell survival rates. The CCK-8 assay results showed that the survival rate of M20– pre-treated MPMs under 20 μM concentration was greater than 80%, which indicated the low toxicity of the compound (**Figure 3B**).

As the secretion of pro-inflammatory cytokines is the most intuitive indicator of inflammation, ELISA assay was first carried out to evaluate the function of M20 in LPS-induced MPMs. As shown in **Figures 3C,D**, the M20–pre-treated group showed the

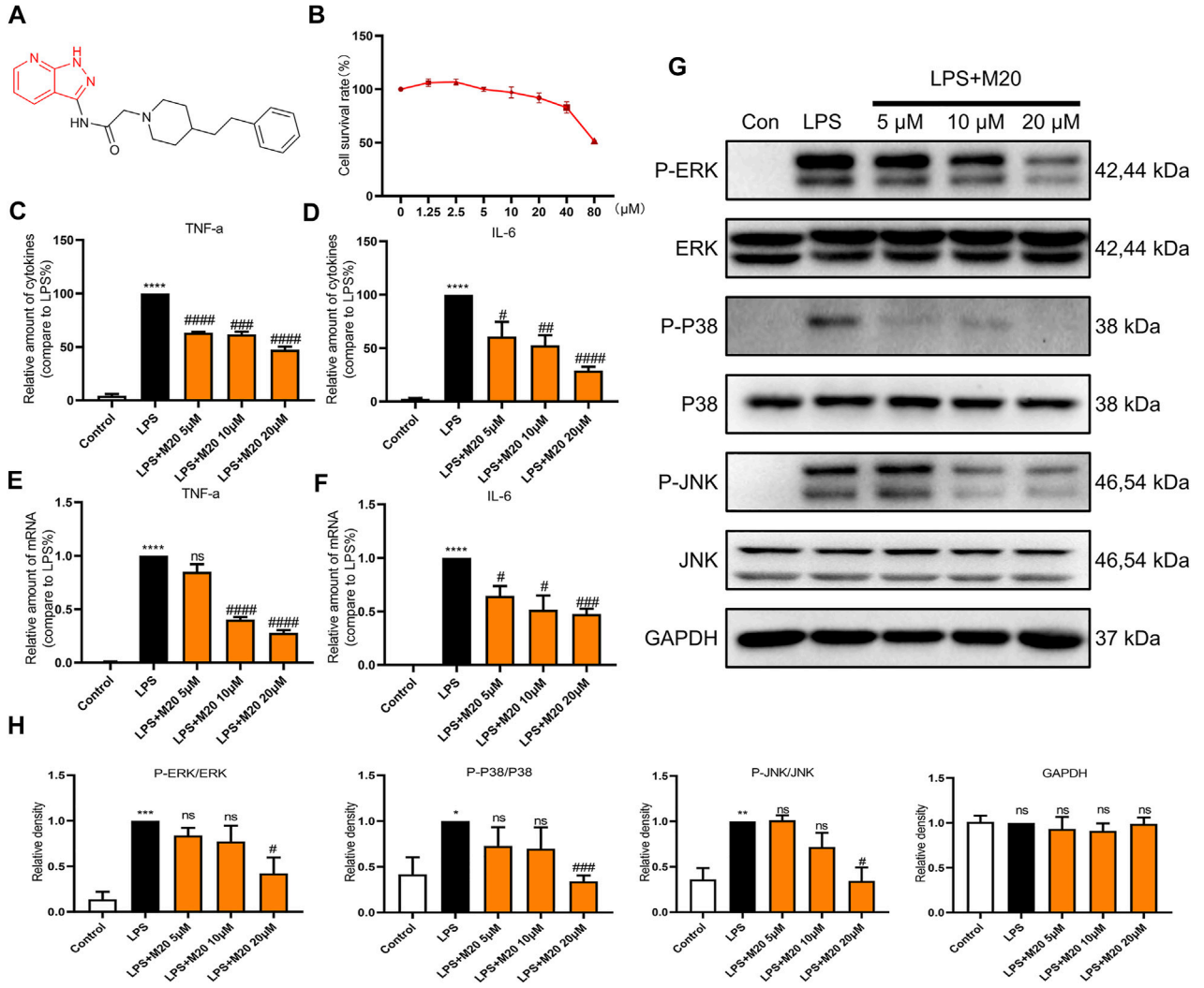

FIGURE 3 | M20 is a potent compound that inhibits LPS-induced inflammation *in vitro*. **(A)** The structure of M20. **(B)** The cell survival rates of M20 (1.25, 2.5, 5, 10, 20, 40, and 80 μM) in MPMs. The concentrations of TNF-α **(C)** and IL-6 **(D)** in supernatants from MPMs that were measured by ELISA. The TNF-α **(E)** and IL-6 **(F)** mRNA levels of MPMs that were determined by RT-qPCR. **(G)** The protein levels of the P-ERK, P-P38 and P-JNK that were detected by western blot. **(H)** Densitometric quantification was presented as the mean ± SEM ($n = 3$) in the lower panel. Data were expressed as the mean ± SEM as indicated. Different groups were compared with Student's *t* test. It was utilized for the statistical analysis, and significant differences were indicated as * or #. ****$p < 0.0001$ vs the control group; #$p < 0.05$, ##$p < 0.01$, ###$p < 0.005$, and ####$p < 0.0001$ vs the LPS alone group.

prominent inhibition of TNF-α and IL-6, two classical pro-inflammatory cytokines observed in the inflammatory response. The corresponding changes in mRNA levels of TNF-α and IL-6 were also seen during the LPS stimulation periods (**Figure 3E–F**). M20 downregulated the expression levels of the two inflammatory factors in a dose-dependent manner. At 20 μM, it exhibited favorable inhibition capability (TNF-α > 70%, IL-6 > 50%).

In addition, in order to better comprehend whether M20 would affect signal transduction under LPS stimulation, we further examined its performance in the phosphorylation of key proteins (ERK, P38, and JNK) in the MAPK signaling pathway since MyD88 is upstream of the classical inflammation pathway MAPK. Treatment of LPS-induced MPMs with M20 for 1 h resulted in a dose-dependent inhibition of ERK phosphorylation (**Figures 3G,H**), while the total amount of the target protein remained unchanged. The same decreasing trends were also observed in the phosphorylation levels of P38 and JNK (**Figures 3G,H**).

Collectively, these findings support the conclusion that M20 is a potent compound that can significantly mitigate LPS-induced inflammation *in vitro*.

M20 Alleviates Sepsis-Induced ALI in Vivo

To better evaluate the anti-inflammatory activity of M20 *in vivo*, we used the sepsis-induced ALI mice model to investigate the therapeutic capability of it. When ALI occurs, type II alveolar epithelial cells are extensively damaged, leading to decreased synthesis and activity of alveolar surfactant. These changes

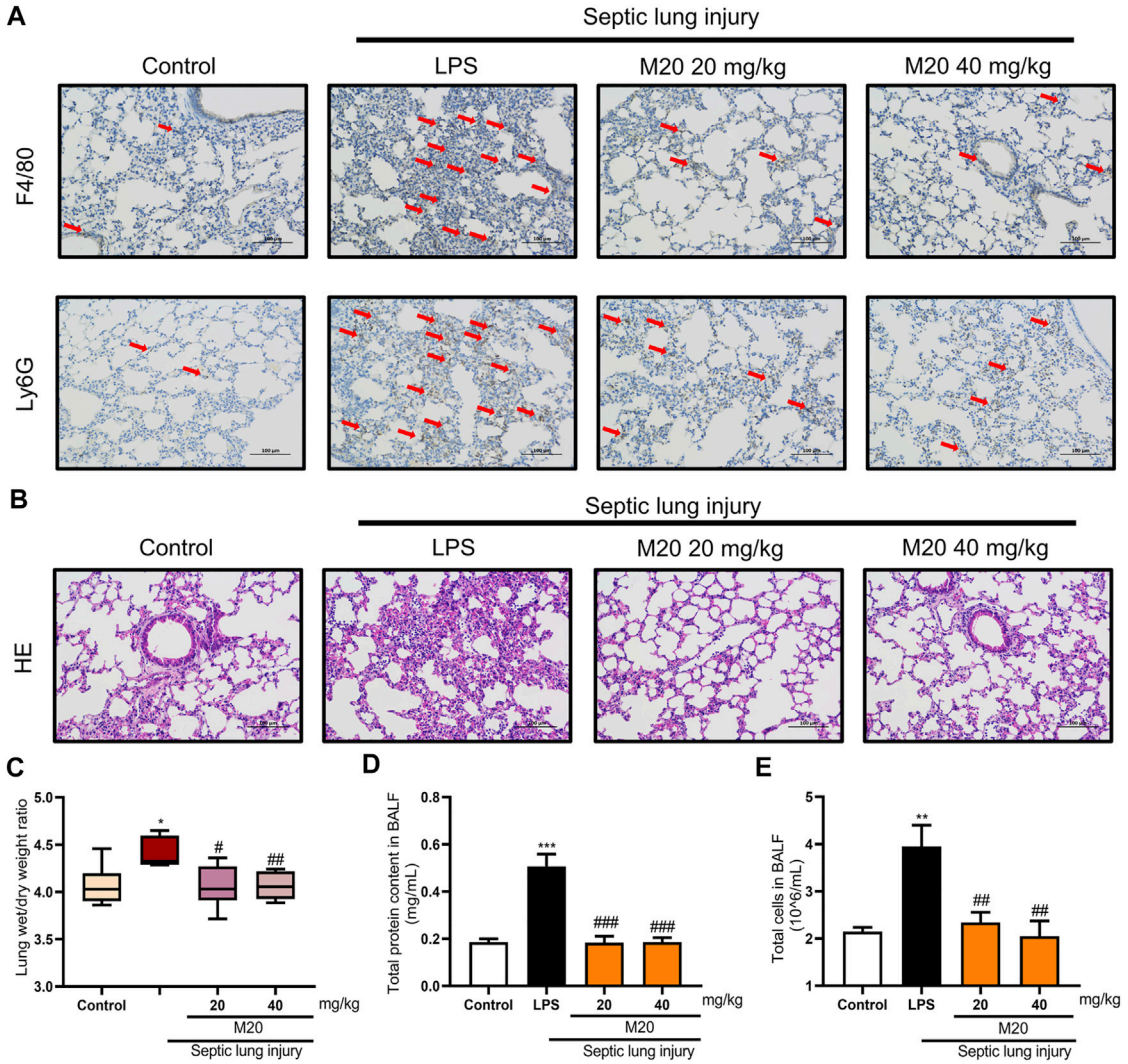

FIGURE 4 | M20 alleviates sepsis-induced ALI *in vivo*. **(A)** IHC staining was used to observe the distribution of neutrophil positive spots. **(B)** H&E staining was used to observe histopathological changes. The lung wet/dry weight ratio **(C)** and total protein content in BALF **(D)** were measured to evaluate pulmonary edema. **(E)** The total cells in BALF were measured to evaluate inflammatory infiltration. The data were presented as the mean ± SEM ($n = 6$). Different groups were compared with Student's *t* test. It was utilized for the statistical analysis, and significant differences were indicated as * or #. ****$p < 0.0001$ vs the control group; #$p < 0.05$, ##$p < 0.01$, ###$p < 0.005$, and ####$p < 0.0001$ vs the Septic lung injury alone group.

result in damage to the respiratory membrane, followed by alveolar collapse and pulmonary edema (Yao et al., 2017). Pathological analysis was first carried out to characterize the pathohistological appearance of the lung, which is considered one of the important phenotypes of the ALI pattern. As shown in **Figures 4A,B**, LPS alone led to obvious destruction of the alveolar structure and induced appearance of emphysema in connective tissue. However, when M20 was applied, the signs of lung injury were significantly alleviated (**Figure 4A,B**). To assess neutrophil infiltration, we detected Ly6G and F4/80—two classic neutrophils. Neutrophils, observed as brown dots in the lung interstitial area, increased significantly in ALI mice; however, this increase was markedly mitigated by the pre-treatment with M20 (**Figure 4A**).

Pulmonary edema is another vital indicator of ALI, which can be measured by the wet/dry ratio of the lung tissues. As shown in **Figures 4C,D**, the wet/dry ratio of the lung tissues in the ALI group was increased, and it was accompanied by a significant increase in BALF protein content as well. In contrast, M20 treatment reversed the pulmonary edema. Next, we further measured the protein concentration in the alveolar lavage; it was found that the M20–pre-treated group effectively reduced the damage to the pulmonary microvascular barrier (**Figure 4E**).

Additionally, while detecting the pro-inflammatory cytokines of lung tissue homogenate supernatant, serum, and alveolar lavage fluid, we found that when challenged with a high dose of LPS, the levels of pro-inflammatory cytokines were elevated in ALI mice (**Figures 5A–F**). Moreover, the levels of the two inflammatory

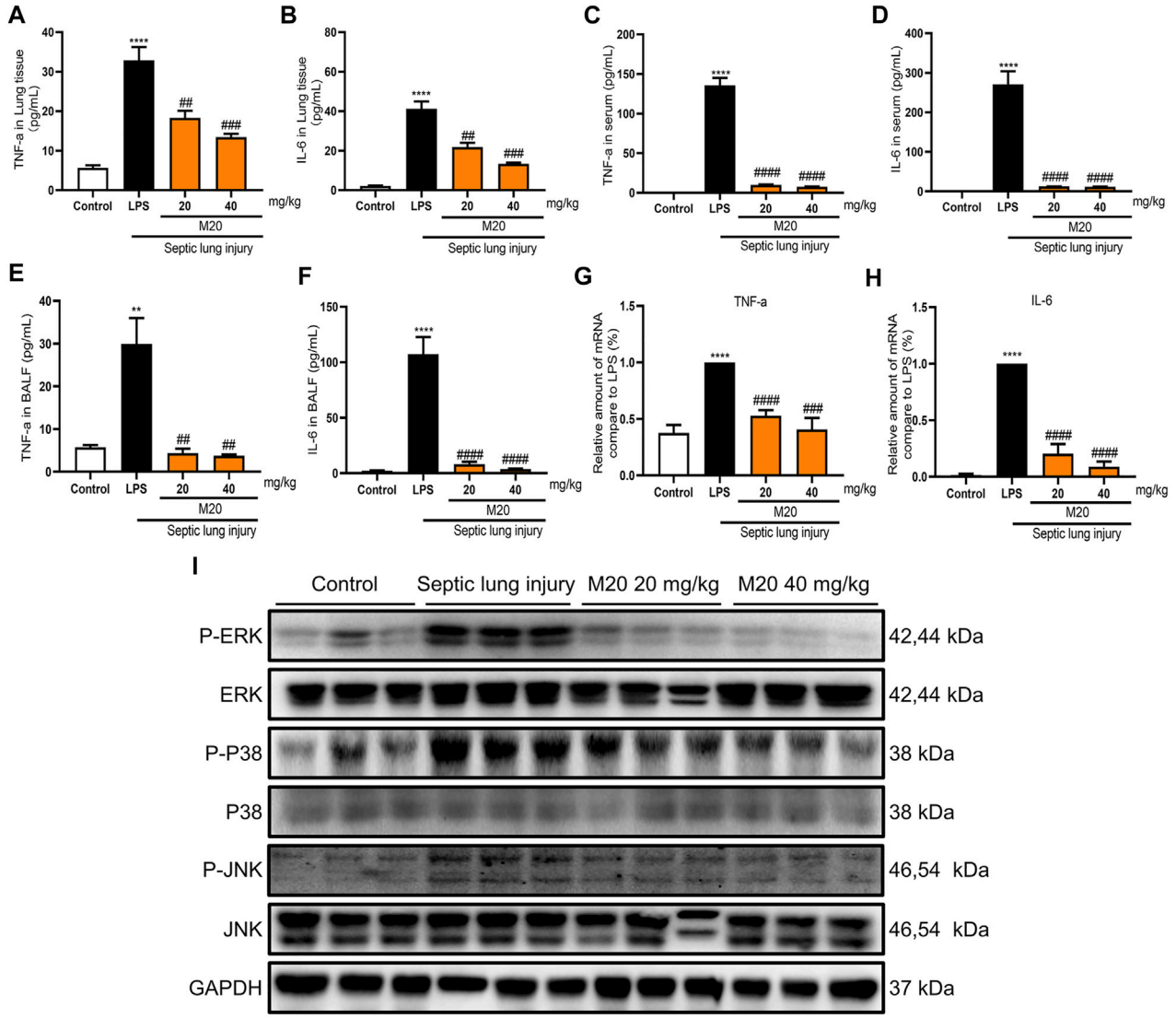

FIGURE 5 | M20 alleviates sepsis-induced ALI *in vivo*. The release levels of TNF-α **(A)** and IL-6 **(B)** in lung tissues were measured by ELISA ($n = 6$). The release levels of TNF-α **(C)** and IL-6 **(D)** in serum were measured by ELISA ($n = 6$). The release levels of TNF-α **(E)** and IL-6 **(F)** in BALF were measured by ELISA($n = 6$). The mRNA levels of TNF-α **(G)** and IL-6 **(H)** in lung tissues were measured by RT-qPCR ($n = 6$). **(I)** The protein levels of the P-ERK, P-P38 and P-JNK in lung tissues that were detected by western blot. The data were expressed as the mean ± SEM as indicated. Different groups were compared with Student's *t* test. It was utilized for the statistical analysis, and significant differences were indicated as * or #. ****$p < 0.0001$ vs the control group; #$p < 0.05$, ##$p < 0.01$, ###$p < 0.005$, and ####$p < 0.0001$ vs the Septic lung injury alone group.

factors in the ALI–alone group were higher than those in the control group, which demonstrated the success of our modeling. What motivated us most was that the M20–pre-treated group successfully inhibited the release of pro-inflammatory cytokines with more than 90% inhibition rates when compared with the ALI-alone group (**Figures 5C,D**). Subsequently, we produced further evidence that this compound significantly reversed inflammation in the lungs of ALI mice by measuring the levels of activated ERK, P38, and JNK protein. The western blot results showed that 6 h of sepsis promoted the MAPK signaling pathway activation; however, the M20–pre-treated group showed a dose-dependent mitigation effect (**Figure 5I**). To further investigate the anti-inflammatory effect of M20, we detected the level of inflammatory gene fluctuations from the mice lungs. Compared with the ALI model group, the gene expression levels of TNF-α and IL-6 in the M20–pre-treated group were reduced in a dose-dependent manner (**Figures 5G,H**). ALI can cause peripheral neutrophils, macrophages, and other immune cells to infiltrate and accumulate in lung tissues, whereas M20 significantly improves acute pulmonary edema and the secretion of inflammatory factors, eventually preventing the trigger of the "inflammation waterfall" cascade effect.

In summary, all of the above results further provide us with strong evidence that M20 is a promising candidate with a novel chemical scaffold in pre-treatment of ALI and potentially other

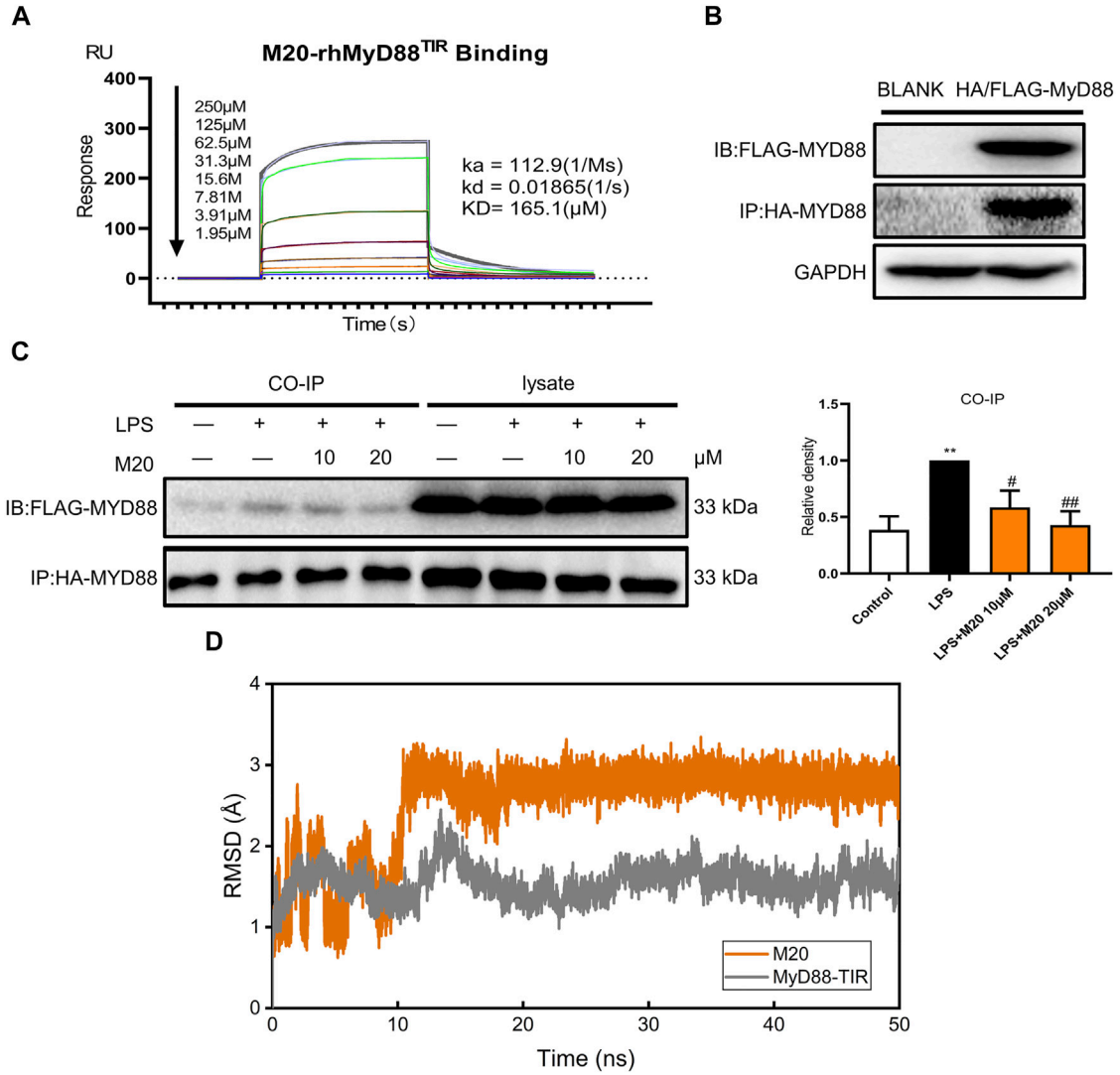

FIGURE 6 | Explore the binding mode of M20 and MyD88. **(A)** SPR shows direct interactions between M20 and MyD88 in a concentration-dependent manner. **(B)** The transfection efficacy of HEK293T cells that were cotransfected with HA-MyD88 and FLAG-MyD88 for 24 h. **(C)** The effect of M20 in inhibiting MyD88 dimerization. Densitometric quantification was presented as the mean ± SEM (n = 3) in the right panel. **(D)** Root mean square deviation of the CA atoms in MyD88-TIR domain (gray) and heavy atoms in M20 (orange). The data were expressed as the mean ± SEM as indicated. Different groups were compared with Student's t test. It was utilized for the statistical analysis, and significant differences were indicated as * or #. $^{****}p < 0.0001$ vs the control group; $^{\#}p < 0.05$, $^{\#\#}p < 0.01$, $^{\#\#\#}p < 0.005$, and $^{\#\#\#\#}p < 0.0001$ vs the LPS alone group.

inflammatory injuries. Next, we explored the stability of the MyD88/M20 complex and the potential binding mode.

Explore the Binding Mode of M20 and MyD88

Previous studies have proven that M20 is a bioactive molecule with great potential, but it remains unknown whether M20 could inhibit MyD88 homodimerization and thereby inhibit inflammation. Whether M20 could truly conform to the initial concept of previous modeling and screening predictions, instead of merely exhibiting anti-inflammatory activity, was still remains a mystery. Thus, SPR was used to further investigate the binding of M20 with MyD88. As we can see, M20 showed a relatively optimal binding affinity toward the MyD88 protein in a dose-dependent manner (K_D = 165.1 μM, **Figure 6A**). To better confirm that the immunomodulatory function of M20 attributed to the inhibition of MyD88 homodimerization, co-immunoprecipitation was used to study the interactions of tag-proteins *in vitro*. Two plasmids encoding HA-MyD88 and FLAG-MyD88 were co-transfected into HEK-293T cells using Liposome 3,000. Western blotting showed that FLAG-MyD88 and HA-MyD88 were effectively co-expressed in HEK293T cells after 24 h (**Figure 6B**). Then, the transfected cells were incubated with the compound M20 for 1 h. Western blot analysis was performed 15 min after LPS induction. The results showed that M20 inhibited the formation of the MyD88-TIR domain homodimer (**Figure 6C**).

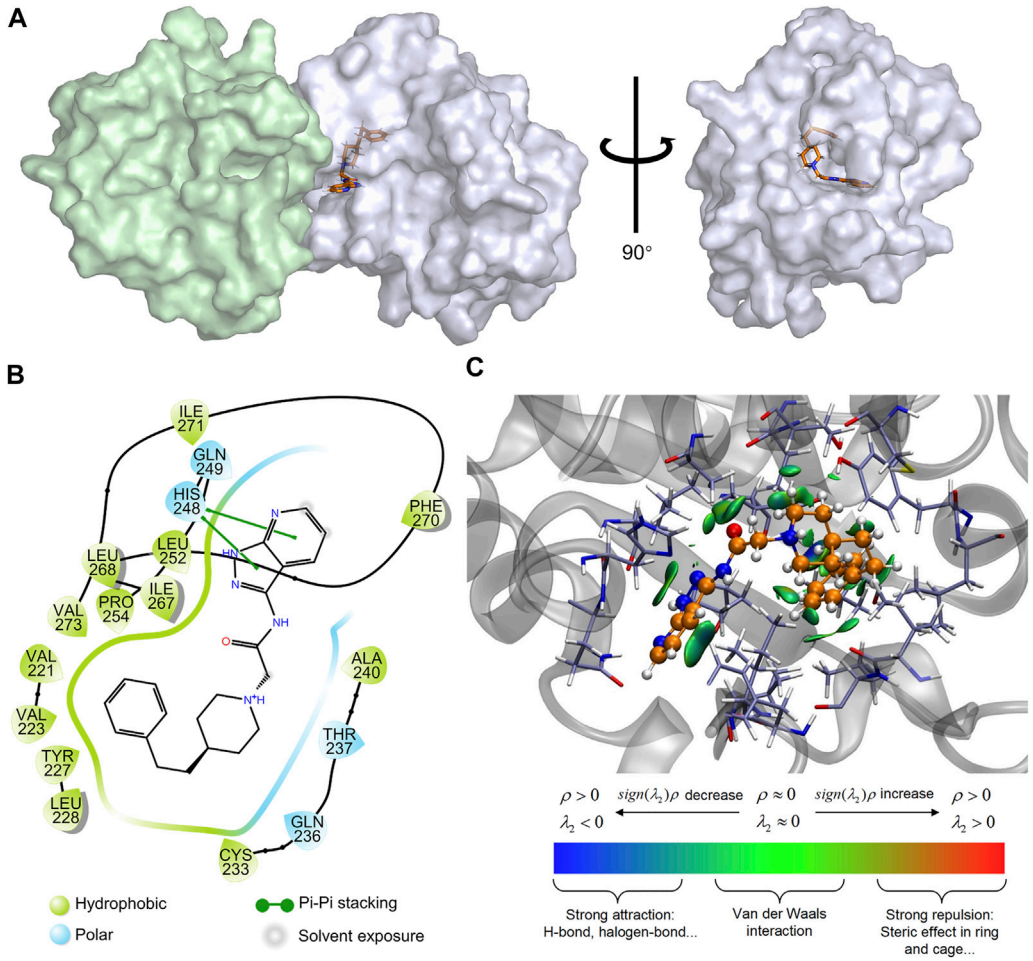

FIGURE 7 | Prediction of the binding mechanism of M20 and MyD88. **(A)** The prediction of the binding mode of M20 with MyD88. M20 was depicted as orange licorice, the left region of MyD88 oligomer was colored in palegreen and the right region was colored in bluewhite. **(B)** The 2D-binding mode of M20 with MyD88-TIR domain. **(C)** The 3D-binding mode of M20 with MyD88-TIR domain with the isosurfaces of IGM and colorbar. M20 was colored in orange, and the surrounding residues of the binding pockets were colored in iceblue. The backbone of the receptor was depicted as a gray cartoon.

Once the binary complex of M20 and MyD88 is formed, it interferes with the recruitment of IRAK2/IRAK4 (Sun et al., 2016) into the active site of MyD88, thereby resulting in the inability to activate the MAPK signaling pathway.

Additionally, to further investigate the binding mode of M20 with the MyD88-TIR domain, a 50 ns MD simulation under 300 K was carried out, and the docking outputs were adopted as the initial structure in this calculation. The RMSD plot of heavy atoms in M20 experienced fluctuation initially until 10 ns and then stabilized (**Figure 6D**). In addition, considering the stable RMSD fluctuation in the last 40 ns of the simulation, the last snapshot of the simulation trajectory was chosen as the binding mode of M20 with the MyD88-TIR domain. The pocket diagrams of M20 and MyD88 help in predicting the state of M20 in the protein, which lies in a suitable position in the large hydrophobic binding pocket formed by αC′–βD–αD (**Figure 7A**). The 2D-demonstrated binding mode (**Figure 7B**) showed a wide hydrophobic interaction surrounding M20 with some polar interactions. For visualization of the structure and its interactions, we conducted an Independent Gradient Model (IGM) analysis (Lefebvre et al., 2017) by Multiwfn (Lu and Chen, 2012) and 3D-visualized the isosurfaces and structure by VMD (Humphrey et al., 1996). The δg^{inter} isosurfaces (**Figure 7C**) exhibited that the main interaction of M20 with the MyD88-TIR domain is van der Waals interactions that occurred without strong repulsions between our compound and residues.

Apparently, the van der Waals interactions around M20 make it stably bind to the MyD88-TIR domain. With a relatively small structure, M20 can be flexibly embedded into the hydrophobic pocket, thereby changing the protein morphology and promoting MyD88 into a low-activity state. Eventually, the compound occupied most of the surface of αC′ and αD on the "Open pose" and finally achieved the purpose of inhibiting homodimerization. These results above indicated that the preferred compound, M20, could stably bind to the target protein MyD88 and owns the capability of inhibiting protein self-aggregation. At the same time, the good bioactivity of M20 demonstrated that the MyD88-targeted drug design ideas based on virtual screening to exploit more novel MyD88 inhibitors are advisable and favorable.

DISCUSSION

ALI is a severe clinical syndrome, and its common manifestation is diffuse pulmonary edema. Usually, it is characterized by an overwhelming inflammatory response leading to excessive damage of the alveolar epithelium. Among various causes of ALI, the most common is septic pneumonia caused by LPS. In LPS-induced TLR4 signaling pathway, MyD88 is a typical partner and plays an adaptor protein role in regulating the inflammatory response (Chen et al., 2020). The concept of combating with the TLR and interleukin receptor signaling, demonstrates that MyD88 inhibitors may have enormous potential in the treatment of acute and chronic respiratory diseases (Di Padova et al., 2018). Therefore, developing new types of MyD88 inhibitors is particularly significant for the treatment of ALI.

In recent years, researches on MyD88 inhibitors have mostly focused on the BB-loop, whereas from the surface of αC′ and αD in the "Open pose", we discovered a druggable pocket based on these abnormal dynamic properties as well. Currently, studies have shown the standpoint that L252P mutation could promote the polymerization of MyD88 (Ngo et al., 2011; Loiarro et al., 2013; Vyncke et al., 2016; O'Carroll et al., 2018). It was noticed that this mutation is exactly located in the hydrophobic core of αC′–βD–αD screening pocket. Therefore, a mechanism of L252P mutation may have a significant impact on the αC′–βD–αD hydrophobic core discovered in this study. Additionally, it is the first time that this reliable and valid druggable pocket has been discovered and reported, which could be further employed in discovering inhibitors that block the polymerization of MyD88-TIR domain.

After flexibility exploration of the target protein MyD88, pocket detection, inhibitor screening, and multiple rounds of *in vivo* and *in vitro* activity tests, M20 stood out as a potential candidate to combat inflammatory diseases. M20, a novel MyD88 inhibitor with a pyrazolo [3,4-b] pyridine skeleton, which is totally different from previously reported inhibitors, such as peptidomimetic and its modified compounds. As a new type of MyD88 inhibitor, it broadens the structure developmental platform of MyD88 inhibitors. Computational chemistry, SPR, and co-immunoprecipitation assay have all demonstrated the crucial role of M20 in the inhibition of MyD88 homodimerization. Meanwhile, the release of the IL-6 inhibition rates of M20 in serum and BALF were more than 90% respectively, proving that it has great potential in combating with further MyD88-related diseases. In general, our work provides a lead compound for MyD88 inhibitors as well as a valuable novel drug candidate for LPS-stimulated inflammatory response, such as acute lung injury.

Moreover, the favorable compound shares a new pyrazolo [3,4-b] pyridine skeleton, which could be adopted as a lead compound for further chemical optimization. In the same batch of compounds, the five heterocyclic chain amide compounds M4, M7, M10, M13, and M19 also showed suitable anti-inflammatory effects. Compared with the core structure of M20, we speculate that the next step of structural modification of these candidates requires the introduction of larger heterocycles to enhance their biological activity. Overall, our data represent valuable progress in the development of MyD88 targeted drug candidates, which reveals the significant advancement in promoting the development and modification of more novel MyD88 inhibitors. Furthermore, considering that the co-crystallization structure of MyD88 and M20 has not yet been revealed, we conjecture that the preferred lead compound M20 will bind to the target protein in a more diverse form. Further studies on structural optimization and biological activities of the inhibitor are underway in our laboratory. We are committed to exploring this mechanism in more depth and will plan to report future findings.

High Lights

1. A brand-new virtual screening pocket was discovered for the first time via the exploration of αC′ and αD flexible regions, and was successfully applied.
2. Computational chemistry, SPR, and co-immunoprecipitation verified that the best hit M20 could interact with MyD88 directly and inhibited the homodimerization.
3. M20 exhibited significant anti-inflammatory activities in LPS-induced responses, especially in ALI mice model mediated by sepsis.
4. The discovery of a new skeleton, pyrazolo [3,4-b] pyridine, revealed the significant implications in the development and transformation for MyD88 inhibitors.

DATA AVAILABILITY STATEMENT

The datasets used and analyzed during the current study are available from the corresponding author on reasonable request.

ETHICS STATEMENT

The animal study was reviewed and approved by the Wenzhou Medical College Animal Policy and Welfare Committee. School of Pharmaceutical Sciences, Wenzhou Medical University.

AUTHOR CONTRIBUTIONS

JS, DC, and YC designed the research. JS and DC performed the research. JS, DC, and YP wrote the paper. XS, QL, XL, and XX contributed to data collection and analysis. YC and GC reviewed and modified the paper.

FUNDING

This work was supported by the National Natural Science Foundation of China (21877085, 81473242, 82073705).

SUPPLEMENTARY MATERIAL

The Supplementary Material for this article can be found online at: https://www.frontiersin.org/articles/10.3389/fphar.2021.775117/full#supplementary-material

REFERENCES

Chen, L., Chen, H., Chen, P., Zhang, W., Wu, C., Sun, C., et al. (2019). Development of 2-Amino-4-Phenylthiazole Analogues to Disrupt Myeloid Differentiation Factor 88 and Prevent Inflammatory Responses in Acute Lung Injury. *Eur. J. Med. Chem.* 161, 22–38. doi:10.1016/j.ejmech.2018.09.068

Chen, L., Zheng, L., Chen, P., and Liang, G. (2020). Myeloid Differentiation Primary Response Protein 88 (MyD88): The Central Hub of TLR/IL-1R Signaling. *J. Med. Chem.* 63 (22), 13316–13329. doi:10.1021/acs.jmedchem.0c00884

Clabbers, M. T. B., Holmes, S., Muusse, T. W., Vajjhala, P. R., Thygesen, S. J., Malde, A. K., et al. (2021). MyD88 TIR Domain Higher-Order Assembly Interactions Revealed by Microcrystal Electron Diffraction and Serial Femtosecond Crystallography. *Nat. Commun.* 12 (1), 2578. doi:10.1038/s41467-021-22590-6

Di Padova, F., Quesniaux, V. F. J., and Ryffel, B. (2018). MyD88 as a Therapeutic Target for Inflammatory Lung Diseases. *Expert Opin. Ther. Targets* 22 (5), 401–408. doi:10.1080/14728222.2018.1464139

Dickson, K., and Lehmann, C. (2019). Inflammatory Response to Different Toxins in Experimental Sepsis Models. *Int. J. Mol. Sci.* 20 (18). doi:10.3390/ijms20184341

Ding, Z., Zhong, R., Xia, T., Yang, Y., Xing, N., Wang, W., et al. (2020). Advances in Research into the Mechanisms of Chinese Materia Medica against Acute Lung Injury. *Biomed. Pharmacother.* 122, 109706. doi:10.1016/j.biopha.2019.109706

Drayman, N., DeMarco, J. K., Jones, K. A., Azizi, S. A., Froggatt, H. M., Tan, K., et al. (2021). Masitinib Is a Broad Coronavirus 3CL Inhibitor that Blocks Replication of SARS-CoV-2. *Science* 373 (6557), 931–936. doi:10.1126/science.abg5827

Fantò, N., Gallo, G., Ciacci, A., Semproni, M., Vignola, D., Quaglia, M., et al. (2008). Design, Synthesis, and *In Vitro* Activity of Peptidomimetic Inhibitors of Myeloid Differentiation Factor 88. *J. Med. Chem.* 51 (5), 1189–1202. doi:10.1021/jm070723u

Humphrey, W., Dalke, A., and Schulten, K. (1996). VMD: Visual Molecular Dynamics. *J. Mol. Graph* 14, 33–38. doi:10.1016/0263-7855(96)00018-5

Jiang, Z., Georgel, P., Li, C., Choe, J., Crozat, K., Rutschmann, S., et al. (2006). Details of Toll-like Receptor:adapter Interaction Revealed by Germ-Line Mutagenesis. *Proc. Natl. Acad. Sci. U S A.* 103 (29), 10961–10966. doi:10.1073/pnas.0603804103

Kräutler, V., Van Gunsteren, W. F., and Hünenberger, P. H. (2001). A Fast SHAKE Algorithm to Solve Distance Constraint Equations for Small Molecules in Molecular Dynamics Simulations. *J. Comput. Chemco* 22 (5), 501–508. doi:10.1002/1096-987X(20010415)22:5<501:AID-JCC1021>3.0

Kumar, V. (2020). Pulmonary Innate Immune Response Determines the Outcome of Inflammation during Pneumonia and Sepsis-Associated Acute Lung Injury. *Front. Immunol.* 11, 1722. doi:10.3389/fimmu.2020.01722

Lefebvre, C., Rubez, G., Khartabil, H., Boisson, J. C., Contreras-García, J., and Hénon, E. (2017). Accurately Extracting the Signature of Intermolecular Interactions Present in the NCI Plot of the Reduced Density Gradient versus Electron Density. *Phys. Chem. Chem. Phys.* 19 (27), 17928–17936. doi:10.1039/C7CP02110K

Lim, K. H., and Staudt, L. M. (2013). Toll-like Receptor Signaling. *Cold Spring Harb Perspect. Biol.* 5 (1), a011247. doi:10.1101/cshperspect.a011247

Liu, J. H., He, L., Zou, Z. M., Ding, Z. C., Zhang, X., Wang, H., et al. (2018). A Novel Inhibitor of Homodimerization Targeting MyD88 Ameliorates Renal Interstitial Fibrosis by Counteracting TGF-B1-Induced EMT *In Vivo* and *In Vitro*. *Kidney Blood Press. Res.* 43 (5), 1677–1687. doi:10.1159/000494745

Liu, Q., Yan, H., Zheng, X., Fu, L., Bao, Y., Zheng, H., et al. (2021). A Novel Indazole Derivative, Compound Cyy-272, Attenuates LPS-Induced Acute Lung Injury by Inhibiting JNK Phosphorylation. *Toxicol. Appl. Pharmacol.* 428, 115648. doi:10.1016/j.taap.2021.115648

Loiarro, M., Sette, C., Gallo, G., Ciacci, A., Fantò, N., Mastroianni, D., et al. (2005). Peptide-mediated Interference of TIR Domain Dimerization in MyD88 Inhibits Interleukin-1-dependent Activation of NF-{kappa}B. *J. Biol. Chem.* 280 (16), 15809–15814. doi:10.1074/jbc.C400613200

Loiarro, M., Volpe, E., Ruggiero, V., Gallo, G., Furlan, R., Maiorino, C., et al. (2013). Mutational Analysis Identifies Residues Crucial for Homodimerization of Myeloid Differentiation Factor 88 (MyD88) and for its Function in Immune Cells. *J. Biol. Chem.* 288 (42), 30210–30222. doi:10.1074/jbc.M113.490946

Lu, T., and Chen, F. (2012). Multiwfn: a Multifunctional Wavefunction Analyzer. *J. Comput. Chem.* 33 (5), 580–592. doi:10.1002/jcc.22885

Maier, J. A., Martinez, C., Kasavajhala, K., Wickstrom, L., Hauser, K. E., and Simmerling, C. (2015). ff14SB: Improving the Accuracy of Protein Side Chain and Backbone Parameters from ff99SB. *J. Chem. Theor. Comput* 11 (8), 3696–3713. doi:10.1021/acs.jctc.5b00255

Ngo, V. N., Young, R. M., Schmitz, R., Jhavar, S., Xiao, W., Lim, K. H., et al. (2011). Oncogenically Active MYD88 Mutations in Human Lymphoma. *Nature* 470 (7332), 115–119. doi:10.1038/nature09671

O'Carroll, A., Chauvin, B., Brown, J. W. P., Meagher, A., Coyle, J., Schill, J., et al. (2018). Pathological Mutations Differentially Affect the Self-Assembly and Polymerisation of the Innate Immune System Signalling Adaptor Molecule MyD88. *BMC Biol.* 16 (1), 149. doi:10.1186/s12915-018-0611-7

Ohnishi, H., Tochio, H., Kato, Z., Orii, K. E., Li, A., Kimura, T., et al. (2009). Structural Basis for the Multiple Interactions of the MyD88 TIR Domain in TLR4 Signaling. *Proc. Natl. Acad. Sci. U S A.* 106 (25), 10260–10265. doi:10.1073/pnas.0812956106

Olson, M. A., Lee, M. S., Kissner, T. L., Alam, S., Waugh, D. S., and Saikh, K. U. (2015). Discovery of Small Molecule Inhibitors of MyD88-dependent Signaling Pathways Using a Computational Screen. *Sci. Rep.* 5 (1), 14246. doi:10.1038/srep14246

Sagui, C., and Darden, T. A. (1999). MOLECULAR DYNAMICS SIMULATIONS of BIOMOLECULES: Long-Range Electrostatic Effects. *Annu. Rev. Biophys. Biomol. Struct.* 28 (1), 155–179. doi:10.1146/annurev.biophys.28.1.155

Salomon-Ferrer, R., Case, D. A., and Walker, R. C. (2013). An Overview of the Amber Biomolecular Simulation Package. *Wires Comput. Mol. Sci.* 3 (2), 198–210. doi:10.1002/wcms.1121

Singh, A., Kumar, A., Kumar, P., Nayak, N., Bhardwaj, T., Giri, R., et al. (2021). A Novel Inhibitor L755507 Efficiently Blocks C-Myc-MAX Heterodimerization and Induces Apoptosis in Cancer Cells. *J. Biol. Chem.* 297 (1), 100903. doi:10.1016/j.jbc.2021.100903

Sun, J., Li, N., Oh, K. S., Dutta, B., Vayttaden, S. J., Lin, B., et al. (2016). Comprehensive RNAi-Based Screening of Human and Mouse TLR Pathways Identifies Species-specific Preferences in Signaling Protein Use. *Sci. Signal.* 9 (409), ra3. doi:10.1126/scisignal.aab2191

Thabault, L., Liberelle, M., and Frédérick, R. (2021). Targeting Protein Self-Association in Drug Design. *Drug Discov. Today* 26 (5), 1148–1163. doi:10.1016/j.drudis.2021.01.028

Ve, T., Vajjhala, P. R., Hedger, A., Croll, T., DiMaio, F., Horsefield, S., et al. (2017). Structural Basis of TIR-Domain-Assembly Formation in MAL- and MyD88-dependent TLR4 Signaling. *Nat. Struct. Mol. Biol.* 24 (9), 743–751. doi:10.1038/nsmb.3444

Vyncke, L., Bovijn, C., Pauwels, E., Van Acker, T., Ruyssinck, E., Burg, E., et al. (2016). Reconstructing the TIR Side of the Myddosome: a Paradigm for TIR-TIR Interactions. *Structure* 24 (3), 437–447. doi:10.1016/j.str.2015.12.018

Wang, J., Wolf, R. M., Caldwell, J. W., Kollman, P. A., and Case, D. A. (2004). Development and Testing of a General Amber Force Field. *J. Comput. Chem.* 25 (9), 1157–1174. doi:10.1002/jcc.20035

Xie, L., Jiang, F. C., Zhang, L. M., He, W. T., Liu, J. H., Li, M. Q., et al. (2016). Targeting of MyD88 Homodimerization by Novel Synthetic Inhibitor TJ-M2010-5 in Preventing Colitis-Associated Colorectal Cancer. *J. Natl. Cancer Inst.* 108 (4). doi:10.1093/jnci/djv364

Yao, H., Sun, Y., Song, S., Qi, Y., Tao, X., Xu, L., et al. (2017). Protective Effects of Dioscin against Lipopolysaccharide-Induced Acute Lung Injury through Inhibition of Oxidative Stress and Inflammation. *Front. Pharmacol.* 8, 120. doi:10.3389/fphar.2017.00120

Yu, H., and Huang, H. (2014). Engineering Proteins for Thermostability through Rigidifying Flexible Sites. *Biotechnol. Adv.* 32 (2), 308–315. doi:10.1016/j.biotechadv.2013.10.012

Yu, H., Yan, Y., Zhang, C., and Dalby, P. A. (2017). Two Strategies to Engineer Flexible Loops for Improved Enzyme Thermostability. *Sci. Rep.* 7 (1), 41212. doi:10.1038/srep41212

Zhan, C., Qi, R., Wei, G., Guven-Maiorov, E., Nussinov, R., and Ma, B. (2016). Conformational Dynamics of Cancer-Associated MyD88-TIR Domain Mutant L252P (L265P) Allosterically Tilts the Landscape toward Homo-Dimerization. *Protein Eng. Des. Sel* 29 (9), 347–354. doi:10.1093/protein/gzw033

Zhang, L. M., Liu, J. H., Xue, C. B., Li, M. Q., Xing, S., Zhang, X., et al. (2016). Pharmacological Inhibition of MyD88 Homodimerization Counteracts Renal Ischemia Reperfusion-Induced Progressive Renal Injury *In Vivo* and *In Vitro*. *Sci. Rep.* 6, 26954. doi:10.1038/srep26954

Conflict of Interest: The authors declare that the research was conducted in the absence of any commercial or financial relationships that could be construed as a potential conflict of interest.

Publisher's Note: All claims expressed in this article are solely those of the authors and do not necessarily represent those of their affiliated organizations, or those of the publisher, the editors and the reviewers. Any product that may be evaluated in this article, or claim that may be made by its manufacturer, is not guaranteed or endorsed by the publisher.

frontiers in Pharmacology

ORIGINAL RESEARCH
published: 09 December 2021
doi: 10.3389/fphar.2021.770910

Screening of Microbial Natural Products and Biological Evaluation of Trichomicin as Potential Anti-Cytokine Storm Agents

Yu Chen[1,2†], *Zhuochen Zhuang*[2†], *Jing Yang*[1*] *and Liping Bai*[2*]

[1]School of Basic Medicine and Forensic Medicine, Baotou Medical College, Baotou, China, [2]NHC Key Laboratory of Biotechnology of Antibiotics, CAMS Key Laboratory of Synthetic Biology for Drug Innovation, Institute of Medicinal Biotechnology, Chinese Academy of Medical Sciences & Peking Union Medical College, Beijing, China

OPEN ACCESS

Edited by:
Tharmarajan Ramprasath, Georgia State University, United States

Reviewed by:
Senthamizharasi Manivasagam, The University of Iowa, United States
Stalinraja Maruthamuthu, University of California, San Francisco, United States
Rekha Balakrishnan, City of Hope National Medical Center, United States

***Correspondence:**
Jing Yang
yangjing2569@126.com
Liping Bai
lipingbai1973@163.com

[†]These authors have contributed equally to this work

Specialty section:
This article was submitted to Inflammation Pharmacology, a section of the journal Frontiers in Pharmacology

Received: 05 September 2021
Accepted: 11 November 2021
Published: 09 December 2021

Citation:
Chen Y, Zhuang Z, Yang J and Bai L (2021) Screening of Microbial Natural Products and Biological Evaluation of Trichomicin as Potential Anti-Cytokine Storm Agents. Front. Pharmacol. 12:770910. doi: 10.3389/fphar.2021.770910

COVID-19 has remained an uncontained, worldwide pandemic. Most of the infected people had mild symptoms in the early stage, and suddenly worsened or even died in the later stage which made the cytokine release syndrome (CRS) once again aroused people's attention. CRS is an excessive immunity of the body to external stimuli such as viruses, bacteria, and nanomaterials, which can cause tissue damage, local necrosis or even death. Lipopolysaccharide (LPS) is one of the most effective CRS inducers, which can activate macrophages to release cytokines, including tumor necrosis factor (TNF-α), interleukin-1β (IL-1β), IL-6 and chemokines. We used RT-PCR to detect the expression of representative cytokines in mouse and human cells at different concentrations of Trichomicin, Ebosin, and 1487B after LPS stimulation. The results showed that the expression of TNF-α, IL-1β, IL-6, and CXCL10 all increased after LPS stimulation. Among the various drugs, Trichomicin had the most obvious inhibitory effect on cytokine expression *in vitro*, and it was further verified *in vivo* that Trichomicin can improve the survival rate of mice stimulated with LPS. Finally, it was proved that Trichomicin inhibited the Stat3 and NF-κB pathways and reduced the phosphorylation of Stat3 and p65 after LPS stimulation, thereby inhibiting the response of macrophages to pro-inflammatory stimuli. The article clarified the inhibitory activity and mechanism of action of Trichomicin on CRS, and laid the foundation for the research on the anti-cytokine storm activity of microbial natural products.

Keywords: cytokine storm, Trichomicin, microbial natural products, LPS, COVID-19

INTRODUCTION

Coronavirus disease 19 (COVID-19) is caused by severe acute respiratory syndrome coronavirus 2 (SARS-CoV-2). WHO declared a COVID-19 pandemic in January 2020. The virus rapidly spread across the world through travelers and the number of world-wide cases has exceeded 72 million with over one million deaths as of December 14, 2020 (Chung et al., 2021). Most of patients have mild symptoms, but a significant proportion of patients have developed a severe acute hyperimmune response characterized by cytokine storm (Caricchio et al., 2021). It includes systemic hyperinflammation, acute respiratory distress syndrome (ARDS) and multiorgan failure. In fact, the ultimate culprit is not caused by the virus itself, but the body's own immune system that the virus

intervenes, and its excessive immune response brews into a cytokine storm, which causes the dysfunction of the body's organs. This is one of the important reasons that cause the sudden increase in the condition of the new crown infection and even the death (Shinya et al., 2012; Casadevall and Pirofski, 2014).

Cytokine storm, also known as cytokine release syndrome (CRS), is an excessive and uncontrollable release of inflammatory cytokines and chemokines, leading to a self-balancing detrimental process, and is considered to be a major cause of COVID-19 disease severity (Coperchini et al., 2021). It has been shown that several cytokines such as IL-6 and IL-1 are involved in the severity of COVID-19 disease (Kim et al., 2021). The elevated serum levels of IL-6 in COVID-19 patients and its circulating levels are positively correlated with the severity of disease, indicating that IL-6 plays a key role in the pathogenesis of CRS (McGonagle et al., 2020; Ragab et al., 2020; Zhang et al., 2020).

In CRS, the three most important cytokines in the IL-1 family are IL-1β, IL-18 and IL-33, in which IL-1β cytokine has been studied the most (Ye et al., 2020). IL-1β plays a pro-inflammatory role in recruiting immune cells and inducing secondary cytokine production, leading to an acute phase response. Coperchini et al. proposed that COVID-19 patients have high levels of the pro-inflammatory cytokines IL-1β, IL-6, TNF-α, INF-γ and chemokines CXCL10, CXCL9 levels (Coperchini et al., 2020). In addition, circulating levels of CXCL10 are elevated at admission and remain high during disease progression (Coperchini et al., 2021). Various cytokines promote or inhibit the expression of each other in the body, forming a complicated cytokine regulatory network (Zhang et al., 2013a). However, when body is severely infected, the balance between immune-promoting and immune-inhibiting mechanisms promoted by cytokines will be broken, which may result in CRS, a leading cause of death of COVID-19 patients (Ragab et al., 2020). Therefore, suppression of CRS can effectively prevent the aggravation of COVID-19 patients.

At present, there is no specific treatment for CRS and ARDS in clinical practice, and treatment measures such as administration of anti-infective drugs, glucocorticoids, and artificial ventilation assistance are mostly used. IL-6 antagonists such as tocilizumab and stutuzumab can block downstream signal transduction through receptor binding, effectively controlling CRS without affecting the efficacy of CAR-T cells (Maude et al., 2014; Wang et al., 2018a). Glucocorticoids can combine with corticosteroid binding protein and albumin to form a complex, and a small amount of free hormones diffused through the cell membrane to bind to the glucocorticoid receptor in the cytoplasm, and enters the nucleus to induce or inhibit the expression of inflammation-related genes and exert anti-inflammatory effects (Zhang and Jiang, 2015). Cytokine blockers such as Etanercept and Anakinra can also bind to their targeting cytokines to inhibit CRS (Zou et al., 2017; Giavridis et al., 2018; Norelli et al., 2018). In addition, catecholamine modulators such as atrial natriuretic peptide and α-methyltyrosine (Staedtke et al., 2018), sphingosine analogs such as Siponimod (Zhang et al., 2013a), Ulinastatin (Tao et al., 2017) and the plasma of recovered patients also show varying therapeutic potential for CRS. However, among the above-mentioned drugs, cytokine blockers have single target, and glucocorticoids may cause side effects such as double infection and diabetes, osteoporosis and high blood pressure. Therefore, the development of new drugs that effectively inhibit CRS has become an urgent need.

Ebosin is a novel exopolysaccharide (EPS) isolated from the fermentation culture of *Streptomyces* sp. 139 (Zhang et al., 2016). Preliminary pharmacodynamic research showed that Ebosin has significant therapeutic effect in rat type II collagen-induced arthritis (CIA) models and adjuvant rheumatoid arthritis animal models. Following its treatment, the expression level of IL-1β and TNF-α decreased significantly *in vivo*, indicating that the inhibitory effect of Ebosin on rheumatoid arthritis may be attributed to the reduced levels of related inflammatory cytokines (Zhang et al., 2013b; Zhang et al., 2016). Trichomicin is a small molecule compound with new structure isolated from *Trichoderma harzianum* (*T. harzianum*) in our laboratory (Zhu et al., 2020). Early *in vitro* studies confirmed that Trichomicin has significant anti-inflammatory and anti-tumor activities, and inhibits the growth of colon tumor (Qi et al., 2011; Zhao et al., 2020). Furthermore, our laboratory also used the anti-inflammatory model to screen the new structure small molecule compound 1487B. Pharmacodynamic studies showed that 1487B has a significant inhibitory effect on the acute inflammation model of mouse ear swelling (Ma et al., 2015). The above results suggest that Ebosin, Trichomicin and 1487B may have anti-inflammatory activities, and we speculate that they may also have an inhibitory effect on CRS.

Lipopolysaccharide (LPS) is one of the most effective CRS inducers. It can activate monocytes/macrophages to release cytokines, including tumor necrosis factor (TNF-α), interleukin-1β (IL-1β), IL-6, chemokines, and other inflammatory cytokines (Cavaillon, 2018). Not only that, LPS can induce sepsis and toxic shock syndrome in mice. Therefore, relevant research always uses LPS to induce the release of pro-inflammatory cytokines in both *in vivo* and *in vitro* models. In this study, we used LPS to stimulate cells or mice, and used RT-PCR and western blot methods to conduct a preliminary study to compare the anti-cytokine storm activities of Trichomicin, Ebosin and 1487B, and further discuss their possible mechanisms of action. This study aims to lay the foundation for the research on the anti-cytokine storm activity of a variety of microbial natural products.

MATERIALS AND METHODS

Materials

Ebosin (50 mg/ml), 1487B (20 mM) and Lipopolysaccharide (LPS, 1 mg/ml, Beyotime, China) were dissolved in Phosphate-Buffered Saline (PBS, Corning, Manassas, United States). Filtered through a 0.22 μm filter, they were stored at −80°C until use. Trichomicin (4 mM) and PMA (10 mM, Sigma, GER) were dissolved in DMSO, and were further diluted with medium (for cell assays). Sodium carboxymethyl cellulose (CMC-Na, Selleckchem, United States) was dissolved in double distilled water at 0.5 mg/ml and used as a solvent for animal experiments.

Cell Lines and Culture

RAW264.7, NR8383, J774A.1 and THP-1 cells were purchased from Cell Resource Center, Institute of Basic Medical Sciences, Chinese Academy of Medical Sciences (CAMS, Beijing, China). U937 and HL-60 cells were derived from Beijing BeNa Culture Collection (BNCC) Biotechnology Company. RAW, J774A.1 and NR8383 cells were conventionally cultivated in Dulbecco ¯s modified Eagle medium (DMEM) with high glucose (Corning, Manassas, United States). THP-1 and U937 cells were routinely cultivated in RPMI 1640 medium (Corning, Manassas, United States). HL-60 cells were routinely cultivated in Iscove's modified Dubecco's medium (IMDM, Corning, Manassas, United States). The media were supplemented with 10% fetal bovine serum (FBS, Invitrogen, Carlsbad, CA, United States) and antibiotics (penicillin and streptomycin, 100 U/mL) (Corning, Manassas, United States) under standard conditions (37°C, 5% CO_2).

To generate macrophage-like differentiated cells, THP-1, U937 and NR8383 cells were incubated with 160 nM PMA, HL-60 cells were incubated with 1.25% DMSO at 37°C for 24 h (Aldo et al., 2013). After incubation, the PMA/DMSO-containing medium was removed and replaced with medium for subsequent experiments.

Experimental Animals

Female BALB/c mice of bodyweight 18–22 g were purchased from Beijing Huafukang Biotechnology Co., Ltd., allowed to acclimate to a new SPF surrounding (temperature: 22 ± 2°C, humidity: 40–60%, light/dark cycle: 12 h) for 1 week, with food and water supplied ad libitum. Animal experimental protocols were performed under NO. IMB-20210601$D_7$01 according to the Chinese National Guidelines for the Care and Use of Laboratory Animals and approved by the Animal Experimental Ethics Committee of Institute of Medicinal Biotechnology, Chinese Academy of Medical Sciences & Peking Union Medical College.

Cell Viability Assay

The sensitivities of the cell lines RAW, NR8383, THP-1 and HL-60 to Trichomicin, Ebosin and 1487B compounds were evaluated by MTT assay. Each cell line was seeded in a 96-well plate. After 24 h incubation, the medium was changed and Trichomicin/Ebosin/1487B was added to cell culture medium with different concentrations. The cells were cultured for 72 h, supplemented with 10 μl MTT (Boster, Wuhan, China) solution, and incubated for another 4 h, after which the medium was removed and 100 μl of DMSO was added. Finally, the absorbance at 570 nm of each well was measured with a Victor X5 multi-label microplate detector (PerkinElmer, MA, United States).

RNA Purification, cDNA Synthesis, and Real-Time Reverse Transcription PCR (RT-PCR)

Total mRNA was extracted from cells with TRIzol Reagents (TransGen Biotech, Beijing, China), and was transcribed into cDNA with TransScript One-Step gDNA Removal and cDNA Synthesis SuperMix according to the manufacturer's instructions. The amplification protocol consists of an initial step of 30 s at 94°C followed by 45 cycles of 5 s at 94°C and 30 s at 60°C on a Bio-Rad CFX96 (Bio-Rad, United States) using PerfectStart Green qPCR SuperMix (TransGen Biotech, Beijing, China). The relative expression levels were normalized to gapdh level using the $2^{-\Delta\Delta CT}$ method. The primer sequences are listed in **Table 1**.

Western Blot

Total protein samples of cells were prepared by RIPA buffer (Boster, China) with phosphatase inhibitor (1:1,000, Applygen, Beijing, China) on ice-bath for 1 h. The supernatant was collected by centrifugation at 14,000 rpm for 20 min at 4°C, and the protein concentration was measured by a BCA protein assay kit (Applygen, Beijing, China). The protein samples were loaded to an 10% SDS-PAGE gel and was transferred to a PVDF membrane. The PVDF membranes were blocked with 5% (w/v) skimmed milk powder in TBST for 2 h, and were subsequently incubated with primary anti-phospho-NF-κB p65 (#3033, Cell Signaling Technology, Boston, United States), anti-NF-κB p65 (#8242, Cell Signaling Technology, Boston, United States), anti phospho-Stat3 (#9145S, Cell Signaling Technology, Boston, United States), anti Stat3 (#JA9179, Calbiochem, NJ, United States), anti-phospho-IKKα/β (#2697, Cell Signaling Technology, Boston, United States), anti-IKKβ (#8943, Cell Signaling Technology, Boston, United States) and anti GAPDH (AMM04703G, Santa Cruz Biotechnology, Beijing, China) at 4°C overnight. Then the membranes were washed with TBST and were incubated with secondary HRP-conjugated goat anti-rabbit or antimouse IgG antibody (1: 10,000) for 2 h at room temperature. The blots were detected with an enhanced chemiluminescence method on a Bio-Rad Gel imaging system (733BR-2008, Bio-Rad, CA, United States) and were analyzed by ImageJ software.

Model and Animal Treatment

In the LPS-induced inflammation model, mice were randomly divided into four groups (n = 8): placebo (CMC-Na) group, LPS only model group (4 mg/kg), LPS with Trichomicin low dose (15 mg/kg) and high dose (30 mg/kg) treatment groups. Placebo and Trichomicin groups were applied intragastrically from day 1 to day 14. At day 8, mice within the model group and treatment group were intraperitoneally injected with LPS (4 mg/kg) 1 h after administration to establish the model. The changes in the weight of mice were monitored and their survival were observed every day. All mice were euthanized at day 14.

Statistical Analysis

All data were analyzed using Graph Pad Prism 8.4.2 (Graph Pad Software, Inc., San Diego, CA) and presented as mean ± SD of at least three independent experiments. Differences between two groups were evaluated using Student's t test. $p < 0.05$ was considered to be statistically significant, $p < 0.01$ was considered to be highly statistically significant, $p < 0.001$ was considered to be extremely statistically significant.

TABLE 1 | The primers used for RT-PCR.

Gene name	Forward primer (5′-3′)	Reverse primer (5′-3′)
human il-1β	CTGTCCTGCGTGTTGAAAGA	TTCTGCTTGAGAGGTGCTGA
human tnf-α	TGTAGCAAACCCTCAAGCTG	TTGATGGCAGAGAGGAGGTT
human-il-6	CCACACAGACAGCCACTCAC	TTTCACCAGGCAAGTCTCCT
human cxcl10	TCTAAGTGGCATTCAAGGAGTACC	GGACAAAATTGGCTTGCAGGA
human-gapdh	GGAGCGAGATCCCTCCAAAAT	GGCTGTTGTCATACTTCTCATGG
mouse-il-1β	TGCCACCTTTTGACAGTGAT	AAGGTCCACGGGAAAGACAC
mouse-tnfα	GTCCCCAAAGGGATGAGAAGT	TTTGCTACGACGTGGGCTAC
mouse-il-6	AGTTGCCTTCTTGGGACTGA	CAGAATTGCCATTGCACAAC
mouse-cxcl10	GTCTGAGTGGGACTCAAGGGAT	AGGCTCGCAGGGATGATTTC
mouse-gapdh	AACAGCAACTCCCACTCTTC	CCTGTTGCTGTAGCCGTATT

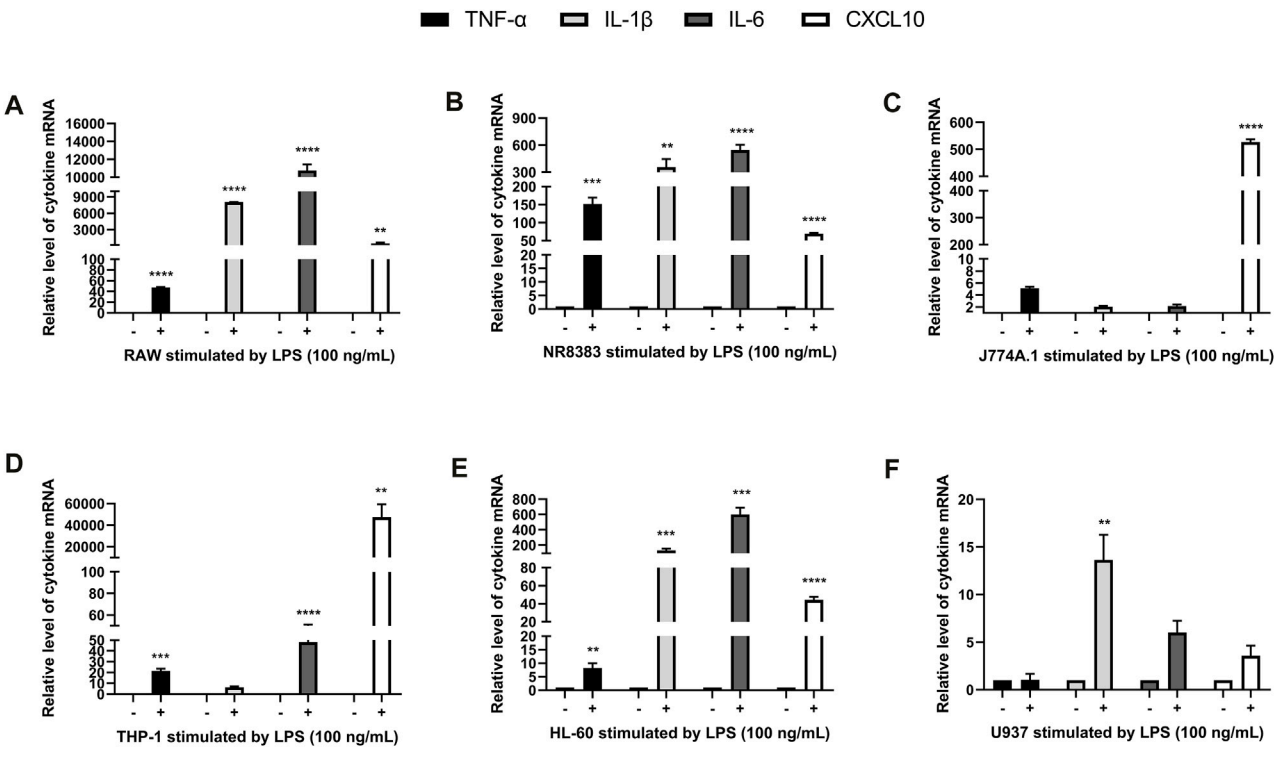

FIGURE 1 | LPS stimulated cytokine expression in mouse and human macrophages. RT-PCR quantification of TNF-α, IL-6, IL-1β, and CXCL10 mRNA expression in RAW **(A)**, NR8383 **(B)**, J774A.1 **(C)**, THP-1 **(D)**, HL-60 **(E)** and U937 **(F)** cells stimulated with LPS. (mean ± SD, $n = 3$). $^{**}p < 0.01$, $^{***}p < 0.001$, $^{****}p < 0.0001$ vs. Control group.

RESULTS

Expression of Cytokines in Mouse and Human Macrophages Induced by Lipopolysaccharide

In order to observe the effect of LPS on the expression of different cytokines in mouse and human cells, we used LPS to induce RAW, NR8383, J774A.1, THP-1, U937, and HL-60 cells, and then RT-PCR to quantitatively analyze the expression of IL-1β, TNF-α, IL-6, and CXCL10. Preliminary analyses of cytokine expressions induced by LPS showed that the concentration of 100 ng/ml for 4 h was most significant (data not shown). For mouse RAW and NR8383 cells the mRNA expression levels of IL-1β, TNF-α, IL-6 and CXCL10 cytokines increased significantly after LPS stimulation ($p < 0.01$), especially IL-6 and IL-1β. However, in J774A.1 cells, except for CXCL10, the changes in other cytokines were not obvious (**Figures 1A–C**). For human THP-1 and HL-60 cells, the mRNA expression levels of the four cytokines all increased significantly after LPS stimulation ($p < 0.01$). But in U937 cells, the expression levels of various cytokines had almost no significant changes compared with the control (**Figures 1D–F**). The above data suggested that LPS induced a significant increase in cytokine levels in human and mouse

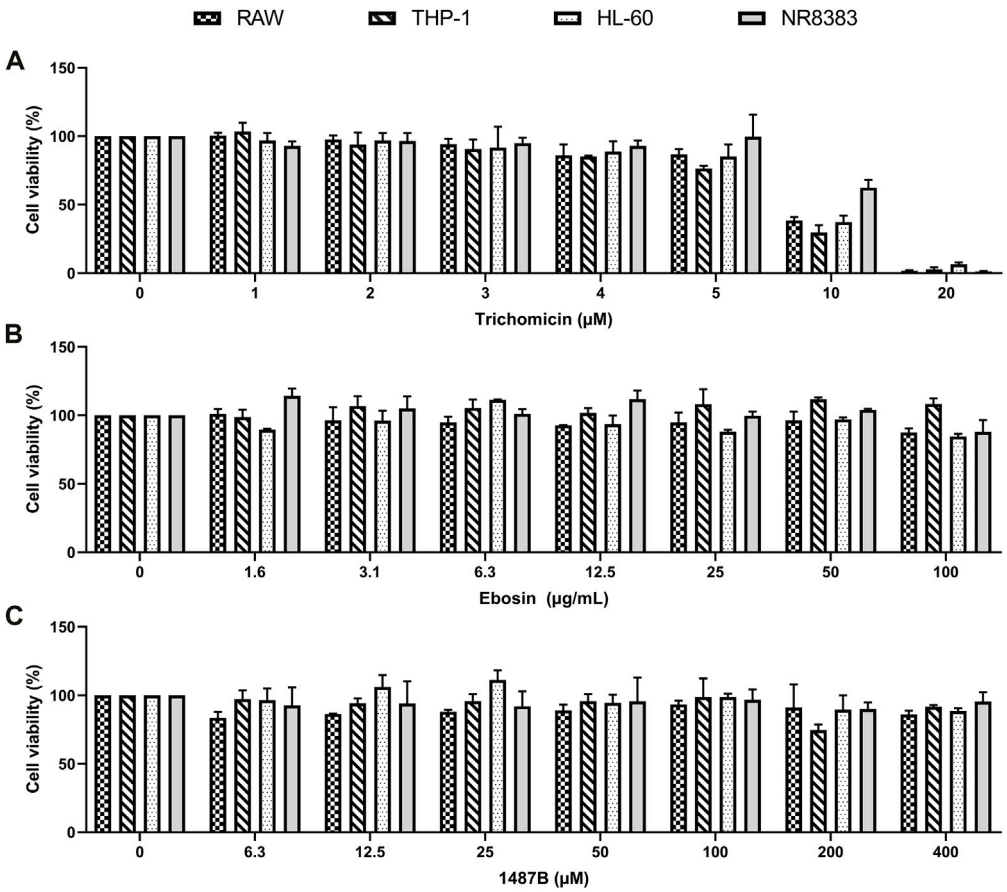

FIGURE 2 | Effects of Trichomicin, Ebosin and 1487B on the viability of RAW, THP-1, NR8383, and HL-60 cells. **(A)** MTT assay of viability in the cells treatment with 1, 2, 3, 4, 5, 10, and 20 μM Trichomicin. **(B)** MTT assay of viability in the cells treatment with 1.6, 3.1, 6.3, 12.5, 25, 50, and 100 μg/ml Ebosin. **(C)** MTT assay of viability in the cells treatment with 6.3, 12.5, 25, 50, 100, 200, and 400 μM 1487B. (mean ± SD, $n = 6$).

macrophages, and the changes in cytokine levels in mouse cells were more obvious.

Effects of Trichomicin, Ebosin, and 1487B on the Cytotoxicity of RAW, NR8383, HL-60, and THP-1 Cells

To further explore the anti-cytokine storm activity of Trichomicin, Ebosin and 1487B, cell viability assay was performed. Cell lines sensitive to LPS induction, including Raw, NR8383, THP-1 and HL-60, were selected. The cells were cultured with Trichomicin (0, 1, 2, 3, 4, 5, 10, 20 μM), Ebosin (0, 1.6, 3.1, 6.3, 12.5, 25, 50, 100 μg/ml) and 1487B (0, 6.3, 12.5, 25, 50, 100, 200, 400 μM) for 72 h, and cell viability was determined by MTT assay. As shown in **Figure 2**, within the experimental concentrations, Ebosin and 1487B were almost non-toxic to the four cells. However, 20 μM of Trichomicin was toxic to cells, and 10 μM of Trichomicin was slightly toxic to cells, so the Trichomicin concentration in subsequent experiments should be lower than 10 μM.

Cytokine Transcription Levels in RAW, NR8383, HL-60 and THP-1 Cells Were Inhibited by Trichomicin, Ebosin and 1487B

Cytokines such as IL-1β, TNF-α, IL-6, and CXCL10 are central players in CRS, thus we further investigated the effects of Trichomicin, Ebosin and 1487B on the expression of these cytokines in different macrophages. Based on the results induced by LPS (**Figure 1**), RAW, NR8383 mouse cells and THP-1, HL-60 human cells were selected for the experiment. According to the results of the cell viability assay (**Figure 2**), maximum concentrations of Trichomicin, Ebosin, and 1487B were 8 μM, 12,800 ng/ml and 400 μM, respectively. The cells were treated with Trichomicin, Ebosin, and 1487B for 30 min, and then stimulated with LPS for 4 h. Then RNA was extracted, and the expression of IL-1β, TNF-α, IL-6 and CXCL10 was quantitatively analyzed by RT-PCR after reverse transcription.

As shown in **Figure 3**, Trichomicin had a significant inhibitory effect on the expression of TNF-α, IL-6, IL-1β and CXCL10 in a dose-dependent manner, with the exception of IL-1β in NR8383

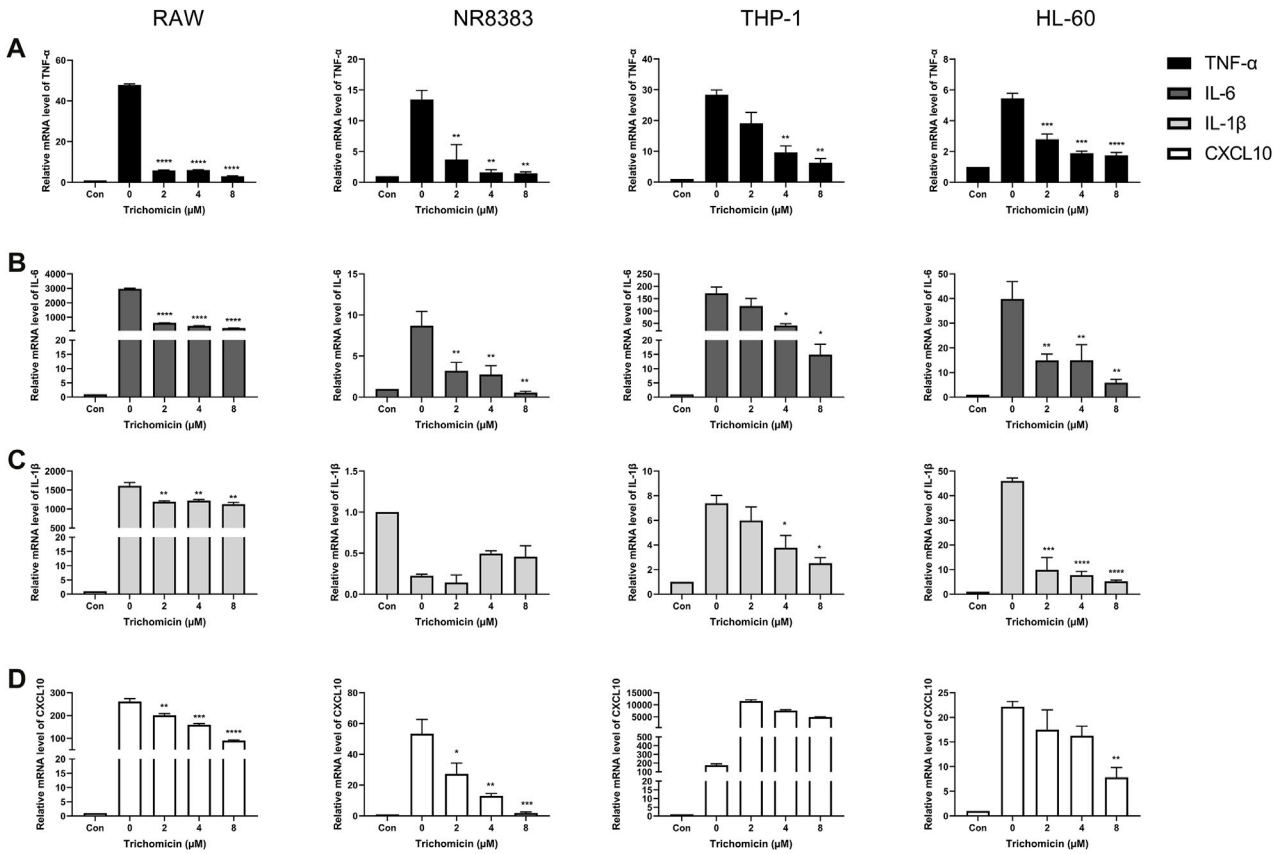

FIGURE 3 | Trichomicin inhibits the expression of TNF-α, IL-6, IL-1β, and CXCL10 in macrophages. RT-PCR quantitation of TNF-α **(A)**, IL-6 **(B)**, IL-1β **(C)** and CXCL10 **(D)** mRNA expression in RAW, NR8383, THP-1, and HL-60 cells stimulated with LPS (100 ng/ml) following treatment with 2, 4, and 8 μM Trichomicin. (mean ± SD, $n = 3$). *$p < 0.05$, **$p < 0.01$, ***$p < 0.001$, ****$p < 0.0001$ vs. LPS-induced group.

and CXCL10 in THP-1. Among them, Trichomicin had the most significant inhibitory effect on the TNF-α and IL-6 factors of RAW and NR8383 mouse cells, especially RAW cells. In RAW cells stimulated with LPS, the expression of TNF-α mRNA was decreased to 6.0 ± 0.2 ($p < 0.001$), 5.9 ± 0.2 ($p < 0.001$), and 3.0 ± 0.5 ($p < 0.001$), and the expression of IL-6 mRNA was decreased to 601.9 ± 6.4 ($p < 0.001$), 401.5 ± 8.7 ($p < 0.001$), and 243.8 ± 11.5 ($p < 0.001$) in response to 2, 4, and 8 μM Trichomicin, respectively. Compared with RAW cells stimulated by LPS, the expression of TNF-α was reduced by 15.3 times and the expression of IL-6 was reduced by 11.2 times in cells treated with 8 μM of Trichomicin. Similarly, Ebosin had a significant inhibitory effect on the four factors in mouse cells, all of which are statistically significant (**Figure 4**). Obviously, the IL-6 expression level in NR8383 cells treated with the maximum concentration of Ebosin was 482.6 times lower than cells treated with LPS (**Figure 4B**). Furthermore, the expression levels of TNF-α and IL-6 in all cells tend to decrease with the increase of 1487B concentration, but not significant (**Figure 5**).

In summary, the three drugs had obvious inhibitory effects on the expression of TNF-α and IL-6 in all cells, of which Trichomicin was the most significant. It was also found that the three drugs inhibited the expression of cytokines in mouse cells in a more significant manner. Therefore, we believe that the three drugs have inhibitory activity on the cytokine storm caused by LPS, of which Trichomicin is the one with best activity.

Effect of Trichomicin on Mortality and Weight Changes in a Mouse Model

According to the results of the RT-PCR experiment, the three drugs inhibited various cytokines in mouse cells, and the inhibition of Trichomicin was the most obvious. We further explored the inhibitory activity of Trichomicin *in vivo*. After preliminary dose exploration, 4 mg/kg LPS was used for modeling, and Trichomicin at 15 and 30 mg/kg were used in the low-dose and high-dose treatment groups. As shown in **Figure 6**, both low-dose and high-dose of Trichomicin reduced the mortality of mice compared with the control, and high-dose of Trichomicin was more effective. In addition, following treatment with LPS, the body weight of mice within the model and Trichomicin treatment groups were significantly lower than that of the blank control, and their body weight were gradually recovered after 3 days of treatment.

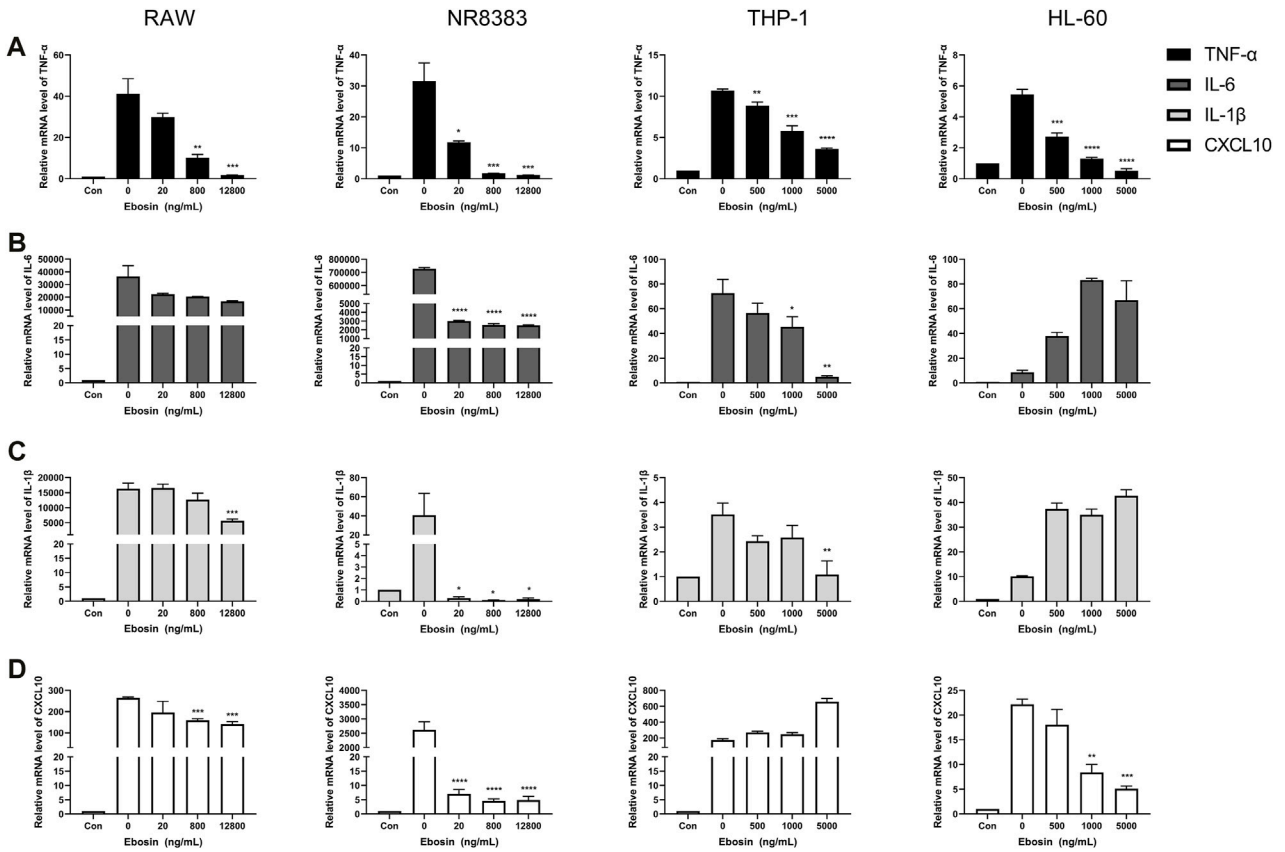

FIGURE 4 | Ebosin inhibits the expression of TNF-α, IL-6, IL-1β, and CXCL10 in macrophages. RT-PCR quantitation of TNF-α **(A)**, IL-6 **(B)**, IL-1β **(C)** and CXCL10 **(D)** mRNA expression in RAW and NR8383 cells stimulated with LPS (100 ng/ml) following treatment with 20, 800, and 12,800 ng/ml Ebosin, and in THP-1 and HL-60 cells stimulated with LPS (100 ng/ml) following treatment with 500, 1,000, and 5,000 ng/ml Ebosin. (mean ± SD, $n = 3$) $^{*}p < 0.05$, $^{**}p < 0.01$, $^{***}p < 0.001$, $^{****}p < 0.0001$ vs. LPS-induced group.

Trichomicin Downregulates Lipopolysaccharide–Induced NF-κB Pathway Activation and Blocks Basal Stat3 Phosphorylation in Macrophages

Macrophages have historically been considered to be the main source of IL-6 and TNF-α. To further elucidate the role of Trichomicin in the CRS, we evaluated signaling transduction pathways associated with TNF-α and IL-6 expression in macrophages by immunoblotting. Due to the fact that Trichomicin inhibited the expression of cytokines in mouse cells more significantly, we decided to use RAW and NR8383 mouse cells in this assay. Followed by a 4 h's stimulation with LPS, macrophages were preincubated with various concentrations of Trichomicin for 30 min, and then the phosphorylation of NF-κB p65, IKKα/β and Stat3 were analyzed. The results showed that phosphorylation of Stat3 and phosphorylation of NF-κB p65 were significantly inhibited by treatment with 4 and 8 μM Trichomicin ($p < 0.05$) (**Figure 7**). It can be concluded that Trichomicin inhibited the NF-κB and Stat3 pathways, and then inhibited the response of macrophages to pro-inflammatory stimuli.

DISCUSSION

The cause of cytokine storm is generally considered to be the overreaction of immune system to new and highly pathogenic pathogens, that is, the imbalance of immune regulatory network. The lack of negative feedback and the continuous self-amplification of positive feedback make a variety of cytokines abnormally increasing, eventually leading to single or multiple organ damage, functional failure and death. As early as 1989, in the clinical application of the anti-T cell antibody OKT3, it was discovered that following the first treatment, patients would have a series of uncomfortable symptoms such as elevated body temperature, headache, nausea, and releasement of a large number cytokines. These symptoms will be relieved following glucocorticoid treatment, and the concept of CRS has also been formally put forward (Chatenoud et al., 1989). The CRS caused by SARS infection in 2003 would cause multiple organ failures, resulting in extremely high mortality rates, thus has attracted more attention (de Jong et al., 2006). This COVID-19 epidemic has pushed the research of CRS to a climax, making it a key research direction.

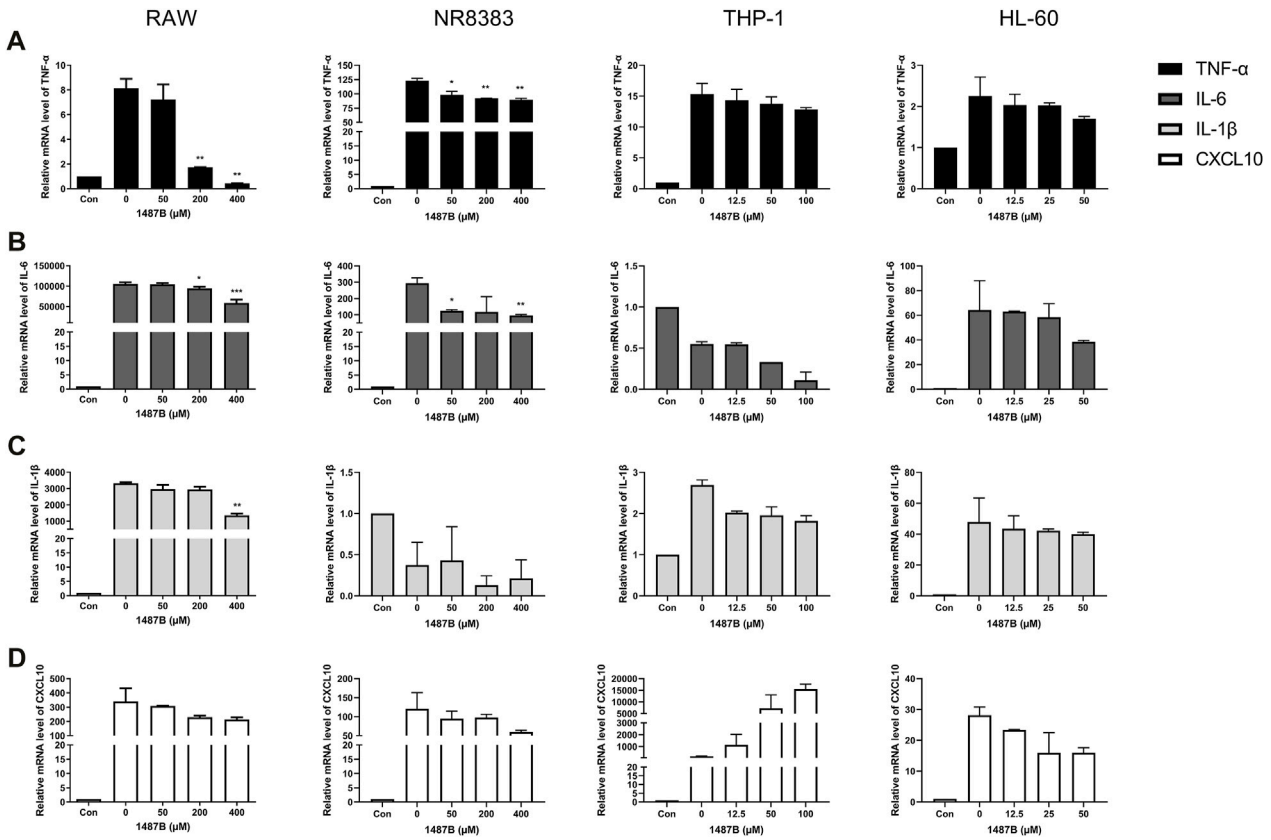

FIGURE 5 | 1487B inhibits the expression of TNF-α, IL-6, IL-1β, and CXCL10 in macrophages. RT-PCR quantitation of TNF-α **(A)**, IL-6 **(B)**, IL-1β **(C)** and CXCL10 **(D)** mRNA expression in RAW and NR8383 cells stimulated with LPS (100 ng/ml) following treatment with 50, 200, and 400 μM 1487B, and in THP-1 cell stimulated with LPS (100 ng/ml) following treatment with 12.5, 50, and 100 μM 1487B, and in HL-60 cell stimulated with LPS (100 ng/ml) following treatment with 12.5, 25, and 50 μM 1487B. (mean ± SD, $n = 3$) $^{*}p < 0.05$, $^{**}p < 0.01$, $^{***}p < 0.001$ vs. LPS-induced group.

When the body is infected or traumatized, its immune system produces immune response to eliminate or destroy antigens. When a pathogen invades the body, the innate immune system first takes effect. Epithelial cells infected by the pathogen produce a small amount of cytokines such as IFN-α/β, IL-1β, IL-8, etc. NK cells stimulated by IFN-α/β release a small amount of INF-γ to activate macrophages, and activated macrophages release large amounts of IL-6, TNF-α, IL-12 and other cytokines, which in turn activate NK cells. Therefore, "positive feedback" is formed between NK cells and macrophages, and cytokines being released increase drastically (Wang et al., 2018b). At the same time, pathogens are processed by the innate immune system and are recognized as antigens, and the adaptive immune system composed of B cells and T cells begins to play a role. A large amount of IL-12 and IFN-γ cytokines released by T-helper-1 (Th1) cells not only stimulate their own division and proliferation, but also stimulate the activation of macrophages to further activate the innate immune system, which can also generate "positive feedback" (Shimabukuro-Vornhagen et al., 2018). Normally, once the body controls the invading pathogen under the regulation of "positive feedback," the signal presented by the antigen to the adaptive immune system is weakened, the release of cytokines begins to decrease, and the inflammatory response gradually gets weakened, resulting in "negative feedback." Moreover, there are some inhibitory cytokines in the immune system, such as IL-10, TGF-β, and sphingosine 1-phosphate (S1P), which act on vascular endothelial cells to regulate excessive immune response and carry out "negative feedback" regulation on the body (Tisoncik et al., 2012). However, when the body is attacked by a violent virus such as COVID-19, the human immune system will release a large amount of cytokines under the action of "positive feedback," and the cytokine signals will be extremely amplified. The body's "negative feedback" regulation is too weak and too late, which will lead to an imbalance in the body's immune regulatory network, causing a CRS and worsening the disease.

LPS enters the cell by binding to receptors such as CD14 and Toll-like receptor 4 (TLR4) located on the membrane of monocytes/macrophages. A series of enzymatic reactions are activated through signal transduction pathways to promote activation or translocation of transcription factors into the nucleus, thereby regulate the expression of many genes (Zhang and Cao, 2003). Specifically, TLR4 activates host defenses by rapidly triggering the inflammatory response in the LPS recognition pathway, transferring to CD14 and presenting

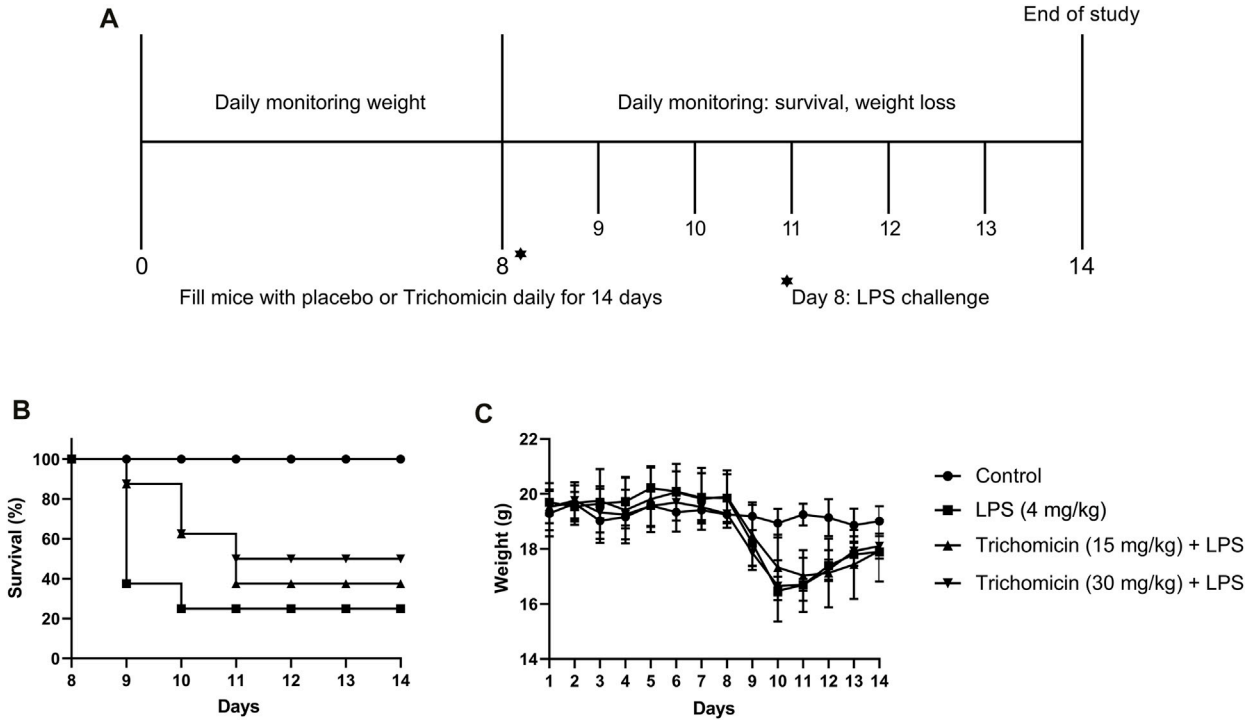

FIGURE 6 | Trichomicin protected mice from LPS challenge. **(A)** Overview of studies investigating the use of Trichomicin as a therapeutic for LPS infection. BALB/c mice were challenged with 4 mg/kg of LPS. Mice received a 14-day's intragastrically treatment of Trichomicin or placebo. **(B)** Survival rate within the 14 days' study. **(C)** Weight changes during the 14 days.

LPS to the TLR4-MD2 complex, thereby dimerizes from the plasma membrane and initiates the TIRAP-MyD88-dependent pathway, leading to NF-κB activation. NF-κB activation is essential for maintaining NF-κB-dependent transcription of genes encoding inflammatory cytokine, especially in macrophages (Granucci, 2018). Subsequently, it induces the phosphorylation of nuclear transcription factor-κB (NF-κB) p65 protein and its IKKα in the Stat3 signaling pathway, leading to the production of tumor necrosis factor (TNF)-α, interleukin (IL-1β and IL-6) cytokines and chemokines (Zusso et al., 2019). Being injected with LPS, most tissues and organs can be activated to produce pro-inflammatory factors, and monocytes/macrophages are the main secreting cells of these factors. For example, rats were injected with LPS or *E. coli*, and *in situ* analysis showed that a large amount of IL-α and IL-β were produced in the spleen (Ge et al., 1997). The bone marrow mononuclear cells of mice treated with endotoxin showed overexpression of TNF-α (Schmauder-Chock et al., 1994). Chensue et al. found that in the LPS-induced sepsis mouse model, liver Kupffer cells were a major source of TNF and IL-1 production (Chensue et al., 1991). In this study, it was confirmed that after macrophages were stimulated by LPS, RT-PCR showed that the mRNA expression of TNF-α, IL-1β, IL-6 and CXCL10 in the cells was increased.

Other cytokines, such as MIP-1 and CRP, which also are the major underlying factors of CRS. CCL3 (MIP-1alpha), CCL4 (MIP-1beta), CCL9/10 (MIP-1delta) and CCL15 (MIP-1gamma) were produced by many cells, especially macrophages, dendritic cells and lymphocytes. MIP-1 proteins, which act via G-protein-coupled cell surface receptors (CCR1, 3, 5), expressed by lymphocytes and monocytes/macrophages, are best known for their chemotactic and proinflammatory effects but can also promote homoeostasis. Moreover, CRP, ferritin, and procalcitonin are sensitive markers of COVID-19 disease in the acute phase. The elevated CRP level of COVID-19 patients is strongly correlated with disease severity and prognosis. The severity of COVID-19 can be assessed by detecting inflammatory biomarkers, including high levels of IL-6 and plasma CRP, and the release of these factors is closely related to ARDS. In addition, high levels of CRP and procalcitonin in the serum are also the main factors for poor prognosis.

Our study proves that Trichomicin, Ebosin and 1487B inhibited the expression of TNF-α, IL-1β, IL-6 and CXCL10 factors in mouse macrophages in varying degrees, while Trichomicin is the most effective one (**Figures 3–5**). Subsequent western blot experiments found that Trichomicin inhibited the Stat3 and NF-κB pathways and reduced the phosphorylation of Stat3 and p65 following LPS stimulation (**Figure 7**). Through comparison, the anti-cytokine storm activity of Trichomicin was significantly stronger than that of entecavir (Su et al., 2020). Trichomicin also showed good oral absorption and rapid uptake (Zhu et al., 2020). In addition, Scarneo et al. have

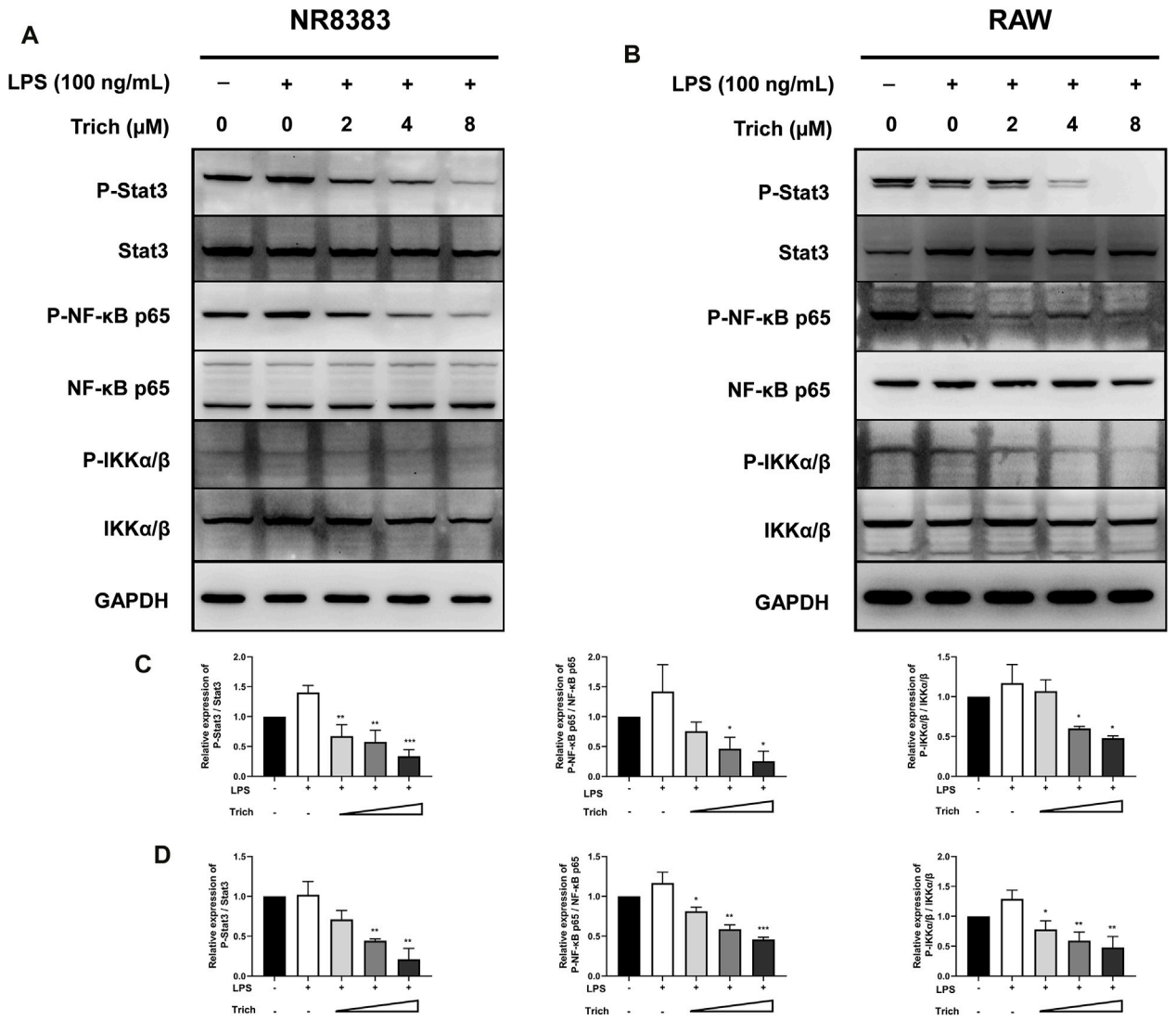

FIGURE 7 | Western blot analysis of LPS-induced NF-κB p65, IKKα/β and Stat3 phosphorylation in NR8383 **(A,C)** and RAW **(B,D)** cells treated with Trichomicin. (mean ± SD, $n = 3$). $^{*}p < 0.05$, $^{**}p < 0.01$, $^{***}p < 0.001$ vs. LPS-induced group.

proved that the new TAK1 inhibitor Takinib could inhibit the response of macrophages to pro-inflammatory stimuli. Also, Takinib reduced the phosphorylation of downstream proteins p-38, c-Jun, and NF-κB following LPS stimulation (Scarneo et al., 2018). Liu et al. established a U937 cell model based on human monocytes for high-throughput anti-influenza drug screening. Expression of three cytokine indicators CCL2, CXCL10 and viral NA were selected to screen immunomodulators and antiviral agents for the treatment of influenza. It was verified that at cellular level, the NF-κB pathway mainly regulates the expression of IL-6, IL-8, TNF-α, CCL2, CCL3, and CCL5 (Liu et al., 2019). On the other hand, *in vivo* studies have found that Clopidogrel, Sarpogrelate and Cilostazol all had inhibitory effects on the expression of TNF mRNA in the blood after LPS stimulation. Further study of the mechanism found that Cilostazol attenuated TNF-mediated phosphorylation of MAPKs and NF-κB p65 (Lee et al., 2020). LMT-28 could alleviate arthritis and acute pancreatitis in mice, reduce the secretion of TNF-α in serum, and inhibit IL-6-induced phosphorylation of Stat3, gp130 and JAK2 proteins (Hong et al., 2015). The above findings corroborate the results of this article, i.e., the phosphorylation of downstream Stat3 and p65 following LPS stimulation can be reduced by agents, eventually inhibits CRS. Based on these results, two indicators of IL-6 and TNF-α have been selected to establish a RAW cell model for the screening of anti-cytokine storm activity. The results of the three drugs purified in our laboratory show that Trichomicin has the best activity.

In summary, we used RT-PCR to detect the expression of representative cytokines in mouse and human cells treated with different concentrations of Trichomicin, Ebosin and 1487B following LPS stimulation. The results showed that the expression of TNF-α, IL-1β, IL-6, and CXCL10 in both cell lines increased after LPS stimulation, and the three drugs inhibited the expression of various factors to varying degrees. Trichomicin had the most obvious inhibitory activity on the expression of cytokines, and the change of cytokine expression is more significant in mouse cells. We subsequently verified that Trichomicin can improve the survival rate of mice treated with LPS, and the survival rate of high-dose group is higher. Furthermore, our research on the mechanism of Trichomicin inhibiting cytokine expression in mouse cells showed that Trichomicin inhibited the Stat3 and NF-κB pathways, thereby inhibiting the response of macrophages to pro-inflammatory stimuli.

The article clarifies that the inhibitory activity of the three drugs on CRS and its mechanism of action have important scientific significance and application value, which lays a foundation for the screening of anti-cytokine storm activity from microbial natural products. Although it was reported that blocking cytokine signaling may impair clearance of influenza virus, increase the risk of secondary infections, and lead to worse outcomes (Koch et al., 2018), until now we found no reports that blocking cytokine signaling may impair clearance of SARS-CoV-2. Trichomicin has the potential to be developed as a treatment for COVID-19, however, we will maintain sustained attention about secondary infections of SARS-CoV-2 after blocking cytokine signaling.

DATA AVAILABILITY STATEMENT

The original contributions presented in the study are included in the article/Supplementary Material, further inquiries can be directed to the corresponding authors.

ETHICS STATEMENT

The animal study was reviewed and approved by Animal Experimental Ethics Committee of Institute of Medicinal Biotechnology, Chinese Academy of Medical Sciences & Peking Union Medical College.

AUTHOR CONTRIBUTIONS

YC and ZZ performed the research work and drafted the manuscript. JY and LB designed the research and revised the paper. All authors contributed to the article and approved the submitted version.

FUNDING

This research was supported by grants from National Key Research and Development Program of China (2018YFA0902000), and National Natural Science Foundation of China (31870059 & 82173721).

REFERENCES

Aldo, P. B., Craveiro, V., Guller, S., and Mor, G. (2013). Effect of Culture Conditions on the Phenotype of THP-1 Monocyte Cell Line. *Am. J. Reprod. Immunol.* 70 (1), 80–86. doi:10.1111/aji.12129

Caricchio, R., Gallucci, M., Dass, C., Zhang, X., Gallucci, S., Fleece, D., et al. (2021). Preliminary Predictive Criteria for COVID-19 Cytokine Storm. *Ann. Rheum. Dis.* 80 (1), 88–95. doi:10.1136/annrheumdis-2020-218323

Casadevall, A., and Pirofski, L. A. (2014). Microbiology: Ditch the Term Pathogen. *Nature* 516 (7530), 165–166. doi:10.1038/516165a

Cavaillon, J. M. (2018). Exotoxins and Endotoxins: Inducers of Inflammatory Cytokines. *Toxicon* 149, 45–53. doi:10.1016/j.toxicon.2017.10.016

Chatenoud, L., Ferran, C., Reuter, A., Legendre, C., Gevaert, Y., Kreis, H., et al. (1989). Systemic Reaction to the Anti-T-cell Monoclonal Antibody OKT3 in Relation to Serum Levels of Tumor Necrosis Factor and Interferon-Gamma [corrected]. *N. Engl. J. Med.* 320 (21), 1420–1421. doi:10.1056/NEJM198905253202117

Chensue, S. W., Terebuh, P. D., Remick, D. G., Scales, W. E., and Kunkel, S. L. (1991). *In Vivo* biologic and Immunohistochemical Analysis of Interleukin-1 Alpha, Beta and Tumor Necrosis Factor during Experimental Endotoxemia. Kinetics, Kupffer Cell Expression, and Glucocorticoid Effects. *Am. J. Pathol.* 138 (2), 395–402.

Chung, J. Y., Thone, M. N., and Kwon, Y. J. (2021). COVID-19 Vaccines: The Status and Perspectives in Delivery Points of View. *Adv. Drug Deliv. Rev.* 170, 1–25. doi:10.1016/j.addr.2020.12.011

Coperchini, F., Chiovato, L., Croce, L., Magri, F., and Rotondi, M. (2020). The Cytokine Storm in COVID-19: An Overview of the Involvement of the Chemokine/Chemokine-Receptor System. *Cytokine Growth Factor. Rev.* 53, 25–32. doi:10.1016/j.cytogfr.2020.05.003

Coperchini, F., Chiovato, L., Ricci, G., Croce, L., Magri, F., and Rotondi, M. (2021). The Cytokine Storm in COVID-19: Further Advances in Our Understanding the Role of Specific Chemokines Involved. *Cytokine Growth Factor. Rev.* 58, 82–91. doi:10.1016/j.cytogfr.2020.12.005

de Jong, M. D., Simmons, C. P., Thanh, T. T., Hien, V. M., Smith, G. J., Chau, T. N., et al. (2006). Fatal Outcome of Human Influenza A (H5N1) is Associated with High Viral Load and Hypercytokinemia. *Nat. Med.* 12 (10), 1203–1207. doi:10.1038/nm1477

Ge, Y., Ezzell, R. M., Clark, B. D., Loiselle, P. M., Amato, S. F., and Warren, H. S. (1997). Relationship of Tissue and Cellular Interleukin-1 and Lipopolysaccharide After Endotoxemia and Bacteremia. *J. Infect. Dis.* 176 (5), 1313–1321. doi:10.1086/514127

Giavridis, T., van der Stegen, S. J. C., Eyquem, J., Hamieh, M., Piersigilli, A., and Sadelain, M. (2018). CAR T Cell-Induced Cytokine Release Syndrome Is Mediated by Macrophages and Abated by IL-1 Blockade. *Nat. Med.* 24 (6), 731–738. doi:10.1038/s41591-018-0041-7

Granucci, F. (2018). The Family of LPS Signal Transducers Increases: The Arrival of Chanzymes. *Immunity* 48 (1), 4–6. doi:10.1016/j.immuni.2017.12.016

Hong, S. S., Choi, J. H., Lee, S. Y., Park, Y. H., Park, K. Y., Lee, J. Y., et al. (2015). A Novel Small-Molecule Inhibitor Targeting the IL-6 Receptor β Subunit, Glycoprotein 130. *J. Immunol.* 195 (1), 237–245. doi:10.4049/jimmunol.1402908

Kim, J. S., Lee, J. Y., Yang, J. W., Lee, K. H., Effenberger, M., Szpirt, W., et al. (2021). Immunopathogenesis and Treatment of Cytokine Storm in COVID-19. *Theranostics* 11 (1), 316–329. doi:10.7150/thno.49713

Koch, R. M., Diavatopoulos, D. A., Ferwerda, G., Pickkers, P., de Jonge, M. I., and Kox, M. (2018). The Endotoxin-Induced Pulmonary Inflammatory Response Is Enhanced during the Acute Phase of Influenza Infection. *Intensive Care Med. Exp.* 6 (1), 15. doi:10.1186/s40635-018-0182-5

Lee, H. R., Park, K. Y., Jeong, Y. J., and Heo, T. H. (2020). Comparative Effectiveness of Different Antiplatelet Agents at Reducing TNF-Driven

Inflammatory Responses in a Mouse Model. *Clin. Exp. Pharmacol. Physiol.* 47 (3), 432–438. doi:10.1111/1440-1681.13211

Liu, G., Chen, S., Hu, A., Zhang, L., Sun, W., Chen, J., et al. (2019). The Establishment and Validation of the Human U937 Cell Line as a Cellular Model to Screen Immunomodulatory Agents Regulating Cytokine Release Induced by Influenza Virus Infection. *Virol. Sin* 34 (6), 648–661. doi:10.1007/s12250-019-00145-w

Ma, M., Zhang, Y., Guo, L. H., Bai, L. P., Jiang, R., and Li, Y. (2015). Suppression Activity and Mechanism of Compound 1487B on TNF-α Expression. *Chin. Pharm. J.* 50 (20), 1806–1810.

Maude, S. L., Barrett, D., Teachey, D. T., and Grupp, S. A. (2014). Managing Cytokine Release Syndrome Associated with Novel T Cell-Engaging Therapies. *Cancer J.* 20 (2), 119–122. doi:10.1097/PPO.0000000000000035

McGonagle, D., Sharif, K., O'Regan, A., and Bridgewood, C. (2020). The Role of Cytokines Including Interleukin-6 in COVID-19 Induced Pneumonia and Macrophage Activation Syndrome-like Disease. *Autoimmun. Rev.* 19 (6), 102537. doi:10.1016/j.autrev.2020.102537

Norelli, M., Camisa, B., Barbiera, G., Falcone, L., Purevdorj, A., Genua, M., et al. (2018). Monocyte-derived IL-1 and IL-6 Are Differentially Required for Cytokine-Release Syndrome and Neurotoxicity Due to CAR T Cells. *Nat. Med.* 24 (6), 739–748. doi:10.1038/s41591-018-0036-4

Qi, X. Q., Zhu, F. C., Zhang, Y., Guo, L. H., Jiang, R., He, Q. Y., et al. (2011). Study of a Novel Compound 2460A with Activities Produced by Fungus. *Yao Xue Xue Bao* 46 (2), 165–169. doi:10.16438/j.0513-4870.2011.02.016

Ragab, D., Salah Eldin, H., Taeimah, M., Khattab, R., and Salem, R. (2020). The COVID-19 Cytokine Storm; What we Know so Far. *Front. Immunol.* 11, 1446. doi:10.3389/fimmu.2020.01446

Scarneo, S. A., Mansourati, A., Eibschutz, L. S., Totzke, J., Roques, J. R., Loiselle, D., et al. (2018). Genetic and Pharmacological Validation of TAK1 Inhibition in Macrophages as a Therapeutic Strategy to Effectively Inhibit TNF Secretion. *Sci. Rep.* 8 (1), 17058. doi:10.1038/s41598-018-35189-7

Schmauder-Chock, E. A., Chock, S. P., and Patchen, M. L. (1994). Ultrastructural Localization of Tumour Necrosis Factor-Alpha. *Histochem. J.* 26 (2), 142–151. doi:10.1007/BF00157963

Shimabukuro-Vornhagen, A., Gödel, P., Subklewe, M., Stemmler, H. J., Schlößer, H. A., Schlaak, M., et al. (2018). Cytokine Release Syndrome. *J. Immunother. Cancer* 6 (1), 56. doi:10.1186/s40425-018-0343-9

Shinya, K., Gao, Y., Cilloniz, C., Suzuki, Y., Fujie, M., Deng, G., et al. (2012). Integrated Clinical, Pathologic, Virologic, and Transcriptomic Analysis of H5N1 Influenza Virus-Induced Viral Pneumonia in the Rhesus Macaque. *J. Virol.* 86 (11), 6055–6066. doi:10.1128/JVI.00365-12

Staedtke, V., Bai, R. Y., Kim, K., Darvas, M., Davila, M. L., Riggins, G. J., et al. (2018). Disruption of a Self-Amplifying Catecholamine Loop Reduces Cytokine Release Syndrome. *Nature* 564 (7735), 273–277. doi:10.1038/s41586-018-0774-y

Su, L., Tu, Y., Kong, D. P., Chen, D. G., Zhang, C. X., Zhang, W. N., et al. (2020). Drug Repurposing of Anti-infective Clinical Drugs: Discovery of Two Potential Anti-Cytokine Storm Agents. *Biomed. Pharmacother.* 131, 110643. doi:10.1016/j.biopha.2020.110643

Tao, G. F., Zhang, S. S., Zhu, L. Y., Li, W., and Liu, W. Z. (2017). Pharmacological Mechanism and Clinical Application of Ulinastatin. *China Pharm.* 28 (35), 5020–5023. doi:10.6039/j.issn.1001-0408.2017.35.34

Tisoncik, J. R., Korth, M. J., Simmons, C. P., Farrar, J., Martin, T. R., and Katze, M. G. (2012). Into the Eye of the Cytokine Storm. *Microbiol. Mol. Biol. Rev.* 76 (1), 16–32. doi:10.1128/MMBR.05015-11

Wang, J. F., Jin, B., and Cao, F. L. (2018). Advances in the Study of Cytokine Release Syndrome Induced by CAR-T Cell Therapy. *J. Chin. Prac. Diag. Ther.* 32 (12), 1228–1231. doi:10.13507/j.issn.1674-3474.2018.12.028

Wang, Q., Zhang, T., Su, F., and Fang, Y. (2018). Research Status of Adverse Reactions of Cytokine Release Syndrome. *Chin. J. Clin. Pharmacol.* 34 (7), 906–909. doi:10.13699/j.cnki.1001-6821.2018.07.049

Ye, Q., Wang, B., and Mao, J. (2020). The Pathogenesis and Treatment of the 'Cytokine Storm' in COVID-19. *J. Infect.* 80 (6), 607–613. doi:10.1016/j.jinf.2020.03.037

Zhang, C., Wu, Z., Li, J. W., Zhao, H., and Wang, G. Q. (2020). Cytokine Release Syndrome in Severe COVID-19: Interleukin-6 Receptor Antagonist Tocilizumab May be the Key to Reduce Mortality. *Int. J. Antimicrob. Agents* 55 (5), 105954. doi:10.1016/j.ijantimicag.2020.105954

Zhang, H. Y., Xie, X., Zhang, K. J., and Hu, J. (2013). Effects of Cytokine Storm on Influenza Virus Infection and its Prevention and Treatment. *Chin. J. Cell Mol. Imm.* 29 (5), 556–559. doi:10.13423/j.cnki.cjcmi.006831

Zhang, S. C., and Cao, Z. W. (2003). "Structure and Biogenetic Characteristics of Endotoxin," in *Endotoxin Basic and Clinical*. (Beijing: Science Press), 1–21.

Zhang, Y., Wang, L., Bai, L., Jiang, R., Guo, L., Wu, J., et al. (2016). Effect of Ebosin on Modulating Interleukin-1β-Induced Inflammatory Responses in Rat Fibroblast-like Synoviocytes. *Cell Mol. Immunol.* 13, 584–592. doi:10.1038/cmi.2015.36

Zhang, Y. L., and Jiang, C. Y. (2015). Cytokine Storms: the Dominant Hand in Acute Respiratory Distress Syndrome. *Life Sci.* 27 (5), 554–557. doi:10.13376/j.cbls/2015073

Zhang, Y., Wang, L. F., Bai, J. Y., Guan, M. Z., Jiang, R., Guo, L. H., et al. (2013). Anti-Inflammatory Effect of Ebosin on Rat Collagen-Induced Arthritis through Suppressing Production of Interleukin-1β, Interleukin-6 and Tumor Necrosis Factor-α. *Eur. J. Inflamm.* 11, 697–708. doi:10.1177/1721727x1301100313

Zhao, X., Qi, X., Lian, W., Tong, X., Wang, H., Su, L., et al. (2020). Trichomicin Suppresses Colorectal Cancer via Comprehensive Regulation of IL-6 and TNFα in Tumor Cells, TAMs, and CAFs. *Front. Pharmacol.* 11 (11), 386. doi:10.3389/fphar.2020.00386

Zhu, F., Zhao, X., Li, J., Guo, L., Bai, L., and Qi, X. (2020). A New Compound Trichomicin Exerts Antitumor Activity through STAT3 Signaling Inhibition. *Biomed. Pharmacother.* 121, 109608. doi:10.1016/j.biopha.2019.109608

Zou, Y., Fan, L., Xu, W., and Li, J. Y. (2017). Progress of Cytokine Release Syndrome Caused by Chimeric Antigen Receptor T-Cell Immunotherapy. *J. Leuk. Lymph.* 26 (11), 697–701. doi:10.3760/cma.j.issn.1009-9921.2017.11.016

Zusso, M., Lunardi, V., Franceschini, D., Pagetta, A., Lo, R., Stifani, S., et al. (2019). Ciprofloxacin and Levofloxacin Attenuate Microglia Inflammatory Response via TLR4/NF-kB Pathway. *J. Neuroinflamm.* 16 (1), 148. doi:10.1186/s12974-019-1538-9

Conflict of Interest: The authors declare that the research was conducted in the absence of any commercial or financial relationships that could be construed as a potential conflict of interest.

Publisher's Note: All claims expressed in this article are solely those of the authors and do not necessarily represent those of their affiliated organizations, or those of the publisher, the editors and the reviewers. Any product that may be evaluated in this article, or claim that may be made by its manufacturer, is not guaranteed or endorsed by the publisher.

frontiers in Pharmacology

ORIGINAL RESEARCH
published: 18 January 2022
doi: 10.3389/fphar.2021.773150

Autophagy Induced by Micheliolide Alleviates Acute Irradiation-Induced Intestinal Injury *via* Inhibition of the NLRP3 Inflammasome

Dong-ming Wu[1,2,3†], Jing Li[2,3†], Rong Shen[1†], Jin Li[2,3], Ye Yu[2,3], Li Li[2,3], Shi-hua Deng[2,3], Teng Liu[2,3], Ting Zhang[2,3], Ying Xu[2,3] and De-gui Wang[1]**

[1]School of Basic Medical Sciences, Lanzhou University, Lanzhou, China, [2]The First Affiliated Hospital of Chengdu Medical College, Chengdu, China, [3]School of Clinical Medicine, Chengdu Medical College, Chengdu, China

Radiation-induced enteropathy (RIE) is one of the most common and fatal complications of abdominal radiotherapy, with no effective interventions available. Pyroptosis, a form of proinflammatory regulated cell death, was recently found to play a vital role in radiation-induced inflammation and may represent a novel therapeutic target for RIE. To investigate this, we found that micheliolide (MCL) exerted anti-radiation effects *in vitro*. Therefore, we investigated both the therapeutic effects of MCL in RIE and the possible mechanisms by which it may be therapeutic. We developed a mouse model of RIE by exposing C57BL/6J mice to abdominal irradiation. MCL treatment significantly ameliorated radiation-induced intestinal tissue damage, inflammatory cell infiltration, and proinflammatory cytokine release. In agreement with these observations, the beneficial effects of MCL treatment in RIE were abolished in *Becn1*$^{+/-}$ mice. Furthermore, super-resolution microscopy revealed a close association between NLR pyrin domain three and lysosome-associated membrane protein/light chain 3-positive vesicles following MCL treatment, suggesting that MCL facilitates phagocytosis of the NLR pyrin domain three inflammasome. In summary, MCL-mediated induction of autophagy can ameliorate RIE by NLR pyrin domain three inflammasome degradation and identify MCL as a novel therapy for RIE.

Keywords: autophagy, irradiation-induced intestinal injury, NLR pyrin domain 3, micheliolide, pyroptosis

OPEN ACCESS

Edited by:
Nandakumar Natarajan, University of California, San Francisco, United States

Reviewed by:
StalinRaja MaruthaMuthu, University of California, San Francisco, United States
Wei Chen, Stanford University, United States

***Correspondence:**
Ying Xu
yingxu825@126.com
De-gui Wang
wangdegui@lzu.edu.cn

[†]These authors have contributed equally to this work

Specialty section:
This article was submitted to Inflammation Pharmacology, a section of the journal Frontiers in Pharmacology

Received: *09 September 2021*
Accepted: *20 December 2021*
Published: *18 January 2022*

Citation:
Wu D-m, Li J, Shen R, Li J, Yu Y, Li L, Deng S-h, Liu T, Zhang T, Xu Y and Wang D-g (2022) Autophagy Induced by Micheliolide Alleviates Acute Irradiation-Induced Intestinal Injury via Inhibition of the NLRP3 Inflammasome. Front. Pharmacol. 12:773150. doi: 10.3389/fphar.2021.773150

INTRODUCTION

Radiotherapy is an important treatment strategy for several malignancies including lung cancer, prostate cancer, and renal cell carcinoma. However, despite significant improvements in radiotherapy delivery methods, incidence of irradiation induced bowel disease is a huge challenge for clinical, exposure to radiation causes lesions, which can result in several complications such as hematopoietic and gastrointestinal dysfunction and death (Seong, 2009; Hazell et al., 2020; Miccio et al., 2020; Sipaviciute et al., 2020; Molitoris et al., 2021). The small intestine is a highly radiosensitive organ, and radiation-induced enteropathy (RIE) tends to emerge quickly after radiation exposure. To date, RIE remains the most common and severe complication of the treatment of abdominal malignancies (Nussbaum et al., 1993; Lu et al., 2019). The well-known symptoms of RIE, including gastrointestinal hemorrhage, endotoxemia, bacterial infection, anorexia,

nausea, vomiting, diarrhea, and loss of electrolytes and fluid, limit the therapeutic potential of radiotherapy in patients with abdominal malignancies and prevent further use of fractionated radiotherapy (Shadad et al., 2013; Hauer-Jensen et al., 2014). Patients with RIE appear nausea and vomiting, abdominal pain and diarrhea, tenesmus and other clinical symptoms, significantly reduce the life quality of patients, even cause serious complications such as colon stenosis, intestinal fibrosis and aggravate patients, greatly restricts the implementation of radiotherapy for patients with malignant tumors (Takemura et al., 2018; Akahane et al., 2020). Currently, the pathogenesis of RIE remains unclear, and there are no effective clinical interventions. Therefore, it is increasingly necessary to develop novel radioprotective agents with fewer adverse effects to protect patients from RIE.

The nucleotide-binding domain, leucine-rich repeat-containing receptor contains the NLR pyrin domain 3 (NLRP3) inflammasome, which is a cytosolic sensor of pathogens and endogenous damage-associated molecular patterns (Jiang et al., 2020; Seoane et al., 2020). Upon activation, NLRP3 facilitates the assembly of the apoptosis-associated speck-like protein containing a caspase recruitment domain (ASC) and the cysteine protease caspase-1 (Wang and Hauenstein, 2020). The formation of this complex cleaves the precursor of caspase-1 (pro-casp1) to its active form, caspase-1 (casp1-p20), and induces the cleavage of gasdermin D (GSDMD). This cascade results in pore formation on the plasma membrane and mediates a process known as pyroptosis (He et al., 2015; Ives et al., 2015). Pyroptosis is an inflammatory programmed cell death event that is distinct from apoptosis (Tang et al., 2020; Yu et al., 2021). Cells that undergo pyroptosis swell, release cytosolic contents, and release damage-associated molecular pattern molecules such as adenosine triphosphate, DNA, and the proinflammatory cytokines interleukin (IL)-18 and IL-1β into the extracellular milieu, thus initiating an inflammatory cascade in the affected tissue (Shi et al., 2017). Accumulating evidence suggests that NLRP3 inflammasome-mediated pyroptosis participates in radiation-induced damage and thus could be a novel therapeutic target for the treatment of RIE (Wei et al., 2019).

Autophagy is an intracellular self-digestive process that can deliver damaged organelles or proteins from the cytoplasm to lysosomes for degradation in order to maintain cellular homeostasis in response to external stimuli (Eskelinen, 2019; Haq et al., 2019; Pohl and Dikic, 2019). Numerous environmental stimuli, such as starvation or organelle damage, can induce autophagy (Haq et al., 2019). There is a growing appreciation that autophagy negatively regulates the activation of the NLRP3 inflammasome, thereby inhibiting inflammatory responses and reducing inflammatory injury of tissues in a disease state (Mehto et al., 2019; Fu et al., 2020; Peng et al., 2021). For example, it has been demonstrated that autophagy induced by the Axl receptor tyrosine kinase alleviates acute liver injury *via* inhibition of the NLRP3 inflammasome in mice (Han et al., 2016). Furthermore, administration of hydrogen-rich saline alleviated hyperpathia and microglial activation *via* autophagy-mediated inhibition of the NLRP3 inflammasome in a rat model of neuropathic pain (Chen et al., 2019). Collectively, these reports suggest that the modulation of autophagy in inflammatory conditions may be a novel strategy against RIE.

Radiation protective drugs for the prevention or treatment of RIE can significantly improve the life quality of patients (Wu et al., 2018). 441 compounds in Pyroptosis Compound Library (Selleck) was used in order to screening radiation protective drugs. Of which, Micheliolide (MCL) presents the strongest protective effect. MCL, isolated from the Michelia compressa and Michelia champaca plants, is a natural guaianolide sesquiterpene lactone derivative of parthenolide, and has shown promising anti-inflammatory, immunomodulatory, and therapeutic efficacy against multiple forms of cancer (Qin et al., 2016; Jiang et al., 2017; Sun et al., 2017). A previous study showed that MCL blocks doxorubicin-induced cardiotoxicity by ameliorating inflammation and necrosis through the repression of the PI3K/Akt/NF-kB signaling pathway (Kalantary-Charvadeh et al., 2019). Moreover, it was recently reported that MCL induces upregulation of peroxisome proliferator-activated receptor-γ expression, thereby alleviating NF-κB-mediated inflammation and activating autophagy in liver steatosis (Zhong et al., 2018). Based on these promising findings and the critical role that inflammation plays in RIE progression, we postulated that MCL may also play a promising role in the treatment of RIE. In the present study, we investigated the therapeutic effects of MCL in RIE, and evaluated the possible mechanisms by which it may be therapeutic.

MATERIALS AND METHODS

Reagents

Pyroptosis Compound Library (L7400) were purchased from Selleck (Houston, TX, United States). Primary antibodies against NLRP3 (ab4207), GSDMD N-terminus (GSDMD-N; ab215203), caspase-1 (ab179515), LAMP-1 (ab208943), ASC (ab127537), P62 (ab109012), and beclin 1 (ab207612) were obtained from Abcam (Cambridge, MA, United States). The anti-light chain 3 (LC3) primary antibody (FNab04716) was obtained from Abcam Fine Test (Beijing, China). The horseradish peroxidase-conjugated secondary antibody (SA00001-1) and anti-glyceraldehyde-3-phosphate dehydrogenase antibody (60004-1-1g) were purchased from Proteintech (Wuhan, China). The following immunoglobulinG (H + L) antibodies were purchased from Beyotime Biotechnology (Shanghai, China): Cy3-labeled goat anti-rabbit (A0516), Cy3-labeled goat anti-mouse (A0521), Alexa Fluor 488-labeled goat anti-rabbit (A0423), and Alexa Fluor 488-labeled goat anti-mouse (A0428).

Cell Culture and Radiation Treatment

The human intestinal epithelial cell (HIEC) line was purchased from the Cell Bank of the Chinese Academy of Sciences (Shanghai, China) and cultured in RPMI-1640 medium (Hyclone, Hudson, NH, United States) containing 10% fetal bovine serum and 1% penicillin-streptomycin in an incubator at 37°C, containing 5% carbon dioxide (CO_2). Cells were treated

with the desired dose (0, 5, 10, or 20 Gy) of X-ray irradiation at a rate of 2 Gy/min. Cell viability and lactate dehydrogenase (LDH) release assays were performed after irradiation for 24 or 48 h. In some experiments, HIECs were pretreated with different concentrations (0, 2.5, 5, or 10 μM) of MCL (Houston, TX, United States; s9309) for 2 h, and exposed to 10 Gy radiation. After 48 h, cell viability, LDH release, flow cytometry assays, and propidium iodide (PI) staining assays were performed.

Cell Viability Analysis of an FDA-Approved Compound Library

A high throughput pyroptosis drug library was purchased from Selleck Chemicals (Houston, TX, United States). Compounds were stored as 10 mM stock solutions in dimethyl sulfoxide at 4 °C until use. HIECs in the logarithmic growth phase were plated in a 96-well plate at a density of 5 × 103 cells per well and incubated overnight in a cell incubator at 37°C and 5% CO_2. Cells were treated with 10 μM of a compound for 2 h and then exposed to 10 Gy radiation. After 48 h, cell viability was measured using the cell counting kit-8 (Shanghai, China). Candidate drugs were selected based on the average cell viability in the replicate wells.

LDH Release Assay

HIECs in the logarithmic growth phase were inoculated in a 96-well plate at a density of 5 × 103 cells per well and incubated overnight in a cell incubator at 37°C and 5% CO_2. After receiving the corresponding treatment, LDH release assay was checked according to the operation steps of the LDH Cytotoxicity Assay Kit (Shanghai, China) instructions.

Flow Cytometry

HIEC viability was measured by flow cytometry using an Annexin V-FITC/PI apoptosis detection kit (KeyGEN, Jiangsu, China; KGA1015-1018), as previously described (Li et al., 2020).

PI Staining

HIECs were pretreated with different concentrations (0, 2.5, 5, or 10 μM) of MCL for 2 h and exposed to 10 Gy radiation. After 48 h, a PI solution (Shanghai, China) was added to the medium and further incubated for 30 min at 37°C in the dark.

Animals and Irradiation

Wild-type (WT), *Nlrp3*$^{-/-}$, and *Becn1*$^{+/-}$ mice on a C57BL/6J background were purchased from Beijing Weishanglide Biotechnology Co., Ltd. All mice were housed under the following conditions: 12-h light/dark cycle (lights on: 7:00, lights off: 19:00), temperature of 22 ± 2°C, humidity of 50 ± 10%, and standard diet and water. The WT mice were divided into the following groups (n = 15 per group): control, irradiation (IR), MCL (50 mg/kg), and MCL (10, 20, and 50 mg/kg)+IR. All *Nlrp3*$^{-/-}$ and *Becn1*$^{+/-}$ mice received IR either with or without MCL (50 mg/kg; n = 15 per group). An X-RAD 160-225 instrument (Precision X ray Inc, Branford, CT, United States; filter: 2 mm, AI; 42 cm, 225 kv/s, 12.4 mA, and 2.0 Gy/min) was used for abdominal irradiation. Except for the control and MCL groups, all other groups were exposed to 10 Gy radiation.

MCL Treatment

For drug-treated groups, MCL was injected intraperitoneally (10, 20, and 50 mg/kg) 2 h before IR, and again daily for 5 days following IR. Mice were weighed every other day, and survival was recorded for 14 days. On day 8, the mice were sacrificed, and their serum was collected. The mice were then carefully and quickly dissected on ice trays, and their small intestines were removed to be used for subsequent analyses.

Enzyme-Linked Immunosorbent Assay of Inflammatory Cytokines

Cell culture supernatant and mouse serum were collected, and the levels of IL-1β, IL-18, TNF-α, TGF-β1 and IFN-γ were detected using Enzyme-linked Immunosorbent assay kits (Shanghai, China) according to the kit instructions.

Caspase-1 Activity Assay

Caspase-1 activity in mouse intestinal tissue was detected using the caspase-1 activity assay kit (Shanghai, China).

Western Blotting

Protein samples were resolved by sodium dodecyl sulfate polyacrylamide gel electrophoresis (SDS-PAGE) on 12% gels, transferred to nitrocellulose membranes, blocked for 1 h at room temperature using Tris-buffered saline containing 0.1% Tween 20 and 5% fat-free milk, and probed with primary antibodies for 18 h at 4°C. Membranes were then stained at 37°C for 1 h with secondary antibodies conjugated with horseradish peroxidase, and immunoreactive signals were detected by enhanced chemiluminescence (SuperSignal; Pierce, Rockford, IL, United States). Protein signals were detected using the Chemi Doc XRS instrument plus Image Lab Software.

Co-Immunoprecipitation Assays

The intestinal tissue lysates were incubated with primary antibody and shaken slowly overnight at 4°C. The next day, protein A + G agarose was added and shaken slowly at 4°C for 3 h. The samples were centrifuged, and the supernatant was aspirated. The pellet was washed five times with phosphate-buffered saline (PBS) containing 1× phenylmethyl-sulfonyl fluoride protease inhibitors. The supernatant was aspirated, and the pellet was resuspended in 1×SDS-PAGE electrophoresis loading buffer and incubated in a boiling water bath for 5 min. Samples were then used for SDS-PAGE electrophoresis.

Hematoxylin and Eosin (H&E) Staining and Immunohistochemistry (IHC)

The small intestine tissue was fixed in 4% paraformaldehyde and embedded in paraffin after dehydration. Sections 4–6 μm thick were used for H&E staining or IHC. The sections were stained according to the instructions for the H&E staining kit (Beijing, China).

IHC was performed using an SPlink Detection Kit (ZSGB-BIO Technology Co., Ltd, Beijing, China). In short, the sections were

deparaffinized and rehydrated, followed by antigen retrieval. Hydrogen peroxide was added to block the activity of endogenous peroxidase, and 5% goat serum was added dropwise for blocking. Sections were incubated in the primary antibody overnight at 4°C. The sections were the incubated at room temperature in peroxidase-labeled universal secondary antibody. Sections were then developed and counter-stained, and five high-powered field of view (10 × 40) images were randomly taken for each sample.

Immunofluorescence (IF)

Sections were prepared as described above, and were then deparaffinized and rehydrated. Sections were blocked with 5% goat serum for 30 min at room temperature; thereafter, they were incubated overnight with the NLRP3 (1:100) and ASC (1:100) primary antibodies at 4°C. The next day, after washing with PBS, the sections were incubated in fluorescence-labeled secondary antibody solution for 2 h at 37°C, and washed again in PBS before staining with 4′,6-dimidyl-2-phenylindole for 5 min. Finally, slices were washed with PBS three times (5 min each time) and treated with anti-fluorescence quenching and sealing tablets. An Olympus inverted fluorescence microscope was used to capture fluorescence images over time.

Confocal Microscopy

HIECs were seeded on sterile coverslips in a 24-well plate. MCL (50 pg/ml) was added to the wells for 2 h, followed by 10 Gy radiation treatment. IF staining was performed 48 h later, followed by 4',6-dimidyl-2-phenylindole counterstaining. A confocal laser scanning microscope was used to collect the images.

Cell Transfections

For NLRP3 silencing, HIEC cells were transfected with NLRP3 small interfering RNA (5′-AGAAATGGATTGAAGTGAAA-3′; RIBOBIO, Guangzhou, China), following the manufacturer's instructions. The Opti-MEM (Gibco, Grand Island, NY, United States) transfection medium was replaced with a complete culture medium 5 h after transfection. All experiments were performed 48 h after transfection. The expression of NLRP3 was measured by real-time quantitative polymerase chain reaction (PCR).

Real Time Fluorescent Quantitative PCR

Total RNA was extracted using an RNAprep FastPure kit (TSP413, TSINGKE, Shanghai, China), according to the manufacturer's instructions. Total RNA was then reverse-transcribed using an RT6 cDNA synthesis kit (TSK302M, TSINGKE, Shanghai, China) to synthesize complementary DNA. Real-time fluorescent quantitative PCR was performed using a CFX96 Real-time System (Bio-Rad) with SYBR Green I (TSE202, TSINGKE, Shanghai, China). The 2-ΔΔCT method was used to calculate relative expression levels. The primer sense and antisense sequences were as follows: β-actin: 5′-CCTGGCACCCAGCACAAT-3′(sense); 5′-GGGCCGGAC TCGTCATAC-3′ (anti-sense). β-actin was used as an internal control for quantification. For NLRP3: F, 5′-GAGCTGGACCTCAGTGACAATGC-3′(sense); R, 5′-ACC AATGCGAGATCCTGACAACAC-3′ (antisense).

Statistical Analysis

All experiments were repeated independently at least three times. All animals were randomly assigned to experimental groups. Survival was analyzed using a log-rank test. Statistical significance among groups was determined using one-way analysis of variance or paired t-tests. Statistical significance was set at $p < 0.05$. Statistical analyses were performed using GraphPad Prism 7 (GraphPad Software, Inc, La Jolla, CA, United States).

RESULTS

MCL Protects Against Ionizing Radiation in HIECs

To identify compounds with radioprotective effects, we first established a radiation-induced cell damage model in HIECs. We observed that cell viability was significantly decreased in a dose-dependent manner following treatment with radiation for 24, 48, or 72 h (**Figure 1A**, and lactate dehydrogenase (LDH) release increased in a time-and dose-dependent manner (**Figure 1B**). From these data, we chose a radiation dose of 10 Gy and a time point of 48 h for all subsequent experiments.

Next, we used the radiation-induced cell damage model to screen the compounds in the pyroptosis drug library. Among the 441 tested compounds, MCL elicited the strongest reversal of the reduced cell viability observed following radiation exposure (**Figure 1C**). Therefore, MCL was used in the subsequent experiments.

To further analyze the radioprotective effects of MCL, we pretreated HIECs with different concentrations of MCL prior to radiation exposure. Our results showed that cell viability with MCL exposure increased and LDH release decreased in a dose-dependent manner (**Figure 1D,E**). Furthermore, secretion of the inflammatory factors IL-18 and IL-1β decreased in a dose-dependent manner (**Figure 1F,G**). Moreover, the flow cytometry and PI staining indicate that 10 μM MCL is the most effective dose for promoting cell survival (**Figure 1H,I**). Altogether, these results indicate a protective role of MCL against radiation-induced cell damage.

MCL Attenuates Radiation-Induced Intestinal Toxicity and Inflammatory Responses in Mice

First, we tested the effect of MCL on the survival of WT C57BL/6 mice treated with a 10 Gy radiation dose. Mice in the IR group began to die by the ninth day after irradiation, with a survival rate of 26.6% on the 14th day (**Figure 2A**). The survival rates of MCL (10, 20, and 50 mg/kg) groups reached 26.7, 46.7, and 60%, respectively. Moreover, the survival rate of MCL 50 mg/kg group was significantly higher than that of other groups ($p < 0.001$; **Figure 2A**). Radiation-induced intestinal injury is characterized by diarrhea, sparse stools, and visible blood in

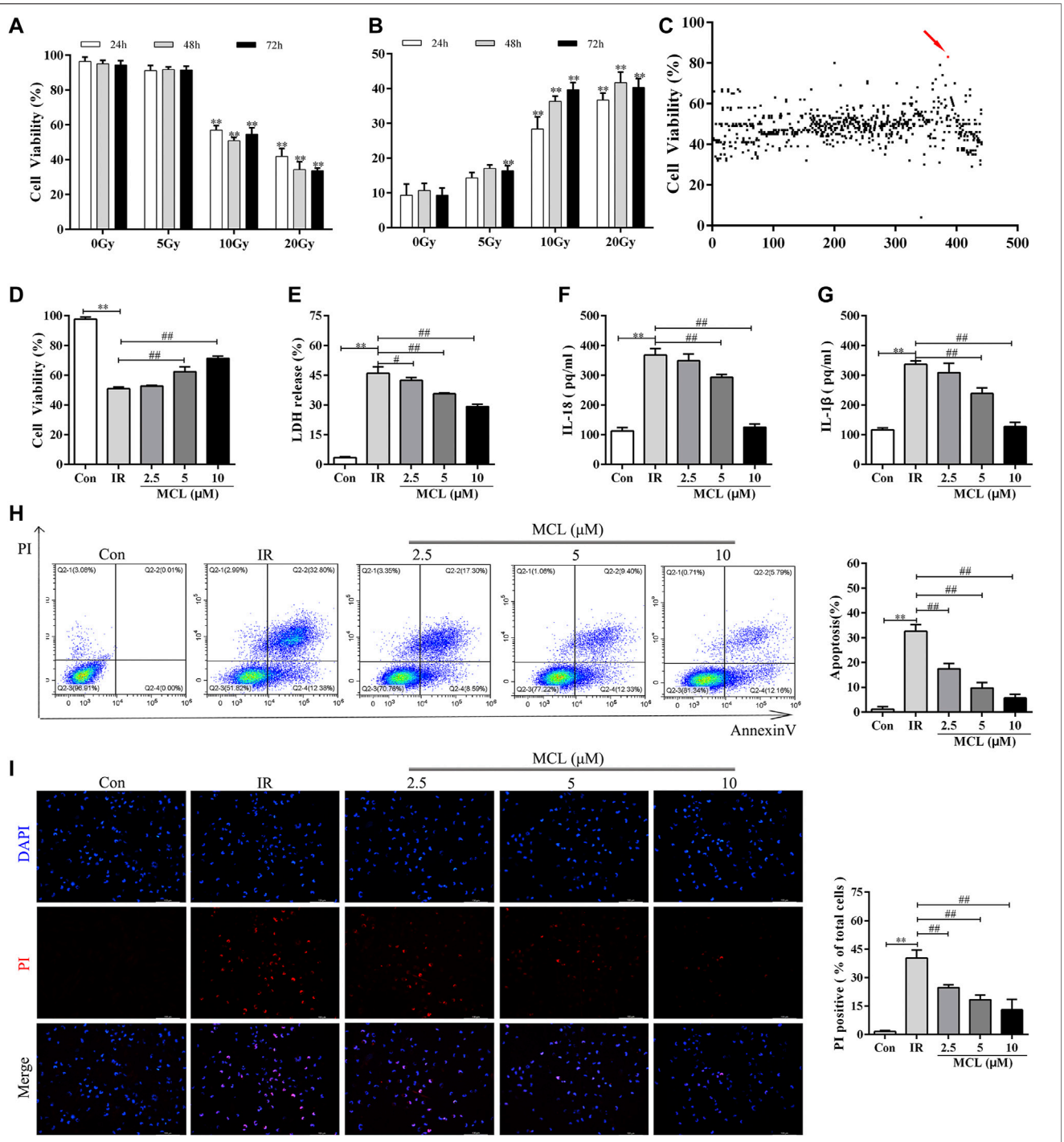

FIGURE 1 | MCL protects against radiation in HIECs **(A)** Cell viability was significantly decreased in a dose-dependent manner following treatment with radiation (0, 5, 10, or 20 Gy) for 24, 48, or 72 h **(B)** LDH release increased in a time-and dose-dependent manner following radiation (0, 5, 10, or 20 Gy) **(C)** Cells were treated with 10 μM of the drug candidate library for 2 h and then exposed to radiation (10 Gy). Cell viability of HIECs exposed to the drug candidate library. Each point represents the percentage of cell viability of the compounds at a concentration of 10 μM **(D)** MCL increased cell viability following radiation (10 Gy) in a dose-dependent (0, 2.5, 5, or 10 μM) manner **(E)** MCL decreased LDH release following radiation (10 Gy) in a dose-dependent (0, 2.5, 5, or 10 μM) manner **(F)** MCL decreased cell culture supernatant IL-18 release following radiation (10 Gy) in a dose-dependent (0, 2.5, 5, or 10 μM) manner **(G)** MCL decreased cell culture supernatant IL-1β release following radiation (10 Gy) in a dose-dependent (0, 2.5, 5, or 10 μM) manner **(H)** HIECs were pretreated with different concentrations (0, 2.5, 5, or 10 μM) of MCL for 2 h and exposed to 10 Gy radiation. Representative flow cytometry scatter plots **(I)** HIECs were pretreated with different concentrations (0, 2.5, 5, or 10 μM) of MCL for 2 h and exposed to 10 Gy radiation. Representative propidium iodide staining fluorescence image. *$p < 0.05$, **$p < 0.01$, ***$p < 0.001$, ****$p < 0.0001$, two-tailed Student's t-test. HIEC, human intestinal epithelial cell; LDH, lactate dehydrogenase; MCL, micheliolide; IL, interleukin.

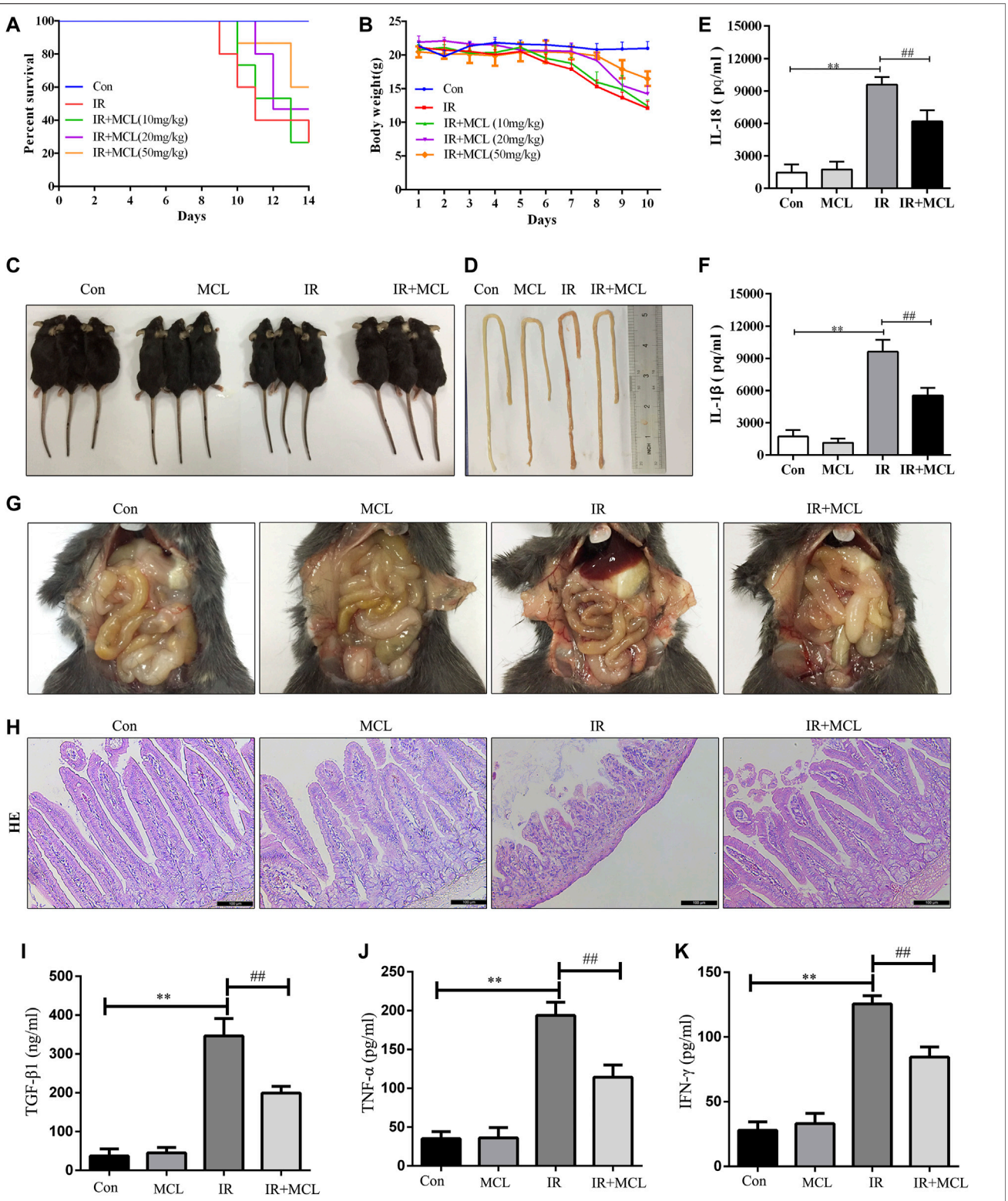

FIGURE 2 | Micheliolide (MCL) attenuates radiation-induced intestinal toxicity and inflammatory responses in wild-type (WT) mice **(A)** Survival curves of all experimental groups following radiation **(B)** Weight loss following radiation exposure **(C)** Representative images of mice following radiation **(D, G)** Representative macroscopic appearance of the small intestine following radiation with MCL treatment **(E)** Serum interleukin (IL)-18 levels **(F)** Serum IL-1β levels **(I)** Serum TGF-β1 levels **(J)** Serum TNF-α levels **(K)** Serum IFN-γ levels **(H)** Representative intestinal hematoxylin and eosin staining. Con, untreated WT mice; IL, interleukin; IR, irradiation group; MCL (10 mg/kg)+ IR, mice pre-treated with MCL (10 mg/kg) prior to irradiation; MCL (20 mg/kg)+ IR, mice pre-treated with MCL (20 mg/kg) prior to irradiation; MCL (50 mg/kg)+ IR, mice pre-treated with MCL (50 mg/kg) prior to irradiation; MCL + IR, mice pre-treated with MCL (50 mg/kg) prior to irradiation; and MCL, mice treated with MCL (50 mg/kg) without irradiation. N = 15/group. $^{*}p < 0.05$, $^{**}p < 0.01$, $^{***}p < 0.001$, $^{****}p < 0.0001$, two-tailed Student's t-test.

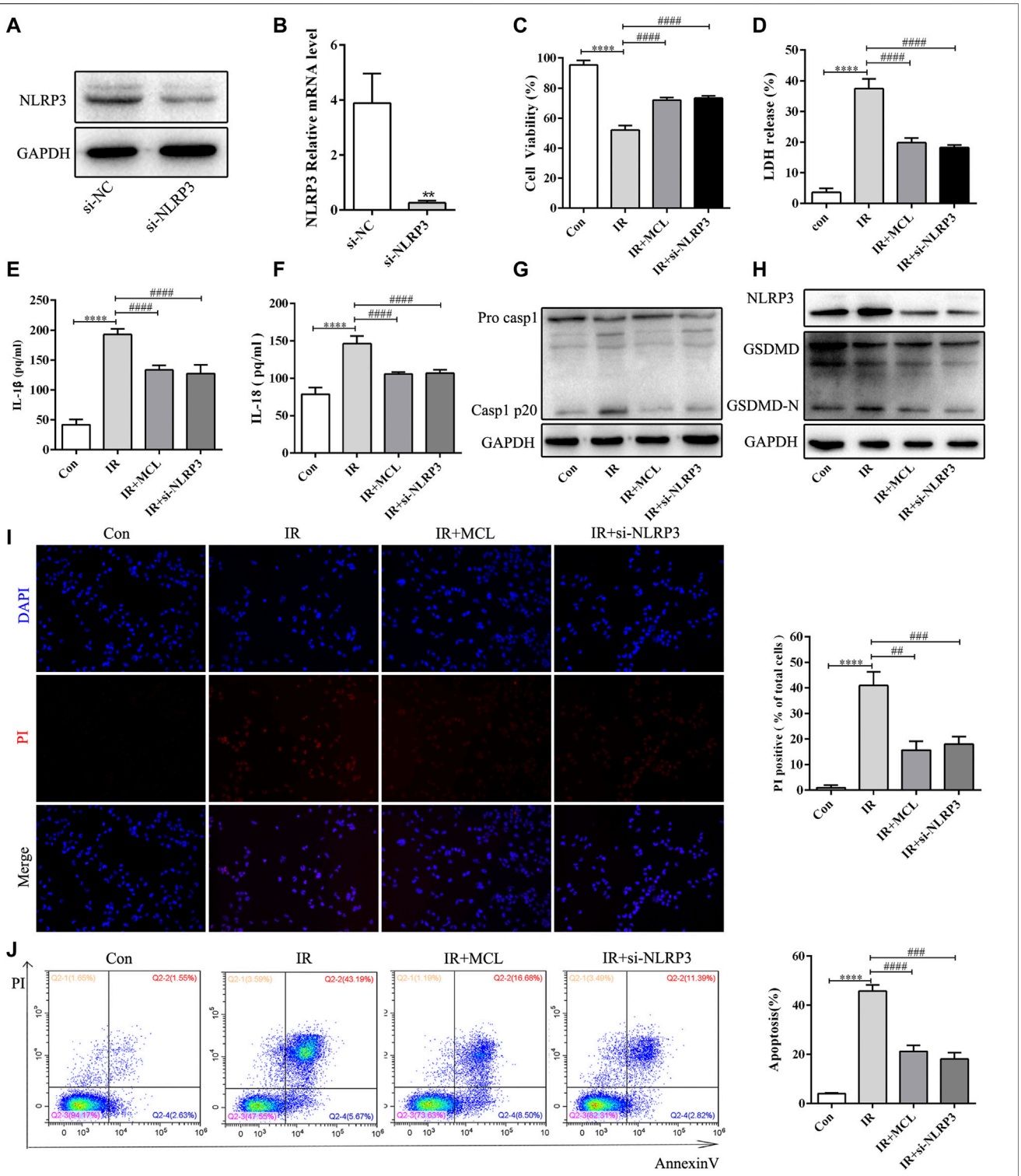

FIGURE 3 | Micheliolide (MCL) inhibits radiation-induced NLRP3 inflammasome-dependent pyroptosis *in vitro* **(A,B)** Expression of NLRP3 in control (Ctl) and NLRP3-silenced (si-NLRP3) cells was detected by western blotting and quantitative real-time polymerase chain reaction **(C)** Cell viability was significantly increased by MCL (10 μM) treatment and NLRP3 knockout manner following treatment with radiation (10 Gy) for 48 h **(D)** LDH release was significantly decreased by MCL (10 μM) treatment and NLRP3 knockout manner following treatment with radiation (10 Gy) for 48 h **(E)** Cell culture supernatant IL-1β levels **(F)** Cell culture supernatant IL-18 levels **(G,H)** Expression of pro-casp1, casp1 p20, NLRP3, GSDMD, and GSDMD-N in si-NLRP3 cells and si-NC cells treated with MCL (10 μM) following irradiation (10 Gy) **(I)** Representative propidium iodide staining fluorescence image **(J)** Representative flow cytometry scatter plots. $^{*}p < 0.05$, $^{**}p < 0.01$, $^{***}p < 0.001$, $^{****}p < 0.0001$, two-tailed Student's t-test. IL, interleukin; NLRP3, nucleotide binding domain leucine-rich repeat-containing receptor-pyrin domain containing three; GSDMD, gasdermin D.

the stool, which leads to significant weight loss. We observed that weight loss after radiation exposure was significantly attenuated in the MCL (50 mg/kg)+IR mice (**Figure 2B,C**). Therefore, an MCL dose of 50 mg/kg was used in subsequent experiments.

In the IR mice, histology, H&E staining revealed pathological changes including mucosal injury, necrosis, loss of tissue structure, edema, and inflammatory cell infiltration when compared with the control group (**Figure 2D,H**). MCL treatment significantly improved these pathological changes (**Figure 2D,G,H**). Furthermore, enzyme-linked immunosorbent assay analysis demonstrated that the secretion of IL-1β, IL-18,TGF-β1,TNF-αand IFN-γ in the blood was lower in the MCL (50 mg/kg)+IR group than the IR-group (**Figure 2E,F,I–K**). Altogether, these results suggest that MCL reduces the damage and inflammation caused by RIE. Importantly, MCL (50 mg/kg) administered alone without radiation had no significant effects on intestinal tissue, suggesting that there are no adverse effects of our experimental dose of MCL.

MCL Inhibits Radiation-Induced NLRP3 Inflammasome-dependent Pyroptosis *in vitro*

To establish whether the activation of the NLRP3 inflammasome is involved in the underlying mechanism of RIE, we identified an effective RNAi oligonucleotide to silence NLRP3 expression in HIEC cells. We generated NLRP3-knockdown HIEC cell lines. NLRP3 knockdown was confirmed by western blot and real-time quantitative PCR (**Figure 3A,B**). We exposed HIEC/si-NLRP3 cells to 10 Gy of radiation and observed the cell viability after 48 h, and at the same time, detected the production of LDH, IL-1β, and IL-18 in the supernatant after 48 h. As expected, the HIEC/IR cell viability was significantly decreased (**Figure 3C**); the levels of LDH, IL-1β, and IL-18 in the HIEC/IR cells supernatant were dramatically increased compared with those in the control cells, whereas opposite effects were observed in HIEC/IR/si-NLRP3 cells and HIEC/IR/MCL (**Figure 3D–F**). In addition, GSDMD, which is essential for NLRP3-mediated pyroptosis, was cleaved by active caspase-1. In our study, we found that NLRP3 knockdown and MCL treatment suppressed the expression levels of active caspase-1 and GSDMD-N proteins (**Figure 3H**). PI staining also showed that IR exposure increased PI uptake by HIEC, and this increase was reduced by NLRP3 knockdown and MCL treatment (**Figure 3I**). Radiation-induced NLRP3 inflammasome-dependent pyroptosis was further confirmed by the flow cytometry results, which showed the inhibitory effect of MCL treatment on the proportion of double-positive HIEC (**Figure 3J**).

MCL Inhibits Radiation-Induced NLRP3 Inflammasome-dependent Pyroptosis in Mice

To establish whether the activation of the NLRP3 inflammasome is involved in the pathogenesis of RIE, NLRP3−/− and WT mice were administered abdominal radiotherapy at a dose of 10 Gy. NLRP3−/− mice exhibited significantly reduced inflammation following radiation than their WT counterparts (**Figure 4A**). **Figure 4** show that after radiation of *NLRP3* knockout mice, the levels of IL-1β, IL-18, TGF-β1, TNF-α and IFN-γ (**Figure 2B–F**) in the blood were significantly lower in $NLRP3^{-/-}$ mice than in WT mice after radiation. These results indicate that the activation of the NLRP3 inflammasome contributes to the inflammation observed in RIE and may promote RIE progression after irradiation.

Next, we evaluated whether MCL exerted anti-inflammatory effects through inhibition of the NLRP3 inflammasome. As shown in **Figure 4**, the activity of caspase-1 (**Figure 4G**)and the expression of cleaved caspase-1 and GSDMD-N proteins (**Figure 4H**) were significantly increased in IR-treated WT mice. MCL-treated WT mice and $NLRP3^{-/-}$ mice exhibited reduced expression of these proteins after radiation. In addition, co-immunoprecipitation assays revealed that the NLRP3-ASC complex was increased significantly in the intestinal tissue of IR-treated WT animals (**Figure 4I**). This finding was confirmed with IF, in which the number of cells positive for both NLRP3 and ASC was increased in IR-treated animals (**Figure 4J**). MCL-treated WT animals and NLRP3−/− mice exhibited a significantly reduced assembly of the NLRP3 inflammasome following radiation (**Figure 4I,J**).

MCL Enhances Autophagy in Mice Intestinal Tissue and HIECs After Radiotherapy

To further explore whether MCL can regulate autophagy, we performed IF to detect the aggregation of the autophagosome component LC3. When compared with IR-only HIEC, the aggregation levels of LC3 significantly increased in the MCL + IR group (**Figure 5A**). Transmission electron microscopy was employed to detect autophagosomes and autolysosomes in the HIEC and the intestinal tissue. The number of autophagosomes was increased in the MCL + IR group compared with IR-only HIEC and mice (**Figure 5B,E**). In addition, we performed western blot to detect the expression levels of autophagy markers LC3, p62, and beclin 1 in the HIEC. The levels of LC3 and beclin 1 were higher, and levels of p62 were lower in the HIEC of MCL + IR-treated than in the HIEC of IR-treated, indicating that MCL treatment significantly increased autophagy (**Figure 5C**). Furthermore, IHC and western blot analysis of the same proteins recapitulated these results in mouse intestinal tissues (**Figure 5D,F**). Altogether, these results indicate that MCL enhances autophagy in mouse intestinal tissues following radiation.

MCL Mediates Autophagy of the NLRP3 Inflammasome

After the autophagosome matures, lysosomes and autophagosomes fuse to form an autophagolysosome, which leads to the degradation of the autophagosome (Zhao and Zang, 2019). To determine whether autophagy is involved in the degradation of the NLRP3 inflammasome, we evaluated the co-localization of NLRP3 with LC3 and lysosome-associated membrane protein (LAMP-1). Fluorescent confocal microscopy showed that NLRP3 and LC3 were co-localized, and NLRP3 was surrounded by the lysosomal marker LAMP-1, suggesting that the NLRP3 inflammasome is fused

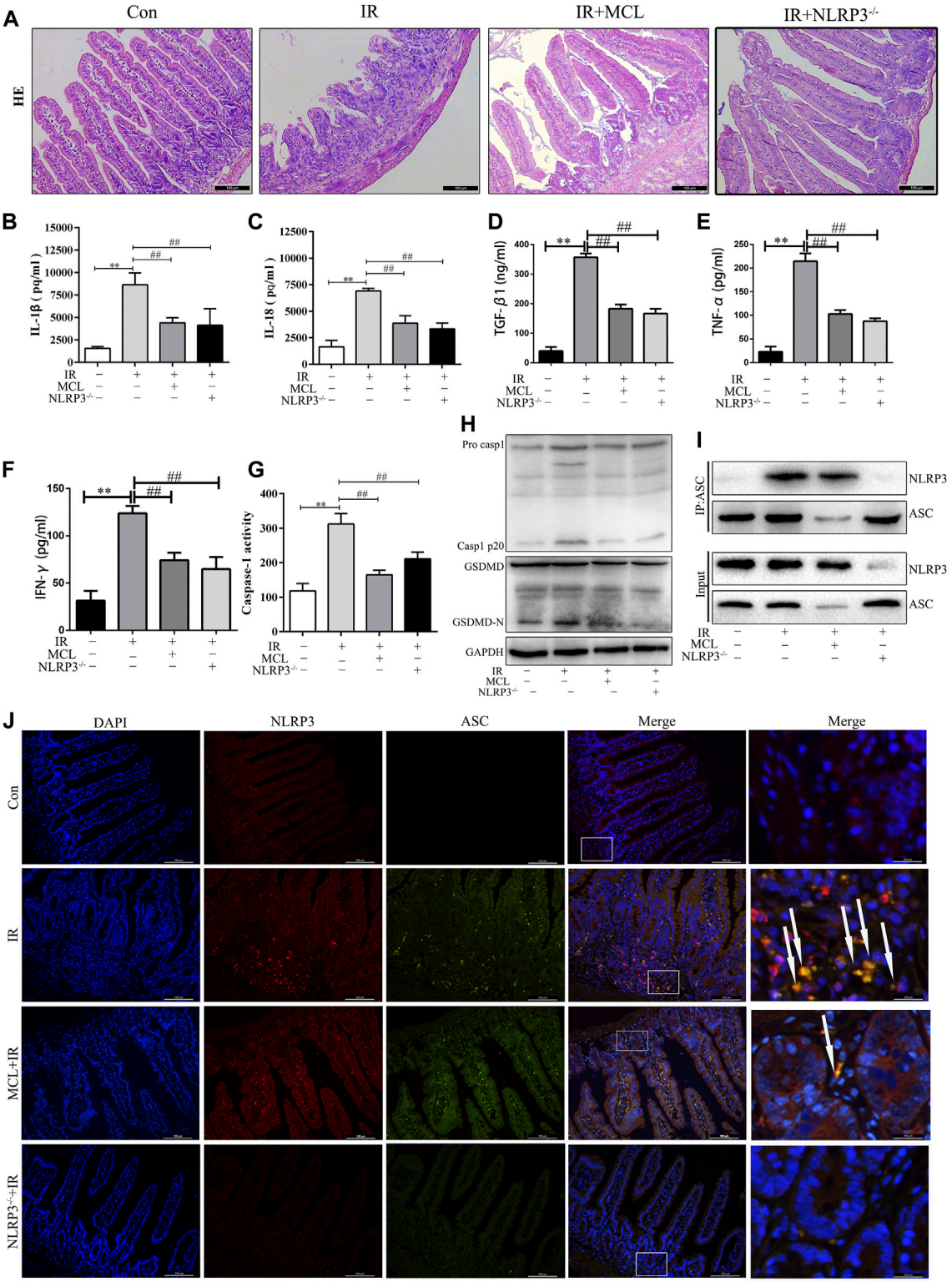

FIGURE 4 | Micheliolide (MCL) inhibited irradiation-induced NLRP3 inflammasome activation in mice **(A)** Representative small intestine hematoxylin and eosin staining from NLRP3−/− and wild-type (WT) mice following irradiation **(B)** Serum IL-1β levels in NLRP3−/− and WT mice following irradiation **(C)** Serum IL-18 levels in NLRP3−/− and WT mice following irradiation (D) Serum TGF-β1 levels in NLRP3−/− and WT mice following irradiation **(E)** Serum TNF-α levels in NLRP3−/− and WT mice following irradiation (F) Serum IFN-γ levels in NLRP3−/− and WT mice following irradiation **(G)** Caspase-1 activity in the small intestine of NLRP3−/− and WT mice treated with MCL following irradiation (H) Expression of pro-casp1, casp1 p20, GSDMD, and GSDMD-N in NLRP3−/− and WT mice treated with MCL following

(*Continued*)

FIGURE 4 | irradiation **(I)** Formation of the NLRP3 and ASC complex in NLRP3−/− and WT mice treated with MCL following irradiation **(J)** Representative image of immunofluorescencent co-localization (arrows) between NLRP3 and ASC in small intestine tissue. *$p < 0.05$, **$p < 0.01$, ***$p < 0.001$, ****$p < 0.0001$, two-tailed Student's t-test. Con, untreated WT mice; IR, WT mice that were treated with irradiation (10 Gy); MCL + IR, mice pre-treated with MCL prior to irradiation (10 Gy); NLRP3−/− + IR, NLRP3 knockout mice exposed to radiation (10 Gy); IL, interleukin; NLRP3, nucleotide binding domain leucine-rich repeat-containing receptor-pyrin domain containing three; GSDMD, gasdermin D. N = 15/group.

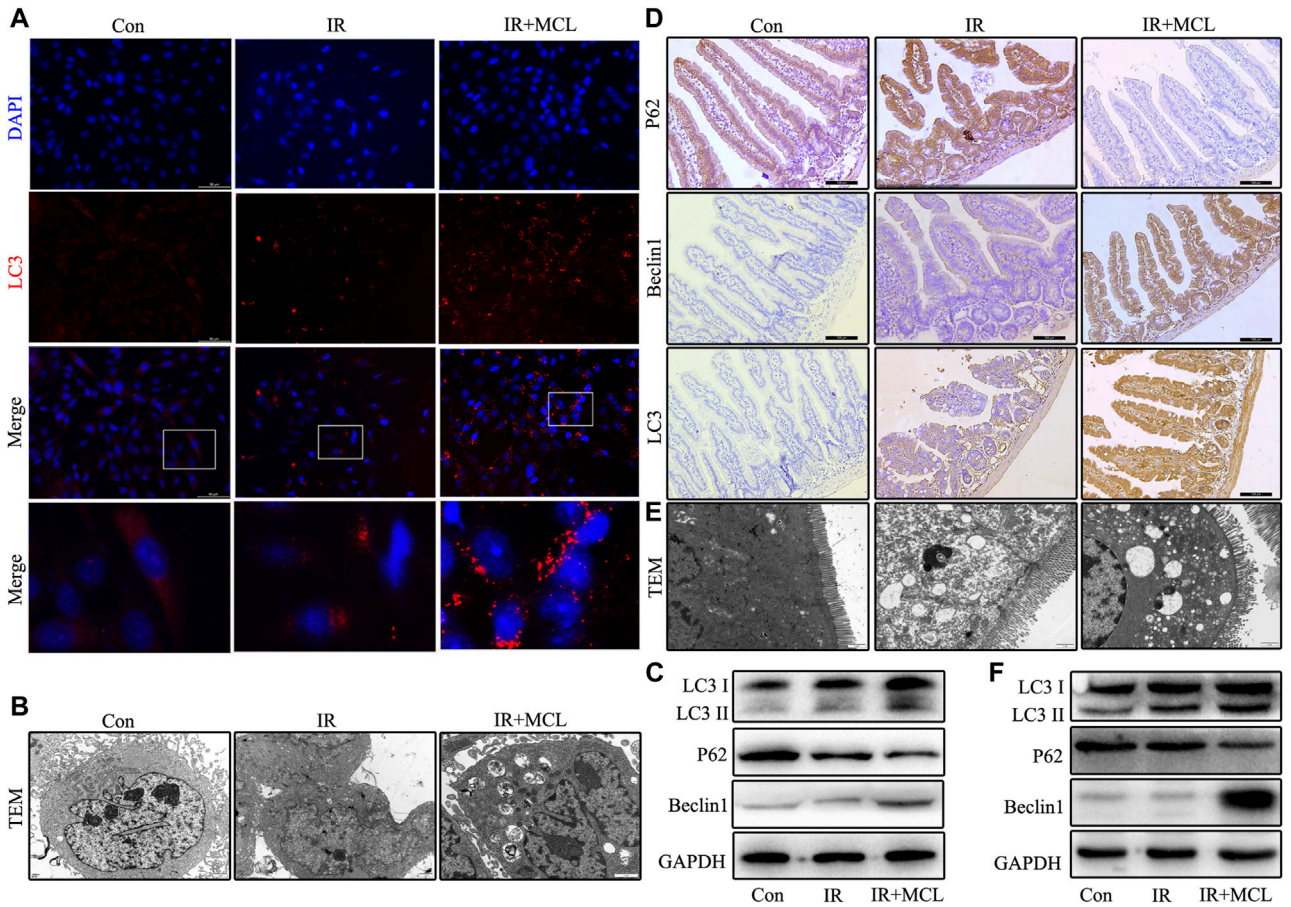

FIGURE 5 | MCL enhances autophagy in mice intestinal tissue and HIEC after radiotherapy. Con, untreated HIECs; IR, HIECs that were treated with irradiation (10 Gy); MCL + IR, HIECs pre-treated with MCL (10 μM) prior to irradiation **(A)** Representative immunofluorescence image of LC3 aggregation in HIECs **(B)** Autophagosomes (arrows) in HIEC detected by transmission electron microscopy **(C)** Western blot of p62, beclin 1, and LC3 protein expression in HIEC. Con, untreated WT mice; IR, WT mice that were treated with irradiation (10 Gy); MCL + IR, WT mice pre-treated with MCL (50 mg/kg) prior to irradiation (10 Gy) **(D)** Immunohistochemical staining of p62, beclin 1, and LC3B in small intestine tissues **(E)** Autophagosomes (arrows) in small intestine tissue detected by transmission electron microscopy **(F)** Western blot of p62, beclin 1, and LC3 protein expression in small intestine tissues. *$p < 0.05$, **$p < 0.01$, ***$p < 0.001$, ****$p < 0.0001$, two-tailed Student's t-test. IR, irradiation; HIEC, human intestinal epithelial cell; MCL, micheliolide.

with autophagosomes and lysosomes (**Figure 6A,B**). These data indicate that MCL can promote the formation of autophagic lysosomes which degrade NLRP3 inflammasomes.

MCL Inhibits the NLRP3 Inflammasome via the Activation of Autophagy

To evaluate the role of autophagy in MCL-mediated protection following radiation, we examined whether MCL was protective against RIE in heterozygous beclin-1 knockout mice ($Becn^{+/-}$). We observed that the MCL-mediated protection against histopathological changes following radiation was abolished in $Becn^{+/-}$ mice (**Figure 7A**). Furthermore, MCL-induced autophagy following radiation was abolished in *Becn*+/-mice (**Figure 7B,C**). Moreover, heterozygous knockout of beclin 1 reversed the MCL-mediated downregulation of IL-1β, IL-18, TGF-β1, TNF-α and IFN-γ following radiation (**Figure 7D–H**).

To determine whether MCL-mediated suppression of the NLRP3 inflammasome is dependent on autophagy, we evaluated the expression of NLRP3-associated proteins in $Becn^{+/-}$ mice. Similar to previous experiments, the expression of GSDMD-N and casp1 p20 was increased following radiation in

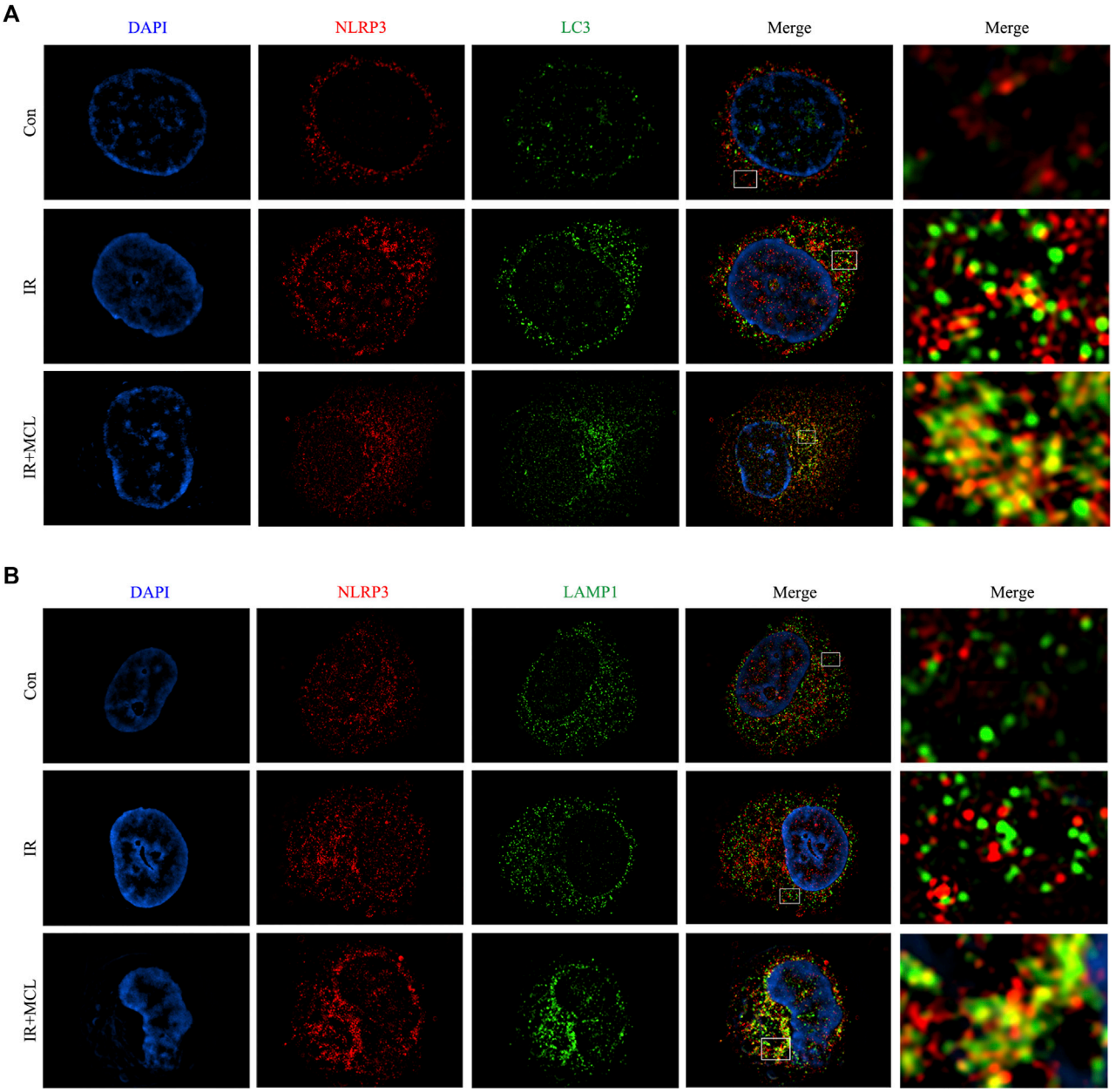

FIGURE 6 | Micheliolide (MCL) mediates autophagy of the NLRP3 inflammasome **(A–B)** HIECs were stained for LC3/LAMP1 (green) and NLRP3 (red) and analyzed by confocal microscopy. Co-localization of NLRP3 (arrows) and LC3/LAMP1 (arrowheads) is apparent. *$p < 0.05$, **$p < 0.01$, ***$p < 0.001$, ****$p < 0.0001$, two-tailed Student's t-test. Con, untreated HIECs; IR, HIECs exposed to radiation (10 Gy); IR + MCL, HIECs pretreated with MCL (10 μM) prior to radiation (10 Gy) exposure; HIEC, human intestinal epithelial cell; LC3/LAMP1, light chain three/lysosome-associated membrane protein.

WT mice, an effect which was inhibited by MCL treatment (**Figure 7J**). In contrast, MCL-mediated inhibition of caspase 1 activity (**Figure 7I**), and expression of GSDMD-N and casp1 p20 was abolished in *Becn*$^{+/-}$ mice (**Figure 7J**). Concordantly, co-localization of NLRP3 with ASC was observed in MCL-treated *Becn*$^{+/-}$ mice following radiation (**Figure 7K**). Altogether, these data indicate that MCL inhibits the activation of the NLRP3 inflammasome in an autophagy-dependent manner.

DISCUSSION

Radiotherapy is regarded as a vital treatment for abdominal and pelvic tumors (Miccio et al., 2020). However, the intestines are relatively sensitive to irradiation, and normal tissues surrounding the tumor, especially the small intestines, may be damaged by radiation exposure (Lu et al., 2019). Currently, there are no effective therapeutic agents to prevent intestinal injury resulting from radiotherapy in cancer patients (Hauer-Jensen

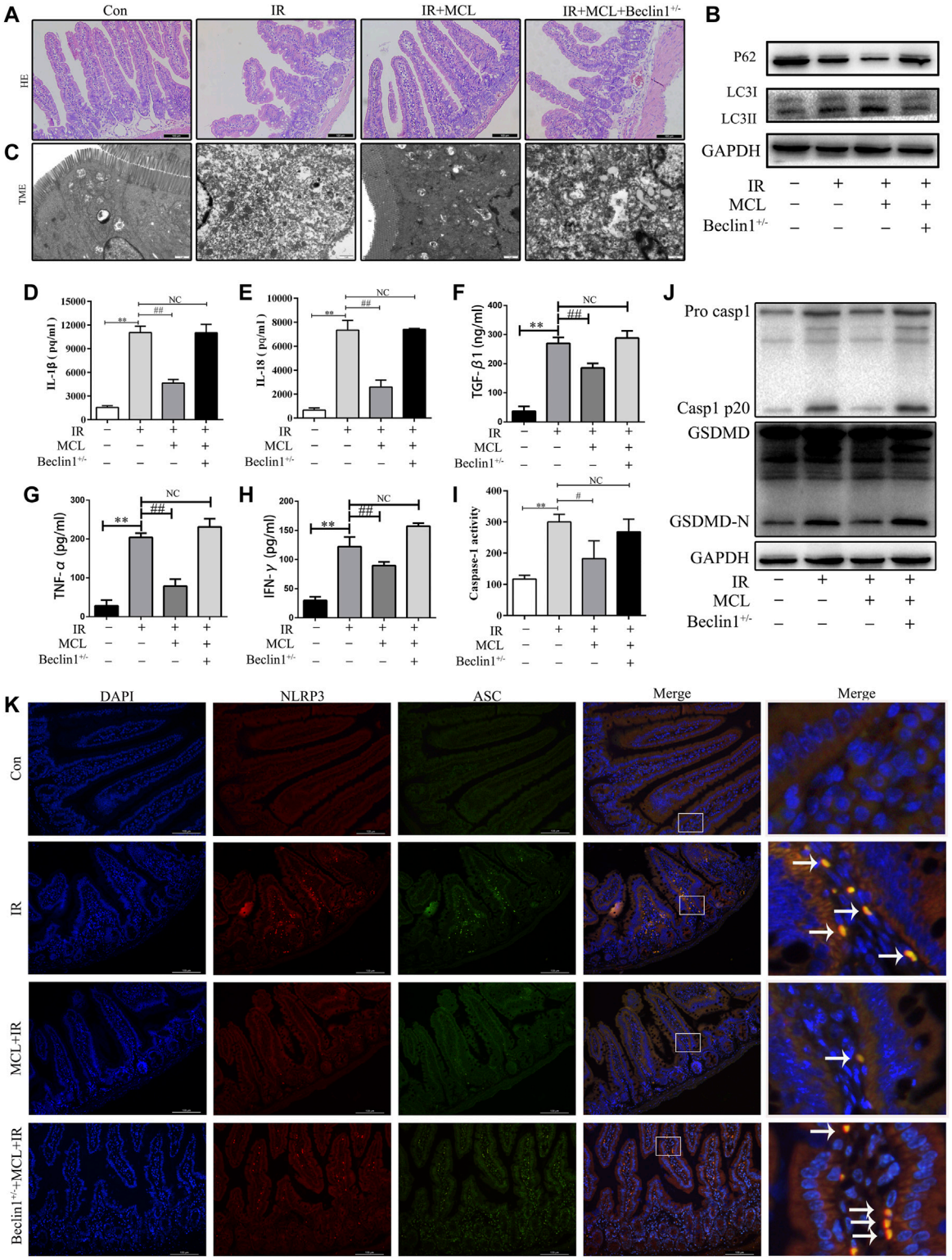

FIGURE 7 | Micheliolide (MCL) inhibits the NLRP3 inflammasome via the activation of autophagy **(A)** Representative small intestine hematoxylin and eosin staining from Beclin1+/-and wild-type (WT) mice following irradiation **(B)** Western blot of p62 and LC3 protein expression **(C)** Autophagosomes in small intestine tissue detected by transmission electron microscopy **(D)** Serum IL-1β levels in MCL-treated heterozygous beclin 1 knockout mice following radiation **(E)** Serum IL-18 levels in MCL-treated heterozygous beclin 1 knockout mice following radiation **(F)** Serum TGF-β1 levels in MCL-treated heterozygous beclin 1 knockout mice following radiation **(G)** Serum TNF-α levels in MCL-treated heterozygous beclin 1 knockout mice following radiation **(H)** Serum IFN-γ levels in MCL-treated heterozygous beclin 1 knockout

(*Continued*)

FIGURE 7 | mice following radiation **(I)** Caspase-1 activation in the small intestine **(J)** Expression of pro casp1, casp1 p20, GSDMD, and GSDMD-N was examined by western blot in MCL-treated heterozygous beclin 1 knockout mice. **(K)** Representative immunofluorescence image of the co-localization (arrows) between NLRP3 and ASC in the small intestine tissue. *$p < 0.05$, **$p < 0.01$, ***$p < 0.001$, ****$p < 0.0001$, two-tailed Student's t-test. Con, untreated WT mice; IR, WT mice that were treated with irradiation (10 Gy); MCL + IR, mice pre-treated with MCL (50 mg/kg) prior to irradiation (10 Gy); MCL + IR + Beclin1$^{+/-}$, Beclin1+/-mice with MCL (50 mg/kg) prior to irradiation (10 Gy); IL, interleukin; NLRP3, nucleotide binding domain leucine-rich repeat-containing receptor-pyrin domain containing three; GSDMD, gasdermin D; LC3, anti-light chain 3.

et al., 2014). Therefore, novel compounds that can prevent or reverse RIE are urgently needed. In this study, we screened a drug library and identified MCL as a potentially therapeutic agent for RIE. We demonstrated that MCL effectively inhibited NLRP3 inflammasome activity and blocked pyroptosis in RIE, which may be associated with the ability of MCL to induce autophagy of the NLRP3 inflammasome.

In a previous study, it was demonstrated that pyroptosis plays an important role in radiation-induced inflammatory injury (Wu et al., 2018). The intact intestinal epithelium acts as an effective barrier against external stimuli, regulates intestinal homeostasis, and is sensitive to radiotherapy (Kessler et al., 2018). Therefore, we screened the pyroptosis-drug compound library in a HIEC model of radiation-induced intestinal injury. Of all the drugs in this library, MCL was found to exert the strongest effect on cell viability following radiation exposure. Furthermore, our results showed that MCL dose-dependently inhibited radiation-induced cell death and LDH release. Based on these findings, we hypothesized that MCL would attenuate radiation-induced intestinal injury in an animal model. To test this hypothesis, we exposed WT C57BL/6J mice to 10 Gy of radiation and evaluated the subsequent inflammatory response and cell damage in the intestinal tissue. The data gathered indicated that irradiation induces an inflammatory reaction accompanied by abundant production of pro-inflammatory cytokines, including IL-1β and IL-18. Interestingly, MCL alleviated radiation-induced intestinal damage and downregulated cytokine levels, consistent with previous reports (Liu et al., 2019; Tian et al., 2020).

The NLRP3 inflammasome is a multi-protein platform. It has been shown that the NLRP3-associated protein, caspase-1, is activated upon cellular infection or stress and leads to a form of programmed cell death called pyroptosis (Luan et al., 2018; Wang & Hauenstein, 2020). In the process of pyroptosis, cleaved caspase-1 specifically cleaves the linker between GSDMD-N and the carboxy-terminal domain of GSDMD, triggering the secretion of IL-1β and IL-18, which are required for pyroptosis and expansion of the inflammatory reaction (Ives et al., 2015; Kovacs and Miao, 2017). A recent study reported that radiation exposure induces NLRP3 inflammasome pathway activation, which participates in the inflammatory response to radiation damage in mouse lungs and intestines (Wei et al., 2019). Based on these findings, we speculated that MCL would mitigate RIE in mice through the inhibition of the NLRP3 inflammasome and pyroptosis. We observed that the damaging responses to radiation were attenuated in NLRP3−/− mice, suggesting NLRP3 involvement in RIE-induced damage. Furthermore, MCL treatment reduced the expression of Casp1 p20 and GSDMD-N, thereby inhibiting pyroptosis in RIE, suggesting that the therapeutic effects of MCL may be mediated by inhibition of the NLRP3 inflammasome (Gong et al., 2019; Sui et al., 2020).

The autophagy pathway is known to play a crucial role in regulating inflammation (Cao et al., 2019). Impaired autophagy may contribute to the aberrant activation of signaling pathways, leading to uncontrolled inflammation and cell death (Han et al., 2019). An increasing number of studies have indicated that the modulation of autophagy could protect against multiple organ injuries by inhibiting the NLRP3 inflammasome (Chen et al., 2020; Qiu et al., 2020; Peng et al., 2021). Moreover, research suggests that MCL mitigates the severity of liver steatosis by enhancing autophagy and attenuating NF-κB-mediated inflammation (Zhong et al., 2018). Additionally, it has been reported that resveratrol can inhibit the activation of the NLRP3 inflammasome by inducing autophagy, which ameliorates IgA nephropathy (Wu et al., 2020; Chen et al., 2021). Considering this evidence, we speculated that MCL may alleviate radiation-induced pyroptosis by promoting autophagy and subsequently inhibiting the activation of the NLRP3 inflammasome. Therefore, we evaluated the involvement of several autophagy-related genes in this study. BECN1, encoding beclin 1, is a protein essential for autophagy, which acts in cooperation with the PtdIns3K pathway to enhance the formation of the autophagic vacuole. We found that the heterozygous deletion of beclin 1 in mice reduces the radioprotective capacity of MCL. Furthermore, the inhibition of NLRP3-ASC co-localization by MCL was absent in *Becn1*$^{+/-}$ mice. Collectively, these results suggest that MCL may regulate autophagy to inhibit the NLRP3 inflammasome and exert a radioprotective effect.

No research performed to date has evaluated the effect of MCL on the relationship between the NLRP3 inflammasome and autophagy. LC3 is a protein associated with phagophores, the precursor to the autophagosome (Kabeya et al., 2000; Wirawan et al., 2012; Katsuragi et al., 2015). Previous studies have described the clearance of the NLRP3 inflammasome via autophagy. In this process, the NLRP3 inflammasome is entirely enclosed by LC3 and delivered to lysosomes for destruction (Mehto et al., 2019; Biasizzo and Kopitar-Jerala, 2020). Given this evidence, we hypothesized that MCL would promote targeting of NLRP3 inflammasomes to autophagolysosomes, thereby increasing their degradation. Direct visualization by super-resolution microscopy in our HIEC model of RIE confirmed that NLRP3 is completely enclosed by LC3 positive structures, which was increased with MCL treatment. Furthermore, we demonstrated the direct co-

localization of NLRP3 with the lysosomal protein LAMP1. Altogether, these results indicate that MCL attenuates RIE by targeting NLRP3 inflammasomes for degradation.

Nonetheless, this study has some limitations. We did not determine other potential molecular targets of MCL in this study, and we were unable to determine whether NLRP3 can bind to multitarget proteins involved in inflammatory or autophagy processes. Future studies should evaluate the specific target proteins of NLRP3 binding.

In summary, we demonstrated that MCL ameliorates RIE via inhibition of the NLRP3 inflammasome, which is likely a result of enhanced autophagy leading to NLRP3 inflammasome degradation. These data suggest that MCL may be a novel drug candidate for the treatment of RIE.

DATA AVAILABILITY STATEMENT

The original contributions presented in the study are included in the article/supplementary material, further inquiries can be directed to the corresponding authors.

ETHICS STATEMENT

The animal study was reviewed and approved by Laboratory Animal Ethical Committee at Chengdu Medical College.

AUTHOR CONTRIBUTIONS

D-gW and YX: conceptualization and data curation. YX: funding acquisition. D-gW and YX: project administration. JL and D-mW: writing—original draft preparation. D-gW, YX, JL, and RS: writing—review and editing. LJ and YY: visualization. LL and S-hD: software. LJ, TL, and TZ: data curation. D-mW, LJ, LL, and RS: methodology.

FUNDING

This research was funded by the National Natural Science Foundation of China (81972977 and 81802955), the Foundation of Health Commission of Sichuan Province (20ZD016), the Foundation of Sichuan Science and Technology Agency (2018JY0648 and 2019YJ0589), the Foundation of The First Affiliated Hospital of Chengdu Medical College (CYFY2017ZD03, CYFY2018ZD02, CYFY2019ZD06, and CYFY2020YB05), and the Foundation of Collaborative Innovation Center of Sichuan for Elderly Care and Health, Chengdu Medical College (20Z096).

ACKNOWLEDGMENTS

We would like to thank Editage (www.editage.cn) for English language editing.

REFERENCES

Akahane, K., Shirai, K., Wakatsuki, M., Ogawa, K., Minato, K., Hamamoto, K., et al. (2020). Severe Esophageal Stenosis in a Patient with Metastatic colon Cancer Following Palliative Radiotherapy, Ramucirumab, and Chemotherapy. *Clin. Case Rep.* 8 (5), 919–922. doi:10.1002/ccr3.2751

Biasizzo, M., and Kopitar-Jerala, N. (2020). Interplay between NLRP3 Inflammasome and Autophagy. *Front. Immunol.* 11, 591803. doi:10.3389/fimmu.2020.591803

Cao, Z., Wang, Y., Long, Z., and He, G. (2019). Interaction between Autophagy and the NLRP3 Inflammasome. *Acta Biochim. Biophys. Sin (Shanghai)* 51, 1087–1095. doi:10.1093/abbs/gmz098

Chen, H., Zhou, C., Xie, K., Meng, X., Wang, Y., and Yu, Y. (2019). Hydrogen-rich saline Alleviated the Hyperpathia and Microglia Activation via Autophagy Mediated Inflammasome Inactivation in Neuropathic Pain Rats. *Neuroscience* 421, 17–30. doi:10.1016/j.neuroscience.2019.10.046

Chen, W., Shen, Y., Fan, J., Zeng, X., Zhang, X., Luan, J., et al. (2021). IL-22-mediated Renal Metabolic Reprogramming via PFKFB3 to Treat Kidney Injury. *Clin. Transl Med.* 11 (2), e324. doi:10.1002/ctm2.324

Chen, W., Zai, W., Fan, J., Zhang, X., Zeng, X., Luan, J., et al. (2020). Interleukin-22 Drives a Metabolic Adaptive Reprogramming to Maintain Mitochondrial Fitness and Treat Liver Injury. *Theranostics* 10 (13), 5879–5894. doi:10.7150/thno.43894

Eskelinen, E. L. (2019). Autophagy: Supporting Cellular and Organismal Homeostasis by Self-Eating. *Int. J. Biochem. Cel Biol.* 111, 1–10. doi:10.1016/j.biocel.2019.03.010

Fu, C., Zhang, X., Lu, Y., Wang, F., Xu, Z., Liu, S., et al. (2020). Geniposide Inhibits NLRP3 Inflammasome Activation via Autophagy in BV-2 Microglial Cells Exposed to Oxygen-Glucose Deprivation/reoxygenation. *Int. Immunopharmacol.* 84, 106547. doi:10.1016/j.intimp.2020.106547

Gong, W., Zhang, S., Zong, Y., Halim, M., Ren, Z., Wang, Y., et al. (2019). Involvement of the Microglial NLRP3 Inflammasome in the Anti-inflammatory Effect of the Antidepressant Clomipramine. *J. Affect. Disord.* 254, 15–25. doi:10.1016/j.jad.2019.05.009

Han, J., Bae, J., Choi, C. Y., Choi, S. P., Kang, H. S., Jo, E. K., et al. (2016). Autophagy Induced by AXL Receptor Tyrosine Kinase Alleviates Acute Liver Injury via Inhibition of NLRP3 Inflammasome Activation in Mice. *Autophagy* 12, 2326–2343. doi:10.1080/15548627.2016.1235124

Han, X., Sun, S., Sun, Y., Song, Q., Zhu, J., Song, N., et al. (2019). Small Molecule-Driven NLRP3 Inflammation Inhibition via Interplay between Ubiquitination and Autophagy: Implications for Parkinson Disease. *Autophagy* 15, 1860–1881. doi:10.1080/15548627.2019.1596481

Haq, S., Grondin, J., Banskota, S., and Khan, W. I. (2019). Autophagy: Roles in Intestinal Mucosal Homeostasis and Inflammation. *J. Biomed. Sci.* 26, 19. doi:10.1186/s12929-019-0512-2

Hauer-Jensen, M., Denham, J. W., and Andreyev, H. J. (2014). Radiation Enteropathy-Ppathogenesis, Treatment and Prevention. *Nat. Rev. Gastroenterol. Hepatol.* 11, 470–479. doi:10.1038/nrgastro.2014.46

Hazell, S. Z., Mai, N., Fu, W., Hu, C., Friedes, C., Negron, A., et al. (2020). Hospitalization and Definitive Radiotherapy in Lung Cancer: Incidence, Risk Factors and Survival Impact. *BMC Cancer* 20, 334. doi:10.1186/s12885-020-06843-z

He, W. T., Wan, H., Hu, L., Chen, P., Wang, X., Huang, Z., et al. (2015). Gasdermin D Is an Executor of Pyroptosis and Required for Interleukin-1β Secretion. *Cell Res* 25, 1285–1298. doi:10.1038/cr.2015.139

Ives, A., Nomura, J., Martinon, F., Roger, T., LeRoy, D., Miner, J. N., et al. (2015). Xanthine Oxidoreductase Regulates Macrophage IL1β Secretion upon NLRP3 Inflammasome Activation. *Nat. Commun.* 6, 6555. doi:10.1038/ncomms7555

Jiang, H., Gong, T., and Zhou, R. (2020). The Strategies of Targeting the NLRP3 Inflammasome to Treat Inflammatory Diseases. *Adv. Immunol.* 145, 55–93. doi:10.1016/bs.ai.2019.11.003

Jiang, X., Wang, Y., Qin, Y., He, W., Benlahrech, A., Zhang, Q., et al. (2017). Micheliolide Provides protection of Mice against *Staphylococcus aureus* and MRSA Infection by Down-Regulating Inflammatory Response. *Sci. Rep.* 7, 41964. doi:10.1038/srep41964

Kabeya, Y., Mizushima, N., Ueno, T., Yamamoto, A., Kirisako, T., Noda, T., et al. (2000). LC3, a Mammalian Homologue of Yeast Apg8p, Is Localized in Autophagosome Membranes after Processing. *EMBO J.* 19, 5720–5728. doi:10.1093/emboj/19.21.5720

Kalantary-Charvadeh, A., Sanajou, D., Hemmati-Dinarvand, M., Marandi, Y., Khojastehfard, M., Hajipour, H., et al. (2019). Micheliolide Protects against Doxorubicin-Induced Cardiotoxicity in Mice by Regulating PI3K/Akt/NF-kB Signaling Pathway. *Cardiovasc. Toxicol.* 19, 297–305. doi:10.1007/s12012-019-09511-2

Katsuragi, Y., Ichimura, Y., and Komatsu, M. (2015). p62/SQSTM1 Functions as a Signaling Hub and an Autophagy Adaptor. *FEBS J.* 282, 4672–4678. doi:10.1111/febs.13540

Kessler, S. P., Obery, D. R., Nickerson, K. P., Petrey, A. C., McDonald, C., and de la Motte, C. A. (2018). Multifunctional Role of 35 Kilodalton Hyaluronan in Promoting Defense of the Intestinal Epithelium. *J. Histochem. Cytochem.* 66, 273–287. doi:10.1369/0022155417746775

Kovacs, S. B., and Miao, E. A. (2017). Gasdermins: Effectors of Pyroptosis. *Trends Cel Biol* 27, 673–684. doi:10.1016/j.tcb.2017.05.005

Li, J., Wu, D. M., Han, R., Yu, Y., Deng, S. H., Liu, T., et al. (2020). Low-Dose Radiation Promotes Invasion and Migration of A549 Cells by Activating the CXCL1/NF-Kb Signaling Pathway. *Onco. Targets Ther.* 13, 3619–3629. doi:10.2147/OTT.S243914

Liu, W., Chen, X., Wang, Y., Chen, Y., Chen, S., Gong, W., et al. (2019). Micheliolide Ameliorates Diabetic Kidney Disease by Inhibiting Mtdh-Mediated Renal Inflammation in Type 2 Diabetic Db/db Mice. *Pharmacol. Res.* 150, 104506. doi:10.1016/j.phrs.2019.104506

Lu, L., Li, W., Chen, L., Su, Q., Wang, Y., Guo, Z., et al. (2019). Radiation-induced Intestinal Damage: Latest Molecular and Clinical Developments. *Future Oncol.* 15, 4105–4118. doi:10.2217/fon-2019-0416

Luan, J., Zhang, X., Wang, S., Li, Y., Fan, J., Chen, W., et al. (2018). NOD-like Receptor Protein 3 Inflammasome-dependent IL-1β Accelerated ConA-Induced Hepatitis. *Front. Immunol.* 9, 758. doi:10.3389/fimmu.2018.00758

Mehto, S., Chauhan, S., Jena, K. K., Chauhan, N. R., Nath, P., Sahu, R., et al. (2019). IRGM Restrains NLRP3 Inflammasome Activation by Mediating its SQSTM1/p62-dependent Selective Autophagy. *Autophagy* 15, 1645–1647. doi:10.1080/15548627.2019.1628544

Miccio, J. A., Oladeru, O. T., Jun Ma, S., and Johung, K. L. (2020). Radiation Therapy for Patients with Advanced Renal Cell Carcinoma. *Urol. Clin. North. Am.* 47, 399–411. doi:10.1016/j.ucl.2020.04.011

Molitoris, J. K., Alexander, G. S., Siddiqui, O., Cohen, J., Mishra, M. V., and Rana, Z. (2021). High-risk, Recurrent and Oligometastatic Prostate Cancer: Recent Developments on the Role of Radiation. *Curr. Opin. Oncol.* 33, 238–243. doi:10.1097/CCO.0000000000000720

Nussbaum, M. L., Campana, T. J., and Weese, J. L. (1993). Radiation-induced Intestinal Injury. *Clin. Plast. Surg.* 20, 573–580. doi:10.1016/s0094-1298(20)31199-8

Peng, W., Peng, F., Lou, Y., Li, Y., Zhao, N., Shao, Q., et al. (2021). Autophagy Alleviates Mitochondrial DAMP-Induced Acute Lung Injury by Inhibiting NLRP3 Inflammasome. *Life Sci.* 265, 118833. doi:10.1016/j.lfs.2020.118833

Pohl, C., and Dikic, I. (2019). Cellular Quality Control by the Ubiquitin-Proteasome System and Autophagy. *Science* 366, 818–822. doi:10.1126/science.aax3769

Qin, X., Jiang, X., Jiang, X., Wang, Y., Miao, Z., He, W., et al. (2016). Micheliolide Inhibits LPS-Induced Inflammatory Response and Protects Mice from LPS challenge. *Sci. Rep.* 6, 23240. doi:10.1038/srep23240

Qiu, W. Q., Pan, R., Tang, Y., Zhou, X. G., Wu, J. M., Yu, L., et al. (2020). Lychee Seed Polyphenol Inhibits Aβ-Induced Activation of NLRP3 Inflammasome via the LRP1/AMPK Mediated Autophagy Induction. *Biomed. Pharmacother.* 130, 110575. doi:10.1016/j.biopha.2020.110575

Seoane, P. I., Lee, B., Hoyle, C., Yu, S., Lopez-Castejon, G., Lowe, M., et al. (2020). The NLRP3-Inflammasome as a Sensor of Organelle Dysfunction. *J. Cel Biol.* 219, e2020061942020. doi:10.1083/jcb.202006194

Seong, J. (2009). Challenge and hope in Radiotherapy of Hepatocellular Carcinoma. *Yonsei Med. J.* 50 (5), 601–612. doi:10.3349/ymj.2009.50.5.601

Shadad, A. K., Sullivan, F. J., Martin, J. D., and Egan, L. J. (2013). Gastrointestinal Radiation Injury: Prevention and Treatment. *World J. Gastroenterol.* 19, 199–208. doi:10.3748/wjg.v19.i2.199

Shi, J., Gao, W., and Shao, F. (2017). Pyroptosis: Gasdermin-Mediated Programmed Necrotic Cell Death. *Trends Biochem. Sci.* 42, 245–254. doi:10.1016/j.tibs.2016.10.004

Sipaviciute, A., Sileika, E., Burneckis, A., and Dulskas, A. (2020). Late Gastrointestinal Toxicity after Radiotherapy for Rectal Cancer: a Systematic Review. *Int. J. Colorectal Dis.* 35, 977–983. doi:10.1007/s00384-020-03595-x

Sui, X., Yang, J., Zhang, G., Yuan, X., Li, W., Long, J., et al. (2020). NLRP3 Inflammasome Inhibition Attenuates Subacute Neurotoxicity Induced by Acrylamide *In Vitro* and *In Vivo*. *Toxicology* 432, 152392. doi:10.1016/j.tox.2020.152392

Sun, Z., Li, G., Tong, T., and Chen, J. (2017). Micheliolide Suppresses LPS-Induced Neuroinflammatory Responses. *PLoS One* 12, e0186592. doi:10.1371/journal.pone.0186592

Takemura, N., Kurashima, Y., Mori, Y., Okada, K., Ogino, T., Osawa, H., et al. (2018). Eosinophil Depletion Suppresses Radiation-Induced Small Intestinal Fibrosis. *Sci. Transl Med.* 10 (429), eaan0333. doi:10.1126/scitranslmed.aan0333

Tang, R., Xu, J., Zhang, B., Liu, J., Liang, C., Hua, J., et al. (2020). Ferroptosis, Necroptosis, and Pyroptosis in Anticancer Immunity. *J. Hematol. Oncol.* 13, 110. doi:10.1186/s13045-020-00946-7

Tian, Z. G., Yao, M., and Chen, J. (2020). Micheliolide Alleviates Ankylosing Spondylitis (AS) by Suppressing the Activation of the NLRP3 Inflammasome and Maintaining the Balance of Th1/Th2 via Regulating the NF-Kb Signaling Pathway. *Ann. Transl. Med.* 8, 991. doi:10.21037/atm-20-4987

Wang, L., and Hauenstein, A. V. (2020). The NLRP3 Inflammasome: Mechanism of Action, Role in Disease and Therapies. *Mol. Aspects Med.* 76, 100889. doi:10.1016/j.mam.2020.100889

Wei, J., Wang, H., Wang, H., Wang, B., Meng, L., Xin, Y., et al. (2019). The Role of NLRP3 Inflammasome Activation in Radiation Damage. *Biomed. Pharmacother.* 118, 109217. doi:10.1016/j.biopha.2019.109217

Wirawan, E., Lippens, S., Vanden Berghe, T., Romagnoli, A., Fimia, G. M., Piacentini, M., et al. (2012). Beclin1: a Role in Membrane Dynamics and beyond. *Autophagy* 8, 6–17. doi:10.4161/auto.8.1.16645

Wu, C. Y., Hua, K. F., Yang, S. R., Tsai, Y. S., Yang, S. M., Hsieh, C. Y., et al. (2020). Tris DBA Ameliorates IgA Nephropathy by Blunting the Activating Signal of NLRP3 Inflammasome through SIRT1- and SIRT3-Mediated Autophagy Induction. *J. Cel Mol. Med.* 24, 13609–13622. doi:10.1111/jcmm.15663

Wu, D., Han, R., Deng, S., Liu, T., Zhang, T., Xie, H., et al. (2018). Protective Effects of Flagellin a N/c against Radiation-Induced NLR Pyrin Domain Containing 3 Inflammasome-dependent Pyroptosis in Intestinal Cells. *Int. J. Radiat. Oncol. Biol. Phys.* 101, 107–117. doi:10.1016/j.ijrobp.2018.01.035

Yu, P., Zhang, X., Liu, N., Tang, L., Peng, C., and Chen, X. (2021). Pyroptosis: Mechanisms and Diseases. *Sig Transduct Target. Ther.* 6, 128. doi:10.1038/s41392-021-00507-5

Zhao, Y. G., and Zhang, H. (2019). Autophagosome Maturation: An Epic Journey from the ER to Lysosomes. *J. Cel Biol.* 218, 757–770. doi:10.1083/jcb.201810099

Zhong, J., Gong, W., Chen, J., Qing, Y., Wu, S., Li, H., et al. (2018). Micheliolide Alleviates Hepatic Steatosis in Db/db Mice by Inhibiting Inflammation and Promoting Autophagy via PPAR-γ-Mediated NF-κB and AMPK/mTOR Signaling. *Int. Immunopharmacol.* 59, 197–208. doi:10.1016/j.intimp.2018.03.036

Conflict of Interest: The authors declare that the research was conducted in the absence of any commercial or financial relationships that could be construed as a potential conflict of interest.

Publisher's Note: All claims expressed in this article are solely those of the authors and do not necessarily represent those of their affiliated organizations, or those of the publisher, the editors and the reviewers. Any product that may be evaluated in this article, or claim that may be made by its manufacturer, is not guaranteed or endorsed by the publisher.

frontiers in Pharmacology

ORIGINAL RESEARCH
published: 17 February 2022
doi: 10.3389/fphar.2022.822833

An RRx-001 Analogue With Potent Anti-NLRP3 Inflammasome Activity but Without High-Energy Nitro Functional Groups

Hualong Lin[1,2,3], *Mingyang Yang*[4], *Cong Li*[1,2,3], *Bolong Lin*[1,2,3], *Xianming Deng*[4]*, *Hongbin He*[1,2,3]* and *Rongbin Zhou*[1,2,3]*

[1]Department of Geriatrics, First Affiliated Hospital of USTC, Division of Life Sciences and Medicine, University of Science and Technology of China, Hefei, China, [2]CAS Key Laboratory of Innate Immunity and Chronic Disease, School of Basic Medical Sciences, Division of Life Sciences and Medicine, University of Science and Technology of China, Hefei, China, [3]Chinese Academy of Sciences Centre for Excellence in Cell and Molecular Biology, University of Science and Technology of China, Hefei, China, [4]State Key Laboratory of Cellular Stress Biology, Innovation Center for Cell Signaling Network, School of Life Sciences, Xiamen University, Xiamen, China

OPEN ACCESS

Edited by:
Tharmarajan Ramprasath, Georgia State University, United States

Reviewed by:
Rosalinda Sorrentino, University of Salerno, Italy
Venkata Naga Lakshmi Ramarao Sure, Tulane University, United States

***Correspondence:**
Xianming Deng
xmdeng@xmu.edu.cn
Hongbin He
hhb123@ustc.edu.cn
Rongbin Zhou
zrb1980@ustc.edu.cn

Specialty section:
This article was submitted to Inflammation Pharmacology, a section of the journal Frontiers in Pharmacology

Received: 26 November 2021
Accepted: 18 January 2022
Published: 17 February 2022

Citation:
Lin H, Yang M, Li C, Lin B, Deng X, He H and Zhou R (2022) An RRx-001 Analogue With Potent Anti-NLRP3 Inflammasome Activity but Without High-Energy Nitro Functional Groups. Front. Pharmacol. 13:822833. doi: 10.3389/fphar.2022.822833

NLRP3 inflammasome is involved in the pathology of multiple human inflammatory diseases but there are still no clinically available medications targeting the NLRP3 inflammasome. We have previously identified RRx-001 as a highly selective and potent NLRP3 inhibitor, however, it contains high-energy nitro functional groups and may cause potential processing problems and generates highly toxic oxidants. Here, we show that compound 149-01, an RRx-001 analogue without high-energy nitro functional groups, is a potent, specific and covalent NLRP3 inhibitor. Mechanistically, 149-01 binds directly to cysteine 409 of NLRP3 to block the NEK7-NLRP3 interaction, thereby preventing NLRP3 inflammasome complex assembly and activation. Furthermore, treatment with 149-01 effectively alleviate the severity of several inflammatory diseases in mice, including lipopolysaccharide (LPS)-induced systemic inflammation, monosodium urate crystals (MSU)-induced peritonitis and experimental autoimmune encephalomyelitis (EAE). Thus, our results indicate that 149-01 is a potential lead for developing therapeutic agent for NLRP3-related inflammatory diseases.

Keywords: RRx-001 analogues, NLRP3 inflammasome, anti-inflammation, NLRP3-related inflammatory diseases, NLRP3 inhibitor

INTRODUCTION

The NLRP3 inflammasome is a multimeric protein complex consisted of innate immune sensor NLRP3 (NLR family, Pyrin domain containing 3), adaptor protein ASC and effector cysteine protease caspase-1, it plays a pivotal role in host defense against microbial infection and inflammation (Schroder and Tschopp, 2010; Davis et al., 2011). Unlike other sensor proteins, NLRP3 can be activated by a wide range of factors derived from microbes, the host and the environment (Broz and Dixit, 2016). Upon activation, NLRP3 recruits ASC, which then interacts with pro-caspase-1 to induce NLRP3 inflammasome complex assembly. This results in the cleavage and activation of caspase-1, which subsequently promotes the maturation and secretion of IL-1β and IL-18 and induces pyroptosis, a type of inflammatory cell death (Shi et al., 2015; Swanson et al., 2019). However, aberrant activation of NLRP3 inflammasome has been reported to promote the

development of several human diseases, including gout, type 2 diabetes (T2D), inflammatory bowel disease (IBD), atherosclerosis, neurodegenerative diseases and others (Martinon et al., 2006; Bauer et al., 2010; Duewell et al., 2010; Masters et al., 2010; Wen et al., 2012; Heneka et al., 2013; Guo et al., 2015). Therefore, NLRP3 inflammasome is considered as a novel therapeutic target for these inflammatory diseases.

Currently, biologic agents targeting IL-1β are clinically used to treat NLRP3-driven diseases, including canakinumab (a neutralizing IL-1β monoclonal antibody), anakinra (a recombinant non-glycosylated IL-1 receptor antagonist), and rilonacept (a soluble decoy IL-1β receptor) (Dinarello et al., 2012). These agents have been proven to be effective in the treatment of Cryopyrin-associated periodic syndromes (CAPS) caused by NLRP3 gene mutations and have also been applied in clinical trials for other NLRP3-associated disorders (Dinarello et al., 2012; Dinarello and van der Meer, 2013). However, the NLRP3 inflammasome activation induces not only IL-1β production, but also drives pyroptosis and other proinflammatory cytokines production such as IL-18, which may also contribute to the pathogenesis of inflammatory diseases (Nowarski et al., 2015). Moreover, IL-1β can also be produced by other inflammasomes or in an inflammasome-independent manner (Davis et al., 2011; Netea et al., 2015), so blockage of IL-1β may lead to a higher risk of infection. Therefore, compared with biologic agents that target IL-1β, inhibitors that directly target NLRP3 inflammasome may be a better therapeutic option for NLRP3-related diseases.

In recent years, several small molecules, including MCC950, CY-09, OLT1177, oridonin, tranilast, INF39 and others, have been proposed to inhibit the NLRP3 inflammasome activation and exert remarkable therapeutic effects for NLRP3-associated disorders in animal models (Coll et al., 2015; Daniels et al., 2016; Jiang et al., 2017; He et al., 2018; Huang et al., 2018; Marchetti et al., 2018; Zhang et al., 2020; Shi et al., 2021). However, considering the safety, efficacy and specificity of these inhibitors, only a few have entered clinical trials, such as the MCC950-related agents (Inzomelid and IZD334), IFM-2427, OLT1177 (Mullard, 2019; Kluck et al., 2020). Although these agents hold promise for the treatment of NLRP3-related diseases, their clinical efficacy and safety remain to be further determined.

We previously described RRx-001 (1-bromoacetyl-3,3-dinitroazetidine), an antitumor agent in phase III clinical trials, as a novel potent NLRP3 inhibitor (Kim et al., 2016; Oronsky et al., 2019; Chen et al., 2021). However, RRx-001 is a small-molecule compound developed from the defense and aerospace industry and contains unique high-energy nitro functional groups (Oronsky et al., 2016). The gem-dinitroazetidine can decompose rapidly and may be sensitive to heat, impact, friction and electrostatic discharge (Ning et al., 2012; Straessler et al., 2012). Due to its inherent energy properties, the gem-dinitroazetidine can cause potential processing problems. In addition, these geminal dinitro-groups undergo decomposition under hypoxic conditions *in vivo*, producing the gaseous multifunctional free radical, nitric oxide (NO) (Fens et al., 2011; Oronsky et al., 2017). Further chemical interaction between NO and ROS (reactive oxygen species) can generate highly toxic oxidants, including nitrogen dioxide and peroxynitrite (van der Vliet et al., 2000; Oronsky et al., 2017). Moreover, our previous study has shown that removal of geminal dinitro-groups from RRx-001 resulted in a nearly 32-fold decrease in its inhibitory activity (Chen et al., 2021).

In this study, we tried to identify RRx-001 analogues with potent anti-NLRP3 inflammasome activity but without high-energy nitro functional groups. Our results showed that 149-01, an RRx-001 analogue, had comparable activity with RRx-001. Mechanistically, 149-01 blocked the NEK7-NLRP3 interaction by binding directly to cysteine 409 of NLRP3, thereby preventing the assembly of NLRP3 inflammasome complex. Moreover, 149-01 treatment effectively attenuated several NLRP3-related inflammatory diseases in mice, including LPS-induced systemic inflammation, MSU-induced peritonitis and EAE. Taken together, our findings demonstrate that 149-01 is active both *in vitro* and *in vivo*, suggesting that 149-01 is a potential lead for developing therapeutic agent for NLRP3-related human inflammatory diseases.

MATERIALS AND METHODS

Mice

C57BL/6J mice were obtained from Shanghai SLAC Laboratory Animal Limited Liability Company (Shanghai, China). The generation of *Nlrp3*$^{-/-}$ mice were as previously described (Martinon et al., 2006). Mice were maintained in a SPF facility under a 12/12 h light/dark cycle (lights on at 07:00 and off at 19:00). All animal studies were performed in accordance with the guidelines of the Ethics Committee of University of Science and Technology of China.

Reagents

ATP, Nigericin, MSU, and poly (A/T) were purchased from Sigma-Aldrich. Ultrapure LPS, Lipofextamine 2000, Pam3CSK4, MQAE, MitoSOX, MitoTracker, DAPI were acquired from Invitrogen. The Salmonella strain was a gift from Dr. Cai Zhang (Shandong University, Shandong, China). The C3 toxin was a gift from Dr. Tengchuan Jin (University of Science and Technology of China, Hefei, China). CY-09 was synthesized from Dr. Xianming Deng (Xiamen University, Xiamen, China). Protein G agarose (16-266) and anti-Flag (A2220) beads were bought from Millipore and Sigma-Aldrich, respectively. Anti-Flag (F2555) and anti-VSV (V4888) antibodies were from Sigma-Aldrich. The anti-mouse NLRP3 (AG-20B-0014) and the anti-mouse caspase-1 (AG-20B-0042) antibodies was from AdipoGen. The anti-mouse IL-1β antibody (AF-401-NA) was obtained from R&D Systems. The anti-β-actin antibody (66009-1-Ig) was from Proteintech Group. The anti-mouse ASC antibody (67824S) was from Cell Signaling Technology. The anti-mouse NEK7 antibody (ab133514) was from Abcam.

Cell Preparation and Stimulation

BMDMs (bone marrow-derived macrophages) were collected from the bone marrow of 6–8 weeks old mice and cultured in

DMEM supplemented with 10% FBS and 20 ng/ml murine M-CSF (Novoprotein). Human PBMCs (peripheral blood mononuclear cells) were obtained by Human Lymphocyte Separation Medium (catalog no. P8610-200, Solarbio) and cultured in RPMI 1640 medium containing 10% FBS.

To stimulate inflammasome activation, BMDMs (5×10^5/well) or PBMCs (1×10^6/well) were seeded into 12-well plates and cultured overnight. Cells were primed for 3 h in Opti-MEM with LPS (50 ng/ml) or Pam3CSK4 (400 ng/ml, for noncanonical inflammasome activation), followed by treatment with 149-01 for 30 min, and then stimulated with various inflammasome agonists: 3 μM nigericin (30 min); 150 μg/ml MSU (4 h); 2.5 mM ATP (30 min); S. typhimurium (4 h, multiplicity of infection (MOI)); 30 μM CL097 (1 h) or 0.5 μg/ml C3 toxin (6 h). 0.5 μg/ml poly (A/T) or 500 ng/ml LPS were transfected into BMDMs with Lipofectamine 2000 for 4 h or 16 h, respectively. The release of lactate dehydrogenase (LDH) was measured by LDH Cytotoxicity Assay Kit (Beyotime). Precipitated supernatants and cell lysates were further detected using western blotting.

In vitro, 149-01 was dissolved in DMSO, and the DMSO was used as vehicle control in all figures.

ELISA

Cell culture supernatants and serum samples were analyzed for mouse IL-6, TNF-α or IL-1β and for human TNF-α or IL-1β with ELISA kit (all from R&D except human IL-1β from BD, 557953) according to the manufacturer's instructions.

Western Blotting

Sample buffer was added to resuspend precipitated supernatants or to lyse cells, and the cell lysates were transferred to 1.5 ml EP tube. All protein samples were further boiled at 100°C for 10 min and separated by 8% or 15% SDS–PAGE gels at 80 V for 0.5 h and at 120 V for 1 h. After that, proteins were transferred to PVDF membranes at 90 V for 1 h. The membranes were blocked with PBST containing 5% nonfat milk at room temperature for 1 h and then incubated with primary and conjugated secondary antibodies as described previously (Chen et al., 2021). After washing the membranes with PBST, protein bands were acquired after visualization by enhanced chemiluminescence.

Detection of Intracellular K^+ and Cl^- Levels

To determine intracellular K^+ concentration, BMDMs (1×10^6/well) seeded in 6-well plates were stimulated with nigericin to trigger NLRP3 inflammasome activation as described above. After that, cell culture supernatants were thoroughly removed and cells were lysed with ultrapure HNO_3. Cell lysates were further boiled at 100°C for 30 min and then the precipitated products were dissolved with ddH_2O. K^+ concentrations were measured using PerkinElmer Optima 2000 DV spectrometer.

To determine intracellular Cl^- concentration, BMDMs seeded in 12-well plates were also stimulated to activate NLRP3 inflammasome. After stimulation, the culture supernatants were thoroughly discarded and cells were lysed with ddH_2O (200 μl/well) at 37°C for 30 min. Cell lysates were transferred to 1.5 ml EP tube, centrifuged at 10,000×g for 5 min and then supernatants were mixed with MQAE (10 μM). The absorbance of the mixture was determined using BioTek Multi-Mode Microplate Readers (Synergy2). A control was set for each experiment to measure the extracellular residual Cl^- level after removal of the culture supernatant.

Confocal Microscopy

BMDMs (2×10^5/well) were seeded on coverslips (Thermo Fisher Scientific) and cultured overnight in 12-well plates. The next day, LPS-primed mouse BMDMs were stained with 5 μM MitoSOX or 50 nM MitoTracker Red and stimulated with nigericin. After stimulation, the culture supernatants were removed, and the cells were fixed *in situ* with 4% paraformaldehyde (PFA) in PBS for 15 min after washing by ice-cold PBS three times. Then, the cells were washed three times with PBST. Confocal microscopic analyses were utilized to detect mitochondrial damage by using a Zeiss LSM 700.

Immunoprecipitation

To detect endogenous interaction, LPS-primed BMDMs were stimulated with nigericin in 6-well plates, then lysed in NP-40 lysis buffer containing protease inhibitor cocktail. The cell lysates were centrifuged at 10,000 rpm at 4°C for 10 min and the supernatants were then incubated with primary antibodies and Protein G Mag Sepharose overnight with rotation at 4°C. The protein-antibody complex was pulled down by protein G beads and determined using immunoblot analysis.

To detect exogenous interaction, plasmids were transfected into HEK-293T cells in 6-well plates via polyethylenimine (PEI). 24 h after transfection, cells were collected and lysed in NP-40 lysis buffer. After centrifugation, supernatants of cell lysates were co-incubated with anti-Flag antibody–coated beads. Then, immunocomplex proteins were pulled down by beads and analyzed using immunoblotting.

ASC Oligomerization Assay

BMDMs (1×10^6/well) were plated in 6-well plates and treated with nigericin. After stimulation, the cells were washed with ice-cold PBS and then lysed in NP-40 lysis buffer at 4°C for 30 min. The cell lysates were centrifuged at 330×*g* at 4°C for 10 min. The pellets were washed with ice-cold PBS three times and re-suspended in 500 μl PBS, then cross-linked with 2 mM disuccinimidyl suberate (DSS, Sangon Biotech, C100015) at room temperature for 30 min with rotation. The crosslinked pellets were collected after centrifugation at 330 *g* for 10 min and dissolved directly in 30 μl sample buffer, and analyzed using immunoblotting.

Protein Expression and Purification

To purify human Flag-NLRP3 protein, human Flag-NLRP3 plasmid was transfected into HEK-293T cells via PEI and expressed for 48 h. The cells were then washed with ice-cold PBS and lysed in lysis buffer (50 mM HEPES, pH 7.4, 150 mM NaCl, and 0.4% CHAPS) at 4°C for 30 min. The cell lysates were centrifuged at 14,000 rpm at 4°C for 15 min. After centrifugation, supernatants of cell lysates were co-incubated with anti-Flag antibody–coated beads at 4°C for

2.5 h with rotation. The beads were collected after centrifugation and incubated with Flag peptide (Sigma-Aldrich, F3290) in elution buffer (50 mM HEPES, pH 7.4, 500 mM NaCl and 0.1% CHAPS) at 4°C for 90 min with rotation to elute Flag-NLRP3 protein. The eluents containing Flag-NLRP3 protein were collected and concentrated by ultrafiltration device (UFC910024; Merck Millipore) to remove proteins <100 kD. Meanwhile, 10 μl eluent was dissolved in sample buffer, separated by 8% SDS–PAGE gels, followed by detection using anti-Flag antibody.

To purify human GFP-NLRP3 protein, human His-GFP-NLRP3 plasmid was transfected into HEK-293T cells *via* PEI and expressed for 48 h. The cells were lysed in lysis buffer at 4°C for 30 min and sonicated. The supernatants of cell lysates were then collected by centrifuging at 14,000 rpm at 4°C for 15 min. The His-GFP-NLRP3 proteins were preliminarily isolated using nickel–nitrilotriacetic acid matrices (QIAGEN) at room temperature for 45 min, and the pulled down proteins were washed twice with lysis buffer. After that, proteins were eluted in elution buffer and the eluents were concentrated by ultrafiltration device to remove proteins <10 kD after filtration through a 0.45 μm syringe filter. Then, the final eluents were added to a Superdex 200 10/300 GL column (GE Healthcare) for further purification in 50 mM HEPES (pH 7.4) and 150 mM NaCl on an GE Healthcare AKTA purifier. The solutions containing His-GFP-NLRP3 protein were collected together and concentrated by ultrafiltration device to remove proteins <100 kD. Meanwhile, 10 μl solution was dissolved in sample buffer and analyzed using immunoblotting.

NLRP3 ATPase Activity Assay

Purified human NLRP3 protein (1.4 ng/μl) was incubated with indicated doses of 149-01 or 1 μM CY-09 in reaction buffer at 37°C for 15 min and then ATP (25 μm, Ultra-Pure ATP) was added. After further incubation at 37°C for 40 min, the amount of ATP converted into ADP in the mixture was measured by luminescent ADP detection using ADP-Glo Kinase Assay kit (Promega, Madison, MI, United States). The data were presented as percentage of residual enzyme activity versus vehicle-treated enzyme activity.

Microscale Thermophoresis Assay

A Monolith NT.115 instrument (NanoTemper Technologies) was used to measure the K_D value. Purified His-GFP-NLRP3 protein (200 nM) was incubated at room temperature with a range of doses of 149-01 (from 1 μM to 0.0169 nM) in assay buffer (50 mM HEPES, 10 mM $MgCl_2$, 100 mM NaCl, pH 7.5, and 0.05% Tween 20) for 40 min. After the mixtures were loaded onto the NanoTemper glass capillaries, measurements were performed using 80% MST power and 100% LED power. K_D value calculations were done using the mass action equation through NanoTemper software from duplicate reads of an experiment.

Drug Affinity Responsive Target Stability Assays

Assays were performed according to published protocols. BMDMs primed with LPS (3 h) or HEK-293T cells transfected with plasmid (24 h) were collected and lysed in NP-40 lysis buffer containing protease inhibitor cocktail. The cell lysates were centrifuged at 12,000×*g* at 4°C for 10 min and the supernatants were then measured by Pierce BCA Protein Assay Kit (Beyotime) to determine the protein concentration. After that, lysates (8 μg of protein lysate per reaction) were incubated at 4°C with indicated doses of 149-01 overnight with rotation. The mixtures were further incubated with protease pronase (25 ng of enzyme per μg of protein, Sigma) at room temperature for another 30 min. Then, the samples were dissolved directly in sample buffer and analyzed using immunoblotting.

NLRP3 Reconstitution

Nlrp3$^{-/-}$ BMDMs were seeded into 12-well plates and cultured overnight. Then, cells were transduced with lentivirus (pLEX vector, Thermo Fisher) encoding mouse NLRP3 or their indicated mutant (C405A). After 6 h, the culture supernatant was removed and replaced with DMEM containing 10% FBS and 20 ng/ml murine M-CSF. After 48 h, BMDMs were stimulated with nigericin.

Histological Analysis

Mouse spinal cords were fixed in 4% PFA at 4°C for 24 h, embedded in paraffin, and sectioned. Then, sections were stained with H&E or LFB according to standard procedures. Histological analysis for inflammatory cell infiltration and demyelination was performed with a Nikon ECL IPSE Ci biological microscope, and images were recorded using a Nikon DS-U3 color digital camera.

Quantitative Real-Time PCR

Total RNA from tissues was extracted using TRIzol reagent (Takara). To synthesize cDNA, 800 ng of total RNA from each sample was reverse transcribed with Moloney murine leukemia virus (M-MLV) reverse transcriptase (Invitrogen). Then qPCR analysis was performed with SYBR Green premix (Takara Bio). All data were individually normalized to *Gapdh*. The primer sequences are shown as follows:

for mouse *Gapdh*: forward, GGTGAAGGTCGGTGTGAACG; reverse, CTCGCTCCTGGAAGATGGTG; for mouse *Il1b*: forward, TGCCACCTTTTGACAGTGATG; reverse, AAGGTCCACGGGAAAGACAC; for mouse *Tnf*: forward, CGATGGGTTGTACCTTGTC; reverse, CGGACTCCGCAAAGTCTAAG; for mouse *Il6*: forward, GTCCTTCCTACCCCAATTTCC; reverse, GCACTAGGTTTGCCGAGTAGA.

LPS-Induced Systemic Inflammation

8-week-old male mice were injected intraperitoneally with 5 mg/kg 149-01 or vehicle control (90% PBS plus 10% DMSO) for 30 min and then challenged with 20 mg/kg LPS. After 4 h,

mice were sacrificed and the secretion of IL-1β and TNF-α in serum was detected by ELISA.

MSU-Induced Peritonitis

8-week-old male mice pretreated with 5 mg/kg 149-01 or vehicle (90% PBS plus 10% DMSO) for 30 min were intraperitoneally injected with 1 mg MSU (dissolved in 0.5 ml PBS). After 6 h, mice were sacrificed and peritoneal cavities were washed with 10 ml ice-cold PBS. The proportion of polymorph nuclear neutrophils was detected by flow cytometry and the number of peritoneal exudate cells was counted. In addition, the secretion of IL-1β in lavage fluid or serum was also measured using ELISA.

Induction and Assessment of EAE

8-week-old male mice were subcutaneously immunized with 300 μg MOG_{35-55} peptide emulsified in CFA supplemented with 5 mg/ml (0.5 mg/mouse) of heat-killed Mycobacterium tuberculosis. Mice were intravenously injected with 150 ng pertussis toxin on days 0 and 2.149-01 (5 mg/kg) was administered intraperitoneally to mice on the day of induction and every 2 days thereafter. Control mice were given vehicle (90% PBS plus 10% DMSO) at the same time points. Clinical disease scores were recorded according to the following standard scale: 0, no abnormalities; 1, limp tail or waddling gait with tail tonicity; 2, wobbly gait; 3, hind limb paralysis; 4, hind limb and forelimb paralysis; 5, death. Mononuclear cells isolated from both the brain and spinal cord using 30% Percoll separation were analyzed by flow cytometry.

Statistical Analyses

All data are presented as mean ± s.e.m. Statistical analysis was carried out with one-way ANOVA (GraphPad Software) for data in all figures (except **Figure 7** and **Supplementary Figure S7**) or with unpaired Student's t-tests (GraphPad Software) for data in **Figure 7** and **Supplementary Figure S7**, and differences were considered significant at $p < .05$. No values were excluded.

RESULTS

149-01 Blocks NLRP3 Inflammasome Activation

Several RRx-001 analogues were screened for their NLRP3 inhibitory activity in **Supplementary Figure S1A** and their chemical structure were depicted in **Supplementary Table S1**. In the screening results of RRx-001 analogues, 149-01 showed comparable NLRP3 inhibitory activity with RRx-001. To further evaluate the inhibitory effect of 149-01 on NLRP3 inflammasome activation, mouse bone marrow-derived macrophages (BMDMs) were first primed with LPS, then pretreated with 149-01 for 30 min, lastly stimulated with the NLRP3 stimulus nigericin. We found that 149-01 dose-dependently inhibited IL-1β release and caspase-1 activation at the doses of 200-600 nM (**Figures 1A–C**). Consistently, 149-01 also suppressed nigericin-induced release of lactate dehydrogenase (LDH) (**Figure 1D**), but LPS-dependent IL-6 and TNF-α secretion was not affected (**Figures 1E,F**), which suggests that 149-01 inhibits NLRP3-dependent cytokine production and pyroptosis. To ascertain whether 149-01 only blocked NLRP3 activation induced by nigericin, we tested the effects of 149-01 on NLRP3 activation triggered by two additional agonists, ATP and MSU. We observed that 149-01 inhibited IL-1β release and caspase-1 activation triggered by both NLRP3 agonists (**Figures 1G,H**). In addition, 149-01 also dose-dependently suppressed intracellular LPS-induced noncanonical NLRP3 inflammasome activation (**Supplementary Figures S2A,B**) but did not reduce LDH release (**Supplementary Figure S2C**). As previously reported, intracellular LPS induced LDH release was independent of NLRP3 (Coll et al., 2015). These results demonstrate that 149-01 displays potent and broad inhibitory effects on both canonical and non-canonical NLRP3 activation.

We next investigated whether 149-01 was effective for human cells. We isolated human peripheral blood mononuclear cells (PBMCs), treated LPS-primed cells with 149-01 for 30 min and then activated NLRP3 inflammasome with nigericin. We observed that 149-01 treatment reduced IL-1β release in a dose-dependent manner but not TNF-α production (**Figures 1I,J**). Furthermore, LPS alone induced alternative NLRP3 inflammasome activation was also suppressed by 149-01 in PBMCs (**Supplementary Figures S2D,E**). These results together indicate that 149-01 can prevent NLRP3 inflammasome activation in both mouse and human cells.

Because RRx-001 is reported to inhibit pro-IL-1β expression in macrophages (Yu et al., 2019; Chen et al., 2021), we then tested whether 149-01 influenced LPS-induced priming phase of NLRP3 inflammasome activation. We found that at concentrations of 200-600 nM, 149-01 treatment before or after LPS stimulation did not affect LPS-induced pro-IL-1β, NLRP3 production and IL-6, TNF-α secretion (**Supplementary Figures S3A–C**), indicating that 149-01 does not influence LPS-induced priming phase at concentrations that blocks NLRP3 activation. Although at higher concentrations of 1–4 μM, 149-01 treatment before LPS stimulation markedly inhibited LPS-induced pro-IL-1β and IL-6 production but did not affect NLRP3 or TNF-α expression (**Supplementary Figures S4A–C**), 149-01 showed approximately 9 times inhibitory activity against IL-1β release than that against IL-6 production (**Supplementary Figures S4D,E**). Besides, higher concentrations (one to four μM) of 149-01 treatment after LPS stimulation did not affect LPS-induced pro-IL-1β, NLRP3 production and IL-6, TNF-α secretion (**Supplementary Figures S4A–C**).

149-01 Does Not Affect AIM2, NLRC4, or Pyrin Inflammasomes Activation

Besides NLRP3, several other sensors were also proposed to trigger inflammasome complex assembly (Xu et al., 2014; Broz and Dixit, 2016). To explore the specificity of 149-01's inhibitory activity against NLRP3 inflammasome, we examined whether 149-01 could suppress the activation of three other well-characterized inflammasome. Murine BMDMs were first primed with LPS, then transfected with double-stranded DNA analog poly (A/T) to induce the AIM2 (Absent In Melanoma 2) inflammasome activation or infected with S. typhimurium to

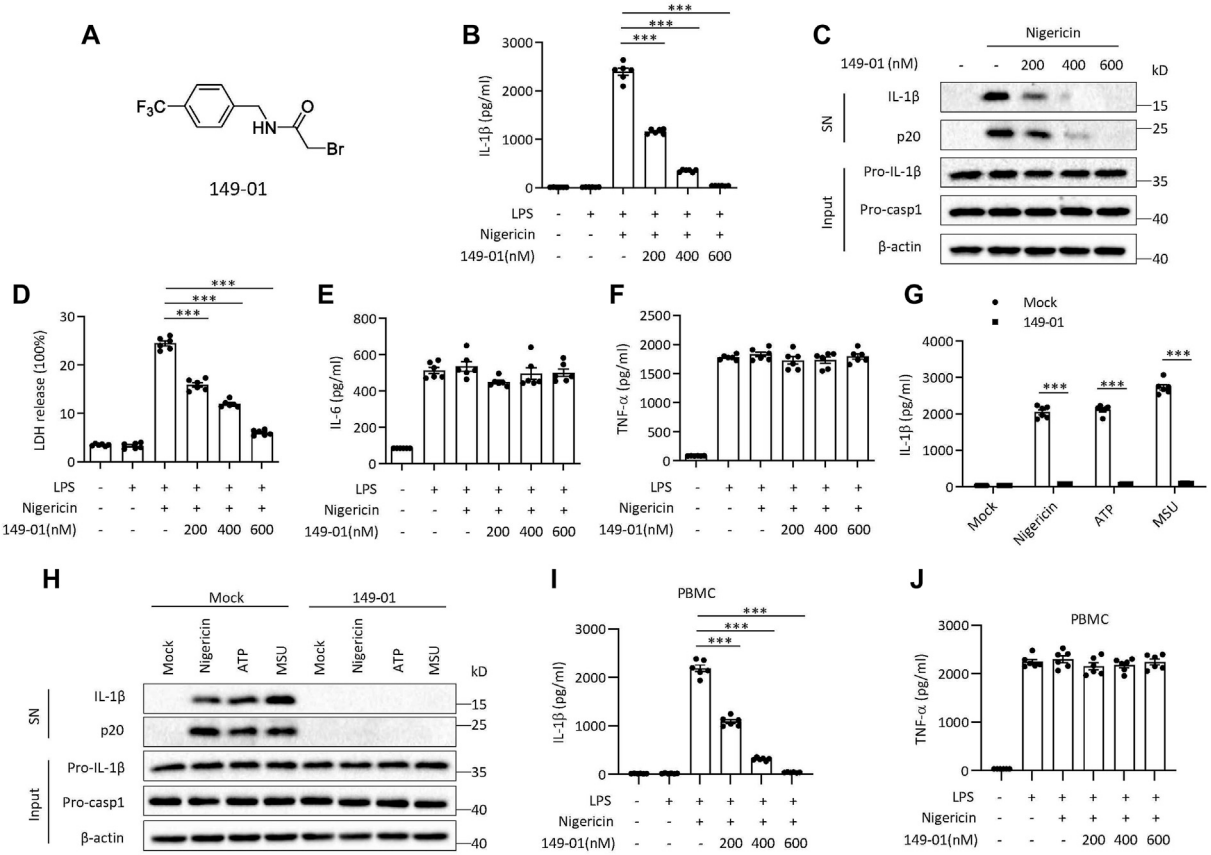

FIGURE 1 | Identification of 149-01 as a highly potent inhibitor for NLRP3 inflammasome. **(A)** 149-01 structure. **(B–F)** BMDMs were first primed with LPS for 3 h, then pretreated with indicated doses of 149-01 (200-600 nM) for 30 min, lastly stimulated with nigericin. **(B)** IL-1β releases in supernatants were detected by ELISA. **(C)** Active IL-1β and p20 (cleaved caspase-1) in supernatants (SN) and pro-IL-1β, pro-caspase-1 and *β*-actin in cell lysates (Input) were measured by western blot. **(D)** The release of LDH in supernatants. **(E)** IL-6 and **(F)** TNF-α secretion levels in supernatants were determined by ELISA. **(G,H)** BMDMs were first primed with LPS, then treated with or without 149-01 (600 nM) for 30 min, lastly stimulated with nigericin, ATP or MSU. **(G)** IL-1β releases in supernatants were detected by ELISA. **(H)** Active IL-1β and p20 in supernatants and pro-IL-1β, pro-caspase-1 and *β*-actin in cell lysates were measured by western blot. **(I,J)** PBMCs were first primed with LPS for 3 h, then pretreated with indicated doses of 149-01 for 30 min, lastly stimulated with nigericin. **(I)** IL-1β and **(J)** TNF-α secretion levels in supernatants were determined by ELISA. Data are obtained from three independent experiments, each with two biological replicates and are expressed as mean ± s. e.m (n = 6) **(B,D–G,I,J)**, or are representative of three independent experiments **(C,H)**. One-way ANOVA was applied to calculate statistical significance: ***p < .001.

induce the NLRC4 (NLR Family CARD Domain Containing 4) inflammasome activation or stimulated with C3 toxin to induce the Pyrin inflammasome activation. In contrast to its potent inhibitory effects on NLRP3 inflammasome activation, 149-01 could not inhibit IL-1β release or caspase-1 activation following AIM2 or NLRC4 inflammasome activation (**Figures 2A,B**). In addition, 149-01 also could not attenuate IL-1β release triggered by Pyrin inflammasome activation (**Figure 2C**). Collectively, our data show that 149-01 selectively suppresses NLRP3 inflammasome activation.

149-01 Suppresses the Assembly of NLRP3 Inflammasome by Preventing the NEK7-NLRP3 Interaction

Next, we sought to identify the precise mechanism by which 149-01 prevents NLRP3 inflammasome activation. Potassium (K^+) efflux and chloride (Cl^-) efflux are proposed to be upstream events required for NLRP3 activation (Munoz-Planillo et al., 2013; Tang et al., 2017). To determine whether 149-01 abrogates NLRP3 activation by affecting these upstream events, we tested intracellular levels of K^+ and Cl^- after nigericin stimulation. We found that pretreatment with 149-01 in BMDMs did not prevent the nigericin-induced decrease in intracellular K^+ and Cl^- (**Supplementary Figures S5A,B**). Consistent with this, we also observed that 149-01 could dose-dependently suppress NLRP3 inflammasome activation induced by CL097, which is a K^+ efflux-independent NLRP3 agonist (**Supplementary Figure S5C**) (Gross et al., 2016). In addition, mitochondrial damage is considered to be another upstream event required for NLRP3 activation (Zhou et al., 2011; Gurung et al., 2015). We next detected the mitochondrial status of BMDMs after nigericin stimulation and observed abnormal mitochondrial fission, clustering, and enhanced ROS production. However, pretreatment with 149-01 did not significantly affect these processes (**Supplementary Figure S5D**). Taken together, our

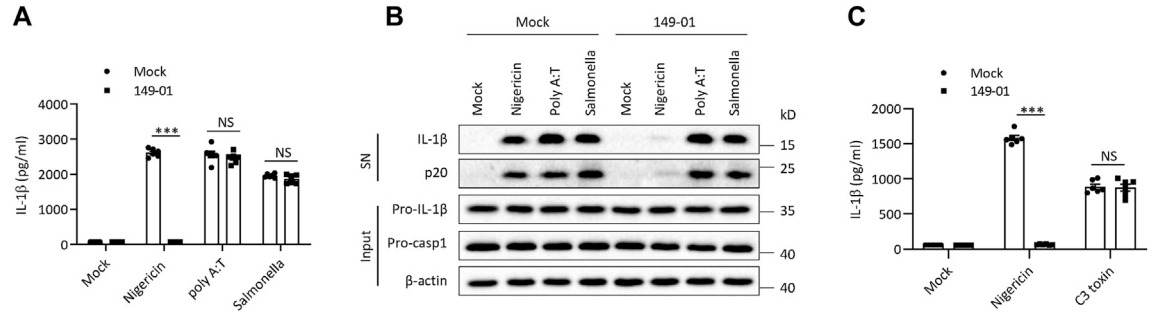

FIGURE 2 | 149-01 does not affect the activation of AIM2, NLRC4, or Pyrin inflammasomes. **(A–C)** BMDMs were first primed with LPS, then treated with or without 149-01 (600 nM) for 30 min, lastly stimulated with nigericin, poly (A/T), Salmonella or C3 toxin. **(A,C)** IL-1β releases in supernatants were detected by ELISA. **(B)** Active IL-1β and p20 in supernatants and pro-IL-1β, pro-caspase-1 and β-actin in cell lysates were measured by western blot. Data are obtained from three independent experiments, each with two biological replicates and are expressed as mean ± s. e.m ($n = 6$) **(A,C)**, or are representative of three independent experiments **(B)**. One-way ANOVA was applied to calculate statistical significance: ***$p < .001$, NS, not significant.

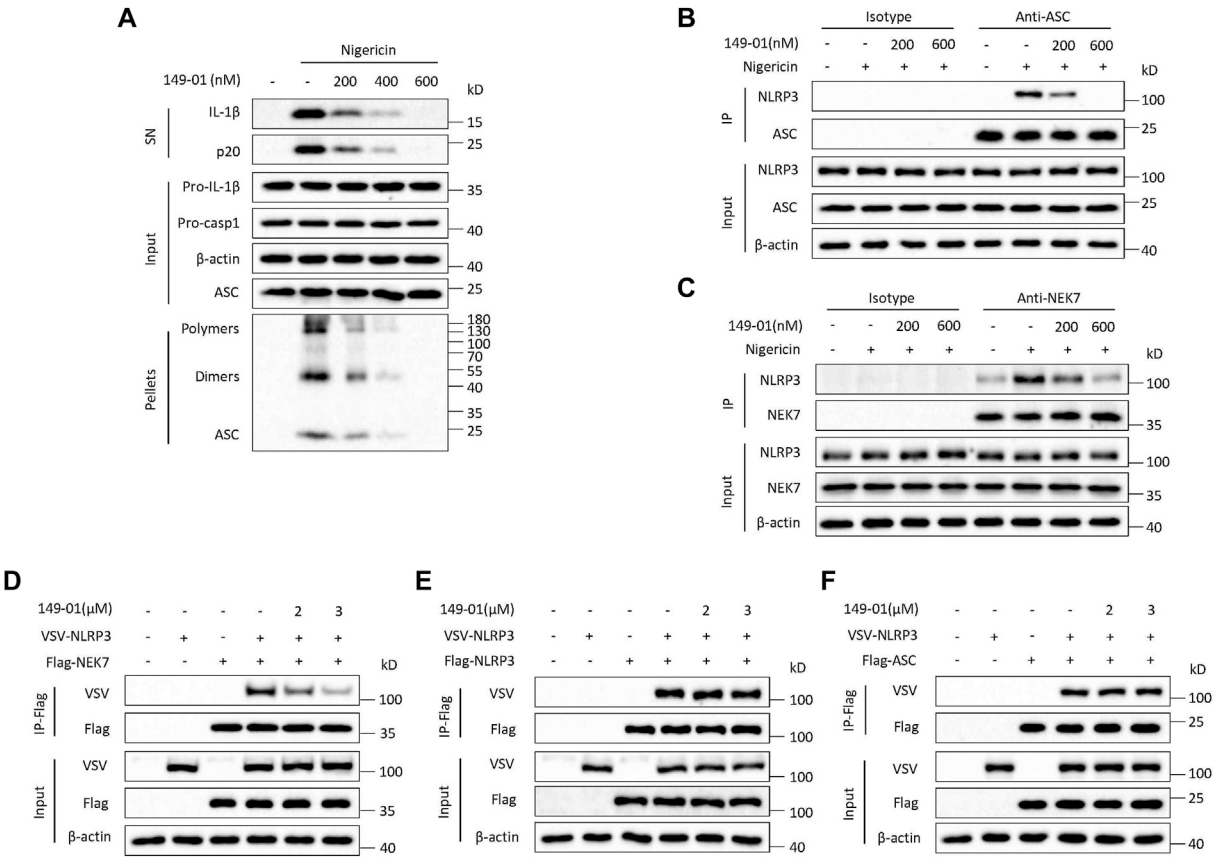

FIGURE 3 | 149-01 blocks the assembly of NLRP3 inflammasome by preventing the interaction between NEK7 and NLRP3. **(A)** Supernatants, cell lysates and DSS-crosslinked pellets from LPS-primed BMDMs treated with indicated doses of 149-01 for 30 min before nigericin stimulation were analyzed by western blot. **(B)** The endogenous NLRP3-ASC interaction in LPS-primed BMDMs treated with indicated doses of 149-01 for 30 min before nigericin stimulation was detected by immunoprecipitation (IP) and western blot. **(C)** The endogenous NEK7-NLRP3 interaction in LPS-primed BMDMs treated with indicated doses of 149-01 for 30 min before nigericin stimulation was detected by IP and western blot. **(D)** The NEK7–NLRP3 interaction in HEK-293T cells transfected with Flag-NEK7, VSV-NLRP3 plasmids and treated with indicated doses of 149-01 was evaluated by IP and western blot. **(E)** The NLRP3–NLRP3 interaction in HEK-293T cells transfected with Flag-NLRP3, VSV-NLRP3 plasmids and treated with indicated doses of 149-01 was evaluated by IP and western blot. **(F)** The NLRP3–ASC interaction in HEK-293T cells transfected with Flag-ASC, VSV-NLRP3 plasmids and treated with indicated doses of 149-01 was evaluated by IP and western blot. Data are representative of three independent experiments.

findings indicate that 149-01 blocks NLRP3 activation by acting downstream of K^+ efflux, Cl^- efflux and mitochondrial damage.

We then tested whether 149-01 could block NLRP3 activation by influencing NLRP3 inflammasome complex assembly. A critical step for NLRP3 inflammasome complex assembly and subsequent caspase-1 activation is ASC oligomerization (Lu et al., 2014; Dick et al., 2016), which can be detected after chemical cross-linking followed by western blotting. Consistent with inhibition of IL-1β release and caspase-1 activation, 149-01 markedly suppressed ASC oligomerization induced by nigericin at the doses of 200-600 nM without affecting ASC expression in cell lysates (**Figure 3A**), indicating that 149-01 prevents NLRP3 activation by acting upstream of ASC oligomerization. Next, we examined by coimmunoprecipitation whether 149-01 could block NLRP3-ASC interaction, which is essential for ASC recruitment and subsequent ASC oligomerization (Swanson et al., 2019). We observed that 149-01 dramatically attenuated the interaction between endogenous NLRP3 and ASC in nigericin stimulated BMDMs (**Figure 3B**). Moreover, we investigated if 149-01 influenced NEK7–NLRP3 interaction, which is imperative for NLRP3 oligomerization and subsequent NLRP3-ASC complex formation (He et al., 2016; Shi et al., 2016). We found that 149-01 substantially abolished the nigericin-mediated endogenous NEK7-NLRP3 interaction (**Figure 3C**). Collectively, these findings reveal that 149-01 may prevents NLRP3 inflammasome complex assembly by blocking the NEK7-NLRP3 interaction.

To validate this hypothesis, we overexpressed Flag-NEK7 and VSV-NLRP3 in HEK-293T cells, and explored by coimmunoprecipitation whether 149-01 could inhibit direct NEK7-NLRP3 interaction. The results showed that 149-01 treatment blocked the direct NEK7-NLRP3 interaction (**Figure 3D**). In contrast, 149-01 treatment had no impact on the direct NLRP3-NLRP3 or NLRP3-ASC interaction (**Figures 3E,F**). Therefore, these results suggest that 149-01 inhibits NLRP3 inflammasome activation by abrogating the direct NEK7-NLRP3 interaction, rather than by affecting NLRP3 oligomerization or subsequent NLRP3-ASC complex formation. Consistent with this, we found that 149-01 did not impact the NLRP3 ATPase activity (**Supplementary Figure S6A**), which is critical for the NLRP3 self-oligomerization (Duncan et al., 2007). In the same experiment, the known NLRP3 inflammasome inhibitor CY-09 was used as a positive control (Jiang et al., 2017). In addition, NEK7 has also been reported to act downstream of NEK9 and contribute to mitotic progression (Haq et al., 2015). However, 149-01 treatment did not affect the interaction between NEK7 and NEK9 (**Supplementary Figure S6B**).

149-01 Binds Directly to Cys409 of NLRP3

We next determined whether the activation of NLRP3 inflammasome inhibited by 149-01 was reversible. LPS-primed mouse BMDMs were first treated with 149-01 for 15 min, then washed every 5 min for three times to remove unbound 149-01, and lastly stimulated with nigericin. We observed that nigericin-induced IL-1β release remained inhibited after removal of unbound 149-01, suggesting that 149-01's inhibitory effect on NLRP3 activation is essentially irreversible (**Figure 4A**). In contrast, the inhibitory effects of CY-09 on NLRP3 activation is reversible (**Supplementary Figure S6C**). Together these data suggest that 149-01 may bind its target protein in a covalent manner.

Based on the result that 149-01 blocks the direct NEK7-NLRP3 interaction, we inferred that 149-01 may prevents NLRP3 inflammasome complex assembly by directly targeting NEK7 or NLRP3. To confirm this conjecture, we performed the drug affinity responsive target stability (DARTS) assay (Lomenick et al., 2009; Coll et al., 2019), which exploits the target protein's reduced sensitivity to protease when it interacts with small molecules. We incubated the LPS-primed BMDMs cell lysates with different concentrations of 149-01, then digested with the protease pronase, and observed that 149-01 dose-dependently reduced proteolysis of NLRP3 by pronase (**Figure 4B**), suggesting that 149-01 directly interacts with NLRP3. However, incubation with 149-01 did not affect pronase mediated degradation of other NLRP3 inflammasome components, including NEK7, pro-casp1 and ASC (**Figure 4B**), indicating that 149-01 specifically targets NLRP3. To further validate the direct binding of 149-01 to NLRP3, we employed microscale thermophoresis (MST) assay to quantify the direct interaction between 149-01 and purified GFP-NLRP3. The data revealed that 149-01 interacted with purified GFP-NLRP3 with an equilibrium dissociation constant (K_D) of 48.2 nM (**Figure 4C**). Therefore, our results reveal that 149-01 binds directly to NLRP3 with high affinity. To investigate whether 149-01 interacted with other inflammasome sensors, we overexpressed flag-tagged NLRP3, NLRP1b, AIM2 or NLRC4 in HEK-293T cells and then performed DARTS experiments. The results showed that 149-01 protected only NLRP3 but not NLRP1b, AIM2 or NLRC4 from pronase-induced proteolysis in a dose-dependent manner (**Figures 4D–G**).

We next overexpressed three functional domains of NLRP3 in HEK-293T cells, NACHT, LRR and PYD, respectively, to explore which domain is responsible for interacting with 149-01. We found that only the NACHT domain but not the LRR or PYD domain could be protected by 149-01 from pronase-mediated proteolysis (**Figures 5A–C**). These results together demonstrate that 149-01 directly and specifically targets the NACHT domain of NLRP3. Next, we sought to determine the 149-01-binding residue within the NLRP3 NACHT domain. Since RRx-001 has been reported to bind to cysteine 409 (Chen et al., 2021), we tested whether 149-01 also targeted the C409 site of the NACHT domain. Flag-tagged the NACHT domain with the C409A mutation was overexpressed in HEK-293T cells and then performed DARTS assay. We observed that the C409A mutation abrogated the interaction between 149-01 and the NACHT domain (**Figure 5D**). Furthermore, the C409A mutation had no effect on the NEK7-NLRP3 interaction, but abolished 149-01's inhibitory effect on this interaction (**Figure 5E**), suggesting that 149-01 binds directly to C409 of NLRP3. We then reconstituted *NLRP3*$^{-/-}$ BMDMs with mouse WT NLRP3 or mutant NLRP3 (C405A, corresponding to human NLRP3-C409A) and found that nigericin-induced NLRP3

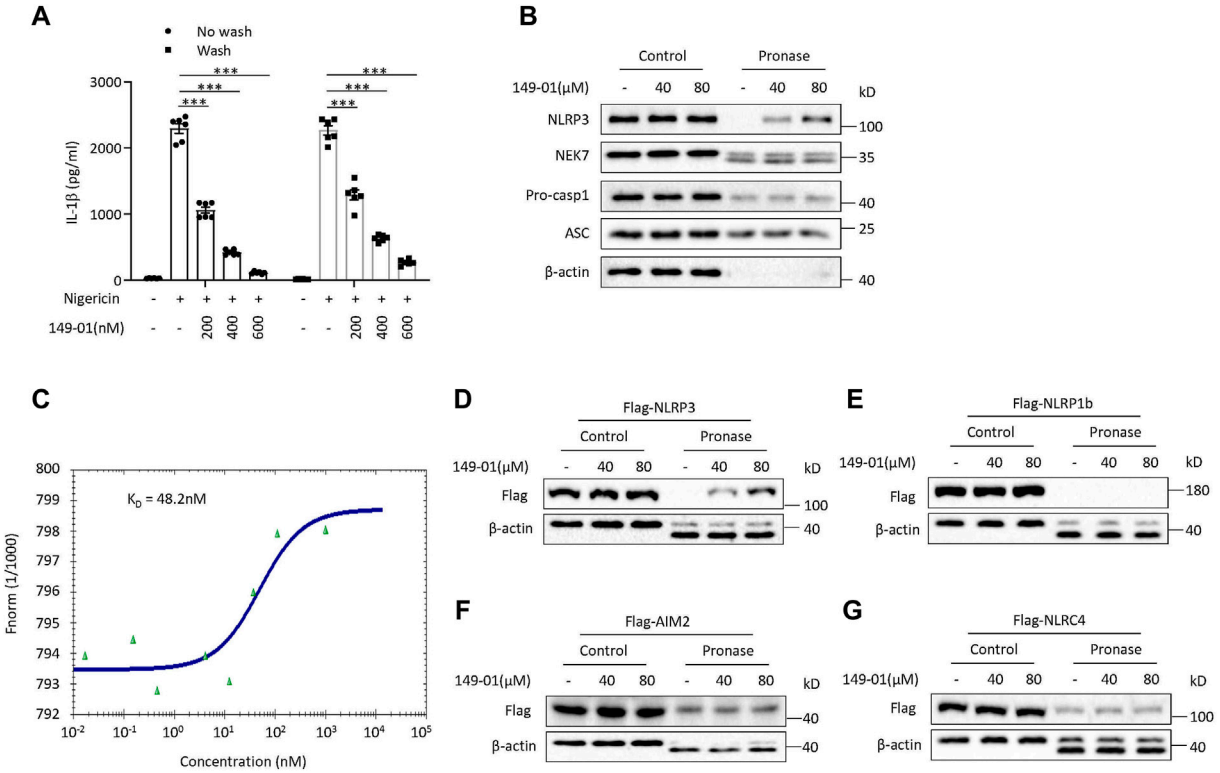

FIGURE 4 | 149-01 irreversibly, directly, and specifically binds to NLRP3. **(A)** IL-1β releases in supernatants from LPS-primed BMDMs treated with indicated doses of 149-01 for 15 min, washed three times before nigericin stimulation were detected by ELISA. **(B)** LPS-primed BMDMs cell lysates incubated overnight with indicated doses of 149-01 before pronase digestion were detected by western blot using antibodies for NLRP3, NEK7, pro-caspase-1, ASC and *β*-actin. **(C)** Binding affinity of 149-01 to purified GFP-NLRP3 protein was analyzed by MST. HEK-293T cells transfected with Flag-tagged NLRP3 **(D)**, NLRP1b **(E)**, AIM2 **(F)**, or NLRC4 **(G)** were lysed and the cell lysates incubated overnight with indicated doses of 149-01 before pronase digestion were detected by western blot. Data are obtained from three independent experiments, each with two biological replicates and are expressed as mean ± s. e.m (n = 6) **(A)**, or are representative of three independent experiments **(B–G)**. One-way ANOVA was applied to calculate statistical significance: ***$p < .001$.

activation was blocked by 149-01 in cells reconstituted with WT NLRP3 but remained intact in cells reconstituted with mutant NLRP3 (**Figures 5F,G**). Collectively, our results suggest that 149-01 binds directly to cysteine 409 of NLRP3 and then prevents the NEK7-NLRP3 interaction and ultimately inhibits NLRP3 inflammasome activation.

149-01 Suppresses NLRP3 Inflammasome *in vivo*

Since 149-01 disrupts NLRP3 inflammasome activation *in vitro*, we next tested the therapeutic efficacy of 149-01 in NLRP3-dependent septic shock disease model, in which intraperitoneal injection of LPS could elicit NLRP3-driven IL-1β production (He et al., 2013). Mice were injected with 149-01 intraperitoneally before challenge with LPS and were evaluated 4 h later. The data revealed that pretreatment with 149-01 markedly downregulated serum IL-1β level without considerably decreasing NLRP3-independent TNF-α production in serum (**Figures 6A,B**). These findings indicate that 149-01 suppresses LPS-induced NLRP3-related systemic inflammation *in vivo*.

MSU crystal-induced peritonitis is another well-established NLRP3-dependent acute inflammatory model characterized by IL-1β secretion and massive neutrophil infiltration in peritoneal cavity (Martinon et al., 2006). To investigate the inhibitory activity of 149-01 in peritonitis model, mice were pretreated with 149-01 before intraperitoneal injection of MSU. As expected, pretreatment with 149-01 efficiently inhibited IL-1β secretion and neutrophil recruitment (**Figures 6C–E**). Our results suggest that 149-01 significantly alleviates MSU-induced peritonitis in mice.

The experimental autoimmune encephalomyelitis (EAE) mouse model, which effectively simulates human multiple sclerosis disease, is characterized by inflammation and demyelination. Considering that NLRP3 inflammasome acts a key role in the pathogenesis of EAE and exacerbates neuroinflammation (Sutton et al., 2006; Gris et al., 2010; Lalor et al., 2011), we then assessed whether 149-01 could alleviate the severity of EAE *via* targeting NLRP3 inflammasome. We induced EAE by subcutaneous immunizing mice with myelin oligodendrocyte glycoprotein (MOG) peptide (MOG_{35-55}) and recorded clinical disease scores on a daily basis. Compared with the vehicle-treated group, treatment of mice with 149-01

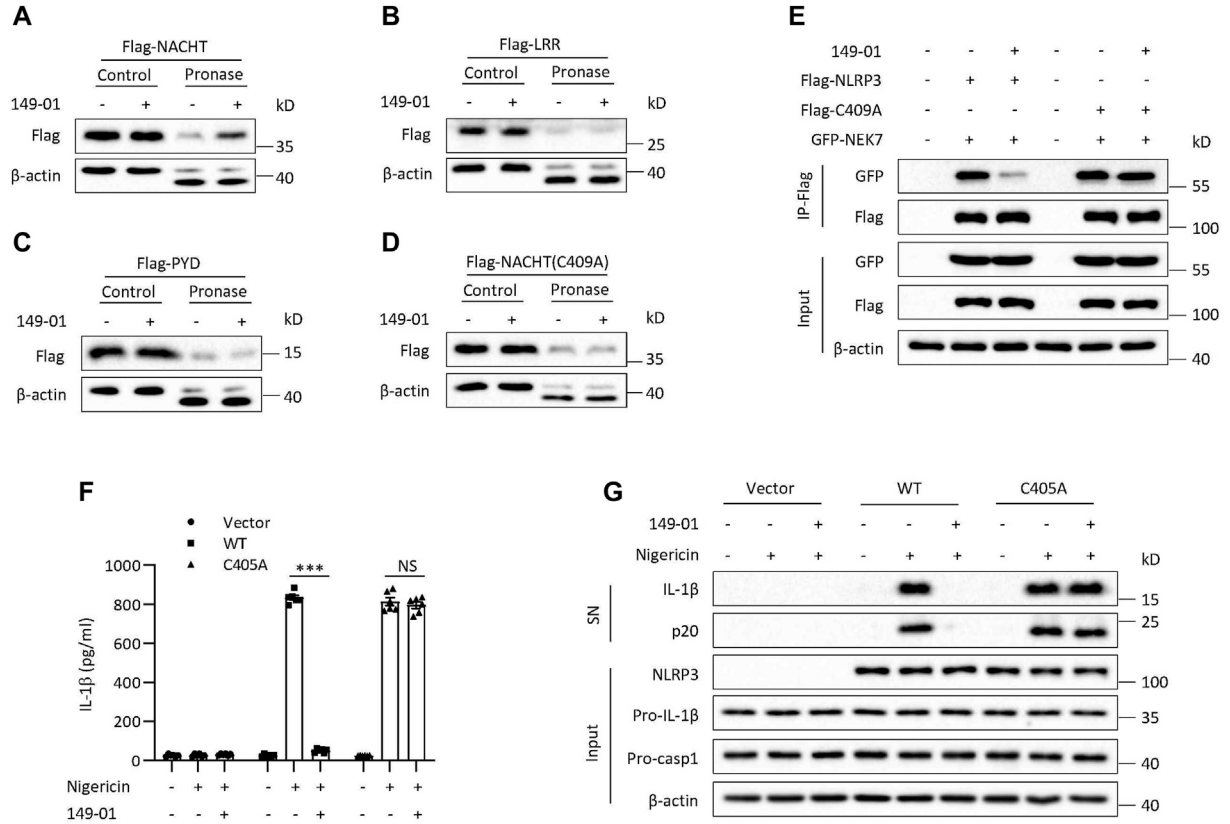

FIGURE 5 | 149-01 targets Cys409 of NLRP3. HEK-293T cells transfected with Flag-tagged NACHT **(A)**, LRR **(B)**, PYD **(C)**, or NACHT (C409A) **(D)** were lysed and the cell lysates incubated overnight with or without 149-01 (80 μM) before pronase digestion were detected by western blot. **(E)** The interactions between NEK7 and WT or mutant NLRP3 in HEK-293T cells treated with or without 149-01 (3 μM) were evaluated by IP and western blot. **(F,G)** *Nlrp3*$^{-/-}$ BMDMs reconstituted with mouse WT or mutant NLRP3 were first primed with LPS, then treated with or without 149-01 (600 nM) for 30 min, lastly stimulated with nigericin. **(F)** IL-1β releases in supernatants were detected by ELISA. **(G)** Active IL-1β and p20 in supernatants and NLRP3, pro-IL-1β, pro-caspase-1 and *β*-actin in cell lysates were measured by western blot. Data are obtained from three independent experiments, each with two biological replicates and are expressed as mean ± s. e.m (n = 6) **(F)**, or are representative of three independent experiments **(A–E,G)**. One-way ANOVA was applied to calculate statistical significance: ***p < .001, NS, not significant.

improved their clinical behaviors (**Figure 7A**). Consistent with this phenotype, in mice 14 days after EAE induction, HE staining revealed that 149-01 treatment ameliorated inflammatory cell infiltration in the spinal cord and LFB staining showed that 149-01 treatment reduced spinal cord demyelination (**Figure 7B**). In addition, the proportions and absolute numbers of infiltrated T cells ($CD8^+$ and $CD4^+$), total lymphocytes ($CD11b^-$ $CD45^{hi}$), activated resident microglial cells and myeloid cells ($CD11b^+$ $CD45^{hi}$) gated on $CD45^{hi}$ cell populations in the CNS were markedly reduced in 149-01-treated mice (**Figures 7C,D**). Further investigation of inflammation in EAE mice showed that 149-01 treatment significantly inhibited the expression of inflammatory cytokines in the CNS, including IL-1β, IL-6 and TNF-α (**Figure 7E**). Furthermore, 149-01 treatment significantly reduced protein levels for IL-1β, caspase-1 and NLRP3 in the spinal cords of EAE mice (**Figures 7F,G**). Collectively, these findings suggest that the disease progression of EAE can be attenuated effectively by 149-01 administration. To confirm that 149-01 mitigate EAE severity through suppression of NLRP3 inflammasome, we induced EAE in *NLRP3* knockout mice. We found that treatment of *NLRP3*$^{-/-}$ mice with 149-01 did not affect the clinical disease scores of EAE (**Figure 7H**) or the proportions and numbers of infiltrated immune cells in the CNS (**Figures 7I,J**). We also evaluated the safety profile of 149-01 in naive mice. Mice were intraperitoneally injected with 5 mg/kg 149-01 or vehicle control once a day for 4 weeks, and the results showed that 149-01 treatment did not affect the metabolic parameters and serum chemistry of naive mice (**Supplementary Figure S7**). Taken together, our results demonstrate that 149-01 is active *in vivo* and can mitigate the progression of inflammatory diseases by targeting NLRP3 inflammasome.

DISCUSSION

In this study, we identify compound 149-01, an RRx-001 analogue, as a potent, specific and covalent NLRP3 inhibitor, which can effectively inhibit the NLRP3 inflammasome activation both *in vitro* and *in vivo*. Our study suggests that 149-01 may be a useful small molecule tool to investigate the mechanism of NLRP3 inflammasome activation and a potential lead for

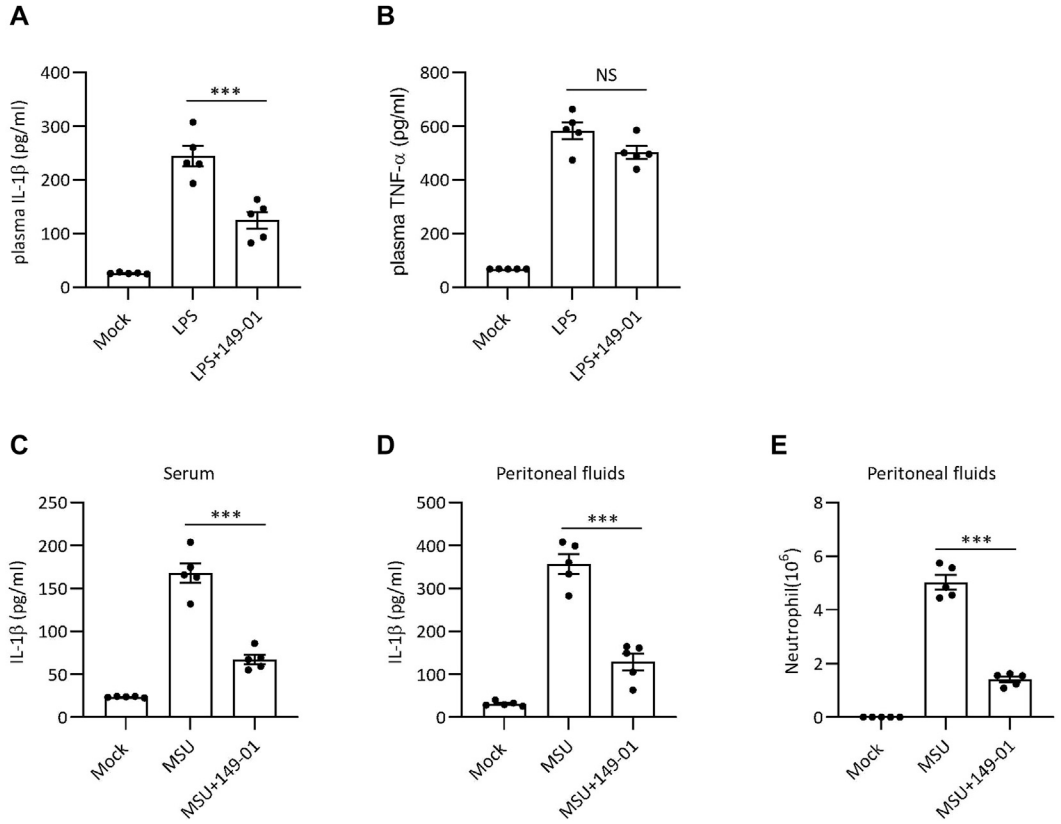

FIGURE 6 | 149-01 alleviates LPS-induced systemic inflammation and MSU-induced peritonitis in mice. **(A,B)** Serum IL-1β **(A)** and TNF-α **(B)** levels in mice intraperitoneally injected with 149-01 (5 mg/kg) or vehicle before challenge with LPS (20 mg/kg) were measured by ELISA. **(C–E)** Mice were intraperitoneally injected with 149-01 (5 mg/kg) or vehicle before challenge with MSU (1 mg/mouse). IL-1β in the serum **(C)** or peritoneal cavity **(D)** were measured by ELISA. **(E)** Neutrophil numbers in the peritoneal cavity were determined by FACS. Data are expressed as mean ± s. e.m (n = 5). One-way ANOVA was applied to calculate statistical significance: ***p < .001, NS, not significant.

developing therapeutic agent for NLRP3-driven inflammatory diseases.

Our results showed that the IC50 (half-maximal inhibitory concentration) value of 149-01 inhibiting IL-1β release is 182.8 nM, indicating that its inhibitory activity is stronger than most of the reported NLRP3 inhibitors, and 149-01 exhibits comparable inhibitory activity against NLRP3 inflammasome as RRx-001 (Chen et al., 2021). At the doses of 200-600 nM, 149-01 dose-dependently suppressed canonical and non-canonical NLRP3 activation in mouse cells and canonical and alternative NLRP3 activation in human cells. Meanwhile, 149-01 had no effect on the activation of AIM2, NLRC4, or Pyrin inflammasome, nor did it affect the priming phase of NLRP3 inflammasome at this concentration. These results demonstrate that 149-01 displays potent, broad and specific inhibitory effects on NLRP3 activation. We also observed that 149-01 treatment before LPS stimulation significantly inhibited LPS-induced pro-IL-1β and IL-6 production at higher doses of 1–4 μM, and the concentration required to inhibit IL-6 release is ~9 times higher than that required to inhibit IL-1β release, suggesting that 149-01 may have better therapeutic activity in NLRP3-related inflammatory disorders than in other inflammatory disorders. However, the specific mechanism by which high doses of 149-01 inhibits LPS-induced pro-IL-1β and IL-6 production and its possible effects remain unclear. One possibility is that high doses of 149-01 also affect the function of other proteins, and high doses of 149-01 affect pro-IL-1β and IL-6 production by targeting other proteins.

Mechanistically, our data indicated that 149-01 does not block NLRP3 inflammasome activation by affecting upstream events, including K^+ efflux, Cl^- efflux and mitochondrial damage (Zhou et al., 2011; Munoz-Planillo et al., 2013; Gurung et al., 2015; Tang et al., 2017), suggesting that 149-01 may directly affect the assembly of NLRP3 inflammasome complex. Indeed, 149-01 blocked the interaction between NEK7 and NLRP3 by irreversibly targeting cysteine 409 of NLRP3, ultimately inhibiting the NLRP3 inflammasome assembly and activation. However, according to the determined cryo-electron microscopy structure of human NLRP3-NEK7 complex (Sharif et al., 2019), we found that cysteine 409 is not at the interface of NLRP3-NEK7 interaction. We speculate that 149-01 binding to the C409 site of NLRP3 may cause a conformational change of NLRP3, resulting in the blockage of the NLRP3-NEK7 interaction, but

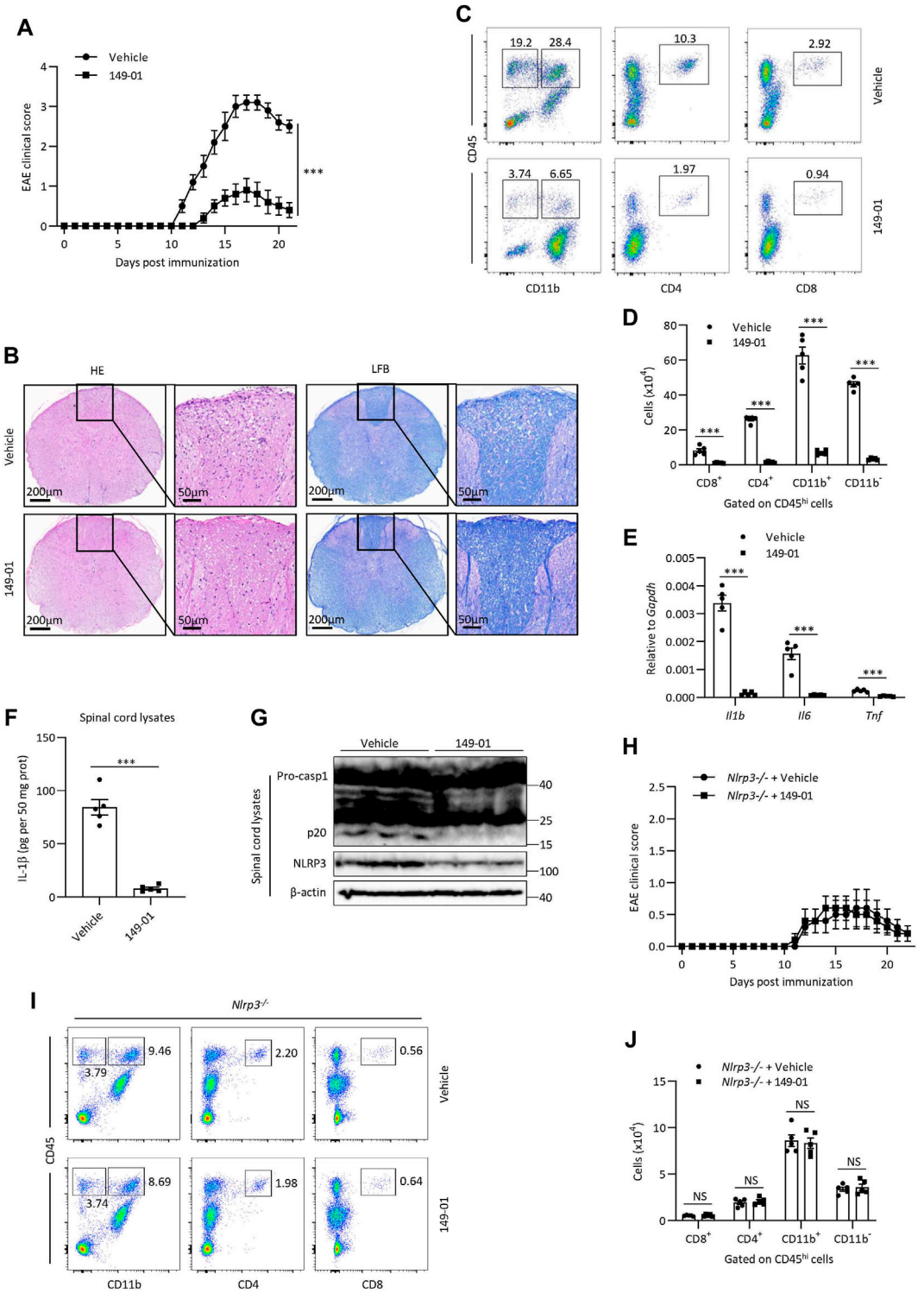

FIGURE 7 | 149-01 attenuates the progression of EAE *via* inhibition of NLRP3 inflammasome. **(A–G)** Mice were intraperitoneally injected with 149-01 (5 mg/kg) or vehicle on the day of EAE induction and every 2 days thereafter. **(A)** EAE clinical scores. **(B)** Representative spinal cord sections were stained with H&E or Luxol fast blue (LFB) to visualize inflammatory cell infiltration or demyelination at day 14 after EAE induction. **(C,D)** The percentages of representative plots **(C)** and total numbers **(D)** of infiltrated $CD8^+$, $CD4^+$, $CD11b^+$ and $CD11b^-$ cells gated on $CD45^{hi}$ cell populations in the CNS were determined by FACS at day 14 after EAE induction. **(E)** The expression of indicated inflammatory cytokines in the CNS were detected by qPCR at day 14 after EAE induction. **(F,G)** The protein levels of IL-1β, caspase-1 and NLRP3 in the spinal cords were detected by ELISA **(F)** or western blot **(G)** at day 14 after EAE induction. **(H–J)** *Nlrp3*$^{-/-}$ mice were intraperitoneally injected with 149-01

(*Continued*)

FIGURE 7 | (5 mg/kg) or vehicle on the day of EAE induction and every 2 days thereafter. **(H)** EAE clinical scores. **(I,J)** The percentages of representative plots **(I)** and total numbers **(J)** of infiltrated $CD8^+$, $CD4^+$, $CD11b^+$ and $CD11b^-$ cells gated on $CD45^{hi}$ cell populations in the CNS were determined by FACS at day 14 after EAE induction. Data are expressed as mean ± s. e.m ($n = 5$) **(A,D–F,H,J)** or are representative of five mice **(B,C,G,I)**. Unpaired Student's t-tests were applied to calculate statistical significance: ***$p < .001$, NS, not significant.

how 149-01 binds to the cysteine 409 of NLRP3 and how this combination changes the conformation of NLRP3 remain to be further studied.

Our data revealed that 149-01 effectively alleviate LPS-induced systemic inflammation, MSU-induced peritonitis and EAE at a dose of 5 mg/kg and its therapeutic effect is dependent on NLRP3. In previous study, the dosage of 10 mg/kg RRx-001, was used in the treatment of multiple NLRP3-dependent disease models (Chen et al., 2021), indicating that 149-01 may possess *in vivo* therapeutic efficacy comparable to or better than RRx-001. Notably, in EAE mice model, 149-01 treatment significantly inhibited the expression of inflammatory cytokines in the CNS such as IL-6 and TNF-α in contrast to *in vitro* results. We suggested that the reduced inflammatory cytokines in the CNS may result from 1) 149-01 treatment alleviated the infiltration of inflammatory cell that produce these inflammatory cytokines; and 2) 149-01 treatment inhibited the expression of IL-1β which could mediate these inflammatory cytokines production via IL-1 receptors (Mori et al., 2011; Dinarello, 2018). Since RRx-001 has been shown to have a high safety profile in clinical trials (Reid et al., 2015; Oronsky et al., 2017; Oronsky et al., 2019), its analogue, 149-01, may have a higher potential to enter clinical trials.

Compared with RRx-001, the structure of 149-01 does not contain high-energy nitro functional groups, which avoids the side effects of NO production on the treatment of NLRP3-related diseases. In addition, 149-01 also avoids potential processing problems, for example, 1) the gem-dinitroazetidine can decompose rapidly, resulting in decreased yields; and 2) the gem-dinitroazetidine is sensitive to heat, impact, friction and electrostatic discharge, causing potential safety hazards (Straessler et al., 2012).

It has been proposed that inhibitors directly targeting NLRP3 have certain advantages over biologic agents targeting IL-1β in the treatment of NLRP3-related inflammatory disorders (Jiang et al., 2017), but there are still no clinically available therapeutic drugs. Although at least some small molecules have entered clinical trials, their clinical efficacy and safety remain to be further confirmed (Mullard, 2019; Kluck et al., 2020).

Considering the potent and specific inhibitory effect of 149-01 on NLRP3 inflammasome both *in vitro* and *in vivo*, and the high safety of RRx-001 in clinical trials (Reid et al., 2015; Oronsky et al., 2017; Oronsky et al., 2019), we consider that 149-01, as an analogue of RRx-001, has promising therapeutic potential for NLRP3-related diseases. However, as mentioned above, there are some concerns remain to be further investigated, which may limit the application of 149-01 as a NLRP3 inhibitor.

DATA AVAILABILITY STATEMENT

The original contributions presented in the study are included in the article/**Supplementary Materials**, further inquiries can be directed to the corresponding authors.

ETHICS STATEMENT

The studies involving human participants were reviewed and approved by The University of Science and Technology of China. The patients/participants provided their written informed consent to participate in this study. The animal study was reviewed and approved by The University of Science and Technology of China.

AUTHOR CONTRIBUTIONS

HL, MY, CL, and BL performed the experiments of this work. XD, HH, and RZ designed the research. HL and RZ wrote the manuscript. HH and RZ supervised the project.

FUNDING

This research was supported by the National Key research and development program of China (grant numbers 2018YFA0507403 and 2019YFA0508503), the Strategic Priority Research Program of the Chinese Academy of Sciences (grant number XDB29030102), the National Natural Science Foundation of China (grant numbers 82003765, 81821001, 31770991, and 82130107), the Fundamental Research Funds for the Central Universities, the University Synergy Innovation Program of Anhui Province (GXXT-2019-026) and the Natural Science Foundation of Anhui Province (1908085QC99).

SUPPLEMENTARY MATERIAL

The Supplementary Material for this article can be found online at: https://www.frontiersin.org/articles/10.3389/fphar.2022.822833/full#supplementary-material

REFERENCES

Bauer, C., Duewell, P., Mayer, C., Lehr, H. A., Fitzgerald, K. A., Dauer, M., et al. (2010). Colitis Induced in Mice with Dextran Sulfate Sodium (DSS) Is Mediated by the NLRP3 Inflammasome. *Gut* 59 (9), 1192–1199. doi:10.1136/gut.2009.197822

Broz, P., and Dixit, V. M. (2016). Inflammasomes: Mechanism of Assembly, Regulation and Signalling. *Nat. Rev. Immunol.* 16 (7), 407–420. doi:10.1038/nri.2016.58

Chen, Y., He, H., Lin, B., Chen, Y., Deng, X., Jiang, W., et al. (2021). RRx-001 Ameliorates Inflammatory Diseases by Acting as a Potent Covalent NLRP3 Inhibitor. *Cell Mol. Immunol.* 18 (6), 1425–1436. doi:10.1038/s41423-021-00683-y

Coll, R. C., Robertson, A. A., Chae, J. J., Higgins, S. C., Muñoz-Planillo, R., Inserra, M. C., et al. (2015). A Small-Molecule Inhibitor of the NLRP3 Inflammasome for the Treatment of Inflammatory Diseases. *Nat. Med.* 21 (3), 248–255. doi:10.1038/nm.3806

Coll, R. C., Hill, J. R., Day, C. J., Zamoshnikova, A., Boucher, D., Massey, N. L., et al. (2019). MCC950 Directly Targets the NLRP3 ATP-Hydrolysis Motif for Inflammasome Inhibition. *Nat. Chem. Biol.* 15 (6), 556–559. doi:10.1038/s41589-019-0277-7

Daniels, M. J., Rivers-Auty, J., Schilling, T., Spencer, N. G., Watremez, W., Fasolino, V., et al. (2016). Fenamate NSAIDs Inhibit the NLRP3 Inflammasome and Protect against Alzheimer's Disease in Rodent Models. *Nat. Commun.* 7, 12504. doi:10.1038/ncomms12504

Davis, B. K., Wen, H., and Ting, J. P. (2011). The Inflammasome NLRs in Immunity, Inflammation, and Associated Diseases. *Annu. Rev. Immunol.* 29, 707–735. doi:10.1146/annurev-immunol-031210-101405

Dick, M. S., Sborgi, L., Rühl, S., Hiller, S., and Broz, P. (2016). ASC Filament Formation Serves as a Signal Amplification Mechanism for Inflammasomes. *Nat. Commun.* 7, 11929. doi:10.1038/ncomms11929

Dinarello, C. A., and van der Meer, J. W. (2013). Treating Inflammation by Blocking Interleukin-1 in Humans. *Semin. Immunol.* 25 (6), 469–484. doi:10.1016/j.smim.2013.10.008

Dinarello, C. A., Simon, A., and van der Meer, J. W. (2012). Treating Inflammation by Blocking Interleukin-1 in a Broad Spectrum of Diseases. *Nat. Rev. Drug Discov.* 11 (8), 633–652. doi:10.1038/nrd3800

Dinarello, C. A. (2018). Overview of the IL-1 Family in Innate Inflammation and Acquired Immunity. *Immunol. Rev.* 281 (1), 8–27. doi:10.1111/imr.12621

Duewell, P., Kono, H., Rayner, K. J., Sirois, C. M., Vladimer, G., Bauernfeind, F. G., et al. (2010). NLRP3 Inflammasomes Are Required for Atherogenesis and Activated by Cholesterol Crystals. *Nature* 464 (7293), 1357–1361. doi:10.1038/nature08938

Duncan, J. A., Bergstralh, D. T., Wang, Y., Willingham, S. B., Ye, Z., Zimmermann, A. G., et al. (2007). Cryopyrin/NALP3 Binds ATP/dATP, Is an ATPase, and Requires ATP Binding to Mediate Inflammatory Signaling. *Proc. Natl. Acad. Sci. U S A.* 104 (19), 8041–8046. doi:10.1073/pnas.0611496104

Fens, M. H. A. M., Larkin, S. K., Morris, C. R., Fitch, B., Scicinski, J., Oronsky, B., et al. (2011). NO or No NO, Increased Reduction of Nitrite to Nitric Oxide by Modified Red Blood Cells. *Blood* 118 (21), 2125. doi:10.1182/blood.V118.21.2125.2125

Gris, D., Ye, Z., Iocca, H. A., Wen, H., Craven, R. R., Gris, P., et al. (2010). NLRP3 Plays a Critical Role in the Development of Experimental Autoimmune Encephalomyelitis by Mediating Th1 and Th17 Responses. *J. Immunol.* 185 (2), 974–981. doi:10.4049/jimmunol.0904145

Gross, C. J., Mishra, R., Schneider, K. S., Médard, G., Wettmarshausen, J., Dittlein, D. C., et al. (2016). K+ Efflux-independent NLRP3 Inflammasome Activation by Small Molecules Targeting Mitochondria. *Immunity* 45 (4), 761–773. doi:10.1016/j.immuni.2016.08.010

Guo, H., Callaway, J. B., and Ting, J. P. (2015). Inflammasomes: Mechanism of Action, Role in Disease, and Therapeutics. *Nat. Med.* 21 (7), 677–687. doi:10.1038/nm.3893

Gurung, P., Lukens, J. R., and Kanneganti, T. D. (2015). Mitochondria: Diversity in the Regulation of the NLRP3 Inflammasome. *Trends Mol. Med.* 21 (3), 193–201. doi:10.1016/j.molmed.2014.11.008

Haq, T., Richards, M. W., Burgess, S. G., Gallego, P., Yeoh, S., O'Regan, L., et al. (2015). Mechanistic Basis of Nek7 Activation through Nek9 Binding and Induced Dimerization. *Nat. Commun.* 6, 8771. doi:10.1038/ncomms9771

He, Y., Franchi, L., and Núñez, G. (2013). TLR Agonists Stimulate Nlrp3-dependent IL-1β Production Independently of the Purinergic P2X7 Receptor in Dendritic Cells and *In Vivo*. *J. Immunol.* 190 (1), 334–339. doi:10.4049/jimmunol.1202737

He, Y., Zeng, M. Y., Yang, D., Motro, B., and Núñez, G. (2016). NEK7 Is an Essential Mediator of NLRP3 Activation Downstream of Potassium Efflux. *Nature* 530 (7590), 354–357. doi:10.1038/nature16959

He, H., Jiang, H., Chen, Y., Ye, J., Wang, A., Wang, C., et al. (2018). Oridonin Is a Covalent NLRP3 Inhibitor with strong Anti-inflammasome Activity. *Nat. Commun.* 9 (1), 2550. doi:10.1038/s41467-018-04947-6

Heneka, M. T., Kummer, M. P., Stutz, A., Delekate, A., Schwartz, S., Vieira-Saecker, A., et al. (2013). NLRP3 Is Activated in Alzheimer's Disease and Contributes to Pathology in APP/PS1 Mice. *Nature* 493 (7434), 674–678. doi:10.1038/nature11729

Huang, Y., Jiang, H., Chen, Y., Wang, X., Yang, Y., Tao, J., et al. (2018). Tranilast Directly Targets NLRP3 to Treat Inflammasome-Driven Diseases. *EMBO Mol. Med.* 10 (4), e8689. doi:10.15252/emmm.201708689

Jiang, H., He, H., Chen, Y., Huang, W., Cheng, J., Ye, J., et al. (2017). Identification of a Selective and Direct NLRP3 Inhibitor to Treat Inflammatory Disorders. *J. Exp. Med.* 214 (11), 3219–3238. doi:10.1084/jem.20171419

Kim, M. M., Parmar, H., Cao, Y., Pramanik, P., Schipper, M., Hayman, J., et al. (2016). Whole Brain Radiotherapy and RRx-001: Two Partial Responses in Radioresistant Melanoma Brain Metastases from a Phase I/II Clinical Trial: A TITE-CRM Phase I/II Clinical Trial. *Transl. Oncol.* 9 (2), 108–113. doi:10.1016/j.tranon.2015.12.003

Klück, V., Jansen, T. L. T. A., Janssen, M., Comarniceanu, A., Efdé, M., Tengesdal, I. W., et al. (2020). Dapansutrile, an Oral Selective NLRP3 Inflammasome Inhibitor, for Treatment of Gout Flares: an Open-Label, Dose-Adaptive, Proof-Of-Concept, Phase 2a Trial. *Lancet Rheumatol.* 2 (5), e270–e280. doi:10.1016/s2665-9913(20)30065-5

Lalor, S. J., Dungan, L. S., Sutton, C. E., Basdeo, S. A., Fletcher, J. M., and Mills, K. H. (2011). Caspase-1-processed Cytokines IL-1beta and IL-18 Promote IL-17 Production by Gammadelta and CD4 T Cells that Mediate Autoimmunity. *J. Immunol.* 186 (10), 5738–5748. doi:10.4049/jimmunol.1003597

Lomenick, B., Hao, R., Jonai, N., Chin, R. M., Aghajan, M., Warburton, S., et al. (2009). Target Identification Using Drug Affinity Responsive Target Stability (DARTS). *Proc. Natl. Acad. Sci. U S A.* 106 (51), 21984–21989. doi:10.1073/pnas.0910040106

Lu, A., Magupalli, V. G., Ruan, J., Yin, Q., Atianand, M. K., Vos, M. R., et al. (2014). Unified Polymerization Mechanism for the Assembly of ASC-dependent Inflammasomes. *Cell* 156 (6), 1193–1206. doi:10.1016/j.cell.2014.02.008

Marchetti, C., Swartzwelter, B., Gamboni, F., Neff, C. P., Richter, K., Azam, T., et al. (2018). OLT1177, a β-sulfonyl Nitrile Compound, Safe in Humans, Inhibits the NLRP3 Inflammasome and Reverses the Metabolic Cost of Inflammation. *Proc. Natl. Acad. Sci. U S A.* 115 (7), E1530–E1539. doi:10.1073/pnas.1716095115

Martinon, F., Pétrilli, V., Mayor, A., Tardivel, A., and Tschopp, J. (2006). Gout-associated Uric Acid Crystals Activate the NALP3 Inflammasome. *Nature* 440 (7081), 237–241. doi:10.1038/nature04516

Masters, S. L., Dunne, A., Subramanian, S. L., Hull, R. L., Tannahill, G. M., Sharp, F. A., et al. (2010). Activation of the NLRP3 Inflammasome by Islet Amyloid Polypeptide Provides a Mechanism for Enhanced IL-1β in Type 2 Diabetes. *Nat. Immunol.* 11 (10), 897–904. doi:10.1038/ni.1935

Mori, T., Miyamoto, T., Yoshida, H., Asakawa, M., Kawasumi, M., Kobayashi, T., et al. (2011). IL-1 and TNF -initiated IL-6-STAT3 Pathway Is Critical in Mediating Inflammatory Cytokines and RANKL Expression in Inflammatory Arthritis. *Int. Immunol.* 23 (11), 701–712. doi:10.1093/intimm/dxr077

Mullard, A. (2019). NLRP3 Inhibitors Stoke Anti-inflammatory Ambitions. *Nat. Rev. Drug Discov.* 18 (6), 405–407. doi:10.1038/d41573-019-00086-9

Muñoz-Planillo, R., Kuffa, P., Martínez-Colón, G., Smith, B. L., Rajendiran, T. M., and Núñez, G. (2013). K^+ Efflux Is the Common Trigger of NLRP3 Inflammasome Activation by Bacterial Toxins and Particulate Matter. *Immunity* 38 (6), 1142–1153. doi:10.1016/j.immuni.2013.05.016

Netea, M. G., van de Veerdonk, F. L., van der Meer, J. W., Dinarello, C. A., and Joosten, L. A. (2015). Inflammasome-independent Regulation of IL-1-family Cytokines. *Annu. Rev. Immunol.* 33, 49–77. doi:10.1146/annurev-immunol-032414-112306

Ning, S., Bednarski, M., Oronsky, B., Scicinski, J., Saul, G., and Knox, S. J. (2012). Dinitroazetidines Are a Novel Class of Anticancer Agents and Hypoxia-Activated Radiation Sensitizers Developed from Highly Energetic Materials. *Cancer Res.* 72 (10), 2600–2608. doi:10.1158/0008-5472.CAN-11-2303

Nowarski, R., Jackson, R., Gagliani, N., de Zoete, M. R., Palm, N. W., Bailis, W., et al. (2015). Epithelial IL-18 Equilibrium Controls Barrier Function in Colitis. *Cell* 163 (6), 1444–1456. doi:10.1016/j.cell.2015.10.072

Oronsky, B., Scicinski, J., Ning, S., Peehl, D., Oronsky, A., Cabrales, P., et al. (2016). Rockets, Radiosensitizers, and RRx-001: an Origin story Part I. *Discov. Med.* 21 (115), 173–180.

Oronsky, B., Paulmurugan, R., Foygel, K., Scicinski, J., Knox, S. J., Peehl, D., et al. (2017). RRx-001: a Systemically Non-toxic M2-To-M1 Macrophage Stimulating and Prosensitizing Agent in Phase II Clinical Trials. *Expert Opin. Investig. Drugs* 26 (1), 109–119. doi:10.1080/13543784.2017.1268600

Oronsky, B., Reid, T. R., Larson, C., Caroen, S., Quinn, M., Burbano, E., et al. (2019). REPLATINUM Phase III Randomized Study: RRx-001 + Platinum Doublet versus Platinum Doublet in Third-Line Small Cell Lung Cancer. *Future Oncol.* 15 (30), 3427–3433. doi:10.2217/fon-2019-0317

Reid, T., Oronsky, B., Scicinski, J., Scribner, C. L., Knox, S. J., Ning, S., et al. (2015). Safety and Activity of RRx-001 in Patients with Advanced Cancer: a First-In-Human, Open-Label, Dose-Escalation Phase 1 Study. *Lancet Oncol.* 16 (9), 1133–1142. doi:10.1016/S1470-2045(15)00089-3

Schroder, K., and Tschopp, J. (2010). The Inflammasomes. *Cell* 140 (6), 821–832. doi:10.1016/j.cell.2010.01.040

Sharif, H., Wang, L., Wang, W. L., Magupalli, V. G., Andreeva, L., Qiao, Q., et al. (2019). Structural Mechanism for NEK7-Licensed Activation of NLRP3 Inflammasome. *Nature* 570 (7761), 338–343. doi:10.1038/s41586-019-1295-z

Shi, J., Zhao, Y., Wang, K., Shi, X., Wang, Y., Huang, H., et al. (2015). Cleavage of GSDMD by Inflammatory Caspases Determines Pyroptotic Cell Death. *Nature* 526 (7575), 660–665. doi:10.1038/nature15514

Shi, H., Wang, Y., Li, X., Zhan, X., Tang, M., Fina, M., et al. (2016). NLRP3 Activation and Mitosis Are Mutually Exclusive Events Coordinated by NEK7, a New Inflammasome Component. *Nat. Immunol.* 17 (3), 250–258. doi:10.1038/ni.3333

Shi, Y., Lv, Q., Zheng, M., Sun, H., and Shi, F. (2021). NLRP3 Inflammasome Inhibitor INF39 Attenuated NLRP3 Assembly in Macrophages. *Int. Immunopharmacol.* 92, 107358. doi:10.1016/j.intimp.2020.107358

Straessler, N. A., Lesley, M. W., and Cannizzo, L. F. (2012). Development of a Safe and Efficient Two-step Synthesis for Preparing 1-Bromoacetyl-3,3-Dinitroazetidine, a Novel Clinical Anticancer Candidate. *Org. Process. Res. Dev.* 16, 512–517. doi:10.1021/op2003216

Sutton, C., Brereton, C., Keogh, B., Mills, K. H., and Lavelle, E. C. (2006). A Crucial Role for Interleukin (IL)-1 in the Induction of IL-17-producing T Cells that Mediate Autoimmune Encephalomyelitis. *J. Exp. Med.* 203 (7), 1685–1691. doi:10.1084/jem.20060285

Swanson, K. V., Deng, M., and Ting, J. P. (2019). The NLRP3 Inflammasome: Molecular Activation and Regulation to Therapeutics. *Nat. Rev. Immunol.* 19 (8), 477–489. doi:10.1038/s41577-019-0165-0

Tang, T., Lang, X., Xu, C., Wang, X., Gong, T., Yang, Y., et al. (2017). CLICs-Dependent Chloride Efflux Is an Essential and Proximal Upstream Event for NLRP3 Inflammasome Activation. *Nat. Commun.* 8 (1), 202. doi:10.1038/s41467-017-00227-x

van der Vliet, A., Eiserich, J. P., and Cross, C. E. (2000). Nitric Oxide: a Pro-inflammatory Mediator in Lung Disease? *Respir. Res.* 1 (2), 67–72. doi:10.1186/rr14

Wen, H., Ting, J. P., and O'Neill, L. A. (2012). A Role for the NLRP3 Inflammasome in Metabolic Diseases-Ddid Warburg Miss Inflammation? *Nat. Immunol.* 13 (4), 352–357. doi:10.1038/ni.2228

Xu, H., Yang, J., Gao, W., Li, L., Li, P., Zhang, L., et al. (2014). Innate Immune Sensing of Bacterial Modifications of Rho GTPases by the Pyrin Inflammasome. *Nature* 513 (7517), 237–241. doi:10.1038/nature13449

Yu, W., Wang, Z., Zhang, K., Chi, Z., Xu, T., Jiang, D., et al. (2019). One-Carbon Metabolism Supports S-Adenosylmethionine and Histone Methylation to Drive Inflammatory Macrophages. *Mol. Cel* 75 (6), 1147. doi:10.1016/j.molcel.2019.06.039

Zhang, X., Xu, A., Lv, J., Zhang, Q., Ran, Y., Wei, C., et al. (2020). Development of Small Molecule Inhibitors Targeting NLRP3 Inflammasome Pathway for Inflammatory Diseases. *Eur. J. Med. Chem.* 185, 111822. doi:10.1016/j.ejmech.2019.111822

Zhou, R., Yazdi, A. S., Menu, P., and Tschopp, J. (2011). A Role for Mitochondria in NLRP3 Inflammasome Activation. *Nature* 469 (7329), 221–225. doi:10.1038/nature09663

Conflict of Interest: The authors declare that the research was conducted in the absence of any commercial or financial relationships that could be construed as a potential conflict of interest.

frontiers in Pharmacology

ORIGINAL RESEARCH
published: 18 March 2022
doi: 10.3389/fphar.2022.845959

Saikosaponin D Inhibited IL-1β Induced ATDC 5 Chondrocytes Apoptosis *In Vitro* and Delayed Articular Cartilage Degeneration in OA Model Mice *In Vivo*

Xinhui Wu[1,2†], *Kangxian Zhao*[1,2†], *Xiaoxin Fang*[3,4], *Feng Lu*[3,4], *Pu Cheng*[1,2], *Xiaoting Song*[1,2], *Weikang Zhang*[1,2], *Can Yao*[1], *Jiling Zhu*[2] *and Haixiao Chen*[1,2,4*]

[1]Department of Orthopedics, Taizhou Hospital of Zhejiang Province Affiliated to Wenzhou Medical University, Linhai, China, [2]Wenzhou Medical University, Wenzhou, China, [3]Zhejiang University School of Medicine, Hangzhou, China, [4]Taizhou Hospital of Zhejiang Province, Zhejiang University, Linhai, China

OPEN ACCESS

Edited by:
Peramaiyan Rajendran,
King Faisal University, Saudi Arabia

Reviewed by:
Lin Wang,
Shandong Agricultural University, China
Ranjan K. C.,
Children's Hospital of Philadelphia, United States

***Correspondence:**
Haixiao Chen
drchx@126.com

[†]These authors have contributed equally to this work and share first authorship

Specialty section:
This article was submitted to Inflammation Pharmacology, a section of the journal Frontiers in Pharmacology

Received: 30 December 2021
Accepted: 24 February 2022
Published: 18 March 2022

Citation:
Wu X, Zhao K, Fang X, Lu F, Cheng P, Song X, Zhang W, Yao C, Zhu J and Chen H (2022) Saikosaponin D Inhibited IL-1β Induced ATDC 5 Chondrocytes Apoptosis In Vitro and Delayed Articular Cartilage Degeneration in OA Model Mice In Vivo. Front. Pharmacol. 13:845959. doi: 10.3389/fphar.2022.845959

Osteoarthritis (OA) is the most common joint disease in the elderly, characterized by cartilage degradation and proliferation of subchondral bone. The pathogenesis of OA involves a variety of inflammatory mediators, including nitric oxide (NO), prostaglandin E2 (PGE2), tumor necrosis factor (TNF)-α, and interleukin (IL)-1β. From the molecular mechanism, the nuclear factor-erythroid 2-related factor (Nrf2)/heme oxygenase-1 (HO-1) pathway and the expression of ROS regulated the production of the above inflammatory mediators. Saikosaponin D (SSD), which is an active ingredient isolated from Bupleurum, has various biological functions. In this study, IL-1β was used as a pro-inflammatory factor to create an *in vitro* OA model. According to the results of high-density culture, qPCR, ROS measurement, Western blot, and immunofluorescence, SSD activated the Nrf2/HO-1/ROS axis, inhibited the production of inflammatory mediators, and protected against ECM destruction. The DMM mouse model was used as a model of OA in mice. From the results of safranin O/fast green staining, hematoxylin–eosin staining, tartrate-resistant acid phosphatase (TRAP) staining, and OARSI scores, SSD protected against the mice knee articular cartilage degeneration and reduced the number of osteoclasts in the subchondral bone. Experimental results found that SSD suppressed IL-1β–induced differentiated ATDC 5 chondrocytes apoptosis *via* the Nrf2/HO-1/ROS axis *in vitro*. SSD delayed the progression of OA in DMMs model mice *in vivo*. Therefore, SSD has the potential to become a drug for clinical treatment of OA.

Keywords: Saikosaponin D, osteoarthritis, Nrf2, HO-1, ROS, NF-κB, therapy

INTRODUCTION

Osteoarthritis (OA) is one of the most common chronic degenerative joint diseases, characterized by narrowing of the joint space, cartilage degradation, and proliferation of subchondral bone (Martel-Pelletier et al., 2016). The pathology of this disease is very complicated, and the specific mechanism is still controversial. A large amount of evidence indicates that pro-inflammatory factors such as tumor necrosis factor (TNF)-α and interleukin (IL)-1β play a key role in the pathogenesis of OA (Kapoor et al., 2011; Chu

et al., 2014). IL-1β could induce the expression of inflammatory mediators including nitric oxide (NO) and prostaglandin E2 (PGE2) (Kapoor et al., 2011; Wojdasiewicz et al., 2014). These inflammatory mediators accumulated for a long time and destroyed the extracellular matrix (ECM), which is the main component of cartilage including collagen II and aggrecan. Eventually, the imbalance between ECM anabolism and catabolism leads to continuous chondrocyte apoptosis and cartilage degradation, which is considered to be a sign of the progression of OA (Guilak et al., 2018). Because of the lack of reliable drugs to reverse and delay OA, most patients will eventually need joint replacement surgery, leaving a huge burden on society and the economy (Cao et al., 2020; Latourte et al., 2020). Therefore, we urgently need a safe and effective drug to deal with this kind of degenerative joint disease.

Nuclear factor-erythroid 2-related factor (Nrf2) directly regulates the expression of heme oxygenase-1 (HO-1) (Saha et al., 2020). Studies demonstrated that the Nrf2/HO-1 signaling pathway could suppress the production of pro-inflammatory cytokines by immune cells. When the Nrf2 gene was knocked out, the expression of inflammatory cytokines such as COX-2, iNOS, IL-6, and TNF-α increased significantly. In addition, when the Nrf2/HO-1 axis of vascular smooth muscle cells is activated, the expression of COX2 and iNOS decreases remarkably (Ho et al., 2007). The activated Nrf2/HO-1 pathway is closely related to the inhibition of ROS and the regulated NF-κB signaling pathway (Bellezza et al., 2010; Rigoglou and Papavassiliou, 2013; Zhai et al., 2018). After IL-1β stimulation, the activation of pathways such as NF-κB and MAPKs accelerated the production of a series of inflammatory factors which caused the catabolism of chondrocytes (Sondergaard et al., 2010). The activated NF-κB pathway will cause IKBα to be degraded by the proteasome in the cytoplasm and rapidly phosphorylated. P65 enters the nucleus and specifically binds to the promoter region of downstream genes to initiate the inflammatory cascade (Sun, 2017). Therefore, the activation of the Nrf2/HO-1/ROS axis could be used as a treatment for patients with OA.

Bupleurum is a common Chinese herbal medicine with a long history and is widely used to treat inflammation and infectious diseases in Asian countries (Yuan et al., 2017). Saikosaponin D (SSD), which is an active ingredient isolated from *Bupleurum*, has anti-inflammatory, antitumor, and antiviral effects. Studies have shown that SSD can effectively inhibit late-stage autophagy and prevent EV-A71 virus infection (Li et al., 2019). Lai et al. found that SSD can target the MKK4-JNK axis to inhibit the growth of pancreatic cancer cells (Lai et al., 2020). However, the therapeutic effects of SSD on OA mice are not clear. This study aimed to investigate whether SSD treatment could suppress the IL-1β–mediated differentiated ATDC 5 chondrocytes apoptosis *in vitro*. In addition, we established a mice DMMs model to observe the protective effects of SSD treatment on articular cartilage *in vivo*.

MATERIALS AND METHODS

Reagents and Antibodies

Saikosaponin D (purity >98%) was purchased from MCE (New Jersey, United States). DMSO (Meilunbio, Dalian, China) was used to dissolve Saikosaponin D and diluted in the cell culture until DMSO <0.1%. Recombinant mouse IL-1β was obtained from Peprotech (United States). Safranin-O and Fast Green and tartrate-resistant acid phosphatase staining (TRAP) were acquired from Solarbio (Beijing, China). Primary antibodies were applied in this study: antibodies against P65 (#8242), p-P65 (#3033), IκBα (#4814), p-IκBα (#2859), ERK (#4695), p-ERK (#4370), JNK (#9252), p-JNK (#9255), P38 (#8690), and p-P38 (#4511S) were acquired from CST (1:1,000, Cambridge, MA, United States). Anti-iNOS (1:1,000, ab178945), anti-COX2 (1:4,000, ab179800), anti-Aggrecan (1:1,000, ab3778), and anti-ADAMTS5 (1:250, ab41037) were purchased from Abcam (Cambridge, United Kingdom). Antibodies against MMP13 (1:2000, 18165-1-AP), Collagen II (1:1,000, 28459-1-AP), Nrf2 (1:2000, 66504-1-Ig), HO-1 (1:1,500, 27282-1-AP), Lamin B (1:10000, 66095-1-Ig), and Actin β (1:8,000, 66009-1-Ig) were obtained from Proteintech (Wuhan, China). Goat anti-mouse and goat anti-rabbit were acquired from Thermo Fisher (United States).

ATDC 5 Chondrocytes Culture and Differentiation

The mice chondrocyte cell line ATDC 5 was obtained from Jennio Biotech (GuangZhou, China).

ATDC 5 chondrocytes were maintained in monolayer culture in Dulbecco's modified Eagle's medium (DMEM)/F12 (Hyclone; Logan, UT, United States) containing 5% fetal bovine serum (FBS; Gibco, United States) and 1% bovine serum albumin (BSA; Hyclone; United States). To induce ATDC 5 chondrocytes to the mature chondrocytes, we added insulin, transferrin, and selenium (ITS) to the culture medium. The differentiation period was 14 days, and the culture medium was changed every other day. According to previous studies, cartilage nodule formation and the elevated expression levels of type II collagen, type X collagen, and aggrecan mRNA are observed after ATDC 5 chondrocyte differentiation (Gómez et al., 2009; Morimoto et al., 2013; Abella et al., 2016).

Cell Viability

The cytotoxicity of SSD on ATDC 5 chondrocytes was determined using a CCK-8 kit (Beyotime, Shanghai, China) according to the manufacturer's protocol. A 6-well plate were planted with cells at a density of 8,000 cells per well and incubated with or without SSD (0, 0.5, 1, 2, 4, 8, 16, and 32 μmol/L) for 24 and 48 h. In addition, the cells were stimulated by IL-1β (10 ng/ml) or not and incubated with multiple concentrations of SSD (0, 1, 2, and 4 μmol/L) for 24 and 48 h. Each concentration of SSD was repeated 3 times. At each experimental end point, 10 μL CCK-8 kit diluted in the 100 μL DMEM/F12 was added into each well and then further incubated for 3 h at 37°C with 5% CO_2. The absorbance of all wells was calculated using a microplate photometer at OD 450 nm (Thermo Fisher, Waltham, MA, United States).

High-Density Culture

The mature chondrocytes at a density of 10^8 cells/ml were seeded in a 24-well plate, 10 μl per well. After 6 h, 1 ml complete medium

TABLE 1 | Mouse Primers for qPCR.

Gene	Forward primer	Reverse primer
β-actin	5′- AGC CAT GTA CGT AGC CAT CC-3′	5′- CTC TCA GCA GTG GTG GTG AA-3′
COX-2	5′-TCC TCA CAT CCC TGA GAA CC-3′	5′- GTC GCA CAC TCT GTT GTG CT-3′
iNOS	5′-GAC GAG ACG GAT AGG CAG AG-3′	5′-CAC ATG CAA GGA AGG GAA CT-3′
IL-6	5′-CCG GAG AGG AGA CTT CAC AG-3′	5′-TCC ACG ATT TCC CAG AGA AC-3′
TNF-α	5′-CCG GAG AGG AGA CTT CAC AG-3′	5′- GTG GGT GAG GAG CAC GTA GT- 3′

was added to each well and cultured for 5 days. The cells were fixed using 4% paraformaldehyde at room temperature for 15 min. After washing extensively with PBS thrice, toluidine blue o solution (solarbio, United States) was used to stain the cells. The images of the cells in a 24-well plate were observed using an EPSON V600 photo scanner (Tokyo, Japan).

Apoptosis Detection

A 6-well plate were seeded with the cells at a density of 2×10^5 cells per well. After 6 h, different concentrations of SSD (0, 2, and 4 μmol/L) were used to treat the cells under the stimulation of IL-1β (1 μmol/L) or not. An Annexin V-FITC Apoptosis Detection Kit was used to treat the cells according to the manufacturer's instructions. The apoptosis rate of cells was quantified by flow cytometry (Moflo XDP, United States). Annexin V positive and PI negative cells were regarded as early apoptotic cells. Annexin V positive cells and PI positive cells were regarded as late apoptotic chondrocytes.

Reactive Oxygen Species Measurement

The Reactive Oxygen Species Assay Kit (Beyotime) was used to detect the generation of cellular ROS. After special treatment of the cells in the 6-well plate (2×10^5), DCFH-DA was diluted with DMEM/F12 medium (1:1,000) and added to the 6-well plate at 37°C in a cell incubator for 20 min. After washing the cells thrice with DMEM/F12 medium, the fluorescence intensity of dichlorofluorescein (DCF) fluorescence was observed using a confocal microscope (Zeiss, Japan). The cellular ROS fluorescence intensity was quantified using Image Pro Plus 6.0 software (Media Cybernetics, MD, United States).

Quantitative Reverse Transcription Polymerase Chain Reaction Assay

A 6-well plate was planted with the cells at a density of 2×10^5 cells. Various concentrations of SSD (0, 1, 2, and 4 μmol/L) were used to pretreat the cells for 30 min. The cells were then treated with or without IL-1β (10 ng/ml) and incubated with different concentrations of SSD for a day. The total RNA was extracted from the chondrocytes using TRIzol Reagent (Thermo Fisher Scientific). A cDNA synthesis kit (Cwbio; Beijing, China) was used to perform reversing transcription on the extracted RNA template to synthesize cDNA. Then ChamQ Universal SYBR qPCR Master Mix (Vazyme; Nanjing, China) was used to perform real-time quantitative PCR (qPCR) on cDNA samples according to the manufacturer's instructions. The specific mouse sequence primers are shown in **Table 1**, and β-actin is used as an internal control.

Western Blot

The cells (density, 2×10^5/well) were seeded in 6-well plates. The cells stimulated with 10 ng/ml IL-1β or not were incubated with different concentrations of SSD (0, 1, 2, and 4 μmol/L). At the end point, the cells were washed twice with ice-cold PBS and then extracted using RIPA (AMEKO, Shanghai, China) supplemented with phosphatase inhibitor and phenylmethanesulfonyl fluoride (PMSF). The concentration of total protein was normalized using a BCA protein kit (Takara, Dalian). The protein samples were separated using 12% sodium dodecylsulfate-polyacrylamide gel electrophoresis (SDS-PAGE) and subsequently transferred to 0.22-μm polyvinylidene difluoride (PVDF) membranes (Millipore, Boston, United States). After incubating with QuickBlock™ Blocking Buffer at room temperature for 30 min, the blocked PVDF membranes were incubated with the primary antibodies overnight at 4°C. On the 2nd day, tris-buffered saline with Tween 20 (TBST) was used to wash the PVDF membranes thrice and the membranes were incubated with the respective secondary antibodies for 1 h on the laboratory shaker at 37°C. Finally, the bands were acquired with an enhanced chemiluminescence reagent (Millipore, Boston, United States). ImageJ software was used to observe the density of these bands.

Immunofluorescence Analysis

The cells were planted in 6-well plates at 2×10^5 cells/well. The cells were treated with or without SSD (4 μmol/L) and stimulated with IL-1β (10 ng/ml) or not for 24 h. At the end point, the cells were then washed twice using PBS and fixed by 4% paraformaldehyde for 15 min at room temperature. The cells and nuclear membranes were permeabilized by the 0.1% Triton -100 dissolved in PBS for 5 min at room temperature and blocked with QuickBlock™ Blocking Buffer for Immunol Staining (Beyotime) for 30 min. Primary antibodies collagen (1:1,000) and P65 (1:1,000) were added to the 6-well plate and incubated with the cells overnight at 4°C. On the 2nd day, the 6-well plate was washed twice using PBS and Alexa Fluor® 488-labeled secondary antibody or Alexa Fluor® 594-labeled secondary antibody was added to it, and the cells were incubated at room temperature in the dark for 1 h. Finally, the nucleus was stained with DAPI for 5 min. Images of the cells were acquired by immunofluorescence microscopy (Zeiss, Japan). The fluorescence intensity was observed using Image Pro Plus 6.0 software.

Small Interfering RNA Transfection

siRNA Nrf2 Small Interfering RNA (si-Nrf2) and siRNA negative control (si-NC) were obtained and constructed from Invitrogen (Carlsbad, United States). The special synthetic sequence of si-Nrf2 is constructed as follows: sense, 5-UUG GGA UUC ACG CAU AGG AGC ACU G3′, antisense, 5-CAG UGC UCC UAU GCG GAA UCC CAA-3′. In accordance with the protocol, lipofectamine 2000 siRNA transfection reagent (Thermo Fisher, UT, United States) was used to conduct transfection of si-NC and si-Nrf2 into the cells. The next step was to extract total cell protein for Western blot analysis.

Construction of Binding Mode Between Saikosaponin D and Nrf2 Protein

The SSD molecular structure was constructed using ChemDraw, and we performed geometric optimization and energy minimization using Chem3D. We obtained the Nrf2 target protein crystal structure from the protein database (https://www.rcsb.org/). SSD was regarded as the small molecule ligand and Nrf2 protein target as the receptor. The center position of the Grid Box (x_center = −2.949, y_center = −3.867, z_center = 3.259) was determined based on the interaction between the small molecule and the target, and the length, width, and height are set to 60 × 60 × 60. Finally, batch molecular docking was performed using AutoDock and the results of molecular docking were analyzed. The binding effect of SSD and Nrf2 protein was visualized using Pymol2.1 software. In the calculation process, Lamarckian genetic algorithm was used for molecular docking calculation. According to the interaction between SSD and protein residues, we scored the docking of the reference compound and inferred whether the compound had a certain activity.

A Mouse Model of Destabilization of the Medial Meniscus

Shanghai Laboratory Animal Center (SLAC) provided 24 8-week-old male C57 WT mice. To determine the effects of SSD on the mouse OA model, the mice were subjected or not to the destabilization of the medial meniscus (DMM) surgery as previously described (Ma et al., 2007; Huang et al., 2017; Jeon et al., 2020). Briefly, a 5- to 6-mm incision was made in the medial skin of the mouse right knee using a pointed blade to open the knee capsule and expose the medial meniscus. Ophthalmic scissors cut the medial collateral ligament attached to the medial tibial plateau. Finally, the joint capsule and epidermis are sutured sequentially using 6–0 sutures. According to the IACUC protocol, analgesia and antibiotics treatments were administered for 3 days after DMM surgery. The Institutional Animal Ethics Committee of Taizhou Hospital approved all animal experiments (ethic code: tzy-2021170). The Health Guide for Care and Use of Laboratory Animals was regarded as the guideline for the care and use of our experimental animals. There were four groups to which we randomly assigned mice (n = 6): sham group, OA group (intra-articular injection with PBS), OA treated with low-dose SSD group (intra-articular injection with 2 mg/kg SSD), and OA treated with high-dose SSD group (intra-articular injection with 4 mg/kg SSD). The dosage of SSD is determined by referring to the relevant literature (Li et al., 2020; Qin et al., 2020). Pentobarbital (40 mg/kg) by intraperitoneal injection was used to anesthetize mice, and the DMM surgery was conducted on the right knee of each mouse except the sham group. After 1 week of the DMM surgery, PBS or SSD dissolved in PBS was intraperitoneally injected every other day during the 8-week period. The mice were allowed to get food, water, and free movements in the same way after surgery. All animals were maintained at a 12-h light/dark cycle, a relative humidity of 50 ± 10% within a constant temperature of 20 ± 2°C. The mice were euthanized at the end point, and all right knee joints were fixed by 4% PFA paraformaldehyde for further analysis.

Knee Joints Tissue Section Analysis

All knee joint specimens were decalcified in 10% ethylenediaminetetraacetic acid (EDTA) for 2 weeks. The decalcified samples were embedded in paraffin and cut into 4-μm sections. We used Safranin-O (S-O), hematoxylin and eosin (HE), and tartrate-resistant acid phosphatase staining (TRAP) staining reagents to stain the sections as previously described (Kim et al., 2014; Zhu et al., 2019). Finally, the Osteoarthritis Research Society International (OARSI) scoring system was used to evaluate the degree of destruction of articular cartilage (Glasson et al., 2010). Image ProPlus 6.0 software (MD, United States) was used to measure the number of TRAP-positive cells in the subchondral bone.

Statistical Analysis

All experimental data were presented as mean ± S.D. The experiments *in vitro* were performed at least three times. Each group of animal experiments was randomly assigned to 6 mice. SPSS statistical software version 20.0 (IBM Corp, Armonk, NY, United States) was used for statistical analysis. Two sets of data were compared using Student's *t*-test or the Kruskal–Wallis test. The significance between various groups was examined with one-way analysis of variance (ANOVA) with Tukey's post hoc test. p values < 0.05 were considered statistically significant.

RESULTS

Effects of Saikosaponin D and IL-1β on ATDC 5 Chondrocytes Viability

The chemical structure of SSD is shown in **Figure 1A**. The morphology of ATDC 5 chondrocytes under the microscope is shown in **Figure 1B**. In order to determine the potential cytotoxicity of SSD, the ATDC 5 chondrocytes were incubated with or without SSD at various concentrations (0.5, 1, 2, 4, 8, 16, and 32 μmol/L) for 24 and 48 h. The cellular viability was determined using a CCK-8 assay kit. **Figure 1C** shows that SSD show no apparent cytotoxicity to the cells at concentrations of ≤4 μmol/L after a day or 2 days. Therefore, the concentrations of SSD (1, 2, or 4 μmol/L) were used in the following experiments. The cell viability of ATDC 5 chondrocytes decreased significantly under the stimulation of IL-1β (10 ng/ml),

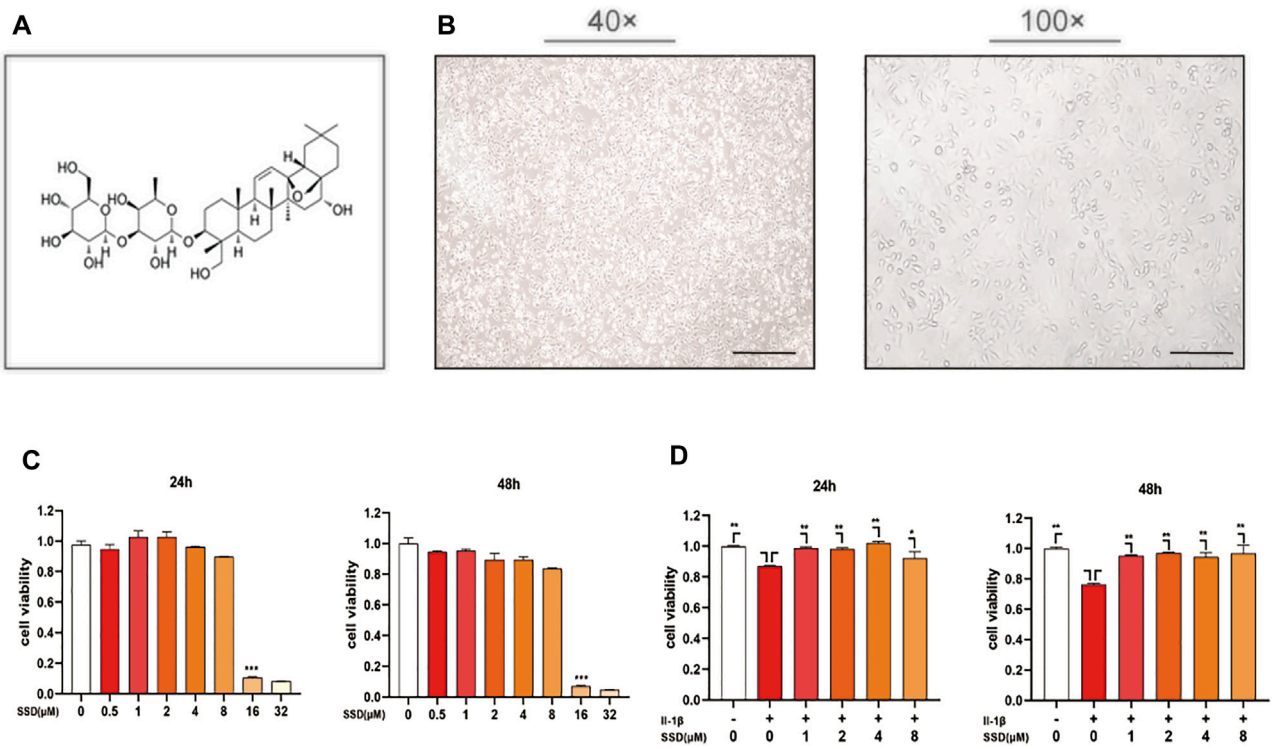

FIGURE 1 | SSD improved the cell viability of the cells stimulated by IL-1β and prevented cell death. **(A)** The chemical structure of SSD. **(B)** The morphology of ATDC 5 chondrocytes under the microscope (40×; 100×; Scale, 200 μm). **(C)** Effects of various concentrations of SSD on the cell viability. **(D)** The protective effects of SSD on the cells stimulated by IL-1β.

and the treatment of SSD reversed this phenomenon**.** Compared with IL-1β stimulation alone, ATDC 5 chondrocytes had a better viability after SSD treatment (**Figure 1D**).

Saikosaponin D Attenuated IL-1β–Induced Differentiated ATDC 5 Chondrocyte Apoptosis

As shown in **Figure 2A**, the protective effects of SSD (1, 2, and 4 μmol/L) on the mature chondrocytes stimulated by IL-1β were detected. The results of high-density culture showed that the cells' density increased significantly and the area of toluidine blue o solution staining was larger than the cells treated with IL-1β alone after SSD treatment. According to the results of flow cytometry (**Figures 2B,C**), the cell apoptosis under IL-1β stimulation was inhibited by SSD in a dose-dependent manner. Especially when the SSD concentration was 4 μmol/L, the cellular apoptosis rate was significantly lower than that of the IL-1β group.

The Inhibition of Saikosaponin D on the Secretion of Inflammatory Factors by the Mature Chondrocytes

The cells were treated with different concentrations of SSD (0, 1, 2, and 4 μmol/L) under IL-1β–induced inflammatory conditions. Related inflammatory factors were detected by Western blot and qPCR. According to our experimental results, IL-1β upregulated the expression level of inflammation-related maker genes: TNF-α, IL-6, COX2, and INOS, whereas high concentration of SSD (4 mol/L) could decrease the degree to baseline (**Figure 3A**). Similarly, **Figures 3B,C** shows that SSD significantly decreased the protein level of COX2 and INOS in a dose-dependent manner. Together, these data found that SSD could reverse the upregulation trend of inflammatory cytokines under IL-1β stimulation at the gene and protein levels.

Saikosaponin D Inhibited IL-1β–Induced Production of Extracellular Matrix Catabolic

To evaluate the protective effects of SSD on IL-1β–induced degradation of the ECM, the ECM components of chondrocytes were determined by using Western blot analysis and immunofluorescence. As shown in **Figures 3D,E**, IL-1β stimulation remarkably accelerated the production of ADAMTS 5 and MMP13 compared with the negative control group, while this trend was reversed by SSD pretreatment. Meanwhile, the expression levels of type II collagen and aggrecan decreased significantly after stimulation with IL-1β (10 ng/ml) for 24 h. SSD treatment protected these two kinds of ECM compositions from damage. In addition, the immunofluorescence results showed

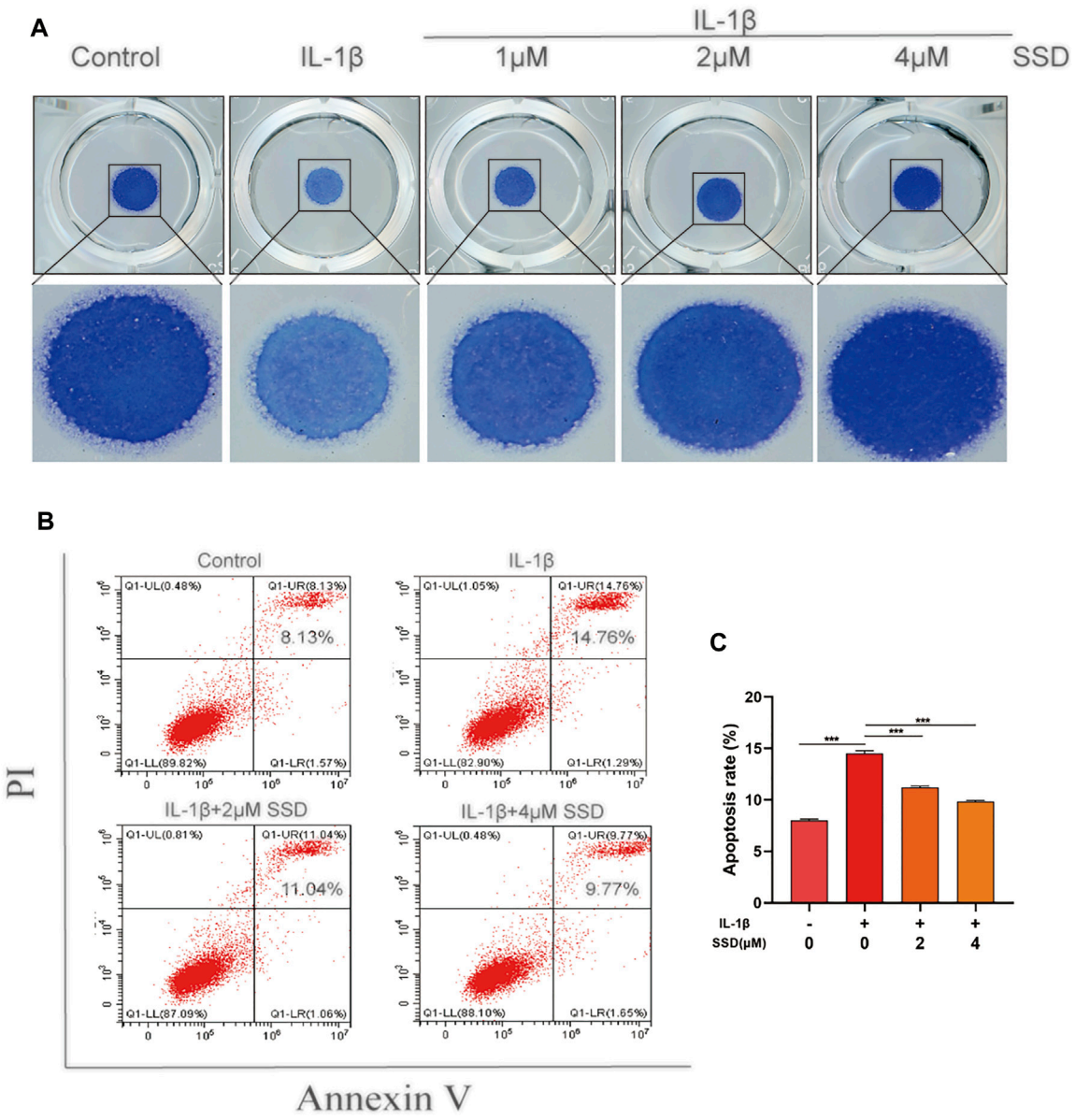

FIGURE 2 | SSD prevented IL-1β–induced differentiated ATDC 5 chondrocyte apoptosis. **(A)** The cells (density, 10^8/ml) stimulated by IL-1β were seeded in 24-well plates and treated with or without different concentrations of SSD for 5 days. Images of the cells stained with toluidine blue o solution. **(B)** The cellular apoptotic ratios in different groups were quantified by flow cytometry. **(C)** Statistical analysis of the cellular apoptosis results between groups. Mean ± SD was applied with all data. The experiments *in vitro* were performed independently at least 3 times. ***$p < 0.001$, **$p < 0.01$, *$p < 0.05$.

that the fluorescence intensity of type II collagen significantly decreased when the cells were stimulated with IL-1β alone, but the fluorescence intensity was increased after SSD treatment (**Figures 3F,G**). Therefore, SSD could promote ECM anabolism and suppress ECM catabolism.

The Binding Mode Between Saikosaponin D and Nrf2 Protein

According to the results of molecular docking, SSD has a strong binding effect with NrF2 target protein (binding energy of −8.19 kcal/mol) (**Figures 4A–C**). From the binding mode of SSD and Nrf2 protein, the amino acid residues that SSD binds to the active site of Nrf2 protein include LEU-86, ARG-84, LYS-83, CYS-81, ASN-80, ALA-78, LYS-39, PRO-34, VAL-90, etc. (**Figure 4D**). One end of the SSD is very hydrophobic. Multiple hydrophobic amino acids (LEU-86, ALA-78, PRO-34, and VAL-90) of the target protein form a strong hydrophobic interaction with the SSD, which helps stabilize the small molecules in the protein pocket. The other end of the SSD has more active groups, which can form strong hydrogen bond interactions with LYS-83, LYS-39, and GLN-79

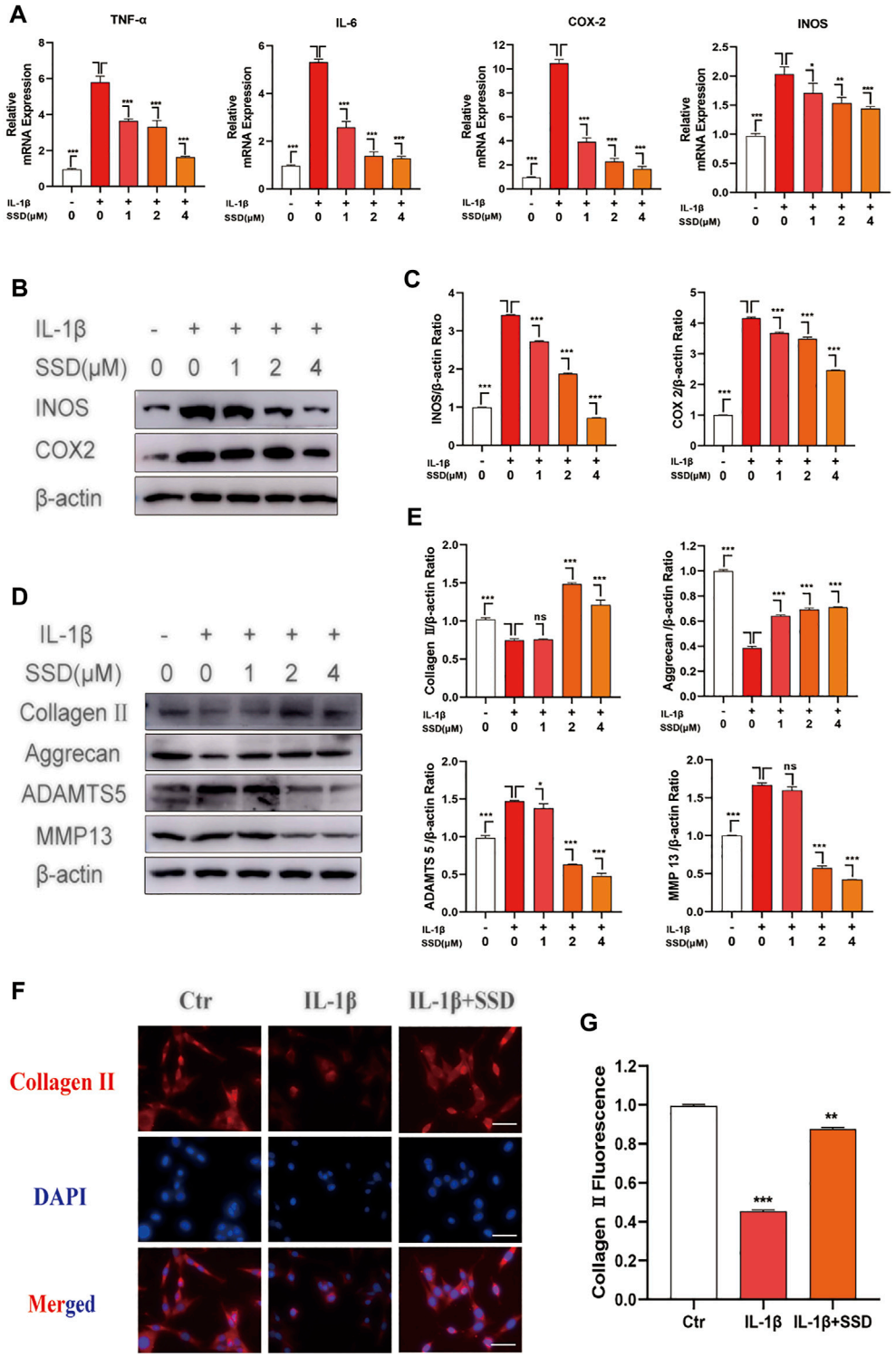

FIGURE 3 | SSD attenuated the production of inflammation-related factors and protected the ECM from damage under the stimulation of IL-1β. The mature chondrocytes stimulated by 10 ng/ml IL-1β or not were incubated with different concentrations of SSD (0, 1, 2, and 4 μM) for 2 days. The extracted RNA and total protein were used for further analysis by Western blot and qPCR. **(A)** SSD inhibited the expression level of inflammatory cytokine related marker genes in a dose-dependent manner. **(B)** SSD suppressed the production of INOS and COX2, especially at 4 μM. **(C)** The quantification of INOS and COX2 protein expression levels. **(D)** SSD reduced the expression level of ADAMTS 5 and MMP13 and increased the expression level of Aggrecan and Collagen II in a dose-dependent manner. **(E)** The quantification of ADAMTS 5, MMP13, Aggrecan, and Collagen II protein expression levels. **(F)** Immunofluorescence was conducted to visualize Collagen II. **(G)** The quantification of Collagen II fluorescence intensity (original magnification, ×200; scale, 15 μm). Mean ± SD was applied with all data. The experiments *in vitro* were performed independently at least 3 times. ***$p < 0.001$, **$p < 0.01$, *$p < 0.05$.

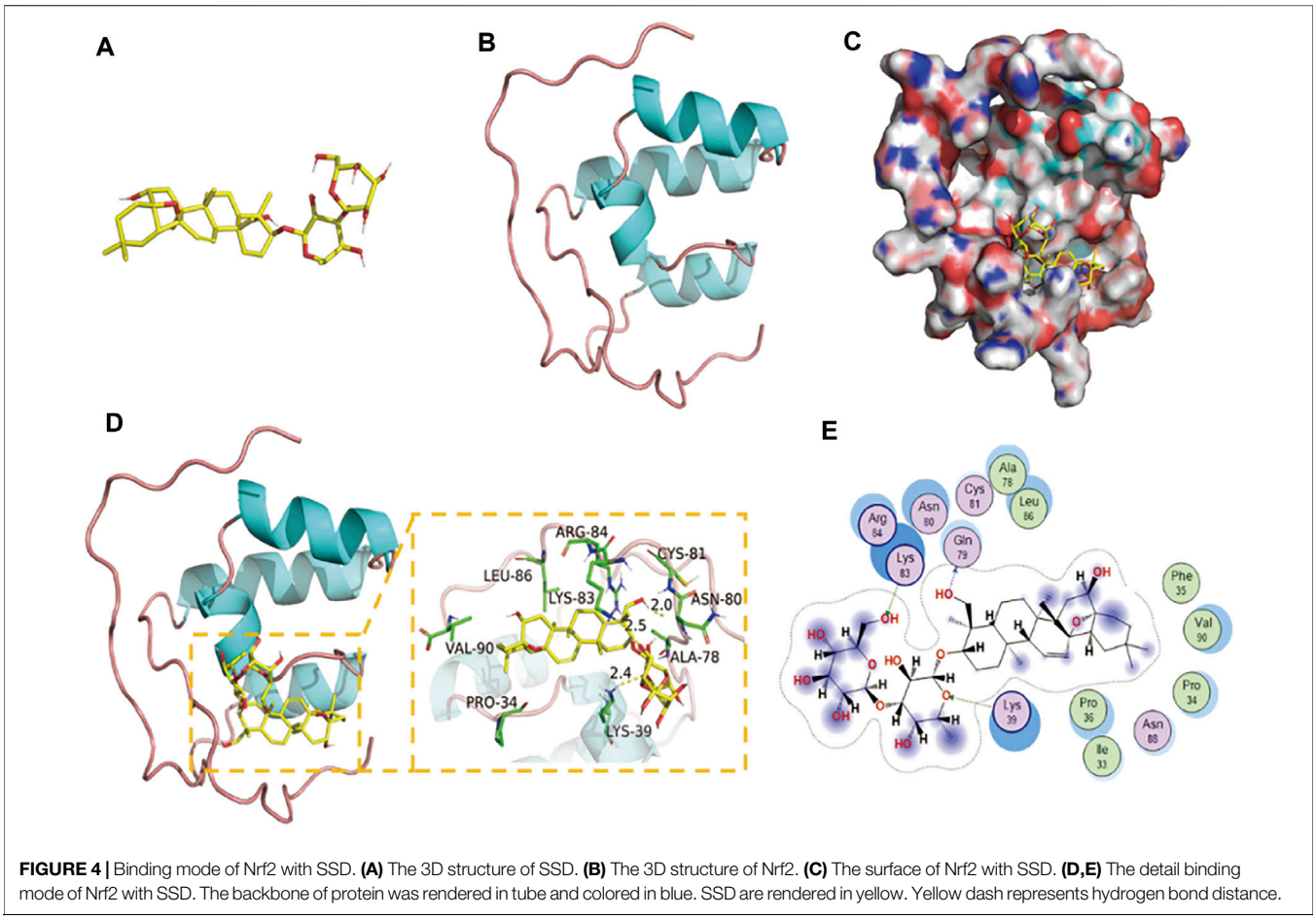

FIGURE 4 | Binding mode of Nrf2 with SSD. **(A)** The 3D structure of SSD. **(B)** The 3D structure of Nrf2. **(C)** The surface of Nrf2 with SSD. **(D,E)** The detail binding mode of Nrf2 with SSD. The backbone of protein was rendered in tube and colored in blue. SSD are rendered in yellow. Yellow dash represents hydrogen bond distance.

(**Figure 4E**). The hydrogen bond distances are 2.5, 2.4, and 2.0 Å, respectively. In summary, the SSD and Nrf2 protein are well matched and strongly bound, and the complex formed is relatively stable.

The Activation of Saikosaponin D on the Nrf2/HO-1/Reactive Oxygen Species Axis

According to previous studies, Nrf2 is maintained in the cytoplasm by Keap1 (Lu et al., 2016; Yamamoto et al., 2018). When Nrf2 is activated, Nrf2 is phosphorylated and translocated to the nucleus and quickly accelerates the expression of downstream HO-1 (Loboda et al., 2016). The activated Nrf2/HO-1 axis suppresses the production of ROS and the NF-κB signaling pathway in rheumatoid arthritis fibroblast like-synoviocytes (RA-FLSs) (Zhai et al., 2018). From the results in **Figures 5A,B**, SSD treatment significantly increased the expression of Nrf2 and HO-1 in a dose-dependent manner regardless of whether the cells were stimulated with IL-1β. Similarly, the results of ROS detection showed that SSD significantly reduced the fluorescence intensity of cellular ROS compared to the IL-1β group (**Figures 5C,D**). The results showed that SSD could activate the Nrf2/HO-1 axis and reduce the generation of ROS.

Nrf2 siRNA Suppressed the Activation of the Nrf2/HO-1 Pathway and the Generation of Reactive Oxygen Species

According to the results of Western blot, Nrf2 knockdown significantly reduced the expression level of HO-1. Compared with the si-NC group, SSD could not activate the Nrf2/HO-1 signal pathway after Nrf2 was knocked down (**Figures 5E,F**). In addition, the results of ROS detection indicated that the production of ROS was significantly increased in the si-NC group (**Figures 5G,H**). At this time, SSD could not play the role of activating the Nrf2/HO-1/ROS axis.

Effects of Saikosaponin D on NF-κB and Mapks Signaling Pathways in Differentiated ATDC 5 Chondrocytes

To further investigate the molecular mechanism of SSD on the NF-κB and Mapks signaling pathways in differentiated ATDC 5 chondrocytes, related protein expression levels in these signaling pathways were measured by Western blot analysis. **Figures 6A,B** showed that IκBα was degraded after IL-1β stimulation compared with the negative control group. The phosphorylation of p65 and IκBα was remarkably upregulated

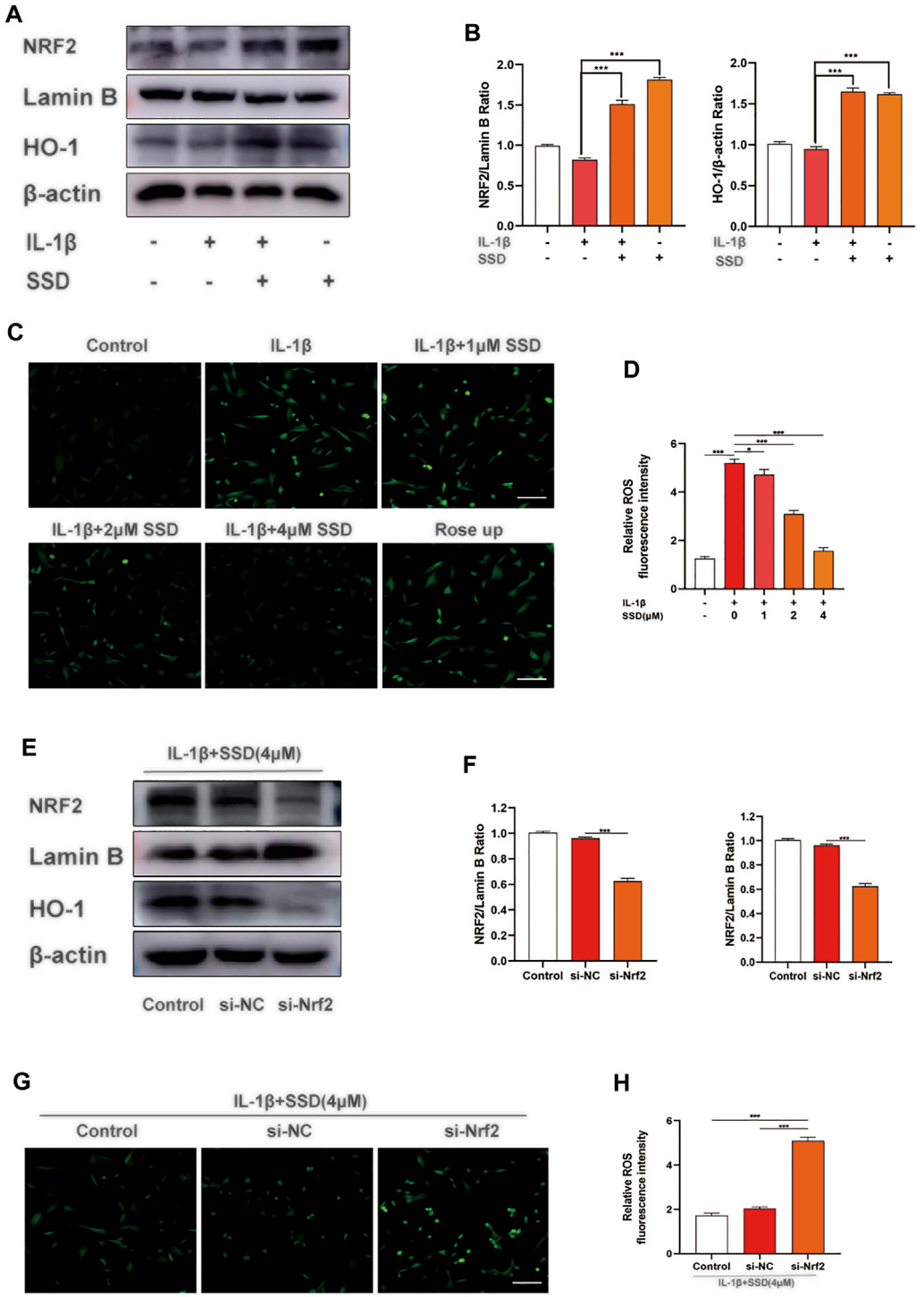

FIGURE 5 | SSD activated the Nrf2/HO-1 pathway and suppressed the generation of ROS. **(A)** SSD increased the expression levels of Nrf2 and HO-1regardless of the existence of IL-1β stimulation. **(B)** The quantification of Nrf2 and HO-1 protein expression levels. **(C)** Immunofluorescence was conducted to visualize ROS level. SSD decreased cellular ROS immunofluorescence intensity under IL-1β stimulation. **(D)** The quantification of ROS immunofluorescence intensity. **(E)** SSD could not increase the expression level of HO-1 after Nrf2 was knocked out. **(F)** The quantification of Nrf2 and HO-1 protein expression levels. **(G)** SSD has no effects on cellular ROS level under IL-1β stimulation after Nrf2 was knocked out. **(H)** The quantification of immunofluorescence intensity (original magnification, ×200; scale, 15 μm). Mean ± SD was applied with all data. The experiments *in vitro* were performed independently at least 3 times. ***$p < 0.001$, **$p < 0.01$, *$p < 0.05$.

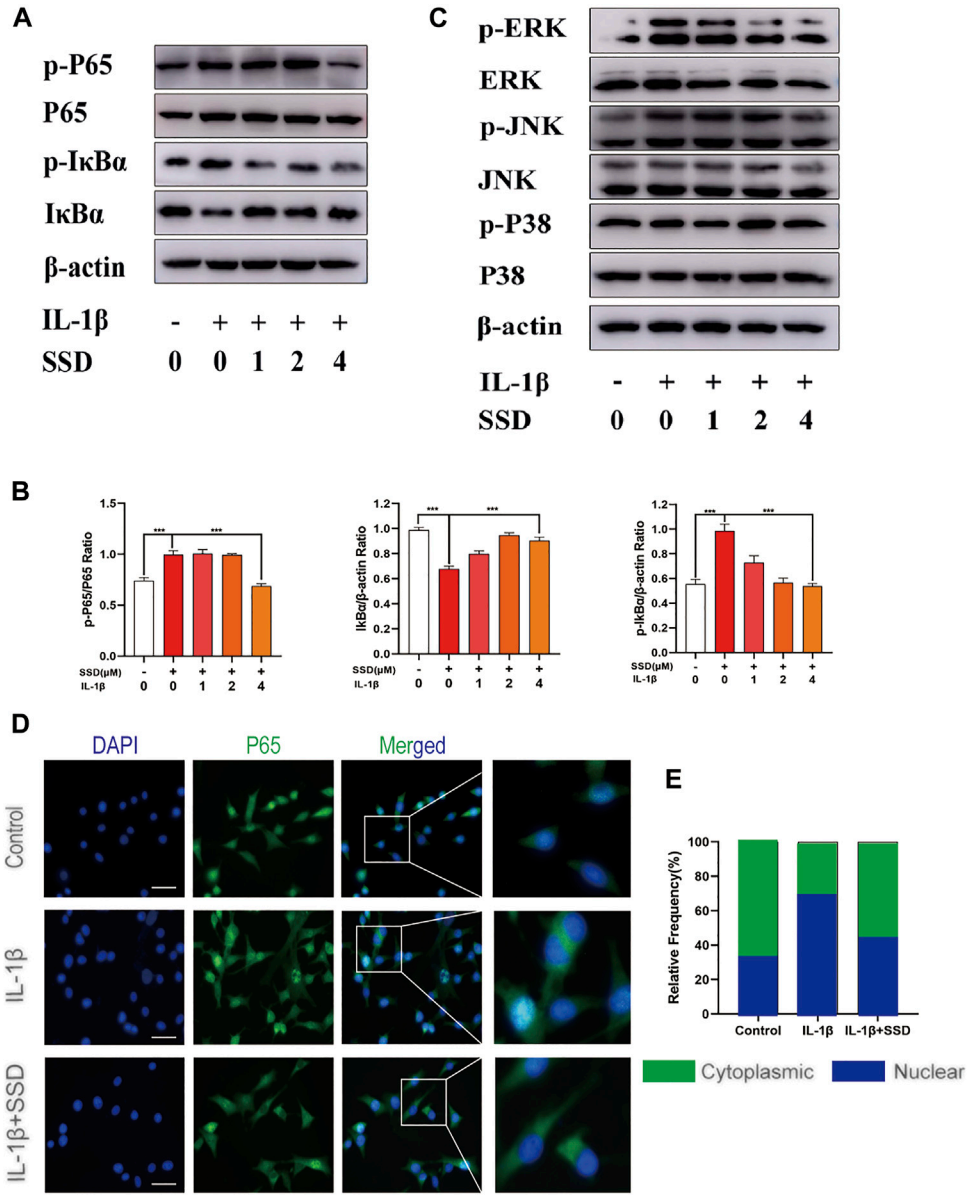

FIGURE 6 | Inhibition of SSD on the NF-κB signaling pathway. **(A)** SSD prevented IκBα from being degraded and inhibited the phosphorylation level of p-P65 and p-IκBα. **(B)** Above protein expression level was quantified using ImageJ. **(C)** SSD had no effects on Mapks signaling pathway–related proteins including P38, p-P38, ERK, p-ERK, JNK, and p-JNK. **(D)** Immunofluorescence was conducted to detect the P65 nuclear translocation. **(E)** The quantification of P65 fluorescence intensity (original magnification, ×200; scale, 15 μm). Mean ± SD was applied with all data. The experiments *in vitro* were performed independently at least 3 times. ***p < 0.001, **p < 0.01, *p < 0.05.

in the IL-1β group. However, the phosphorylation levels of P65 and IκBα was decreased significantly by SSD treatment. The Mapks play a key regulatory role in the production of pro-inflammatory factors. We observed that IL-1β enhanced the phosphorylation level of ERK, JNK, and P38, but SSD could not significantly reduce related phosphorylation levels (**Figure 6C**). Consistent with the results of immunofluorescence, P65 had a higher fluorescence intensity in the nucleus in the IL-1β group and SSD treatment reduced the fluorescence intensity (**Figures 6D,E**). The results indicated that SSD prevented the P65 nuclear translocation mediated by the IκBα pathway.

Saikosaponin D Attenuated the Progression of Cartilage Degeneration in Osteoarthritis Model Mice

Based on the results *in vitro*, an *in vivo* OA model mouse was established to further investigate whether SSD could delay the progression of OA. OARSI score, H&E staining, S-O staining, and

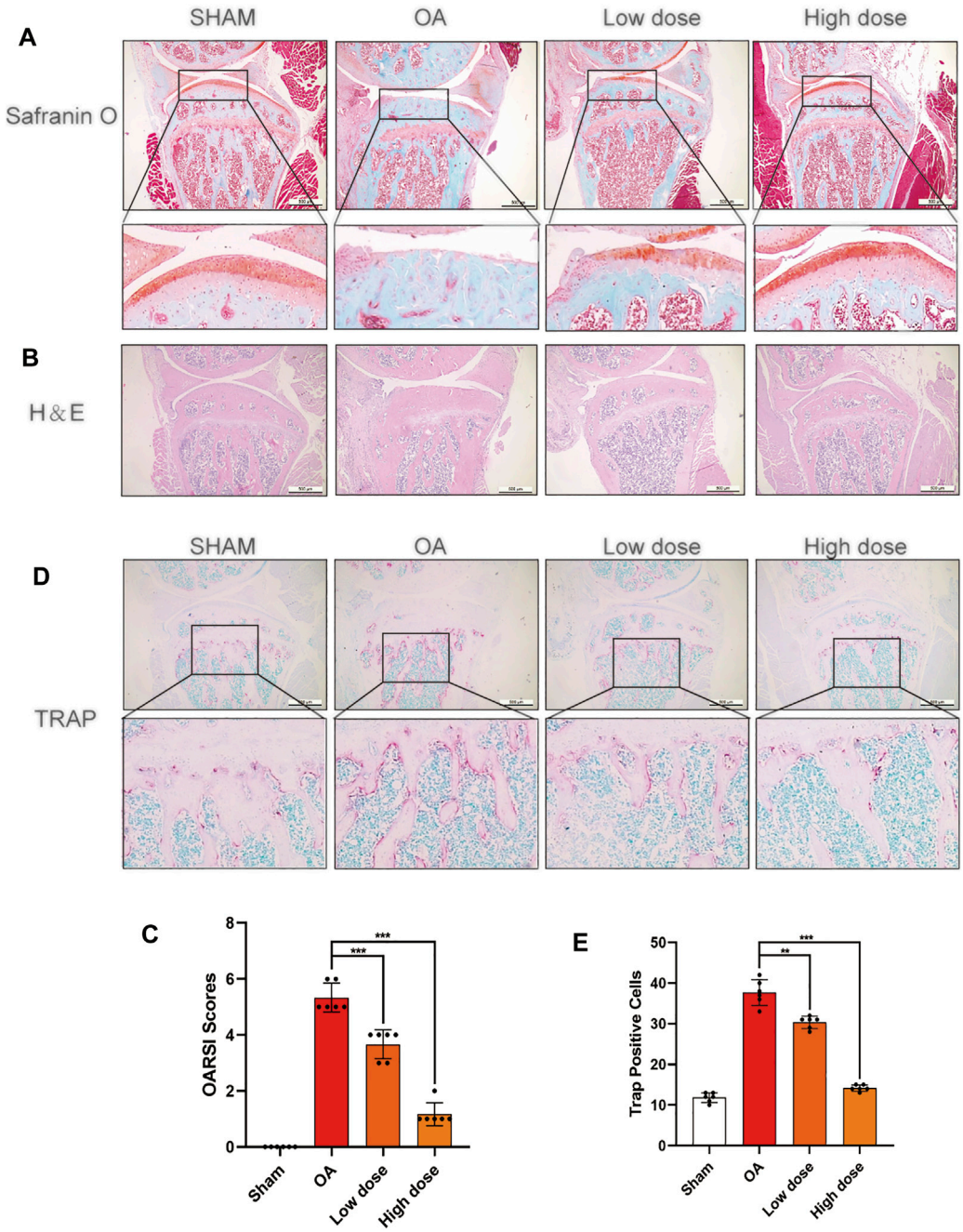

FIGURE 7 | SSD treatment delayed the progression of cartilage destruction in OA mice and decreased the osteoclasts in the knee joints' subchondral bone. **(A,B)** The S-O staining and H&E staining images of the right knee articular cartilage of 8-week-old male mice. SSD protected the mouse's right knee articular cartilage from damage. **(C)** The knee joint damage of each group was evaluated according to Osteoarthritis Research Society International (OARSI) scores. **(D)** The images of subchondral bone TRAP staining in male mice at 8 weeks. The activity of osteoclasts was weakened in the subchondral bone of mice right joints after SSD treatment. **(E)** The TRAP-positive cells were measured in the subchondral bone of each group using ImageJ. Mean ± SD was applied with all data. There were 6 randomly assigned male mice in each group. ***$p < 0.001$, **$p < 0.01$, *$p < 0.05$.

TRAP staining were used to perform histological analysis on mice of each group. The ratio of the red-stained area to the total area (red/total area) in the OA histone proteoglycan S-O staining was reduced in the OA group, indicating that the associated cartilage matrix was degraded. However, the red area ratio increased significantly in SSD intraperitoneal injection groups (low- and high-dose groups) (**Figure 7A**). For the H&E staining results, the number of chondrocytes decreased remarkably and the thickness and shape of the articular cartilage was irregular in the OA group. The shape of the articular cartilage was more regular and there were more chondrocytes in SSD low- and high-dose groups (**Figure 7B**). According to the results of TRAP staining of

histological sections, the number of TRAP-positive cells were decreased in SSD low- and high-dose groups compared with the OA group (**Figures 7D,E**). Consistent with the above results, the OARSI scores of SSD treatment groups were significantly lower than that of the OA group and closer to that of the sham group (**Figure 7C**). Therefore, SSD intraperitoneal injection suppressed the progression of cartilage degeneration in OA model mice.

DISCUSSION

Osteoarthritis (OA) is a common joint degenerative disease in the elderly. Both systemic and local factors are involved in the development of the disease (Martel-Pelletier et al., 2016). The clinical features of OA mainly include pain, joint dysfunction, and destruction of articular cartilage, resulting in restricted daily activities and even physical disability (Bijlsma et al., 2011). IL-1β and TNF-α are key pro-inflammatory cytokines involved in the pathophysiology of OA (Hosseinzadeh et al., 2016). Inhibiting the production of IL-1β and TNF-α could protect articular cartilage and reduce knee joint degeneration (Kapoor et al., 2011). However, the main purpose of current OA treatment is to relieve pain and improve joint function, including NSAIDs, analgesics, and joint lubricants (Kapoor et al., 2011). More and more studies have shown that plant and fruit extracts can be used in the treatment of related pro-inflammatory factor–mediated diseases (Azab et al., 2016). A recent study found that tangeretin downregulates IL-1β–induced secretion of inflammatory mediators and delays OA progression in mice (Shi et al., 2022). In our study, SSD is a triterpene saponin compound extracted from Bupleurum, which has various pharmacological activities such as anti-inflammatory, anti-oxidant, and antitumor activities (Li et al., 2019; Lai et al., 2020). This study found that SSD inhibited the expression level of inflammatory factors in the mature chondrocytes stimulated with IL-1β and increased the synthesis of the ECM *in vitro*.

Studies have found that IL-1β is an important inflammatory cytokine, which is significantly elevated in the knee synovial fluid of OA patients, and is closely related to the occurrence and development of OA. Therefore, the *in vitro* model of OA could be simulated by IL-1β–induced chondrocyte damage. The mature chondrocytes induced by IL-1β have an inflammatory response, and the expression of iNOS and COX2 increased at the mRNA and protein levels (Huang et al., 2009; Wojdasiewicz et al., 2014). Among them, iNOS belongs to the family of nitric oxide synthase (NOS) enzymes and is involved in NO synthesis (Cinelli et al., 2020). COX-2 can produce PGE2, an important inflammatory factor in the development of OA (Tong et al., 2018). Overexpression of inflammatory factors such as PGE2 and NO can disrupt the balance between ECM anabolism and catabolism (Amin et al., 2000). Studies have shown that inhibition of PGE2 and NO has a positive effect on the protection of articular cartilage (Wojdasiewicz et al., 2014). In addition, NO and PGE2 can induce chondrocytes to synthesize and release matrix metalloproteinases (MMPs) after reaching a certain amount of accumulation. MMPs are a major member of the proteolytic enzyme family, which participate in the process of chondrocyte apoptosis and destroy ECM components (aggrecan and collagen II). According to the results of previous studies, with the progress of OA, the levels of MMP-3 and MMP-13 increased significantly (Mehana et al., 2019). ADAMTS5 belongs to the ADAMTS protein family and participates in cartilage degradation during the OA progression. Studies have shown that ADAMTS5 cleaves proteoglycans in the early stages of OA. The loss of aggrecan in human OA cartilage explants is significantly reduced after transfection with siRNA, indicating that it may be a potential therapeutic target for OA (Hoshi et al., 2017; Malemud, 2019). When the ECM is destroyed, chondrocytes exposed to non-physiological load undergo apoptosis. At the same time, the high concentration of proteolytic enzymes accumulated by apoptosis will degrade aggrecan and collagen II. These factors lead to the further development of OA.

The NF-κB pathway involved in the progression of OA disease was regulated by the Nrf2/HO-1 axis (Bellezza et al., 2010). In the resting state, NF-κB binds to IκBα and is located in the cytoplasm. When stimulated by IL-1β, IκBα degraded and released P65 into the nucleus. The expression level of related inflammatory genes was accelerated, including COX-2, iNOS, MMPs, and ADAMTS (Rigoglou and Papavassiliou, 2013). As mentioned earlier, these inflammatory factors destroyed the balance between anabolism and catabolism of the ECM. Our experimental results showed that SSD activated the Nrf2/HO-1/ROS pathway and suppressed the IL-1β–induced NF-κB signaling pathway activation in the mature chondrocytes. Therefore, SSD attenuated IL-1β–induced chondrocyte apoptosis *via* the Nrf2/HO-1/ROS axis.

We performed mice DMM surgery on an *in vivo* research model of OA (Jia et al., 2019; Yan et al., 2020). Compared with the sham group, mice undergoing DMM surgery experienced joint space stenosis, cartilage erosion, and a decrease in the number of chondrocytes. Compared with the sham group, there were larger cartilage matrixes, more chondrocytes, fewer osteoclasts, and lower OARSCI scores in SSD intraperitoneal injection groups. Our experimental results showed that SSD could suppress cartilage destruction and chondrocyte loss *in vivo* OA model mice.

In summary, this study demonstrated that SSD inhibited differentiated ATDC 5 chondrocytes inflammatory apoptosis *via* the Nrf2/HO-1/ROS axis *in vitro* and suppressed cartilage destruction and chondrocyte loss *in vivo*. All above findings showed that SSD might have the potential to become a therapeutic drug for human OA in the future.

DATA AVAILABILITY STATEMENT

The original contributions presented in the study are included in the article/Supplementary Materials, further inquiries can be directed to the corresponding author.

ETHICS STATEMENT

The animal study was reviewed and approved by The Institutional Animal Ethics Committee of Taizhou Hospital (ethic code: tzy-2021170). The Health Guide for Care and Use of Laboratory Animals was regarded as the guideline for the care and use of our experimental animals. Written informed consent was obtained from the owners for the participation of their animals in this study.

AUTHOR CONTRIBUTIONS

HC and KZ designed the study. XW, XF, FL and PC participated in experiments. XS, WZ, CY, and JZ analyzed the results. XW wrote the manuscript and all authors reviewed the manuscript.

FUNDING

The research was funded by the Natural Science Foundation of Zhejiang Province (No. LY20H060006) and the Experimental Animal Science Project of Zhejiang Province (No. LGD19H310001).

REFERENCES

Abella, V., Scotece, M., Conde, J., López, V., Pirozzi, C., Pino, J., et al. (2016). The Novel Adipokine Progranulin Counteracts IL-1 and TLR4-Driven Inflammatory Response in Human and Murine Chondrocytes via TNFR1. *Sci. Rep.* 6, 20356. doi:10.1038/srep20356

Amin, A. R., Dave, M., Attur, M., and Abramson, S. B. (2000). COX-2, NO, and Cartilage Damage and Repair. *Curr. Rheumatol. Rep.* 2 (6), 447–453. doi:10.1007/s11926-000-0019-5

Azab, A., Nassar, A., and Azab, A. N. (2016). Anti-Inflammatory Activity of Natural Products. *Molecules* 21 (10), 1321. doi:10.3390/molecules21101321

Bellezza, I., Mierla, A. L., and Minelli, A. (2010). Nrf2 and NF-Kb and Their Concerted Modulation in Cancer Pathogenesis and Progression. *Cancers (Basel)* 2 (2), 483–497. doi:10.3390/cancers2020483

Bijlsma, J. W., Berenbaum, F., and Lafeber, F. P. (2011). Osteoarthritis: an Update with Relevance for Clinical Practice. *Lancet* 377 (9783), 2115–2126. doi:10.1016/s0140-6736(11)60243-2

Cao, P., Li, Y., Tang, Y., Ding, C., and Hunter, D. J. (2020). Pharmacotherapy for Knee Osteoarthritis: Current and Emerging Therapies. *Expert Opin. Pharmacother.* 21 (7), 797–809. doi:10.1080/14656566.2020.1732924

Chu, C. R., Millis, M. B., and Olson, S. A. (2014). Osteoarthritis: From Palliation to Prevention: AOA Critical Issues. *J. Bone Jt. Surg Am* 96 (15), e130. doi:10.2106/JBJS.M.01209

Cinelli, M. A., Do, H. T., Miley, G. P., and Silverman, R. B. (2020). Inducible Nitric Oxide Synthase: Regulation, Structure, and Inhibition. *Med. Res. Rev.* 40 (1), 158–189. doi:10.1002/med.21599

Glasson, S. S., Chambers, M. G., Van Den Berg, W. B., and Little, C. B. (2010). The OARSI Histopathology Initiative - Recommendations for Histological Assessments of Osteoarthritis in the Mouse. *Osteoarthritis Cartilage* 18 (Suppl. 3), S17–S23. doi:10.1016/j.joca.2010.05.025

Gómez, R., Lago, F., Gómez-Reino, J. J., Dieguez, C., and Gualillo, O. (2009). Expression and Modulation of ghrelinO-Acyltransferase in Cultured Chondrocytes. *Arthritis Rheum.* 60 (6), 1704–1709. doi:10.1002/art.24522

Guilak, F., Nims, R. J., Dicks, A., Wu, C. L., and Meulenbelt, I. (2018). Osteoarthritis as a Disease of the Cartilage Pericellular Matrix. *Matrix Biol.* 71-72, 40–50. doi:10.1016/j.matbio.2018.05.008

Ho, F. M., Kang, H. C., Lee, S. T., Chao, Y., Chen, Y. C., Huang, L. J., et al. (2007). The Anti-inflammatory Actions of LCY-2-CHO, a Carbazole Analogue, in Vascular Smooth Muscle Cells. *Biochem. Pharmacol.* 74 (2), 298–308. doi:10.1016/j.bcp.2007.04.008

Hoshi, H., Akagi, R., Yamaguchi, S., Muramatsu, Y., Akatsu, Y., Yamamoto, Y., et al. (2017). Effect of Inhibiting MMP13 and ADAMTS5 by Intra-articular Injection of Small Interfering RNA in a Surgically Induced Osteoarthritis Model of Mice. *Cell Tissue Res* 368 (2), 379–387. doi:10.1007/s00441-016-2563-y

Hosseinzadeh, A., Kamrava, S. K., Joghataei, M. T., Darabi, R., Shakeri-Zadeh, A., Shahriari, M., et al. (2016). Apoptosis Signaling Pathways in Osteoarthritis and Possible Protective Role of Melatonin. *J. Pineal Res.* 61 (4), 411–425. doi:10.1111/jpi.12362

Huang, C.-Y., Hung, L.-F., Liang, C.-C. T., and Ho, L.-J. (2009). COX-2 and iNOS are Critical in Advanced Glycation End Product-Activated Chondrocytes in vitro. *Eur. J. Clin. Invest.* 39, 417–428. doi:10.1111/j.1365-2362.2009.02106.x

Huang, H., Skelly, J. D., Ayers, D. C., and Song, J. (2017). Age-dependent Changes in the Articular Cartilage and Subchondral Bone of C57BL/6 Mice after Surgical Destabilization of Medial Meniscus. *Sci. Rep.* 7, 42294. doi:10.1038/srep42294

Jeon, J., Noh, H. J., Lee, H., Park, H. H., Ha, Y. J., Park, S. H., et al. (2020). TRIM24-RIP3 axis Perturbation Accelerates Osteoarthritis Pathogenesis. *Ann. Rheum. Dis.* 79 (12), 1635–1643. doi:10.1136/annrheumdis-2020-217904

Jia, Y., Pang, C., Zhao, K., Jiang, J., Zhang, T., Peng, J., et al. (2019). Garcinol Suppresses IL-1β-Induced Chondrocyte Inflammation and Osteoarthritis via Inhibition of the NF-Kb Signaling Pathway. *Inflammation* 42 (5), 1754–1766. doi:10.1007/s10753-019-01037-7

Kapoor, M., Martel-Pelletier, J., Lajeunesse, D., Pelletier, J. P., and Fahmi, H. (2011). Role of Proinflammatory Cytokines in the Pathophysiology of Osteoarthritis. *Nat. Rev. Rheumatol.* 7 (1), 33–42. doi:10.1038/nrrheum.2010.196

Kim, J. H., Jeon, J., Shin, M., Won, Y., Lee, M., Kwak, J. S., et al. (2014). Regulation of the Catabolic cascade in Osteoarthritis by the Zinc-ZIP8-MTF1 axis. *Cell* 156 (4), 730–743. doi:10.1016/j.cell.2014.01.007

Lai, M., Ge, Y., Chen, M., Sun, S., Chen, J., and Cheng, R. (2020). Saikosaponin D Inhibits Proliferation and Promotes Apoptosis through Activation of MKK4-JNK Signaling Pathway in Pancreatic Cancer Cells. *Onco Targets Ther.* 13, 9465–9479. doi:10.2147/OTT.S263322

Latourte, A., Kloppenburg, M., and Richette, P. (2020). Emerging Pharmaceutical Therapies for Osteoarthritis. *Nat. Rev. Rheumatol.* 16 (12), 673–688. doi:10.1038/s41584-020-00518-6

Li, C., Huang, L., Sun, W., Chen, Y., He, M. L., Yue, J., et al. (2019). Saikosaponin D Suppresses Enterovirus A71 Infection by Inhibiting Autophagy. *Signal. Transduct Target. Ther.* 4, 4. doi:10.1038/s41392-019-0037-x

Li, P., Wu, M., Xiong, W., Li, J., An, Y., Ren, J., et al. (2020). Saikosaponin-d Ameliorates Dextran Sulfate Sodium-Induced Colitis by Suppressing NF-Kb Activation and Modulating the Gut Microbiota in Mice. *Int. Immunopharmacol* 81, 106288. doi:10.1016/j.intimp.2020.106288

Loboda, A., Damulewicz, M., Pyza, E., Jozkowicz, A., and Dulak, J. (2016). Role of Nrf2/HO-1 System in Development, Oxidative Stress Response and Diseases: an Evolutionarily Conserved Mechanism. *Cell Mol Life Sci* 73 (17), 3221–3247. doi:10.1007/s00018-016-2223-0

Lu, M. C., Ji, J. A., Jiang, Z. Y., and You, Q. D. (2016). The Keap1-Nrf2-ARE Pathway as a Potential Preventive and Therapeutic Target: An Update. *Med. Res. Rev.* 36 (5), 924–963. doi:10.1002/med.21396

Ma, H. L., Blanchet, T. J., Peluso, D., Hopkins, B., Morris, E. A., and Glasson, S. S. (2007). Osteoarthritis Severity Is Sex Dependent in a Surgical Mouse Model. *Osteoarthritis Cartilage* 15 (6), 695–700. doi:10.1016/j.joca.2006.11.005

Malemud, C. J. (2019). Inhibition of MMPs and ADAM/ADAMTS. *Biochem. Pharmacol.* 165, 33–40. doi:10.1016/j.bcp.2019.02.033

Martel-Pelletier, J., Barr, A. J., Cicuttini, F. M., Conaghan, P. G., Cooper, C., Goldring, M. B., et al. (2016). Osteoarthritis. *Nat. Rev. Dis. Primers* 2, 16072. doi:10.1038/nrdp.2016.72

Mehana, E. E., Khafaga, A. F., and El-Blehi, S. S. (2019). The Role of Matrix Metalloproteinases in Osteoarthritis Pathogenesis: An Updated Review. *Life Sci.* 234, 116786. doi:10.1016/j.lfs.2019.116786

Morimoto, H., Baba, R., Haneji, T., and Doi, Y. (2013). Double-stranded RNA-dependent Protein Kinase Regulates Insulin-Stimulated Chondrogenesis in Mouse Clonal Chondrogenic Cells, ATDC-5. *Cel Tissue Res* 351 (1), 41–47. doi:10.1007/s00441-012-1521-6

Qin, T., Yuan, Z., Yu, J., Fu, X., Deng, X., Fu, Q., et al. (2020). Saikosaponin-d Impedes Hippocampal Neurogenesis and Causes Cognitive Deficits by Inhibiting the Survival of Neural Stem/progenitor Cells via Neurotrophin Receptor Signaling in Mice. *Clin. Transl Med.* 10 (8), e243. doi:10.1002/ctm2.243

Rigoglou, S., and Papavassiliou, A. G. (2013). The NF-Kb Signalling Pathway in Osteoarthritis. *Int. J. Biochem. Cel Biol* 45 (11), 2580–2584. doi:10.1016/j.biocel.2013.08.018

Saha, S., Buttari, B., Panieri, E., Profumo, E., and Saso, L. (2020). An Overview of Nrf2 Signaling Pathway and its Role in Inflammation. *Molecules* 25 (22), 25. doi:10.3390/molecules25225474

Shi, Y., Chen, J., Li, S., Wu, Y., Yu, C., Ni, L., et al. (2022). Tangeretin Suppresses Osteoarthritis Progression via the Nrf2/NF-Kb and MAPK/NF-κB Signaling Pathways. *Phytomedicine* 98, 153928. doi:10.1016/j.phymed.2022.153928

Sondergaard, B. C., Schultz, N., Madsen, S. H., Bay-Jensen, A. C., Kassem, M., and Karsdal, M. A. (2010). MAPKs Are Essential Upstream Signaling Pathways in Proteolytic Cartilage Degradation-Ddivergence in Pathways Leading to Aggrecanase and MMP-Mediated Articular Cartilage Degradation. *Osteoarthritis Cartilage* 18 (3), 279–288. doi:10.1016/j.joca.2009.11.005

Sun, S. C. (2017). The Non-canonical NF-Kb Pathway in Immunity and Inflammation. *Nat. Rev. Immunol.* 17 (9), 545–558. doi:10.1038/nri.2017.52

Tong, D., Liu, Q., Wang, L. A., Xie, Q., Pang, J., Huang, Y., et al. (2018). The Roles of the COX2/PGE2/EP axis in Therapeutic Resistance. *Cancer Metastasis Rev.* 37 (2-3), 355–368. doi:10.1007/s10555-018-9752-y

Wojdasiewicz, P., Poniatowski, Ł. A., and Szukiewicz, D. (2014). The Role of Inflammatory and Anti-inflammatory Cytokines in the Pathogenesis of Osteoarthritis. *Mediators Inflamm.* 2014, 561459. doi:10.1155/2014/561459

Yamamoto, M., Kensler, T. W., and Motohashi, H. (2018). The KEAP1-NRF2 System: a Thiol-Based Sensor-Effector Apparatus for Maintaining Redox Homeostasis. *Physiol. Rev.* 98 (3), 1169–1203. doi:10.1152/physrev.00023.2017

Yan, Z., Qi, W., Zhan, J., Lin, Z., Lin, J., Xue, X., et al. (2020). Activating Nrf2 Signalling Alleviates Osteoarthritis Development by Inhibiting Inflammasome Activation. *J. Cel Mol Med* 24 (22), 13046–13057. doi:10.1111/jcmm.15905

Yuan, B., Yang, R., Ma, Y., Zhou, S., Zhang, X., and Liu, Y. (2017). A Systematic Review of the Active Saikosaponins and Extracts Isolated from Radix Bupleuri and Their Applications. *Pharm. Biol.* 55 (1), 620–635. doi:10.1080/13880209.2016.1262433

Zhai, K. F., Duan, H., Khan, G. J., Xu, H., Han, F. K., Cao, W. G., et al. (2018). Salicin from Alangium Chinense Ameliorates Rheumatoid Arthritis by Modulating the Nrf2-HO-1-ROS Pathways. *J. Agric. Food Chem.* 66 (24), 6073–6082. doi:10.1021/acs.jafc.8b02241

Zhu, X., Chen, F., Lu, K., Wei, A., Jiang, Q., and Cao, W. (2019). PPARγ Preservation via Promoter Demethylation Alleviates Osteoarthritis in Mice. *Ann. Rheum. Dis.* 78 (10), 1420–1429. doi:10.1136/annrheumdis-2018-214940

Conflict of Interest: The authors declare that the research was conducted in the absence of any commercial or financial relationships that could be construed as a potential conflict of interest.

Publisher's Note: All claims expressed in this article are solely those of the authors and do not necessarily represent those of their affiliated organizations, or those of the publisher, the editors, and the reviewers. Any product that may be evaluated in this article, or claim that may be made by its manufacturer, is not guaranteed or endorsed by the publisher.

frontiers | Frontiers in Pharmacology

ORIGINAL RESEARCH
published: 06 April 2022
doi: 10.3389/fphar.2022.842730

N-Acetyldopamine Dimer Attenuates DSS-Induced Ulcerative Colitis by Suppressing NF-κB and MAPK Pathways

Li-Jun Huang[1†], Yu-Mei Wang[1†], Lei-Qiang Gong[2], Chao Hu[1], Yu Gui[1], Chen Zhang[2], Xue Tan[1], Xian-Kuo Yu[1], Yi-Le Liao[1], Yan Luo[1], Yu-Qin Tang[1], Yi-Fei Dai[3], Yun Deng[2], Dong Wang[1]* and Da-le Guo[2]**

[1]State Key Laboratory of Southwestern Chinese Medicine Resources, School of Basic Medical Sciences, Chengdu University of Traditional Chinese Medicine, Chengdu, China, [2]School of Pharmacy, Chengdu University of Traditional Chinese Medicine, Chengdu, China, [3]Department of Basic Medical Sciences, School of Medicine, Tsinghua University, Beijing, China

OPEN ACCESS

Edited by:
Peramaiyan Rajendran,
King Faisal University, Saudi Arabia

Reviewed by:
Jennifer Catherine Brazil,
University of Michigan, United States
Erin C Steinbach,
University of North Carolina at Chapel Hill, United States
Chang-Jiang Yu,
Georgia State University, United States

***Correspondence:**
Yun Deng
dengyun@cdutcm.edu.cn
Dong Wang
dwang@cdutcm.edu.cn
Da-le Guo
guodale@cdutcm.edu.cn

[†]These authors have contributed equally to this work

Specialty section:
This article was submitted to Inflammation Pharmacology, a section of the journal Frontiers in Pharmacology

Received: 24 December 2021
Accepted: 03 March 2022
Published: 06 April 2022

Citation:
Huang L-J, Wang Y-M, Gong L-Q, Hu C, Gui Y, Zhang C, Tan X, Yu X-K, Liao Y-L, Luo Y, Tang Y-Q, Dai Y-F, Deng Y, Wang D and Guo D-l (2022) N-Acetyldopamine Dimer Attenuates DSS-Induced Ulcerative Colitis by Suppressing NF-κB and MAPK Pathways. Front. Pharmacol. 13:842730. doi: 10.3389/fphar.2022.842730

Ulcerative Colitis (UC) is a major form of chronic inflammatory bowel disease of the colonic mucosa and exhibits progressive morbidity. There is still a substantial need of small molecules with greater efficacy and safety for UC treatment. Here, we report a N-acetyldopamine dimer (NADD) elucidated (2R,3S)-2-(3′,4′-dihydroxyphenyl)-3-acetylamino-7-(N-acetyl-2″-aminoethyl)-1,4-benzodioxane, which is derived from traditional Chinese medicine *Isaria cicadae*, exhibits significant therapeutic efficacy against dextran sulfate sodium (DSS)-induced UC. Functionally, NADD treatment effectively relieves UC symptoms, including weight loss, colon length shortening, colonic tissue damage and expression of pro-inflammatory factors in pre-clinical models. Mechanistically, NADD treatment significantly inhibits the expression of genes in inflammation related NF-κB and MAPK signaling pathways by transcriptome analysis and western blot, which indicates that NADD inhibits the inflammation in UC might through these two pathways. Overall, this study identifies an effective small molecule for UC therapy.

Keywords: N-acetyldopamine dimer, ulcerative colitis, inflammation, NF-κB pathway, MAPK pathway

INTRODUCTION

Ulcerative Colitis (UC) is a chronic inflammatory bowel disease that shows increasing incidence worldwide (Ordás et al., 2012; Ng et al., 2017). The incidence of UC in North America, Europe, and Oceania is greater than 15 per 100,000 person-years (Du and Ha, 2020). The annual incidence of UC, among Asian countries, is relatively high in China with a mean of 1.18 per 100,000 person-years (Zhou et al., 2021). The occurrence of UC is influenced by many factors, including genetic, environmental, and luminal factors (Ordás et al., 2012). The pathophysiology of UC is multifaceted and its etiology is still not completely understood.

Mucosal inflammation in UC usually starts from the rectum and gradually extends to part of or the entire colon (Ordás et al., 2012). Intestinal barrier disruption caused by an inflammatory cascade may lead to UC chronicity. Medical treatment of UC mainly focuses on reducing inflammation and uses mesalazine, corticosteroids, immune-suppressive drugs, and TNF-α monoclonal antibodies (Ordás et al., 2012). Nevertheless, side effect, safety, and tolerance issues with these drugs indicate an

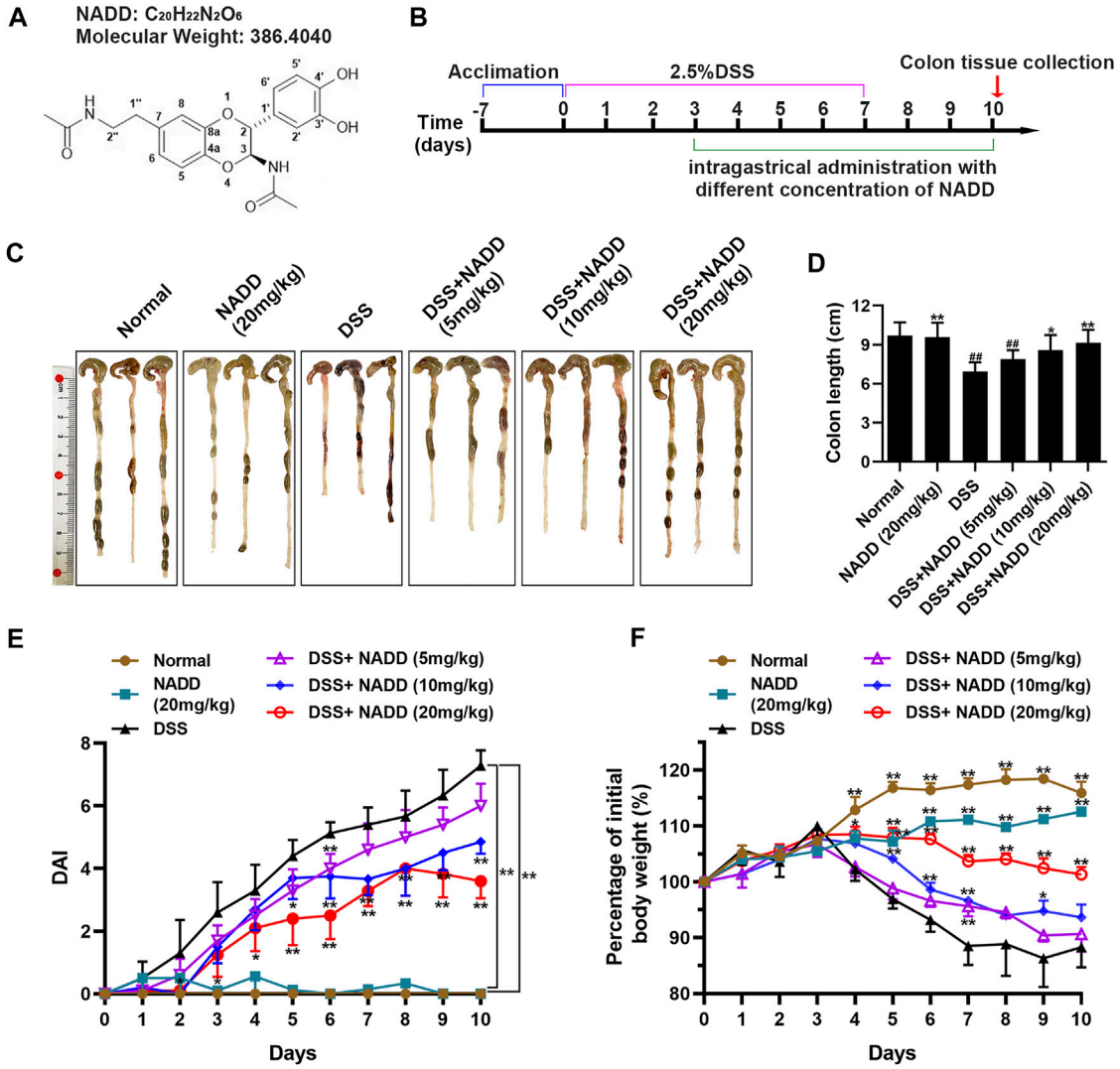

FIGURE 1 | The therapeutic effect of NADD on UC. **(A)** Molecular structures of NADD **(B)** Experiment flow diagram. **(C)** Images of murine colons among different groups of mice **(D)** Histogram of colon length after treatment with different concentrations of NADD. **(E)** DAI of mice among different treatment groups. **(F)** Body weight changes of mice among different treatment groups. Differences were statistically significant when compared with mice in the DSS group (*$p < 0.05$, **$p < 0.01$).

urgent need for effective agents with fewer unwanted properties. Natural products from traditional Chinese medicine might be promising resources of such molecules for UC treatment.

Isaria cicadae is a homologous medicine and food that displays anti-oxidation, anti-aging, anti-inflammation, and antitumor properties, ameliorates renal dysfunction, and shows remarkable immune modulation (Hua et al., 2016; Xu et al., 2018). *I. cicadae* has been used to cure inflammatory bowel disease in traditional Chinese medicine. The Compendium of Materia Medica, for instance, indicates that *I. cicadae* can cure malaria. A phytochemical search for active constituents in *I. cicadae* led to the isolation an N-acetyl dopamine dimer (NADD, **Figure 1A**), which was elucidated as (2R,3S)-2-(3′,4′-dihydroxyphenyl)-3-acetylamino-7-(N-acetyl-2″-aminoethyl)-1,4-benzodioxane. It was reported this compound exhibits antioxidant and anti-inflammatory properties (Xu et al., 2006), but its efficacy for the treatment of UC and underlying mechanism of anti-inflammatory activity are unclear.

Dextran sulfate sodium (DSS) induces changes in the gut microbiome, especially causing an increase in the number of gram-negative anaerobes (Okayasu et al., 1990). Mice treated with DSS mimic severe pathophysiological damage seen in human UC (Okayasu et al., 1990; Cooper et al., 1993; Ohkawara et al., 2002; Forbes et al., 2004). Clinical manifestations of UC induced by DSS include weight loss, diarrhea, and occult blood in stools. These issues are summarized with the DAI (Perse and Cerar, 2012). Hence, DSS-induced UC mice are considered a good model to study the effects and potential mechanisms of pharmacologic agents in treating inflammatory colon disease (Cooper et al., 1993).

This study evaluated the efficacy of NADD toward UC and explored underlying anti-inflammatory mechanisms. DSS-induced

UC mouse model was used to evaluate protective effects of NADD. Endpoints for assessing disease activity index (DAI), colon length, histopathological changes, as well as the secretion and gene expression of cytokines. Subsequently, lipopolysaccharide (LPS)-induced RAW264.7 macrophages were employed to investigate anti-inflammatory mechanisms. Transcriptional analysis combined with western blotting of LPS-induced RAW264.7 macrophages before and after NADD treatment was used to reveal related signaling pathways.

MATERIALS AND METHODS

Materials

I. cicadae was collected from a suburb of Ya'an, Sichuan province, China. DSS (40 KD) was purchased from Seebio Biotechnology Co., Ltd (Shanghai, China). TLR4 protein (purity ≥ 87%) was purchased from Sino biological. Bovine serum albumin (BSA) was purchased from Gemini. Animal Total RNA Isolation and Cell Total RNA Isolation Kits (RE-03014 and RE-03014113, respectively), RT EasyTM II (Master Premix for first-strand cDNA synthesis for Real-Time PCR RT-01022), and Real-Time PCR EasyTM-SYBR Green I (QP-01012) were purchased from Foregene (Chengdu, China). RNA Isolater Total RNA Extraction Reagent was purchased from Vazyme (R401-01, Nanjing, China). The Immobilon Western Chemiluminescent HRP Substrate was from Millipore (WBKLS0500, United States).

Preparation and Characterization of the NADD

Air-dried powder of *I. cicadae* (10 Kg) was extracted using 95% aqueous MeOH (3 × 100 l) under reflux. A crude extract was obtained after removing the solvent under reduced pressure. This extract was then suspended in distilled water (10 l) and placed on a macro-porous resin D101 column (D × L: 20 × 120 cm). The column was eluted with MeOH-H_2O (0:100, 30:70, 60:40, 100:0, V/V) to yield four fractions (A-D). Fraction C (150 g) was placed on a silica gel column (100–200 mesh, D × L: 15 × 80 cm) and eluted with a PE-acetone gradient (100:0→1:1, V/V) to afford eight subfractions (C1-C8). Fractions C2 (4.1 g), C3 (1.9 g), and C4 (3.9 g) were combined, guided by TLC, and passed through a Sephadex LH-20 column (D × L: 2 × 180 cm, $CHCl_3$-MeOH, 1:1). Finally, the combined fractions were further purified by preparative HPLC (5 μm, 120 A, D × L: 10 × 250 mm) with MeOH-H_2O (30:70, 10 ml/min) to yield NADD (1.26 g, purity ≥98%, (**Supplementary Figures S1, S2**).

Animals

All animal experiments were conducted as per protocols accredited by the Animal Welfare Committee of Chengdu University of Traditional Chinese Medicine, and in accordance with the National Institutes of Health Guide for the Care and Use of Laboratory Animals.

Imprinting control region male mice (7 weeks old, 30–35 g) were supplied by Specific Pathogen Free (SPF) Biotechnology Co., Ltd (Beijing, China) and housed in the animal facility of the Laboratory Animal Center of Chengdu University of Traditional Chinese Medicine, under standard conditions. All mice were provided food and distilled water. Animal experiments were designed following reported procedures (Ma et al., 2018; Shi et al., 2020; Wang et al., 2021; Zhang et al., 2021). After one week of acclimatization, mice were randomly divided into six groups (n = 8 per group): normal group (normal), NADD administration group (NADD (20 mg/kg)), UC model group (DSS), rescue UC model groups administrated different concentrations of NADD—DSS + NADD (5 mg/kg), DSS + NADD (10 mg/kg), DSS + NADD (20 mg/kg). NADD was dissolved in normal saline.

Mice administered DSS or DSS combined with NADD were supplied with freely accessible 2.5% DSS in drinking water for first 7 days. DSS was discontinued in favor of distilled water for the last 3 days (days 8–10). Normal mice and mice administered NADD (20 mg/kg) were provided with only distilled water for all 10 days. From the third day, mice in DSS + NADD (5 mg/kg), DSS + NADD (10 mg/kg), DSS + NADD (20 mg/kg) groups were administrated low, middle, and high concentrations of NADD by gavage. Mice in normal and DSS groups were administrated the same volume of normal saline by gavage as parallel controls. Body weight and DAI were recorded daily during the experiment. DAI was evaluated on the last day as the sum of body weight loss, diarrhea, and fecal bleeding (Wang et al., 2021). All groups of mice were sacrificed and colon tissues were obtained; colon length of each mouse was measured. Colon tissues were divided into five parts for different analyses.

Morphological Analysis

Colon tissues were fixed with 4% paraformaldehyde for 24 h and dehydrated with 30% sucrose at 4°C for 72 h. Tissues were then embedded in paraffin. Embedded tissues were cut into 5 μm-thick sections and stained with hematoxylin-eosin (HE) or Periodic Acid-Schiff (PAS) (Naeem et al., 2020). Stained sections were visualized and images were captured by light microscopy.

RT-PCR of Colon Tissues

Total RNA of colon tissues was isolated using an Animal Total RNA Isolation Kit, and mRNA was reverse transcribed into cDNA using an RT EasyTM II Kit following the manufacture's protocol. Expression of target genes was assessed with RT-PCR using Analytikjena (qTOWER3 G, Germany) and Real-Time PCR EasyTM-SYBR Green I. Sequences of primers TNF-α, IL-1β, iNOS, IL-6 and β-actin were previously reported (Wang et al., 2014). The primer sequences of Ikbkb, CCL2, Rela (p65), Nfkb1 (p50) and Nfkb2 (p52) were designed as previously described (Listwak et al., 2013).

ELISA Analysis of Colon Tissues

Colon tissues were lysed in PBS using a tissuelyzer (Servicebio, KZ-III F, China), then centrifuged and supernatants collected. TNF-α, IL-1β and IL-6 in supernatants were assessed using enzyme-linked immunosorbent assay (ELISA) kits (Multi Science, China), following the manufactures instruction. Absorbance was measured at 450 nm.

Cell Culture

Murine leukemic monocyte macrophage cells (RAW264.7 macrophages) were cultured in a DMEM complete medium with 10% fetal bovine serum and 1% penicillin-streptomycin at 37°C in a humidified atmosphere with 5% CO_2. In cell culture experiments, both NADD and LPS were dissolved in DMSO, therefore, DMSO was used as control.

Cell Viability Assay

RAW 264.7 macrophages were seeded into 96-well plates at a density of 8×10^3 cells/well. Cells achieved a density of 60–70% by the next day. Cells were then pre-treated with different concentrations of NADD (0 μM, 10 μM, 30 μM, 60 μM, 100 μM, 200 μM) for 1 h, followed by co-treating with or without 1 ug/mL LPS for 24 h. Subsequently, 10 μl of Cell Counting Kit-8 reagent (CCK8, MCE, HY-K0301) was added to each well and incubation continued for 3 h. Finally, optical density of formazan was measured at 450 nm using a microplate reader to assess cell viability (Thermo, Varioskan, MA, United States).

Transcriptome Sequencing (RNA-Seq)

RAW264.7 macrophages were seeded into 10 cm plates. When cells achieved a density of 60–70%, they were pre-treated with NADD at the concentration of 60 μM or without NADD for 1 h, followed by co-treatment with or without 1 μg/ml LPS for 24 h and generated three groups (DMSO group, LPS group, NADD + LPS group). A total of 5×10^6 cells were collected and lysed with RNA Isolater Total RNA Extraction Reagent. Lysates or fresh colon tissues were sent for transcriptome sequencing at Annoroad Biotechnology Co., Ltd (Zhejiang, China): Purity, concentration, and integrity of total RNA samples were assessed before further analysis. A cDNA library was obtained after amplification and purification. Finally, the cDNA library was sequenced using the Illumina NovaSeq 6000 platform with a 150-bp pair-end sequencing strategy to generate raw reads. Clean reads were obtained after removing adapter, poly-N sequences, and inferior quality reads. These reads were mapped to the *Mus musculus* (GRCm39 (Howe et al., 2021)) reference genome sequence using HISAT2 (Kim D. et al., 2019) tools. We assembled transcripts using HTSeq (Anders et al., 2015) for each sample to obtain gene read counts. Differential gene expression was assessed using DESeq2. Only genes with p-value < 0.05 and fold change value ≥ 1.5 were considered as significantly differentially expressed. We use cluster profiler (Wu et al., 2021) to assess KEGG pathway enrichment of DEGs. Volcano and heatmap plots were drawn in R. We used the upregulated genes and downregulated genes after LPS treatment as the background gene sets datasets, respectively. The upregulated and downregulated genes after LPS + NADD treatment were sorted according to the fold changes and used as input data for GSEA analysis. The related results showed whether the upregulated and downregulated genes were enriched in the term of background gene sets.

Western Blotting

RAW264.7 macrophages were seeded into 6-well plates at a density of 5×10^5 cells/well. When the cells achieved a density of 60–70%, they were pre-treated with different concentrations of NADD (10 μM, 30 μM, 60 μM) for 1 h, followed by co-treatment with or without 1 ug/mL LPS for 24 h. Subsequently, cells were collected and lysed with RIPA lysis buffer at 4°C for 30 min, centrifuged, and supernatants collected. The protein concentrations were then analyzed using a BCA protein assay kit (Beyotime, P0012, China) following the manufacturer's instructions. Aliquots with equal amounts of protein were loaded into wells of SDS-PAGE gels, subjected to electrophoresis and protein transferred to PVDF membranes (Ju et al., 2021). After blocking with 10% BSA, membranes were incubated with primary antibodies at 4°C overnight. Primary antibodies were: TLR4 (1:4000, Proteintech, 66350-1-Ig, China), IKK-α (1:1,000, CST, 11930 s, United States), p-IKK-α (1:1,000, CST, 2,697 s, United States), NF-κB-P65 (1:1,000, CST, 8,242 s, United States), p-NF-KB-P65 (1:1,000, CST, 3,033 s, United States), IκB-α (1:1,000, CST, 4812 s, United States), p-IκB-α (1:1,000, CST, 5,209 s, United States), P38 (1:1,000, CST, 8,690 s, UnitedStates), p-P38 (1:1,000, CST, 4511s, United States), R-iNOS (1:1,000, NOVCCS, NB300-605SS, United States), COX-2 (1:1,000, abcam, ab179800, United States), α-tubulin (1:20,000, proteintech, 66031-1-Ig, China). Membranes were washed three times, and incubated with species-specific secondary antibodies at room temperature for 2 h: HRP-Anti-mouse-IgG (1:5,000, servicebio, GB23301, China), and HRP-Anti-rabbit-IgG (1:5,000, servicebio, GB23303, China). Finally, targeted proteins were visualized using HRP substrate for immunoblotting and detected using a Chemiluminescent Imaging System (MiniChemi 610, China). The immunoblots of targeted proteins were analyzed using ImageJ.

Statistical Analysis

All inter-group comparisons were assessed using one-way analysis of variance by SPSS 26 and reported as mean ± standard deviation (SD). $p < 0.05$ was considered statistically significant, and a post-hoc analysis was done to determine which comparisons were significant.

RESULTS

NADD Alleviates Colitis Symptoms

The UC model was specifically constructed by receiving 2.5% DSS in drinking water on days 0–7, followed by normal drinking water for the last 3 days before sacrifice. Subsequently, different concentrations of NADD were administered orally from the fourth day to assess their impact on colitis. Parallel control groups (normal and DSS) were administrated with normal saline (**Figure 1B**). The UC model was constructed successfully as indicated by findings in normal and DSS group mice (**Figures 1C–E**). Further, mice administered NADD were compared to UC model mice to assess the therapeutic effect of NADD. The colon in DSS group mice appeared red, bleeding and shortened. In contrast, the colon for animals administered NADD gradually improved and became similar to normal mice. No differences were observed between colons from normal and NADD treated mice. Colon length shortened

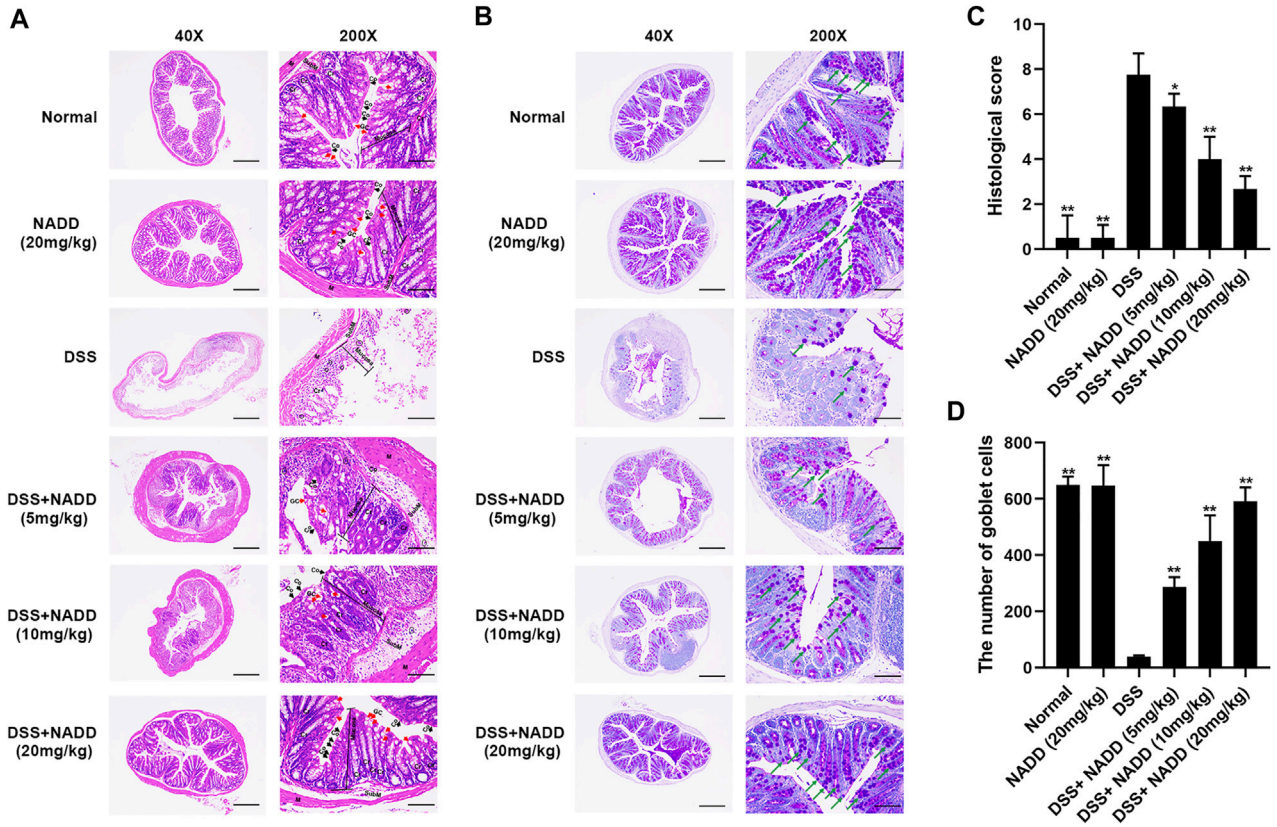

FIGURE 2 | HE and PAS staining. **(A)** Representative images of HE staining sections of colon; GC, goblet cells (red arrows); Cr, Crypts; Co, Columnar colonocytes (black arrows); SubM: Submucosa; Cells in the circle are Neutrophils. **(B)** Representative images of PAS staining; Amaranth granules are mucin glycoproteins (green arrows). **(C)** Histological scores of colon tissues with or without DSS induction and with or without administration of NADD. **(D)** The number of goblet cells of colon tissues with or without DSS induction and with or without administration of NADD. Differences were statistically significant when compared with the DSS group mice (*p < 0.05, **p < 0.01).

significantly in mice exposed to DSS when compared with normal animals (**Figure 1C**, $^{\#\#}p < 0.01$). However, NADD administration gradually reversed this shortening increasing oral dose (**Figure 1D**, *p < 0.05, **p < 0.01). No changes in DAI were noted between colons from normal and NADD treated mice. Compared with normal and NADD treated mice, all the DAI increased with time in DSS and DSS + NADD treated animals. However, the increase of DAI in DSS group was most notable over time, because NADD administration reversed this increase of DAI induced by DSS in a dose-dependent manner (**Figure 1E**, *p < 0.05, **p < 0.01). The body weight of DSS-exposed mice decreased over time, while the body weight of normal and NADD treated animals increased gradually. Compared with DSS group mice, the body weight of DSS + NADD treated animals increased significantly each day: In the low concentration group [DSS + NADD (5 mg/kg)], there were a trend of body weight increasing on days 5–10, but only on day 7, the increase was significantly; In the middle concentration group [DSS + NADD (10 mg/kg)], the trends of body weight increasing were more notable on days 4–10, and there were significantly increasing of body weight on days 5, 6, 7, and 9; In the highest concentration group [DSS + NADD (20 mg/kg)], the trends of body weight increasing were most notable, and there were significantly increasing of body weight on days 4, 5, 6, 7, 8, 9, and 10. To sum up, increases were most significant for mice administered NADD+20 (mg/kg) (**Figure 1F**, *p < 0.05, **p < 0.01). NADD thus relieved the symptoms of DSS-induced UC in a dose-dependent manner.

NADD Reduced Histologic Injury of Colitis Induced by DSS

Histological damage in colon tissues from DSS-induced UC reflected injury seen in human UC. Pathology included the disappearance of colonocytes, mucin depletion, decreases in goblet cells and crypts, neutrophil infiltration of lamina propria, and submucosa, and edematous submucosa (Perse and Cerar, 2012). Normal mucosa, thin submucosa and muscularis was found in the colon of normal and NADD (20 mg/kg) treated mice, and columnar colonocytes, goblet cells and long crypts were found in the mucosa (**Figure 2A**). The mucosa layer in DSS-exposed mice was disrupted, colonocytes and goblet cells disappeared, long crypts loosened, submucosa was edematous, and a large number of neutrophils infiltrated into the mucosa and submucosa, accompanied by crypt

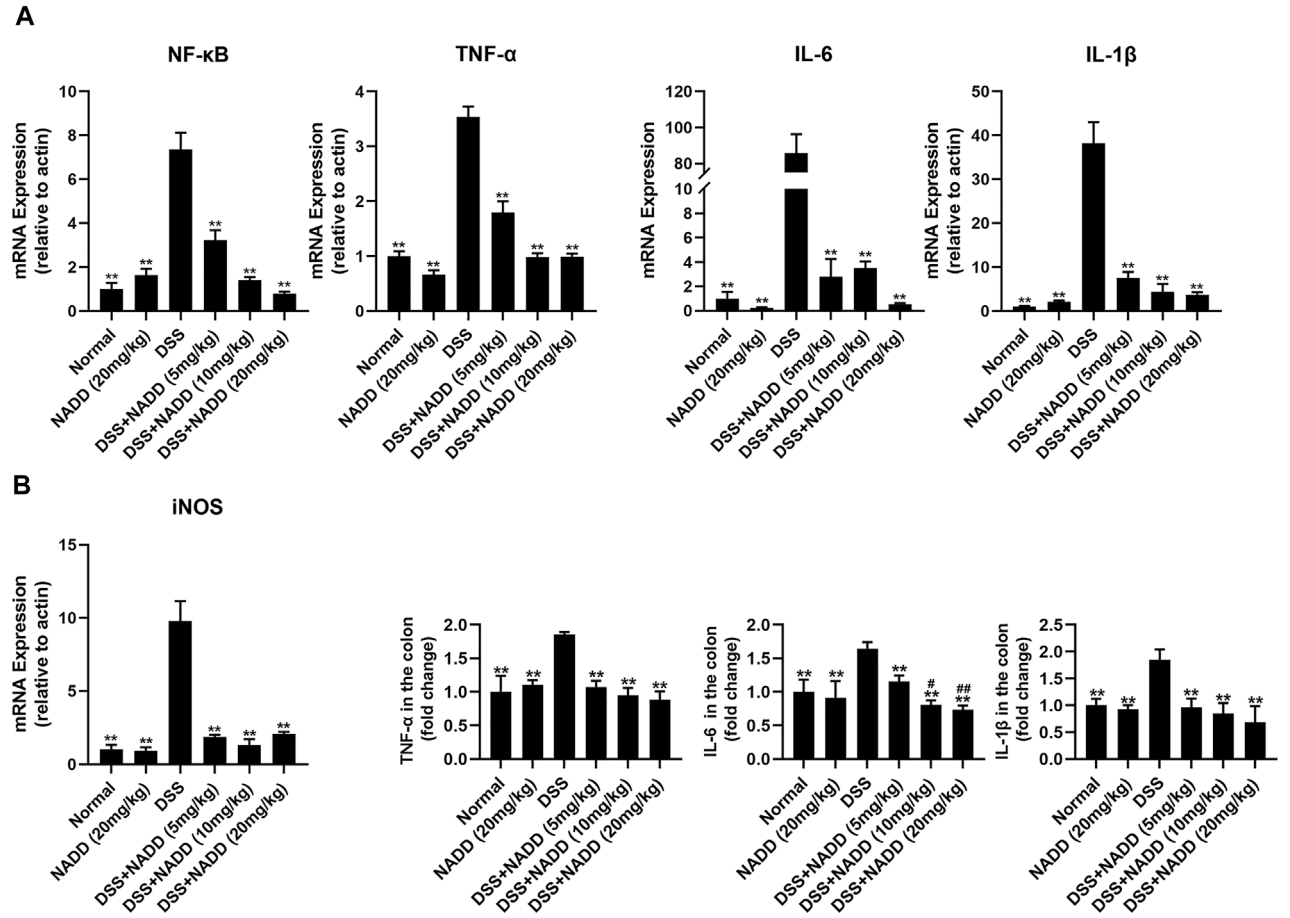

FIGURE 3 | Gene expressions and protein levels of proinflammatory factors. **(A)** mRNA expression levels of NF-κB, TNF-α, IL-6, IL-1β, and iNOS in colon tissues from mice in different treatment groups. **(B)** ELISA results of proinflammatory factor levels, including TNF-α, IL-6, IL-1β, in colon tissues from mice in different treatment groups. Differences were statistically significant when compared with the DSS group mice ($^{*}p < 0.05$, $^{**}p < 0.01$), and compared with the mice treated with DSS + NADD (5 mg/kg) ($^{\#}p < 0.01$, $^{\#\#}p < 0.01$).

abscesses. However, NADD administration protected colon tissues from damage induced by DSS. Colonocytes, goblet cells and long crypts increased, the submucosa became thinner, and neutrophil infiltration was less prominent. These protective effects of NADD became more obvious with increasing concentration. Conversely, PAS was used to identify goblet cells by staining secreted mucin glycoproteins. Mucin layers are considered protective factors against colitis (Chen et al., 2019). Colons from normal and NADD group mice showed mucin glycoprotein (**Figure 2B**). NADD increased mucin glycoproteins in a concentration-dependent manner. The grading of histological score was refer to references (Cooper et al., 1993; Kim S. E. et al., 2019). The pathohistological scores increased and the number of goblet cells lost significantly in the DSS only group than Normal and NADD only groups. However, the administration of NADD significantly decreased the pathohistological scores and increased the number of goblet cells in a concentration-dependent manner (**Figures 2C,D**). NADD thus protected against morphological changes induced by DSS exposure.

NADD Downregulated mRNA and Protein Levels of Proinflammatory Factors

UC is typically accompanied by the secretion of various proinflammatory factors, including TNF-α, IL-6, IL-1β, and NF-κB. For example, NF-κB induces an increase in NO concentrations by activating inducible nitric oxide synthase (iNOS) (Kimura et al., 2000). In this study, transcription levels of NF-κB, TNF-α, IL-6, IL-1β and iNOS were increased significantly in the colon tissues of DSS group mice compared with that of the normal and NADD only group animals ($^{**}p < 0.01$). Thus, DSS exposure successfully induced inflammation of colon tissues in mice (**Figure 3A**). Transcription levels were downregulated in a concentration-dependent manner by NADD ($^{**}p < 0.01$). Similarly, protein levels of TNF-α, IL-6, and IL-1β were also highest in DSS group mice, and became lower following NADD treatment ($^{**}p < 0.01$). IL-6 levels of DSS + NADD (10 mg/ml) and DSS + NADD (20 mg/ml) groups also decreased significantly ($^{\#}p < 0.01$, $^{\#\#}p < 0.01$) compared with mice treated with the low concentration of NADD (DSS + NADD

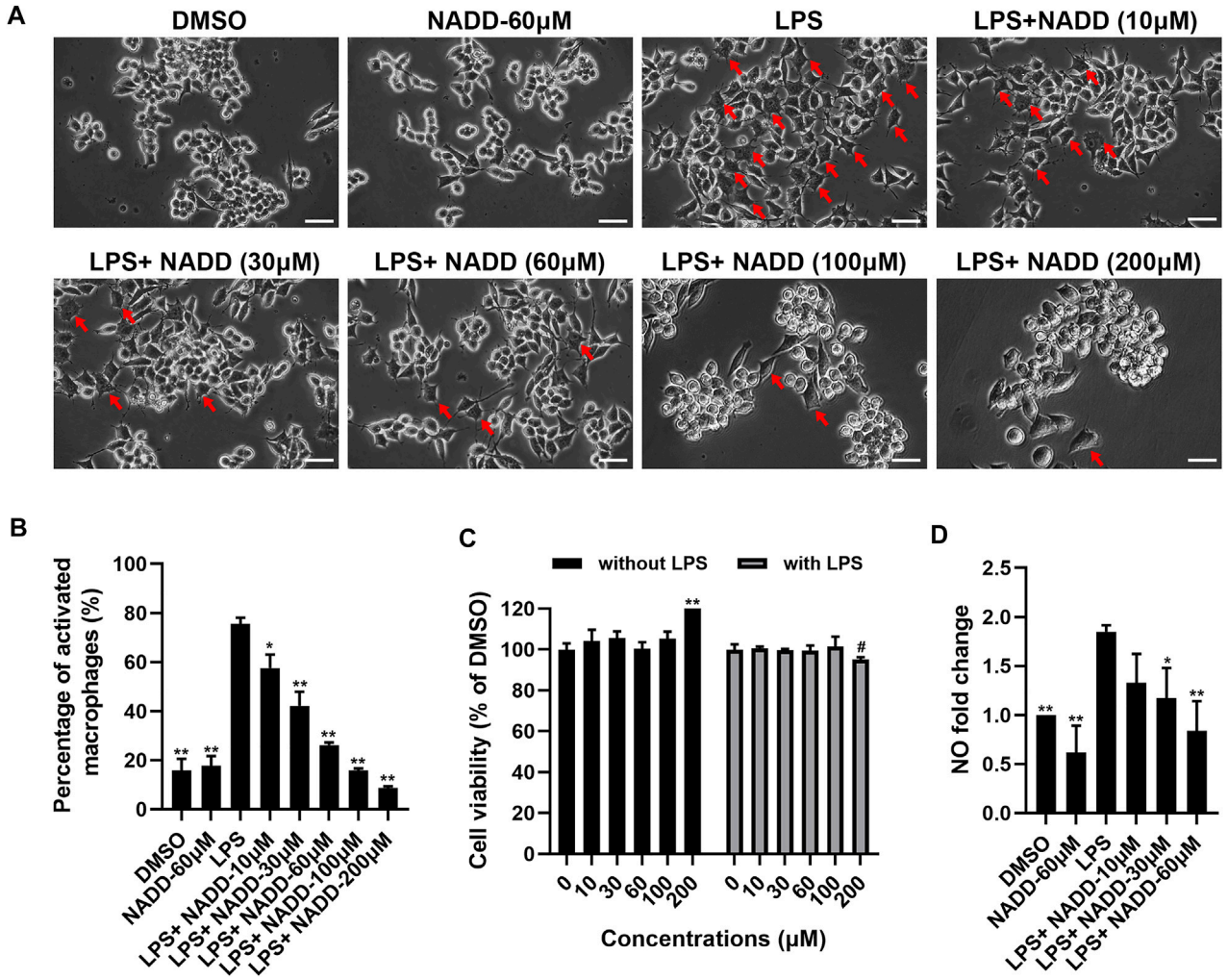

FIGURE 4 | The effect of NADD on LPS-induced inflammation *in vitro*. **(A)** The morphology of RAW264.7 macrophages treated with DMSO, NADD-60 μM, LPS, LPS + NADD-10 μM, LPS + NADD-30 μM, LPS + NADD-60 μM, LPS + NADD-100 μM, and LPS + NADD-200 μM. Red arrows indicate activated macrophages; white bar = 100 μm. **(B)** The statistical analysis of morphologic changes of RAW264.7 macrophages treated with DMSO, NADD-60 μM, LPS, LPS + NADD-10 μM, LPS + NADD-30 μM, LPS + NADD-60 μM, LPS + NADD-100 μM, and LPS + NADD-200 μM. Differences were statistically significant when compared with the LPS group (*$p < 0.05$, **$p < 0.01$). **(C)** Cell viability by CCK8; without LPS: RAW264.7 macrophages were not stimulated by LPS; with LPS: RAW264.7 macrophages were stimulated with LPS after cells were pre-treated with different concentrations of NADD. Differences were statistically significant when compared with the 0 μM group (**$p < 0.01$, without LPS; $^{\#}p < 0.05$, with LPS). **(D)** NO in culture supernatant from different groups of cells. Differences were statistically significant when compared with the LPS group (*$p < 0.05$, **$p < 0.01$).

(5 mg/ml)) (**Figure 3B**). NADD thus shows anti-inflammation activity for DSS-induced UC.

NADD Inhibits LPS-Stimulated Inflammation in a Concentration-Dependent Manner

RAW264.7 macrophages are a monocyte/macrophage-like cell linage (Kong et al., 2019) and LPS stimulates RAW264.7 to induce inflammation. This activity is accompanied by the expression of proinflammatory cytokines and iNOS (Plociennikowska et al., 2015; Kong et al., 2019). RAW264.7 macrophages activated by LPS change morphology from round to irregular and pseudopodia are expanded (**Figure 4A**). Cells treated with DMSO and 60 μM NADD were round and small, basically with no pseudopodia. After LPS exposure, most cells became irregular, cell bodies enlarged, and pseudopodia expanded. RAW264.7 macrophages treated with NADD showed reduced numbers of activated cells, and greater numbers of normal cells in a concentration-dependent manner. The statistical analysis showed that the morphological changes were significant as compared with the LPS group (**Figure 4B**). Further, NADD significantly decreased the generation of NO. This effect was also concentration-dependent (**Figure 4D**, *$p < 0.05$, **$p < 0.01$). Compared with 10 μM and 30 μM NADD, the higher concentration of NADD

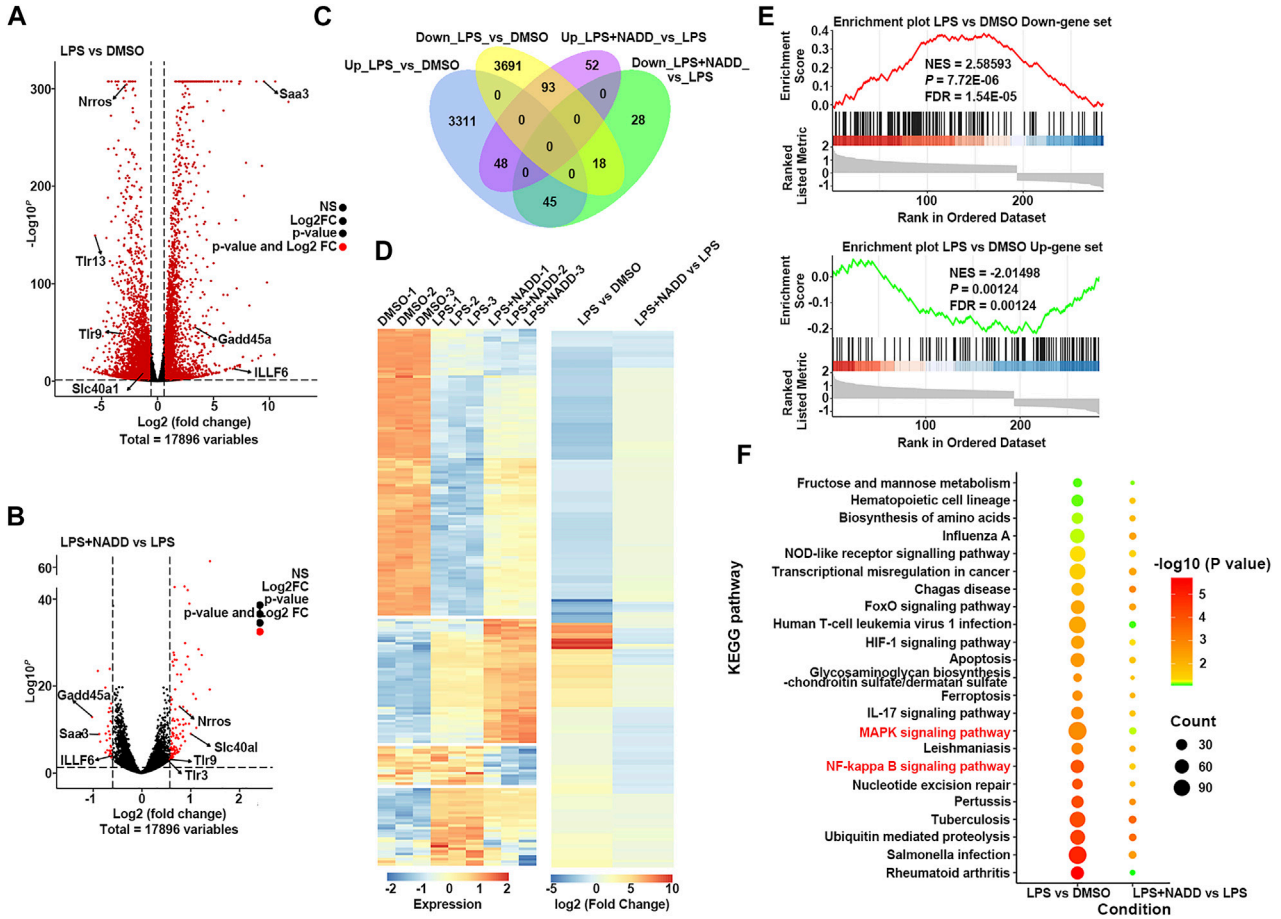

FIGURE 5 | The result of RNA-seq. **(A)** The volcano plot of DEGs between LPS and DMSO treated RAW264.7 macrophages; The red dots show significantly DEGs. **(B)** Volcano plot of DEGs between LPS + NADD LPS treated RAW264.7 macrophages; the red dots show significantly DEGs **(C)** Venn diagrams of overlapping genes with LPS only treatment and LPS + NADD treated RAW264.7 macrophages. **(D)** Heatmap of 204 common DEGs in LPS and LPS + NADD treated RAW264.7 macrophages. **(E)** GSEA analysis result of DEGs. **(F)** KEGG enrichment analysis of DEGs. The DEGs were defined by |foldchange| > 2 and $p < 0.05$.

(60 μM) induced a better anti-inflammation (**Figure 4D**) effect without adverse impacts on cell phenotype and viability with or without LPS stimulation (**Figures 4A,C**). NADD thus shows anti-inflammatory activity *in vitro*.

NADD Treatment Reversed LPS-Induced Changes of Gene Expressions

Transcriptome analysis was used to assess anti-inflammatory mechanisms of NADD. First, RAW264.7 macrophages were treated with LPS for 24 h to induce inflammation *in vitro*. Cells treated with DMSO served as a parallel control. Another group of cells were pre-treated with NADD (60 μM) for 1 h followed by LPS treatment for the next 24 h. Genome-wide profiles of differentially expressed genes (DEGs) were obtained by RNA-seq from all groups of cells. Cut-off criteria for volcano plots was fold change≥1.5 and $p < 0.05$ to identify DEGs. Many more DEGs were observed when comparing LPS and DMSO treated cells than when comparing LPS + NADD and LPS treated cells. Almost all genes downregulated by LPS treatment were upregulated after LPS treatment plus NADD treatment (**Figures 5A,B**), for example, *Nrros*, which downregulates ROS production (Bonini and Malik, 2014). Also, almost all genes upregulated by LPS treatment were downregulated after LPS treatment plus NADD treatment (**Figures 5A,B**), for example, *Saa3*, which is an inflammatory ligand that stimulates the production of IL-6 and TNF-α (Zhuang et al., 2017). The Venn diagrams (**Figure 5C**) showed 7,206 DEGs between LPS and DMSO treated cells, and 284 DEGs between LPS + NADD and LPS treated cells. Notably, almost 72% of the LPS + NADD affected genes (204/284) were also DEGs affected by LPS treatment alone. 93 DEGs that were down-regulated by LPS could be up-regulated by treatment of LPS + NADD, and 45 DEGs that were up-regulated by LPS could be down-regulated by treatment of LPS + NADD. The heat-map (**Figure 5D**) also shows that expression changes after LPS treatment are reversed by NADD treatment (fold change≥1.5, $p < 0.05$): Downregulated genes after LPS treatment were upregulated by NADD and vice-versa.

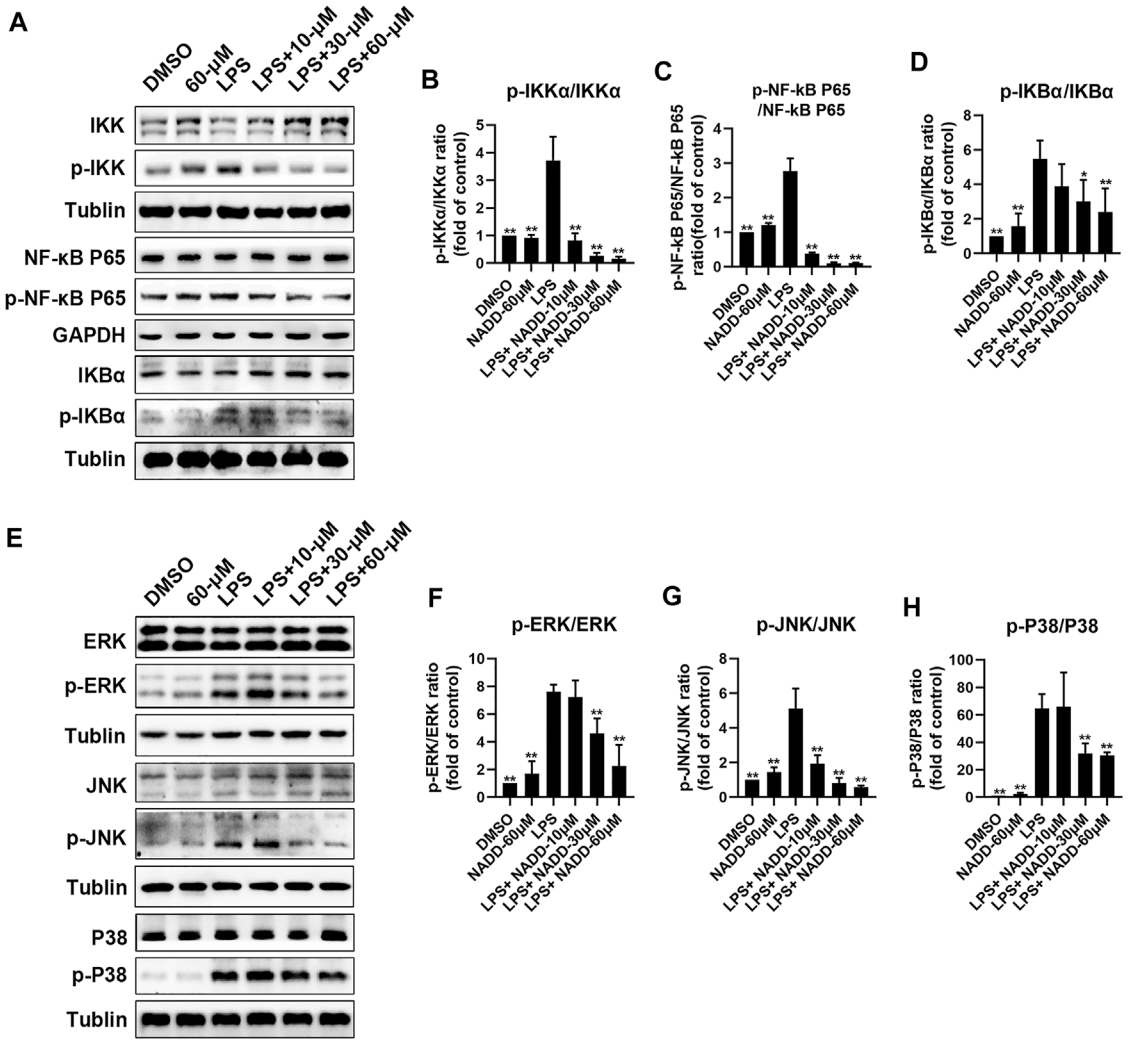

FIGURE 6 | Protein levels of NF-kB and MAPK pathway factors after LPS and NADD treatments. **(A)** Expression of IKK, p-IKK (LPS stimulated 30 min), NF-kB p65, p-NF-kB p65 (LPS stimulated 60 min), IKBα and p-IKBα (LPS stimulated 60 min) in the NF-kB pathway. Tubulin were internal reference proteins. Bar charts showing expression of p-IKK/IKK **(B)**, p-NF-kB p65/NF-kB p65 **(C)** and p-IKBα/ IKBα **(D)**. **(E)** expressions of ERK, p-ERK (LPS stimulated 15 min), JNK, p-JNK (LPS stimulated 30 min), P38 and p-P38 (LPS stimulated 30 min) in the MAPK pathway; Tubulin was the internal reference protein; Bar charts showing expression of p-ERK/ERK **(F)**, p-JNK/JNK **(G)** and p-IKBα/IKBα **(H)**. Differences were statistically significant when compared with the LPS treated cells (*$p < 0.05$, **$p < 0.01$).

Furthermore, gene set enrichment analysis (GSEA) illustrated the gene sets of up-regulated and down-regulated genes following LPS + NADD treatment (**Figure 5E**). As expected, NADD could reprogram the expressions of LPS regulated gene sets (**Figure 5E**). The intersection pathways enriched by both conditions were showed in **Figure 5F**, and the results showed that DEGs under both conditions were enriched in NF-kB and MAPK pathways. These findings suggest that NADD reverses LPS-induced inflammation at a transcriptional level. NADD inhibited LPS-induced Inflammation through TLR4/NF-kB and MAPK pathways.

RAW264.7 macrophages were treated with LPS and different concentrations of NADD to further explore anti-inflammatory effects of NADD *in vitro*. Western blotting was used to detect representative proteins involved in inflammatory signaling. Protein levels of p-IKK/IKK, p-NF-κB p65/ NF-κB p65, and p-IκBα/ IκBα in the NF-κB pathway were significantly elevated in LPS treated cells compared with DMSO and 60-μM treated cells. However, this effect was reversed significantly by NADD in a concentration-dependent manner (*$p < 0.05$, **$p < 0.01$) (**Figures 6A–D**). LPS treatment also significantly upregulated protein levels of p-JNK/JNK, p-ERK/ERK and p-P38/P38 compared with DMSO and 60 μM treated cells, and NADD reduced the levels of these proteins in a concentration-dependent manner (*$p < 0.05$, **$p < 0.01$) (**Figures 6E–H**). NADD thus suppress inflammation through modulation of NF-κB and MAPK pathways.

DISCUSSION

The etiology of UC is murky and complicated (Eisenstein, 2018). Hence, an effective strategy for screening compounds for useful clinical activity is to use pathological phenotype, including body weight, DAI, colon length, and histological changes. The latter may include disruption of epithelial barriers, goblet cell depletion, and damage to mucosa (Perse and Cerar, 2012; Chen et al., 2019). Damage to the epithelial barrier caused by UC allows gut microorganism invasion and enhances serious inflammation (Eisenstein, 2018). Hence, anti-inflammatory drugs are expected to be effective in treating UC. In this study, NADD was extracted from *I. cicadae*. The utility of this compound for treating UC has been observed and anti-inflammatory mechanisms were partially revealed.

NADD was found to significantly reduce DSS-induced DAI, improve colon length shortening, and reduce body weight loss. Especially, NADD decreases DAI, which reflects the main signs UC. Further, NADD administration significantly restored DSS-induced disruption or loss of the mucosal layer, columnar colonocytes, goblet cells and long crypts, and rescued submucosa edema and neutrophil infiltration into mucosa and submucosa. The actions of NADD were concentration-dependent. Therefore, NADD displayed the ability to relieve signs and symptoms of DSS-induced UC. In **Figure 1F**, although there were decreases of body weights in NADD group (**Supplementary Figure S3**), considered that NADD did not change the DAI when compared with normal group, we suspected that NADD may have a role of weight loss. However, the specific reason and underlying mechanism of decreasing of body weight need further studies in future.

DSS-induced UC is usually accompanied by disruption of the intestinal mucosal barrier accompanied by immune cell infiltration of mucosa and submucosa (Perse and Cerar, 2012). Further, bacterial invasion is also typical (Johansson et al., 2010). The main structural component of gram-negative bacteria is formed by LPS. The LPS receptor is the TLR4/MD-2 complex. This complex plays an important role in inflammation initiated by bacterial invasion (Kogut et al., 2005; St Paul et al., 2012; Yao et al., 2019). NF-κB is a downstream molecule of TLR4 signaling (Luo et al., 2012) and is often upregulated or over-activated in inflammatory disorders (Atreya et al., 2008; Danese and Mantovani, 2010). Activated NF-κB enters the nucleus and promotes the transcription of important cytokines (Thompson and Van Eldik, 2009; Cao et al., 2018). NF-κB is activated by phosphorylation, following ubiquitination and degradation of IκBs, IκBs phosphorylated by phosphorylated IKK (Atreya et al., 2008; Napetschnig and Wu, 2013). The MAPK pathway involves well-known proteins, such as P38, ERK, and JNK (Chang and Karin, 2001), TLR4 activation also activates this pathway (Hofmann et al., 2017). Briefly, TLR4 actives MyD88 and MyD88 activates TAK1. Subsequently, P38, ERK, and JNK are activated by TAK1, which activates activator protein 1 (AP-1). This protein promotes the production of proinflammatory cytokines and the initiation of inflammation (Palsson-McDermott and O'Neill, 2004; Moresco et al., 2011; Zhang et al., 2020).

In this study, NADD suppressed transcriptional and protein expression of proinflammatory cytokines, including TNF-α, IL-6 and IL-1β, and NF-κB induced by DSS *in vivo* (**Figure 4**). Although the pinnacle of LPS-induced transcriptional changes in macrophages is 4–6 h, we detected some interested gene changes of $LPS^{+/-}$NADD on macrophages after 24 h, because we analyzed transcripts of TNF-α, IL-6 and IL-1β after 4 h of $LPS^{+/-}$NADD treatment, the results showed that NADD reversed the increasing transcription level of TNF-α, IL-6 and IL-1β after 4 h of LPS treatment in a concentration dependent manner (**Supplementary Figure S4**). This result was consistent with the RNA-seq result. RNA-seq of macrophages showed that NADD reversed the gene signature generated by LPS exposure *in vitro*. Thus, results *in vivo* and *in vitro* are consistent. Subsequent western blotting showed that NADD significantly reduced phosphorylation of IKK, NF-κB p65, and IKBα in the NF-κB pathway, and suppressed the activation of JNK/ERK/P38 in the MAPK pathway. Considering the important role of LPS receptor TLR4 in the inflammation both *in vitro* and *in vivo*, we have predicted whether there was an interaction between NADD and TLR4 by molecular docking, and the result showed that NADD could docking with the pocket of the TLR4/MD-2 (**Supplementary Figure S5**), and this result indicated NADD may combine directly with the TLR4/M2 complexes, prevent them from combining to TLR4 receptor. Thus, TLR4 signaling may be prevented by NADD, as well as the downstream pathways NF-κB and MAPK. NF-κB and MAPK pathways are closely linked and therefore NADD may alleviate DSS-induced UC through modulation of both pathways.

CONCLUSION

The present study shows that NADD significantly alleviates DSS-induced UC symptoms, such as increased DAI and histopathological changes including weight loss, colon length shortening, colonic tissue damage, as well as expression of proinflammatory factors *in vivo*. NADD also reverses LPS-induced gene signatures and LPS-related inflammatory signaling pathways including NF-κB and MAPK pathways *in vitro*. Hence, NADD may be a hit compound for UC therapy.

DATA AVAILABILITY STATEMENT

The datasets presented in this study can be found in online repositories. The names of the repository/repositories and accession number(s) can be found below: https://www.ncbi.nlm.nih.gov, accession ID: PRJNA788753.

ETHICS STATEMENT

The animal study was reviewed and approved by Ethics Committee of Chengdu University of Traditional Chinese Medicine.

AUTHOR CONTRIBUTIONS

D-LG designed and supervised the article. L-JH and Y-MW performed the experiments and collected, analyzed and plotted the data. L-QG extracted NADD, Y-FD, CH, X-KY, XT, Y-LL, CZ, YG, Y-LL, and Y-QT participated in the animal experiments. L-JH and Y-MW wrote and finalized the manuscript. D-LG, DW, and YD contribute to the writing of this manuscript. All authors contributed to this manuscript read and approved the submitted version.

FUNDING

This work was supported by the National Natural Science Foundation of China (82172723, 81673460, U19A2011), Key Projects of Science and Technology Plan of Inner Mongolia Autonomous Region (201,802115), Project of Department of Science and Technology of Sichuan Province (2021YFN0134, 2021ZYD0079), Sichuan Youth Science and Technology Innovation Research Team of Experimental Formulology (2020JDTD0022), the Project of First-Class Disciplines Development supported by Chengdu University of Traditional Chinese Medicine (CZYJC 1905) and "Xinglin Scholars" scientific research promotion plan of Chengdu University of Traditional Chinese Medicine (BSH2019017).

ACKNOWLEDGMENTS

The authors thank State Key Laboratory of Southwestern Chinese Medicine Resources, Research and Innovation Center of Basic Medical Sciences, Chengdu University of Traditional Chinese Medicine for using of some instruments.

SUPPLEMENTARY MATERIAL

The Supplementary Material for this article can be found online at: https://www.frontiersin.org/articles/10.3389/fphar.2022.842730/full#supplementary-material

REFERENCES

Anders, S., Pyl, P. T., and Huber, W. (2015). HTSeq--a Python Framework to Work with High-Throughput Sequencing Data. *Bioinformatics* 31 (2), 166–169. doi:10.1093/bioinformatics/btu638

Atreya, I., Atreya, R., and Neurath, M. F. (2008). NF-kappaB in Inflammatory Bowel Disease. *J. Intern. Med.* 263 (6), 591–596. doi:10.1111/j.1365-2796.2008.01953.x

Bonini, M. G., and Malik, A. B. (2014). Regulating the Regulator of ROS Production. *Cell Res.* 24 (8), 908–909. doi:10.1038/cr.2014.66

Cao, H., Liu, J., Shen, P., Cai, J., Han, Y., Zhu, K., et al. (2018). Protective Effect of Naringin on DSS-Induced Ulcerative Colitis in Mice. *J. Agric. Food Chem.* 66 (50), 13133–13140. doi:10.1021/acs.jafc.8b03942

Chang, L., and Karin, M. (2001). Mammalian MAP Kinase Signalling Cascades. *Nature* 410, 37–40. doi:10.1038/35065000

Chen, Y., Yang, B., Ross, R. P., Jin, Y., Stanton, C., Zhao, J., et al. (2019). Orally Administered CLA Ameliorates DSS-Induced Colitis in Mice via Intestinal Barrier Improvement, Oxidative Stress Reduction, and Inflammatory Cytokine and Gut Microbiota Modulation. *J. Agric. Food Chem.* 67 (48), 13282–13298. doi:10.1021/acs.jafc.9b05744

Cooper, H. S., Murthy, S. N., Shah, R. S., and Sedergran, D. J. (1993). Clinicopathologic Study of Dextran Sulfate Sodium Experimental Murine Colitis. *Lab. Invest.* 69 (2), 238–249.

Danese, S., and Mantovani, A. (2010). Inflammatory Bowel Disease and Intestinal Cancer: a Paradigm of the Yin-Yang Interplay between Inflammation and Cancer. *Oncogene* 29 (23), 3313–3323. doi:10.1038/onc.2010.109

Du, L., and Ha, C. (2020). Epidemiology and Pathogenesis of Ulcerative Colitis. *Gastroenterol. Clin. North. Am.* 49 (4), 643–654. doi:10.1016/j.gtc.2020.07.005

Eisenstein, M. (2018). Ulcerative Colitis: towards Remission. *Nature* 563 (7730), S33. doi:10.1038/d41586-018-07276-2

Forbes, E., Murase, T., Yang, M., Matthaei, K. I., Lee, J. J., Lee, N. A., et al. (2004). Immunopathogenesis of Experimental Ulcerative Colitis Is Mediated by Eosinophil Peroxidase. *J. Immunol.* 172 (9), 5664–5675. doi:10.4049/jimmunol.172.9.5664

Hofmann, S. R., Kapplusch, F., Girschick, H. J., Morbach, H., Pablik, J., Ferguson, P. J., et al. (2017). Chronic Recurrent Multifocal Osteomyelitis (CRMO): Presentation, Pathogenesis, and Treatment. *Curr. Osteoporos. Rep.* 15 (6), 542–554. doi:10.1007/s11914-017-0405-9

Howe, K. L., Achuthan, P., Allen, J., Allen, J., Alvarez-Jarreta, J., Amode, M. R., et al. (2021). Ensembl 2021. *Nucleic Acids Res.* 49 (D1), D884–D891. doi:10.1093/nar/gkaa942

Hua, R., Huang, H. R., He, R., and Tai, L. M. (2016). Magical Medicinal Fungus-Cordyceps Cicadae. *Edible Fungi of China* 35 (4), 84–86.

Johansson, M. E., Gustafsson, J. K., Sjöberg, K. E., Petersson, J., Holm, L., Sjövall, H., et al. (2010). Bacteria Penetrate the Inner Mucus Layer before Inflammation in the Dextran Sulfate Colitis Model. *PLoS One* 5 (8), e12238. doi:10.1371/journal.pone.0012238

Ju, F., Kuang, Q. X., Li, Q. Z., Huang, L. J., Guo, W. X., Gong, L. Q., et al. (2021). Aureonitol Analogues and Orsellinic Acid Esters Isolated from Chaetomium Elatum and Their Antineuroinflammatory Activity. *J. Nat. Prod.* 84 (12), 3044–3054. doi:10.1021/acs.jnatprod.1c00783

Kim, D., Paggi, J. M., Park, C., Bennett, C., and Salzberg, S. L. (2019). Graph-based Genome Alignment and Genotyping with HISAT2 and HISAT-Genotype. *Nat. Biotechnol.* 37 (8), 907–915. doi:10.1038/s41587-019-0201-4

Kim, S. E., Kawaguchi, K., Hayashi, H., Furusho, K., and Maruyama, M. (2019). Remission Effects of Dietary Soybean Isoflavones on DSS-Induced Murine Colitis and an LPS-Activated Macrophage Cell Line. *Nutrients* 11 (8), 1746. doi:10.3390/nu11081746

Kimura, H., Weisz, A., Kurashima, Y., Hashimoto, K., Ogura, T., D'Acquisto, F., et al. (2000). Hypoxia Response Element of the Human Vascular Endothelial Growth Factor Gene Mediates Transcriptional Regulation by Nitric Oxide: Control of Hypoxia-Inducible Factor-1 Activity by Nitric Oxide. *Blood* 95 (1), 189–197. doi:10.1182/blood.v95.1.189.001k05_189_197

Kogut, M. H., Iqbal, M., He, H., Philbin, V., Kaiser, P., and Smith, A. (2005). Expression and Function of Toll-like Receptors in Chicken Heterophils. *Dev. Comp. Immunol.* 29 (9), 791–807. doi:10.1016/j.dci.2005.02.002

Kong, L., Smith, W., and Hao, D. (2019). Overview of RAW264.7 for Osteoclastogensis Study: Phenotype and Stimuli. *J. Cel. Mol. Med.* 23 (5), 3077–3087. doi:10.1111/jcmm.14277

Listwak, S. J., Rathore, P., and Herkenham, M. (2013). Minimal NF-Kb Activity in Neurons. *Neuroscience* 250, 282–299. doi:10.1016/j.neuroscience.2013.07.013

Luo, H., Guo, P., and Zhou, Q. (2012). Role of TLR4/NF-Kb in Damage to Intestinal Mucosa Barrier Function and Bacterial Translocation in Rats Exposed to Hypoxia. *PLoS One* 7 (10), e46291. doi:10.1371/journal.pone.0046291

Ma, X., Hu, Y., Li, X., Zheng, X., Wang, Y., Zhang, J., et al. (2018). Periplaneta americana Ameliorates Dextran Sulfate Sodium-Induced Ulcerative Colitis in Rats by Keap1/Nrf-2 Activation, Intestinal Barrier Function, and Gut Microbiota Regulation. *Front. Pharmacol.* 9, 944. doi:10.3389/fphar.2018.00944

Moresco, E. M., LaVine, D., and Beutler, B. (2011). Toll-like Receptors. *Curr. Biol.* 21 (13), R488–R493. doi:10.1016/j.cub.2011.05.039

Naeem, M., Lee, J., Oshi, M. A., Cao, J., Hlaing, S. P., Im, E., et al. (2020). Colitis-targeted Hybrid Nanoparticles-In-Microparticles System for the Treatment of Ulcerative Colitis. *Acta Biomater.* 116, 368–382. doi:10.1016/j.actbio.2020.09.017

Napetschnig, J., and Wu, H. (2013). Molecular Basis of NF-Kb Signaling. *Annu. Rev. Biophys.* 42, 443–468. doi:10.1146/annurev-biophys-083012-130338

Ng, S. C., Shi, H. Y., Hamidi, N., Underwood, F. E., Tang, W., Benchimol, E. I., et al. (2017). Worldwide Incidence and Prevalence of Inflammatory Bowel Disease in the 21st century: a Systematic Review of Population-Based Studies. *Lancet* 390 (10114), 2769–2778. doi:10.1016/s0140-6736(17)32448-0

Ohkawara, T., Nishihira, J., Takeda, H., Hige, S., Kato, M., Sugiyama, T., et al. (2002). Amelioration of Dextran Sulfate Sodium-Induced Colitis by Anti-macrophage Migration Inhibitory Factor Antibody in Mice. *Gastroenterology* 123 (1), 256–270. doi:10.1053/gast.2002.34236

Okayasu, I., Hatakeyama, S., Yamada, M., Ohkusa, T., Inagaki, Y., and Nakaya, R. (1990). A Novel Method in the Induction of Reliable Experimental Acute and Chronic Ulcerative Colitis in Mice. *Gastroenterology* 98 (3), 694–702. doi:10.1016/0016-5085(90)90290-h

Ordás, I., Eckmann, L., Talamini, M., Baumgart, D. C., and Sandborn, W. J. (2012). Ulcerative Colitis. *Lancet* 380 (9853), 1606–1619. doi:10.1016/s0140-6736(12)60150-0

Pålsson-McDermott, E. M., and O'Neill, L. A. (2004). Signal Transduction by the Lipopolysaccharide Receptor, Toll-like Receptor-4. *Immunology* 113 (2), 153–162. doi:10.1111/j.1365-2567.2004.01976.x

Perše, M., and Cerar, A. (2012). Dextran Sodium Sulphate Colitis Mouse Model: Traps and Tricks. *J. Biomed. Biotechnol.* 2012, 1–13. doi:10.1155/2012/718617

Płóciennikowska, A., Hromada-Judycka, A., Borzęcka, K., and Kwiatkowska, K. (2015). Co-operation of TLR4 and Raft Proteins in LPS-Induced Pro-inflammatory Signaling. *Cell. Mol. Life Sci.* 72 (3), 557–581. doi:10.1007/s00018-014-1762-5

Shi, H., Zhao, X., Gao, J., Liu, Z., Liu, Z., Wang, K., et al. (2020). Acid-resistant ROS-Responsive Hyperbranched Polythioether Micelles for Ulcerative Colitis Therapy. *Chin. Chem. Lett.* 31 (12), 3102–3106. doi:10.1016/j.cclet.2020.03.039

St Paul, M., Mallick, A. I., Read, L. R., Villanueva, A. I., Parvizi, P., Abdul-Careem, M. F., et al. (2012). Prophylactic Treatment with Toll-like Receptor Ligands Enhances Host Immunity to Avian Influenza Virus in Chickens. *Vaccine* 30 (30), 4524–4531. doi:10.1016/j.vaccine.2012.04.033

Thompson, W. L., and Van Eldik, L. J. (2009). Inflammatory Cytokines Stimulate the Chemokines CCL2/MCP-1 and CCL7/MCP-3 through NFkB and MAPK Dependent Pathways in Rat Astrocytes [corrected]. *Brain Res.* 1287, 47–57. doi:10.1016/j.brainres.2009.06.081

Wang, T., Wu, F., Jin, Z., Zhai, Z., Wang, Y., Tu, B., et al. (2014). Plumbagin Inhibits LPS-Induced Inflammation through the Inactivation of the Nuclear Factor-Kappa B and Mitogen Activated Protein Kinase Signaling Pathways in RAW 264.7 Cells. *Food Chem. Toxicol.* 64, 177–183. doi:10.1016/j.fct.2013.11.027

Wang, X., Gu, H., Zhang, H., Xian, J., Li, J., Fu, C., et al. (2021). Oral Core-Shell Nanoparticles Embedded in Hydrogel Microspheres for the Efficient Site-specific Delivery of Magnolol and Enhanced Antiulcerative Colitis Therapy. *ACS Appl. Mater. Inter.* 13 (29), 33948–33961. doi:10.1021/acsami.1c09804

Wu, T., Hu, E., Xu, S., Chen, M., Guo, P., Dai, Z., et al. (2021). clusterProfiler 4.0: A Universal Enrichment Tool for Interpreting Omics Data. *The Innovation* 2 (3), 100141. doi:10.1016/j.xinn.2021.100141

Xu, M. Z., Lee, W. S., Han, J. M., Oh, H. W., Park, D. S., Tian, G. R., et al. (2006). Antioxidant and Anti-inflammatory Activities of N-Acetyldopamine Dimers from Periostracum Cicadae. *Bioorg. Med. Chem.* 14 (23), 7826–7834. doi:10.1016/j.bmc.2006.07.063

Xu, Z., Yan, X., Song, Z., Li, W., Zhao, W., Ma, H., et al. (2018). Two Heteropolysaccharides from Isaria Cicadae Miquel Differ in Composition and Potentially Immunomodulatory Activity. *Int. J. Biol. Macromol.* 117, 610–616. doi:10.1016/j.ijbiomac.2018.05.164

Yao, D., Dong, M., Dai, C., and Wu, S. (2019). Inflammation and Inflammatory Cytokine Contribute to the Initiation and Development of Ulcerative Colitis and its Associated Cancer. *Inflamm. Bowel Dis.* 25 (10), 1595–1602. doi:10.1093/ibd/izz149

Zhang, C., Chen, Z., He, Y., Xian, J., Luo, R., Zheng, C., et al. (2021). Oral colon-targeting Core-Shell Microparticles Loading Curcumin for Enhanced Ulcerative Colitis Alleviating Efficacy. *Chin. Med.* 16 (1), 92. doi:10.1186/s13020-021-00449-8

Zhang, P., Yang, M., Chen, C., Liu, L., Wei, X., and Zeng, S. (2020). Toll-Like Receptor 4 (TLR4)/Opioid Receptor Pathway Crosstalk and Impact on Opioid Analgesia, Immune Function, and Gastrointestinal Motility. *Front. Immunol.* 11, 1455. doi:10.3389/fimmu.2020.01455

Zhou, T., Sheng, Y., Guan, H., Meng, R., and Wang, Z. (2021). Cost-Effectiveness Analysis of Vedolizumab Compared with Infliximab in Anti-TNF-α-naïve Patients with Moderate-To-Severe Ulcerative Colitis in China. *Front. Public Health* 9, 704889. doi:10.3389/fpubh.2021.704889

Zhuang, Y. T., Xu, D. Y., Wang, G. Y., Sun, J. L., Huang, Y., and Wang, S. Z. (2017). IL-6 Induced lncRNA MALAT1 Enhances TNF-α Expression in LPS-Induced Septic Cardiomyocytes via Activation of SAA3. *Eur. Rev. Med. Pharmacol. Sci.* 21 (2), 302–309.

Conflict of Interest: The authors declare that the research was conducted in the absence of any commercial or financial relationships that could be construed as a potential conflict of interest.

Publisher's Note: All claims expressed in this article are solely those of the authors and do not necessarily represent those of their affiliated organizations, or those of the publisher, the editors and the reviewers. Any product that may be evaluated in this article, or claim that may be made by its manufacturer, is not guaranteed or endorsed by the publisher.

frontiers | Frontiers in Pharmacology

ORIGINAL RESEARCH
published: 20 April 2022
doi: 10.3389/fphar.2022.835697

Orphan Nuclear Receptor NR4A2 Is Constitutively Expressed in Cartilage and Upregulated in Inflamed Synovium From hTNF-Alpha Transgenic Mice

Cullen M. Lilley[1], *Andrea Alarcon*[1], *My-Huyen Ngo*[1], *Jackeline S. Araujo*[1], *Luis Marrero*[2] *and Kimberlee S. Mix*[1]*

[1]Department of Biological Sciences, Loyola University New Orleans, New Orleans, LA, United States, [2]Department of Orthopaedic Surgery, Louisiana State University Health Sciences Center, New Orleans, LA, United States

Orphan nuclear receptor 4A2 (NR4A2/Nurr1) is a constitutively active transcription factor with potential roles in the onset and progression of inflammatory arthropathies. NR4A2 is overexpressed in synovium and cartilage from individuals with rheumatoid arthritis (RA), psoriatic arthritis, and osteoarthritis. This study documents the expression and tissue localization of NR4A2 and upstream regulator nuclear factor kappa B (NF-κB) in the human tumor necrosis factor-alpha (hTNF-α) transgenic mouse model of RA. Since TNF-α is a potent inducer of NR4A2 *in vitro*, we hypothesized that NR4A2 would also be upregulated and active during disease progression in this model. Expression levels of NR4A2, related receptors NR4A1 (Nur77) and 3 (NOR1), and NF-κB_1 transcripts were quantified by RT-qPCR in hTNF-α and wild-type joints at three stages of disease. The protein distribution of NR4A2 and NF-κB subunit RelA (p65) was analyzed by quantitative immunohistochemistry. Global gene expression of 88 RA-related genes was also screened and compared between groups. Consistent with previous reports on the hTNF-α model, transgenic mice exhibited significant weight loss and severely swollen paws by 19 weeks of age compared to age-matched wild-type controls. NR4A1-3 and NF-κB_1 were constitutively expressed at disease onset and in healthy joints. NF-κB_1 transcript levels increased 2-fold in hTNF-α paws with established disease (12 weeks), followed by a 2-fold increase in NR4A2 at the late disease stage (19 weeks). NR4A2 and RelA proteins were overexpressed in inflamed synovium prior to symptoms of arthritis, suggesting that gene expression changes documented in whole paws were largely driven by elevated expression in diseased synovium. Broader screening of RA-related genes by RT-qPCR identified several differentially expressed genes in hTNF-α joints including those encoding inflammatory cytokines and chemokines, matrix-degrading enzymes and inhibitors, cell surface receptors, intracellular signaling proteins and transcription factors. Consensus binding sites for NR4A receptors and NF-κB_1 were enriched in the promoters of differentially expressed genes suggesting central roles for these transcription factors in this model. This study is the first comprehensive analysis of NR4A2 in an animal model of RA and validates the hTNF-α model for testing of small molecules and genetic strategies targeting this transcription factor.

Keywords: nuclear receptors, NR4A2 gene, NFkB (RelA), TNF-α, cartilage, synovium, inflammation, rheumatoid arthritis

OPEN ACCESS

Edited by:
Evelyn P. Murphy,
University of Limerick, Ireland

Reviewed by:
Sadiq Umar,
University of Illinois at Chicago, United States
Elena Izquierdo,
CEU San Pablo University, Spain

***Correspondence:**
Kimberlee S. Mix
kmix@loyno.edu

Specialty section:
This article was submitted to Inflammation Pharmacology, a section of the journal Frontiers in Pharmacology

Received: *14 December 2021*
Accepted: *04 April 2022*
Published: *20 April 2022*

Citation:
Lilley CM, Alarcon A, Ngo M-H, Araujo JS, Marrero L and Mix KS (2022) Orphan Nuclear Receptor NR4A2 Is Constitutively Expressed in Cartilage and Upregulated in Inflamed Synovium From hTNF-Alpha Transgenic Mice. Front. Pharmacol. 13:835697. doi: 10.3389/fphar.2022.835697

INTRODUCTION

Rheumatoid arthritis (RA) is a chronic inflammatory arthropathy with an estimated global population prevalence of 0.46% (Almutairi et al., 2021). RA is characterized by synovial membrane hyperplasia, leukocyte infiltration, and irreversible cartilage and bone destruction in multiple joints. Biological therapies targeting the inflammatory cytokine tumor necrosis factor-alpha (TNF-α) serve as robust treatment options for attenuating chronic inflammation in RA (Mitoma et al., 2018; Kerschbaumer et al., 2020). However, these agents are expensive and 30%–40% of RA patients have inadequate clinical responses (Rubbert-Roth et al., 2019). Furthermore, blocking TNF-α results in broad-spectrum immunosuppression that increases the risk of serious infections and some types of cancer (Sartori et al., 2019; Sepriano et al., 2020; Li et al., 2021). Elucidating molecular pathways downstream of TNF-α may lead to the development of more selective drugs capable of attenuating joint damage without compromising essential immune functions.

The orphan nuclear receptor 4A2 (NR4A2/Nurr1) may be a promising therapeutic target downstream of TNF-α and nuclear factor kappa B (NF-κB) signaling pathways. This transcription factor is a member of the NR4A family of receptors along with NR4A1 (Nur77) and NR4A3 (NOR1). The NR4A receptors share a high degree of homology and may have functional redundancy in some cellular contexts (Crean and Murphy, 2021). In contrast to other nuclear receptors, the NR4A receptors are presumed to be constitutively active, ligand-independent factors regulated at the level of expression and post-translational modification (Zhao and Bruemmer, 2010). In response to inflammation, NF-κB and cyclic adenosine monophosphate response element binding protein (CREB) bind directly to the NR4A2 promoter and rapidly induce its expression in chondrocytes, synoviocytes, endothelial cells, and immune cells (McEvoy et al., 2002; Ralph et al., 2005; Pei et al., 2006; Mix et al., 2007). NR4A2 is also highly expressed in inflamed synovial tissues from individuals with RA and psoriatic arthritis as well as in cartilage from individuals with osteoarthritis (OA) (Murphy et al., 2001; McEvoy et al., 2002; Ralph et al., 2005; Mix et al., 2007; Aherne et al., 2009; Ralph et al., 2010; Mix et al., 2012). Over-expression of NR4A2 in synovial fibroblasts enhances proliferation, anchorage-independent growth, and invasion, suggesting critical roles for this receptor in synovial hyperplasia (Mix et al., 2012). At the transcriptional level, NR4A2 regulates expression of the chemokine interleukin 8 (IL-8), cartilage-degrading matrix metalloproteinases-1 and 13 (MMP-1, 13), and the immunomodulatory peptide hormone prolactin (Davies et al., 2005; Mix et al., 2007; Aherne et al., 2009; Mix et al., 2012; McCoy et al., 2015). While analyses of human joint tissues and cells have yielded important insight into NR4A2-dependent mechanisms, a comprehensive analysis of receptor mRNA expression levels and protein distribution has not been performed in an animal model of arthritis.

This study provides a detailed analysis of gene expression levels and joint tissue distribution patterns of the NR4A receptors and NF-κB in a transgenic mouse model of RA driven by chronic expression of the human TNF-α cytokine (hTNF-α, Taconic model 1006). Transgenic models expressing hTNF-α have demonstrated great utility for pre-clinical validation of therapies and insight into RA mechanisms (Douni et al., 2004; Zwerina et al., 2004; Delavallée et al., 2009; Binder et al., 2013; Li et al., 2016; Karagianni et al., 2019; Ubah et al., 2019). The hTNF-α transgenic mice studied here exhibit spontaneous and progressive inflammation leading to severe polyarthritis by 20 weeks of age. Since TNF-α is a potent inducer of NF-κB and NR4A2 in human joint cells, we hypothesized that these transcription factors would also be upregulated and active during disease progression in the hTNF-α model. To test this, we quantified NR4A1-3 and NF-κB mRNA levels by RT-qPCR and measured protein distribution by immunohistochemistry in joints from hTNF-α mice at different disease stages. In addition, a broader screen of RA-related genes was conducted and potential NR4A and NF-κB target genes were identified through promoter analyses. Our results provide the first spatiotemporal map of NR4A2 distribution in an animal model of RA and validate the hTNF-α model for testing of small molecules and genetic therapies targeting this transcription factor.

METHODS AND MATERIALS

Animals

Male hTNF-α transgenic and C57BL6/N wild-type mice were obtained from Taconic Biosciences (Model 1006; Hudson, NY, United States). The hTNF-α model was generated using a 2.8 kb transgene containing the human TNF-α gene with the full-length promoter and coding region. The endogenous 3′ untranslated region (UTR) of the human TNF-α gene was replaced with the human beta-globin 3′ UTR which served to stabilize the transcript (Keffer et al., 1991). The transgenic line was produced by pronuclear microinjection of B6SLJ (F2) hybrid zygotes and mice were backcrossed for over 20 generations onto the C57BL6/N genetic background. For this study, transgenic and wild-type littermates were maintained at Taconic Biosciences until 8 (n = 5), 12 (n = 4), and 19 weeks of age (n = 4), representing early, established, and late stages of RA (Taconic Biosciences, 2022). Mice were group-housed in a barrier facility with a 12-h light cycle and access to food and water ad libitum. At the end of the study, body mass was measured and clinical scores were assessed by Taconic Biosciences using a 24-point scoring system as follows: 20 digits scored as 0 (normal) or 0.2 (one or more swollen joints) for a maximum total digit score of 4, each paw scored as 0 (normal), 1 (noticeably swollen) or 2 (severely swollen) for a maximum total paw score of 8, each wrist scored as 0 (normal), 1 (noticeably swollen), or 2 (severely swollen) for a maximum total wrist score of 4 and each ankle scored as 0 (normal), 2 (noticeably swollen), or 4 (severely swollen) for a maximum total ankle score of 8 (Taconic Biosciences, 2022). Immediately after euthanasia, paws were dissected proximal to the ankle/wrist joints and transferred to RNAlater (left paws) and 10% neutral buffered formalin (right paws) for RT-qPCR and histology, respectively. Protocols were approved by the

Institutional Animal Care and Use Committees at Taconic Biosciences and Loyola University New Orleans.

Immunohistochemistry and Imaging

Hind paws (n = 13 per genotype) were fixed in neutral-buffered formalin followed by decalcification with formic acid-based Decalcifier I (Leica), paraffin processed and embedded sagittally for microtomy. Serial 5 µm-thick sections were cut and mounted on Trubond 380 slides (Electron Microscopy Sciences). Slides were then heated for 45 min at 59°C, deparaffinized, re-hydrated, and formaldehyde cross-links were dissociated by submerging slides in pressure-heated citrate buffer (pH 6.0). Endogenous peroxidases were removed by treatment with 3% H_2O_2 in methanol and non-specific binding was reduced by incubation in Protein Block (Abcam). Sections were incubated overnight at 4°C with either rabbit polyclonal anti-NR4A2 (Novus NB110-40415), rabbit monoclonal anti-RelA (Abcam ab32536), rabbit IgG isotype control (Abcam 172730) or antibody diluent only. After washing, sections were incubated for 30 min in anti-rabbit Ig (H + L) secondary conjugated to horseradish peroxidase (Vector ImPRESS). The reaction product of Diaminobenzidine and H_2O_2 was used as substrate to visualize the tagged epitopes. Slides were counterstained with hematoxylin, mounted, and images collected with an Olympus BX51 microscope equipped with a digital camera driven by CellSens software (Olympus). Semi-quantitative scoring of RelA and NR4A2-positive cells in synovium and cartilage from at least two 400× fields per section was conducted by two blinded observers. Representative images from hTNF-α and wild-type joints at 400× magnification are shown.

RNA Extraction and RT-qPCR

Contralateral paws were dissected proximal to the ankle/wrist joints and the skin was removed. Tissue was coarsely minced with a scalpel and homogenized with a TissueTearor (Thomas Scientific, Swedesboro, NJ, United States). Total RNA was extracted using RNeasy fibrous tissue mini columns (Qiagen, Germantown, MD, United States), eluted into RNase-free water and quantified with a NanoDrop spectrophotometer (Thermo Fisher Scientific). RNA was reverse transcribed into complementary DNA (cDNA) using the iSCRIPT reverse transcriptase master mix (Bio-Rad, Hercules, CA, United States). Twenty microliter reactions were prepared with 1 µg of total RNA from each paw (50 ng/µl cDNA). Control reactions were prepared with the negative control master mix provided with the kit. Reactions were incubated in a Bio-Rad C1000 thermocycler for 5 min at 25°C, 30 min at 42°C, and 5 min at 85°C. Quantitative PCR was performed using iTaq Universal SYBR Green SuperMix (Bio-Rad, Hercules, CA, United States) and validated primers spanning exon-intron junctions in the mouse TATA-Box Binding Protein (TBP), NR4A1, NR4A2, NR4A3, and NF-κB_1 genes (Bio-Rad, Hercules, CA, United States). Twenty microliter reactions were prepared in triplicate with 50 ng of cDNA from each sample and incubated in a CFX96 Real-Time PCR Detection System (Bio-Rad, Hercules, CA, United States) for 30 s at 95°C, 5 s at 95°C, 30 s at 60°C (40 cycles), followed by melting curve analysis from 65°C–95°C using CFX Manager Software (Bio-Rad, Hercules, CA, United States). Relative gene expression was calculated by the $2^{-\Delta\Delta Ct}$ method (Livak and Schmittgen, 2001) with target gene levels normalized to TBP.

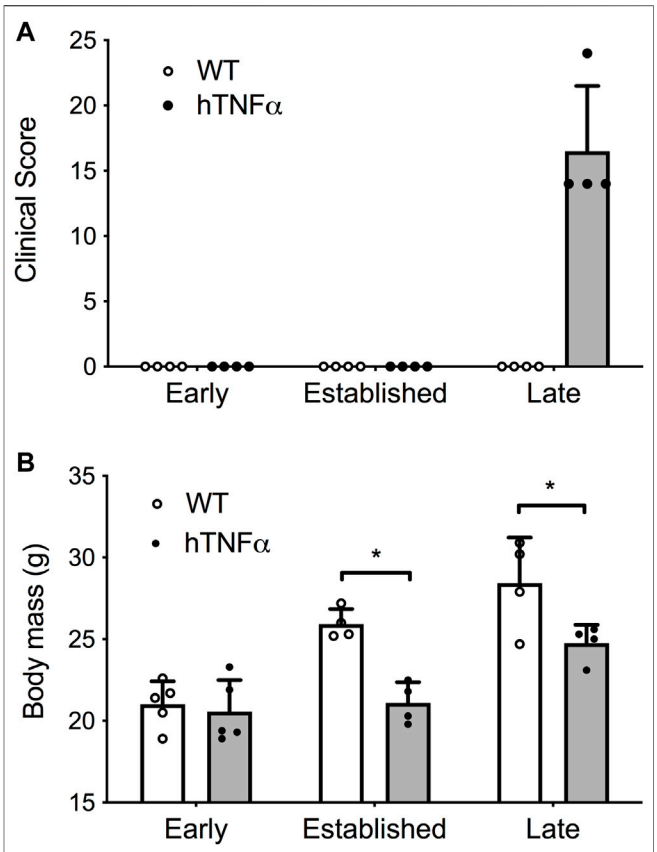

FIGURE 1 | Progression of arthritis in hTNF-α transgenic mice. Wild-type and hTNF-α mice were studied at three stages of disease: early (8 weeks), established (12 weeks), and late (19 weeks). **(A)** Mean clinical score based on total paw swelling ±standard deviation. **(B)** Mean body mass (g) ± standard deviation. Unpaired t-test, $^*p < 0.05$.

RT-qPCR Panels and Promoter Analysis

Pre-designed PrimePCR panels were used to analyze 88 mouse genes associated with RA and reference genes (Rheumatoid Arthritis Tier 1 M96, Bio-Rad, Hercules, CA, United States). Pooled cDNA from transgenic or wild-type paws (n = 4/group) at early or late time points was mixed with iTaq Universal SYBR Green SuperMix (Bio-Rad, Hercules, CA, United States) and added to each well of the PrimePCR reaction plates containing lyophilized primers. Reactions were incubated for 30 s at 95°C, 5 s at 95°C, 30 s at 60°C (40 cycles), followed by melting curve analysis from 65°C–95°C. Target gene expression was normalized to TBP and Glyceraldehyde 3-phosphate dehydrogenase (GAPDH) using the gene study analysis in the CFX Manager Software. Control assays included on each PrimePCR plate confirmed RNA integrity and the absence of contaminating genomic DNA. Thresholds for induced and

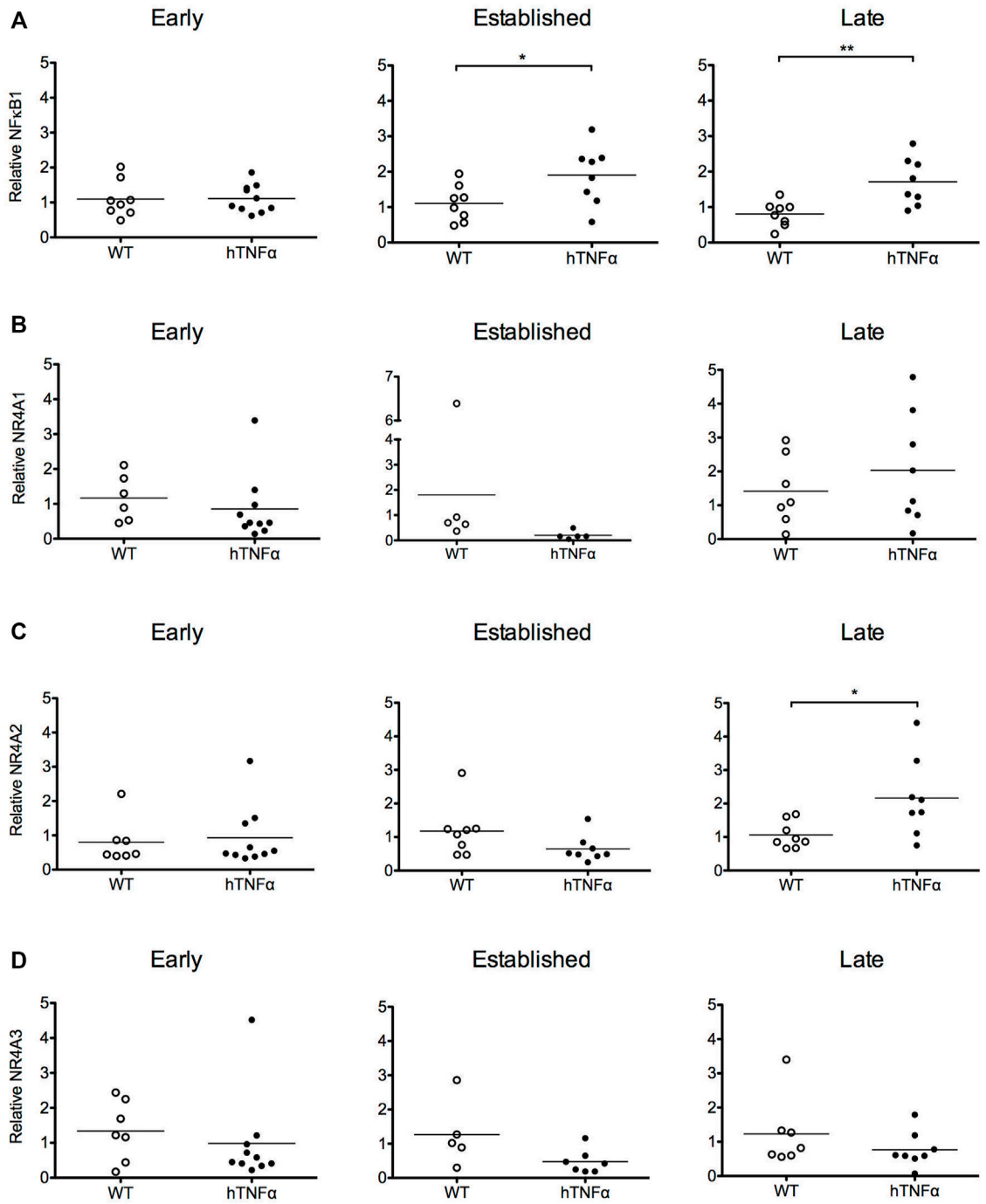

FIGURE 2 | Gene expression analysis of target transcription factors. RNA was extracted from the paws of wild-type and hTNF-α transgenic mice at early, established, and late timepoints. Relative levels of NF-κB$_1$ **(A)**, NR4A1 **(B)**, NR4A2 **(C)**, NR4A3 mRNA **(D)** were measured by RT-qPCR and normalized to TBP. Horizontal bars represent mean expression levels for each group. Mann Whitney test, $^{*}p < 0.05$, $^{**}p < 0.005$.

repressed genes in hTNF-α mice were set at a >2-fold increase or a >0.5-fold decrease, respectively. Genes were classified as stable if fold-change values were between these thresholds. LASAGNA (Length-Aware Site Alignment Guided by Nucleotide Association)-Search, an integrated web tool for predicting transcription factor binding sites with the LASAGNA algorithm, was used to analyze gene promoters in all expressed genes (Lee and Huang, 2013). Promoter regions of mouse genes (−1,000 bp to 0) were scanned for NR4A2 (AAGGTCAC) and NF-κB$_1$ (GGGGATTCCCC) binding sites using matrix derived JASPAR CORE models of consensus vertebrate binding sites, with a p-value threshold of <0.001.

Statistical Analysis

GraphPad Prism software (version 9.3.1) was used to generate graphs and compare gene and protein expression data between groups of age-matched transgenic and wild-type mice. Normality was confirmed with the D'Agostino-Pearson test and the unpaired *t*-test was applied to data in **Figures 1**, **3**, **4** with the threshold of statistical significance at $p < 0.05$. The Mann Whitney test was used to analyze RT-qPCR data with deviations from normality in **Figure 2** with a threshold of statistical significance at $p < 0.05$.

RESULTS

Symptoms and physical signs of arthritis were monitored in hTNF-α transgenic mice at early (8 weeks), established (12 weeks), and late (19 weeks) disease stages. Transgenic mice appeared healthy at 8 weeks of age but demonstrated impaired mobility and reduced digit splaying by 12 weeks. Severe polyarthritis was evident in all transgenic mice by 19 weeks and elevated clinical scores reflected severely swollen digits, paws, and ankle joints (**Figure 1A**). Consistent with previous studies in this model (Taconic Biosciences, 2022), synovial hyperplasia, leukocyte infiltration, cartilage destruction, fibrosis, and subchondral bone erosion were observed in digit and ankle joints (data not shown). Furthermore, hTNF-α mice demonstrated a significant decrease in body mass at 12 and 19 weeks (**Figure 1B**, $p < 0.05$), consistent with RA-induced cachexia. In contrast, wild-type mice remained healthy and demonstrated a steady increase in body mass.

To investigate transcriptional pathways activated by hTNF-α signaling in this model, NF-κB and orphan nuclear receptor NR4A1-3 mRNA levels were measured in whole paws from transgenic and wild-type mice by RT-qPCR. NF-κB_1 mRNA was expressed at similar levels between transgenic and wild-type groups at 8 weeks and increased 2-fold at established and late disease stages (**Figure 2A**, $p < 0.05$). All three NR4A receptors were detected without differential expression at 8 and 12 weeks (**Figures 2B–D**). At the late disease stage, NR4A2 was selectively upregulated 2-fold (**Figure 2C**, $p < 0.05$), while NR4A1 and 3 remained equivalent to wild-type levels. These gene expression results reflect the net expression patterns of NF-κB_1 and the NR4A receptors in whole paws composed of multiple tissues and cell types.

To expand on these findings and measure the histological distribution of NF-κB and NR4A2 proteins, sections of contralateral paws from hTNF-α and wild-type mice were assayed by immunohistochemistry. RelA was detected in chondrocytes from wild-type and hTNF-α joints (**Figures 3A,D,E,F**). At the early stage of disease, 80% of hTNF-α chondrocytes in the resting zone of the articular surfaces stained positive for RelA (**Figure 3I**, $p < 0.005$). However, at the established and late disease stages, RelA positivity in cartilage decreased to wild-type levels without significant differences between groups **Figures 3E,F,I**. Synovial hyperplasia was observed with concurrent increases in RelA signal in synoviocytes (**Figures 3B,H**, >70%, $p < 0.005$) and cells in synovio-entheseal compartments (**Figure 3C**). Isotype controls confirmed the absence of background staining on paw sections (**Figure 3G**).

NR4A2 was detected in a similar distribution pattern in both cartilage and synovium and ubiquitously expressed in superficial chondrocytes from hTNF-α and wild-type joints at the early timepoint (**Figures 4A,D,I**). A 10% decrease in NR4A2 positive chondrocytes was observed in both groups at late stage, but statistical significance was limited to the hTNF-α groups (**Figure 4E,F,I**, $p < 0.05$). Synovial hyperplasia coincided with increases in NR4A2 in the synovium (>80%) and abundant expression in synoviocytes at the sites of membrane insertion to the cartilage (**Figures 4B,C,H**, $p < 0.0005$). Isotype controls confirmed the absence of background staining on paw sections (**Figure 4G**). Taken together, elevated RelA and NR4A2 protein levels in synoviocytes suggest that gene expression changes noted in whole paws (**Figure 2**) are largely driven by disease changes in the synovium.

To further investigate arthritis-related molecular mechanisms in the hTNF-α model, global gene expression patterns were examined in paws using RT-qPCR panels specific for 88 genes implicated in RA. A set of 48 genes was upregulated at the early stage of disease relative to wild-type controls, of which 22 remained elevated at the late stage along with nine additional induced genes (**Figures 5A,C,E**). Upregulated genes included inflammatory cytokines and chemokines (IL-1β, IL-6, IL-1, IL-4, CCL5, CXCL10, CXCL12), matrix degrading enzymes and inhibitors (MMP2, MMP9, TIMP1, TIMP2), cell surface receptors (ICAM1, VCAM1, CD14, CCR5, CXCR4, KDR), intracellular signaling proteins (AKT3, SOCS3, PRKCB, S100A4) and transcription factors (JUN, HIF1-alpha, STAT1, PPAR-alpha, CREB1). Endogenous mouse TNF-α was elevated by 3.5-fold (**Figure 5C**), consistent with autoregulation of this cytokine in response to chronic hTNF-α signaling. Validating RT-qPCR results presented earlier, NR4A2 (+4.4-fold) and NF-κB transcripts (NFKB1 +11.8-fold, RELA +2.9-fold) were also upregulated in hTNF-α paws (**Figures 5A,C**). Notably, four genes were repressed at the early stage (BCL2, MUC1, PTGS2, SLC16A3) and two were repressed at the late stage (UBC, IL-4) (**Figures 5B,D**). Differential expression was not observed for the remaining genes detected on the panels (early = 28, late = 51, **Supplementary Table S1**).

Next, the promoters of all genes detected in the panel experiment were scanned for putative binding sites for NF-κB_1 (GGGGATTCCCC) and NR4A receptors (AAGGTCAC) using matrix derived JASPAR CORE models of consensus vertebrate binding sites (Lee and Huang, 2013). Consensus binding sites for these factors were enriched in the promoters of differentially expressed genes relative to the stably expressed groups (**Table 1**). Over half of the early induced promoters contained at least one NR4A or NF-κB_1 binding site and 38% of the promoters contained sites for both factors. Furthermore, NR4A consensus binding sites were predicted in 8 of the 10 most highly induced promoters (CCL5, ICAM1, CD14, TNFRSF1B, NFκB_1, H2-AB1, TNFAIP3, TNFRSF1A) (**Supplementary Table S2**). These trends

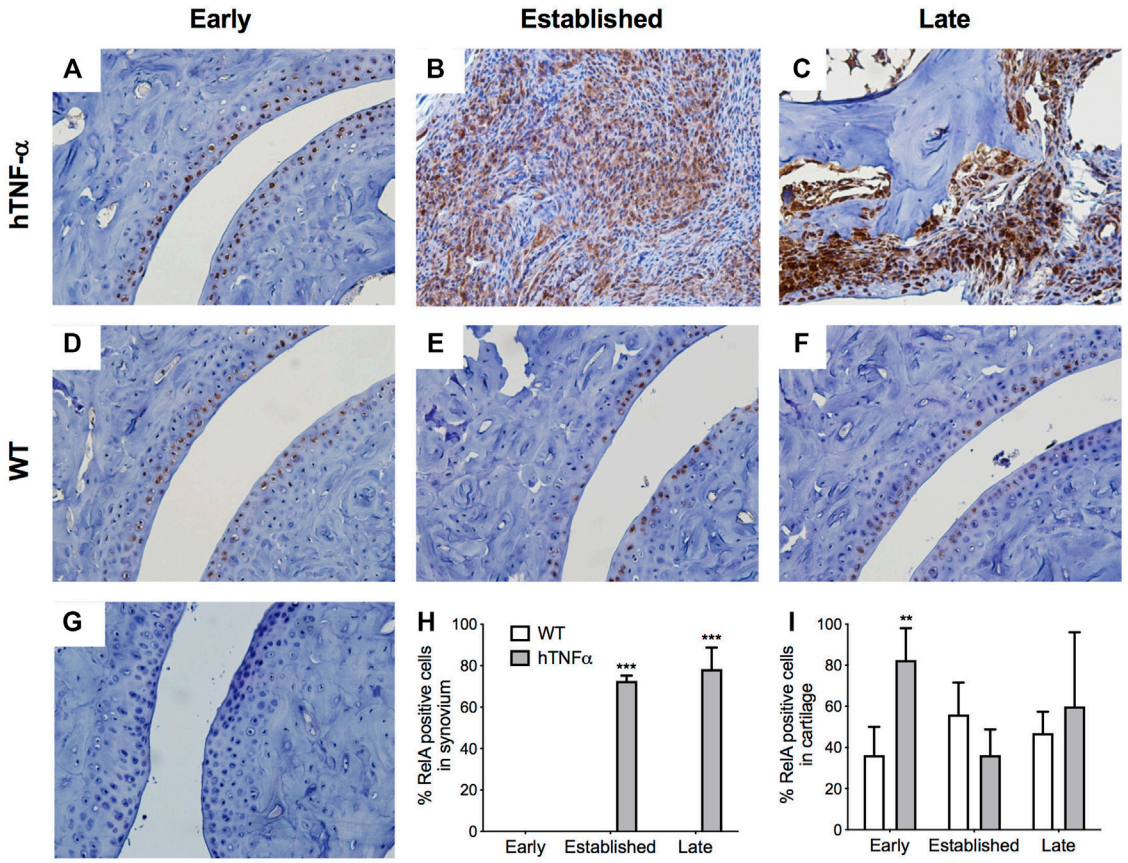

FIGURE 3 | Localization of RelA in cartilage and synovium. RelA was detected in paws of wild-type and hTNF-α mice at early **(A,D)**, established **(B,E)**, and late **(C,F)** stages of disease by immunohistochemistry. Isotype control was applied to a transgenic section from the late stage of disease **(G)**. Representative images at 400× magnification are shown. Scoring of RelA positive cells in synovium **(H)** and cartilage **(I)**. Unpaired *t*-test, $^{**}p < 0.005$, $^{***}p < 0.0005$.

were evident in differentially expressed genes from early and late stages of disease, suggesting that NF-κB and NR4A receptors regulate transcriptional pathways central to this model.

DISCUSSION

This study provides the first comprehensive analysis of the NR4A receptors and NF-κB in a transgenic mouse model of RA driven by the human TNF-α cytokine. Since TNF-α is a potent inducer of NF-κB and NR4A receptors in human joint cells, we hypothesized that these transcription factors would also be expressed in arthritic joints *in vivo*. NF-κB_1 and NR4A2 mRNA transcripts were upregulated in whole paws from hTNF-α mice, while NR4A1 and NR4A3 were not differentially expressed (**Figure 2**). Consistent with transcriptional induction of NR4A2 by NF-κB in human joint cells (McEvoy et al., 2002; Ralph et al., 2005; Mix et al., 2007), we documented an increase in NF-κB_1 mRNA prior to NR4A2 upregulation at the late disease stage. Furthermore, we detected potent increases in RelA and NR4A2 proteins in inflamed synovium by immunohistochemistry (**Figures 3**, **4**), suggesting that gene expression patterns in whole paws are largely driven by changes in the synovium. In contrast, NR4A2 was constitutively expressed in the resting zone of cartilage but decreased at the late stage of disease. Since NR4A2 is a constitutively active transcription factor tightly regulated at the level of expression, the detection of NR4A2 protein in articular surfaces and synovium suggests this receptor is transcriptionally active in resident chondrocytes and synoviocytes.

Our results in the hTNF-α model are consistent with tissue-specific activities for the NR4A receptors in joints. In human synovial fibroblasts, NR4A2 exacerbates inflammation and tissue degradation by upregulating IL-8, MMP-13, prolactin, CRH, and CRH-receptor1 (Murphy et al., 2001; Davies et al., 2005; Ralph et al., 2007; Aherne et al., 2009; Mix et al., 2012; McCoy et al., 2015). In human chondrocytes, NR4A2 antagonizes MMP-1, 3, and 9 gene expression and contributes to chondroprotection (Mix et al., 2007). However, depletion of NR4A1-3 in human chondrocytes antagonizes histamine-dependent regulation of RANKL expression, providing evidence for differential modulation of genes involved in cartilage degradation (Marzaioli et al., 2012). In addition, studies in rat chondrocytes support a protective function for NR4A1 through suppression of COX-2, iNOS, and MMP expression

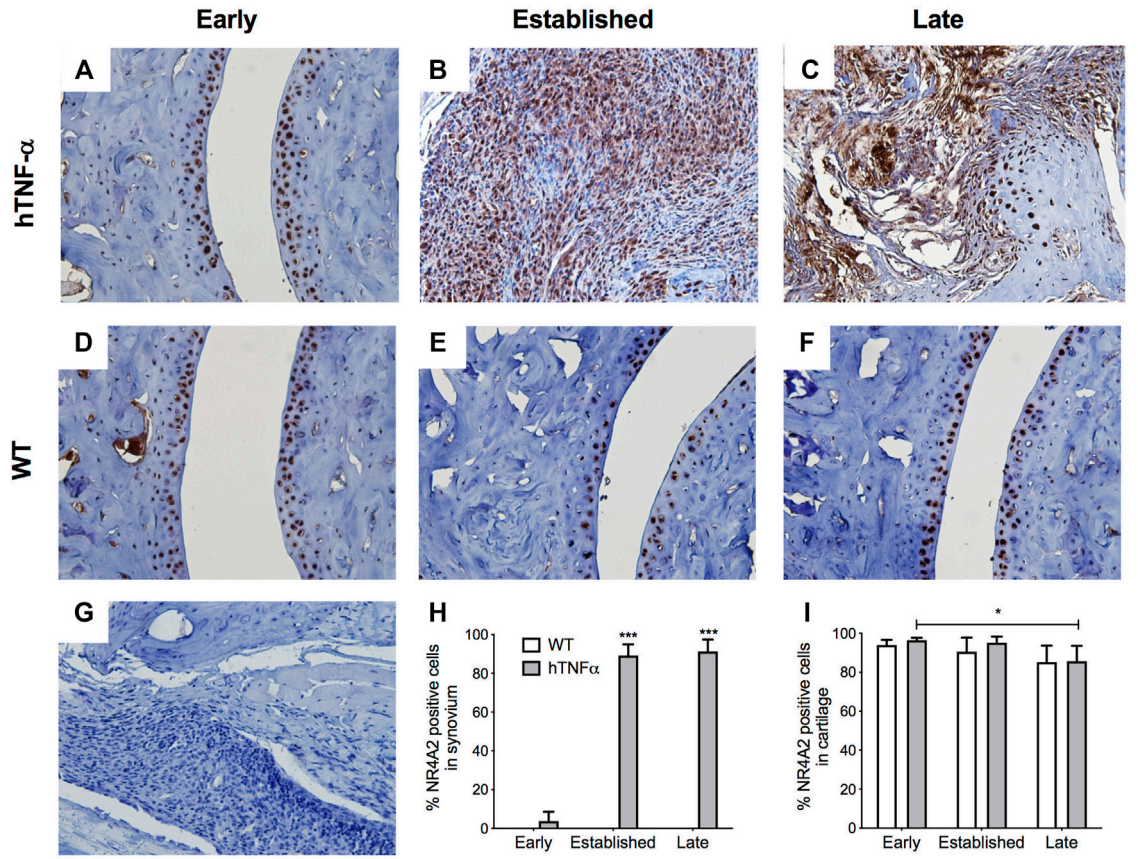

FIGURE 4 | Localization of NR4A2 in cartilage and synovium. NR4A2 protein was detected in paws of wild-type and hTNF-α mice at early **(A,D)**, established **(B,E)**, and late **(C,F)** stages of disease by immunohistochemistry. Isotype control was applied to a transgenic section from the late stage of disease **(G)**. Representative images at 400× magnification are shown. Scoring of NR4A2 positive cells in synovium **(H)** and cartilage **(I)**. Unpaired *t*-test, $^{*}p < 0.05$, $^{***}p < 0.0005$.

(Xiong et al., 2020), while other studies suggest that NR4A3 has opposing effects (Ma et al., 2020).

By screening a broader panel of genes implicated in RA, we generated evidence of increased expression of various inflammatory cytokines and chemokines, matrix degrading enzymes and inhibitors, cell surface receptors, intracellular signaling proteins and transcription factors that support the hTNF-α mouse as a model of RA (**Figure 5**). Of these, IL-1β and CCL5 were the most potently induced genes, consistent with the known activation of these promoters in response to increased TNF-α signaling (Turner et al., 1989; Lee et al., 2000). Additionally, NR4A2, NF-κB$_1$, and RelA were also upregulated concurrent with increases in endogenous murine TNF-α. This screen focused on a select group of genes involved in RA and as such our results do not reflect the full spectrum of aberrant gene expression changes that may be occurring within hTNF-α joints.

Promoter analysis of differentially expressed genes supports central roles for NF-κB and NR4A transcription factors in the hTNF-α model. Consensus binding sites for NF-κB$_1$ were predicted in the promoters of 58% of the induced genes in contrast to only 36% of the stable genes (**Table 1**). Several of these differentially expressed genes have been previously recognized as transcriptional targets of NF-κB. NR4A monomeric binding sites known as Nurr binding response elements (NBRE: AAACCGTA) were also enriched in the promoters of differentially expressed genes. Among the genes containing these promoter elements (**Supplementary Table S2**), NR4A receptors have been reported to regulate BCL-2, IL-6, CXCL-12, CXCR-4, and MMP-9 in various cellular contexts (Johnson et al., 2011, Bonta et al., 2006, Mix et al., 2007, Duren et al., 2016). NR4A receptors can also modulate gene expression through heterodimeric binding with retinoid X receptors (RXR) and interactions with NF-κB and erythroblast transformation specific (ETS) transcription factors (Mix et al., 2007; Aherne et al., 2009; Saijo et al., 2009; Duren et al., 2016; McEvoy et al., 2017).

Our findings are supported by recent gene expression studies highlighting the importance of NF-κB and NR4A receptors in the pathophysiology of arthritis. Integrative transcriptome analysis of a distinct hTNF-α transgenic model with rapid onset of symptomatic arthropathy (Tg197, Keffer et al., 1991) ranked NF-κB as the most important transcription factor in this model (Karagianni et al., 2019). Interestingly, the NR4A receptors exhibited disparate expression patterns in limbs from the Tg197 model; NR4A1 and 3 were downregulated and NR4A2

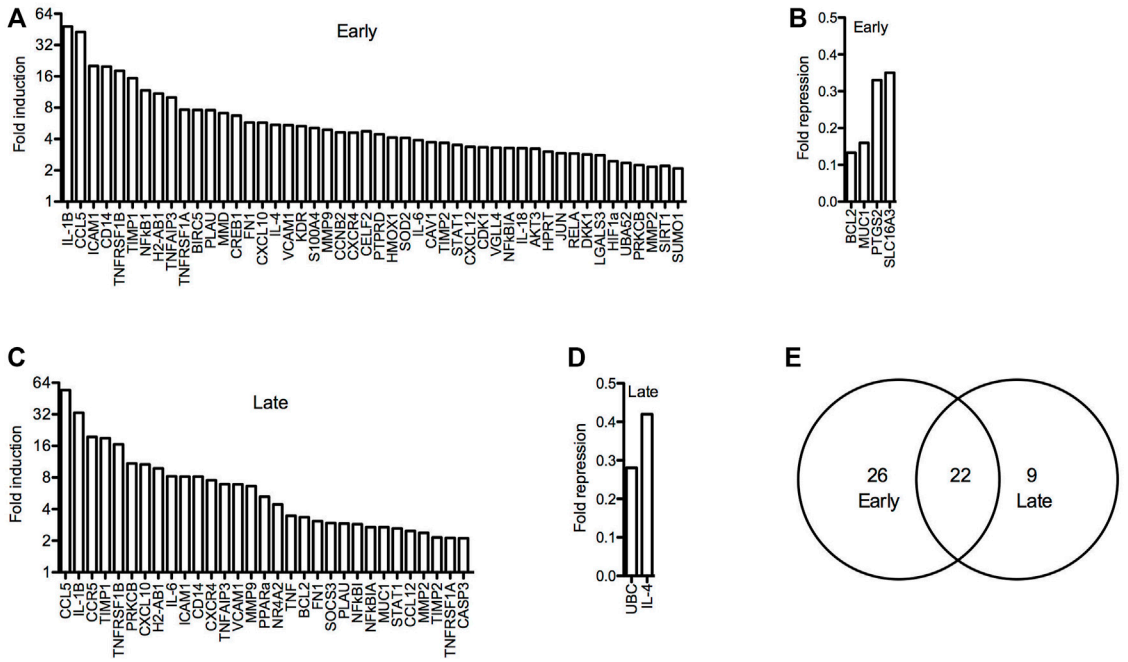

FIGURE 5 | Global gene expression profiles in hTNF-α joints. RT-qPCR panels were used to measure the expression of 88 genes associated with RA in wild-type and hTNF-α paws at early and late stages of disease. **(A)** Genes induced by greater than 2-fold at early stage. **(B)** Genes repressed by greater than 0.5-fold at early stage. **(C)** Genes induced by greater than 2-fold at late stage. **(D)** Genes repressed by greater than 0.5-fold at late stage. **(E)** Comparison of induced genes at early and late stages.

TABLE 1 | Consensus binding sites in promoters of differentially and stably expressed genes.

	Early stage			Late stage		
	Induced	**Repressed**	**Stable**	**Induced**	**Repressed**	**Stable**
Number of expressed genes	48	4	28	30	2	51
Promoters with NR4A sites	30 (63%)	1 (25%)	10 (36%)	19 (63%)	2 (100%)	22 (43%)
Promoters with NF-κB_1 sites	28 (58%)	3 (75%)	10 (36%)	16 (53%)	2 (100%)	25 (47%)
Promoters with both sites	18 (38%)	0 (0%)	3 (10%)	12 (40%)	2 (100%)	8 (16%)

was not significantly altered. The hTNF-α model used here expresses significantly lower levels of hTNF-α and exhibits a gradual onset of symptoms that more closely models chronic RA (Hayward et al., 2007). Another study of synovial gene expression profiles in OA identified NR4A2 as one of the top 10 transcription factors linked to differentially expressed genes from multiple microarray datasets (Fei et al., 2016). However, NR4A2 was categorized as a downregulated gene in these OA synovial datasets, in contrast to its upregulation in OA cartilage (Mix et al., 2007), RA synovium (Murphy et al., 2001; McEvoy et al., 2002; Ralph et al., 2005; Aherne et al., 2009; Ralph et al., 2010), and hTNF-α joints in this study.

NR4A expression and pharmacological targeting have been investigated in other mouse models of arthritis, providing broader insight into the therapeutic potential of these receptors. In the K/BxN serum-induced model of RA (Christianson et al., 2012), NR4A1-3 mRNA levels were elevated in inflamed ankles and NR4A2 expression was potently suppressed by dexamethasone and intra-articular injections of salmon calcitonin and hyaluronic acid (Ryan et al., 2013). In $CD4^+$ T-cells isolated from DBA/1 mice with collagen-induced arthritis (CIA), NR4A1-3 mRNA levels were reduced relative to naïve controls and the NR4A agonist cytosporone B improved clinical scores *in vivo* (Saini et al., 2019). NR4A2 protein was detected in inflamed synovium and cartilage of ankle joints from the $TNF^{-delta\text{-}ARE}$ model of chronic inflammation (Kontonyiannis et al., 1999; Smyth et al., 2019) and also in joints from the antigen-induced arthritis model in a pilot study (Everett et al., 2015). Further investigation of the NR4A receptors in animal models of arthritis will provide greater insight into the mechanisms linking these transcription factors to inflammation and cartilage degradation *in vivo*.

Recent advances in synthetic NR4A ligands and endogenous receptor modulators have provided new strategies for targeting the NR4A receptors *in vitro* and *in vivo*. The ligand-binding domain of NR4A2 was once thought to be incompatible with the

binding of endogenous ligands (Wang et al., 2003), however structural studies have revealed that unsaturated fatty acids can bind to the canonical NR4A ligand-binding pocket and transactivate the NR4A2 receptor (de Vera et al., 2016; de Vera et al., 2019). Probing interactions between unsaturated fatty acids and NR4A receptors may lead to the development of new synthetic agents for selective receptor targeting. The purine anti-metabolite 6-mercaptopurine activates the NR4A receptors *in vitro,* suggesting some of the therapeutic actions of this widely used chemotherapeutic agent may also be mediated through the NR4A receptors (Ordentlich et al., 2003; Wansa et al., 2003; Wansa and Muscat, 2005). Furthermore, multiple structurally-diverse agents have been identified that can regulate NR4A expression and transcriptional activity as selective agonists or antagonists (Safe et al., 2016; Munoz-Tello et al., 2020). Most relevant to the current study, the synthetic NR4A2 agonist 1,1-bis(3′-indolyl)-1-(p-chlorophenyl) methane (C-DIM12) blocked TNF-α induction of adhesion molecules and NF-κB regulated genes in primary murine synovial fibroblasts (Afzali et al., 2018), suggesting that this agent may be a candidate for *in vivo* testing in arthritis models.

Our study has limitations but presents opportunities for in-depth studies of the impact of NR4A receptors on structural and symptomatic arthritis *in vivo*. This study was restricted to male hTNF-α mice since they exhibit earlier symptoms and a higher degree of arthritis severity (Hayward et al., 2007). Female mice should be included in future studies to address mechanisms of sexual dimorphism in the model. Microdissection of joint tissues would provide greater insight into the distribution of transcription factors and their potential target genes within hTNF-α joints. Furthermore, determining the cell-type-specific expression patterns of the NR4A receptors within the hTNF-α synovium would refine pharmacotherapeutic targeting strategies.

In conclusion our results provide the first spatiotemporal map of NR4A2 distribution in an animal model of arthritis and validate the hTNF-α model for future testing of synthetic ligands and genetic strategies targeting this transcription factor *in vivo*.

DATA AVAILABILITY STATEMENT

The original contributions presented in the study are included in the article/**Supplementary Materials**, further inquiries can be directed to the corresponding author.

ETHICS STATEMENT

The animal study was reviewed and approved by Institutional Animal Care and Use Committees at Taconic Biosciences and Loyola University New Orleans.

AUTHOR CONTRIBUTIONS

KSM conceived and designed the study, supervised all data collection, performed statistical analysis, prepared figures and tables, and drafted the manuscript. CML, AA, M-HN, and JSA contributed to RNA analysis and histology and drafted sections of the manuscript. CML conducted the RT-qPCR panel experiments and gene expression analysis. KSM and LM optimized histology methods and conducted immunohistochemistry. All authors contributed to manuscript revision and approved the submitted version.

FUNDING

This study was supported by the Mullahy Biology Research Fund, a Marquette Faculty Fellowship (KSM), a Carter Fellowship (KSM) and a faculty research grant (KSM) from Loyola University New Orleans, and an Irvin Cahen Research Grant (KSM) from the Department of Orthopaedic Surgery at LSUHSC.

ACKNOWLEDGMENTS

This study was largely conducted by undergraduate researchers and we express gratitude to all faculty and staff in the Department of Biological Sciences at Loyola University New Orleans for supporting the thesis work of CML, AA, M-HN, and JSA. Engaging in undergraduate research was transformative and it paved the way for success in medical school (CML and M-HN), graduate school (JSA and CML), and business school (AA). Appreciation is also given to the Science Without Borders scholarship program from the Brazilian government that enabled JSA to study abroad and conduct research at Loyola. We thank Dr. Rosalie Anderson for helpful discussions and the use of her TissueTearor and microscope, as well as Elma Selva for editorial support. Appreciation is also given to Drs. Jennifer Simkin, Vinod Dasa, and Matt Cable in the Department of Orthopaedic Surgery at LSUHSC for helpful discussions and the Morphology and Imaging Core of the LSUHSC School of Medicine for technical support.

SUPPLEMENTARY MATERIAL

The Supplementary Material for this article can be found online at: https://www.frontiersin.org/articles/10.3389/fphar.2022.835697/full#supplementary-material

REFERENCES

Afzali, M. F., Popichak, K. A., Burton, L. H., Klochak, A. L., Wilson, W. J., Safe, S., et al. (2018). A Novel Diindolylmethane Analog, 1,1-Bis(3'-Indolyl)-1-(p-Chlorophenyl) Methane, Inhibits the Tumor Necrosis Factor-Induced Inflammatory Response in Primary Murine Synovial Fibroblasts through a Nurr1-dependent Mechanism. *Mol. Immunol.* 101, 46–54. doi:10.1016/j.molimm.2018.05.024

Aherne, C. M., McMorrow, J., Kane, D., FitzGerald, O., Mix, K. S., and Murphy, E. P. (2009). Identification of NR4A2 as a Transcriptional Activator of IL-8

Expression in Human Inflammatory Arthritis. *Mol. Immunol.* 46 (16), 3345–3357. doi:10.1016/j.molimm.2009.07.019

Almutairi, K., Nossent, J., Preen, D., Keen, H., and Inderjeeth, C. (2021). The Global Prevalence of Rheumatoid Arthritis: A Meta-Analysis Based on a Systematic Review. *Rheumatol. Int.* 41 (5), 863–877. doi:10.1007/s00296-020-04731-0

Binder, N. B., Puchner, A., Niederreiter, B., Hayer, S., Leiss, H., Blüml, S., et al. (2013). Tumor Necrosis Factor-Inhibiting Therapy Preferentially Targets Bone Destruction but Not Synovial Inflammation in a Tumor Necrosis Factor-Driven Model of Rheumatoid Arthritis. *Arthritis Rheum.* 65, 608–617. doi:10.1002/art.37797

Bonta, P. I., van Tiel, C. M., Vos, M., Pols, T. W., van Thienen, J. V., Ferreira, V., et al. (2006). Nuclear Receptors Nur77, Nurr1, and NOR-1 Expressed in Atherosclerotic Lesion Macrophages Reduce Lipid Loading and Inflammatory Responses. *Arterioscler Thromb. Vasc. Biol.* 26 (10), 2288–2294. doi:10.1161/01.ATV.0000238346.84458.5d

Christianson, C. A., Corr, M., Yaksh, T. L., and Svensson, C. I. (2012). K/BxN Serum Transfer Arthritis as a Model of Inflammatory Joint Pain. *Methods Mol. Biol.* 851, 249–260. doi:10.1007/978-1-61779-561-9_19

Crean, D., and Murphy, E. P. (2021). Targeting Nr4a Nuclear Receptors to Control Stromal Cell Inflammation, Metabolism, Angiogenesis, and Tumorigenesis. *Front Cel Dev Biol* 9, 589770. doi:10.3389/fcell.2021.589770

Davies, M. R., Harding, C. J., Raines, S., Tolley, K., Parker, A. E., Downey-Jones, M., et al. (2005). Nurr1 Dependent Regulation of Pro-inflammatory Mediators in Immortalised Synovial Fibroblasts. *J. Inflamm. (Lond)* 2, 15. doi:10.1186/1476-9255-2-15

de Vera, I. M., Giri, P. K., Munoz-Tello, P., Brust, R., Fuhrmann, J., Matta-Camacho, E., et al. (2016). Identification of a Binding Site for Unsaturated Fatty Acids in the Orphan Nuclear Receptor Nurr1. *ACS Chem. Biol.* 11 (7), 1795–1799. doi:10.1021/acschembio.6b00037

de Vera, I. M. S., Munoz-Tello, P., Zheng, J., Dharmarajan, V., Marciano, D. P., Matta-Camacho, E., et al. (2019). Defining a Canonical Ligand-Binding Pocket in the Orphan Nuclear Receptor Nurr1. *Structure* 27 (1), 66–e5. e5. doi:10.1016/j.str.2018.10.002

Delavallée, L., Semerano, L., Assier, E., Vogel, G., Vuagniaux, G., Laborie, M., et al. (2009). Active Immunization to Tumor Necrosis Factor-Alpha Is Effective in Treating Chronic Established Inflammatory Disease: a Long-Term Study in a Transgenic Model of Arthritis. *Arthritis Res. Ther.* 11, R195. doi:10.1186/ar2897

Douni, E., Sfikakis, P. P., Haralambous, S., Fernandes, P., and Kollias, G. (2004). Attenuation of Inflammatory Polyarthritis in TNF Transgenic Mice by Diacerein: Comparative Analysis with Dexamethasone, Methotrexate and Anti-TNF Protocols. *Arthritis Res. Ther.* 6, R65–R72. doi:10.1186/ar1028

Duren, R. P., Boudreaux, S. P., and Conneely, O. M. (2016). Genome Wide Mapping of Nr4a Binding Reveals Cooperativity with Ets Factors to Promote Epigenetic Activation of Distal Enhancers in Acute Myeloid Leukemia Cells. *PLoS One* 11 (3), e0150450. doi:10.1371/journal.pone.0150450

Everett, J., Gravallese, E., and Mix, K. S. (2015). Nr4a2 Expression Patterns in Mouse Models of Rheumatoid Arthritis. *J. Stud. Res.* 4 (1), 136–143. doi:10.47611/jsr.v4i1.213

Fei, Q., Lin, J., Meng, H., Wang, B., Yang, Y., Wang, Q., et al. (2016). Identification of Upstream Regulators for Synovial Expression Signature Genes in Osteoarthritis. *Jt. Bone Spine* 83 (5), 545–551. doi:10.1016/j.jbspin.2015.09.001

Hayward, M. D., Jones, B. K., Saparov, A., Hain, H. S., Trillat, A. C., Bunzel, M. M., et al. (2007). An Extensive Phenotypic Characterization of the hTNFalpha Transgenic Mice. *BMC Physiol.* 7, 13. doi:10.1186/1472-6793-7-13

Johnson, M. M., Michelhaugh, S. K., Bouhamdan, M., Schmidt, C. J., and Bannon, M. J. (2011). The Transcription Factor Nurr1 Exerts Concentration-dependent Effects on Target Genes Mediating Distinct Biological Processes. *Front. Neurosci.* 5, 135. doi:10.3389/fnins.2011.00135

Karagianni, N., Kranidioti, K., Fikas, N., Tsochatzidou, M., Chouvardas, P., Denis, M. C., et al. (2019). An Integrative Transcriptome Analysis Framework for Drug Efficacy and Similarity Reveals Drug-specific Signatures of Anti-TNF Treatment in a Mouse Model of Inflammatory Polyarthritis. *Plos Comput. Biol.* 15 (5), e1006933. doi:10.1371/journal.pcbi.1006933

Keffer, J., Probert, L., Cazlaris, H., Georgopoulos, S., Kaslaris, E., Kioussis, D., et al. (1991). Transgenic Mice Expressing Human Tumour Necrosis Factor: A Predictive Genetic Model of Arthritis. *EMBO J.* 10 (13), 4025–4031. doi:10.1002/j.1460-2075.1991.tb04978.x

Kerschbaumer, A., Sepriano, A., Smolen, J. S., van der Heijde, D., Dougados, M., van Vollenhoven, R., et al. (2020). Efficacy of Pharmacological Treatment in Rheumatoid Arthritis: a Systematic Literature Research Informing the 2019 Update of the EULAR Recommendations for Management of Rheumatoid Arthritis. *Ann. Rheum. Dis.* 79, 744–759. doi:10.1136/annrheumdis-2019-216656

Kontoyiannis, D., Pasparakis, M., Pizarro, T. T., Cominelli, F., and Kollias, G. (1999). Impaired On/off Regulation of TNF Biosynthesis in Mice Lacking TNF AU-Rich Elements: Implications for Joint and Gut-Associated Immunopathologies. *Immunity* 10 (3), 387–398. doi:10.1016/s1074-7613(00)80038-2

Lee, A. H., Hong, J. H., and Seo, Y. S. (2000). Tumour Necrosis Factor-Alpha and Interferon-Gamma Synergistically Activate the RANTES Promoter through Nuclear Factor kappaB and Interferon Regulatory Factor 1 (IRF-1) Transcription Factors. *Biochem. J.* 350 Pt 1 (Pt 1), 131–138. doi:10.1042/bj3500131

Lee, C., and Huang, C. H. (2013). LASAGNA: A Novel Algorithm for Transcription Factor Binding Site Alignment. *BMC Bioinformatics* 14, 108. doi:10.1186/1471-2105-14-108

Li, G., Wu, Y., Jia, H., Tang, L., Huang, R., Peng, Y., et al. (2016). Establishment and Evaluation of a Transgenic Mouse Model of Arthritis Induced by Overexpressing Human Tumor Necrosis Factor Alpha. *Biol. Open* 5, 418–423. doi:10.1242/bio.016279

Li, J., Zhang, Z., Wu, X., Zhou, J., Meng, D., and Zhu, P. (2021). Risk of Adverse Events after Anti-TNF Treatment for Inflammatory Rheumatological Disease. A Meta-Analysis. *Front. Pharmacol.* 12, 746396. doi:10.3389/fphar.2021.746396

Livak, K. J., and Schmittgen, T. D. (2001). Analysis of Relative Gene Expression Data Using Real-Time Quantitative PCR and the 2(-delta delta C(t)) Method. *Methods* 25 (4), 402–408. doi:10.1006/meth.2001.1262

Ma, C., Wu, L., Song, L., He, Y., Adel Abdo Moqbel, S., Yan, S., et al. (2020). The Pro-inflammatory Effect of NR4A3 in Osteoarthritis. *J. Cel Mol Med* 24 (1), 930–940. doi:10.1111/jcmm.14804

Marzaioli, V., McMorrow, J. P., Angerer, H., Gilmore, A., Crean, D., Zocco, D., et al. (2012). Histamine Contributes to Increased RANKL to Osteoprotegerin Ratio through Altered Nuclear Receptor 4A Activity in Human Chondrocytes. *Arthritis Rheum.* 64 (10), 3290–3301. doi:10.1002/art.34554

McCoy, J. M., Walkenhorst, D. E., McCauley, K. S., Elaasar, H., Everett, J. R., and Mix, K. S. (2015). Orphan Nuclear Receptor NR4A2 Induces Transcription of the Immunomodulatory Peptide Hormone Prolactin. *J. Inflamm. (Lond)* 12 (1), 13. doi:10.1186/s12950-015-0059-2

McEvoy, A. N., Murphy, E. A., Ponnio, T., Conneely, O. M., Bresnihan, B., FitzGerald, O., et al. (2002). Activation of Nuclear Orphan Receptor NURR1 Transcription by NF-Kappa B and Cyclic Adenosine 5'-monophosphate Response Element-Binding Protein in Rheumatoid Arthritis Synovial Tissue. *J. Immunol.* 168 (6), 2979–2987. doi:10.4049/jimmunol.168.6.2979

McEvoy, C., de Gaetano, M., Giffney, H. E., Bahar, B., Cummins, E. P., Brennan, E. P., et al. (2017). NR4A Receptors Differentially Regulate NF-Kb Signaling in Myeloid Cells. *Front. Immunol.* 8, 7. doi:10.3389/fimmu.2017.00007

Mitoma, H., Horiuchi, T., Tsukamoto, H., and Ueda, N. (2018). Molecular Mechanisms of Action of Anti-TNF-α Agents - Comparison Among Therapeutic TNF-α Antagonists. *Cytokine* 101, 56–63. doi:10.1016/j.cyto.2016.08.014

Mix, K. S., Attur, M. G., Al-Mussawir, H., Abramson, S. B., Brinckerhoff, C. E., and Murphy, E. P. (2007). Transcriptional Repression of Matrix Metalloproteinase Gene Expression by the Orphan Nuclear Receptor Nurr1 in Cartilage. *J. Biol. Chem.* 282 (13), 9492–9504. doi:10.1074/jbc.M608327200

Mix, K. S., McMahon, K., McMorrow, J. P., Walkenhorst, D. E., Smyth, A. M., Petrella, B. L., et al. (2012). Orphan Nuclear Receptor NR4A2 Induces Synoviocyte Proliferation, Invasion, and Matrix Metalloproteinase 13 Transcription. *Arthritis Rheum.* 64 (7), 2126–2136. doi:10.1002/art.34399

Munoz-Tello, P., Lin, H., Khan, P., de Vera, I. M. S., Kamenecka, T. M., and Kojetin, D. J. (2020). Assessment of Nr4a Ligands that Directly Bind and Modulate the Orphan Nuclear Receptor Nurr1. *J. Med. Chem.* 63 (24), 15639–15654. doi:10.1021/acs.jmedchem.0c00894

Murphy, E. P., McEvoy, A., Conneely, O. M., Bresnihan, B., and FitzGerald, O. (2001). Involvement of the Nuclear Orphan Receptor NURR1 in the Regulation

of Corticotropin-Releasing Hormone Expression and Actions in Human Inflammatory Arthritis. *Arthritis Rheum.* 44 (4), 782–793. doi:10.1002/1529-0131(200104)44:4<782::AID-ANR134>3.0.CO;2-H

Ordentlich, P., Yan, Y., Zhou, S., and Heyman, R. A. (2003). Identification of the Antineoplastic Agent 6-mercaptopurine as an Activator of the Orphan Nuclear Hormone Receptor Nurr1. *J. Biol. Chem.* 278 (27), 24791–24799. doi:10.1074/jbc.M302167200

Pei, L., Waki, H., Vaitheesvaran, B., Wilpitz, D. C., Kurland, I. J., and Tontonoz, P. (2006). NR4A Orphan Nuclear Receptors Are Transcriptional Regulators of Hepatic Glucose Metabolism. *Nat. Med.* 12 (9), 1048–1055. doi:10.1038/nm1471

Ralph, J. A., Ahmed, A. U., Santos, L. L., Clark, A. R., McMorrow, J., Murphy, E. P., et al. (2010). Identification of NURR1 as a Mediator of MIF Signaling during Chronic Arthritis: Effects on Glucocorticoid-Induced MKP1. *Am. J. Pathol.* 177 (5), 2366–2378. doi:10.2353/ajpath.2010.091204

Ralph, J. A., McEvoy, A. N., Kane, D., Bresnihan, B., FitzGerald, O., and Murphy, E. P. (2005). Modulation of Orphan Nuclear Receptor Nurr1 Expression by Methotrexate in Human Inflammatory Joint Disease Involves Adenosine A2a Receptor-Mediated Responses. *J. Immunol.* 175 (1), 555–565. doi:10.4049/jimmunol.175.1.555

Ralph, J. A., Zocco, D., Bresnihan, B., Fitzgerald, O., McEvoy, A. N., and Murphy, E. P. (2007). A Role for Type 1alpha Corticotropin-Releasing Hormone Receptors in Mediating Local Changes in Chronically Inflamed Tissue. *Am. J. Pathol.* 170 (3), 1121–1133. doi:10.2353/ajpath.2007.061000

Rubbert-Roth, A., Szabó, M. Z., Kedves, M., Nagy, G., Atzeni, F., and Sarzi-Puttini, P. (2019). Failure of Anti-TNF Treatment in Patients with Rheumatoid Arthritis: The Pros and Cons of the Early Use of Alternative Biological Agents. *Autoimmun. Rev.* 18, 102398. doi:10.1016/j.autrev.2019.102398

Ryan, S. M., McMorrow, J., Umerska, A., Patel, H. B., Kornerup, K. N., Tajber, L., et al. (2013). An Intra-articular salmon Calcitonin-Based Nanocomplex Reduces Experimental Inflammatory Arthritis. *J. Control. Release* 167 (2), 120–129. doi:10.1016/j.jconrel.2013.01.027

Safe, S., Jin, U. H., Morpurgo, B., Abudayyeh, A., Singh, M., and Tjalkens, R. B. (2016). Nuclear Receptor 4A (NR4A) Family - Orphans No More. *J. Steroid Biochem. Mol. Biol.* 157, 48–60. doi:10.1016/j.jsbmb.2015.04.016

Saijo, K., Winner, B., Carson, C. T., Collier, J. G., Boyer, L., Rosenfeld, M. G., et al. (2009). A Nurr1/CoREST Pathway in Microglia and Astrocytes Protects Dopaminergic Neurons from Inflammation-Induced Death. *Cell* 137 (1), 47–59. doi:10.1016/j.cell.2009.01.038

Saini, A., Mahajan, S., Bhagyaraj, E., Kalra, R., Nanduri, R., Gupta, R., et al. (2019). An accord of Nuclear Receptor Expression in Cd4+ T Cells in Rheumatoid Arthritis. *ImmunoHorizons* 3 (8), 402–411. doi:10.4049/immunohorizons.1900043

Sartori, N. S., Picon, P., Papke, A., Neyeloff, J. L., and da Silva Chakr, R. M. (2019). A Population-Based Study of Tuberculosis Incidence Among Rheumatic Disease Patients under Anti-TNF Treatment. *PLoS One* 14, e0224963. doi:10.1371/journal.pone.0224963

Sepriano, A., Kerschbaumer, A., Smolen, J. S., van der Heijde, D., Dougados, M., van Vollenhoven, R., et al. (2020). Safety of Synthetic and Biological DMARDs: a Systematic Literature Review Informing the 2019 Update of the EULAR Recommendations for the Management of Rheumatoid Arthritis. *Ann. Rheum. Dis.* 79, 760–770. doi:10.1136/annrheumdis-2019-216653

Smyth, A., Gogarty, M., Crean, D., and Murphy, E. P. (2019). Subcellular Localization of Nr4a2 Orphan Nuclear Receptor Expression in Human and Mouse Synovial Joint Tissue. *Methods Mol. Biol. (Clifton, N.J.)* 1966, 17–26. doi:10.1007/978-1-4939-9195-2_3

Taconic Biosciences (2022). Human TNFα Transgenic Mouse Model of Spontaneous Arthritis.On-Demand Webinar and Presentation Slides by Dr. Andreas Pahl. AvaliableAt: https://www.taconic.com/resources/webinars/human-tnf-alpha-transgenic-mouse-model-of-spontaneous-arthritis.html (Accessed 30 3, 22).

Turner, M., Chantry, D., Buchan, G., Barrett, K., and Feldmann, M. (1989). Regulation of Expression of Human IL-1 Alpha and IL-1 Beta Genes. *J. Immunol.* 143 (11), 3556–3561.

Ubah, O. C., Steven, J., Porter, A. J., and Barelle, C. J. (2019). An Anti-hTNF-α Variable New Antigen Receptor Format Demonstrates Superior *In Vivo* Preclinical Efficacy to Humira® in a Transgenic Mouse Autoimmune Polyarthritis Disease Model. *Front. Immunol.* 10, 526. doi:10.3389/fimmu.2019.00526

Wang, Z., Benoit, G., Liu, J., Prasad, S., Aarnisalo, P., Liu, X., et al. (2003). Structure and Function of Nurr1 Identifies a Class of Ligand-independent Nuclear Receptors. *Nature* 423 (6939), 555–560. doi:10.1038/nature01645

Wansa, K. D., Harris, J. M., Yan, G., Ordentlich, P., and Muscat, G. E. (2003). The AF-1 Domain of the Orphan Nuclear Receptor NOR-1 Mediates Trans-activation, Coactivator Recruitment, and Activation by the Purine Anti-metabolite 6-mercaptopurine. *J. Biol. Chem.* 278 (27), 24776–24790. doi:10.1074/jbc.M300088200

Wansa, K. D., and Muscat, G. E. (2005). TRAP220 Is Modulated by the Antineoplastic Agent 6-Mercaptopurine, and Mediates the Activation of the NR4A Subgroup of Nuclear Receptors. *J. Mol. Endocrinol.* 34 (3), 835–848. doi:10.1677/jme.1.01739

Xiong, Y., Ran, J., Xu, L., Tong, Z., Adel Abdo, M. S., Ma, C., et al. (2020). Reactivation of Nr4a1 Restrains Chondrocyte Inflammation and Ameliorates Osteoarthritis in Rats. *Front. Cel Dev Biol* 8, 158. doi:10.3389/fcell.2020.00158

Zhao, Y., and Bruemmer, D. (2010). NR4A Orphan Nuclear Receptors: Transcriptional Regulators of Gene Expression in Metabolism and Vascular Biology. *Arterioscler Thromb. Vasc. Biol.* 30 (8), 1535–1541. doi:10.1161/ATVBAHA.109.191163

Zwerina, J., Hayer, S., Tohidast-Akrad, M., Bergmeister, H., Redlich, K., Feige, U., et al. (2004). Single and Combined Inhibition of Tumor Necrosis Factor, Interleukin-1, and RANKL Pathways in Tumor Necrosis Factor-Induced Arthritis: Effects on Synovial Inflammation, Bone Erosion, and Cartilage Destruction. *Arthritis Rheum.* 50, 277–290. doi:10.1002/art.11487

Conflict of Interest: The authors declare that the research was conducted in the absence of any commercial or financial relationships that could be construed as a potential conflict of interest.

Publisher's Note: All claims expressed in this article are solely those of the authors and do not necessarily represent those of their affiliated organizations, or those of the publisher, the editors and the reviewers. Any product that may be evaluated in this article, or claim that may be made by its manufacturer, is not guaranteed or endorsed by the publisher.

frontiers | Frontiers in Pharmacology

BRIEF RESEARCH REPORT
published: 25 April 2022
doi: 10.3389/fphar.2022.872736

Histamine Potentiates SARS-CoV-2 Spike Protein Entry Into Endothelial Cells

*Somasundaram Raghavan and M. Dennis Leo**

Department of Pharmaceutical Sciences, University of Tennessee Health Science Center, Memphis, TN, United States

Severe acute respiratory syndrome coronavirus 2 (SARS-CoV-2) which causes coronavirus disease (COVID-19) is one of the most serious global health crises in recent history. COVID-19 patient symptoms range from life-threatening to mild and asymptomatic, which presents unique problems in identifying, quarantining, and treating the affected individuals. The emergence of unusual symptoms among survivors, now referred to as "Long COVID", is concerning, especially since much about the condition and the treatment of it is still relatively unknown. Evidence so far also suggests that some of these symptoms can be attributed to vascular inflammation. Although famotidine, the commonly used histamine H2 receptor (H2R) blocker, was shown to have no antiviral activity, recent reports indicate that it could prevent adverse outcomes in COVID-19 patients. Histamine is a classic proinflammatory mediator, the levels of which increase along with other cytokines during COVID-19 infection. Histamine activates H2R signaling, while famotidine specifically blocks H2R activation. Investigating the effects of recombinant SARS-CoV-2 spike protein S1 Receptor-Binding Domain (Spike) on ACE2 expression in cultured human coronary artery endothelial cells, we found that the presence of histamine potentiated spike-mediated ACE2 internalization into endothelial cells. This effect was blocked by famotidine, protein kinase A inhibition, or by H2 receptor protein knockdown. Together, these results indicate that histamine and histamine receptor signaling is likely essential for spike protein to induce ACE2 internalization in endothelial cells and cause endothelial dysfunction and that this effect can be blocked by the H2R blocker, famotidine.

Keywords: SARS-CoV-2, histamine, famotidine, spike, angiotensin-converting enzyme-2

OPEN ACCESS

Edited by:
Nandakumar Natarajan, The University of Texas Health Science Center at Tyler, United States

Reviewed by:
Tlili Barhoumi, King Abdullah International Medical Research Center, Saudi Arabia
Ravinder Reddy Gaddam, The University of Iowa, United States

****Correspondence:***
M. Dennis Leo
mleo@uthsc.edu

Specialty section:
This article was submitted to Inflammation Pharmacology, a section of the journal Frontiers in Pharmacology

Received: *09 February 2022*
Accepted: *23 March 2022*
Published: *25 April 2022*

Citation:
Raghavan S and Leo MD (2022) Histamine Potentiates SARS-CoV-2 Spike Protein Entry Into Endothelial Cells. Front. Pharmacol. 13:872736. doi: 10.3389/fphar.2022.872736

INTRODUCTION

Severe acute respiratory syndrome coronavirus 2 (SARS-CoV-2) virus, which causes coronavirus disease (COVID-19), has swept across the globe over the last 2 years, inflicting enormous damage on both personal health and societal well-being (Ackermann et al., 2020; Wiersinga et al., 2020; Hu et al., 2021; Nalbandian et al., 2021). While most patients are either asymptomatic or show mild-to-moderate symptoms, around 15% of affected individuals might require hospitalization and ~ 5% might need intensive care (Nalbandian et al., 2021). While several studies that have been carried out so far have broadened our understanding of the acute phase of the disease, it has become clear that many individuals who had been infected but recovered have developed mysterious and wide-ranging health issues. These varied symptoms are now collectively referred to as "Long COVID" and include

several symptoms that suggest vascular inflammation and dysfunction (Ackermann et al., 2020; Marshall, 2020; Maxwell et al., 2021; Varga et al., 2020; Vassiliou et al., 2020).

The "cytokine storm" that occurs in acute-COVID-19 infection is associated with a massive surge in the circulating levels of several proinflammatory cytokines, but the relevance of histamine, a classic proinflammatory mediator, has been controversial (Ghosh et al., 2020; Loffredo et al., 2021; Ennis and Tiligada, 2021; Malone et al., 2021). Mast cells infected with SARS-CoV-2 release histamine (Conti et al., 2020), while famotidine, a histamine receptor-2 (H2R) blocker, itself does not inhibit virus replication (Conti et al., 2020), and it has been suggested that it might have potentially beneficial effects over the course of the disease (Malone et al., 2021).

ACE2 is a type I membrane-localized glycoprotein that is highly expressed in several cell types and is the primary receptor used by SARS-CoV-2 for cellular entry (Walls et al., 2020). While present in abundance in the heart, conflicting reports have emerged on its expression in vascular cells, specifically endothelial cells, and if the virus can directly infect endothelial cells. Previous evidence had revealed that the virus did not readily infect endothelial cells *in vitro* requiring ACE2 overexpression (Nascimento Conde et al., 2020), while another study reported that there were differences in viral entry into the endothelial cells from different human arteries (Wagner et al., 2021).

The SARS-CoV-Spike (S, spike) protein, which binds ACE2, is a structural protein comprising S1 and S2 subunits with the "Receptor Binding Domain" in the S1 subunit (Zhang H. et al., 2020; Huang et al., 2020). We had also shown previously that the recombinant spike protein added alone to normal cultured endothelial cells required ~ 12 h for observable downregulation of endothelial barrier function (Raghavan et al., 2021). Based on the available data so far, we hypothesized that histamine signaling through the endothelial H2 receptors could accelerate spike-induced ACE2-internalization in the endothelial cells to then trigger endothelial dysfunction. Our results here show that in healthy, untreated, and primary human coronary artery endothelial cells, the addition of the recombinant spike protein did not induce ACE2 internalization immediately but took around 6–12 h for internalization and degradation. The addition of histamine to endothelial cells accelerated spike-ACE2 internalization with observable intracellular ACE2 protein within 30 min of treatment. Blocking the H2R signaling pathway with either famotidine, the protein kinase A inhibitor, PKI, or knockdown of histamine receptor (H2R) inhibited spike-induced ACE2 internalization. Thus, these results suggest that histamine might be an important cofactor for internalization of the ACE2 and likely plays a significant role in accelerating spike protein entry into endothelial cells.

MATERIALS AND METHODS

Cell culture

The human primary coronary artery endothelial cells were purchased from Cell Biologics Inc. The cells were cultured in the endothelial cell medium containing (0.5 ml VEGF, Heparin, EGF, FGF, Hydrocortisone, L-Glutamine, and Antibiotic–Antimycotic Solution) supplemented with 2% fetal bovine serum.

Reagents

The SARS-CoV-2 (COVID-19) S1 Recombinant Protein (cat. no. 97-092) was purchased from ProSci Inc. (Poway, CA) and used at a final concentration of 10 μg/ml. The endothelial cells were treated with spike protein at the final concentration for the required time before surface biotinylation experiments were carried out. The ACE2 antibody was purchased from Abnova (Taipei, Taiwan, cat. no. PAB13443). Histamine, famotidine, and PKI were purchased from Sigma-Aldrich (St. Louis, MO, United States). siRNA to H2 receptor and scrambled siRNA were purchased from Thermo Fisher Scientific Inc.

Surface Biotinylation of Intact Endothelial Cells

Surface biotinylation was performed as we have done previously for intact arteries with slight modifications (Leo et al., 2017; Leo et al., 2018; Hasan et al., 2019; Leo et al., 2021). Briefly, live endothelial cell cultures were treated with appropriate reagents for specified times. After the treatment period, the reagents were washed with warm phosphate-buffered saline (PBS), and the cell culture plates were immediately placed on ice to inhibit all protein trafficking. The cell-impermeable biotinylation reagents dissolved in PBS are then added to the cultures and allowed to incubate at 4°C with gentle shaking for 30 min. The biotinylation reagents are removed with a PBS wash, and the reaction is quenched with 100 mM glycine. Protein lysates are prepared from each culture, and protein content is estimated. An equal quantity of protein from each group is passed through an avidin bead column to separate the biotinylated surface protein, which is eluted from the beads and prepared as the "surface fraction." The unbound protein was collected as the intracellular fraction. Each sample was then run as contiguous lanes on an SDS-gel as surface (denoted as 'S') and intracellular (denoted as 'I') fractions. The analysis was carried out by semi-quantitative comparison between the surface band intensities compared to the untreated or scrambled siRNA controls and was expressed as the ACE2 surface protein, % untreated control.

Western Blotting

Western blotting for protein was carried out following the standard protocols. After separation of surface and intracellular fractions, the proteins were separated on 7.5% SDS-polyacrylamide gels and transferred onto nitrocellulose membranes. The membranes were blocked with 5% non-fat milk and incubated with the ACE2 antibody overnight at 4°C. The membranes were washed and incubated with the horseradish peroxidase–conjugated secondary antibodies at room temperature. The blots were physically cut to allow for probing of two different proteins without the need for stripping. The protein bands were imaged using a ChemiDoc gel imaging system and quantified using Quantity One software (Biorad).

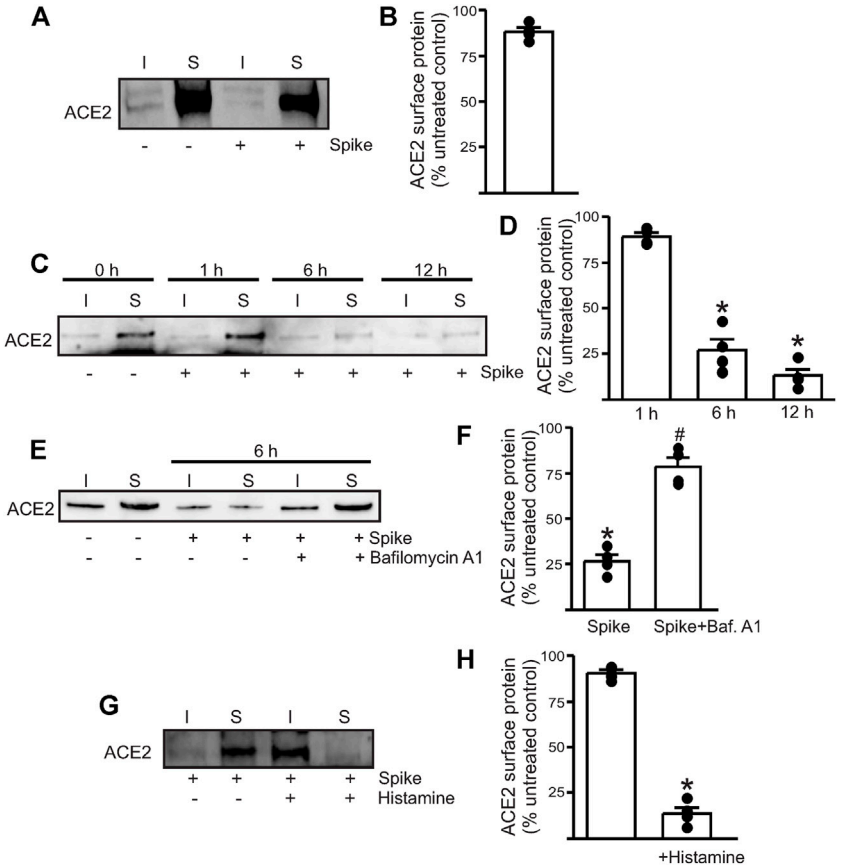

FIGURE 1 | Spike-induced ACE2 internalization is enhanced in the presence of histamine. **(A)** Representative Western blotting after surface biotinylation of intact endothelial cells with or without spike treatment for 30 min. **(B)** Mean data. **(C)** Representative Western blot after surface biotinylation showing that increased incubation time after spike treatment induced ACE2 internalization and degradation. **(D)** Mean data. *$p < 0.05$ *vs*. surface band intensity of the untreated control. **(E)** Representative Western blot after surface biotinylation showing the effect of bafilomycin A1 on spike-induced ACE2 degradation. **(F)** Mean data, *$p < 0.05$ *vs*. untreated, #$p < 0.05$ *vs*. spike treated. **(G)** Representative Western blot after surface biotinylation showing that histamine potentiates spike-induced ACE2 internalization within 30 min of treatment. **(H)** Mean data, *$p < 0.05$ *vs*. surface band intensity of untreated control. $n = 4$ for all the experimental sets. I- indicates intracellular fraction, S-denotes surface or plasma membrane fraction.

Statistics

Statistical analysis was performed using OriginLab and GraphPad InStat software. The data are shown as the mean ± SE and expressed as % change compared to the untreated surface ACE2 band intensities. Student's t-test and Mann–Whitney U test were implemented, where appropriate $p < 0.05$ was considered statistically significant.

RESULTS

Recombinant Spike Protein Does Not Readily Induce Endothelial Cell ACE2 Internalization

To determine if the spike can induce endothelial cell ACE2 internalization, we performed surface biotinylation of live endothelial cells. Recombinant spike (10 μg/ml) was added to a confluent plate of endothelial cells and allowed to incubate for 30 min. After this time, warm PBS was used to replace the media, and then the biotinylation reagents dissolved in PBS were added to the cells, and surface biotinylation was performed for 30 min at room temperature. First, the results showed that ACE2 is predominantly a plasma membrane (surface)–localized protein in healthy endothelial cells with >85% of the protein located on the surface (**Figures 1A,B**) Second, the addition of the spike protein alone to normal, healthy endothelial cells did not induce any ACE2 internalization at 30 min (**Figures 1A,B**). Previously, we had shown that the spike protein induced endothelial junctional protein degradation after 12-h treatment of mouse endothelial cells (Raghavan et al., 2021). Hence, we next tested if longer incubation times would induce ACE2 internalization and degradation. The results showed that spike treatment for 6 h reduced the ACE2 total and surface expression by ~ 70% compared to that of the untreated controls and by ~ 85% after 12 h of spike treatment (**Figures 1C,D**). In separate experiments, the endothelial cells were first pretreated for 30 min with bafilomycin A1, a lysosomal H^+-ATPase inhibitor, and then

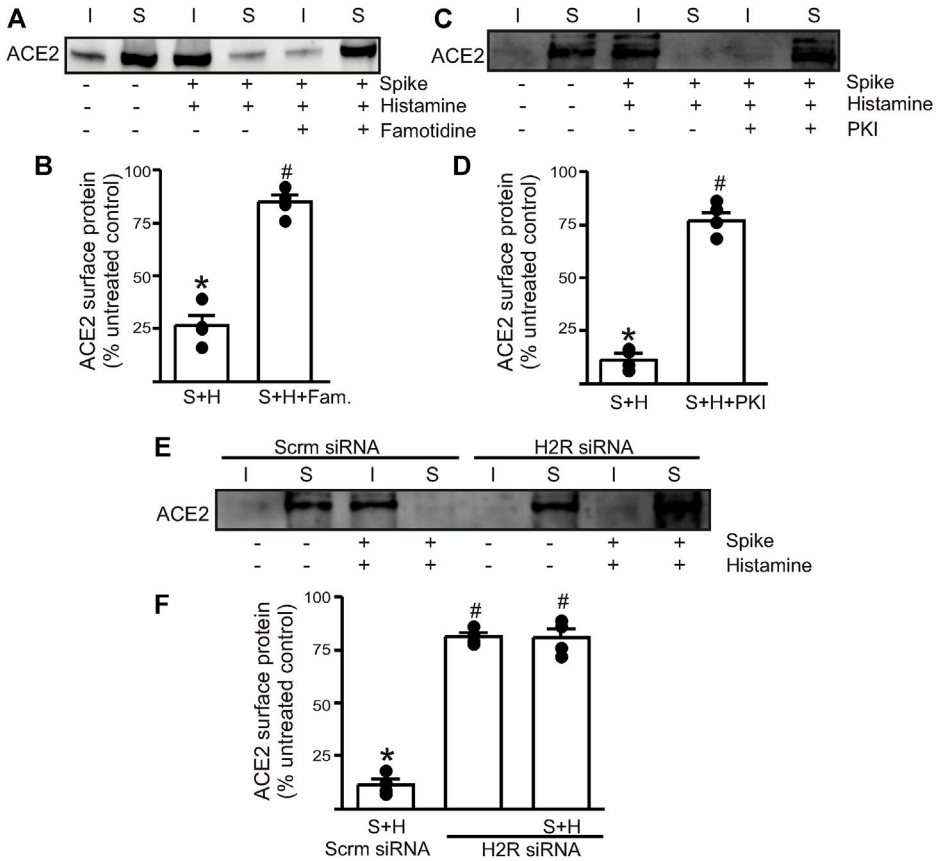

FIGURE 2 | Histamine H2 receptor signaling is involved in histamine potentiating spike–ACE2 internalization. **(A)** Representative Western blot after surface biotinylation of the intact endothelial cells showing the effect of famotidine on the potentiating effect of histamine on spike-ACE2 internalization. **(B)** Mean data. **(C)** Representative Western blot after surface biotinylation showing the effect of the protein kinase A inhibitor, PKI, in preventing histamine-induced spike–ACE2 internalization. **(D)** Mean data. *$p < 0.05$ *vs*. the untreated control, #$p < 0.05$ *vs*. spike + histamine. **(E)** Representative Western blot after surface biotinylation showing the effect of H2 receptor protein knockdown on spike + histamine treatment. Scrm-scrambled siRNA. **(F)** Mean data. *$p < 0.05$ *vs*. untreated control, #$p < 0.05$ *vs*. spike + histamine scrambled control. $n = 4$ for all the experimental sets. I- indicates intracellular fraction, S-denotes surface or plasma membrane fraction.

treated with the spike protein for 6 h in the presence of the inhibitor. The results show that bafilomycin A1 rescued ACE2 protein from spike-induced degradation which was then retrafficked to the cell surface (**Figures 1E,F**). This suggests that internalized ACE2 undergoes degradation *via* the lysosomal pathway. Taken together, these results indicate that in the healthy endothelial cells, the presence of the spike protein alone does not induce immediate internalization of the ACE2 receptor. Prolonged exposure to spike protein induces ACE2 internalization. The results also show that the internalized ACE2 is degraded and is not stored intracellularly.

Histamine Accelerates Spike Protein–Induced ACE2 Internalization

Since histamine levels are likely to increase during COVID-19 infection, we next tested if the presence of histamine modified the interaction of spike with ACE2. The control endothelial cells were treated with 1 μM histamine along with the spike protein for 30 min after which the reagents were washed off with warm PBS and surface biotinylation was performed at 4°C. Western blotting showed that in the presence of histamine, almost all the surface ACE2 now appeared in the intracellular fraction (**Figures 1G,H**). Given the very brief incubation time with the spike, this result indicates that 1. histamine significantly potentiates the ability of the spike to internalize ACE2 and 2. ACE2 is first internalized into the cell before undergoing degradation, and it is likely that a longer incubation period or sustained spike presence is required for ACE2 to undergo degradation. Overall, this suggests that histamine plays an important role in mediating spike–ACE2 interaction on the cell surface.

Histamine Acts Through Endothelial H2 Receptors to Accelerate Spike–ACE2 Internalization

Next, we wanted to investigate which endothelial signaling pathways were activated in the presence of histamine. We hypothesized that histamine likely acted through the endothelial H2 receptors to increase spike–ACE2

internalization. Accordingly, we pretreated the endothelial cells with famotidine (10 μM), the specific H2R blocker, for 30 min before the addition of spike and histamine. This combination was kept for an additional 30 min after which they were washed from the cell culture dishes with warm PBS and surface biotinylation was performed at 4°C. The results showed that in the presence of famotidine, much of the ACE2 protein was still present at the cell surface after treatment with spike and histamine (**Figures 2A,B**). These data suggest that famotidine, likely by the inhibition of H2R and its downstream signaling, prevented histamine from accelerating the internalization of ACE2.

To further investigate the involvement of H2R, we tried two different approaches. First, we pretreated the endothelial cells with PKI (10 μM), a protein kinase A (PKA) inhibitor. Histamine stimulates H2R to activate downstream PKA signaling, so the blockade of PKA signaling should negate H2R activation. The results showed that pretreatment of endothelial cells with PKI before the addition of spike + histamine completely prevented spike–ACE2 internalization (**Figures 2C,D**), suggesting that downstream PKA signaling after H2R activation was essential to this process. Second, we transfected the control cells with siRNA to H2R to knockdown the H2R protein. The results indicated that in cells where H2R was knocked down, the spike + histamine combination did not affect ACE2 surface expression compared to the scrambled siRNA controls (**Figures 2E,F**).

Together, these data indicate that extracellular histamine *via* the activation of H2R signaling potentiates spike-induced ACE2 internalization and that the inhibition of H2R by famotidine prevents acute internalization of the cell surface–localized ACE2 protein.

DISCUSSION

Here, we investigated the hypothesis that SARS-CoV-2 spike protein-induced ACE2 internalization is accelerated in the presence of histamine and that famotidine, a commonly used histamine receptor blocker, can block endothelial cell–spike protein entry through the ACE2 receptor. Using surface biotinylation to track the cellular localization of ACE2 in the endothelial cells after recombinant spike protein treatment, our data here showed that in the normal human coronary artery endothelial cells, the spike protein alone had a delayed response in internalizing ACE2. The total and surface ACE2 were reduced by ~ 85% only after 12 h of incubation with spike. In contrast, in the presence of histamine, the spike induced ACE2 internalization within 30°min. This effect was blocked when the endothelial cells were pretreated with famotidine, the PKA inhibitor, PKI, or when the H2 receptor was knocked down using siRNA. These results showed that the presence of histamine, acting through the endothelial H2 receptors, potentiated endothelial ACE2 internalization.

Evidence of vascular damage in COVID-19 patients began to emerge even early during the pandemic (Gavriilaki et al., 2020; Siddiqi et al., 2021), but there are contrasting reports on the virus infection of vascular cells, specifically endothelial cells. In opposition to the hypothesis that the virus directly infects endothelial cells, Nascimento Conde et al. (2020) have shown that recombinant ACE2 was required for the virus to infect the endothelial cells (Nascimento Conde et al., 2020), while other authors have argued that the expression of ACE2 in the endothelial cells might be too low to support viral entry (McCracken et al., 2021). In contrast, several other groups have found that human endothelial cells do express ACE2 and that the virus likely uses several additional protein pathways to enter the endothelial cells (Hamming et al., 2004; Zhang J. et al., 2020; Zhao et al., 2020; Albini et al., 2021; Wagner et al., 2021; Zhang et al., 2021; Amraei et al., 2022). In an earlier study, we too have shown that the recombinant spike protein incubated with mouse cerebral endothelial cells for 12 h not only induced ACE2 degradation but also decreased endothelial junctional protein expression, thereby affecting endothelial barrier functionality (Raghavan et al., 2021). Here, we also show that inhibition of the lysosomal degradative pathway rescued the internalized ACE2 from degradation. These results were corroborated in mouse models, where intravenous injections of the spike protein resulted in the protein appearing in several regions of the brain, likely after blood–brain barrier disruption and was found to cause cerebral endothelial microvascular damage and that the lysosomal pathway was involved in the virus uncoating within the cell [(Ballout et al., 2020), (Blaess et al., 2020), (Davenport et al., 2021), (Nuovo et al., 2021), (Rhea et al., 2021), (Shang et al., 2020)]. These contrasting reports not only highlight the complexity of COVID-19 but also suggest that ACE2 expression in the vasculature could be highly variable, thus requiring further investigation.

Famotidine (*Pepcid*®) is a histamine H2 receptor–selective blocker, approved by the FDA for treatment of gastroesophageal reflux disease (GERD) and gastric ulcer. Early in the pandemic, evidence emerged that the hospitalized COVID-19 patients treated with famotidine had a reduced risk of severe outcome and/or mortality (Freedberg et al., 2020; Mather et al., 2020; Sethia et al., 2020). Several groups have hypothesized that this effect of famotidine was likely due to the direct inhibition of the histamine H2 receptor (H2R) rather than antiviral activity (Ghosh et al., 2020; Loffredo et al., 2021; Ennis and Tiligada, 2021). Indeed, famotidine was later shown to have no SARS-CoV-2 antiviral activity (Malone et al., 2021), while conflicting reports on its effectiveness in acute COVID-19 cases and the availability of better COVID-19 treatments saw the drug gradually fall out of favor for this purpose. However, the uptick in abnormal health issues in some COVID-19 survivors, which is now broadly described under the term "Long COVID" and the possibility that some of these symptoms might be associated with the long-term virus-induced inflammatory damage to the vasculature, has re-ignited interest in this drug (Eldanasory et al., 2020; Malone et al., 2021; Mura et al., 2021). A recent outcome study of more than 250,000 COVID-19 infected patients found that the histamine receptor blockade significantly improved the outcomes in patients who needed respiratory support and has suggested that this might be due to the ability of

famotidine to block the proinflammatory signals arising from H2R activation (Mura et al., 2021).

Our brief investigation here has shown that the presence of histamine accelerates the spike protein–induced ACE2 internalization in the endothelial cells. In the absence of histamine, the spike protein alone required between 6 and 12 h for the ACE2 to be internalized and degraded. However, in the presence of histamine, the ACE2 was internalized within 30 min. In addition, this effect was largely blocked by either the knockdown of H2R, inhibition of PKA, the effector of the H2R signaling pathway, and most importantly, by famotidine, or the well-known H2R blocker. These results suggest that histamine and the histamine receptor signaling pathway might play a crucial role in virus entry into the endothelial cells. SARS-CoV-2 elicits an inflammatory reaction in the infected patients, leading to the production of several proinflammatory substances including histamine (Nalbandian et al., 2021). Several of these mediators such as TNF-α and several interleukins can further stimulate inflammatory cells such as mast cells to increase the synthesis and secretion of histamine (Crook et al., 2021; Nalbandian et al., 2021; Raveendran et al., 2021). Similar to what was observed with histamine here, the circulating vimentin has also been shown to facilitate SARS-CoV-2 endothelial cell entry (Amraei et al., 2022). Ours and other such studies suggest that the circulating or local levels of endogenous substances could potentiate the entry of the virus into the endothelial cells. We acknowledge the obvious limitation of this study, which is the concentration of histamine used to treat the cells (1 μM). While it is not likely that this concentration would be achieved in circulation in humans, the possibility remains that the local elevations in histamine levels, for example, in the lung, brain, or the heart could alter the viral entry into the cells in the immediate vicinity. We also utilized the recombinant spike protein of the original SARS-CoV-2 variant. Hence, it will be interesting to study the effects of the highly transmissible variants that appeared later and if the spike proteins from these variants could circumvent the requirement of the circulating cofactors such as vimentin or histamine.

CONCLUSION

COVID-19 is a complex disease and while vaccinations and better treatments options have effectively limited the morbidity and mortality, much remains to be learned about 'Long COVID' and its treatment. While famotidine does not have SARS-CoV-2 antiviral activity, the data presented here suggest that famotidine could be considered a second-line treatment to limit virus-induced vascular inflammation.

DATA AVAILABILITY STATEMENT

The original contributions presented in the study are included in the article/**Supplementary Material**, further inquiries can be directed to the corresponding author.

AUTHOR CONTRIBUTIONS

ML conceived designed research, drafted, edited, and revised the manuscript. SR performed Western blotting and analyzed the data. ML and SR interpreted the results of experiments and approved the final version of the manuscript. SR prepared the figures. All authors contributed to the article and approved the submitted version.

FUNDING

This work was supported by UTHSC-College of Pharmacy-startup funds to ML.

SUPPLEMENTARY MATERIAL

The Supplementary Material for this article can be found online at: https://www.frontiersin.org/articles/10.3389/fphar.2022.872736/full#supplementary-material

REFERENCES

Ackermann, M., Verleden, S. E., Kuehnel, M., Haverich, A., Welte, T., Laenger, F., et al. (2020). Pulmonary Vascular Endothelialitis, Thrombosis, and Angiogenesis in Covid-19. *N. Engl. J. Med.* 383, 120–128. doi:10.1056/NEJMoa2015432

Albini, A., Calabrone, L., Carlini, V., Benedetto, N., Lombardo, M., Bruno, A., et al. (2021). Preliminary Evidence for IL-10-Induced ACE2 mRNA Expression in Lung-Derived and Endothelial Cells: Implications for SARS-Cov-2 ARDS Pathogenesis. *Front. Immunol.* 12, 718136. doi:10.3389/fimmu.2021.718136

Amraei, R., Xia, C., Olejnik, J., White, M. R., Napoleon, M. A., Lotfollahzadeh, S., et al. (2022). Extracellular Vimentin Is an Attachment Factor that Facilitates SARS-CoV-2 Entry into Human Endothelial Cells. *Proc. Natl. Acad. Sci.* 119, e2113874119. doi:10.1073/pnas.2113874119

Ballout, R. A., Sviridov, D., Bukrinsky, M. I., and Remaley, A. T. (2020). The Lysosome: A Potential Juncture between SARS-CoV-2 Infectivity and Niemann-Pick Disease Type C, with Therapeutic Implications. *Faseb j* 34, 7253–7264. doi:10.1096/fj.202000654R

Blaess, M., Kaiser, L., Sauer, M., Csuk, R., and Deigner, H. P. (2020). COVID-19/SARS-CoV-2 Infection: Lysosomes and Lysosomotropism Implicate New Treatment Strategies and Personal Risks. *Int. J. Mol. Sci.* 21, 2020. doi:10.3390/ijms21144953

Conti, P., Caraffa, A., Tetè, G., Gallenga, C. E., Ross, R., Kritas, S. K., et al. (2020). Mast Cells Activated by SARS-CoV-2 Release Histamine Which Increases IL-1 Levels Causing Cytokine Storm and Inflammatory Reaction in COVID-19. *J. Biol. Regul. Homeost Agents* 34, 1629–1632. doi:10.23812/20-2EDIT

Crook, H., Raza, S., Nowell, J., Young, M., and Edison, P. (2021). Long Covid-Mechanisms, Risk Factors, and Management. *BMJ* 374, n1648. doi:10.1136/bmj.n1648

Davenport, B. J., Morrison, T. E., Kedl, R. M., and Klarquist, J. (2021). Conserved and Novel Mouse CD8 T Cell Epitopes within SARS-CoV-2 Spike Receptor Binding Domain Protein Identified Following Subunit Vaccination. *J. Immunol.* 206, 2503–2507. doi:10.4049/jimmunol.2100195

Eldanasory, O. A., Eljaaly, K., Memish, Z. A., and Al-Tawfiq, J. A. (2020). Histamine Release Theory and Roles of Antihistamine in the Treatment of Cytokines Storm of COVID-19. *Trav. Med Infect Dis* 37, 1018742020. doi:10.1016/j.tmaid.2020.101874

Ennis, M., and Tiligada, K. (2021). Histamine Receptors and COVID-19. *Inflamm. Res.* 70 (1), 67–75. doi:10.1007/s00011-020-01422-1

Freedberg, D. E., Conigliaro, J., Wang, T. C., Tracey, K. J., Callahan, M. V., and Abrams, J. A. (2020). Famotidine Use Is Associated with Improved Clinical

Outcomes in Hospitalized COVID-19 Patients: A Propensity Score Matched Retrospective Cohort Study. *Gastroenterology* 159, 1129–e3. e1123. doi:10.1053/j.gastro.2020.05.053

Gavriilaki, E., Anyfanti, P., Gavriilaki, M., Lazaridis, A., Douma, S., and Gkaliagkousi, E. (2020). Endothelial Dysfunction in COVID-19: Lessons Learned from Coronaviruses. *Curr. Hypertens. Rep.* 22, 63. doi:10.1007/s11906-020-01078-6

Ghosh, R., Chatterjee, S., Dubey, S., and Lavie, C. J. (2020). Famotidine against SARS-CoV2: A Hope or Hype? *Mayo Clin. Proc.* 95, 1797–1799. doi:10.1016/j.mayocp.2020.05.027

Hamming, I., Timens, W., Bulthuis, M. L., Lely, A. T., Navis, G., and van Goor, H. (2004). Tissue Distribution of ACE2 Protein, the Functional Receptor for SARS Coronavirus. A First Step in Understanding SARS Pathogenesis. *J. Pathol.* 203, 631–637. doi:10.1002/path.1570

Hasan, R., Leo, M. D., Muralidharan, P., Mata-Daboin, A., Yin, W., Bulley, S., et al. (2019). SUMO1 Modification of PKD2 Channels Regulates Arterial Contractility. *Proc. Natl. Acad. Sci. U S A.* 116, 27095–27104. doi:10.1073/pnas.1917264116

Hu, B., Guo, H., Zhou, P., and Shi, Z-L. (2021). Characteristics of SARS-CoV-2 and COVID-19. *Nat. Rev. Microbiol.* 19 (3), 141–154. doi:10.1038/s41579-020-00459-7

Huang, Y., Yang, C., Xu, X. F., Xu, W., and Liu, S. W. (2020). Structural and Functional Properties of SARS-CoV-2 Spike Protein: Potential Antivirus Drug Development for COVID-19. *Acta Pharmacol. Sin* 41, 1141–1149. doi:10.1038/s41401-020-0485-4

Leo, M. D., Peixoto-Nieves, D., Yin, W., Raghavan, S., Muralidharan, P., Mata-Daboin, A., et al. (2021). TMEM16A Channel Upregulation in Arterial Smooth Muscle Cells Produces Vasoconstriction during Diabetes. *Am. J. Physiol. Heart Circ. Physiol.* 320, H1089–h1101. doi:10.1152/ajpheart.00690.2020

Leo, M. D., Zhai, X., Muralidharan, P., Kuruvilla, K. P., Bulley, S., Boop, F. A., et al. (2017). Membrane Depolarization Activates BK Channels through ROCK-Mediated β1 Subunit Surface Trafficking to Limit Vasoconstriction. *Sci. Signal.* 10. doi:10.1126/scisignal.aah5417

Leo, M. D., Zhai, X., Yin, W., and Jaggar, J. H. (2018). Impaired Trafficking of Beta1 Subunits Inhibits BK Channels in Cerebral Arteries of Hypertensive Rats. *Hypertension* 72 (3), 765–775. doi:10.1161/HYPERTENSIONAHA.118.11147

Loffredo, M., Lucero, H., Chen, D-Y., O'Connell, A., Bergqvist, S., Munawar, A., et al. (2021). The In-Vitro Effect of Famotidine on SARS-CoV-2 Proteases and Virus Replication. *Sci Rep* 11, 5433. doi:10.1038/s41598-021-84782-w

Malone, R. W., Tisdall, P., Fremont-Smith, P., Liu, Y., Huang, X. P., White, K. M., et al. (2021). COVID-19: Famotidine, Histamine, Mast Cells, and Mechanisms. *Front. Pharmacol.* 12, 633680. doi:10.3389/fphar.2021.633680

Marshall, M. (2020). How COVID-19 Can Damage the Brain. *Nature* 585, 342–343. doi:10.1038/d41586-020-02599-5

Mather, J. F., Seip, R. L., and McKay, R. G. (2020). Impact of Famotidine Use on Clinical Outcomes of Hospitalized Patients with COVID-19. *Am. J. Gastroenterol.* 115, 1617–1623. doi:10.14309/ajg.0000000000000832

Maxwell, A. J., Ding, J., You, Y., Dong, Z., Chehade, H., Alvero, A., et al. (2021). Identification of Key Signaling Pathways Induced by SARS-CoV2 that Underlie Thrombosis and Vascular Injury in COVID-19 Patients. *J. Leukoc. Biol.* 109, 35–47. doi:10.1002/JLB.4COVR0920-552RR

McCracken, I. R., Saginc, G., He, L., Huseynov, A., Daniels, A., Fletcher, S., et al. (2021). Lack of Evidence of Angiotensin-Converting Enzyme 2 Expression and Replicative Infection by SARS-CoV-2 in Human Endothelial Cells. *Circulation* 143, 865–868. doi:10.1161/CIRCULATIONAHA.120.052824

Mura, C., Preissner, S., Nahles, S., Heiland, M., Bourne, P. E., and Preissner, R. (2021). Real-world Evidence for Improved Outcomes with Histamine Antagonists and Aspirin in 22,560 COVID-19 Patients. *Signal. Transduct Target. Ther.* 6, 267. doi:10.1038/s41392-021-00689-y

Nalbandian, A., Sehgal, K., Gupta, A., Madhavan, M. V., McGroder, C., Stevens, J. S., et al. (2021). Post-acute COVID-19 Syndrome. *Nat. Med.* 27, 601–615. doi:10.1038/s41591-021-01283-z

Nascimento Conde, J., Schutt, W. R., Gorbunova, E. E., and Mackow, E. R. (2020). Recombinant ACE2 Expression Is Required for SARS-CoV-2 to Infect Primary Human Endothelial Cells and Induce Inflammatory and Procoagulative Responses. *mBio* 11, e03185–20. doi:10.1128/mBio.03185-20

Nuovo, G. J., Magro, C., Shaffer, T., Awad, H., Suster, D., Mikhail, S., et al. (2021). Endothelial Cell Damage Is the central Part of COVID-19 and a Mouse Model Induced by Injection of the S1 Subunit of the Spike Protein. *Ann. Diagn. Pathol.* 51, 151682. doi:10.1016/j.anndiagpath.2020.151682

Raghavan, S., Kenchappa, D. B., and Leo, M. D. (2021). SARS-CoV-2 Spike Protein Induces Degradation of Junctional Proteins that Maintain Endothelial Barrier Integrity. *Front. Cardiovasc. Med.* 8, 687783. doi:10.3389/fcvm.2021.687783

Raveendran, A. V., Jayadevan, R., and Sashidharan, S. (2021). Long COVID: An Overview. *Diabetes Metab. Syndr.* 15, 869–875. doi:10.1016/j.dsx.2021.04.007

Rhea, E. M., Logsdon, A. F., Hansen, K. M., Williams, L. M., Reed, M. J., Baumann, K. K., et al. (2021). The S1 Protein of SARS-CoV-2 Crosses the Blood-Brain Barrier in Mice. *Nat. Neurosci.* 24, 368–378. doi:10.1038/s41593-020-00771-8

Sethia, R., Prasad, M., Jagannath, S., Nischal, N., Soneja, M., and Garg, P.Shalimar (2020). Efficacy of Famotidine for COVID-19: A Systematic Review and Meta-Analysis. *medRxiv*. doi:10.1101/2020.09.28.20203463

Shang, J., Wan, Y., Luo, C., Ye, G., Geng, Q., Auerbach, A., et al. (2020). Cell Entry Mechanisms of SARS-CoV-2. *Proc. Natl. Acad. Sci. U S A.* 117, 11727–11734. doi:10.1073/pnas.2003138117

Siddiqi, H. K., Libby, P., and Ridker, P. M. (2021). COVID-19 - A Vascular Disease. *Trends Cardiovasc. Med.* 31, 1–5. doi:10.1016/j.tcm.2020.10.005

Varga, Z., Flammer, A. J., Steiger, P., Haberecker, M., Andermatt, R., Zinkernagel, A. S., et al. (2020). Endothelial Cell Infection and Endotheliitis in COVID-19. *Lancet* 395, 1417–1418. doi:10.1016/S0140-6736(20)30937-5

Vassiliou, A. G., Kotanidou, A., Dimopoulou, I., and Orfanos, S. E. (2020). Endothelial Damage in Acute Respiratory Distress Syndrome. *Int. J. Mol. Sci.* 21, 8793. doi:10.3390/ijms21228793

Wagner, J. U. G., Bojkova, D., Shumliakivska, M., Luxán, G., Nicin, L., Aslan, G. S., et al. (2021). Increased Susceptibility of Human Endothelial Cells to Infections by SARS-CoV-2 Variants. *Basic Res. Cardiol.* 116, 42. doi:10.1007/s00395-021-00882-8

Walls, A. C., Park, Y. J., Tortorici, M. A., Wall, A., McGuire, A. T., and Veesler, D. (2020). Structure, Function, and Antigenicity of the SARS-CoV-2 Spike Glycoprotein. *Cell* 181, 281–e6. e286. doi:10.1016/j.cell.2020.02.058

Wiersinga, W. J., Rhodes, A., Cheng, A. C., Peacock, S. J., and Prescott, H. C. (2020). Pathophysiology, Transmission, Diagnosis, and Treatment of Coronavirus Disease 2019 (COVID-19): A Review. *JAMA* 324, 782–793. doi:10.1001/jama.2020.12839

Zhang, H., Penninger, J. M., Li, Y., Zhong, N., and Slutsky, A. S. (2020). Angiotensin-converting Enzyme 2 (ACE2) as a SARS-CoV-2 Receptor: Molecular Mechanisms and Potential Therapeutic Target. *Intensive Care Med.* 46, 586–590. doi:10.1007/s00134-020-05985-9

Zhang, J., Tecson, K. M., and McCullough, P. A. (2020). Endothelial Dysfunction Contributes to COVID-19-Associated Vascular Inflammation and Coagulopathy. *Rev. Cardiovasc. Med.* 21, 315–319. doi:10.31083/j.rcm.2020.03.126

Zhang, J., Tecson, K. M., and McCullough, P. A. (2021). Role of Endothelial Cell Receptors in the Context of SARS-CoV-2 Infection (COVID-19). *Baylor Univ. Med. Cent. Proc.* 34, 262–268. doi:10.1080/08998280.2021.1874231

Zhao, Y., Zhao, Z., Wang, Y., Zhou, Y., Ma, Y., and Zuo, W. (2020). Single-Cell RNA Expression Profiling of ACE2, the Receptor of SARS-CoV-2. *Am. J. Respir. Crit. Care Med.* 202, 756–759. doi:10.1164/rccm.202001-0179LE

Conflict of Interest: The authors declare that the research was conducted in the absence of any commercial or financial relationships that could be construed as a potential conflict of interest.

Publisher's Note: All claims expressed in this article are solely those of the authors and do not necessarily represent those of their affiliated organizations, or those of the publisher, the editors, and the reviewers. Any product that may be evaluated in this article, or claim that may be made by its manufacturer, is not guaranteed or endorsed by the publisher.

frontiers | Frontiers in Pharmacology

REVIEW
published: 02 May 2022
doi: 10.3389/fphar.2022.829951

Effects of Dexmedetomidine on Immune Cells: A Narrative Review

Rui Chen[1,2†], *Yan Sun*[1,2†], *Jing Lv*[1,2†], *Xiaoke Dou*[1,2], *Maosha Dai*[1,2], *Shujun Sun*[1,2*] and *Yun Lin*[1,2*]

[1]Institute of Anesthesia and Critical Care Medicine, Union Hospital, Tongji Medical College, Huazhong University of Science and Technology, Wuhan, China, [2]Department of Anesthesiology, Union Hospital, Tongji Medical College, Huazhong University of Science and Technology, Wuhan, China

As we all know, dexmedetomidine (DEX), as a highly selective α_2 adrenergic receptor agonist, exerts sedative, anti-anxiety and hypnotic effects by inhibiting the discharge of norepinephrine neurons in locus coeruleus and GABA-related hypnotic pathways. However, the role of DEX in anti-inflammatory and immune regulation has gradually attracted the attention of researchers in recent years. The α_2 adrenergic receptor is one of the members of the adrenergic receptor family, which is widely present in a variety of immune cells and mediates the biological behavior of the inflammatory immune system. At present, there have been more and more studies on the effects of DEX on immune cells and inflammatory responses, but few studies have systematically explored the anti-inflammatory and immunomodulatory effects of DEX. Here, we comprehensively review the published human and animal studies related to DEX, summarize the effects of DEX on immune cells and its role in related diseases, and propose potential research direction.

Keywords: dexmedetomidine, immune cells, innate immune response, adaptive immune response, inflammatory factors

OPEN ACCESS

Edited by:
Nandakumar Natarajan, The University of Texas Health Science Center at Tyler, United States

Reviewed by:
Awadhesh K. Arya, University of Maryland, Baltimore, United States
Badrinath Narayanasamy, Pusan National University, South Korea

***Correspondence:**
Shujun Sun
sunshunjun@foxmail.com
Yun Lin
franklinyun@hust.edu.cn

[†]*These authors have contributed equally to this work*

Specialty section:
This article was submitted to Inflammation Pharmacology, a section of the journal Frontiers in Pharmacology

Received: *06 December 2021*
Accepted: *11 April 2022*
Published: *02 May 2022*

Citation:
Chen R, Sun Y, Lv J, Dou X, Dai M, Sun S and Lin Y (2022) Effects of Dexmedetomidine on Immune Cells: A Narrative Review. Front. Pharmacol. 13:829951. doi: 10.3389/fphar.2022.829951

1 INTRODUCTION

The adrenergic system is closely linked to the immune system (Keating, 2015). Both innate immune cells and adaptive immune cells express adrenergic receptors and can directly respond to the sympathetic nervous system (Lorton and Bellinger Denise, 2015; Scanzano and Marco, 2015). Primary and secondary lymphoid tissues are regulated by postganglionic sympathetic nerve fibers, mainly secreting norepinephrine as its main neurotransmitter (Sharma and Farrar, 2020). In general, the role of the adrenergic system in immunity is gradually receiving attention and has now become a research hotspot.

Dexmedetomidine (DEX) is a highly selective α_2 adrenergic receptor (AR) agonist, which has a high affinity for the AR family members α_2A and α_2C (Berkowitz et al., 1994; Huang et al., 2021). It can regulate the release of norepinephrine by activating the α_2 receptor located on the presynaptic membrane, which is the basis of its immunomodulatory function. Meanwhile, studies have shown that DEX can regulate cellular immunity, suppress the inflammatory response in the tissues and enhance the immune function of patients (Li et al., 2016; Ferreira and Bissell Brittany, 2018). However, the effects of DEX on immune cells and inflammatory cytokines have not been systematically summarized.

The main purpose of our review is to comprehensively provide the latest evidence on the immune regulation and anti-inflammatory effects of DEX in various immune cells and immune-related diseases. And the future value of DEX in the treatment of some common but troublesome diseases is worth looking forward to.

TABLE 1 | Summary table on effects of DEX on immune cells and inflammatory cytokines.

Target cells	Effects		References
	Suppression	Induction	
Dendritic cells	Pro-inflammatory cytokines (TNF-α, IL-1β IL-6, IFN-γ)	Anti-inflammatory cytokine IL-10	Ueshima et al. (2013)
	Immunomodulatory factor (IL-12, IL-23)		Chen G. et al. (2016)
	Class II MHC and costimulatory molecules (I-Ab And CD86)		Guo et al. (2018) Huang et al. (2021)
Natural killer Cells	Development and metastasis of tumor	Increase the number and maintain the activity	Zhao et al. (2013) Yang et al. (2017) Wu L. et al. (2015)
Eosinophils	Chemokines (eotaxin)	————————————————————	Kalbach et al. (2019)
Mast cells	Degranulation Proteolytic enzyme MMP-9	Proteolytic enzyme MMP-2	Tüfek et al. (2013) Matsumoto (2009)
Neutrophils	Pro-inflammatory cytokines (IL-6, TNF-α, Necrosis factor)	Elimination of pathogen	Chen S. L. et al. (2016)
	Antimicrobial effectors (ROS, RNS, NO, iNOS) Respiratory eruption		Yuan et al. (2020)
	Local aggregation of neutrophils		Cowburn et al. (2008)
Monocytes	The ratio of CD42+/CD14+ Pro-inflammatory cytokines (IL-6, TNF-α)	The ratio of HLADR+/CD14+	Zhou et al. (2017)
	The expression of Cx43, PKC-α, VLA-4 and LFA-1 Monocyte-endothelial cells adhesion		Chai et al. (2020)
Macrophages	Pro-inflammatory cytokines (IL-6, COX-II, PGE2, HMGB1)	TNF-α, IL-1β Transforming growth factor TGF-β1	Martinez Fernando and Gordon (2014)
	Inflammatory protein MIP-2	Anti-inflammatory cytokine (IL-10)	Lai et al. (2009)
		The production of Th1 cells by promoting the secretion of IL-12 Polarization of M2	Zhou et al. (2020)
		Clearance of Neutrophil and autophagy of mitochondrial	Li et al. (2021) Wang K. et al. (2019) Piazza et al. (2016)
B cells		Chemokine (IL-2)	Ma et al. (2017) Liu et al. (2018)
T cells	The amount of CD8+ The amount of CD3+, CD4+, CD4+/CD8+	Pro-inflammatory cytokines (IL-17A) Immune regulatory factors (IFN-γ)	Huang et al. (2021) Yang et al. (2017) Lee et al. (2018) Song et al. (2020)

2 DEX'S REGULATORY EFFECT ON IMMUNE CELLS AND INFLAMMATION

2.1 General Effects

DEX can not only modulate the ability of antigen-presenting cells to uptake and process antigens, and the recruitment, chemotaxis and local aggregation of immune cells in innate immunity, but also regulate the CD4+/CD8+ ratio and balance the quantity of Th1, Th2, Th17 and Regulatory T cells (Tregs) in the adaptive immunity. As well, DEX can reduce the secretion of pro-inflammatory cytokines (IL-1β, IL-6, IL-8, IL-12/23 (p40), IL-17A, IL-18, IFN-γ, TNF-α, Eotaxin, HMGB1, MIP-2, MCP-1) and increase the level of anti-inflammatory factors (IL-2, IL-4, IL-10 and TGF-β1). Therefore, it plays a vital role in immunity and inflammation.

In more details, here below we summarize the main effects of DEX on different immune cell populations, as shown in **Table1**.

2.2 Innate Immune Response

The innate immune response refers to the use of differentiated leukocytes to identify and eliminate foreign substances in organs, tissues, blood and lymph. And, the innate immune response-related cells mainly include dendritic cells (DCs), natural killer cells (NKs), eosinophils, mast cells and phagocytic cells (neutrophils and monocytes/macrophages).

2.2.1 Dendritic Cells (DCs)

DCs are one of the antigen presenting cells in the body. They can efficiently capture, process and present antigens, and induce the generation of specific cytotoxic T lymphocytes (CTLs).

DCs express α_1, α_2 and β-AR on the cell membrane. As an α_2-AR agonist, DEX can inhibit immune responses by inhibiting antigen processing/presentation and migration of DCs (Ueshima et al., 2013). For another, DEX could inhibit the maturation and function of DCs by interfering with the synthesis and secretion of IL-12 and IL-23, thereby negatively regulating human immune function (Chen G. et al., 2016). In addition, DEX can inhibit the protein hydrolysis and migration of phagosomes in DCs, reduce the expression and migration of class II MHC molecule I-Ab and costimulatory molecule CD86 and inhibit the proliferation of cytotoxic T lymphocytes and the secretion of IFN-γ, thereby exerting an immunosuppressive effect (Ueshima et al., 2013; Chen S. L. et al., 2016). However, the interesting phenomena have been found in an animal experiments, in which DEX at

different concentrations may have the opposite effect on the secretion of inflammatory mediators by DCs. At high concentrations (10, 1, and 0.1 μm) of DEX, the expression of mRNA and the contents of TNF-α, IL-1β, IL-6, and IL-10 in DCs stimulated by LPS increased, while DEX at lower concentrations (0.001 μm), the content of these molecules decreased, and the mechanism was related to the activation of NF-κB and JNK-MAPK signaling pathways (Guo et al., 2018). The experiment shows that DEX has a dual regulatory effect on DCs, in which inflammatory factors are increased at high concentrations and decreased at low concentrations. Studies have found that DEX can preserve the number of DCs in patients undergoing oral cancer surgery and enhance the immune function of patients (Huang et al., 2021).

In general, DEX acts on DCs through α_2-AR and exerts immune regulation. Guo et al. (2018) have suggested that DEX may play different roles in different pathological conditions, because other kinds of AR and downstream signals also participate in the reaction. Moreover, the current results of clinical trials are too few, and the actual effects of DEX on DCs need to be further confirmed.

2.2.2 Natural Killer Cells (NKs)

NKs are the important immune cells in the body, participating in non-specific cell-mediated anti-tumor immune regulation. They can kill MHC class I cells without being activated, and when the number of NKs decreases, it means the body's immune function is suppressed (Pilla et al., 2005).

Whether α_2 -AR are expressed on the cell membrane of NKs is unclear. At present, animal studies have found that DEX can maintain the activity of NKs after surgery or general anesthesia (Taniguchi et al., 2004), which decreased after operation or anesthesia originally. In clinical trials, cancer patients who used DEX in the perioperative period showed significantly higher concentrations of NKs from 6 to 24 h after surgery (Barbera-Guillem et al., 2000; Wolf et al., 2003; Zhao et al., 2013; Yang et al., 2017). It has also been found that the decrease in the number of NK cells after DEX treatment in children with brain tumors during the perioperative period was significantly less than that in the control group (Wu Lei et al., 2015).

In fact, it is believed that IL-2, IL-12, IL-18, IFN-α, TNF-α and leucomodulin (LR) have a positive regulatory effect on the activation and differentiation of NK cells, which can significantly improve the killing activity of NK cells. Prostaglandins (PGE1, E2, D2) and adrenocortical hormone can inhibit the activity of NK cells (Alboni et al., 2010; Kallioinen et al., 2019).

In conclusion, DEX can increase the number of NKs and maintain their activity. However, most of the current studies focus on the effect of DEX on the number of NKs, and lack of studies on the effect of DEX on the differentiation and migration of NK cells. Whether DEX can affect the function of NK cells through the above-mentioned inflammatory immune molecules will be the direction of future research.

2.2.3 Eosinophils

Eosinophils have the function of killing bacteria and parasites, which are also considered as the crucial cells in the process of immune and allergic reactions.

It has not been verified that whether α_2-AR are expressed on the cell membrane of eosinophils cells yet. But, Kallioinen et al. (2019) and Dahl. (1991) confirmed that eosinophil chemoattractant factor (eotaxin) decreased significantly in healthy subjects after administration of DEX. Eotaxin is a potent chemotactic agent for eosinophils, which mediates leukocyte recruitment in allergic diseases such as asthma (Cheng et al., 2002), and is also strongly up-regulated in septic mouse models (Kalbach et al., 2019). It means that DEX may be a good choice for anesthesia for patients with asthma and sepsis. However, some studies have found that a large proportion of children with severe asthma require an upgrade from noninvasive positive pressure ventilation to invasive mechanical ventilation when DEX is given as adjunctive therapy (Kalbach et al., 2019).

Generally speaking, there are few studies on the effect of DEX on eosinophils currently, and the clinical effect of DEX on asthma can be used as a future research direction.

2.2.4 Mast Cells

Mast cells are the first cells to be recruited to the site of the injury, then selectively produce pro-inflammatory mediators, thereby enlisting neutrophils, macrophages and other monocytes into the site to activate the inflammatory response (Kennelly et al., 2011; Younan et al., 2011; Theoharides et al., 2012).

It is not known that whether α_2 -AR are expressed on the cell membrane of mast cells. However, early studies have shown that α_2-AR agonist clonidine can regulate the function of mast cells through α_2-AR (Lindgren et al., 1987; Anderson et al., 1987; Lavand'homme and Eisenach, 2003; Lavand'homme Patricia et al., 2002). Compared with clonidine, DEX has 8-fold higher affinity for α_2-AR (Bhana et al., 2000). At present, numerous literatures have shown that DEX may be a strong stabilizer of mast cells, and may inhibit inflammation by preventing degranulation (Tüfek et al., 2013). In the animal models, the application of DEX could reduce oxidative stress (Tüfek et al., 2013). Specifically, it decreased the levels of matrix metalloproteinase-9 (MMP-9) and galectin-3, and increased the level of matrix metalloproteinase-2 (MMP-2) (Matsumoto, 2009). Besides, some studies have found that DEX stabilizes mast cells at the injured site (Tüfek et al., 2013).

There are few studies on the regulation of mast cell function and inhibition of inflammation by DEX, which may be the fields of future research.

2.2.5 Neutrophils

Neutrophils, also known as polymorphonuclear leukocytes (PMN), are the main cell type of the innate immune system, which mainly scavenge pathogens and lead to the acute inflammation (Cowburn et al., 2008). The clearance of pathogens by neutrophils involves a series of physiological processes, including chemotaxis, phagocytosis and killing microorganisms (Kantari et al., 2008; Raffaghello et al., 2008).

It has been identified that α_2-AR are expressed on the cell membrane of neutrophils (Panosian and Marinetti, 1983). And it has been confirmed that a variety of anesthetics, including propofol, midazolam and ketamine, can inhibit the chemotaxis and phagocytosis of neutrophils and the production of superoxide anion, while DEX not (Stevenson et al., 1990;

Mikawa et al., 1998; Nishina et al., 1998). This suggests that DEX may be more suitable for patients with infection, sepsis and systemic inflammation (Nishina et al., 1999).

Whether neutrophils can successfully eliminate pathogens depends on oxidative burst, the main process that kills microorganisms through the formation of reactive oxygen species (ROS) and reactive nitrogen species (RNS) (Cowburn et al., 2008). It was found that DEX could inhibit the oxidative burst stimulated by *E. coli* and the production of nitric oxide (NO) (Chen G. et al., 2016). And studies have found that DEX can inhibit endotoxin induced inflammatory response, reduce the concentration of IL-6, TNF-α and local aggregation of neutrophils, so as to play the role of anti-inflammation and immunosuppression. And the inhibition of DEX on the infiltration of neutrophils may be related to FOXO3a signaling pathway (Yuan et al., 2020).

To sum up, DEX can not only regulate the chemotaxis and phagocytosis of neutrophils, but also inhibit the local aggregation, oxidative burst and the production of reactive oxygen and reactive nitrogen of neutrophils, thereby playing an anti-inflammatory effect. However, the above results are all *in vitro* data, and the clinical situation cannot be simply inferred. Therefore, further studies are needed to elucidate the effect of DEX on function of neutrophils *in vivo*.

2.2.6 Monocytes/Macrophages

2.2.6.1 Monocytes

Monocytes are the precursors of macrophages and DCs, which are involved in immune responses. After phagocytosis of antigen by monocytes, antigenic determinants are transferred to lymphocytes to induce lymphocyte-specific immune responses. And the recruitment of circulating monocytes to inflammatory tissues is one of the important characteristics of acute and chronic inflammatory response.

It has been confirmed that α_2-AR are expressed on the cell membrane of monocytes. And it has been reported that the percentage of monocyte-platelet aggregation (CD42a +/CD14 +) can reflect the level of inflammation and hemostasis, and the percentage of monocyte activated cytokines (HLA DR+/$CD14^+$) can reflect the state of immunosuppression (Monneret et al., 2006). Clinical trials have found that when DEX acts on monocytes, it can inhibit the inflammatory response and enhance immunity by inhibiting the percentage of ($CD42a+/CD14^+$), promoting the percentage of (HLA $DR+/CD14^+$) and reducing the production of proinflammatory cytokines, such as IL-6 and TNF-a (Zhou et al., 2017).

In vitro cell experiments, DEX decreased Cx43 expression and PKC-α of the carboxyl terminal domain of Cx43 protein in monocytes at its clinically relevant concentrations (0.1 and 1 nm). With the downregulation of PKC-α, the NOX2/ROS signaling pathway was inhibited, resulting in the decreased expression of VLA-4 and LFA-1, and finally, decreased monocyte-endothelial cell adhesion (Chai et al., 2020).

At present, there are many known risk factors that increase monocyte-endothelial cell adhesion, including patients undergoing major surgery, intensive care, or long-term bed rest (Sikorski et al., 2011; Ribeiro et al., 2018; Schmitt et al., 2020; Wilhelms et al., 2020; Wu et al., 2020). Therefore, the rational use of DEX in critically ill patients should be concerned. Moreover, whether DEX can affect the phagocytosis and presentation of monocytes remains to be further studied.

2.2.6.2 Macrophages

Macrophages, as the principal phagocytes in the inflammatory stage, are responsible for clearing the necrotic fragments, pathogens of tissues and cells in the body damage. They can phagocytize and absorb polymorphonuclear neutrophils (PMN) with local infiltration and apoptosis, and then inhibit the excessive secretion of pro-inflammatory cytokines. They play a key role in the lysis phase, and participate in the progress and regression of inflammation (Sugimoto et al., 2017).

Macrophages express α_2-AR on their cell membrane. And the ability of macrophages to resist microbial growth depends on the activated state of macrophages. There are two phenotypes of macrophage activation including M1 and M2. M1 macrophages participate in the positive immune response and play the role of immune monitoring by secreting pro-inflammatory cytokines and chemokines, and presenting antigens; M2 macrophages only have weak antigen presenting ability, but play an important role in immune regulation by secreting cytokines such as IL-10 and TGF-β (Martinez Fernando and Gordon, 2014). And DEX can enhance the production of major antibacterial effector molecules, including ROS and NO, and activate macrophages to resist the growth of intracellular pathogens (Rezai, 1968; Ohmori and Hamilton, 1994; MacMicking et al., 1997). It can also activate the antifungal and antibacterial activities of macrophages by combining with macrophages α_2-AR, and regulate the up-regulation of inflammatory molecules induced by endotoxin (Miles et al., 1996; Lai et al., 2009). In an animal experiment, macrophages were pretreated with DEX to increase pro-inflammatory factors, such as TNF-α and IL-6, inhibit the secretion of anti-inflammatory factor IL-10, and promote macrophage M2 polarization in a PPARγ/STAT3 dependent manner (Zhou et al., 2020).

Moreover, Chang et al. (2013) found that DEX could inhibit the transport of HMGB1 from nucleus to cytoplasm and the expression of high mobility group box 1 (HMGB1) mRNA, while HMGB1 is a key pro-inflammatory factor closely related to the mortality of patients with sepsis. Its mechanism may be related to NF-κB signaling pathway and α_2-AR activation (Chang et al., 2013). Li et al. (2021) found that DEX post-treatment, through the increase of F4/80 + Ly6G + macrophages, promotes the secretion of TGF-β1, which leads to the reduction of cytokine storm and accelerates the resolution of inflammation. A series of studies have found that DEX can reduce the secretion of IL-1β and TNF-α in macrophages, increase the expression of LC3-II (autophagy related protein), promote the clearance of damaged mitochondria. The DEX also can promote PTEN-induced putative kinase 1 (PINK1) mediated mitochondrial autophagy, thereby reducing the apoptosis and inflammation of macrophages induced by LPS, and play a protective role in sepsis (Wang K. et al., 2019). Yang et al. (2008) found in animal models that high-dose but not clinically relevant dose DEX can effectively inhibit the concentration of macrophage inflammatory protein 2 (MIP-2), TNF-α and iNOS in the lung,

and significantly reduce the cytokines (IL-1β, IL-6) in ventilator-related lung injury, these effects are at least partially mediated by α_2-AR. However, Lai et al. (2009) discovered that DEX at a higher dose than routinely used in clinics has a significant biphasic effect (first inhibition and then enhancement) on the secretion of inflammatory factors (COX-2, PGE2, TNF-a, IL-1b, IL-6, IL-10, iNOS and NO) after activating mouse macrophages α_2-AR. Meanwhile, it has been found that DEX does not directly inhibit the release of cytokines from human pulmonary macrophages like rodents (Kang et al., 2003; Piazza et al., 2016).

At present, the effect of DEX on phagocytosis of macrophages is still controversial. Wu R. S. et al. (2015) found that DEX could enhance the phagocytic activity of macrophages in mice with endotoxemia. Tippimanchai et al. (2018) suggested that DEX could reduce the number of alveolar macrophages and inhibit their phagocytosis in septic mice. García et al. (2003) suggest that α_2-AR controls phagocytosis and chemotaxis in primary cultured rat peritoneal macrophages, maintaining phagocytosis at optimal levels.

All in all, the difference between the results of animal experiments and clinical trials deserves further study.

2.3 Adaptive Immune Responses

Adaptive immune responses refer to the whole process in which antigen-specific T/B lymphocytes are activated, proliferated and differentiated into effector cells to produce a series of biological effects.

2.3.1 B Cells

B cells participate in the immune responses through a variety of ways: produce antibodies, differentiate into plasma cells, act as APCs, and secrete various cytokines to regulate the activities of other immune systems and immune cells. Under antibody-mediated autoimmune conditions, B cells play a key role in humoral immunity.

Whether α_2-AR are expressed on the surface of B cells is unclear. When DEX is administrated with middle and high doses, it can inhibit the release of IL-1, IL-6, TNF-α and PGE2, increase the release of IL-2, and play an anti-nociceptive role in acute inflammatory visceral pain, thereby inhibiting visceral hypersensitivity (Ma et al., 2017; Liu et al., 2018). Also, DEX activates the B cell signaling pathway by inhibiting the p38 mitogen-activated protein kinase/nuclear factor K-light chain enhancer, increasing the serum IL-2 level of ovarian cancer rats and enhancing the immune function (Cai et al., 2017).

However, it was found that there was no significant difference in the number of B lymphocytes between the DEX group and the control group, suggesting that DEX had little effect on humoral immune response of patients undergoing oral cancer surgery (Huang et al., 2021). Wu R. S. et al. (2015) found that continuous intravenous infusion of DEX during general anesthesia can reduce the number of B cells, which effectively inhibits the perioperative stress response of children with brain tumors. The specific mechanism of the effect of DEX on humoral immune function is still unclear, and its effect on humoral immune function of patients with malignant tumor needs further study.

2.3.2 T Cells

T cells are one of the main members of lymphocytes. They have many biological functions, including killing target cells directly, assisting or inhibiting B cells to produce antibodies, responding to specific antigens and producing cytokines. The immune response caused by T cells belongs to cellular immunity.

2.3.2.1 The Amount of $CD3^+$, $CD4^+$, $CD8^+$ and CD4+/CD8+ Ratio

CD3 molecule is a characteristic mark on the mature T cells and the number of it reflects the total number of T cells, and its increase indicates the enhancement of immune function. $CD4^+$ T cells are auxiliary T cells, which play an accessory role in the induction of cellular and humoral immunity. $CD8^+$ T cells are mainly immunosuppressive cells, which inhibit the function of other immune cells. The decrease of the CD4+/CD8+ ratio indicates poor immune function, and a large decrease often indicates the severity of the disease and poor prognosis (Huang et al., 2021).

Related studies have confirmed that compared with the control group, the amount of $CD3^+$, $CD4^+$ cells and the ratio of CD4+/CD8+ in the DEX group were significantly increased, while the percentage of $CD8^+$ cells was significantly decreased (Wu R. S. et al. (2015); Huang et al., 2021; Wu R. S. et al. (2015); Yang et al., 2017; T. Zhao et al., 2013). Moreover, clinical trials found that intraoperative continuous intravenous infusion of DEX in adults can significantly improve cellular immune function (Liang et al., 2012). Clinical studies also show that DEX can regulate the perioperative immune response of patients undergoing radical surgery for breast cancer, colon cancer and gastric cancer, which is beneficial to enhance the immune function of cancer patients and promote postoperative recovery. And the incidence of gastrointestinal reaction and postoperative cognitive dysfunction in the DEX group are significantly lower than those in the control group (Wang et al., 2015; Yang et al., 2017; Wang and Li, 2018). Related studies believe that DEX can maintain better perioperative cellular immune function, reduce cellular immune suppression and hematogenous metastasis, and play a role in postoperative immune protection. As for cytokines, Yang et al. (2017) considered that the concentrations of IFN-γ, IL-2, IL-10 and IL-6 in DEX group were significantly increased.

2.3.2.2 The Balance Among Th1, Th2, Th17 and Regulatory T Cells (Tregs)

The balance among T cell subsets is crucial for the homeostasis of the immune system and is a hot spot in current research (Zhao et al., 2013). The number of $CD4^+$ T cells accounts for 65% in peripheral blood. The previous studies on $CD4^+$ T cells are more detailed, and we will focus on this review. The Th0 cells is an initial $CD4^+$ T cell unstimulated by antigen and can differentiate into Th1, Th2, Th17, and Treg cells under different cytokine environments.

Th1 mainly secretes IL-2 and IFN-γ, activates T lymphocytes and macrophages, mediates cellular immune response, and reduces postoperative infection (Lee et al., 2018). It is also believed that the increased secretion of IL-2 and TNF-α can activate inflammatory responses, promote leukocyte adhesion,

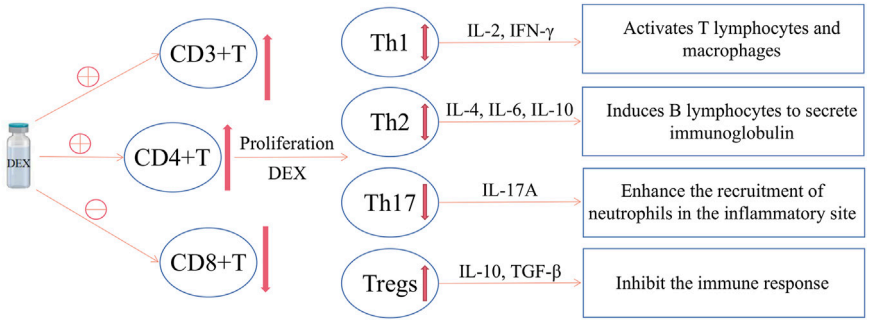

FIGURE 1 | The effect of DEX on T cells. DEX can increase $CD4^+$ T cells, decrease $CD8^+$ T cells, and increase the CD4+/CD8+ value; meanwhile, DEX can promote the differentiation of $CD4^+$ T cells into Tregs, reduce Th17 and the Th17/Tregs value; however, there is currently no consensus on the effect of DEX on Th1 and Th2.

and provide conditions for the further development of inflammation (Jeong et al., 2016; Elmoutaz Mahmoud and Rashwan, 2018). Th2 mainly secretes IL-4, IL-6 and IL-10, induces B lymphocytes to secrete immunoglobulin (Lee et al., 2018), promotes humoral or antibody mediated immunity, and suppresses cell-mediated immune responses (Kurosawa and Kato, 2008; Webster and Galley, 2009). At present, IFN-γ, IL-2 and IL-4 are the main indicators that reflect the balance of Th1 and Th2. However, the effect of DEX on the balance of T cell subsets (Th1/Th2) is controversial.

From the results of the meta-analysis, Wang Y. et al. (2019) belived that DEX increased the ratio of Th1/Th2. Besides, in patients undergoing laparoscopic cholecystectomy, the ratio of IFN -γ/IL-4 and Th1/Th2 cytokines in DEX group were higher than that in control group. In breast cancer patients, the levels of IL-2 and IFN-γ secreted by Th1 in DEX group increased, while the level of IL-4 secreted by Th2 did not change much, indicating that DEX can inhibit the transformation of Th1 to Th2 (Cardinale et al., 2011). DEX attenuates Th2 polarization, maintains a relatively stable balance of Th1/Th2, and reduces surgical stimulation and inflammatory response. Therefore, DEX can maintain the immune balance of the patient population and protect the cellular immune function of the patient (Wang et al., 2015). These findings suggest that DEX may increase the Th1/Th2 ratio, thus playing an immunomodulatory role in patients under stress from surgery and anesthesia (Song et al., 2014).

The above research believes that DEX can shift the balance to Th1, but the following research believes that DEX is more inclined to Th2. Inada et al. (2005) found that DEX reduced the Th1/Th2 ratio, leading to a shift towards Th2. DEX combined with spinal anesthesia could promote the mRNA expression and protein secretion of IL-4 and IL-10 in female patients and newborns after cesarean section, while the mRNA expression and protein secretion of TNF-α and IL-2 in the DEX combined with spinal anesthesia group were significantly lower than that in the control group. Although cesarean section may affect the levels of IL-2 and IL-4, but it turns out that there is no significant difference compared with normal delivery. Therefore, DEX combined with intraspinal anesthesia can reduce the adverse reactions of puerpera after cesarean section, and promote the transformation of Th1 cytokines to Th2 cytokines (Shi and Zhang, 2019). In the anesthesia of patients with colon cancer radical operation, the indexes of Th1 and Th1/Th2 in DEX group were lower than that in the control group, which promoted the transformation of Th1 cytokines to Th2 cytokines, and DEX can significantly inhibit the activation of NF-κB, soluble intercellular adhesion molecule-1 (sICAM-1), IL-8 and IL-6 caused by anesthesia (Wang and Li, 2018). However, it was also found that the ratio of Th1/Th2 in DEX group did not change significantly during anesthesia in healthy patients (Kallioinen et al., 2019).

Th17 cells are another recently discovered helper T cell that differentiates under the stimulation of IL-6 and IL-23. The Th17 secrete IL-17A, which has obvious pro-inflammatory effect (Song et al., 2014), and can enhance the recruitment of neutrophils in the inflammatory site (Zhang et al., 2018a). IL-17A is considered to coordinate the local immune response and host defense against foreign pathogens in the autoimmune system. Regulatory T cells (Tregs) are a subset of T cells that can inhibit the immune response of cancer patients, and closely related to the occurrence of autoimmune diseases. Their abnormal expression can lead to autoimmune diseases, in which IL-17 and IL-10 are the main indicators of Th17 and Tregs, respectively. Moreover, the Th17/Tregs ratio has been reported to play an important role in immune regulation (Park et al., 2005; Singh et al., 2007; Guo et al., 2010; ChangHee and Chen, 2011; Zhang et al., 2011; Gu et al., 2013).

Similarly, there are different opinions about the effect of DEX on the balance of Th17 and Tregs. In patients undergoing radical resection of colon cancer, the number of Tregs in the DEX group was higher than that in the control group, indicating that DEX can promote the transformation of primitive T cells into Tregs (Wang and Li, 2018). However, in laparoscopic cholecystectomy anesthesia, DEX is associated with the decrease of Tregs cytokines IL-4 and IL-10 and can dose-dependently modulate the inflammatory response (Lee et al., 2018). In the mouse model, Song et al. (2020) deemed that DEX could inhibit IL-17A storm induced by acute lung injury to a certain extent, and could significantly reduce the amount of proinflammatory cytokines in bronchoalveolar lavage fluid (BALF).

In general, DEX can regulate the balance of Th1, Th2, Th17 and Tregs, and it can not only inhibit inflammation, but also

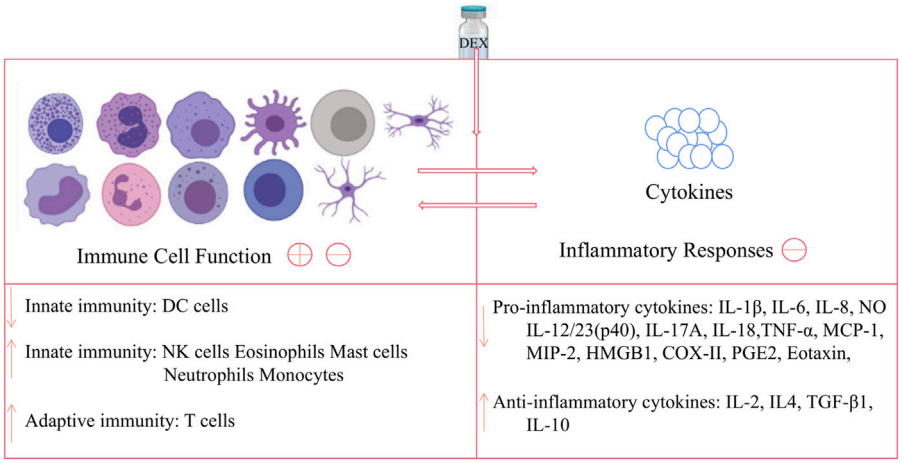

FIGURE 2 | Effects of DEX on immune cell and inflammatory cytokines. DEX can act on DC cells to down-regulate innate immune function, while acting on NK cells, eosinophils, mast cells, neutrophils and monocytes to up-regulate this function; and DEX has no obvious effect on B cells, but can act on T cells upregulate adaptive immunity; meanwhile, DEX can down-regulate pro-inflammatory cytokines and up-regulate anti-inflammatory factors, thereby inhibiting the inflammatory response. Note: The image of the cells in the figure is from https://biorender.com/.

alleviate immunosuppression, so it has strong immunomodulatory effect and better clinical therapeutic effect (Song et al., 2020).

2.3.2.3 Brief Summary

The possible reasons for DEX to improve cellular immunity are as follows: 1) DEX can selectively activate α_2-AR in central and peripheral nervous system, reduce sympathetic activity and serum catecholamine concentration, and further alleviate surgical stress and its coupled immunosuppression (Xu and Wang, 2003); 2) DEX reduces perioperative opioid use and thus reduces the immunosuppressive effects of opioids (Kallioinen et al., 2019); 3) DEX has a certain analgesic effect, and application before surgical trauma stress can prevent the sensitization of the central and peripheral nerves, reduce the pain caused by traumatic stimulation, achieve preemptive analgesia, and enhance the body's immune function (Wu R. S. et al., 2015); 4) DEX has anti-inflammatory and organ protective effects on ischemia and hypoxia injury, thereby maintaining body homeostasis and helping to improve immunity (Wang et al., 2015; Ma et al., 2017). In the future, we will need to study these potential mechanisms at the cellular and molecular levels, analyze immune cells, and detect the mRNA expression levels of transcription factors and chemokines (Huang et al., 2021).

In fact, T cells are mainly divided into T helper cells ($CD4^+$ cells), cytotoxic T cells ($CD8^+$ cells), memory T cells ($CD4^+$ or $CD8^+$ with antigenicity), Tregs, natural killer T cells (NKT cells) and δγ T cells (Chaplin, 2010). However, at present, studies mainly focus on the effect of DEX on the amount of $CD3^+$, CD4 +, $CD8^+$ and the ratio of CD4+/CD8+. The effects of DEX on memory T, NKT and δγ T cells are not involved at present, and there are few studies on molecular level, which may become the direction of future research. **Figure 1** summarizes the effects of DEX on T cells.

2.4 DEX and Cancer

DEX can improve the coagulation and immune function of patients with colon cancer, and the CD4+/CD8+ of the DEX group after surgery is higher than that of the control group (Zhao and Li, 2020). DEX can reduce the immunosuppression of patients with oral cancer by increasing the percentage of $CD3^+$, $CD4^+$, DCs and CD4+/CD8+ ratio (Huang L et al., 2021). DEX can effectively inhibit the activation of IGF2 signal pathway, improve the immune function of ovarian cancer rats, inhibit the invasion and migration of ovarian cancer cells, and significantly increase the percentage of $CD4^+$, $CD8^+$ and the ratio of CD4+/CD8+ (Tian et al., 2019). The DEX infusion may improve the surgical outcomes of ovarian cancer by inhibiting the surgical stress response and the release of stress mediators (Shin et al., 2021). $CD3^+$ T cells and CD4+/CD8+ in DEX group were significantly higher than that in the control group, which could reduce the perioperative inflammatory response and improve the cellular immune function of patients undergoing thoracoscopic radical resection of lung cancer (Kong and Lu, 2018; Zong et al., 2021). DEX may inhibit p38MAPK/NF-κB signaling pathway to enhance the immune function of ovarian cancer rats (Cai et al., 2017). DEX can alleviate the immunosuppression caused by circulatory fluctuation in patients with gastric cancer (Zheng et al., 2020). The levels of IFN-γ and IL-10 in the DEX group were lower than those in the control group, and the percentage of CD4+/CD8+ cells was higher than that in the control group, which reduced the perioperative stress response of rectal cancer patients and protected the cellular immune function (Zhang et al., 2018b). DEX can effectively alleviate the release of inflammatory factors in patients undergoing radical gastrectomy for gastric cancer, possibly by down-regulating the activation of NF-κB. In addition, DEX can also regulate the reduction of $CD3^+$ and $CD4^+$ subsets, so as to improve the impaired immune function (Dong et al., 2017). It also reduces the severity of early postoperative pain and

opioid consumption in patients with uterine cancer (Cho et al., 2021). Continuous intravenous infusion of DEX during general anesthesia can effectively inhibit the perioperative stress response of children with brain tumors and reduce cellular immune suppression (Wu L et al., 2015). All in all, the current evidence shows that DEX can reduce immunosuppression in tumor patients, which may have certain significance in limiting tumor spread and invasion. Of course, the current studies has the problem of insufficient sample size, or most of the studies are based on animal experiments, so high-quality clinical randomized controlled studies in the future are necessary to demonstrate this conclusion.

2.5 DEX and Clonidine

Studies have shown that under acute inflammatory conditions, α_2-AR agonist drugs can regulate the inflammatory process and immune pathways, of which receptor-mediated action is one of the important mechanisms (Flanders et al., 2019). Compared with clonidine, DEX has 8-fold higher affinity for α_2-AR (Bhana et al., 2000). It was found that clonidine and DEX at relevant concentrations did not affect the chemotaxis, phagocytosis or superoxide production of human neutrophils. These findings indicate that when used in patients with infection, sepsis, or systemic inflammation, the type of α_2-AR agonist is not the focus of attention (Nishina et al., 1999). A trial with no risk of bias compared DEX to clonidine found that target sedation was achieved in more patients treated with DEX and less need for additional sedation. Evidence on the use of clonidine in the intensive care unit (ICU) is very limited. DEX can effectively reduce the hospitalization time and extubation time of patients in ICU (Cruickshank et al., 2016). Unlike those reported in rodents, clonidine and DEX do not directly inhibit cytokine release from human lung macrophages (Piazza et al., 2016). In short, DEX and clonidine, which are also α_2-AR, have very few comparative studies on their effects on immune cells, and this may be a future research direction.

3 CONCLUSION AND PERSPECTIVES

The adrenergic signaling pathway has an immunomodulatory effect and has been extensively studied (Sharma and Farrar, 2020). As a highly selective agonist of α_2-AR, DEX plays an important role in the inflammatory immune system, and this new direction has also triggered a series of studies on DEX in clinical diseases.

The article reviews the novel functions of DEX from the aspects of immune cells and related diseases. In general, DEX has double effects on innate immune response: on the one hand, it suppresses DCs function to play an immunosuppressive role; on the other hand, it promotes M2 polarization of macrophages, neutrophils clearance and enhance the amount of NKs to adjust immune function and play an anti-inflammatory role. In adaptive immune responses, DEX has little effect on the humoral response of B cells, but it can enhance cellular immunity by regulating the differentiation, number and proportion of T cell subtypes. And, the overall effect of DEX on immune cell function and inflammatory cytokines is shown in **Figure 2**. Furthermore, DEX can alleviate neuroinflammation and has a good therapeutic effect on autoimmune diseases, such as RA, osteoarthritis, tooth inflammation and colitis.

However, there are a lot of controversies at present. Some studies hold that DEX can inhibit the function of DCs *in vitro*, but some consider that it can increase the number of DCs in cancer patients to enhance immune function in clinical trials; besides, some think that DEX can increase the number of B cells, while others argue that it has little effect; and there are different opinions on the direction in which DEX modulates the balance of Th1/Th2 and Th17/Treg; similarly, there are different opinions on the mechanism of the new effect of DEX.

The reasons for the different results may be as follows: 1) due to the long-term use of DEX in some studies, the sensitivity of α_2-AR may be down regulated, resulting in different results (Banati et al.,1993; Peng et al., 2013); 2) at present, the research on immune cells and inflammatory molecules is not thorough enough, and they may play different roles in different conditions; 3) the DEX may also play a role through other receptors and other mechanisms in different pathological conditions (Guo et al., 2018); 4) the dose was more than the clinical use *in vitro* studies; 5) studies on the effects of DEX on immunity and inflammation mostly focuses on monocytes/macrophages, microglia and T cells, and other immune cells are less involved, so it is normal for controversies to arise; 6) the research objects may be different, some are healthy, some are under the condition of illness; 7) it may be inaccurate to estimate the balance of T cells by measuring plasma cytokine concentration, because all IFN-γ and IL-4 in plasma are not only from Th1 and Th2 cells (Meng et al.,2020); 8) in addition, since most studies on the effect of DEX on immune responses are conducted in a clinical environment, patients have received various drug combinations, and some confounding factors may affect the results; 9) the time of sample collection and detection may be different, some may only detect the immediate reaction after medication, ignoring the results after 1–3 days (Lorton and Bellinger Denise, 2015).

The mechanism of DEX regulating immune cells and inflammatory mediators currently discovered includes: 1) DEX can active α_2-AR on the immune cells membrane in the center and periphery, thereby regulating the expression of related inflammatory mediators; 2) DEX can directly or indirectly regulate the release of sympathetic neurotransmitters; 3) DEX has the direct anti-inflammatory effect, reduces the expression of pro-inflammatory mediators and increases the level of anti-inflammatory mediators; 4) DEX can promote natural sleep (Wu et al., 2016), which protects the body immune function, restores body energy and repairs the potential organ damage in the body (Besedovsky et al., 2012; Irwin and Opp, 2017; Joshua, 2021); 5) DEX can regulate M1/M2 polarization of macrophage and the balance among Th1, Th2, Th17 and Tregs; 6) DEX has a certain analgesic effect and helps to regulate the neuroendocrine immune network; 7) DEX reduces the release of pro-inflammatory factors through the TLR4-NF-κB-MAPK signaling pathway and the cholinergic anti-inflammatory pathway; 8) DEX exerts central anti-inflammatory effect by

down regulating the expression of MCP-1; 9) DEX pretreatment can inhibit the expression of HMGB1, which is well known as a mediator of late inflammation, and it is also an early mediator of aseptic inflammation.

In the future, the role of DEX in different inflammatory and immune conditions, such as atherosclerosis and pulmonary infection, should be considered. DEX can significantly reduce the expression of MCP-1 (Wang et al., 2020), which plays an important role in the occurrence and development of RA, atherosclerosis, coronary heart disease and other inflammatory diseases (Deshmane et al., 2009; Xia and Sui, 2009). Also, DEX can enhance the expression of sirtuin-1 (SIRT1), which has been expected to become a new target for the treatment of cardiovascular diseases (Prola et al., 2017). Similarly, DEX can reduce the expression of VCAM-1 receptor integrin-4 (VLA-4) and lymphocyte associated molecule-1 (LFA-1), which is a good news for patients with atherosclerosis, long-term bedridden and undergoing major surgery. Also, DEX can up adjust PPARγ, which is the key to control the synthesis of pro-inflammatory cytokines, immunosuppression and cancer development (Wu et al., 2012). Moreover, DEX can down regulate HMGB1 in macrophages, which is an important inflammatory mediator in the late stage of sepsis and plays an important role in the pathogenesis of sepsis, tumor, arthritis and other inflammatory diseases (Andersson et al., 2018). Besides, DEX can enhance cellular immune response, so we can focus on its role in enhancing anti-tumor immunity.

All in all, we reviewed the anti-inflammatory and immunomodulatory mechanisms of DEX, comprehensively summarized the effects of DEX on immune cell function and inflammatory molecules, and also explained the role of α_2-AR in the immune system, which provides a theoretical background for the application of DEX in immune-inflammatory related diseases.

AUTHOR CONTRIBUTIONS

All authors listed have made a substantial, direct, and intellectual contribution to the work and approved it for publication. Among them, RC and YS wrote the first draft; JL conducted literature search and data extraction; XD and MD designed the tables and completed the drawings; SS polished the language of the manuscript and revised the content of the manuscript; and YL is the initiator of this project and the coordinator of the research team.

FUNDING

This study was supported by the Wu Jieping Medical Foundation (No. 320.6750.2020-21-12) and the Education Reform Funding (No. 02.03.2019.15-15). The sponsor will not be involved in study design; collection, management, analysis, or interpretation of data; writing of the report; or the decision to submit the report for publication.

REFERENCES

Alboni, S., Cervia, D., Sugama, S., and Conti, B. (2010). Interleukin 18 in the CNS. *J. Neuroinflammation.* 7, 9. doi:10.1186/1742-2094-7-9

Anderson, C. D., Lindgren, B. R., and Andersson, R. G. (1987). Effects of Clonidine on the Dermal Inflammatory Cell Response of Experimental Toxic and Allergic Contact Reactions and Intradermal Hypersensitivity. *Int. Arch. Allergy Appl. Immunol.* 83, 371–376. doi:10.1159/000234371

Andersson, U., Yang, H., and Harris, H. (2018). Extracellular HMGB1 as a Therapeutic Target in Inflammatory Diseases. *Expert Opin. Ther. Targets* 22, 263–277. doi:10.1080/14728222.2018.1439924

Barbera-Guillem, E., Nelson, M. B., Barr, B., Nyhus, J. K., May, K. F., Feng, L., et al. (2000). B Lymphocyte Pathology in Human Colorectal Cancer. Experimental and Clinical Therapeutic Effects of Partial B Cell Depletion. *Cancer Immunol. Immunother.* 48 (10), 541–549. doi:10.1007/PL00006672

Berkowitz, D. E., Price, D. T., Bello, E. A., Page, S. O., and Schwinn, D. A. (1994). Localization of Messenger RNA for Three Distinct Alpha 2-adrenergic Receptor Subtypes in Human Tissues. Evidence for Species Heterogeneity and Implications for Human Pharmacology. *Anesthesiology* 81, 1235–1244. doi:10.1097/00000542-199411000-00018

Besedovsky, L., Lange, T., and Born, J. (2012). Sleep and Immune Function. *Pflugers. Arch.* 463, 121–137. doi:10.1007/s00424-011-1044-0

Bhana, N., Goa, K. L., and McClellan, K. J. (2000). Dexmedetomidine. *Drugs.* 59, 263–268. doi:10.2165/00003495-200059020-00012

Brady, J., Carotta, S., Thong, R. P., Chan, C. J., Hayakawa, Y., Smyth, M. J., et al. (2010). The Interactions of Multiple Cytokines Control NK Cell Maturation. *J. Immunol.* 185, 6679–6688. doi:10.4049/jimmunol.0903354

Cai, Q. H., Tang, Y., Fan, S. H., Zhang, Z. F., Li, H., Huang, S. Q., et al. (2017). *In Vivo* effects of Dexmedetomidine on Immune Function and Tumor Growth in Rats with Ovarian Cancer through Inhibiting the p38MAPK/NF-□b Signaling Pathway. *Biomed. Pharmacother.* 95, 1830–1837. doi:10.1016/j.biopha.2017.09.086

Cardinale, F., Chinellato, I., Caimmi, S., Peroni, D. G., Franceschini, F., Miraglia Del Giudice, M., et al. (2011). Perioperative Period: Immunological Modifications. *Int. J. Immunopathol Pharmacol.* 24 (Suppl. 3), S3–S12. doi:10.1177/03946320110240s302

Chai, Y., Cao, Z., Yu, R., Liu, Y., Yuan, D., and Lei, L. (2020). Dexmedetomidine Attenuates LPS-Induced Monocyte-Endothelial Adherence via Inhibiting Cx43/PKC-/NOX2/ROS Signaling Pathway in Monocytes. *Oxid. Med. Cell. Longev.* 2020, 2930463. doi:10.1155/2020/2930463

Chang, S. H., and Chen, D. (2011). Signaling of Interleukin-17 Family Cytokines in Immunity and Inflammation. *Cell. Signal.* 23, 1069–1075. doi:10.1016/j.cellsig.2010.11.022

Chang., Y., Huang., X., Liu., Z., Han., G., Huang., L., Xiong., Y-C., et al. (2013). Dexmedetomidine Inhibits the Secretion of High Mobility Group Box 1 from Lipopolysaccharide-Activated Macrophages *In Vitro*. *J. Surg. Res.* 181, 308–314. doi:10.1016/j.jss.2012.07.017

Chaplin, D. D. (2010). Overview of the Immune Response. *J. Allergy Clin. Immunol.* 125, S3–S23. doi:10.1016/j.jaci.2009.12.980

Chen, G., Le, Y., Zhou, L., Gong, L., Li, X., Li, Y., et al. (2016). Dexmedetomidine Inhibits Maturation and Function of Human Cord Blood-Derived Dendritic Cells by Interfering with Synthesis and Secretion of IL-12 and IL-23. *Plos. One.* 11 (4), e0153288. doi:10.1371/journal.pone.0153288

Chen, S. L., Zhou, W., and Hua, F. Z. (2016). *In Vitro* effect of Dexmedetomidine on the Respiratory Burst of Neutrophils. *Genet. Mol. Res.* 15 (2). doi:10.4238/gmr.15028069

Cheng., S. S., Lukacs., N. W., and Kunkel, S. L. (2002). Eotaxin/CCL11 Is a Negative Regulator of Neutrophil Recruitment in a Murine Model of Endotoxemia. *Exp. Mol. Pathol.* 73, 1–8. doi:10.1006/exmp.2002.2439

Cho, J. S., Seon, K., Kim, M. Y., Kim, S. W., and Yoo, Y. C. (2021). Effects of Perioperative Dexmedetomidine on Immunomodulation in Uterine Cancer Surgery: A Randomized, Controlled Trial. *Front. Oncol.* 11, 749003. doi:10.3389/fonc.2021.749003

Cowburn, A. S., Condliffe, A. M., Farahi, N., Summers, C., and Chilvers, E. R. (2008). Advances in Neutrophil Biology: Clinical Implications. *Chest* 134, 606–612. doi:10.1378/chest.08-0422

Cruickshank, M., Henderson, L., MacLennan, G., Fraser, C., Campbell, M., Blackwood, B., et al. (2016). Alpha-2 Agonists for Sedation of Mechanically Ventilated Adults in Intensive Care Units: a Systematic Review. *Health Technol. Assess.* 20 (25), 1–117. doi:10.3310/hta20250)

Dahl, R. (1991). The Eosinophil. *Allerg Immunol. (Paris)* 23, 429–431.

Deshmane, S. L., Kremlev, S., Amini, S., and Sawaya, B. E. (2009). Monocyte Chemoattractant Protein-1 (MCP-1): an Overview. *J. Interferon. Cytokine Res.* 29, 313–326. doi:10.1089/jir.2008.0027

Dong, W., Chen, M. H., Yang, Y. H., Zhang, X., Huang, M. J., Yang, X. J., et al. (2017). The Effect of Dexmedetomidine on Expressions of Inflammatory Factors in Patients with Radical Resection of Gastric Cancer. *Eur. Rev. Med. Pharmacol. Sci.* 21 (15), 3510–3515.

Elmoutaz Mahmoud., H., and Rashwan, D. A. E. (2018). Efficacy of Dexmedetomidine versus Ketofol for Sedation of Postoperative Mechanically Ventilated Patients with Obstructive Sleep Apnea. *Crit. Care Res. Pract.* 2018, 1015054. doi:10.1155/2018/1015054

Ferreira, J. A., and Bissell Brittany., D. (2018). Misdirected Sympathy: The Role of Sympatholysis in Sepsis and Septic Shock. *J. Intensive Care Med.* 33, 74–86. doi:10.1177/0885066616689548

Flanders, C. A., Rocke, A. S., Edwardson, S. A., Baillie, J. K., and Walsh, T. S. (2019). The Effect of Dexmedetomidine and Clonidine on the Inflammatory Response in Critical Illness: a Systematic Review of Animal and Human Studies. *Crit. Care* 23 (1), 402. doi:10.1186/s13054-019-2690-4

García, J. J., Carmen Sáez, M., De la. Fuente, M., and Ortega, E. (2003). Regulation of Phagocytic Process of Macrophages by Noradrenaline and its End Metabolite 4-Hydroxy-3-Metoxyphenyl-Glycol. Role of Alpha- and Beta-Adrenoreceptors. *Mol. Cell. Biochem.* 254, 299–304.

Gu, C., Wu, L., and Li, X. (2013). IL-17 Family: Cytokines, Receptors and Signaling. *Cytokine.* 64, 477–485. doi:10.1016/j.cyto.2013.07.022

Guo, N. H., Shi, Q. Z., Hua, J. Y., Li, Z. J., Li, J., He, W. F., et al. (2010). Expression of Regulatory T Cells and Th17 Cells in Idiopathic Thrombocytopenic Purpura and its Significance. *Zhonghua Xue Ye. Xue Za Zhi* 31, 610–612.

Guo., F., Ding., Y., Xue, Y., and Cai., X. (2018). Effect of Dexmedetomidine, Midazolam, and Propofol on Lipopolysaccharide-Stimulated Dendritic Cells. *Exp. Ther. Med.* 15, 5487–5494. doi:10.3892/etm.2018.6094

Huang, L., Qin, C., Wang, L., Zhang, T., and Li, J. (2021). Effects of Dexmedetomidine on Immune Response in Patients Undergoing Radical and Reconstructive Surgery for Oral Cancer. *Oncol. Lett.* 21 (2), 106. doi:10.3892/ol.2020.12367

Inada, T., Shirane, A., Hamano, N., Yamada, M., Kambara, T., and Shingu, K. (2005). Effect of Subhypnotic Doses of Dexmedetomidine on Antitumor Immunity in Mice. *Immunopharmacol. Immunotoxicol.* 27, 357–369. doi:10.1080/08923970500240883

Irwin, M. R., and Opp, M. R. (2017). Sleep Health: Reciprocal Regulation of Sleep and Innate Immunity. *Neuropsychopharmacology* 42, 129–155. doi:10.1038/npp.2016.148

Jeong, S. I., Shin, J. A., ChoSKim, H. W., Lee, J. Y., Kang, J. L., et al. (2016). Resveratrol Attenuates Peripheral and Brain Inflammation and Reduces Ischemic Brain Injury in Aged Female Mice. *Neurobiol. Aging* 44, 7484. doi:10.1016/j.neurobiolaging.2016.04.007

Joshua, E. (2021). *Physiology of Sleep*. Treasure Island (FL): StatPearls Publishing.

Kalbach, N., Schaller, A., Rosene, A., Farley, L., Zani, K., and Saini, A. (2019). 1230: Dexmedetomidine to Facilitate Respiratory Support in Pediatric Severe Asthma. *Crit. Care Med.* 47 (1), 591. doi:10.1097/01.ccm.0000551974.08011.2a

Kallioinen, M., Scheinin, A., Maksimow, M., Långsjö, J., Kaisti, K., Takala, R., et al. (2019). The Influence of Dexmedetomidine and Propofol on Circulating Cytokine Levels in Healthy Subjects. *BMC. Anesthesiol.* 19, 222. doi:10.1186/s12871-019-0895-3

Kang, B. Y., Won, L. S., and Sung, K. T. (2003). Stimulation of Interleukin-12 Production in Mouse Macrophages via Activation of P38 Mitogen-Activated Protein Kinase by Alpha2-Adrenoceptor Agonists. *Eur. J. Pharmacol.* 467, 223–231. doi:10.1016/s0014-2999(03)01628-5

Kantari, C., Pederzoli-Ribeil, M., and Witko-Sarsat, V. (2008). The Role of Neutrophils and Monocytes in Innate Immunity. *Contrib. Microbiol.* 15, 118–146.

Keating, G. M. (2015). Dexmedetomidine: A Review of its Use for Sedation in the Intensive Care Setting. *Drugs* 75, 1119–1130. doi:10.1007/s40265-015-0419-5

Kennelly, R., Conneely, J. B., Bouchier-Hayes, D., and Winter, D. C. (2011). Mast Cells in Tissue Healing: from Skin to the Gastrointestinal Tract. *Curr. Pharm. Des.* 17, 3772–3775. doi:10.2174/138161211798357854

Kong, L., and Lu, X. H. (2018). Effect of Dexmedetomidine on Perioperative Inflammatory Response and Cellular Immune in Patients Undergoing Radical Operation of Thoracoscopic Lung Cancer. *Zhonghua Yi Xue Za Zhi* 98 (36), 2929–2932. doi:10.3760/cma.j.issn.0376-2491.2018.36.011

Kurosawa, S., and Kato, M. (2008). Anesthetics, Immune Cells, and Immune Responses. *J. Anesth.* 22, 263–277. doi:10.1007/s00540-008-0626-2

Lai, Y. C., Tsai, P. S., and Huang, C. J. (2009). Effects of Ddemedetomidine on Regulating Endotoxin-Induced Up-Regulation of Inflammatory Molecules in Murine Macrophages. *J. Surg. Res.* 154, 212. doi:10.1016/j.jss.2008.07.010

Lavand'homme, P. M., and Eisenach, J. C. (2003). Perioperative Administration of the Alpha2-Adrenoceptor Agonist Clonidine at the Site of Nerve Injury Reduces the Development of Mechanical Hypersensitivity and Modulates Local Cytokine Expression. *Pain* 105, 247–254. doi:10.1016/s0304-3959(03)00221-5

Lavand'homme, P. M., Ma, W., De Kock, M., and Eisenach, J. C. (2002). Perineural alpha(2A)-Adrenoceptor Activation Inhibits Spinal Cord Neuroplasticity and Tactile Allodynia after Nerve Injury. *Anesthesiology* 97, 972–980. doi:10.1097/00000542-200210000-00033

Lee, J. M., Han, H. J., Choi, W. K., Yoo, S., Baek, S., and Lee, J. (2018). Immunomodulatory Effects of Intraoperative Dexmedetomidine on T Helper 1, T Helper 2, T Helper 17 and Regulatory T Cells Cytokine Levels and Their Balance: a Prospective, Randomised, Double-Blind, Dose-Response Clinical Study. *BMC. Anesthesiol.* 18 (1), 164. doi:10.1186/s12871-018-0625-2

Li, L. C., Tian, Y., Xiao, J., Yang, Y., Wu, J. N., Chen, Y., et al. (2021). Dexmedetomidine Promotes Inflammation Resolving through TGF-B1 Secreted by F4/80Ly6G Macrophage. *Int. Immunopharmacol.* 95, 107480. doi:10.1016/j.intimp.2021.107480

Li, Y., Wang, B., Zhang, L. L., He, S. F., Hu, X. W., Wong, G. T., et al. (2016). Dexmedetomidine Combined with General Anesthesia Provides Similar Intraoperative Stress Response Reduction when Compared with a Combined General and Epidural Anesthetic Technique. *Anesth. Analg.* 122, 1202–1210. doi:10.1213/ANE.0000000000001165

Liang, Y., Liu, H. Z., Wang, H. B., Wen, X. J., Zhou, Q. L., and Xu, F. (2012). Effects of Dexmedetomidine on Perioperative Cellular Immune Function and Micrometastasis in Blood Circulation in Patients Undergoing Radical Operation for colon Cancer. *Chin. J. Anesthesiology.* 32, 1165–1168.

Lindgren, B. R., Grundström, N., and Andersson, R. G. (1987). Comparison of the Effects of Clonidine and Guanfacine on the Histamine Liberation from Human Mast Cells and Basophils and on the Human Bronchial Smooth Muscle Activity. *Arzneimittelforschung* 37, 551–553.

Liu, Y., Liu, W., Wang, X., Wan, Z., Liu, Y., and Leng, Y. (2018). Dexmedetomidine Relieves Acute Inflammatory Visceral Pain in Rats through the ERK Pathway, Toll-like Receptor Signaling, and TRPV1 Channel. *J. Mol. Neurosci.* 66, 279–290. doi:10.1007/s12031-018-1172-5

Lorton, D., and Bellinger Denise., L. (2015). Molecular Mechanisms Underlying β-adrenergic Receptor-Mediated Cross-Talk between Sympathetic Neurons and Immune Cells. *Int. J. Mol. Sci.* 16, 5635–5665. doi:10.3390/ijms16035635

Ma, X. D., Li, B. P., Wang, D. L., and Yang, W. S. (2017). Postoperative Benefits of Dexmedetomidine Combined with Flurbiprofen Axetil after Thyroid Surgery. *Exp. Ther. Med.* 14, 2148–2152. doi:10.3892/etm.2017.4717

MacMicking, J., Xie, Q. W., and Nathan, C. (1997). Nitric Oxide and Macrophage Function. *Annu. Rev. Immunol.* 15, 323–350. doi:10.1146/annurev.immunol.15.1.323

Martinez Fernando., O., and Gordon, S. (2014). The M1 and M2 Paradigm of Macrophage Activation: Time for Reassessment. *F1000prime Rep.* 6, 13. doi:10.12703/P6-13

Matsumoto, Y. (2009). Park Il-Kwon., Kohyama KunikoMatrix Metalloproteinase (MMP)-9, but Not MMP-2, Is Involved in the Development and Progression of C Protein-Induced Myocarditis and Subsequent Dilated Cardiomyopathy. *J. Immunol.* 183, 4773–4781. doi:10.4049/jimmunol.0900871

Mikawa, K., Akamatsu, H., Nishina, K., Shiga, M., Maekawa, N., Obara, H., et al. (1998). Propofol Inhibits Human Neutrophil Functions. *Anesth. Analg.* 87, 695–700. doi:10.1097/00000539-199809000-00039

Miles, B. A., Lafuse, W. P., and Zwilling, B. S. (1996). Binding of Alpha-Adrenergic Receptors Stimulates the Anti-mycobacterial Activity of Murine Peritoneal

Macrophages. *J. Neuroimmunol.* 71, 19–24. doi:10.1016/s0165-5728(96)00113-0

Monneret, G., Lepape, A., Voirin, N., Bohé, J., Venet, F., Debard, A. L., et al. (2006). Persisting Low Monocyte Human Leukocyte Antigen-DR Expression Predicts Mortality in Septic Shock. *Intensive Care Med.* 32, 1175–1183. doi:10.1007/s00134-006-0204-8

Nishina, K., Akamatsu, H., Mikawa, K., Shiga, M., Maekawa, N., Obara, H., et al. (1998). The Inhibitory Effects of Thiopental, Midazolam, and Ketamine on Human Neutrophil Functions. *Anesth. Analg.* 86, 159–165. doi:10.1097/00000539-199801000-00032

Nishina, K., Akamatsu, H., and Mikawa, K. (1999). The Effects of Clonidine and Dexmedetomidine on Human Neutrophil Functions. *Anesth. Analg.* 88, 452–458. doi:10.1097/00000539-199902000-00042

Ohmori, Y., and Hamilton, T. A. (1994). Regulation of Macrophage Gene Expression by T-Cell-Derived Lymphokines. *Pharmacol. Ther.* 63, 235–264. doi:10.1016/0163-7258(94)90026-4

Panosian, J. O., and Marinetti, G. V. (1983). Alpha 2-Adrenergic Receptors in Human Polymorphonuclear Leukocyte Membranes. *Biochem. Pharmacol.* 32, 2243–2247. doi:10.1016/0006-2952(83)90233-2

Park, H., Li, Z., Yang, X. O., Chang, S. H., Nurieva, R., Wang, Y. H., et al. (2005). A Distinct Lineage of CD4 T Cells Regulates Tissue Inflammation by Producing Interleukin 17. *Nat. Immunol.* 6, 1133–1141. doi:10.1038/ni1261

Piazza, O., Staiano, R. I., De Robertis., E., Conti, G., Di Crescenzo., V., Loffredo, S., et al. (2016). Effect of α2-Adrenergic Agonists and Antagonists on Cytokine Release from Human Lung Macrophages Cultured *In Vitro*. *Transl. Med. Unisa.* 15, 67–73.

Pilla, L., Squarcina, P., Coppa, J., Mazzaferro, V., Huber, V., Pende, D., et al. (2005). Natural Killer and NK-like T-Cell Activation in Colorectal Carcinoma Patients Treated with Autologous Tumor-Derived Heat Shock Protein 96. *Cancer Res.* 65, 3942–3949. doi:10.1158/0008-5472.CAN-04-3493

Prola, A., Pires, Da., Silva, J., Guilbert, A., Lecru, L., Piquereau, J., et al. (2017). SIRT1 Protects the Heart from ER Stress-Induced Cell Death through eIF2α Deacetylation. *Cell. Death Differ.* 24, 343–356. doi:10.1038/cdd.2016.138

Raffaghello, L., Bianchi, G., Bertolotto, M., Montecucco, F., Busca, A., Dallegri, F., et al. (2008). Human Mesenchymal Stem Cells Inhibit Neutrophil Apoptosis: a Model for Neutrophil Preservation in the Bone Marrow Niche. *Stem Cell* 26, 151–162. doi:10.1634/stemcells.2007-0416

Rezai, H. R. (1968). Immunity to Intracellular Bacteria. *Isr. J. Med. Sci.* 4, 315–318.

Ribeiro, M. C., Peruchetti, D. B., Silva, L. S., Silva-Filho, J. L., Souza, M. C., Henriques, M. D. G., et al. (2018). LPS Induces mTORC1 and mTORC2 Activation during Monocyte Adhesion. *Front. Mol. Biosci.* 5, 67. doi:10.3389/fmolb.2018.00067

Scanzano, A., and Marco., C. (2015). Adrenergic Regulation of Innate Immunity: a Review. *Front. Pharmacol.* 6, 171. doi:10.3389/fphar.2015.00171

Schmitt, F. C. F., Lipinski, A., Hofer, S., Uhle, F., Nusshag, C., Hackert, T., et al. (2020). Pulmonary Microbiome Patterns Correlate with the Course of the Disease in Patients with Sepsis-Induced ARDS Following Major Abdominal Surgery. *J. Hosp. Infect.* S0195-6701 (20), 30203–30206. doi:10.1016/j.jhin.2020.04.028

Sharma, D., and Farrar, J. D. (2020). Adrenergic Regulation of Immune Cell Function and Inflammation. *Semin. Immunopathol.* 42, 709–717. doi:10.1007/s00281-020-00829-6

Shi, W., and Zhang, P. (2019). Effect of Dexmedetomidine Combined with Lumbar Anesthesia on Th1/Th2 in Maternal Patients and Neonates Undergoing Caesarean Section. *Exp. Ther. Med.* 18 (2), 1426–1432. doi:10.3892/etm.2019.7648

Shin, S., Kim, K. J., Hwang, H. J., Noh, S., Oh, J. E., and Yoo, Y. C. (2021). Immunomodulatory Effects of Perioperative Dexmedetomidine in Ovarian Cancer: An *In Vitro* and Xenograft Mouse Model Study. *Front. Oncol.* 11, 722743. doi:10.3389/fonc.2021.722743

Sikorski, K., Chmielewski, S., Przybyl, L., Heemann, U., Wesoly, J., Baumann, M., et al. (2011). STAT1-mediated Signal Integration between IFNγ and LPS Leads to Increased EC and SMC Activation and Monocyte Adhesion. *Am. J. Physiol. Cell. Physiol.* 300 (6), C1337–C1344. doi:10.1152/ajpcell.00276.2010

Singh, R., Aggarwal, A., and Misra, R. (2007). Th1/Th17 Cytokine Profiles in Patients with Reactive Arthritis/undifferentiated Spondyloarthropathy. *J. Rheumatol.* 34, 2285–2290.

Song, Q., Lin, L., Chen, L., Cheng, L., and Zhong, W. (2020). Co-administration of N-Acetylcysteine and Dexmedetomidine Plays a Synergistic Effect on protection of LPS-Induced Acute Lung Injury via Correcting Th1/Th2/Th17 Cytokines Imbalance. *Clin. Exp. Pharmacol. Physiol.* 47, 294–301. doi:10.1111/1440-1681.13196

Song, X., Gao, H., and Qian, Y. (2014). Th17 Differentiation and Their Pro-inflammation Function. *Adv. Exp. Med. Biol.* 841, 99–151. doi:10.1007/978-94-017-9487-9_5

Stevenson, G. W., Hall, S. C., Rudnick, S., Seleny, F. L., and Stevenson, H. C. (1990). The Effect of Anesthetic Agents on the Human Immune Response. *Anesthesiology* 72, 542–552. doi:10.1097/00000542-199003000-00024

Sugimoto, M. A., Ribeiro, A. L. C., Costa, B. R. C., Vago, J. P., Lima, K. M., Carneiro, F. S., et al. (2017). Plasmin and Plasminogen Induce Macrophage Reprogramming and Regulate Key Steps of Inflammation Resolution via Annexin A1. *Blood* 129, 2896–2907. doi:10.1182/blood-2016-09-742825

Taniguchi, T., Kidani, Y., Kanakura, H., Takemoto, Y., and Yamamoto, K. (2004). Effects of Dexmedetomidine on Mortality Rate and Inflammatory Responses to Endotoxin-Induced Shock in Rats. *Crit. Care Med.* 32, 1322–1326. doi:10.1097/01.ccm.0000128579.84228.2a

Theoharides, T. C., Alysandratos, K. D., Angelidou, A., Delivanis, D. A., Sismanopoulos, N., Zhang, B., et al. (2012). Mast Cells and Inflammation. *Biochim. Biophys. Acta* 1822, 21–33. doi:10.1016/j.bbadis.2010.12.014

Tian, H., Hou, L., Xiong, Y., Cheng, Q., and Huang, J. (2019). Effect of Dexmedetomidine-Mediated Insulin-like Growth Factor 2 (IGF2) Signal Pathway on Immune Function and Invasion and Migration of Cancer Cells in Rats with Ovarian Cancer. *Med. Sci. Monit.* 25, 4655–4664. doi:10.12659/MSM.915503

Tippimanchai, D. D., Nolan, K., Poczobutt, J., Verzosa, G., Li, H., Scarborough, H., et al. (2018). Adenoviral Vectors Transduce Alveolar Macrophages in Lung Cancer Models. *Oncoimmunology* 7, e1438105. doi:10.1080/2162402X.2018.1438105

Tüfek, A., Kaya, S., Tokgöz, O., Firat, U., Evliyaoğlu, O., Çelik, F., et al. (2013). The Protective Effect of Dexmedetomidine on Bupivacaine-Induced Sciatic Nerve Inflammation Is Mediated by Mast Cells. *Clin. Invest. Med.* 36, E95–E102.

Ueshima, H., Inada, T., and Koh., S. (2013). Suppression of Phagosome Proteolysis and Matrigel Migration with the α_2-adrenergic Receptor Agonist Dexmedetomidine in Murine Dendritic Cells. *Immunopharmacol. Immunotoxicol.* 35, 558–566. doi:10.3109/08923973.2013.822509

Wang, C., Yuan, W., Hu, A., Lin, J., Xia, Z., Yang, C. F., et al. (2020). Dexmedetomidine Alleviated Sepsis-Induced Myocardial Ferroptosis and Septic Heart Injury. *Mol. Med. Rep.* 22, 175–184. doi:10.3892/mmr.2020.11114

Wang, K., Wu, M., Xu, J., Wu, C., Zhang, B., Wang, G., et al. (2019). Effects of Dexmedetomidine on Perioperative Stress, Inflammation, and Immune Function: Systematic Review and Meta-Analysis. *Br. J. Anaesth.* 123: 777–794. doi:10.1016/j.bja.2019.07.027

Wang, K., and Li, C. (2018). Effects of Dexmedetomidine on Inflammatory Factors, T Lymphocyte Subsets and Expression of NF-□b in Peripheral Blood Mononuclear Cells in Patients Receiving Radical Surgery of colon Carcinoma. *Oncol. Lett.* 15, 7153–7157. doi:10.3892/ol.2018.8205

Wang, Y., Mao, X., Chen, H., Feng, J., Yan, M., Wang, Y., et al. (2019). Dexmedetomidine Alleviates LPS-Induced Apoptosis and Inflammation in Macrophages by Eliminating Damaged Mitochondria via PINK1 Mediated Mitophagy. *Int. Immunopharmacol.* 73, 471–481. doi:10.1016/j.intimp.2019.05.027

Wang, Y., Xu, X., Liu, H., and Ji, F. (2015). Effects of Dexmedetomine on Patients Undergoing Radical Gastrectomy. *J. Surg. Res.* 194, 147–153. doi:10.1016/j.jss.2014.10.008

Webster, N. R., and Galley, H. F. (2009). Immunomodulation in the Critically Ill. *Br. J. Anaesth.* 103, 70–81. doi:10.1093/bja/aep128

Wilhelms, S. B., Walther, S. M., Sjöberg, F., and De Geer., L. (2020). Causes of Late Mortality Among ICU-Treated Patients with Sepsis. *Acta Anaesthesiol. Scand.* 64, 961–966. doi:10.1111/aas.13592

Wolf, A. M., Wolf, D., Steurer, M., Gastl, G., Gunsilius, E., and Grubeck-Loebenstein, B. (2003). Increase of Regulatory T Cells in the Peripheral Blood of Cancer Patients. *Clin. Cancer Res.* 9 (2), 606–612.

Wu, L., Lv, H., Luo, W., Jin, S., and Hang, Y. (2015). Effects of Dexmedetomidine on Cellular Immunity of Perioperative Period in Children with Brain Neoplasms. *Int. J. Clin. Exp. Med.* 8 (2), 2748–2753.

Wu, L., Yan, C., Czader, M., Foreman, O., Blum, J. S., Kapur, R., et al. (2012). Inhibition of PPARγ in Myeloid-Lineage Cells Induces Systemic Inflammation, Immunosuppression, and Tumorigenesis. *Blood* 119, 115–126. doi:10.1182/blood-2011-06-363093

Wu, P., Chen, J., Chen, J., Tao, J., Wu, S., Xu, G., et al. (2020). Trimethylamine N-Oxide Promotes apoE Mice Atherosclerosis by Inducing Vascular Endothelial Cell Pyroptosis via the SDHB/ROS Pathway. *J. Cell. Physiol.* 235, 6582–6591. doi:10.1002/jcp.29518

Wu, R. S., Wu, K. C., Huang, C. C., Chiang, Y. Y., Chen, C. C., Liao, C. L., et al. (2015). Different Cellular Responses of Dexmedetomidine at Infected Site and Peripheral Blood of Emdotoxemic BALB/c Mice. *Environ. Toxicol.* 30, 1416–1422. doi:10.1002/tox.22011

Wu, X. H., Cui, F., Zhang, C., Meng, Z. T., Wang, D. X., Ma, J., et al. (2016). Low-dose Dexmedetomidine Improves Sleep Quality Pattern in Elderly Patients after Noncardiac Surgery in the Intensive Care Unit: A Pilot Randomized Controlled Trial. *Anesthesiology* 125, 979–991. doi:10.1097/ALN.0000000000001325

Xia, M., and Sui, Z. (2009). Recent Developments in CCR2 Antagonists. *Expert Opin. Ther. Pat.* 19, 295–303. doi:10.1517/13543770902755129

Xu, H., and Wang, B. G. (2003). Advance in Researches about Operative Stress Responses. *Forei. Med. Sci. (Anesthesio Resus).* 24, 278–281.

Yang, C-L., Pei-Shan, T., and Huang, C-J. (2008). Effects of Dexmedetomidine on Regulating Pulmonary Inflammation in a Rat Model of Ventilator-Induced Lung Injury. *Acta Anaesthesiol. Taiwan.* 46, 151–159. doi:10.1016/S1875-4597(09)60002-3

Yang, X. H., Bai, Q., Lv, M. M., Fu, H. G., Dong, T. L., and Zhou, Z. (2017). Effect of Dexmedetomidine on Immune Function of Patients Undergoing Radical Mastectomy: a Double Blind and Placebo Control Study. *Eur. Rev. Med. Pharmacol. Sci.* 21 (5), 1112–1116.

Younan, G. J., Heit, Y. I., Dastouri, P., Kekhia, H., Xing, W., Gurish, M. F., et al. (2011). Mast Cells Are Required in the Proliferation and Remodeling Phases of Microdeformational Wound Therapy. *Plast. Reconstr. Surg.* 128, 649e–658e. doi:10.1097/PRS.0b013e318230c55d

Yuan, H. X., Chen, C. Y., Li, Y. Q., Ning, D. S., Li, Y., Chen, Y. T., et al. (2020). Circulating Extracellular Vesicles from Patients with Valvular Heart Disease Induce Neutrophil Chemotaxis via FOXO3a and the Inhibiting Role of Dexmedetomidine. *Am. J. Physiol. Endocrinol. Metab.* 319, E217–E231. doi:10.1152/ajpendo.00062.2020

Zhang, Y., Jin, L. J., Zhou, X., Liu, Y., Li, Y., and Wen, L. Y. (2018b). Effect of Dexmedetomidine on Stress Reactions and Cellular Immune Function of Patients in Perioperative Period Following Radial Resection for Rectal Carcinoma. *J. Biol. Regul. Homeost. Agents* 32 (1), 139–145.

Zhang, Y., Jia, S., Gao, T., Zhang, R., Liu, Z., and Wang, Y. (2018a). Dexmedetomidine Mitigate Acute Lung Injury by Inhibiting IL-17-induced Inflammatory Reaction. *Immunobiology* 223, 32–37. doi:10.1016/j.imbio.2017.10.017

Zhang, Y., Ma, D., Zhang, Y., Tian, Y., Wang, X., Qiao, Y., et al. (2011). The Imbalance of Th17/Treg in Patients with Uterine Cervical Cancer. *Clin. Chim. Acta* 412, 894–900. doi:10.1016/j.cca.2011.01.015

Zhao, L., and Li, Y. (2020). Application of Dexmedetomidine Combined with Sufentanil in colon Cancer Resection and its Effect on Immune and Coagulation Function of Patients. *Oncol. Lett.* 20 (2), 1288–1294. doi:10.3892/ol.2020.11643

Zhao., T., Liu., Z., Yu., A., and Zhang., Z. (2013). Effects of Intraoperative Administration of Dexmedetomidine on the Percentage of T-Lymphocyte Subsets and Natural Killer Cells in Patients with Colorectal Cancer. *Open. J. Anesthesiology.* 3, 104–108. doi:10.4236/ojanes.2013.32026

Zheng, L., Zhao, J., Zheng, L., Jing, S., and Wang, X. (2020). Effect of Dexmedetomidine on Perioperative Stress Response and Immune Function in Patients with Tumors. *Technol. Cancer Res. Treat.* 19, 1533033820977542. doi:10.1177/1533033820977542

Zhou, H., Lu, J., Shen, Y., Kang, S., and Zong, Y. (2017). Effects of Dexmedetomidine on CD42a/CD14, HLADR/CD14 and Inflammatory Cytokine Levels in Patients Undergoing Multilevel Spinal Fusion. *Clin. Neurol. Neurosurg.* 160, 54–58. doi:10.1016/j.clineuro.2017.06.012

Zhou, H., Sun, J., Zhong, W., Pan, X., Liu, C., Cheng, F., et al. (2020). Ddemedetomidine Preconditioning Alleviated Murine Liver Ischemia and Reperfusion Injury by Promoting Macrophage M2 Activation via PPARγ/STAT3 Signaling. *Int. Immunopharmacol.* 82, 106363. doi:10.1016/j.intimp.2020.106363

Zong, S., Du, J., Chen, Y., and Tao, H. (2021). Application Effect of Dexmedetomidine Combined with Flurbiprofen Axetil and Flurbiprofen Axetil Monotherapy in Radical Operation of Lung Cancer and Evaluation of the Immune Function. *J. BUON.* 26 (4), 1432–1439.

Conflict of Interest: The authors declare that the research was conducted in the absence of any commercial or financial relationships that could be construed as a potential conflict of interest.

frontiers | Frontiers in Pharmacology

ORIGINAL RESEARCH
published: 01 June 2022
doi: 10.3389/fphar.2022.847605

The XPO1 Inhibitor KPT-8602 Ameliorates Parkinson's Disease by Inhibiting the NF-κB/NLRP3 Pathway

Shuhan Liu[1,2], Shengxiang Wang[1], Runze Gu[1], Na Che[1], Jing Wang[1], Jinbo Cheng[1], Zengqiang Yuan[1,3], Yong Cheng[1,2] and Yajin Liao[1,2,3]**

[1]Center on Translational Neuroscience, College of Life and Environmental Sciences, Minzu University of China, Beijing, China, [2]Key Laboratory of Ecology and Environment in Minority Areas (Minzu University of China), National Ethnic Affairs Commission, Beijing, China, [3]The Brain Science Center, Beijing Institute of Basic Medical Sciences, Beijing, China

Exportin 1 (XPO1) is an important transport receptor that mediates the nuclear export of various proteins and RNA. KPT-8602 is a second-generation inhibitor of XPO1, demonstrating the lowest level of side effects, and is currently in clinical trials for the treatment of cancers. Previous studies suggest that several first-generation inhibitors of XPO1 demonstrate anti-inflammation activities, indicating the application of this drug in inflammation-related diseases. In this study, our results suggested the potent anti-inflammatory effect of KPT-8602 *in vitro* and *in vivo*. KPT-8602 inhibited the activation of the NF-κB pathway by blocking the phosphorylation and degradation of IκBα, and the priming of NLRP3. Importantly, the administration of KPT-8602 attenuated both lipopolysaccharide (LPS)-induced peripheral inflammation and 1-methyl-4-phenyl-1,2,3,6-tetrahydropyridine (MPTP)-induced neuroinflammation *in vivo*. In addition, the tissue damage was also ameliorated by KPT-8602, indicating that KPT-8602 could be used as a novel potential therapeutic agent for the treatment of inflammasome-related diseases such as Parkinson's disease, through the regulation of the NF-κB signaling pathway and the NLRP3 inflammasome.

Keywords: XPO1, KPT-8602, Parkinson's disease, NLRP3 inflammasome, NF-κB

OPEN ACCESS

Edited by:
Ramasamy Subbiah, Madurai Kamaraj University, India

Reviewed by:
Ana María Espinosa Oliva, Sevilla University, Spain
Zhouteng Tao, Shanghai Institute of Materia Medica (CAS), China

****Correspondence:***
Yong Cheng
yongcheng@muc.edu.cn
Yajin Liao
lyajin@muc.edu.cn

Specialty section:
This article was submitted to Inflammation Pharmacology, a section of the journal Frontiers in Pharmacology

Received: *03 January 2022*
Accepted: *13 April 2022*
Published: *01 June 2022*

Citation:
Liu S, Wang S, Gu R, Che N, Wang J, Cheng J, Yuan Z, Cheng Y and Liao Y (2022) The XPO1 Inhibitor KPT-8602 Ameliorates Parkinson's Disease by Inhibiting the NF-κB/NLRP3 Pathway. Front. Pharmacol. 13:847605. doi: 10.3389/fphar.2022.847605

INTRODUCTION

Exportin 1 (XPO1), also referred to as chromosomal maintenance region 1 (CRM1), is a key nuclear transport receptor involved in the export of more than 200 known cargo proteins, including tumor suppressors, anti-inflammatory factors, and growth-regulating proteins (Hutten and Kehlenbach, 2007; Xu et al., 2010; Xu et al., 2012). XPO1 mediates the nuclear transport process by specifically recognizing the leucine-rich nuclear export signal (NES) in cargo proteins (Hutten and Kehlenbach, 2007). Previous studies suggest that XPO1 is involved in the transport of proteins related to oncogenesis, including p53, p73, FOXO, PI3K/AKT, and Wnt/β-catenin, indicating its pivotal regulatory role in cancer therapy (Kau et al., 2004; Turner et al., 2012; Hill et al., 2014). Also, the upregulation of XOP1 causes alterations in the process of cell apoptosis, DNA damage repair, chromosome stability, and angiogenesis (Sun et al., 2016; Wang and Liu, 2019). Therefore, XPO1 is considered an effective target for the treatment of cancer, inflammation, and autoimmune diseases, through the regulation of nuclear–cytoplasmic localization of important proteins (Mao and Yang, 2013; Gravina et al., 2014; Haines et al., 2015; Olazagoitia-Garmendia et al., 2021).

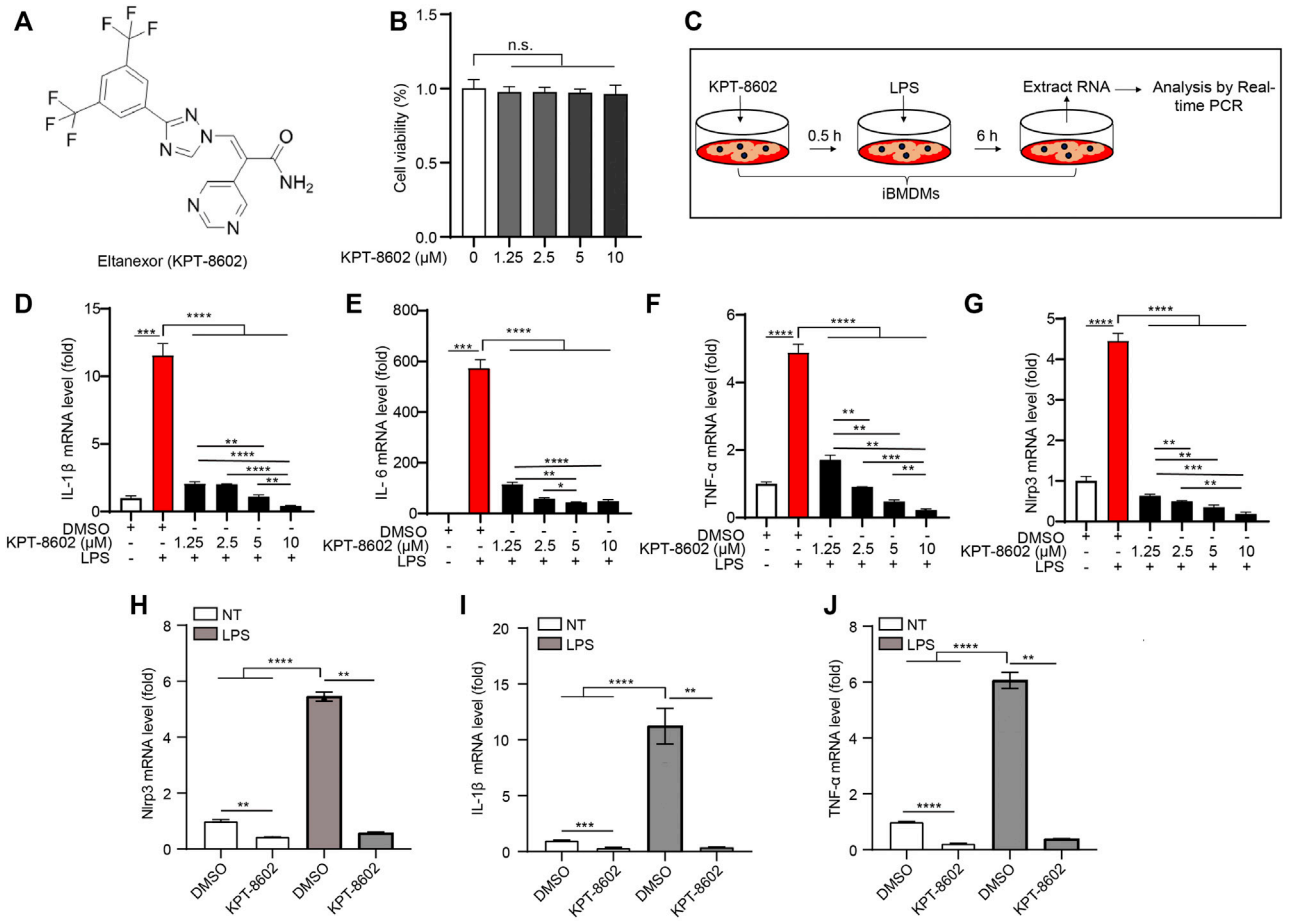

FIGURE 1 | KPT-8602 inhibits LPS-induced high expression of pro-inflammatory cytokines in macrophages. **(A)** Structure of KPT-8602. **(B)** iBMDMs were treated with various doses of KPT-8602 for 6 h, and cell viability was assessed by the CCK-8 assay kit. **(C)** Working model of LPS-induced inflammation. **(D–G)** iBMDMs were pretreated with KPT-8602 at different concentrations and stimulated with LPS for 6 h, and then the mRNA levels of IL-1β **(D)**, IL-6 **(E)**, TNF-α **(F)**, and Nlrp3 **(G)** were analyzed by real-time PCR. **(H–J)** Primary peritoneal macrophages (PMs) pretreated with KPT-8602 (5 μM) were treated with LPS for 6 h, and then the mRNA levels of Nlrp3 **(H)**, IL-1β **(I)**, and TNF-α **(J)** were analyzed by real-time PCR. (** indicates $p < 0.01$, *** indicates $p < 0.001$, **** indicates $p < 0.0001$ by one-way ANOVA). n. s. no significant, NT, no treatment.

In recent years, several small-molecule selective inhibitors of nuclear export (SINE) compounds with anticancer activities are discovered. Selinexor (also called KPT-330), is a first-in-class oral SINE compound that has been shown to induce nuclear aggregation of tumor suppressor proteins and demonstrate anticancer activities in preclinical and clinical research and is currently being evaluated in phase I/II/III clinical trials for its potential use in hematologic and solid tumors (Lang et al., 2019; Taylor-Kashton et al., 2016; Azmi et al., 2021). However, the presence of its systemic toxicities and brain/blood-related adverse reactions limited its clinical application due to safety reasons (Jakubowiak et al., 2019; Chen et al., 2018). Eltanexor (also called KPT-8602, **Figure 1A**) is a second-generation SINE compound developed by Karyopharm to address the high toxicity of selinexor, and it has been shown to have similar efficacy to or even better efficacy than selinexor in hematological malignancies in animal models (Lang et al., 2019). Also, due to its low central nervous system (CNS) penetration rate, eltanexor is therefore better tolerated and can be used in a wider therapeutic window (Hing et al., 2016; Etchin et al., 2017).

The NOD-like receptor protein 3 (NLRP3) inflammasome is one of the major inflammasomes activated by a variety of pathogen-associated molecules and damage-associated molecules (Pan et al., 2021). The activation of the NLRP3 inflammasome is regulated by a 2-step activation process including the priming phase, characterized by the activation of the nuclear factor kappa B (NF-κB) pathway that promotes the expression of NLRP3 and the precursor of IL-1β; and the activation phase, featured by the assembly of the NLRP3 inflammasome induced by stimuli such as nigericin (Nig) (Elliott and Sutterwala, 2015; Shao et al., 2015). Our previous study reveals that aberrant activation of the NLRP3 inflammasome contributes to neurodegenerations and development of Parkinson's disease (PD) through the promotion of inflammation and induction of pyroptosis (Cheng et al., 2020).

In this study, we demonstrated that KPT-8602 suppressed the activation of the NF-κB signaling pathway by inhibiting the phosphorylation and degradation of IκBα, and therefore inhibited the transcription of NLRP3. Moreover, *in vivo* study revealed that lipopolysaccharide (LPS)-induced peripheral inflammation and 1-methyl-4-phenyl-1,2,3,6-tetrahydropyridine (MPTP)-induced neuroinflammation were both downregulated by the administration of KPT-8602. Consistently, the tissue injury was also ameliorated by administration of KPT-8602, suggesting that KPT-8602 is a potential therapeutic agent for the treatment of diseases associated with aberrant activation of the NF-κB signaling pathway and the NLRP3 inflammasome.

MATERIALS AND METHODS

Mice

C57BL/6 mice were purchased from Vital River Laboratory Animal Technology Co., Ltd (Beijing). For the experiment, four to five mice were housed per cage under a 12-h light/dark cycle at 22–24°C and given unrestricted access to food and water. All the animal experimental procedures were approved by the Institutional Animal Care and Use Committee of the Beijing Institute of Basic Medical Sciences.

Cell Culture and Treatment

Immortalized murine bone marrow-derived macrophages (iBMDMs) or BV2 microglial cell lines were maintained in Dulbecco s modified Eagle s medium (#11965–092, Life Technologies, Waltham, MA, United States) supplemented with 10% heat-inactivated fetal bovine serum (FBS, #04-001-1A, Biological Industries, Beit Haemek, Israel) and 1% penicillin–streptomycin solution (#03-031-1B, Biological Industries) at 37°C in a humidified atmosphere with 5% CO_2. For LPS-induced inflammation *in vitro*, iBMDMs were pretreated with 1.25, 2.5, 5, and 10 μM of KPT-8602 for 30 min, and stimulated with LPS (1 μg/ml) for 6 h.

Cell Viability Assay

A Cell Counting Kit-8 (CCK-8) assay (ab228554; Abcam, Cambridge, UK) was used to evaluate cell viability following the manufacturer's instructions. Briefly, iBMDMs were plated at a density of 1×10^5 cells/mL in 96-well plates and exposed to different concentrations of KPT-8602 for 6 h. Subsequently, 10 μL of CCK-8 reagent was added to each well and incubated at 37°C for an additional 2 h. Finally, a Spectra Max i3x (Molecular Devices, Sunnyvale, CA, United States) was used to measure the absorbance at 450 nm.

Isolation and Culture of Primary Macrophages

Primary peritoneal macrophages (PMs) from 8-week-old wild-type mice were isolated and cultured as previously described (Pan et al., 2021). Briefly, the mice were killed by using the cervical dislocation method and 75% ethyl alcohol disinfection for 5–10 min. PMs were collected after washing the peritoneal cavity with 5 ml of an ice-cold serum-free RPMI-1640 medium (#C11875500BT, Gibco, Shanghai, China). After that, the PMs were centrifuged at 300 *g* and 4°C for 5– min, and the cell pellets were resuspended in a fresh RPMI-1640 medium (supplemented with 10% heat-inactivated FBS, 1% penicillin, and 1% streptomycin) and then seeded in culture plates for subsequent experiments.

SiRNA-Mediated Gene Silencing in iBMDMs and PMs

iBMDMs/PMs (3×10^5 cells/mL) were plated in 12-well plates and siRNA (50 nM) was transfected into the cells in each well using Lipofectamine RNAiMAX (Invitrogen) as per the manufacturer's instructions. The siRNA scramble and siRNA against *XPO1* were obtained from Genepharma (Suzhou, China).

Western Blotting

Cells or tissues were lysed with RIPA lysis buffer comprising a cocktail of protease and phosphatase inhibitors, and total protein concentrations were measured by BCA assay and boiled at 100°C for 15 min. The equal amounts of proteins were separated by SDS-PAGE gel at 80 V for 0.5 h and 120 V for 1 h. After that, the protein was transferred to a PVDF membrane (#ISEQ00010, Millipore, Darmstadt, Hessen, Germany) at 250 mA for 1.5 h. The membrane was blocked for 1 h at room temperature using blocking buffer (5% nonfat milk) and was then incubated with primary antibodies overnight at 4°C. The next morning, the membrane was washed with Tris-buffered saline and Tween-20 (TBST) three times for 5 min each, followed by incubated with conjugated secondary antibodies for protein detection. The primary antibodies used in the present study are as follows: anti-phospho-IKKα/β (#2697P, Cell Signaling Technology, MA, United States, 1:1000), anti-phospho-IκBα (#2859, Cell Signaling Technology, 1:1000), anti-IKKα (#A2062, ABclonal Technology, Wuhan, HB, China, 1:1000), anti-IκBα (#4814, Cell Signaling Technology, 1:1000), anti-exportin 1/CRM1 (#46249, Cell Signaling Technology, 1:1000), anti-GAPDH (CW0266A, CWBiotech, Beijing, China, 1:2000), anti-H2B (ab64165, Abcam, 1:1000), anti-phospho-NF-κB p65 (#3033, Cell Signaling Technology, 1:1000), anti-NF-κB p65 (#8242, Cell Signaling Technology, 1:1000 for Western blotting, 1:400 for immunofluorescence), anti-NLRP3 (#AG-20B-0014, AdipoGen, San Diego, CA, United States, 1:1000), anti-caspase-1 (#Ag-20B-0042, AdipoGen, 1:1000), anti-IL-1β (#AF-401-NA, R&D Systems, Minneapolis, MN, United States, 1:1000), anti-ASC (#67824, Cell Signaling Technology, 1:1000 for Western blotting, 1:200 for immunofluorescence), anti-TH (2792, Cell Signaling Technology, 1:1000 for Western blotting, 1:400 for immunochemistry), anti-Iba1 (ab5076, Abcam, 1:1000 for Western blotting, 1:400 for immunofluorescence), anti-β-actin (60008-1-Ig, Proteintech Group, Campbell Park, Chicago, IL, United States, 1:2000 for Western blotting, 1:500 for immunofluorescence), and anti-β-tubulin (#CW0098A, CWBiotech, Taizhou, JS, China, 1:2000 for Western blotting, 1:500 for immunofluorescence).

Enzyme-Linked Immunosorbent Assay

PMs treated with LPS (1 μg/ml) for 3.5 h were further stimulated with Nig for 45 min. Then, the supernatants were collected and centrifuged at 12,000 × *g* and 4°C for 5 min. The concentration of IL-1β in the supernatants (#432604, BioLegend, San Diego, CA, United States) was determined by ELISA following the manufacturer's instructions.

Assessment of LPS-Induced Systemic Inflammation

Eight-week-old C57BL/6 male mice (body weight: 22–25 g) were orally administered with 5 mg/kg KPT-8602 or vehicle (saline) and then intraperitoneally injected with LPS (10 mg/kg). After 4 h, all animals were killed, and tissue samples from the liver, lung, and kidney were collected for subsequent experiments.

Histological Analysis

Tissue samples from the liver, lung, and kidney were fixed with 4% paraformaldehyde (PFA) in 0.1 M phosphate buffer (pH 7.4) for 24 h, and 5 μm coronal paraffinized sections were prepared for histological assessment. The sections of various organs were stained with hematoxylin and eosin (H&E). The pathological scores for these organs were determined as described in previous studies with minor modifications (Maehara et al., 2020) and were mainly determined as the degree of immune cell infiltration and structure disruption, with a scale of 0–3 as follows: 0 = none, 1 = mild, 2 = moderate, and 3 = severe.

Induction and Assessment of MPTP-Induced PD

Eight-week-old C57BL/6 male mice (body weight: 22–25 g) were orally administered 5 mg/kg KPT-8602 or vehicle (saline) for 6 days at 12 h after the MPTP injection (**Figure 6A**). The mice were administered four intraperitoneal injections of 20 mg/kg MPTP as previously described (Wu et al., 2016). At 7 days after the final MPTP injection, all animals were killed, and the substantia nigra and striatum tissue samples of one of the cerebral hemispheres of mice in each group were collected for the Western blot analysis. The other hemispheres were infused with 4% paraformaldehyde in 0.1 M phosphate buffer (pH 7.4), and 40 μm coronal frozen sections were prepared for immunohistochemical assays.

Behavioral Tests

For the rotarod test, the motor capacity of the mice was assessed using a rotarod apparatus (Panlab, Barcelona, Spain, LE8200). Briefly, the mice were placed on a rotation rod, with the rotation speed gradually increased from 4 to 40 rpm over a period of 5 min, and the latency to falling was recorded. Three tests were performed at an interval of 1 h, and the average of the three tests was taken as the final test result. The mice were acclimated to the environment prior to each training and test session.

Immunochemistry

All animals were euthanized with tribromoethanol, then precooled normal saline was infused into the heart and brain tissue was fixed with 4% PFA for at least 24 h. The coronal sections were then immunochemically treated with anti-TH antibody staining and confocal analysis. For TH labeling, briefly, the slices were incubated with rabbit polyclonal anti-TH antibodies (1:400, Cell Signaling Technology) and visualized with biotinylated goat anti-rabbit IgG, followed by streptavidin-conjugated horseradish peroxidase (Vectastain ABC kit, Zhongshanjinqiao, Beijing, China). Positive immunostaining was visualized with 3,3-diaminobenzidine (DAB) peroxidase substrate (DAB kit, Vector Laboratories). Stained sections were mounted onto slides and analyzed by Stereo Investigator software (MicroBrightfield, Williston, VT, United States).

Stereological Analysis

All procedures were performed as previously described (Zheng et al., 2021). Briefly, 40-μm coronal sections were cut throughout the brain, including the substantia nigra and striatum, and every fourth section was used for analysis by Stereo Investigator software.

Multiplex Immunofluorescence Staining

The tyramide signal amplification (TSA)-based Opal staining method was used to stain multiple markers from the same species of SNc sections as described in the previous studies and modified (Fan et al., 2021). Briefly, tissue sections were placed in citrate buffer (10 mM sodium citrate, 0.05% Tween 20, pH 6.0) for 30 min at a sub-boiling temperature, washed twice in PBS, and then blocked in 3% hydrogen peroxide for 20 min at room temperature. The samples were then washed thrice in PBS, blocked in blocking solution (5% fetal bovine serum, 0.5% Triton X-100, 1% bovine serum albumin) for 1 h at room temperature, incubated with anti-rabbit Iba1 antibody (1:400, Abcam) at 4°C for 30 min, and then incubated at room temperature for 30min, washed in PBST (PBS and Tween 20, pH 7.6), incubated in poly-HRP-conjugated secondary antibody, and washed again in PBST before incubation in a tyramide working solution (e.g., AlexaFluor 488 tyramide) for 10 min followed by immediate application of reaction stop reagent working solution. For the second round of staining, tissue sections were first rinsed three times in PBST before being placed in citrate buffer for 30 min and blocked in 3% hydrogen peroxide and blocking solution again before application of anti-rabbit ASC (1: 200, CST) and secondary antibody, followed by treatment with a second tyramide working solution (e.g., AlexaFluor 594 tyramide). For TH marker staining, the process was repeated once more with a third tyramide working solution (e.g., AlexaFluor 647 tyramide). Tissue sections were re-stained with DAPI, covered with slides (CITOGLAS, 188105W) and then dried overnight at 4°C before confocal microscopic imaging.

The number of ASC speck-positive cells was analyzed by the formula as follows: Ratio = the number of ASC speck-positive cells/the number of total cells. The number of Iba-1-positive cells was counted in the same way.

ASC Oligomerization Assay

The ASC oligomerization assay was performed as previously reported (Pan et al., 2021). Briefly, 45 min post-Nig stimulation, primary macrophages were rinsed in ice-cold PBS and then lysed with hypotonic lysis buffer (10 mM KCl, 1.5 mM

$MgCl_2$, 1 mM EDTA, 1 mM EGTA, 0.1mM PMSF, and 20 mM Tris; pH 7.5) and incubated on ice for 30 min, shaking every 5 min. The lysates were centrifuged at 6,000 × *g* for 8 min at 4°C, and then the pellets were washed three times in ice-cold PBS and resuspended in 500 μL CHAPS buffer (0.1% CHAPS, 10 mM KCl, 1.5 mM $MgCl_2$, 1 mM EDTA, 1 mM EGTA, 0.1 mM PMSF, and 20 mM Tris; pH 7.5). The resuspended pellets were incubated with disuccinimidyl suberate (DSS, #S1885, Sigma-Aldrich, 2 mM) for 45 min at 37°C with rotation. The samples were then centrifuged at 6, 000 × *g* for 15 min at 4°C. The cross-linked pellets were resuspended in 60 μL of sample buffer and were then analyzed by Western blotting.

Dual-Luciferase Reporter System

The NF-κB reporter was generated in our laboratory (Li et al., 2020). Briefly, the NF-κB promoter was cloned into a pGL3-luciferase reporter vector (Promega, Madison, United States). Then, HEK293T cells were co-transfected with the pCMV-Renilla plasmid and NF-κB reporter using Lipofectamine 2000 transfection reagent (#11668019, Invitrogen). The cells were lysed 24 hours after transfection, and luciferase activity was measured using a dual-luciferase reporter detection system (Promega).

Real-Time Quantitative Polymerase Chain Reaction

Total RNA was isolated from the cells or tissues using TRIzol reagent (#15596026, Invitrogen), and RNA (1 ug) from each sample was used for reverse transcription with a One-Step First-strand cDNA synthesis kit (#AT311-02, Transgen, Beijing, China). SYBR Green-based real-time qPCR (#A304, GenStar, Beijing, China) was used to measure target gene expression. The sequences of the gene-specific primers used are as follows:

mouse *Il1b* forward, GTCGCTCAGGGTCACAAGAA.
mouse *Il1b* reverse, CTGCTGCCTAATGTCCCCTT.
mouse *Il6* forward, GCTACCAAACTGGATATAATCAGGA.
mouse Il6 reverse, CCAGGTAGCTATGGTACTCCAGAA.
mouse Tnf forward, CAGGCGGTGCCTATGTCTC.
mouse Tnf reverse, CGATCACCCCGAAGTTCAGTAG;
mouse Inos forward, GTTCTCAGCCCAACAATACAAGA.
mouse Inos reverse, GTGGACGGGTCGATGTCAC;
mouse Nlrp3 forward, ATTACCCGCCCGAGAAAGG.
mouse Nlrp3 reverse, TCGCAGCAAAGATCCACACAG.
mouse *β*-actin forward, GGTGAAGGTCGGTGTGAACG.
mouse *β*-actin reverse, CTCGCTCCTGGAAGATGGTG.

Statistical Analysis

The gray values of the Western blot bands were analyzed by ImageJ software (NIH, Bethesda, MD, United States). All the data represent three independent repeat experiments and the significance was performed with the *t*-test for two groups, or one-way ANOVA for multiple groups (GraphPad Software, San Diego, CA, United States). All values are expressed as the mean ± S.E.M. Differences between data were considered significant when the p value was <0.05.

RESULTS

KPT-8602 Inhibits LPS-Induced Inflammation *In Vitro*

To test the potential cytotoxicity of KPT-8602 on cells, we treated iBMDMs with a serial dose of KPT-8602. The results showed that KPT-8602 used the following10 uM displayed no obvious toxic effects on iBMDMs (**Figure 1B**). Then, iBMDMs were pretreated with 1.25, 2.5, 5, and 10 μM of KPT-8602 for 30 min and followed by stimulating with LPS (1 μg/ml) for 6 h (**Figure 1C**), and we found that the expression of IL-1β (**Figure 1D**), IL-6 (**Figure 1E**), and TNF-α (**Figure 1F**) induced by LPS were inhibited by KPT-8602. In addition, LPS-induced upregulation of NLRP3 was also blocked by KPT-8602 (**Figure 1G**), suggesting its inhibitory effect on the transcription of NLRP3. These results indicated that 5 μM KPT-8602 was sufficient to inhibit the expression of pro-inflammatory cytokines and NLRP3, with no obvious cytotoxicity in iBMDMs. In addition, LPS-induced transcription of NLRP3 (**Figure 1H**), IL-1β (**Figure 1I**), and TNF-α (**Figure 1J**) were also significantly inhibited by KPT8602 at 5 μM in PMs. Therefore, the concentration of KPT-8602 used in the subsequent study was five uM. Taken together, these results suggested that KPT-8602 effectively inhibited LPS-induced inflammation *in vitro*.

KPT-8602 Inhibits the Activation of the NLRP3 Inflammasome in Primary Macrophage

As KPT-8602 inhibited the transcription of NLRP3 and IL-1β, we next analyzed the effects of KPT8602 on the activation of the NLRP3 inflammasome (**Figure 2A**). The results displayed that the cleavage of caspase-1 and IL-1β induced by LPS and Nig were significantly reduced by KPT-8602 in PMs (**Figures 2B–F**). Consistently, the concentration of secreted IL-1β in the supernatants was also decreased in KPT-8602-treated PMs (**Figure 2G**). We then analyzed the effects of KPT-8602 on the assembly of the NLRP3 inflammasome and found that the number of ASC specks induced by LPS and Nig were significantly reduced by KPT-8602 (**Figures 2H, I**). In addition, the formation of ASC dimers, tetramers, and oligomers was significantly reduced by KPT-8602 as well (**Figure 2J**; **Supplementary Figure S1**). Together, these results indicate that KPT-8602 inhibited the activation of the NLRP3 inflammasome *in vitro*.

KPT-8602 Exerts Anti-Inflammatory Effects by Blocking the NF-κB Pathway

To further analyze the anti-inflammatory mechanism of KPT-8602, we next investigated the role of KPT-8602 on the activation of the NF-κB signaling pathway (**Figure 3A**). The results revealed that KPT-8602 had no effect on the LPS-induced phosphorylation of IKKα/β. However, we found KPT-8602 significantly inhibited IKKα/β-mediated phosphorylation of IκBα in iBMDMs (**Figures 3B–D**). Consistently, the phosphorylation levels of IκBα induced by LPS in BV2

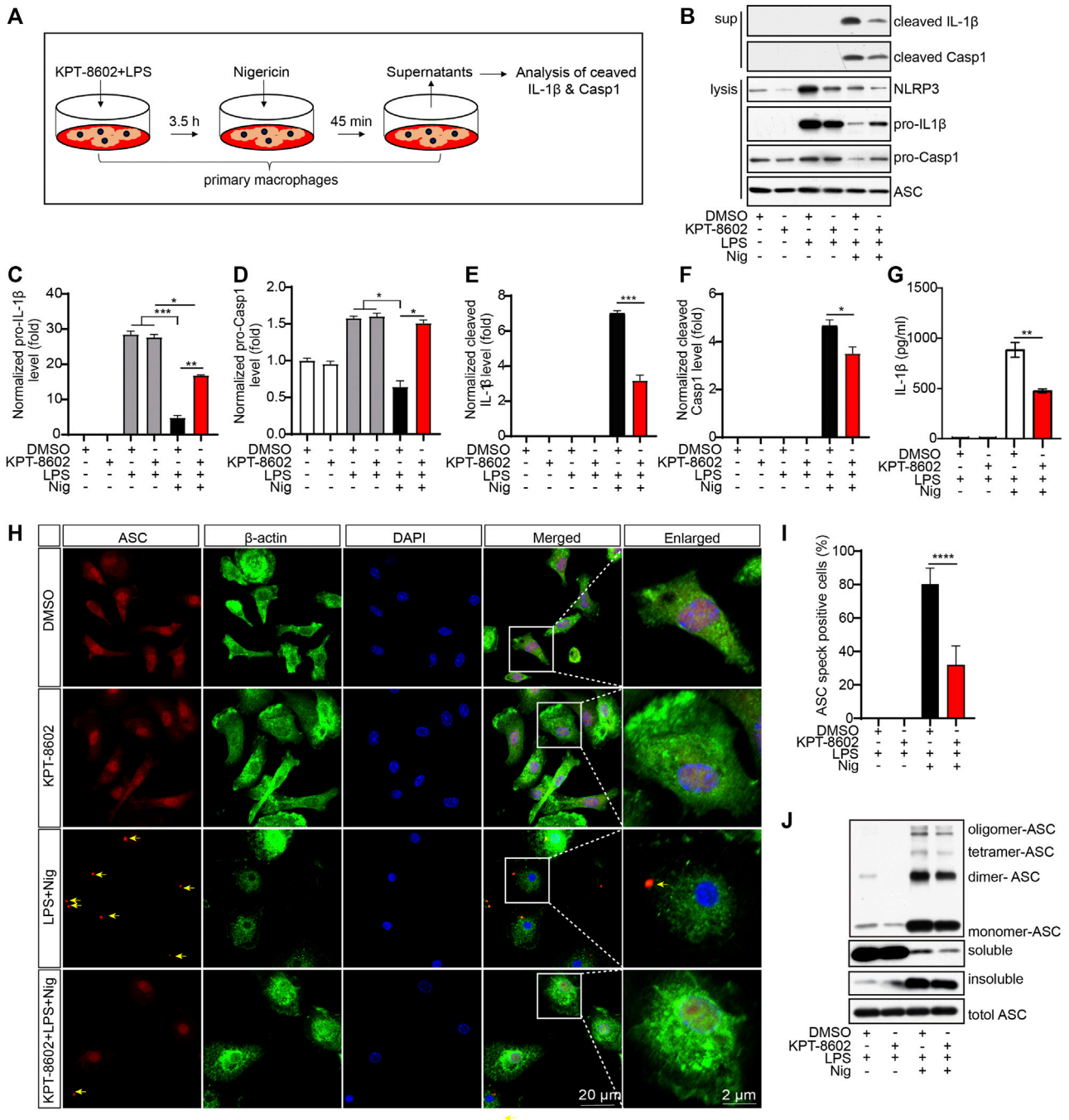

FIGURE 2 | KPT-8602 inhibits the activation and assembly of the NLRP3 inflammasome *in vitro*. **(A)** Working model of the NLRP3 inflammasome activation. **(B–F)** PMs pretreated with LPS were treated with KPT-8602 for 30 min and nigericin (Nig) for 45 min, and the cells and supernatants were harvested for analysis of the expression of NLRP3, pro-IL-1β, pro-caspase-1, cleaved IL-1β, cleaved caspase-1, and ASC by Western blotting **(B)**. Gray values of the pro-IL-1β **(C)**, pro-Casp-1 **(D)**, cleaved IL-1β **(E)**, and cleaved Casp-1 **(F)** bands were analyzed by using ImageJ and were normalized to ASC. **(G)** PMs pretreated with LPS were treated with KPT-8602 for 30 min and nigericin (Nig) for 45 min, and the cells and supernatants were harvested for analysis of the expression of cleaved IL-1β by ELISA. **(H,I)** PMs pretreated with LPS were treated with KPT-8602 for 30 min and nigericin (Nig) for 45 min. Then, the cells were fixed and stained with a rabbit anti-ASC antibody and mouse anti-β-actin antibody **(H)**, and the number of cells containing ASC specks (yellow arrows) was analyzed by ImageJ. **(I)** Scale bars, 20 μm for low-magnification images and 2 μm for high-magnification images, respectively. **(J)** PMs pretreated with LPS were treated with KPT-8602 and Nig for 45 min, and then the cells were harvested and cross-linked with disuccinimidyl suberate (DSS) for analysis of the oligomerization of ASC by Western blotting. (* indicates $p < 0.05$, ** indicates $p < 0.01$, *** indicates $p < 0.001$, **** indicates $p < 0.0001$ by Student's t test or one-way ANOVA).

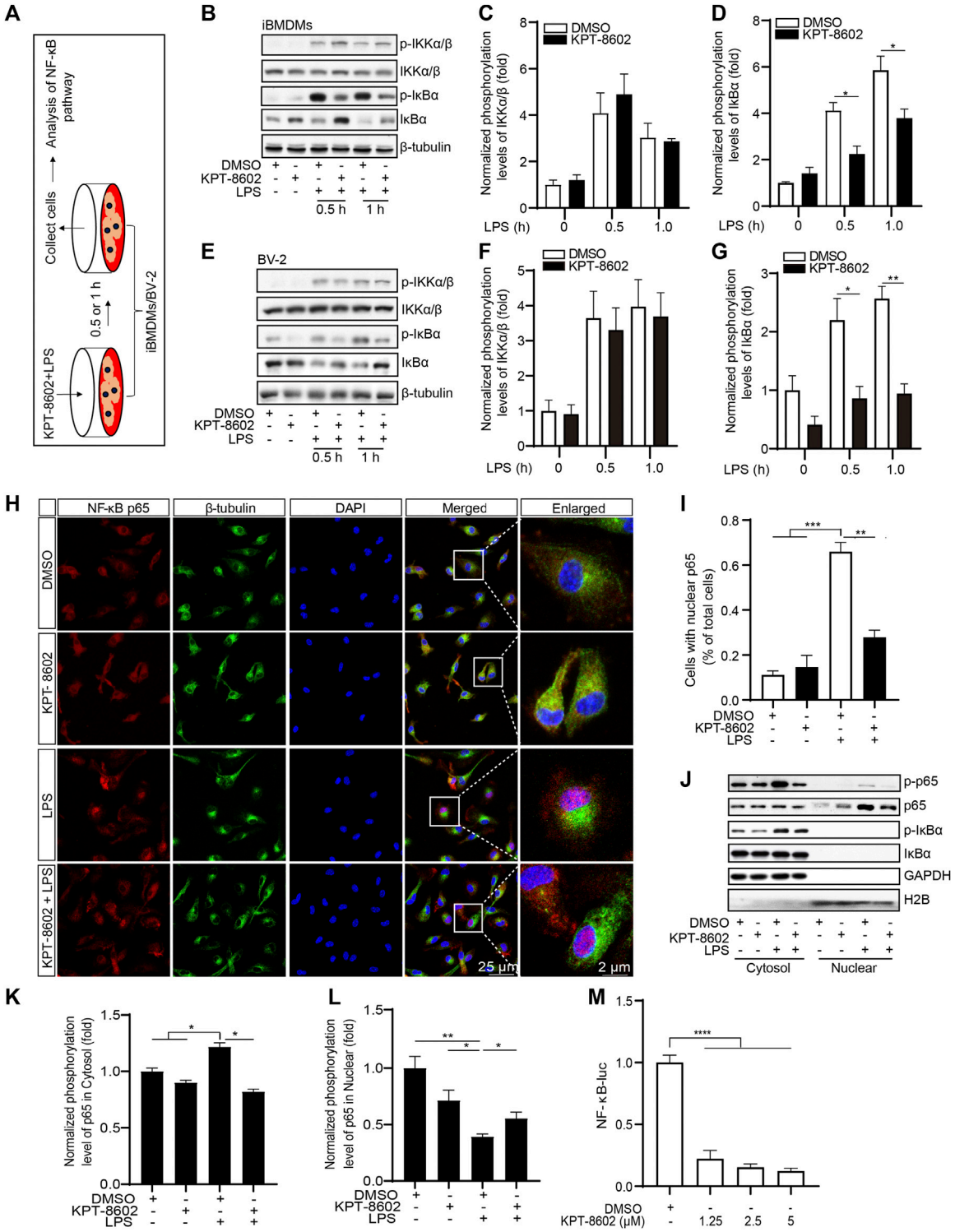

FIGURE 3 | KPT-8602 inhibited LPS-induced activation of the NF-κB signaling pathway. **(A)** iBMDMs or BV-2 were pretreated with or without KPT-8602 (5 μM) and stimulated with LPS for 0.5 and 1 h, respectively, and then the cell lysates were collected for analysis by Western blotting **(B,E)**. The gray values of the phosphorylated and total IKKα/β **(C,F)** and IκBα **(D,G)** bands were analyzed with ImageJ. **(H,I)** PMs were pretreated with KPT-8602 for 30 min and stimulated with LPS for 2 h. Then, the cells were fixed and stained with a rabbit anti-NF-κB p65 antibody and mouse anti-β-tubulin antibody **(H)**, and the number of cells containing nuclear p65 was analyzed by ImageJ **(I)**. Scale bars, 25 μm for low-magnification images and 2 μm for high-magnification images, respectively. **(J,K)** iBMDMs were pretreated with KPT-8602 for 1 h and stimulated with LPS for 2 h, and then extracts from the nucleus and cytoplasm were collected for analysis by Western blotting **(J)**. The gray value of the phosphorylated and total p65 in the nucleus **(K)** and cytoplasm **(L)** were analyzed with ImageJ. H2B served as a nuclear protein marker; GAPDH as a cytosolic protein marker. **(M)** Quantitative analysis of the effect of KPT-8602 on NF-κB luciferase activity. (* indicates $p < 0.05$, ** indicates $p < 0.01$, *** indicates $p < 0.001$, **** indicates $p < 0.0001$ by one-way ANOVA).

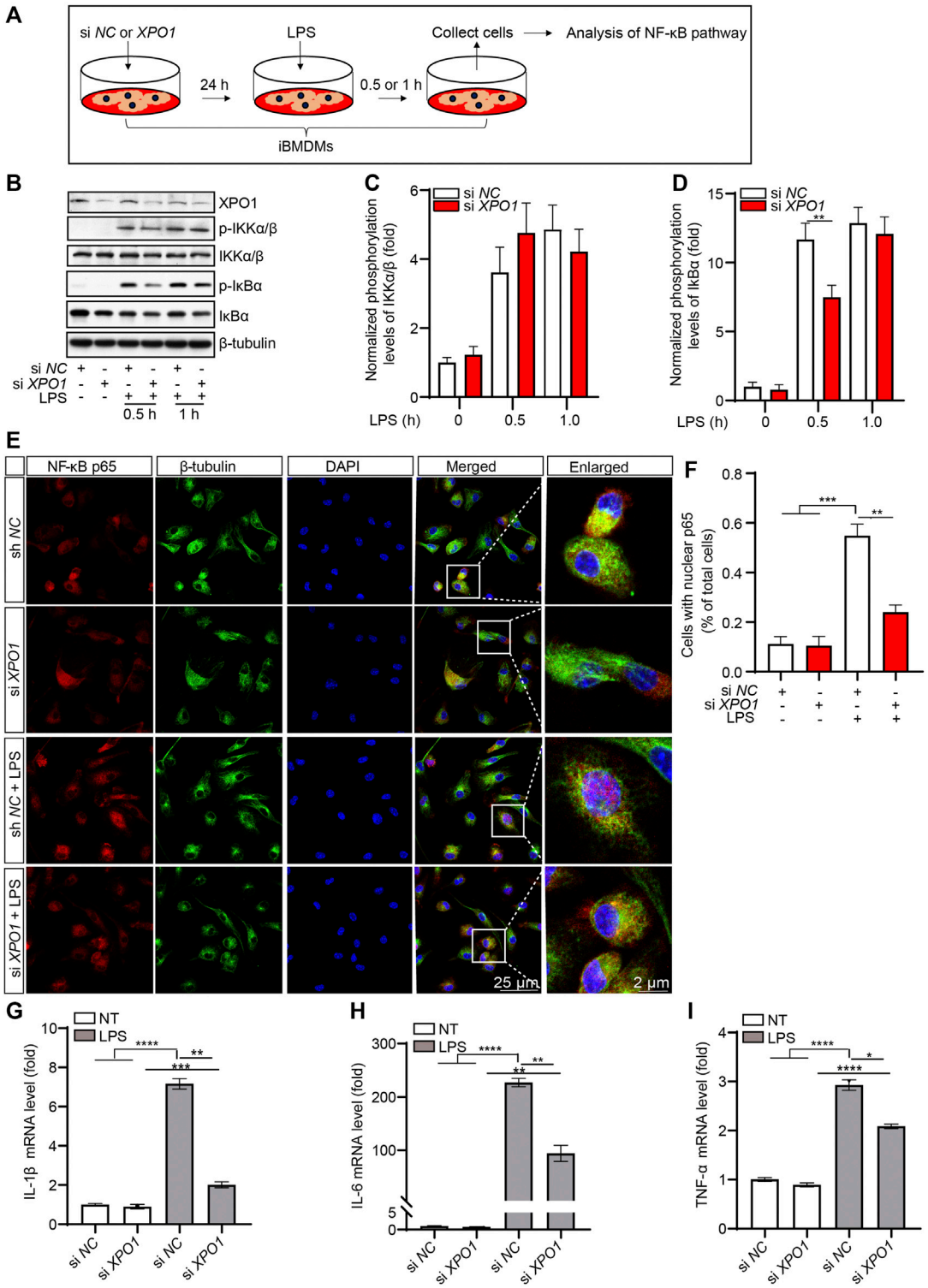

FIGURE 4 | Silencing XPO1 inhibits NF-κB signaling pathway and exerts anti-inflammatory activity. **(A)** iBMDMs transfected with siRNA against XPO1 or scrambled siRNA were treated with LPS for 0.5 and 1 h, respectively, and then the cell lysates were collected for analysis by Western blotting **(B)**. The gray values of the phosphorylated and total IKKα/β **(C)** and IκBα **(D)** bands were analyzed with ImageJ. **(E,F)** PMs transfected with siRNA against XPO1 or scrambled siRNA were stimulated with LPS for 2 h, and then the cells were fixed and stained with a rabbit anti-NF-κB p65 antibody and mouse anti-β-tubulin antibody **(E)**, and the number of cells containing nuclear p65 was analyzed by ImageJ **(F)**. Scale bars, 25 μm for low-magnification images and 2 μm for high-magnification images, respectively. **(G–I)** iBMDMs transfected with siRNA against XPO1 or scrambled siRNA were treated with LPS for 6 h, and then the mRNA levels of IL-1β **(G)**, IL-6 **(H)**, and TNF-α **(I)** were detected by real-time PCR. (* indicates $p < 0.05$, ** indicates $p < 0.01$, *** indicates $p < 0.001$, **** indicates $p < 0.0001$ by one-way ANOVA).

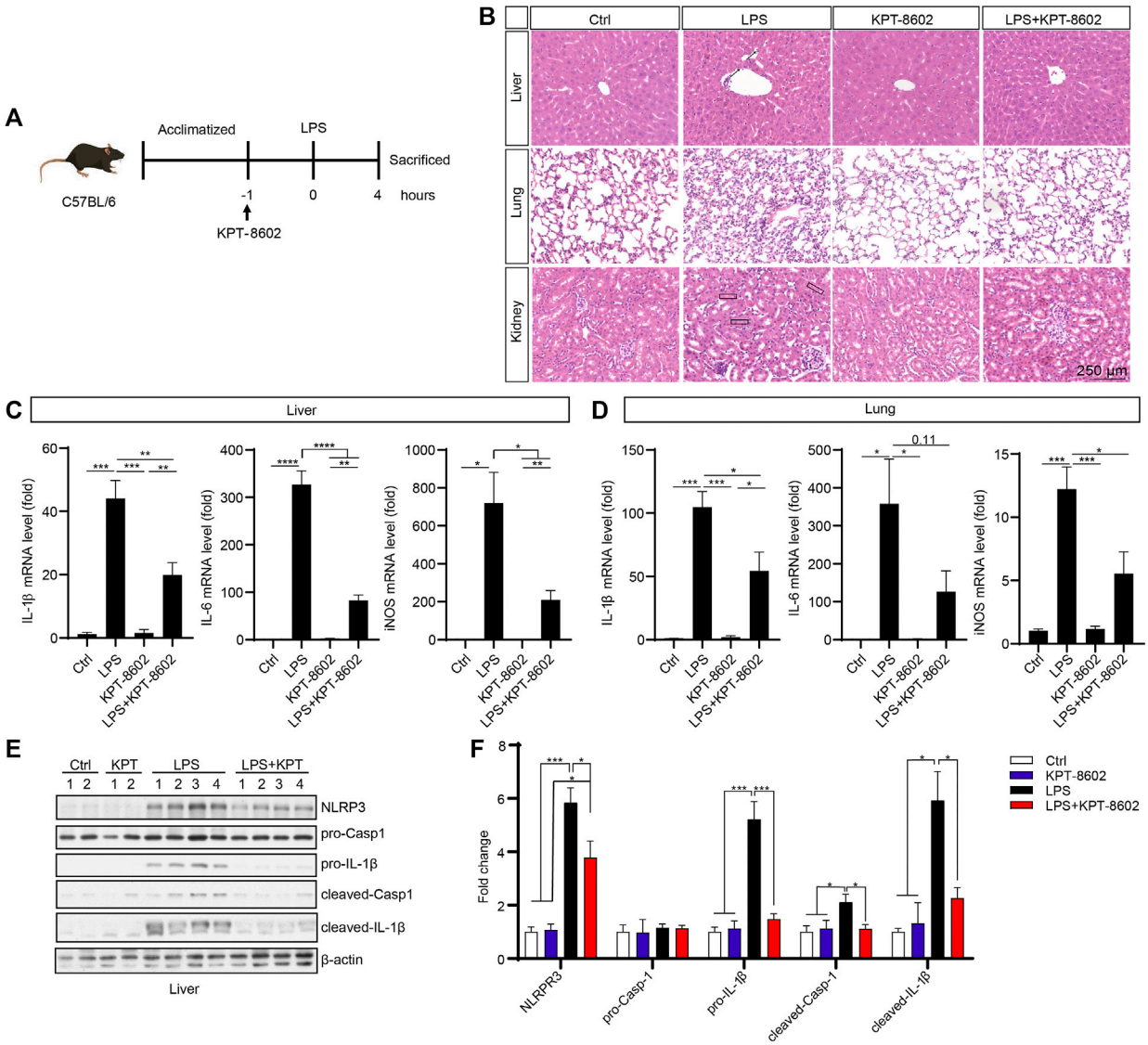

FIGURE 5 | KPT-8602 suppresses LPS-induced systemic inflammation. **(A)** C57BL/6 mice were given LPS (10 mg/kg) intraperitoneally after oral admiration of KPT-8602 (5 mg/kg) or vehicle (5 mice per group). **(B)** Representative photomicrographs of paraffin-embedded sections of the liver, lung, and kidney tissues stained with H&E. Scale bars, 250 μm for images, respectively. The expression levels of IL-1β, IL-6, and iNOS in the liver **(C)** and lung **(D)** were detected by real-time PCR. The expression of NLRP3, pro-caspase-1, pro-IL-1β, cleaved caspase-1, cleaved-IL-1β, and *β*-actin in the liver was analyzed by Western blotting **(E)**, and the gray values of their bands were analyzed by using ImageJ and were normalized to *β*-actin **(F)**. (* indicates $p < 0.05$, ** indicates $p < 0.01$, *** indicates $p < 0.001$, **** indicates $p < 0.0001$ by one-way ANOVA).

microglial cells were also inhibited by KPT-8602 (**Figures 3E–G**). The reduced phosphorylation of IκBα caused decreased degradation of IκBα (**Figures 3B, E**) and decreased nuclear translocation p65 in KPT-8602-treated PMs (**Figures 3H, I**) and iBMDMs (**Figure 3J**). In addition, the LPS-induced phosphorylation of p65 was blocked by KPT-8602 (**Figure 3K–I**). Furthermore, the NF-κB response element reporter activity was also impaired in KPT-8602-treated HEK293T cells (**Figure 3M**).

To investigate whether the knockdown of XPO1 has the same effect on the activation of the NF-κB pathway, we generated XPO1-silenced iBMDMs (**Figure 4A**). As suggested by the results, LPS-induced phosphorylation of IκBα was inhibited in XPO1-silenced iBMDMs. Meanwhile, no significant alteration was observed in the phosphorylation levels of IKKα/β (**Figures 4B–D**). We also found that the nuclear translocation of p65 induced by LPS was also impaired in XPO1-silenced PMs (**Figures 4E, F**). Moreover, LPS-induced transcription of IL-1β (**Figure 4G**), IL-6 (**Figure 4H**), and TNF-α (**Figure 4I**) was inhibited by silencing of XPO1. Taken together, the aforementioned results suggested that KPT-8602 inhibits the activation of the NF-κB pathway by blocking the phosphorylation of IκBα.

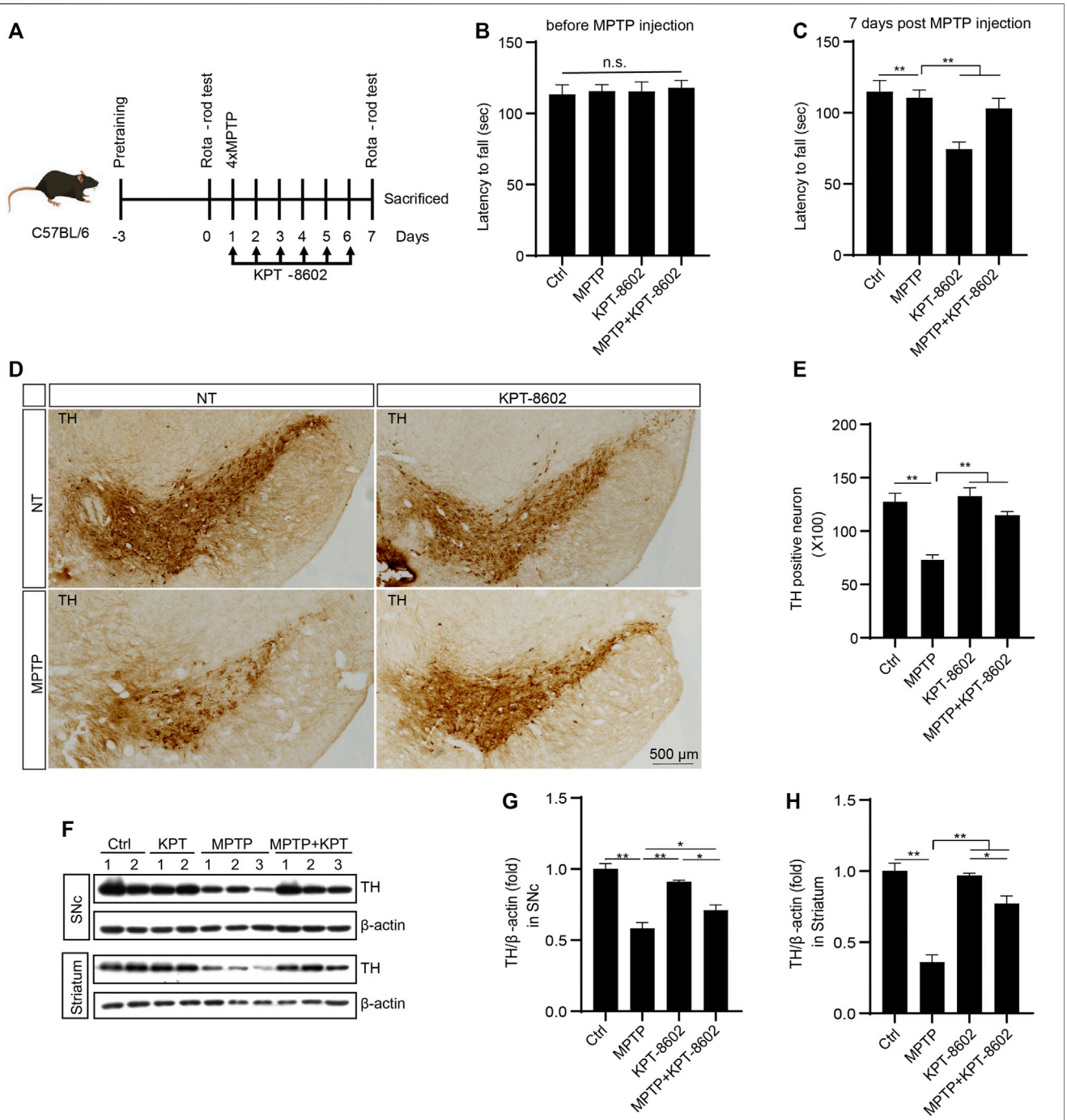

FIGURE 6 | KPT-8602 ameliorates PD model mice severity. C57BL/6 mice were treated with saline or MPTP (four i.p. injections of 20 mg/kg at 2 h intervals). KPT8602 (5 mg/kg) or vehicle were administered daily (7 mice per group). **(A)** Schedule of the PD model establishment and administration of KPT-8602. **(B,C)** Latency of the indicated mice on the rotarod. **(D)** Representative photomicrographs of tyrosine hydroxylase (TH)-stained sections from the substantia nigra compacta (SNc) of mice brain. Scale bars, 500 μm for images, respectively. **(E)** Number of TH-positive neurons was analyzed by ImageJ. The expression of TH and β-actin protein was analyzed by Western blotting **(F)**, and the gray value of their bands in the SNc **(G)** and striatum **(H)** were analyzed by ImageJ. (* indicates $p < 0.05$, ** indicates $p < 0.01$ by one-way ANOVA).

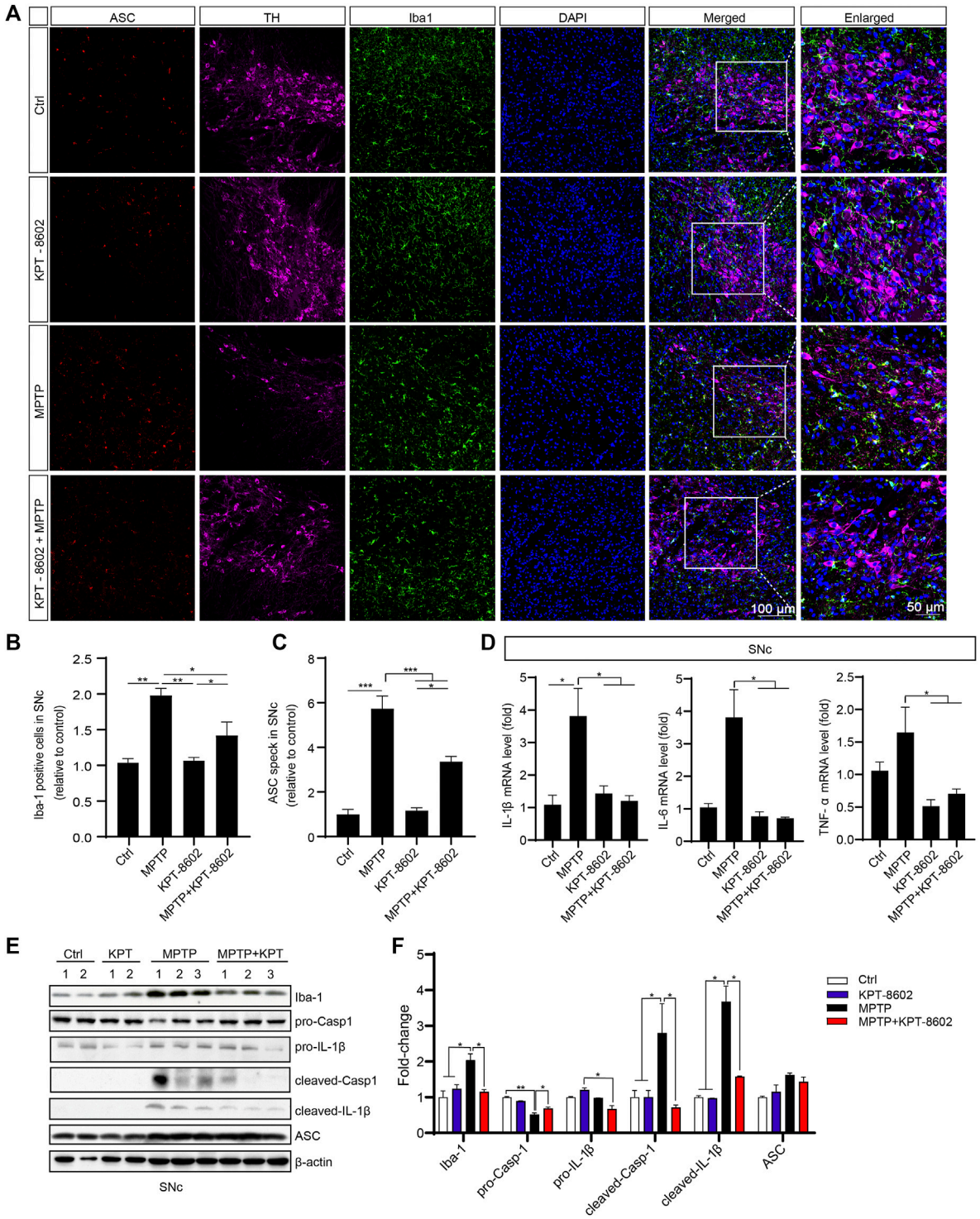

FIGURE 7 | KPT-8602 inhibits activation of the NLRP3 inflammasome *in vivo*. **(A)** Substantia nigra compacta from PD mice administered KPT-8602 or vehicle were stained with an anti-Iba-1 and anti-ASC antibody to evaluate the activation of microglia and the NLRP3 inflammasome (5 mice per group). The number of Iba-1-positive cells **(B)** and ASC specks **(C)** was analyzed by ImageJ. Scale bars, 100 μm for low-magnification images and 50 μm for high-magnification images, respectively. **(D)** Expression levels of IL-1β, IL-6, and TNF-α in the SNc were detected by real-time PCR. The expression of Iba-1, pro-caspase-1, pro-IL-1β, cleaved caspase-1, cleaved-IL-1β, ASC, and *β*-actin in the SNc was analyzed by Western blotting **(E)**, and the gray value of their bands was analyzed by ImageJ **(F)**. (* indicates $p < 0.05$, ** indicates $p < 0.01$, *** indicates $p < 0.001$ by one-way ANOVA).

KPT-8602 Suppresses LPS-Induced Systemic Inflammation *In Vivo*

We further evaluated the potential anti-inflammatory effect of KPT-8602 *in vivo* in an LPS-induced inflammation mice model (**Figure 5A**). We found that the LPS-induced macrophage infiltration (indicated by arrow) in the liver (**Figure 5B**; **Supplementary Figure.3A**), structural destruction (indicated by arrowheads) of the lung (**Figure 5B**; **Supplementary figure.3B**), and the kidney (**Figure 5B**; **Supplementary Figure 3C**) were attenuated by administration of KPT-8602. In addition, the LPS-induced expression of pro-inflammatory cytokines, such as IL-1β, IL-6, and iNOS, in the liver (**Figure 5C**) and lung (**Figure 5D**) were downregulated by KPT-8602 administration. Furthermore, the expression of IL-1β precursor and NLRP3, and mature IL-1β (cleaved IL-1β) in the liver was significantly inhibited by KPT-8602 (**Figures 5E, F**). Consistently, the level of mature IL-1β and expression of NLRP3 induced by LPS was also decreased in the lung in KPT-8602-treated mice (**Supplementary Figures. 3D, E**). Together, these results suggested that KPT-8602 inhibited the activation of the NF-κB pathway and the NLRP3 inflammasome *in vivo*.

KPT-8602 Ameliorates MPTP-Induced Dopaminergic Neuron Loss and Microglial Activation

In this section, we investigated the potential effect of KPT-8602 in inhibiting neuroinflammation and attenuating neurodegeneration in the MPTP-induced PD mouse model (Al-Bachari et al., 2020) (**Figure 6A**). In the rotarod test, KPT-8602 administration attenuated locomotor incoordination caused by MPTP (**Figures 6B, C**). KPT-8602 also significantly increased the number of tyrosine hydroxylase (TH)-positive cells in the substantia nigra compacta (SNc) (**Figures 6D, E**), and increased TH expression in the SNc and striatum (**Figures 6F–H**), suggesting KPT-8602 protected dopaminergic neurons against MPTP-induced cell death.

To determine the role of microglia and the NLRP3 inflammasome activation in this process in the SNc, we co-stained TH and ASC with microglia indicated by ionized calcium-binding adaptor molecule 1 (Iba1). KPT-8602 administration caused a reduced number of amoeboid-like microglia (**Figures 7A, B**) and ASC speck (**Figures 7A, C**) in the SNc of the PD mice model. Consistent with this result, the expression of IL-1β, IL-6, and TNF-α in the SNc area was also reduced in the KPT-8602-treated PD mice model (**Figure 7D**). Consistently, MPTP-induced activation of caspase-1 cleavage and maturation of IL-1β were also ameliorated by KPT-8602 (**Figures 7E, F**). Taken together, these results demonstrated that KPT-8602 demonstrated neuroprotective effects against MPTP-induced dopaminergic neuron loss and the NLRP3 inflammasome activation *in vivo*.

DISCUSSION

In this study, we demonstrate that KPT-8602 exhibits a strong anti-inflammatory effect by blocking the NF-κB pathway and the NLRP3 inflammasome. More importantly, KPT-8602 had significant therapeutic effects on LPS-induced systemic inflammation and MPTP-induced PD in mice. This finding may provide new therapeutic approaches for NF-κB and NLRP3-driven diseases and suggests that KPT-8602 can be used to treat inflammatory diseases in addition to cancer.

Our results indicated that KPT-8602 was identified to block the activation of the NLRP3 inflammasome by inhibiting the NF-κB pathway. The NF-κB pathway is considered the "priming" signal for the NLRP3 inflammasome activation (Zheng et al., 2020). The classical activation of NF-κB is dependent on the phosphorylation of IκBα and p65, followed by degradation of IκBα and nuclear translocation of p65 (Fu et al., 2021). Here, we found that upon the stimulation with LPS, cells pretreated with KPT-8602 displayed decreased phosphorylation of IκBα and p65, especially the phosphorylation and translocation of p65. One possible mechanism is that KPT-8602 might inhibit the expression of XPO1 and thereby reduces the nuclear import of p65. It has been reported that inhibition of the nuclear exporting activity of XPO1 causes the accumulation of p65 in the nuclear (Kashyap et al., 2016). In our result, however, no accumulation of p65 in nuclear was observed in KPT-8602-treated cells and XPO1-silenced cells. This difference was potentially caused by different mechanisms of different inhibitors of XPO1. In addition, we found that cells treated with KPT-8602 displayed a lower level of phosphorylated IκBα, indicating that XPO1 was involved in the process of IKKα/β-mediated phosphorylation of IκBα. However, the mechanism of KPT-8602 in regulating inflammasome is unclear. It is well known that upregulation of NLPR3 and pro-IL-1β is the "priming" signal for the inflammasome activation (Sutterwala et al., 2014). Our results demonstrated that KPT-8602 could directly suppress the transcription of NLRP3 and pro-IL-1β, impeded the assembly of the NLRP3 inflammasome, and thereby decreased the release of mature cytokines.

Increasing evidence indicates that the activation of the NF-κB pathway and the NLRP3 inflammasome is widely involved in different diseases, such as colitis, diabetes, and COVID-19 infection-induced pneumonia in the peripheral tissue (Wang et al., 2018; An et al., 2019; Xian et al., 2021). Aberrant activation of the NLRP3 inflammasome is also involved in the development of several neurodegenerative disorders, such as PD, Alzheimer's disease (AD), and multiple sclerosis (Heneka et al., 2013; Haque et al., 2020; Malhotra et al., 2020). The inhibition of NLRP3 inflammasomes ameliorates the clinical and pathological symptoms of these diseases (Martinon et al., 2006; Duewell et al., 2010; Heneka et al., 2013; Lee et al., 2013; Wang et al., 2019; Pan et al., 2021). However, only a few NLRP3-selective inhibitors are identified up to date, and most of these inhibitors are not available for clinical use (Coll et al., 2015; Jiang et al., 2017; He et al., 2018; Huang et al., 2018). Therefore, new drug development targeting the NF-κB signaling pathway and NLRP3 inflammasome potentially provides a new therapeutic avenue for the treatment of such diseases.

Herein, we demonstrated that KPT-8602 inhibited the activation of the NF-κB pathway and the NLRP3

inflammasome *in vitro*. Most importantly, KPT-8602 protected peripheral tissue injury against LPS-induced systemic inflammation and ameliorated CNS neuronal cell death and neuroinflammation induced by MPTP *in vivo*, suggesting that KPT-8602 was a promising candidate for the clinical treatment of inflammation-associated disease in the peripheral system and CNS. KPT-8602 is a second-generation XPO1-selective inhibitor, and recent studies suggest that XPO1 is involved in a variety of neurological and neuromuscular diseases (Hightower et al., 2020). Inhibition of XPO1 by KPT-350 increases the expression of neuroprotectant proteins and reduces the inflammatory response, leading to improved recovery of motor functions after TBI (Tajiri et al., 2016). Moreover, KPT-8602 is distinctly different from other XPO1 inhibitors due to its poor blood–brain barrier (BBB) permeability. This feature limits its toxicity and anti-inflammatory effects in the CNS. However, when the integrity of BBB is compromised due to diseases such as PD, AD, and stroke, the application of KPT-8602 in the treatment of such diseases is viable (Al-Bachari et al., 2020; Liao et al., 2020). Therefore, our results suggest that KPT-8602 can be used as a potential anti-inflammatory agent in the treatment of a variety of neurodegenerative diseases.

In conclusion, our study suggests that KPT-8602 could be used as an anti-inflammation agent by inhibiting the activation of the NF-κB pathway and the NLRP3 inflammasome. Mechanically, inhibition of XPO1 by KPT-8602 impaired IKKα/β-mediated phosphorylation of IκBα and thereafter decreased the nuclear translocation of p65. In addition, both LPS-induced peripheral inflammation and MPTP-induced neuroinflammation were attenuated by the administration of KPT-8602. Given the pivotal role of the NF-κB pathway and the NLRP3 inflammasome in the pathogenesis of PD, KPT-8602 was suggested to be a promising drug for the clinical treatment of such diseases.

DATA AVAILABILITY STATEMENT

The original contributions presented in the study are included in the article/**Supplementary Material**, further inquiries can be directed to the corresponding authors.

ETHICS STATEMENT

The animal study was reviewed and approved by the Institutional Animal Care and Use Committee of the Beijing Institute of Basic Medical Sciences.

AUTHOR CONTRIBUTIONS

SL and YL designed and performed the experiments and wrote the manuscript. SW, NC, and JW performed the Roto-Rod test. RG, JC, ZY, and YC polished the manuscript. YL and YC supervised the study.

FUNDING

This work was supported by the National Natural Science Foundation of China (82071676, 81703492 to YC); the National Natural Science Foundation of China (81701187 to YJL); the Open Project of Modern Preparation of TCM, Ministry of Education, Jiangxi University of Traditional Chinese Medicine (TCM-201914 to YJL).

SUPPLEMENTARY MATERIAL

The Supplementary Material for this article can be found online at: https://www.frontiersin.org/articles/10.3389/fphar.2022.847605/full#supplementary-material

REFERENCES

Al-Bachari, S., Naish, J. H., Parker, G. J. M., Emsley, H. C. A., and Parkes, L. M. (2020). Blood-Brain Barrier Leakage Is Increased in Parkinson's Disease. *Front. Physiol.* 11, 593026. doi:10.3389/fphys.2020.593026

An, Y., Zhang, H., Wang, C., Jiao, F., Xu, H., Wang, X., et al. (2019). Activation of ROS/MAPKs/NF-κB/NLRP3 and Inhibition of Efferocytosis in Osteoclast-Mediated Diabetic Osteoporosis. *FASEB J.* 33, 12515–12527. doi:10.1096/fj.201802805RR

Azmi, A. S., Uddin, M. H., and Mohammad, R. M. (2021). The Nuclear export Protein XPO1 - from Biology to Targeted Therapy. *Nat. Rev. Clin. Oncol.* 18, 152–169. doi:10.1038/s41571-020-00442-4

Chen, C., Siegel, D., Gutierrez, M., Jacoby, M., Hofmeister, C. C., Gabrail, N., et al. (2018). Safety and Efficacy of Selinexor in Relapsed or Refractory Multiple Myeloma and Waldenstrom Macroglobulinemia. *Blood* 131, 855–863. doi:10.1182/blood-2017-08-797886

Cheng, J., Liao, Y., Dong, Y., Hu, H., Yang, N., Kong, X., et al. (2020). Microglial Autophagy Defect Causes Parkinson Disease-like Symptoms by Accelerating Inflammasome Activation in Mice. *Autophagy* 16, 1–13. doi:10.1080/15548627.2020.1719723

Coll, R. C., Robertson, A. A., Chae, J. J., Higgins, S. C., Muñoz-Planillo, R., Inserra, M. C., et al. (2015). A Small-Molecule Inhibitor of the NLRP3 Inflammasome for the Treatment of Inflammatory Diseases. *Nat. Med.* 21, 248–255. doi:10.1038/nm.3806

Duewell, P., Kono, H., Rayner, K. J., Sirois, C. M., Vladimer, G., Bauernfeind, F. G., et al. (2010). NLRP3 Inflammasomes Are Required for Atherogenesis and Activated by Cholesterol Crystals. *Nature* 464, 1357–1361. doi:10.1038/nature08938

Elliott, E. I., and Sutterwala, F. S. (2015). Initiation and Perpetuation of NLRP3 Inflammasome Activation and Assembly. *Immunol. Rev.* 265, 35–52. doi:10.1111/imr.12286

Etchin, J., Berezovskaya, A., Conway, A. S., Galinsky, I. A., Stone, R. M., Baloglu, E., et al. (2017). KPT-8602, a Second-Generation Inhibitor of XPO1-Mediated Nuclear export, Is Well Tolerated and Highly Active against AML Blasts and Leukemia-Initiating Cells. *Leukemia* 31, 143–150. doi:10.1038/leu.2016.145

Fan, T. W., Higashi, R. M., Song, H., Daneshmandi, S., Mahan, A. L., Purdom, M. S., et al. (2021). Innate Immune Activation by Checkpoint Inhibition in Human Patient-Derived Lung Cancer Tissues. *elife* 10, e69578. doi:10.7554/elife.69578

Fu, Y. J., Xu, B., Huang, S. W., Luo, X., Deng, X. L., Luo, S., et al. (2021). Baicalin Prevents LPS-Induced Activation of TLR4/NF-Kb P65 Pathway and Inflammation in Mice via Inhibiting the Expression of CD14. *Acta Pharmacol. Sin* 42, 88–96. doi:10.1038/s41401-020-0411-9

Gravina, G. L., Senapedis, W., McCauley, D., Baloglu, E., Shacham, S., and Festuccia, C. (2014). Nucleo-cytoplasmic Transport as a Therapeutic Target of Cancer. *J. Hematol. Oncol.* 7, 85. doi:10.1186/s13045-014-0085-1

Haines, J. D., Herbin, O., de la Hera, B., Vidaurre, O. G., Moy, G. A., Sun, Q., et al. (2015). Nuclear export Inhibitors Avert Progression in Preclinical Models of Inflammatory Demyelination. *Nat. Neurosci.* 18, 511–520. doi:10.1038/nn.3953

Haque, M. E., Akther, M., Jakaria, M., Kim, I. S., Azam, S., and Choi, D. K. (2020). Targeting the Microglial NLRP3 Inflammasome and its Role in Parkinson's Disease. *Mov Disord.* 35, 20–33. doi:10.1002/mds.27874

He, H., Jiang, H., Chen, Y., Ye, J., Wang, A., Wang, C., et al. (2018). Oridonin Is a Covalent NLRP3 Inhibitor with strong Anti-inflammasome Activity. *Nat. Commun.* 9, 2550. doi:10.1038/s41467-018-04947-6

Heneka, M. T., Kummer, M. P., Stutz, A., Delekate, A., Schwartz, S., Vieira-Saecker, A., et al. (2013). NLRP3 Is Activated in Alzheimer's Disease and Contributes to Pathology in APP/PS1 Mice. *Nature* 493, 674–678. doi:10.1038/nature11729

Hightower, R. M., Reid, A. L., Gibbs, D. E., Wang, Y., Widrick, J. J., Kunkel, L. M., et al. (2020). The SINE Compound KPT-350 Blocks Dystrophic Pathologies in DMD Zebrafish and Mice. *Mol. Ther.* 28, 189–201. doi:10.1016/j.ymthe.2019.08.016

Hill, R., Cautain, B., de Pedro, N., and Link, W. (2014). Targeting Nucleocytoplasmic Transport in Cancer Therapy. *Oncotarget* 5, 11–28. doi:10.18632/oncotarget.1457

Hing, Z. A., Fung, H. Y., Ranganathan, P., Mitchell, S., El-Gamal, D., Woyach, J. A., et al. (2016). Next-generation XPO1 Inhibitor Shows Improved Efficacy and *In Vivo* Tolerability in Hematological Malignancies. *Leukemia* 30, 2364–2372. doi:10.1038/leu.2016.136

Huang, Y., Jiang, H., Chen, Y., Wang, X., Yang, Y., Tao, J., et al. (2018). Tranilast Directly Targets NLRP3 to Treat Inflammasome-Driven Diseases. *EMBO Mol. Med.* 10 (4), e8689. doi:10.15252/emmm.201708689

Hutten, S., and Kehlenbach, R. H. (2007). CRM1-mediated Nuclear export: to the Pore and beyond. *Trends Cel Biol* 17, 193–201. doi:10.1016/j.tcb.2007.02.003

Jakubowiak, A. J., Jasielec, J. K., Rosenbaum, C. A., Cole, C. E., Chari, A., Mikhael, J., et al. (2019). Phase 1 Study of Selinexor Plus Carfilzomib and Dexamethasone for the Treatment of Relapsed/refractory Multiple Myeloma. *Br. J. Haematol.* 186, 549–560. doi:10.1111/bjh.15969

Jiang, H., He, H., Chen, Y., Huang, W., Cheng, J., Ye, J., et al. (2017). Identification of a Selective and Direct NLRP3 Inhibitor to Treat Inflammatory Disorders. *J. Exp. Med.* 214, 3219–3238. doi:10.1084/jem.20171419

Kashyap, T., Argueta, C., Aboukameel, A., Unger, T. J., Klebanov, B., Mohammad, R. M., et al. (2016). Selinexor, a Selective Inhibitor of Nuclear Export (SINE) Compound, Acts through NF-Kb Deactivation and Combines with Proteasome Inhibitors to Synergistically Induce Tumor Cell Death. *Oncotarget* 7, 78883–78895. doi:10.18632/oncotarget.12428

Kau, T. R., Way, J. C., and Silver, P. A. (2004). Nuclear Transport and Cancer: from Mechanism to Intervention. *Nat. Rev. Cancer* 4, 106–117. doi:10.1038/nrc1274

Lang, Y. D., Chen, H. Y., Ho, C. M., Shih, J. H., Hsu, E. C., Shen, R., et al. (2019). PSPC1-interchanged Interactions with PTK6 and β-catenin Synergize Oncogenic Subcellular Translocations and Tumor Progression. *Nat. Commun.* 10, 5716. doi:10.1038/s41467-019-13665-6

Lee, H. M., Kim, J. J., Kim, H. J., Shong, M., Ku, B. J., and Jo, E. K. (2013). Upregulated NLRP3 Inflammasome Activation in Patients with Type 2 Diabetes. *Diabetes* 62, 194–204. doi:10.2337/db12-0420

Li, X., Liao, Y., Dong, Y., Li, S., Wang, F., Wu, R., et al. (2020). Mib2 Deficiency Inhibits Microglial Activation and Alleviates Ischemia-Induced Brain Injury. *Aging Dis.* 11, 523–535. doi:10.14336/AD.2019.0807

Liao, Y., Cheng, J., Kong, X., Li, S., Li, X., Zhang, M., et al. (2020). HDAC3 Inhibition Ameliorates Ischemia/reperfusion-Induced Brain Injury by Regulating the Microglial cGAS-STING Pathway. *Theranostics* 10, 9644–9662. doi:10.7150/thno.47651

Maehara, T., Higashitarumi, F., Kondo, R., and Fujimori, K. (2020). Prostaglandin F2α Receptor Antagonist Attenuates LPS-Induced Systemic Inflammatory Response in Mice. *FASEB J.* 34, 15197–15207. doi:10.1096/fj.202001481R

Malhotra, S., Costa, C., Eixarch, H., Keller, C. W., Amman, L., Martínez-Banaclocha, H., et al. (2020). NLRP3 Inflammasome as Prognostic Factor and Therapeutic Target in Primary Progressive Multiple Sclerosis Patients. *Brain* 143, 1414–1430. doi:10.1093/brain/awaa084

Mao, L., and Yang, Y. (2013). Targeting the Nuclear Transport Machinery by Rational Drug Design. *Curr. Pharm. Des.* 19, 2318–2325. doi:10.2174/1381612811319120018

Martinon, F., Pétrilli, V., Mayor, A., Tardivel, A., and Tschopp, J. (2006). Gout-associated Uric Acid Crystals Activate the NALP3 Inflammasome. *Nature* 440, 237–241. doi:10.1038/nature04516

Olazagoitia-Garmendia, A., Zhang, L., Mera, P., Godbout, J. K., Sebastian-DelaCruz, M., Mendoza, L. M., et al. (2021). Gluten-induced RNA Methylation Changes Regulate Intestinal Inflammation via Allele-specific XPO1 Translation in Epithelial Cells. *Gut.*71, gutjnl-2020-322566. doi:10.1136/gutjnl-2020-322566

Pan, R. Y., Kong, X. X., Cheng, Y., Du, L., Wang, Z. C., Yuan, C., et al. (2021). 1,2,4-Trimethoxybenzene Selectively Inhibits NLRP3 Inflammasome Activation and Attenuates Experimental Autoimmune Encephalomyelitis. *Acta Pharmacol. Sin.* 42, 1769–1779. doi:10.1038/s41401-021-00613-8

Shao, B. Z., Xu, Z. Q., Han, B. Z., Su, D. F., and Liu, C. (2015). NLRP3 Inflammasome and its Inhibitors: a Review. *Front. Pharmacol.* 6, 262. doi:10.3389/fphar.2015.00262

Sun, Q., Chen, X., Zhou, Q., Burstein, E., Yang, S., and Jia, D. (2016). Inhibiting Cancer Cell Hallmark Features through Nuclear export Inhibition. *Signal. Transduct Target. Ther.* 1, 16010. doi:10.1038/sigtrans.2016.10

Sutterwala, F. S., Haasken, S., and Cassel, S. L. (2014). Mechanism of NLRP3 Inflammasome Activation. *Ann. N. Y Acad. Sci.* 1319, 82–95. doi:10.1111/nyas.12458

Tajiri, N., De La Peña, I., Acosta, S. A., Kaneko, Y., Tamir, S., Landesman, Y., et al. (2016). A Nuclear Attack on Traumatic Brain Injury: Sequestration of Cell Death in the Nucleus. *CNS Neurosci. Ther.* 22, 306–315. doi:10.1111/cns.12501

Taylor-Kashton, C., Lichtensztejn, D., Baloglu, E., Senapedis, W., Shacham, S., Kauffman, M. G., et al. (2016). XPO1 Inhibition Preferentially Disrupts the 3D Nuclear Organization of Telomeres in Tumor Cells. *J. Cel Physiol* 231, 2711–2719. doi:10.1002/jcp.25378

Turner, J. G., Dawson, J., and Sullivan, D. M. (2012). Nuclear export of Proteins and Drug Resistance in Cancer. *Biochem. Pharmacol.* 83, 1021–1032. doi:10.1016/j.bcp.2011.12.016

Wang, A. Y., and Liu, H. (2019). The Past, Present, and Future of CRM1/XPO1 Inhibitors. *Stem Cel Investig* 6, 6. doi:10.21037/sci.2019.02.03

Wang, S., Lin, Y., Yuan, X., Li, F., Guo, L., and Wu, B. (2018). REV-ERBα Integrates colon Clock with Experimental Colitis through Regulation of NF-Kb/nlrp3 axis. *Nat. Commun.* 9, 4246. doi:10.1038/s41467-018-06568-5

Wang, S., Yuan, Y. H., Chen, N. H., and Wang, H. B. (2019). The Mechanisms of NLRP3 Inflammasome/pyroptosis Activation and Their Role in Parkinson's Disease. *Int. Immunopharmacol* 67, 458–464. doi:10.1016/j.intimp.2018.12.019

Wu, R., Chen, H., Ma, J., He, Q., Huang, Q., Liu, Q., et al. (2016). c-Abl-p38α Signaling Plays an Important Role in MPTP-Induced Neuronal Death. *Cell Death Differ* 23, 542–552. doi:10.1038/cdd.2015.135

Xian, H., Liu, Y., Rundberg Nilsson, A., Gatchalian, R., Crother, T. R., Tourtellotte, W. G., et al. (2021). Metformin Inhibition of Mitochondrial ATP and DNA Synthesis Abrogates NLRP3 Inflammasome Activation and Pulmonary Inflammation. *Immunity* 54, 1463–e11. doi:10.1016/j.immuni.2021.05.004

Xu, D., Farmer, A., and Chook, Y. M. (2010). Recognition of Nuclear Targeting Signals by Karyopherin-β Proteins. *Curr. Opin. Struct. Biol.* 20, 782–790. doi:10.1016/j.sbi.2010.09.008

Xu, D., Farmer, A., Collett, G., Grishin, N. V., and Chook, Y. M. (2012). Sequence and Structural Analyses of Nuclear export Signals in the NESdb Database. *Mol. Biol. Cel* 23, 3677–3693. doi:10.1091/mbc.E12-01-0046

Zheng, R., Ruan, Y., Yan, Y., Lin, Z., Xue, N., Yan, Y., et al. (2021). Melatonin Attenuates Neuroinflammation by Down-Regulating NLRP3 Inflammasome via a SIRT1-dependent Pathway in MPTP-Induced Models of Parkinson's Disease. *J. Inflamm. Res.* 14, 3063–3075. doi:10.2147/JIR.S317672

Zheng, X., Hou, Y., He, H., Chen, Y., Zhou, R., Wang, X., et al. (2020). Synthetic Vitamin K Analogs Inhibit Inflammation by Targeting the NLRP3 Inflammasome. *Cell Mol Immunol* 8, 2422–2430. doi:10.1038/s41423-020-00545-z

Conflict of Interest: The authors declare that the research was conducted in the absence of any commercial or financial relationships that could be construed as a potential conflict of interest.

Publisher's Note: All claims expressed in this article are solely those of the authors and do not necessarily represent those of their affiliated organizations, or those of the publisher, the editors, and the reviewers. Any product that may be evaluated in this article, or claim that may be made by its manufacturer, is not guaranteed or endorsed by the publisher.

frontiers | Frontiers in Pharmacology

ORIGINAL RESEARCH
published: 01 June 2022
doi: 10.3389/fphar.2022.778755

Aloperine Ameliorates IMQ-Induced Psoriasis by Attenuating Th17 Differentiation and Facilitating Their Conversion to Treg

Hai-Feng Zhou[1†], Fa-Xi Wang[1†], Fei Sun[1†], Xin Liu[1], Shan-Jie Rong[1], Jia-Hui Luo[1], Tian-Tian Yue[1], Jun Xiao[1,2], Chun-Liang Yang[1], Wan-Ying Lu[1], Xi Luo[1], Qing Zhou[1], He Zhu[1], Ping Yang[1], Fei Xiong[1], Qi-Lin Yu[1], Shu Zhang[1] and Cong-Yi Wang[1]**

[1]NHC Key Laboratory of Respiratory Diseases, Department of Respiratory and Critical Care Medicine, The Center for Biomedical Research, Tongji Hospital, Tongji Medical College, Huazhong University of Sciences and Technology, Wuhan, China, [2]Department of Urology, Tongji Hospital, Tongji Medical College, Huazhong University of Sciences and Technology, Wuhan, China

Aloperine is an anti-inflammatory compound isolated from the Chinese herb *Sophora alopecuroides L.* Previously, our group has reported that the generation of induced Treg was promoted by aloperine treatment in a mouse colitis model. However, the effect of aloperine on effector T cell subsets remains unclear. We therefore carefully examined the effect of aloperine on the differentiation of major subsets of T helper cells. Based on our results, psoriasis, a Th17 dominant skin disease, is selected to explore the potential therapeutic effect of aloperine *in vivo*. Herein, we demonstrated that topical application of aloperine suppressed epidermal proliferation, erythema, and infiltration of inflammatory cells in skin lesions. Mechanistic studies revealed that aloperine suppressed the differentiation of Th17 cells directly through inhibiting the phosphorylation of STAT3 or indirectly through impairing the secretion of Th17-promoting cytokines by dendritic cells. Moreover, aloperine enhanced the conversion of Th17 into Treg *via* altering the pSTAT3/pSTAT5 ratio. Collectively, our study supported that aloperine possesses the capacity to affect Th17 differentiation and modulates Th17/Treg balance, thereby alleviating imiquimod (IMQ)-induced psoriasis in mice.

Keywords: Psoriasis, Aloperine, Th17 differentiation, Th17 to Treg conversion, STAT3/STAT5 pathway

OPEN ACCESS

Edited by:
Nandakumar Natarajan, The University of Texas Health Science Center at Tyler, United States

Reviewed by:
Andrei Adrian Tica, University of Medicine and Pharmacy of Craiova, Romania
Belal Chami, The University of Sydney, Australia
Stalinraja Maruthamuthu, University of California, San Francisco, United States

***Correspondence:**
Shu Zhang
szhang@tjh.tjmu.edu.cn
Cong-Yi Wang
wangcy@tjh.tjmu.edu.cn

†These authors have contributed equally to this work

Specialty section:
This article was submitted to Inflammation Pharmacology, a section of the journal Frontiers in Pharmacology

Received: *17 September 2021*
Accepted: *11 April 2022*
Published: *01 June 2022*

Citation:
Zhou H-F, Wang F-X, Sun F, Liu X, Rong S-J, Luo J-H, Yue T-T, Xiao J, Yang C-L, Lu W-Y, Luo X, Zhou Q, Zhu H, Yang P, Xiong F, Yu Q-L, Zhang S and Wang C-Y (2022) Aloperine Ameliorates IMQ-Induced Psoriasis by Attenuating Th17 Differentiation and Facilitating Their Conversion to Treg. Front. Pharmacol. 13:778755. doi: 10.3389/fphar.2022.778755

INTRODUCTION

$CD4^+$ T helper cells play a pivotal role in the adaptive immune reaction associated with immune defense, immune surveillance, and immune homeostasis. These various functions are achieved through the differentiation of a variety of effector subsets, including Th1, Th2, Th17, follicular helper T cells (Tfh), and regulatory T cells (Treg) (Zhu and Paul, 2008). Upon interaction with the cognate antigen presented by antigen-presenting cells such as dendritic cells (DCs) in the periphery, $CD4^+$ naïve T cells undergo a process of massive proliferation and differentiation into the distinct helper T cell subsets. The process of $CD4^+$ T cell differentiation decision is governed predominantly by the cytokines in the microenvironment and the strength of the interaction of the T cell antigen receptor with the antigen. Many complex inflammatory diseases are caused by the disorder of these processes, such as type 1 diabetes, psoriasis, asthma, and so on (Sun et al., 2021; Yue et al., 2021). Although

many therapies including glucocorticoids and immunomodulators are used in clinics, the development of novel, safe, and effective agents that target $CD4^+$ T cells for treatment is further needed.

Aloperine is a kind of quinolizidine alkaloid extracted from *Sophora alopecuroides L.*, which has been used effectively in the treatment of various clinical disorders, such as dysentery, eczema, furuncle, and other skin inflammatory diseases (Wang et al., 2020). Recent studies including our own revealed that aloperine possesses the bioactivities against cancer, viral infection, oxidative stress, cardiovascular and neurological diseases (Wang et al., 2015; Hu et al., 2016; Fu et al., 2017; Ling et al., 2018; Zhang et al., 2018; Zhao et al., 2018; Chang et al., 2019; Li et al., 2020). Accumulating evidence shows that the clinical effects of the natural plant alkaloid are related to the up- or down-regulation of immune responses (Feng et al., 2006; Furusawa and Wu, 2007). Previously, our group demonstrated that oral administration of aloperine protects the mice against DSS-induced colitis through promoting Treg differentiation and activation (Fu et al., 2017). Thus, the effect of aloperine on the $CD4^+$ T cell differentiation pattern catches our attention.

Psoriasis is a common chronic inflammatory skin disease characterized by the keratinocyte abnormal proliferation and differentiation, dermal blood vessel hyperplasia, and massive inflammatory infiltration (Mak et al., 2009; Lowes et al., 2014). According to epidemiologic survey, the morbidity rate of psoriasis in Asia is below 0.5%, while it is estimated to affect about 2–4% of the population in Western countries (Parisi et al., 2013; Boehncke, 2015). Psoriasis not only is a skin disease but also causes systemic disorders, such as psoriatic arthritis, cardiovascular disease, metabolic syndrome, and so on, which together contribute to a reduced quality of life and represent a mental stress on individuals and considerable economic burden on families and the society (Takeshita et al., 2017). Although the exact etiology of psoriasis is not fully understood, extensive studies have demonstrated it as a multifactorial disease.

As an immune-mediated disease, both innate and adaptive immune cells are involved in the pathogenesis of psoriasis, including different T-cell types such as Th17 cells, Th1 cells and Treg, dermal dendritic cells, macrophages, neutrophils, and natural killer cells (Deng et al., 2016). Robust evidence accumulated in the past years has shown that the IL-23/Th17 axis is central to the psoriatic pathology (Lowes et al., 2013; Girolomoni et al., 2017; Puig, 2017; Conrad and Gilliet, 2018). It is believed that trauma and infection can activate skin-resident dendritic cells and macrophages to produce IL-6, IL-23, and IL-12, which stimulate the maturation of Th17 and Th1 cells, respectively. IL-23 from inflammatory DCs has a great role in the amplification, activation, and pathogenic conversion of Th17 cells (Schirmer et al., 2010). Subsequent secretions of inflammatory cytokines, such as IL-17, IL-22, TNF-α, IFN-γ, and vascular endothelial growth factor (VEGF), stimulate keratinocyte proliferation and angiogenesis, which have important roles both in disease development and progression. On one hand, IL-17A stimulates keratinocyte proliferation and endothelial expression of P-selectins, E-selectins, and integrin ligands, including ICAM-1 and VCAM-1, to enhance neutrophil mobilization. On the other hand, activated keratinocytes produce large amounts of chemokines and antimicrobial peptides, which would in turn promote Th17 cell recruitment and produce more IL-17, resulting in a positive feedback loop that perpetuates the inflammatory response of psoriasis.

Currently, there is no cure for the spectrum of psoriatic diseases. By targeting the cytokine and immune networks in psoriasis, researchers have developed various therapeutic options, including topical agents (such as corticosteroids) and systemic immunosuppressive agents (such as methotrexate and cyclosporine). However, those current medications may have severe side effects, especially the high risk of infection. Thus, better and safer drugs and therapeutic strategies need to be developed. Previously, our group identified the role of aloperine in Treg induction and colitis treatment. In this study, we further revealed that the administration of aloperine modulates Th17/Treg balance by targeting the STAT3/STAT5 signaling pathway and/or indirectly through affecting the recruitment and activation of antigen-presenting cells in psoriatic skin lesions, which render it to be a potential candidate drug to psoriasis in clinical settings.

MATERIALS AND METHODS

Animals

Healthy male C57BL/6 mice (8–10 weeks old) were purchased from Beijing Vital River Laboratory Animal Technology Co., Ltd. (Beijing, China). The mice were bred at the Tongji Medical College and maintained under SPF conditions for at least 1 week before any experiment. All animal studies were approved by the Animal Care and Use Committee in Tongji Hospital (TJH-201612001).

Psoriasis Model and Aloperine Treatment

Aloperine (Shanghai Yuan-ye Bio-Technology Co., Ltd.) was made of 2% cream by mixing in the emollient cream vehicle. Imiquimod (IMQ) cream was purchased from Sichuan Mingxin Pharmaceutical. Twenty mice were randomly divided into the treatment group (2% aloperine + imiquimod) and vehicle control group (vehicle + imiquimod). The mice were shaved on the back, and then subjected to 5% Aldara (a brand of IMQ) at a dose of 62.5 mg daily on the back skin for 5 consecutive days, and aloperine or vehicle cream was administered at the same time or after the psoriasis model was established.

Scoring of Psoriatic Skin Inflammation

The severity of inflammation of the back skin was evaluated by an objective scoring system, which was based on the Psoriasis Area and Severity Index (PASI). Erythema, scaling, and anabrosis were scored independently from 0 to 4 as follows: 0, none; 1, slight; 2, moderate; 3, marked; and 4, very marked. The cumulative score (erythema plus scaling plus thickening) was served to indicate the severity of inflammation (scale 0–12).

Histological Analysis

The skin tissue samples were collected and fixed in 4% paraformaldehyde for 24 h at room temperature and

TABLE 1 | Primers used for the real-time PCR.

Target gene	Forward sequence (5′-3′)	Reverse sequence (5′-3′)
m-IL-6	5′-TACCACTTCACAAGTCGGAGGC-3′	5′-CTGCAAGTGCATCATCGTTGTTC-3′
m-IL-17A	5′-CAGACTACCTCAACCGTTCCAC-3′	5′-TCCAGCTTTCCCTCCGCATTGA-3′
m-IL-23	5′-CATGCTAGCCTGGAACGCACAT-3′	5′-ACTGGCTGTTGTCCTTGAGTCC-3′
m-IL-1β	5′-TGGACCTTCCAGGATGAGGACA-3′	5′-GTTCATCTCGGAGCCTGTAGTG-3′
m-RORγt	5′-GTGGAGTTTGCCAAGCGGCTTT-3′	5′-CCTGCACATTCTGACTAGGACG-3′
m-IL-10	5′-CGGGAAGACAATAACTGCACCC-3′	5′-CGGTTAGCAGTATGTTGTCCAGC-3′
m-Foxp3	5′-CCTGGTTGTGAGAAGGTCTTCG-3′	5′-TGCTCCAGAGACTGCACCACTT-3′
m-TGF-β	5′-TGATACGCCTGAGTGGCTGTCT-3′	5′-CACAAGAGCAGTGAGCGCTGAA-3′
m-IFN-γ	5′-CAGCAACAGCAAGGCGAAAAAGG-3′	5′-TTTCCGCTTCCTGAGGCTGGAT-3′
m-TNF-α	5′-GGTGCCTATGTCTCAGCCTCTT-3′	5′-GCCATAGAACTGATGAGAGGGAG-3′
m-β-actin	5′-CATTGCTGACAGGATGCAGAAGG-3′	5′-TGCTGGAAGGTGGACAGTGAGG-3′

embedded in paraffin. The 4-μm sections were subjected to hematoxylin and eosin (H&E) staining as previously described. Similarly, partial sections were stained with the Ki-67 antibody, and developed by 3,3'-diaminobenzidine as reported (Yue et al., 2021).

Mouse Naïve CD4$^+$ T-Cell Isolation and Differentiation

$CD4^+CD44^{low}CD62L^{high}$ naïve T-cells were extracted from spleens and lymph nodes of 10-week-old C57BL/6 male mice with a mouse naïve $CD4^+$ T-cell isolation kit (catalog number 19782, STEMCELL Technologies EasySep™, CA, United States), and the purity of isolated cells was >90%. The isolated naïve $CD4^+$ T-cells were seeded into culture wells coated with 10 μg/ml anti-CD3 and 10 μg/ml anti-CD28 in sterile phosphate-buffered saline (PBS) and incubated overnight at 4°C. Furthermore, different subsets were differentiated by Th1, Th2, and Th17 polarizing conditions with or without aloperine (10 nM). For the Th1 cells, naïve T-cells were incubated with 10 ng/ml IL-2 (eBioscience, San Diego, CA, United States), 10 ng/ml IL-12 (eBioscience, San Diego, CA, United States), and 10 μg/ml anti-IL-4. For the Th2 cells, naïve T-cells were incubated with 10 ng/ml IL-4 (#214–14) and 10 μg/ml anti-IFN-γ. For the Th17 cells, naïve T-cells were incubated with 10 ng/ml IL-1β, 10 ng/ml IL-6, 10 ng/ml IL-23, 2.5 ng/ml TGF-β, 10 μg/ml anti-IL-4, and 10 μg/ml anti-IFN-γ. For the Th17 cell conversion experiment, Th17 cells were differentiated as described above, and, the medium was then replaced with the Treg differentiation cytokine cocktail after washing three times on day 3 and incubated for 2 days. The cells were next subjected to flow cytometry analysis.

Flow Cytometry Analysis

Single-cell suspensions were prepared from the spleens, skin tissues, and exudates or recovered from cell cultures. The isolated skin tissues were digested with collagenase D (Roche Applied Science) solution (400 U/ml) for 4–6 h at 37°C with periodic agitation. Ethylenediaminetetraacetic acid (10 mM final concentration) was added to the collagenase-digested cells for 1 min and then quenched with cold PBS. The cells were stained with the indicated fluorescently labeled antibodies at 4°C in the dark for 30 min and then washed with fluorescence advanced cell sorting buffer (2% bovine serum albumin in PBS). Detection of intracellular molecules was performed; the cells were permeabilized and stained intracellularly as previously described (Zhong et al., 2014). Flow cytometric measurements were performed with an LSR Fortessa flow cytometer (BD Biosciences, Franklin Lakes, NJ, United States), and FlowJo software was used for the subsequent data analysis as instructed. The PerCP-conjugated antimouse CD45 (#103130), FITC-conjugated antimouse CD4 (#100406), PE-conjugated antimouse CD44 (#103036), APC-conjugated antimouse CD62L (#104412), PE-conjugated antimouse CD11b (#101207), APC-conjugated antimouse CD11C (#117310), PE-conjugated antimouse LY6G (#127607), APC/Cy7-conjugated antimouse Ly6C (#128026), FITC-conjugated antimouse F4/80 (#123108), PE/Cy7-conjugated antimouse IFN-γ (#505826), APC-conjugated antimouse IL-4 (#504106), APC-conjugated antimouse IL-17A (#506916), PE-conjugated antimouse IL-17 (#506904), and Alexa Fluor® 647-conjugated antimouse Foxp3 (#126408) antibodies were purchased from BioLegend (San Diego, CA, United States).

Western-Blot Analysis

Western-blot assays were performed as described previously (He et al., 2018). Briefly, the prepared cell samples were lysed and then separated on 10% (vol/vol) polyacrylamide gels and transferred onto PVDF membranes. The membrane was probed with antibodies (1: 1000 dilution) including P-STAT3, RORγt, P-STAT5 (Cell Signaling Technology, Danvers, MA, United States), and β-actin (Santa Cruz Biotechnology, Santa Cruz, CA, United States), followed by probing to the corresponding horseradish peroxidase-conjugated secondary antibody, respectively. The reactive bands were developed using the established techniques (Yao et al., 2016). The intensity of each band was analyzed using the densitometry feature in the ImageJ software.

Quantitative RT-PCR Analysis

The part of injured skin tissues and spleens or culture cells were collected and subjected to RNA isolation using the Trizol™ reagent (Takara, Japan) as instructed. For the syntheses of complementary DNA, an aliquot containing 1 μg of total RNA was reverse-transcribed using a cDNA synthesis kit (Takara,

Japan). Real-time polymerase chain reaction (PCR) was performed using the SYBR Green PCR master mix (Applied Biosystems, South San Francisco, CA, United States) in an ABI Prism 7500 Sequence Detection System (Applied Biosystems, South San Francisco, United States). The β-actin gene was used as a reference to normalize the data, and the PCR primers used for PCR amplification are listed in **Table 1**. The relative quantitative levels for each of target genes were analyzed using the $2^{-\Delta\Delta CT}$ method as previously reported (Fu et al., 2017).

Air Pouch Model

The air pouch model was created according to the previous studies (Gaspar et al., 2014). Ten mice, whose back sides were cautiously shaved to clean the area, were randomly allocated into two groups: the LPS + PBS group and LPS + aloperine group. Dermal air pouches were generated by injecting the mice on dorsal sites with 3 ml of filtered air (0.20 μm filter) on day 0, and another 3 ml of sterile air was injected on day 3 for re-expansion. On day 6, 1 ml of sterile saline solution containing 10 ng/ml LPS (Sigma, St. Louis, United States) with or without aloperine (4 mg/ml) was injected into the preformed air pouches in mice from the LPS + PBS group and LPS + aloperine group, respectively. Twelve hours later, the exudates of the pouches were collected after injection of 1 ml of saline solution containing 20 U/ml heparin and 2% fetal calf serum (FCS), followed by 1 min of gentle massage. This procedure was repeated twice, and the total collections were washed with cold PBS and centrifuged (5 min, 300 g), followed by suspending with PBS. The number of cells in the pouch fluid samples was determined using a hemocytometer. In addition, different cell types of inflammatory exudates were subjected to flow cytometry analysis as above.

Activation of BMDC and Supernatant Transfer

Bone marrow-derived dendritic cells (BMDCs) were generated from C57BL/6 mice (8–10 weeks old) as previously described (Zhong et al., 2010). Briefly, the mice were sacrificed, and the bone marrow cells were flushed out from the femurs and tibias and then treated with ACK lysis buffer. Pooled cells were suspended to 2×10^6/ml and cultured in RPMI 1640 supplemented with 10% fetal bovine serum, 100 U/ml penicillin, 100 g/ml streptomycin, 50 μM mercaptoethanol, 10 mM *N*-(2-hydroxyethyl)piperazine-*N*'-ethanesulfonic acid, recombinant murine granulocyte macrophage colony stimulating factor (GM-CSF) (10 ng/ml), and interleukin (IL)-4 (10 ng/ml) (#214–14) at 37°C in 5% CO_2 atmosphere. The nonadherent cells were discarded after 48 h of culture, and the adherent cells were cultured with a fresh medium containing rmGM-CSF and IL-4 on alternative days. On day 7, 100 ng/ml LPS (Sigma, St. Louis, United States) was added for 12 h to induce the activation of BMDCs with or without pretreatment of aloperine (10 nM) for 1 h. The cells were next subjected to analysis of RT-PCR, western blotting, and flow cytometry. For supernatant transfer, the LPS + PBS- or LPS + aloperine-treated BMDCs were washed and cultured in the fresh complete medium for another 24 h. Then, the supernatants were collected to culture the $CD4^+$ T-cells in the presence of TCR stimulation. The $CD4^+$ T-cells were harvested for the RT-PCR analysis 48 h later.

Statistical Analysis

All *in vitro* experiments were based on at least three independent biological replications.

An independent Student's t-test was used to examine the significant differences between the two groups. Statistical analysis of the data was performed using the GraphPad Prism 5 software (GraphPad Software Inc., San Diego, CA, United States), and the results were expressed as the mean ± standard error of the mean (SEM). For all statistics, a p value <0.05 was regarded as statistically significant.

RESULTS

Topical Application of Aloperine Ameliorates Psoriasis Induced by IMQ

First of all, we examined the therapeutic effect of aloperine on psoriasis, a skin lesion predominantly mediated by the $CD4^+$ T-cells. To this end, we applied IMQ on the shaved back skin of B6 mice with or without 2% aloperine cream once per day for 5 consecutive days (Chuang et al., 2018). All the mice in the control group manifested significant general skin symptoms, including erythema, silver plaques, and anabrosis after 7 days (**Figure 1A**). Remarkably, topical application of 2% aloperine cream significantly ameliorated pathological situations of skin lesions when compared with the control group (**Figure 1A**). In addition, as a marker of severity in psoriasis, the mice treated with aloperine exhibited lower average PASI scores than the control group (**Figure 1B**).

To further confirm the above data, histological analysis was next conducted. In comparison to the control group, H&E staining of the skin lesion originating from the aloperine treatment group manifested a significantly lower thickness of the epidermis layer along with the attenuated IMQ-induced psoriasis (**Figure 1C**). In terms of Ki-67 immunohistochemistry staining, fewer positive cells with brown particles were observed in the basal layer cells of the lesion skin in the aloperine groups (**Figure 1D**). Additionally, we tested the effect of aloperine on the already established psoriasis to determine whether it has potential to serve as a therapeutic agent. The mouse model of psoriatic dermatitis was first induced by IMQ. Then, the mice received aloperine or control cream (**Supplementary Figure S1A**). The results showed that aloperine significantly alleviated the skin damage compared to control treatment (**Supplementary Figures S1B–D**). Furthermore, aloperine suppressed the local immune response (**Supplementary Figures S2A,B**), which was consistent with the results presented above. Altogether, these results suggested that aloperine treatment ameliorated IMQ-induced psoriatic skin injury in mice.

Aloperine Inhibits the Activation of DCs

Previous studies have reported that specialized APC subsets of the dermal dendritic cells are important in the initiation and

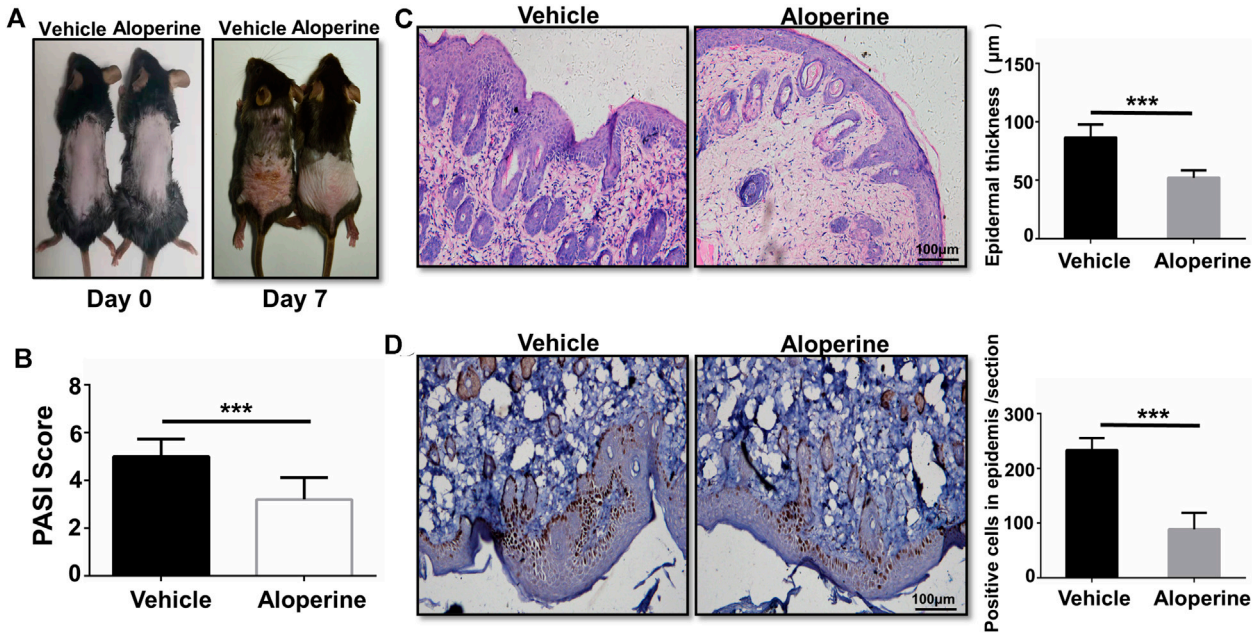

FIGURE 1 | Topical application of aloperine ameliorates psoriasis induced by IMQ. **(A)** Representative presentation of the back skin at day 7 of the IMQ treatment. **(B)** The severity was graded by a modified PASI. **(C)** Histological analysis of the mouse back skin by H&E staining. **(D)** Histological analysis of IHC staining for Ki-67. Corresponding quantification analyses of epidermal thickness and positive proliferation cells were carried out as described. The values are presented as the mean ± SEM (n = 10 mice per group). $*p < 0.05$; $**p < 0.01$; and $***p < 0.001$.

development of psoriatic skin inflammation (Xiao et al., 2017; Wang and Bai, 2020). Also, aloperine has been recognized as a potent anti-inflammatory drug. We thus tested whether aloperine could affect the activation of the dendritic cells, thereby reducing cytokine secretion, especially IL-6 and IL-23, to reduce Th17 differentiation and proliferation indirectly for the improved skin local inflammatory environment. In view of this, we first examined the frequency and activation state of DCs among $CD45^+$ cells in the skin lesion. We observed a decreased DC population along with reduced activation markers (CD80, CD86, MHC-II) in the aloperine group (**Figures 2A–D**). In line with the *in vivo* data, we then checked the effect of aloperine on the activation of DCs *in vitro*. As shown in **Figures 2E–G**, the expressions of CD80, CD86, and MHC-II were significantly decreased upon aloperine treatment. Moreover, aloperine reduced the expression of IL-1β, IL-6, IL-23, and TNF-α in BMDCs (**Figure 2H**). These findings suggest that aloperine plays a crucial role in preventing the activation of skin DCs, which leads to a microenvironment disfavoring Th17 development.

Aloperine Inhibits the Migration and Th17-Inducing Effect of DCs

An important characteristic for psoriasis is the accumulation of myeloid cells, including neutrophils, macrophages, and DCs (Schön et al., 2017; Han et al., 2020; McGinley et al., 2020). Thus, we were interested in whether aloperine would have an effect on the migration of myeloid cells. An air pouch inflammatory model in mice is considered a useful and convenient experiment *in vivo* for determining the anti-inflammatory activity of the testing compounds (Vandooren et al., 2013; Gaspar et al., 2014). A general outline of the method used is shown in **Figure 3A**. As expected, aloperine decreased the total number of inflammatory cells in the exudate induced by LPS (**Figure 3B**). Surprisingly, the neutrophil infiltration was comparable between the groups, suggesting that the decreased neutrophil cellularity in psoriatic lesions might be a result of aloperine-mediated Th17 cell inhibition (**Figure 3C**). In contrast, the trafficking of antigen-presenting cells, DCs in particular, was significantly decreased in the aloperine treatment group (**Figures 3D,E**).

Furthermore, we demonstrated a decreased phosphorylation level of P65 after aloperine treatment (**Figure 3F**), implying that aloperine could inhibit the NF-κB signaling pathway. By supernatant transfer and subsequent RT-PCR analysis, we showed that mRNA levels for the Th17-associated molecules including IL-17A, IL-23, and RORγt were decreased in the $CD4^+$ T-cells receiving the supernatant of DCs pretreated by aloperine (**Figure 3G**). Altogether, these findings support that aloperine could suppress local inflammation in psoriatic skin lesions through inhibiting the migration, activation, and Th17-inducing capacity of the DCs.

Aloperine Decreases the Th17/Treg Ratio in the Psoriasis-like Lesions

To understand the effect of aloperine on the $CD4^+$ T-cells, a single-tissue cell suspension was made from the skin lesion by the digestion of collagenase and hyaluronidase for flow cytometry

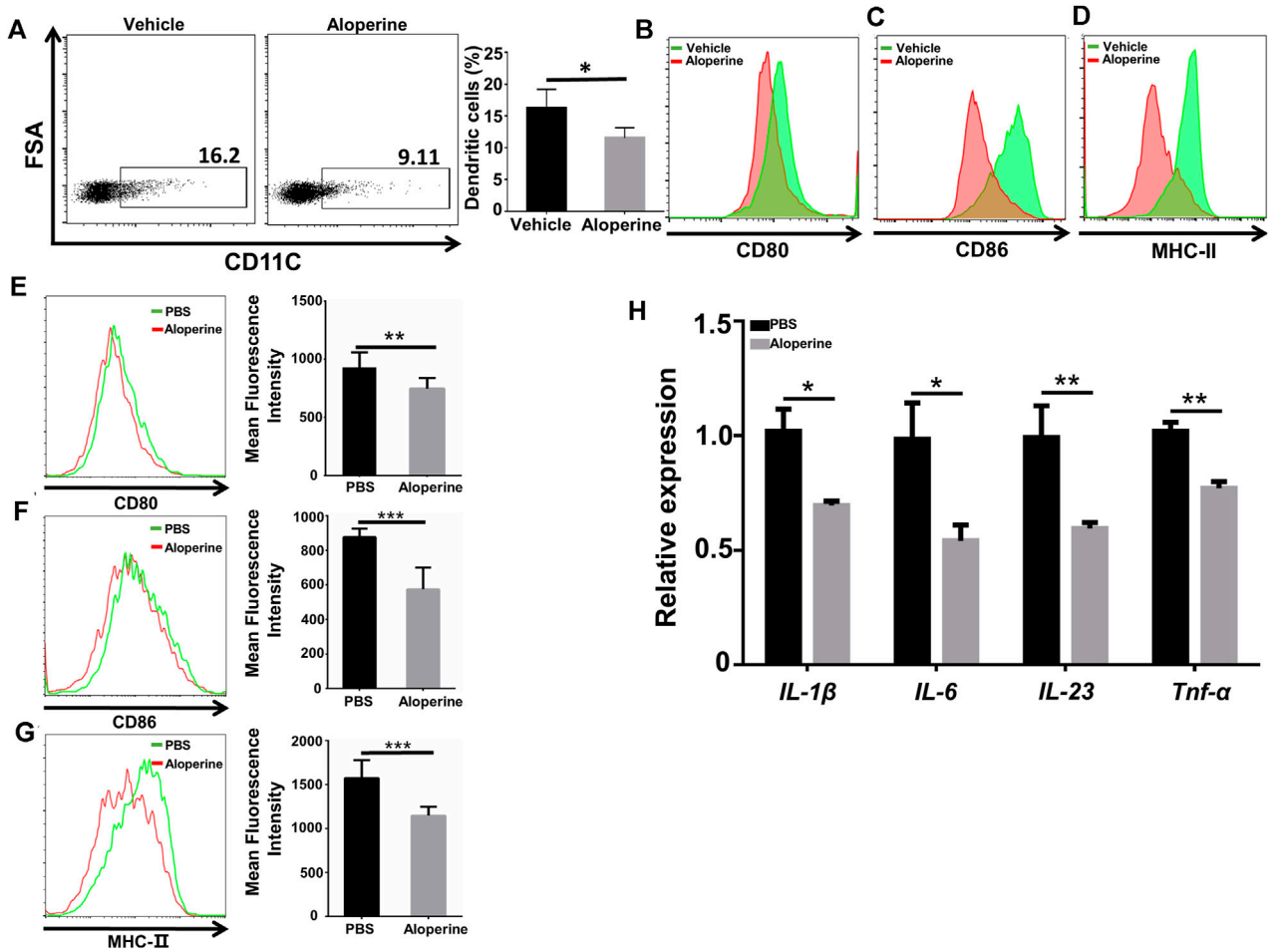

FIGURE 2 | Aloperine inhibits the activation of DCs. **(A)** The proportion of $CD11C^+$ DCs among $CD45^+$ cells in the skin lesion. **(B–D)** Mean Fluorescence Intensity (MFI) analysis of the expression of CD80, CD86, and MHC-II on skin DCs. **(E–G)** MFI analysis of the expression of CD80, CD86, and MHC-II in *in vitro* differentiated BMDCs. **(H)** Real-time PCR analysis of cytokine expression (IL-1β, IL-6, IL-23, and TNF-α) in DCs. The data are shown as the mean ± SEM from three independent experiments. $*p < 0.05$; $**p < 0.01$; and $***p < 0.001$.

analysis when the mice were sacrificed. In comparison to the vehicle control group, aloperine significantly decreased the infiltration of $CD4^+$ and $CD8^+$ T-cells (**Figure 4A**), indicating a reduced adaptive immune response. Furthermore, the frequencies of IL-17^+ Th17 cells were substantially decreased in the aloperine treatment group (**Figure 4B**), while IFN-γ^+ Th1 cells displayed no perceptible difference (**Figure 4C**). On the contrary, as shown in (**Figure 4D**), the Treg cells were significantly increased in the aloperine treatment group.

RT-PCR was next performed to determine the mRNA levels of cytokines and key transcription factors for Th17 and Treg in the skin lesions. Consistent with the flow cytometry results, the levels of IL-17A, IL-23, IL-6, IFN-γ, and RORγt mRNA in the skin lesions were significantly lower than that in vehicle control mice. In contrast, aloperine markedly increased IL-10 and Foxp3 mRNA levels, the characteristic of immunomodulatory Tregs (**Figure 4E**). Taken together, aloperine treatment decreased the Th17/Treg ratio in skin lesions, thereby alleviating immune-mediated pathology in the psoriasis induced by IMQ.

Aloperine Directly Affects Th17 *In Vitro* Differentiation *Via* Inhibiting the STAT3 Signalling

In our previous study, we confirmed that aloperine promoted Treg differentiation and activation through suppressing the PI3K/Akt/mTOR signaling pathway both *in vivo* and *in vitro* (Fu et al., 2017). This phenomenon raised our interest to further examine the effects of aloperine on the $CD4^+$ T-cell differentiation. To address this issue, naïve $CD4^+$ T-cells isolated from WT B6 mice were differentiated toward specific effector populations in the presence of cytokine cocktails and α-CD3/α-CD28 with or without aloperine as described, including Th1, Th2, and Th17 subsets. Apparently, our flow cytometry analysis showed that no change in $CD4^+$ IFN-γ^+ Th1 cell

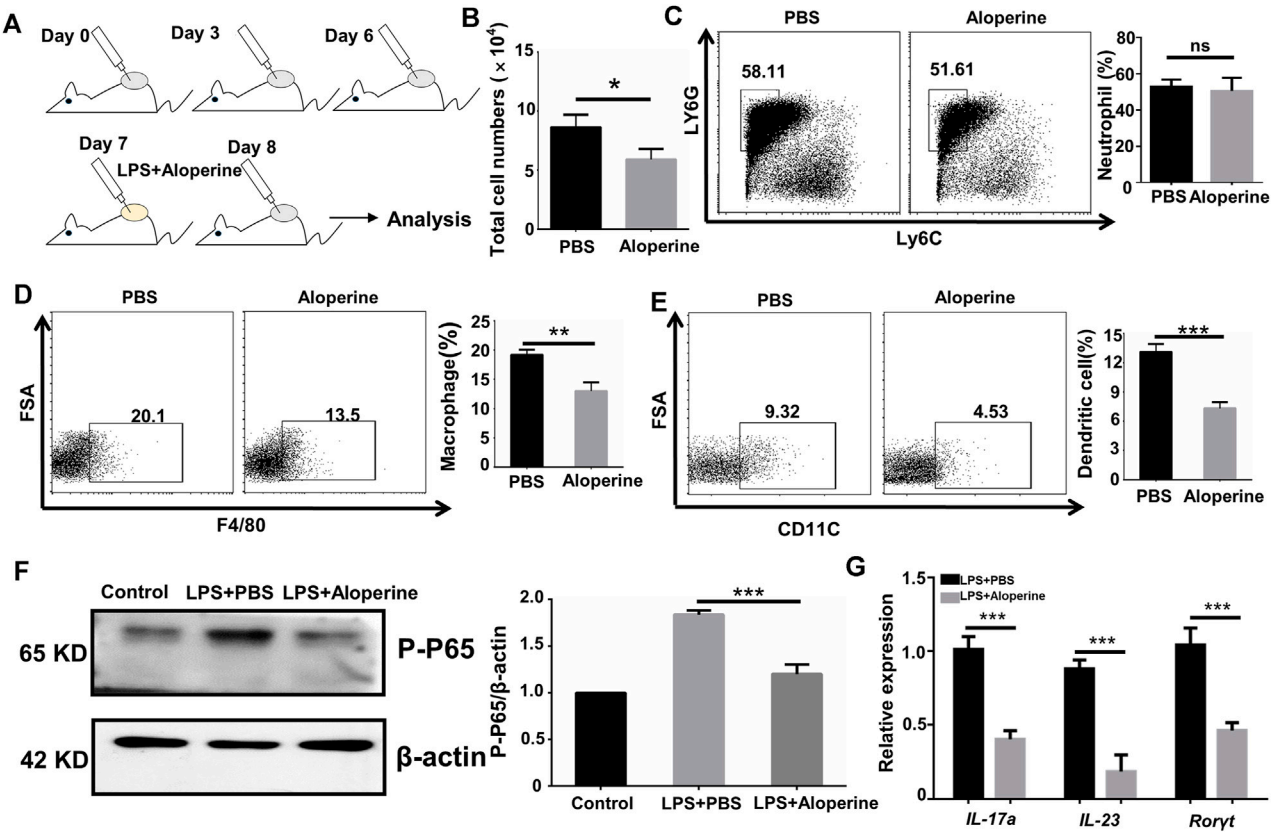

FIGURE 3 | Aloperine inhibits the migration and Th17-inducing effect of DCs. **(A)** A graphical presentation of the air pouch model. On the first day, 3 ml of sterile air was injected subcutaneously into a shaved skin site on the back of each mice. Then, the pouches were settled for 3 days to heal the wound. On the third day, this action was repeated. On the sixth day, LPS was injected into the pouches with or without aloperine. The exudates were collected for subsequent analysis 24 h later. **(B)** Quantitative analysis of total cell numbers in the skin. **(C–E)** Representative flow cytometry analysis of neutrophils ($CD11b^+MHC\text{-}II^-Ly6G^+Ly6C^-$), macrophages ($CD11b^+F4/80^+$), and DCs ($CD11c^+F4/80^-$). **(F)** Western-blot analysis for p-P65 and β-actin. **(G)** Real-time PCR analysis of IL-17A, IL-23, and RORγt in $CD4^+$ T-cells receiving DC cultural supernatant pretreated by LPS + PBS or LPS + aloperine. The values are presented as the mean ± SEM (n = 5 mice per group). $*p < 0.05$; $**p < 0.01$; and $***p < 0.001$.

frequency was observed after aloperine treatment (**Figure 5A**). On the contrary, treatment of aloperine resulted in a moderate increase in the $IL\text{-}4^+$ Th2 cells when compared with the control (**Figure 5B**). Interestingly, aloperine was able to promote a significant decrease in the $CD4^+$ $IL\text{-}17A^+$ Th17 cell frequencies (**Figure 5C**).

Accumulative evidence has shown that the JAK/STAT signaling pathways are essential for the differentiation of Th17 cells. In particular, the phosphorylation of STAT3 is important for the expression of RORγt, which is a key transcription factor in the process of Th17 differentiation, by TGF-β in combination with IL-6 and IL-23. To dissect the mechanism by which aloperine treatment impairs the Th17 program, we examined the phosphorylation of STAT3 by western blotting. Our results showed that aloperine markedly inhibited the phosphorylation of STAT3 and the expression of RORγt under the Th17-polarizing conditions (**Figure 5D**). Collectively, these results indicate that aloperine not only promotes Treg differentiation but also directly impedes the Th17 polarizing program through inhibiting the phosphorylation of STAT3.

Aloperine Facilitates the Conversion of Th17 to Treg

It is well known that Treg is important in the regulation of the local inflammatory environment (Zhang et al., 2016). We showed that the frequencies of Treg were significantly increased in the aloperine treatment group, while the origin for the increased Treg is of great interest to us. Given the fact that Th17 to Treg conversion occurs in animals and humans, we check if aloperine could promote the conversion of Th17 cells into Treg (Obermajer et al., 2014). Interestingly, a significant number of Foxp3/IL-17A double positive cells and Foxp3 single positive cells were observed in the aloperine (plus IL-2 and TGF-β)-treated Th17 cells (**Figure 6A**). However, the frequencies of IL-17A-positive cells were decreased by aloperine. Moreover, western blot analysis showed that the

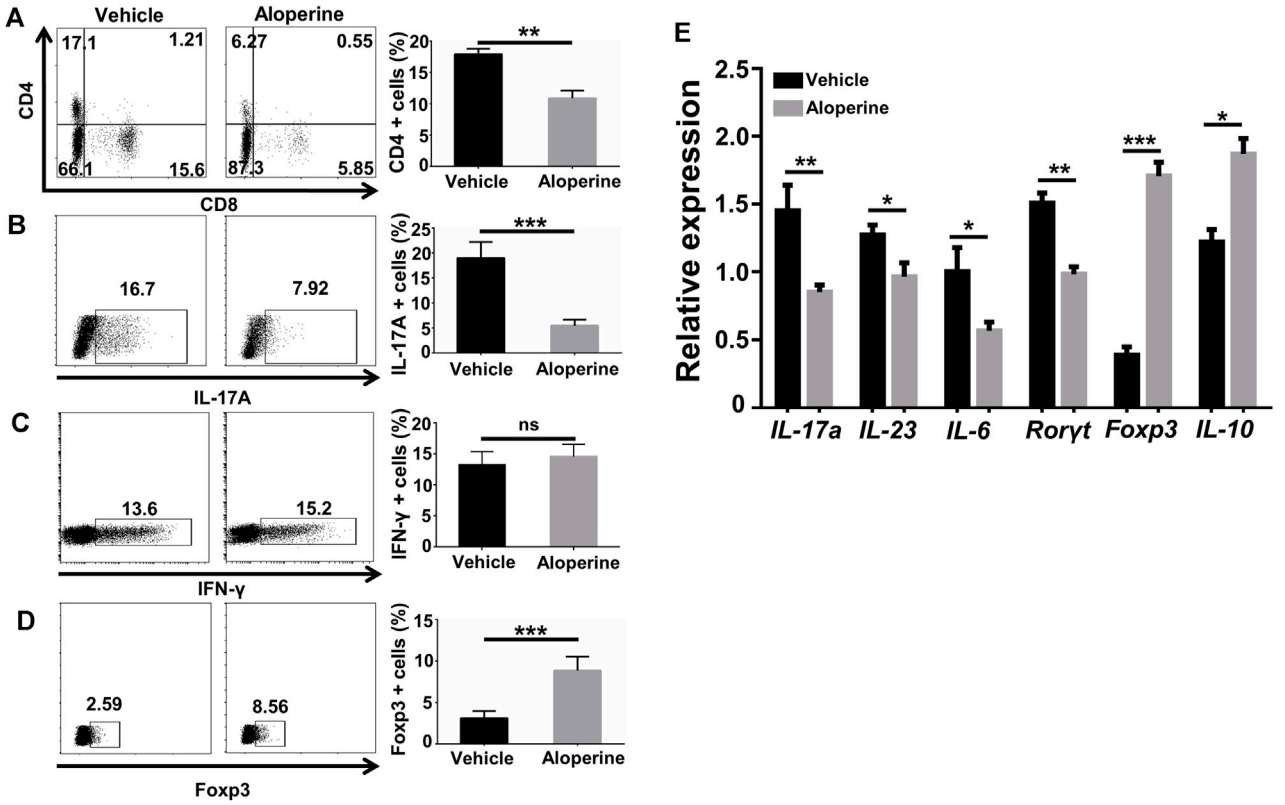

FIGURE 4 | Aloperine decreases the Th17/Treg ratio in the psoriasis-like lesions. **(A–D)** Flow cytometry analysis for CD4, CD8, Th1, Th17, and Treg cells in the skin lesions. **(E)** Real-time PCR analysis of IL-17A, IL-23, IL-6, RORγt, Foxp3, and IL-10. The values are presented as the mean ± SEM (n = 8 mice per group). $*p < 0.05$; $**p < 0.01$; and $***p < 0.001$.

phosphorylation of STAT5 was significantly increased in the aloperine group, but the level of phosphorylated STAT3 was decreased (**Figure 6B**). In addition, RT-PCR revealed that the expression of Foxp3 was increased, while IL-17A and RORγt were decreased in the aloperine-treated Th17 cells (**Figure 6C**). This could explain the lower frequency of Th17 cells and the higher proportion of Treg in the aloperine group during the progressive phase of the disease. In all, these findings indicate that aloperine plays a role in the conversion of Th17 into Treg through tipping the balance of pSTAT5 and pSTAT3.

DISCUSSION

Aloperine is a natural quinolizidine alkaloid extracted from *Sophora alopecuroides L.*, and has been used as an effective therapy in the treatment of inflammatory diseases, such as colitis and ischemia-reperfusion-induced renal injury (Hu et al., 2016). Nevertheless, the detailed mechanism underlying the immune-regulatory role of aloperine is poorly understood. In this study, we sought to investigate the multifaceted effect of aloperine on the Th17 program. Major discoveries in this study are summarized below (**Figure 7**). First, our data suggested that aloperine exerts suppressive effects on DCs by inhibiting their migration, activation, and cytokine secretion, especially those related to Th17 polarization. Western-blot results indicated that aloperine could inhibit the NF-κB signaling pathway in DC, which is consistent with the previous reports (Ye et al., 2020; Hu et al., 2021). Moreover, as far as we know, we provided the first panorama clarifying the effect of aloperine on the $CD4^+$ T-cell differentiation. The results demonstrated that aloperine administration has no effect on $CD4^+IFN\gamma^+$ Th1 differentiation, and moderately increases the $CD4^+IL\text{-}4^+$ Th2 subset, but significantly impairs $CD4^+IL\text{-}17A^+$ Th17 differentiation. Mechanistically, aloperine inhibits the phosphorylation of STAT3, which is essential for the polarization of Th17 cells. Previously, we demonstrated that aloperine promotes Treg differentiation *via* suppressing the PI3K/Akt/mTOR signaling pathway. Based on these data, we conclude that aloperine alleviates inflammatory response partially by modulating the $CD4^+$ T-cell differentiation. Intriguingly, aloperine directly promotes the trans-differentiation of Th17 into Treg by tipping the balance of pSTAT5 and pSTAT3, which implies a more flexible and subtle effect on the adaptive immune response that aloperine confers. In combination with our previous publication on Treg differentiation (Fu et al., 2017), we conclude that aloperine is efficient to restore the Th17/Treg imbalance, thus serving as a

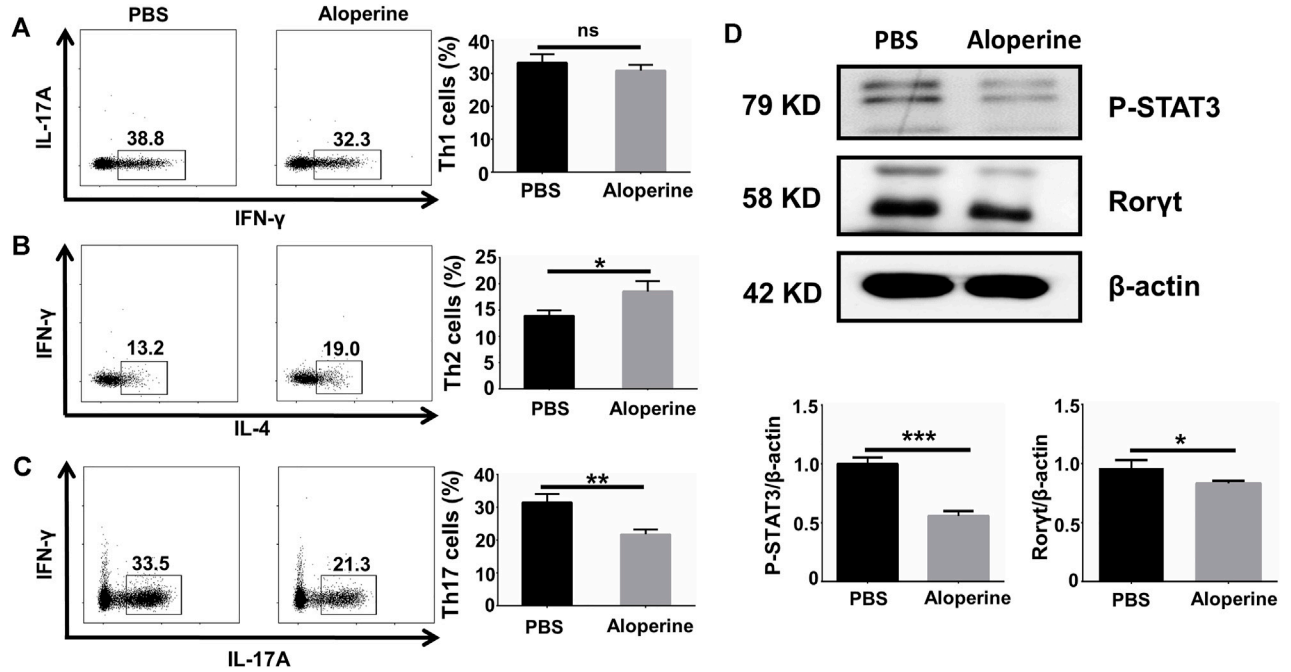

FIGURE 5 | Aloperine directly affects Th17 *in vitro* differentiation by inhibiting the STAT3 signalling. **(A–C)** IFN-γ$^+$ Th1, IL-4$^+$ Th2, and IL-17A$^+$ Th17 polarizing efficiency were analyzed by flow cytometry. **(D)** The levels of RORγt and phosphorylated STAT3 were assessed by western blotting. The results were from three independent experiments. The values are presented as the mean ± SEM. $*p < 0\ 05$; $**p < 0.01$; $***p < 0.001$; and ns, $p \geq 0.05$.

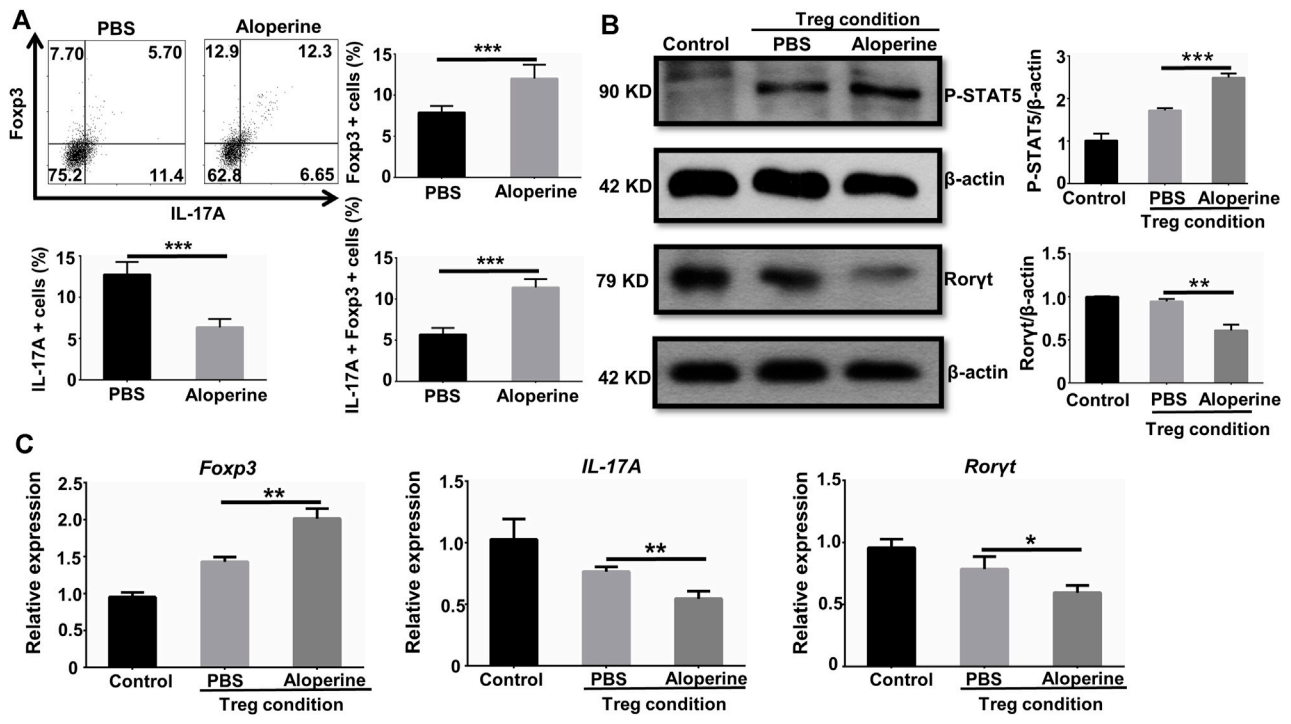

FIGURE 6 | Aloperine facilitates the conversion of Th17 to Treg. **(A)** Flow cytometry analysis of the conversion of Th17 into Treg. **(B)** Western-blot analysis was conducted to assess the influence of aloperine in the phosphorylation of STAT5 and STAT3. **(C)** Real-time PCR analysis of IL-17A, RORγt, and Foxp3 in Th17 cells following 48 h of Treg polarization conditions with or without aloperine. The results were from three independent experiments. The values are presented as the mean ± SEM. $*p < 0.05$; $**p < 0.01$; and $***p < 0.001$.

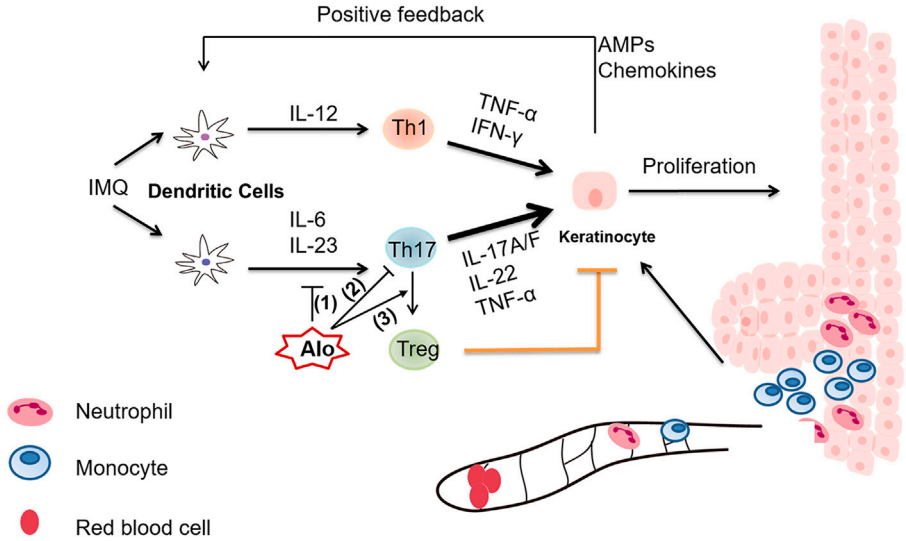

FIGURE 7 | A graphical illustration of aloperine-mediated suppression of the Th17 program in the mouse psoriasis model. (1) Aloperine inhibits the migration, activation, and Th17-inducing capability of DCs. (2) Aloperine directly inhibits Th17 polarization by suppressing the phosphorylation of STAT3. (3) Aloperine promotes the trans-differentiation of Th17 into Treg.

potent therapeutic agent in psoriasis and other immune-related disorders.

Psoriasis is a chronic inflammatory skin disease characterized by skin erythema, plagues, and constant scales derived from excessive proliferation of epithelial cells. IMQ is a TLR7/8 ligand and a potent immune activator of monocytes, macrophages, and DCs, by which it plays a critical role in initiating psoriatic skin inflammation. IMQ-induced psoriasis is established as a rapid and convenient animal model to elucidate the pathogenic mechanism of psoriasis and to screen potential antipsoriasis drugs *in vivo* (Chuang et al., 2018). We therefore explored the therapeutic effect on psoriasis and the related mechanisms in an IMQ-induced psoriasis model. Previous studies demonstrated strong evidence for the role of the IL-23/Th17 axis both in the psoriasis patients and animal models. IL-23, mostly derived from the activated DCs, plays an important role in the proliferation and maintenance of immune response. Intradermal injection of IL-23 in mice led to apparent skin inflammation with histopathological features resembling psoriasis (Lindroos et al., 2011; Rizzo et al., 2011). In the present study, we found that aloperine not only impaired Th17 differentiation directly but also inhibited the activation of dendritic cells, thereby reducing the expression and secretion of proinflammatory cytokines, especially IL-23 and IL-1β. Thus, our data support that aloperine ameliorates IMQ-induced psoriatic skin injury by creating a Th17-disfavoring microenvironment.

Evidence also suggests that neutrophils, monocytes, and monocyte-derived DCs were accumulated in the dermis during the early phase, and macrophages transiently increased in the epidermis and dermis during the late phase (Lee et al., 2018). These findings highlight their key role in inducing the psoriasis-like skin disease. In our study, we observed that aloperine had no effect on the infiltration of neutrophils but could inhibit the migration of DCs and macrophages through the application of an air pouch model. Our finding emphasized the pivotal functions of antigen-presenting cells (DCs in particular) during the early phase of psoriasis development, which could be a perfect time window for the intervention by either aloperine or other chemical compounds.

Th17/Treg imbalance is known to trigger and accelerate the progression of psoriasis (Shi et al., 2019). In psoriatic patients, the impaired function of Treg cells is mediated by the phosphorylation of STAT3 (Yang et al., 2016; Zhang et al., 2016). Treg cells from psoriatic patients could reprogram into IL-17A-producing Th17 cells, which are identified in the peripheral blood and skin lesions, suggesting that the stability of Treg is compromised in the psoriatic inflammation environment (Singh et al., 2013). Our group previously found that aloperine promoted Treg differentiation and activation in mice by inhibiting the PI3K/Akt/mTOR signaling pathway. In this study, we found that the proportion of Treg was increased in the aloperine treatment group, which is consistent with the previous study. We further checked whether increased Treg in the aloperine treatment group was derived from the conversion of Th17 cells. Excitingly, we found that aloperine could alter the pSTAT3/pSTAT5 ratio and promote the conversion from Th17 to Treg cells. These findings suggested that aloperine could improve the skin local immune environment through affecting Th17/Treg balance. Nonetheless, the limitation of this study is that we did not fully identify the specific molecules that interact with aloperine directly, which would be the focus of later investigations.

In summary, topical administration of aloperine ameliorates IMQ-induced psoriasis *via* its versatile suppressive effect on the Th17 program. These findings provide important mechanistic insights into the therapeutic benefits of aloperine, which holds the potential as a candidate drug for the treatment of various inflammatory diseases.

DATA AVAILABILITY STATEMENT

The datasets presented in this study can be found in online repositories. The names of the repository/repositories and accession number(s) can be found in the article/ **Supplementary Material**.

ETHICS STATEMENT

The animal study was reviewed and approved by the Animal Care and Use Committee in Tongji Hospital.

AUTHOR CONTRIBUTIONS

SZ and C-YW designed and supervised the entire study. H-FZ, FS, F-XW, XL (4th author), J-HL, T-TY, JX, C-LY, XL (10th author), QZ, HZ, PY, FX, and Q-LY performed the experiments. H-FZ, F-XW, and FS prepared the manuscript. Q-LY and FX were involved in the data analysis and manuscript revision.

FUNDING

Our study was supported by the National Natural Science Foundation of China (82130023, 81920108009, 82100892, 82070808, 81873656, 82100823, 82100931, 91749207, 81770823 and 81800068), Department of Science and Technology of Hubei Province Program project (2020DCD014), the Postdoctoral Science Foundation of China (54000-0106540081 and 54000-0106540080), Hubei Health Committee Program (WJ2021ZH0002), the Integrated Innovative Team for Major Human Disease Programs of Tongji Medical College, the Huazhong University of Science and Technology, and the Innovative Funding for Translational Research from Tongji Hospital.

SUPPLEMENTARY MATERIAL

The Supplementary Material for this article can be found online at: https://www.frontiersin.org/articles/10.3389/fphar.2022.778755/full#supplementary-material

REFERENCES

Boehncke, W. H. (2015). Etiology and Pathogenesis of Psoriasis. *Rheum. Dis. Clin. North. Am.* 41 (4), 665–675. doi:10.1016/j.rdc.2015.07.013

Chang, Z., Zhang, P., Zhang, M., Jun, F., Hu, Z., Yang, J., et al. (2019). Aloperine Suppresses Human Pulmonary Vascular Smooth Muscle Cell Proliferation via Inhibiting Inflammatory Response. *Chin. J. Physiol.* 62 (4), 157–165. doi:10.4103/cjp.cjp_27_19

Chuang, S. Y., Lin, C. H., Sung, C. T., and Fang, J. Y. (2018). Murine Models of Psoriasis and Their Usefulness for Drug Discovery. *Expert Opin. Drug Discov.* 13 (6), 551–562. doi:10.1080/17460441.2018.1463214

Conrad, C., and Gilliet, M. (2018). Psoriasis: from Pathogenesis to Targeted Therapies. *Clin. Rev. Allergy Immunol.* 54 (1), 102–113. doi:10.1007/s12016-018-8668-1

Deng, Y., Chang, C., and Lu, Q. (2016). The Inflammatory Response in Psoriasis: a Comprehensive Review. *Clin. Rev. Allergy Immunol.* 50 (3), 377–389. doi:10.1007/s12016-016-8535-x

Feng, H., Yamaki, K., Takano, H., Inoue, K., Yanagisawa, R., and Yoshino, S. (2006). Suppression of Th1 and Th2 Immune Responses in Mice by Sinomenine, an Alkaloid Extracted from the Chinese Medicinal Plant Sinomenium Acutum. *Planta Med.* 72 (15), 1383–1388. doi:10.1055/s-2006-951721

Fu, X., Sun, F., Wang, F., Zhang, J., Zheng, B., Zhong, J., et al. (2017). Aloperine Protects Mice against DSS-Induced Colitis by PP2A-Mediated PI3K/Akt/mTOR Signaling Suppression. *Mediators Inflamm.* 2017, 5706152. doi:10.1155/2017/5706152

Furusawa, S., and Wu, J. (2007). The Effects of Biscoclaurine Alkaloid Cepharanthine on Mammalian Cells: Implications for Cancer, Shock, and Inflammatory Diseases. *Life Sci.* 80 (12), 1073–1079. doi:10.1016/j.lfs.2006.12.001

Gaspar, E. B., Sakai, Y. I., and Gaspari, E. D. (2014). A Mouse Air Pouch Model for Evaluating the Immune Response to Taenia Crassiceps Infection. *Exp. Parasitol.* 137, 66–73. doi:10.1016/j.exppara.2013.12.005

Girolomoni, G., Strohal, R., Puig, L., Bachelez, H., Barker, J., Boehncke, W. H., et al. (2017). The Role of IL-23 and the IL-23/TH 17 Immune axis in the Pathogenesis and Treatment of Psoriasis. *J. Eur. Acad. Dermatol. Venereol.* 31 (10), 1616–1626. doi:10.1111/jdv.14433

Han, G., Havnaer, A., Lee, H. H., Carmichael, D. J., and Martinez, L. R. (2020). Biological Depletion of Neutrophils Attenuates Pro-inflammatory Markers and the Development of the Psoriatic Phenotype in a Murine Model of Psoriasis. *Clin. Immunol.* 210, 108294. doi:10.1016/j.clim.2019.108294

He, X., Lai, Q., Chen, C., Li, N., Sun, F., Huang, W., et al. (2018). Both conditional Ablation and Overexpression of E2 SUMO-Conjugating Enzyme (UBC9) in Mouse Pancreatic Beta Cells Result in Impaired Beta Cell Function. *Diabetologia* 61 (4), 881–895. doi:10.1007/s00125-017-4523-9

Hu, R., Chen, L., Chen, X., Xie, Z., Xia, C., and Chen, Y. (2021). Aloperine Improves Osteoporosis in Ovariectomized Mice by Inhibiting RANKL-Induced NF-Kb, ERK and JNK Approaches. *Int. immunopharmacology* 97, 107720. doi:10.1016/j.intimp.2021.107720

Hu, S., Zhang, Y., Zhang, M., Guo, Y., Yang, P., Zhang, S., et al. (2016). Aloperine Protects Mice against Ischemia-Reperfusion (IR)-Induced Renal Injury by Regulating PI3K/AKT/mTOR Signaling and AP-1 Activity. *Mol. Med.* 21 (1), 912–923. doi:10.2119/molmed.2015.00056

Lee, M., Kim, S. H., Kim, T. G., Park, J., Lee, J. W., and Lee, M. G. (2018). Resident and Monocyte-Derived Langerhans Cells Are Required for Imiquimod-Induced Psoriasis-like Dermatitis Model. *J. Dermatol. Sci.* 91 (1), 52–59. doi:10.1016/j.jdermsci.2018.04.003

Li, W., Li, Y., Zhao, Y., and Ren, L. (2020). The Protective Effects of Aloperine against Ox-LDL-Induced Endothelial Dysfunction and Inflammation in HUVECs. *Artif. Cell Nanomed Biotechnol* 48 (1), 107–115. doi:10.1080/21691401.2019.1699816

Lindroos, J., Svensson, L., Norsgaard, H., Lovato, P., Moller, K., Hagedorn, P., et al. (2011). IL-23-Mediated Epidermal Hyperplasia is Dependent on IL-6. *J. Investig. Dermatol.* 131 (5), 1110–1118. doi:10.1038/jid.2010.432

Ling, Z., Guan, H., You, Z., Wang, C., Hu, L., Zhang, L., et al. (2018). Aloperine Executes Antitumor Effects through the Induction of Apoptosis and Cell Cycle Arrest in Prostate Cancer In Vitro and In Vivo. *Onco Targets Ther.* 11, 2735–2743. doi:10.2147/ott.s165262

Lowes, M. A., Russell, C. B., Martin, D. A., Towne, J. E., and Krueger, J. G. (2013). The IL-23/T17 Pathogenic axis in Psoriasis Is Amplified by Keratinocyte Responses. *Trends Immunol.* 34 (4), 174–181. doi:10.1016/j.it.2012.11.005

Lowes, M. A., Suarez-Farinas, M., and Krueger, J. G. (2014). Immunology of Psoriasis. *Annu. Rev. Immunol.* 32, 227–255. doi:10.1146/annurev-immunol-032713-120225

Mak, R. K., Hundhausen, C., and Nestle, F. O. (2009). Progress in Understanding the Immunopathogenesis of Psoriasis. *Actas Dermosifiliogr* 100 (Suppl. 2), 2–13. doi:10.1016/s0001-7310(09)73372-1

McGinley, A. M., Sutton, C. E., Edwards, S. C., Leane, C. M., DeCourcey, J., Teijeiro, A., et al. (2020). Interleukin-17A Serves a Priming Role in

Autoimmunity by Recruiting IL-1β-Producing Myeloid Cells that Promote Pathogenic T Cells. *Immunity* 52, 342–e6. doi:10.1016/j.immuni.2020.01.002

Obermajer, N., Popp, F. C., Soeder, Y., Haarer, J., Geissler, E. K., Schlitt, H. J., et al. (2014). Conversion of Th17 into IL-17A(neg) Regulatory T Cells: a Novel Mechanism in Prolonged Allograft Survival Promoted by Mesenchymal Stem Cell-Supported Minimized Immunosuppressive Therapy. *J. Immunol.* 193 (10), 4988–4999. doi:10.4049/jimmunol.1401776

Parisi, R., Symmons, D. P., Griffiths, C. E., and Ashcroft, D. M. (2013). Global Epidemiology of Psoriasis: a Systematic Review of Incidence and Prevalence. *J. Invest. Dermatol.* 133 (2), 377–385. doi:10.1038/jid.2012.339

Puig, L. (2017). The Role of IL 23 in the Treatment of Psoriasis. *Expert Rev. Clin. Immunol.* 13 (6), 525–534. doi:10.1080/1744666x.2017.1292137

Rizzo, H., Kagami, S., Phillips, K., Kurtz, S., Jacques, S., and Blauvelt, A. (2011). IL-23-Mediated Psoriasis-Like Epidermal Hyperplasia is Dependent on IL-17A. *J. Immunol.* 186 (3), 1495–1502. doi:10.4049/jimmunol.1001001

Schirmer, C., Klein, C., von Bergen, M., Simon, J. C., and Saalbach, A. (2010). Human Fibroblasts Support the Expansion of IL-17-producing T Cells via Up-Regulation of IL-23 Production by Dendritic Cells. *Blood* 116 (10), 1715–1725. doi:10.1182/blood-2010-01-263509

Schön, M. P., Broekaert, S. M. C., and Erpenbeck, L. (2017). Sexy Again: the Renaissance of Neutrophils in Psoriasis. *Exp. Dermatol.* 26 (4), 305–311. doi:10.1111/exd.13067

Shi, Y., Chen, Z., Zhao, Z., Yu, Y., Fan, H., Xu, X., et al. (2019). IL-21 Induces an Imbalance of Th17/Treg Cells in Moderate-To-Severe Plaque Psoriasis Patients. *Front. Immunol.* 10, 1865. doi:10.3389/fimmu.2019.01865

Singh, K., Gatzka, M., Peters, T., Borkner, L., Hainzl, A., Wang, H., et al. (2013). Reduced CD18 Levels Drive Regulatory T Cell Conversion into Th17 Cells in the CD18hypo PL/J Mouse Model of Psoriasis. *J. Immunol.* 190 (6), 2544–2553. doi:10.4049/jimmunol.1202399

Sun, F., Yue, T. T., Yang, C. L., Wang, F. X., Luo, J. H., Rong, S. J., et al. (2021). The MAPK Dual Specific Phosphatase (DUSP) Proteins: A Versatile Wrestler in T Cell Functionality. *Int. Immunopharmacol* 98, 107906. doi:10.1016/j.intimp.2021.107906

Takeshita, J., Grewal, S., Langan, S. M., Mehta, N. N., Ogdie, A., Van Voorhees, A. S., et al. (2017). Psoriasis and Comorbid Diseases: Epidemiology. *J. Am. Acad. Dermatol.* 76 (3), 377–390. doi:10.1016/j.jaad.2016.07.064

Vandooren, J., Berghmans, N., Dillen, C., Van Aelst, I., Ronsse, I., Israel, L. L., et al. (2013). Intradermal Air Pouch Leukocytosis as an In Vivo Test for Nanoparticles. *Int. J. Nanomedicine* 8, 4745–4756. doi:10.2147/ijn.s51628

Wang, A., and Bai, Y. (2020). Dendritic Cells: The Driver of Psoriasis. *J. Dermatol.* 47 (2), 104–113. doi:10.1111/1346-8138.15184

Wang, H., Yang, S., Zhou, H., Sun, M., Du, L., Wei, M., et al. (2015). Aloperine Executes Antitumor Effects against Multiple Myeloma through Dual Apoptotic Mechanisms. *J. Hematol. Oncol.* 8, 26. doi:10.1186/s13045-015-0120-x

Wang, R., Deng, X., Gao, Q., Wu, X., Han, L., Gao, X., et al. (2020). Sophora Alopecuroides L.: An Ethnopharmacological, Phytochemical, and Pharmacological Review. *J. Ethnopharmacol* 248, 112172. doi:10.1016/j.jep.2019.112172

Xiao, C., Zhu, Z., Sun, S., Gao, J., Fu, M., Liu, Y., et al. (2017). Activation of Langerhans Cells Promotes the Inflammation in Imiquimod-Induced Psoriasis-like Dermatitis. *J. Dermatol. Sci.* 85 (3), 170–177. doi:10.1016/j.jdermsci.2016.12.003

Yang, L., Li, B., Dang, E., Jin, L., Fan, X., and Wang, G. (2016). Impaired Function of Regulatory T Cells in Patients with Psoriasis Is Mediated by Phosphorylation of STAT3. *J. Dermatol. Sci.* 81 (2), 85–92. doi:10.1016/j.jdermsci.2015.11.007

Yao, Y., Wang, Y., Zhang, Z., He, L., Zhu, J., Zhang, M., et al. (2016). Chop Deficiency Protects Mice against Bleomycin-Induced Pulmonary Fibrosis by Attenuating M2 Macrophage Production. *Mol. Ther.* 24 (5), 915–925. doi:10.1038/mt.2016.36

Ye, Y., Wang, Y., Yang, Y., and Tao, L. (2020). Aloperine Suppresses LPS-Induced Macrophage Activation through Inhibiting the TLR4/NF-Kb Pathway. *Inflamm. Res. official J. Eur. Histamine Res. Soc.* 69 (4), 375–383. doi:10.1007/s00011-019-01313-0

Yue, T., Sun, F., Wang, F., Yang, C., Luo, J., Rong, S., et al. (2021). MBD2 Acts as a Repressor to Maintain the Homeostasis of the Th1 Program in Type 1 Diabetes by Regulating the STAT1-IFN-Gamma axis. *Cell Death Differ* 29 (1), 218–229. doi:10.1038/s41418-021-00852-6

Zhang, L., Li, Y., Yang, X., Wei, J., Zhou, S., Zhao, Z., et al. (2016). Characterization of Th17 and FoxP3(+) Treg Cells in Paediatric Psoriasis Patients. *Scand. J. Immunol.* 83 (3), 174–180. doi:10.1111/sji.12404

Zhang, X., Lv, X. Q., Tang, S., Mei, L., Li, Y. H., Zhang, J. P., et al. (2018). Discovery and Evolution of Aloperine Derivatives as a New Family of HCV Inhibitors with Novel Mechanism. *Eur. J. Med. Chem.* 143, 1053–1065. doi:10.1016/j.ejmech.2017.12.002

Zhao, J., Zhang, G., Li, M., Luo, Q., Leng, Y., and Liu, X. (2018). Neuro-protective Effects of Aloperine in an Alzheimer's Disease Cellular Model. *Biomed. Pharmacother.* 108, 137–143. doi:10.1016/j.biopha.2018.09.008

Zhong, J., Yang, P., Muta, K., Dong, R., Marrero, M., Gong, F., et al. (2010). Loss of Jak2 Selectively Suppresses DC-mediated Innate Immune Response and Protects Mice from Lethal Dose of LPS-Induced Septic Shock. *PLoS One* 5 (3), e9593. doi:10.1371/journal.pone.0009593

Zhong, J., Yu, Q., Yang, P., Rao, X., He, L., Fang, J., et al. (2014). MBD2 Regulates TH17 Differentiation and Experimental Autoimmune Encephalomyelitis by Controlling the Homeostasis of T-bet/Hlx axis. *J. Autoimmun.* 53, 95–104. doi:10.1016/j.jaut.2014.05.006

Zhu, J., and Paul, W. E. (2008). CD4 T Cells: Fates, Functions, and Faults. *Blood* 112 (5), 1557–1569. doi:10.1182/blood-2008-05-078154

Conflict of Interest: The authors declare that the research was conducted in the absence of any commercial or financial relationships that could be construed as a potential conflict of interest.

Publisher's Note: All claims expressed in this article are solely those of the authors and do not necessarily represent those of their affiliated organizations or those of the publisher, the editors, and the reviewers. Any product that may be evaluated in this article or claim that may be made by its manufacturer is not guaranteed or endorsed by the publisher.

frontiers | Frontiers in Pharmacology

ORIGINAL RESEARCH
published: 15 June 2022
doi: 10.3389/fphar.2022.866228

3,4-Methylenedioxy-β-Nitrostyrene Alleviates Dextran Sulfate Sodium–Induced Mouse Colitis by Inhibiting the NLRP3 Inflammasome

Juanjuan Zheng[1,2,3], *Zhongxin Jiang*[1,2], *Yue Song*[3,4], *Shu Huang*[3], *Yuzhang Du*[3], *Xiaobao Yang*[3], *Yan Xiao*[1,2], *Zhihui Ma*[3], *Dakang Xu*[3]* *and Jing Li*[1,2]*

[1]*Department of Clinical Laboratory, The Affiliated Hospital of Qingdao University, Qingdao, China,* [2]*Department of Inspection, The Medical Faculty of Qingdao University, Qingdao, China,* [3]*Department of Laboratory Medicine, Ruijin Hospital, Shanghai Jiaotong University School of Medicine, Shanghai, China,* [4]*Department of Medical Technology, Qiqihar Medical University, Qiqihar, China*

Inflammatory bowel disease (IBD) has been reported to be associated with NLRP3 inflammasome activation. Therefore inhibiting inflammasome activation could be a new approach to treat IBD. Inflammasome inhibitors NLRP3-IN-2, JC124, and 3,4-methylenedioxy-β-nitrostyrene (MNS) were previously reported to exert anti-inflammatory effects in various disease models but not in the dextran sulfate sodium (DSS)–induced colitis model. Here, we showed that MNS was more efficient in inhibiting the secretion of interleukin-1β (IL-1β) by blocking oligomerization of apoptosis-associated speck-like protein (ASC) than NLRP3-IN-2 and JC124. To investigate the protective effects of MNS on enteritis, we administered intragastric MNS to DSS-induced colitis mice. The results demonstrated that MNS attenuated DSS-induced body weight loss, colon length shortening, and pathological damage. In addition, MNS inhibited the infiltration of macrophages and inflammatory cells and reduced IL-1β and IL-12p40 pro-inflammatory cytokines but had no significant effect on tumor necrosis factor α (TNF-α) and IL-6. Furthermore, we also found that the differentiation of IL-17A$^+$interferon-γ (IFN-γ)$^+$CD4$^+$ T cell was decreased in the colon after MNS treatment, which might be mediated by IL-1β, etc. cytokine release. Taken together, MNS alleviated DSS-induced intestinal inflammation by inhibiting NLRP3 inflammasome activation, which may function as an effective therapeutic for IBD.

Keywords: NLRP3 inflammasome, 3,4-methylenedioxy-β-nitrostyrene, IL-1β, experimental colitis, inflammatory bowel disease

OPEN ACCESS

Edited by:
Nandakumar Natarajan, The University of Texas Health Science Center at Tyler, United States

Reviewed by:
Ting Zhang, First Affiliated Hospital of Chengdu Medical College, China
Velmurugan Meganathan, The University of Texas Health Science Center at Tyler, United States

***Correspondence:**
Dakang Xu
dakang_xu@163.com
Jing Li
qdjingl@163.com

Specialty section:
This article was submitted to Inflammation Pharmacology, a section of the journal Frontiers in Pharmacology

Received: *31 January 2022*
Accepted: *04 May 2022*
Published: *15 June 2022*

Citation:
Zheng J, Jiang Z, Song Y, Huang S, Du Y, Yang X, Xiao Y, Ma Z, Xu D and Li J (2022) 3,4-Methylenedioxy-β-Nitrostyrene Alleviates Dextran Sulfate Sodium–Induced Mouse Colitis by Inhibiting the NLRP3 Inflammasome. Front. Pharmacol. 13:866228. doi: 10.3389/fphar.2022.866228

INTRODUCTION

Inflammatory bowel disease (IBD), including Crohn's disease and ulcerative colitis, is a chronic and intractable inflammatory disease of the gastrointestinal tract (Asquith and Powrie, 2010). The condition is believed to be triggered by environmental factors in genetically susceptible individuals. Beyond this, it is related to an impaired mucosal barrier system and dysregulated intestinal immune responses (Famularo et al., 2002; Kanneganti et al., 2007). The clinical symptoms of IBD include recurrent abdominal pain, diarrhea, and mucopurulent bloody stool, and it severely affects the quality of an individual's life and increases the risk of colon cancer (Kim and Chang, 2014). Some

IBD symptoms can be controlled by conventional drugs such as sulfasalazine and infliximab. However, these drugs are usually accompanied by a relapse of IBD (Patel et al., 2016; Wu et al., 2020). The reagent for anti–tumor necrosis factor α (TNF-α) may elicit good clinical effects, but it is not widely used because of the high cost (Cote-Daigneault et al., 2015; Subramanian et al., 2017). Therefore, it is urgent to find a safe and effective approach for IBD.

To understand dysregulated intestinal inflammation in IBD, an increasing number of recent studies have focused on inflammasome-mediated colitis. In 2002, Martinon et al. identified inflammasomes for the first time and stated that they comprise caspase, ASC, and NACHT leucine-rich-repeat protein 1 (NALP1) (Martinon et al., 2002). Since then, NLR family, pyrin domain containing 3 (NLRP3); NLR family, pyrin domain containing 1 (NLRP1); absent in melanoma 2 (AIM2); NLR family CARD domain-containing protein 4 (NLRC4); interferon alpha-inducible protein 16 (IFI16), and other inflammasomes have been identified one after another (Rock et al., 2010). Among the NLR family, the NLRP3 inflammasome has been studied more extensively due to its key role in the immune system and inflammatory diseases (Agostini et al., 2004; Zhen and Zhang, 2019). NLRP3 inflammasome activation could induce the secretion of pro-inflammatory cytokines, including interleukin-1β (IL-1β) and interleukin-18 (IL-18) (Zhivaki and Kagan, 2021). In patients with IBD, the NLRP3 inflammasome was activated, followed by increased mRNA and protein levels of IL-1β, caspase-1, and NLRP3, which in turn aggravated the severity of IBD (Mahida et al., 1989; Lazaridis et al., 2017). Bauer et al. found that the protein levels of IL-18 and IL-1β from macrophages of DSS-induced wild-type mice colitis were significantly higher than those of mice lacking NLRP3, ASC, and caspase-1 (Bauer et al., 2010). All of this suggests that the NLRP3 inflammasome plays a critical role in intestinal inflammation.

Although the NLRP3 inflammasome acts on a variety of human diseases, its pathogenesis is not fully understood. Therefore, specific NLRP3 inflammasome inhibitors can be used as pharmacological tools to investigate its pathogenic mechanisms and as potential therapeutic approaches. Among these small molecules that inhibit the inflammasome signaling pathway, MNS has previously been reported to promote wound healing by inhibiting the activation of the NLRP3 inflammasome and inhibiting the platelet Glycoprotein IIb/IIIa activation with the classical enteritis drug sulfasalazine (Patel et al., 2012). NLRP3-IN-2 and JC124, chemically synthesized sulfonamide analogs, could inhibit the formation of the NLRP3 inflammasome in cardiomyocytes and limit the infarct size following myocardial ischemia/reperfusion in the mouse, without affecting glucose metabolism (Marchetti et al., 2014; Fulp et al., 2018). To date, there are no results showing the effect of these three inhibitors in colitis.

In this study, we first compared the inhibitory effects of three inhibitors on IL-1β release *in vitro*. Then, we chose MNS, which was more efficient in inhibiting the secretion of interleukin-1β (IL-1β) and explored its efficacy in an experimental enteritis mouse model as it showed better anti-inflammatory effects and IL-17A$^+$ interferon-γ (IFN-γ)$^+$CD4$^+$ T cell–mediated intestinal immune responses. Thus, we proposed MNS as a new therapeutic agent that could promote IBD remission and maintain intestinal immune balance.

MATERIALS AND METHODS

Reagents

NLRP3-IN-2 (4-(2-(5-chloro-2-methoxybenzamido)ethyl) benzenesulfamide), JC124 (5-chloro-2-methoxy-N-(2-(4-(N-methylsulfamoyl)phenyl)-ethyl)benzamide), and MNS (3,4-methylenedioxy-β-nitrostyrene) (purity >99%) were purchased from MedChemExpress (New Jersey, United States).

IL-1β, IL-6, IL-12, and tumor necrosis factor-α (TNF-α) enzyme-linked immunosorbent assay (ELISA) kits were purchased from Thermo Fisher Scientific (Waltham, United States).

Antibodies against NLRP3 (ab270449), ASC (ab175449), IL-1β (ab254360), MUC-2 (ab272692), and HRP Anti-Rabbit IgG (ab288156) were purchased from Abcam Systems (Cambridge, United Kingdom). Antibodies against claudin1 (13050-1-AP) were purchased from Proteintech (Chicago, United States). Antibodies against caspase-1 (24232S), P65 (8242S), P-P65 (3033), β-actin (4970), GAPDH (5174), and Ly-6G (87048) were purchased from Cell Signaling Technology (Boston, United States).

Nigericin (tlrl-nig), ATP (tlrl-atp), MSU (tlrl-msu), and silica (tlrl-sio) were purchased from InvivoGen (San Diego, United States). Disuccinimidyl suberate (DSS) was purchased from MP (Waltham, United States).

Flow cytometry antibodies, FITC-CD45 (109806), Pe-Cy5-CD4 (100540), APC-F4/80 (123116), PE-IL-17A (506904), APC-IFN-γ (505809), PerCP-Cy5.5-CD11b (101228), and the Zombie dye kit (423106), were purchased from Biolegend (San Diego, United States). Fixation/permeabilization buffer and permeabilization buffer were purchased from BD Bioscience (Franklin Lake, United States).

Cell Culture

Bone marrow cells were collected from C57BL/6 mice by flushing dissected tibias and femurs with aseptic PBS. The cells were cultured for 7 days in DMEM with 10% fetal bovine serum and 1% penicillin–streptomycin. 30% L929 cell-conditioned medium was added to promote bone marrow–derived macrophage (BMDM) differentiation. The cells were cultured in a humidified incubator with 5% CO_2 at 37°C.

Cell Viability

BMDMs were plated in 96-well plates (5.0×10^4 cells/well) before being incubated with NLRP3-IN-2, JC124, or MNS (0.5–20 μM) for 2 h and then assayed by a lactate dehydrogenase (LDH) assay kit (Beyotime Biotechnology, Shanghai, China).

Inflammasome Activation

BMDMs were seeded in 24-well plates (1.0×10^6 cells/well) and primed with LPS (100 ng/ml) for 4 h. After that, the cells were incubated with inflammasome inhibitors for 1 h, and then, the cells

were treated with nigericin (5 μg/ml) for 30 min or ATP (5 mM) for 2 h or silica (100 μg/ml) for 6 h or MSU (100 μg/ml) for 6 h.

Cytokine Analysis

The cell supernatant was collected after the activation of the inflammasome and centrifuged at 12,000 g for 1 min. Using relevant ELISA kits, IL-1β and TNF-α were assayed. Similar quality colon tissues were harvested from each group and incubated in DMEM. The culture supernatants were centrifuged for 1 min at 12,000 g and then IL-1β, IL-12p40, IL-6, and TNF-α levels were quantified by ELISA.

Western Blotting

The cells were collected and lysed in lysis buffer. The sample lysates were sonicated and centrifuged at 12,000 g for 5 min, and the supernatant was collected. Protein samples were separated by sodium dodecyl sulfate-polyacrylamide gel electrophoresis and then transferred to nitrocellulose membranes. The membranes were blocked in 5% skim milk in TBS + Tween 20 (TBST) for 1 h at room temperature. After that, the membranes were incubated with primary antibodies (caspase-1, IL-1β, ASC, NLRP3, P65, P-P65, and β-actin) overnight at 4°C. The next day, after washing in TBST, the membranes were incubated with peroxidase-conjugated secondary antibody for 1 h at room temperature. Protein bands were visualized with a high-signal enhanced chemiluminescence Western blotting substrate (Tanon, China) using a Tanon-Chemi imaging system (Tanon-5200).

Immunofluorescence Staining of ASC Specks

BMDMs (6×10^5 cells/well) were placed in 24-well plates. After inflammasome activation, the cells were fixed in 4% paraformaldehyde for 20 min at room temperature, washed with PBS three times, followed by permeabilization with 0.2% Triton X-100, and blocked with 10% goat serum in PBS for 60 min. After that, we poured out the blocking solution and incubated with anti-ASC antibody (1:100) diluted in 5% goat serum in PBS at 4°C overnight. Then, BMDMs were washed with PBS, incubated with Alexa Flour 488 goat anti-rabbit IgG (Invitrogen, Carlsbad, United States) diluted in PBS (1:1000) for 2 h, and nuclei were stained with DAPI (Beyotime Biotechnology, Shanghai, China) for 1 h. The ASC-speck formation was imaged under a positive fluorescence microscope (Nikon, Japan).

Animals and the DSS-Induced Colitis Model

Male C57BL/6 mice (weighing 25–27 g at 8–10 weeks old) were purchased from Charles River Laboratories (Beijing, China). They were kept in a 12 h reverse light/dark cycle, with *ad libitum* access to food and water.

The animals were divided into three groups. The control group ($n = 5$) received no DSS or inhibitors. The DSS group ($n = 5$) was treated with 3% DSS to induce colitis but no inhibitors. Animals in the DSS + MNS group were simultaneously treated with 3% DSS and MNS (30 mg/kg/day) for 5 days. According to a previously described protocol (Zaki et al., 2010), the disease activity index (DAI) was used to record weight loss, fecal diarrhea, and the presence of fecal blood. After 7 days, the mice were humanely killed by cervical dislocation. The colon tissue was excised for subsequent analysis. The animal experiments were conducted in strict accordance with the National Institutes of Health Guide for the Care and Use of Laboratory Animals, approved by the Ethics Committee of Ruijin Hospital, Shanghai Jiao Tong University School of Medicine.

Histological Score

Approximately 1 cm of colon tissue was fixed in 4% formalin. The samples were then dehydrated and embedded in paraffin. Histological sections were stained with hematoxylin and eosin (H&E) and observed under an optical microscope (Nikon, Japan). Colitis severity was evaluated using a lesion score system. 1) Inflammation severity of the intestinal wall (0.5 = extremely mild; 1 = mild; 2 = moderate; 3 = intense inflammation). 2) Lesion severity (1 = mucosal layer; 2 = mucosa; 3 = submucosa or transmural injury). 3) Crypt damage (0 = no significant damage; 1 = 1/3 crypt damage; 2 = 2/3 crypt damage; 3 = crypt loss but surface epithelium intact; and 4 = crypt and surface epithelium missing). The scores were summed up to generate the final score. The average score [mean ± standard error of the mean (SEM)] of each animal in each group was calculated, and t-tests were performed among different groups.

Myeloperoxidase Activity

Neutrophil infiltration into inflamed bowel mucosa was determined by an MPO activity assay using the O-dianisidine method (Qian et al., 2020). The protein extracted from colonic tissue was used to evaluate the MPO level according to the manufacturer's instructions (Beyotime Biotechnology, Shanghai, China).

Immunohistochemistry Staining

Colon tissue sections were deparaffinized, rehydrated, and blocked. Then, the sections were incubated with the following primary antibodies at 4°C overnight: Ly-6G (1:800), claudin-1 (1: 400), and MUC-2 (1:1000) overnight at 4°C. After that, the sections were incubated with an HRP Anti-Rabbit IgG antibody (1:800) for 1 h at room temperature. Positively stained sites were visualized by incubating with peroxidase-labeled streptavidin-complex (Beyotime Biotechnology, Shanghai, China), and the nuclei were counterstained with hematoxylin. The immune-positive sites were recognized by yellowish-brown staining, and the blue or purple staining showed the nuclei. The images were captured with a Nikon confocal microscope (Tokyo, Japan).

Flow Cytometry

The colon tissue was collected when mice were killed and immediately minced and digested with collagenase IV (Sigma-Aldrich, MO, United States) 300 U/ml and a hyaluronidase solution (Sigma-Aldrich, MO, United States) 200 U/ml in Roswell Park Memorial Institute 1640 medium supplemented with penicillin and streptomycin and incubated at 37°C for 1 h. The cell suspension was centrifuged at 12,000 g for 5 min and mechanically dissociated through a sterile nylon mesh filter. For

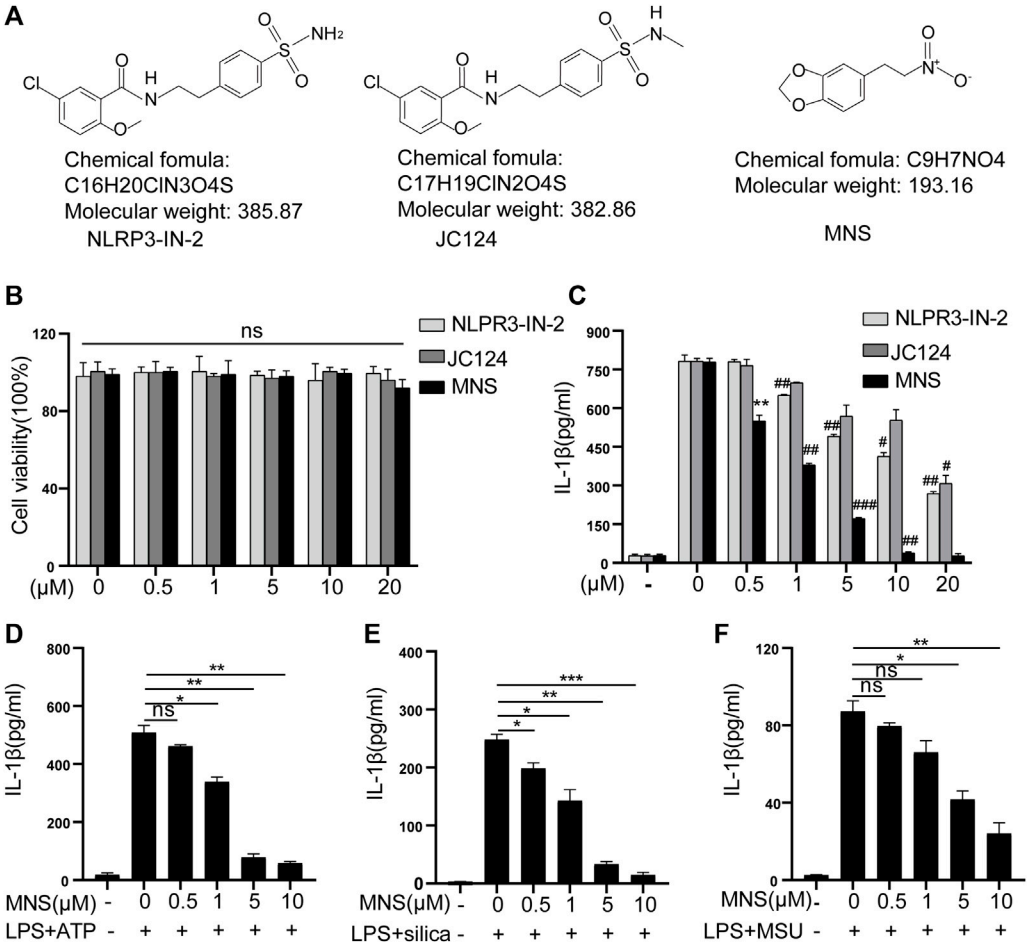

FIGURE 1 | Inflammasome inhibitors inhibited IL-1β secretion. **(A)** Chemical structures of NLRP3-IN-2, JC124, and MNS. **(B)** BMDM viability was measured using the LDH assay after incubation with different doses of inflammasome inhibitors of 0, 0.5, 1, 5, 10, and 20 μM. **(C–F)** After LPS-primed BMDMs were pretreated with MNS (0.5–20 μM), IL-1β secretion was assayed by ELISA upon stimulation with nigericin (15 μM) for 30 min **(C)**, ATP (5 mM) for 2 h **(D)**, silica (100 μg/ml) for 6 h **(E)**, and MSU (100 μg/ml) for 6 h **(F)**. Data were expressed as the mean ± standard error of the mean (SEM) ($n = 3$). Statistical analyses were performed using an unpaired two-tailed Student's t-test; ns = not significant, $^{*}p < 0.05$, $^{**}p < 0.01$, and $^{***}p < 0.001$ vs. without inhibitor treated; $^{\#}p < 0.05$, $^{\#\#}p < 0.01$, and $^{\#\#\#}p < 0.001$ vs. with inhibitor treated.

intracellular cytokine analyses, the cells were stimulated in complete medium plus a Cell Activation Cocktail and Brefeldin A for 4 h at 37°C. The assay antibodies included anti–FITC-CD45, APC-F4/80, Pe-Cy5-CD4, PE-IL-17A, APC-IFN-γ, PerCP-Cy5.5-CD11b, and also a Zombie NIR dye. Data were acquired on an LSR-II system (BD Biosciences) and analyzed using FlowJo software (V10, Becton Dickinson, Ashland, OR, United States).

Statistical Analysis

Statistical analyses were conducted using two-tailed Student's tests for comparisons between two groups and a one-way analysis of variance (ANOVA) followed by Dunnett's test for comparisons between three or more groups. The results were expressed as the mean ± standard error of the mean (SEM). $p < 0.05$ indicated statistical significance. All analyses were carried out by GraphPad Prism v8.0 (La Jolla, San Diego, United States).

RESULTS

The Effects of Inflammasome Inhibitors on IL-1β Secretion

To assess the toxicity of NLRP3-IN-2, JC124, and MNS (**Figure 1A**) on BMDM viability, LDH assays were performed. Treatment with any of the three compounds up to 20 μM did not generate any cytotoxicity (**Figure 1B**). Thus, in the subsequent experiments, we used inhibitors at concentrations of 1–10 μM, a safe range for BMDM viability. NLRP3-IN-2, JC124, and MNS were added before NLRP3 inflammasome activation to investigate their possible inhibition. Of them, MNS showed significant inhibitory effects toward IL-1β production in a concentration-dependent manner (**Figure 1C**). To further confirm the inhibitory effects of MNS on the NLRP3 inflammasome, we stimulated BMDMs with ATP, silica, and MSU (monosodium urate crystals) separately. IL-1β secretion was significantly increased after using these stimulants,

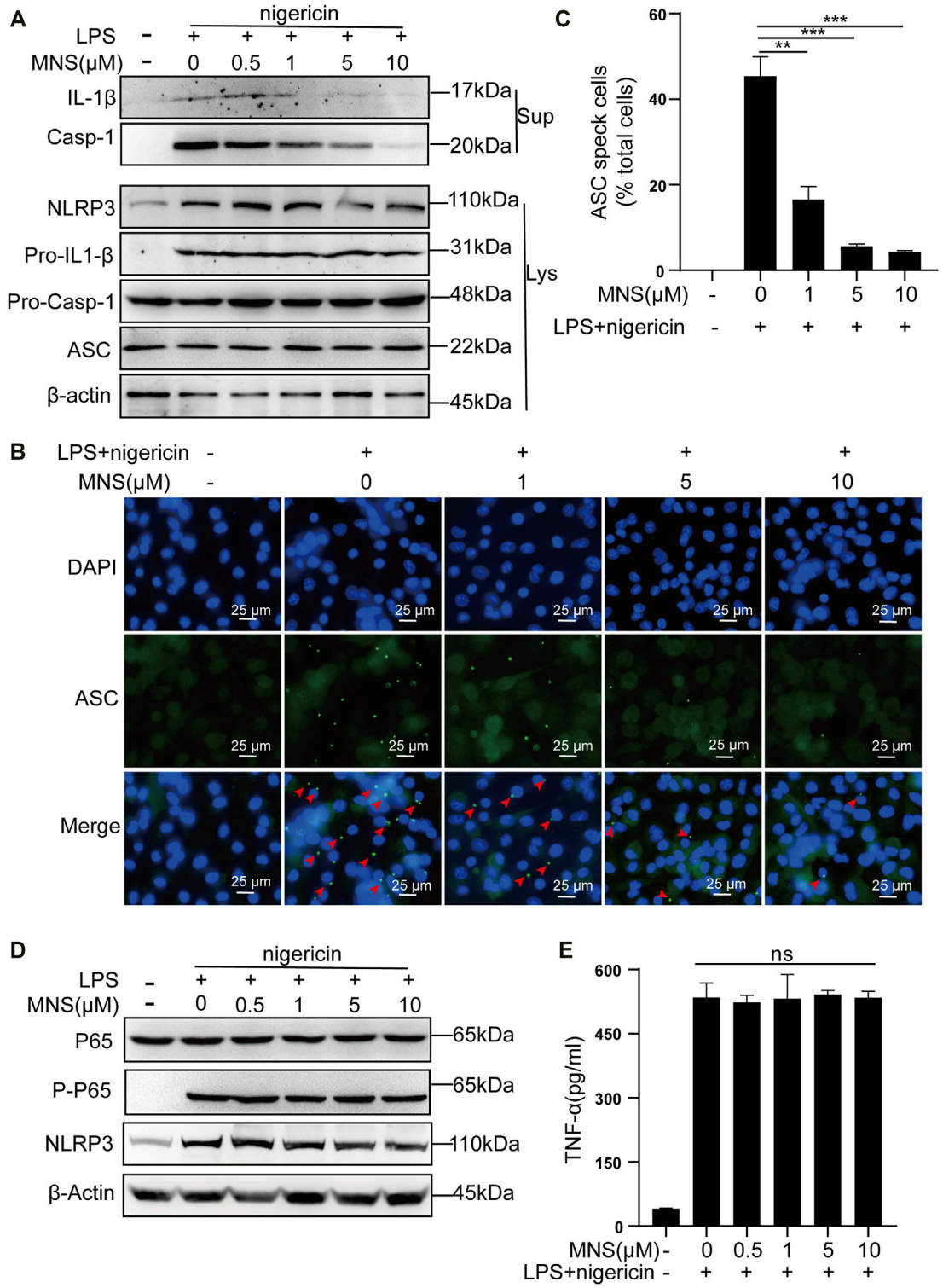

FIGURE 2 | MNS inhibited activation of the NLRP3 inflammasome *in vitro*. **(A–E)** LPS-primed BMDMs were treated with MNS (0.5–10 μM) for 1 h, followed by 15 μM nigericin for 30 min. Mature IL-1β and caspase-1 (Casp-1) were measured in supernatants (Sup); NLRP3, pro–IL-1β, pro–caspase-1(Pro–Casp-1), and ASC were measured in whole-cell lysates (Lys) by immunoblotting **(A)**. BMDMs were stained with anti–ASC antibodies for ASC specks (green) and DAPI for nuclei (blue). ASC specks were marked with red arrows **(B)**. BMDMs with ASC specks were represented as a percentage of total cells **(C)**. BMDM p65 and P-p65 levels were examined by Western blotting. **(D)** TNF-α levels in the supernatant were determined by ELISA **(E)**. Data were expressed as the mean ± standard error of the mean (SEM) ($n = 3$). Statistical analyses were performed using an unpaired two-tailed Student's t-test; ns = not significant; $^{*}p < 0.05$, $^{**}p < 0.01$, and $^{***}p < 0.001$ vs. without MNS treatment.

while it was decreased with the treatment of MNS in a dose-dependent manner (**Figure 1D**). These evidences suggested that MNS could inhibit IL-1β secretion effectively.

MNS Inhibited Activation of the NLRP3 Inflammasome *In Vitro*

The inflammasome contains multiple proteins, and the expression of these proteins affects its activity in turn (Martinon et al., 2002). Therefore, we examined the protein levels of NLRP3, ASC, pro–IL-1β, pro–caspase-1 in cell lysates, and those of caspase-1 and its substrate IL-1β in cell supernatants by immunoblotting. Caspase-1 and IL-1β were reduced, while NLRP3, ASC, pro–IL-1β, and pro–caspase-1 remained unchanged (**Figure 2A**). ASC specks were observed upon ASC oligomerization, which thereby reflected NLRP3 inflammasome activation (He et al., 2014). To investigate whether MNS suppressed IL-1β release by reducing ASC aggregation, we performed immunofluorescence on ASC specks and observed that nigericin triggered ASC speck formation in macrophages in the nigericin group. Compared to this, ASC specks decreased significantly in the MNS-treated group in an MNS dose-dependent manner (**Figures 2B,C**; **Supplementary Figure S1**). Therefore, MNS could inhibit ASC speck formation. We next examined the important proteins of nuclear factor-κB (NF-κB), p65 and P-p65, which are the primary stages of NLRP3 inflammasome formation (Hayden and Ghosh, 2008). Western blotting showed that these protein levels were unchanged (**Figure 2D**). In addition, the effect of MNS on LPS-induced TNF-α secretion levels was investigated, and a negligible change in TNF-α levels was observed at MNS concentrations of 0.5, 1, 5, and 10 μM (**Figure 2E**). Collectively, the inhibitory effects of MNS on NLRP3 inflammasome activation were pronounced, whereas NF-κB expression was unaffected.

MNS Relieved DSS-Induced Colitis Symptoms

To assess whether MNS protects against colitis *in vivo*, we designed an experiment using a DSS-induced colitis mouse model (**Figure 3A**). Both the DSS and DSS + MNS groups recorded weight loss on the fourth day, but with time, weight loss and disease activity index (DAI) in the DSS + MNS group improved compared with those in the DSS group (**Figures 3B,C**). We also observed a significant reduction in colonic length and splenomegaly in the DSS + MNS group compared to that in the DSS group (**Figures 3D,E**; **Supplementary Figures S2A–C**). In conclusion, our data suggest that MNS could significantly alleviate colitis symptoms of mice.

MNS Reduced Histopathological Damage During DSS-Induced Colitis

To observe the effects of MNS on intestinal tissue, we performed H&E staining on colon tissues from each group (**Figure 4A**). DSS treatment caused extensive colonic damage, accompanied by epithelium loss and crypt structure collapse compared with DSS + MNS treatment (**Figures 4A,B**). Myeloperoxidase (MPO) assay and immunohistochemical staining of Ly-6G were used to evaluate the recruitment and infiltration of neutrophils in mouse colon tissue. The results show that neutrophils significantly increased in the DSS group compared with the DSS + MNS group (**Figures 4C,D**). Colonic mucus is the first physical barrier that protects the colon against toxins and pathogenic invasion and is produced and maintained by glycosylated mucin-2 (MUC-2) and claudin-1 (Ambort et al., 2012; Citalán-Madrid et al., 2017; Chen et al., 2021). Immunohistochemistry staining revealed that the protein expression levels of MUC-2 and claudin-1 were significantly reduced in the DSS group, but the levels of these proteins in the DSS + MNS group were similar to those of the control (**Figure 4E**). Thus, MNS treatment retarded histopathological changes, protected the intestinal mucosa from damage, and maintained the intestinal barrier.

MNS Attenuated Macrophage Infiltration and Regulated Cytokine Secretion of Mouse Colon With DSS-Induced Colitis

In patients with IBD, considerable macrophages usually infiltrate the intestine (Bernardo et al., 2018; Wright et al., 2021). To explore this further, we used flow cytometry to examine the number and proportion of F4/80+ and CD11b+ labeled macrophages in colon tissues. Compared with the DSS group, the MNS + DSS group displayed reduced intestinal macrophage infiltration (**Figures 5A,B**). Secretion of macrophage-derived inflammatory cytokines, such as IL-1β, IL-12p40, and TNF-α, is required for T helper 17 (Th17) and T helper 1 (Th1) cell differentiation (Conforti-Andreoni et al., 2011). IL-17A is the marker of Th17, and IFN-γ is the marker of Th1 (Harbour et al., 2015), so we investigated the expression of IL-17A and IFN-γ by flow cytometry. The results showed that $IL\text{-}17A^{+}IFN\text{-}\gamma^{-}CD4^{+}$ T cells (Th17) decreased slightly in the DSS + MNS group compared with those in the DSS group, but there was no significance (**Figures 5C,D**). However, $IL\text{-}17A^{-}IFN\text{-}\gamma^{+}CD4^{+}$ T cells (Th1) and $IL\text{-}17A^{+}IFN\text{-}\gamma^{+}CD4^{+}$ T cells decreased significantly in the DSS + MNS group when compared with the DSS group (**Figures 5C,D**). In addition, the levels of TNF-α, IL-1β, IL-6, and IL-12p40 in colon tissue were measured by ELISA, which were all reduced in DSS + MNS animals, and significance was only observed in IL-1β and IL-12p40 (**Figure 5E**). These data show that MNS attenuated macrophage infiltration and $IL\text{-}17A^{+}IFN\text{-}\gamma^{+}CD4^{+}$ T cell differentiation and IL-1β, IL-12, and IL-6 secretion.

DISCUSSION

IBD is a common clinical disease with a complex pathogenesis. Despite the continuous development of treatments, there are still limitations. Therefore, it is necessary to explore other effective and safe therapeutic drugs. As a cytoplasmic polyprotein complex and an important component of innate immunity, the NLRP3 Inflammasome has been studied by more and more researchers due to its vital role in immune response and diseases, including

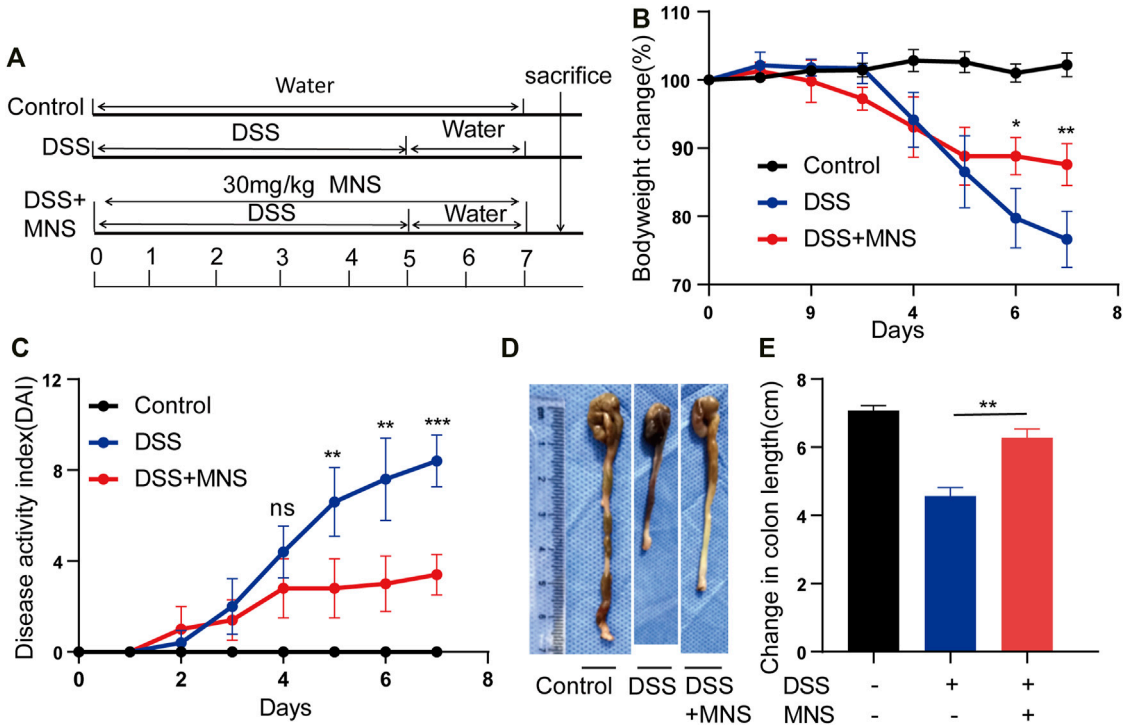

FIGURE 3 | MNS relieved DSS-induced colitis symptoms. **(A)** Experimental DSS-induced colitis protocol. **(B)** Percentage of body weight loss in mice treated with DSS alone (blue line), DSS + MNS (red line), and Control mice (black line). **(C)** Disease activity index (DAI) in mice treated with DSS alone (blue line), DSS + MNS (red line), and Control mice (black line) over 7 days. **(D)** Gross colonic anatomy showing the shortening effects of MNS on DSS-induced colon. **(E)** Colon length was measured at autopsy. N = 3 mice/group. Data were presented as the mean ± standard error of the mean (SEM). In **(B,C,E)** $^{*}p < 0.05$, $^{**}p < 0.01$, and $^{***}p < 0.001$ vs. the DSS group.

infectious diseases and metabolic diseases (Place and Kanneganti, 2019; Tartey and Kanneganti, 2020). It is known that the activation of the NLRP3 inflammasome is achieved through two sequential steps, termed as priming and assembly. The activation of Toll-like receptor 4 (TLR4) by lipopolysaccharide (LPS) provides the priming signal (signal 1), thereby increasing the transcription of NLRP3, pro–IL-1β, and IL-18 through the NF-κB–mediated pathway (Huang et al., 2017; Mangan et al., 2018). Further stimulation by infections and/or tissue damage (e.g., ATP, MSU, and silica) (signal 2) leads to a series of responses, such as K^+ efflux (Mariathasan et al., 2006; Martinon et al., 2006; Dostert et al., 2008), that trigger the assembly of NLRP3 inflammasomes following NLRP3 inflammasome activation (Liu et al., 2014) (**Figure 6**). We have confirmed that MNS has a broad-spectrum inhibitory effect on ATP, MSU, and silica-induced inflammasome activation *in vitro*. As the core of the inflammatory response, the NLRP3 inflammasome may provide new targets for the treatment of various inflammatory diseases. This study is the first description of using compound-MNS on enteritis mice with DSS-induced intestinal inflammation and explored its inhibitory effects on the NLRP3 inflammasome, which may function as an effective therapeutic for IBD.

He et al. identified MNS as one of the most potent inhibitors for NLRP3 inflammasome activation by screening a kinase inhibitor library in 2014 (He et al., 2014). Since then, several studies have confirmed its anti-inflammatory effects on NLRP3, and no effect on NLRC4 or AIM2 inflammasome (He et al., 2014; Xiao et al., 2016; Patel et al., 2018). In addition to reducing the release of mature IL-1β, MNS could also induce other cellular responses, such as cell death and IL-18 maturation, suggesting that directly targeting NLRP3 inflammasome activation may be more effective than blocking IL-1β alone. Several previously identified inhibitors of the NLRP3 inflammasome, such as Bay11-7082 and Parthenolide, acted upstream of the inflammasome pathway and inhibited the activation of the NF-κB pathway, thereby affecting NLRP3 ATPase activity, ASC oligomerization, and reducing IL-1β and TNF-α production (Saadane et al., 2007; Juliana et al., 2010), while recent studies reported that anti-TNF-α agents, such as infliximab, adalimumab, and ustekinumab, could result in severe side effects (Cohen and Sachar, 2017). Therefore, inhibiting upstream molecules of the inflammasome pathway may not be an ideal choice. Our experiments showed that MNS did not affect the activation of NF-κB or the release of TNF-α, suggesting that MNS may have fewer side effects in IBD treatment.

It was also reported that MNS could inhibit Syk kinase that could modulate the activity of the ASC-containing inflammasome in macrophages by regulating the formation of ASC specks (Hara et al., 2013), which was consistent with our results. Interestingly, MNS's inhibitory effects on Syk kinase could inhibit platelet aggregation, which was also consistent with some reports of many antiplatelet drugs having good

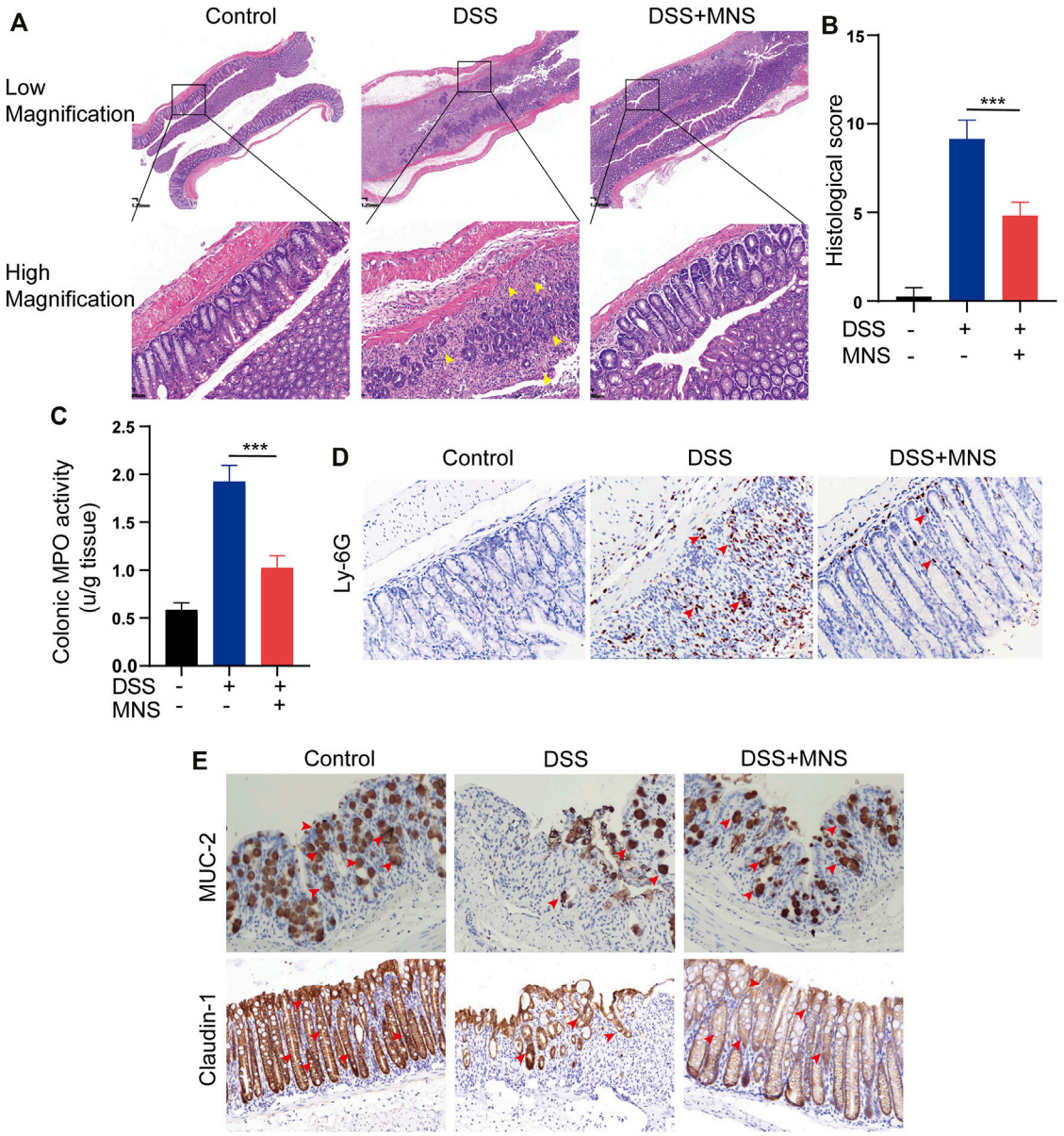

FIGURE 4 | MNS reduced histopathological damage during DSS-induced colitis. **(A)** Hematoxylin and eosin stain of colon tissue, epithelium loss, and crypt structure collapse were marked with yellow arrows. **(B)** Histological scores of blinded sections. **(C)** Colon tissue culture supernatants were assayed for MPO. Immunohistochemistry staining of **(D)** Ly-6G **(E)** MUC-2, and claudin-1 in the colon were marked with red arrows. N = 3 mice/group. Data were presented as the mean ± standard error of the mean (SEM). ***$p < 0.001$ vs. the DSS group.

anti-inflammatory effects (Nannizzi-Alaimo et al., 2003; Friedman et al., 2009; Patil et al., 2010; Petrovic et al., 2020). For example, as the current traditional IBD therapeutic agent, sulfasalazine has been proven to have an anti-platelet aggregation effect (Patel et al., 2012). Considering that MNS may play a role through multiple pathways in the treatment of IBD, which makes it a better therapeutic option.

As synthetic small-molecule inhibitors of the NLRP3 inflammasome, NLRP3-IN-2, JC124, and MNS can all reduce IL-1β secretion in BMDMs. However, in our study, NLRP3-IN-2 and JC124 were not as effective as reported by Marchetti et al. (2014); Kuwar et al. (2019), and MNS was the most effective. The reason for this may be due to different drug sensitivities to different cell lines. Here, we used primary BMDMs because they were superior to tumor cell lines and more closely resembled autologous macrophages, which would make the results more meaningful.

Inflammatory cytokines play an important role in the development of IBD. Clinical studies have shown that the concentration of IL-1β dramatically increased in the serum of IBD patients and inflamed colonic tissues appeared (McAlindon et al., 1998; Ludwiczek et al., 2004). Along with this, mature IL-1β production was also significantly upregulated in our mouse

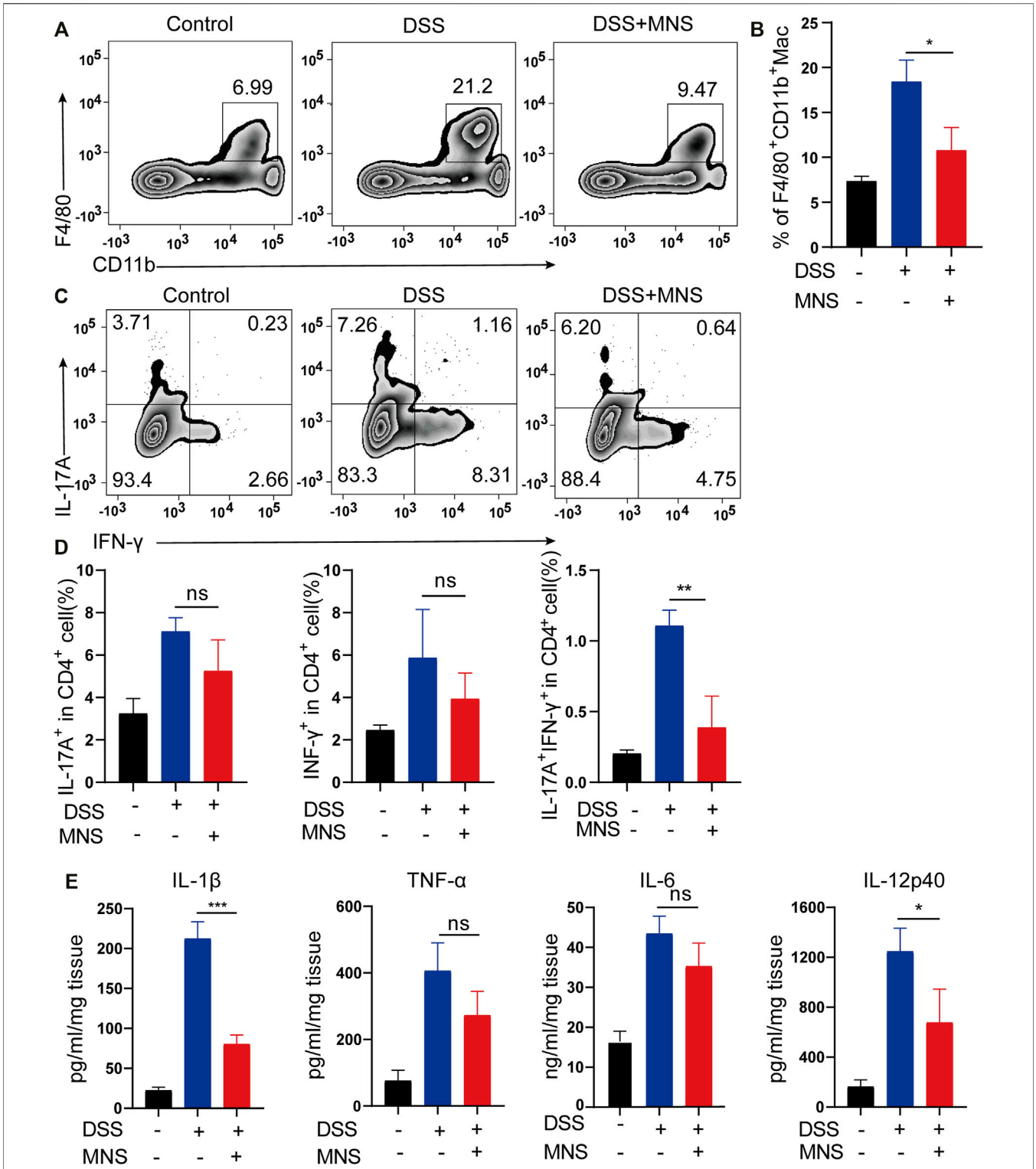

FIGURE 5 | MNS attenuated macrophage infiltration and regulated cytokine secretion of mouse colon with DSS-induced colitis. **(A,B)** F4/80 + CD11b + labeled macrophages in infiltrated colon tissue were detected by flow cytometry. **(C)** IL-17A$^+$IFN-γ$^+$ helper T cells in colon tissue were analyzed by flow cytometry by IL-17A and IFN-γ intracellular staining. **(D)** Proportion analysis of IL-17A$^+$, IFN-γ$^+$, and IL-17A$^+$IFN-γ$^+$ cells in CD4$^+$T cells. **(E)** Washed colon tissues were weighed and cultured *ex vivo* for 24 h, and the supernatants of colon biopsy were analyzed using TNF-α, IL-1β, IL-6, and IL-12p40 ELISA kit. N = 3 mice/group. Data were presented as the mean ± standard error of the mean (SEM); ns = not significant. $^*p < 0.05$, $^{**}p < 0.01$, and $^{***}p < 0.001$ vs. the DSS group.

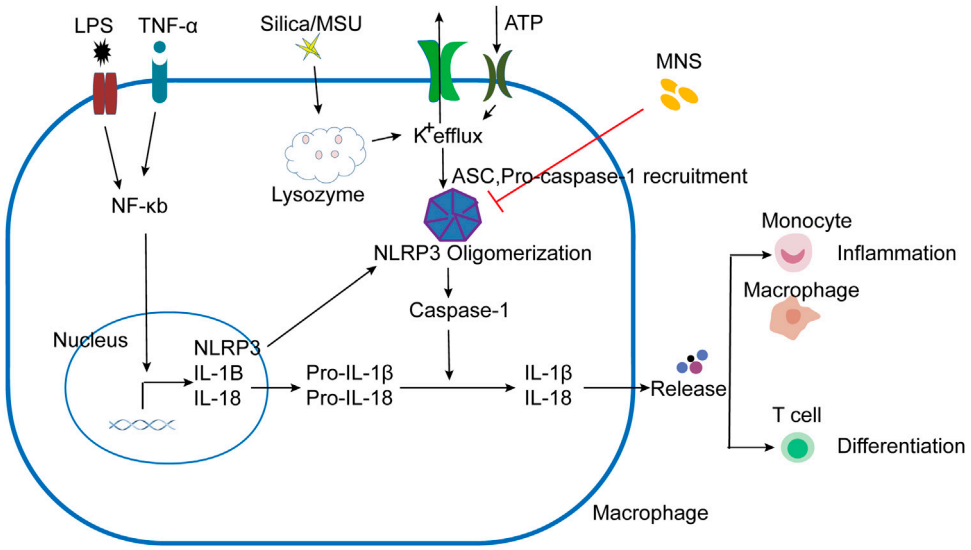

FIGURE 6 | Schematic presentation of MNS-alleviated inflammatory responses. LPS/TNF-α promoted the activation of the NF-κB pathway, increased the transcription of NLRP3, Pro–IL-1β, and Pro–IL-18. NLRP3 responded to stimuli (ATP, MSU, and silica), induced K+ efflux, and ASC and pro–caspase-1 were recruited to assemble and form NLRP3 oligomerization with the active caspase-1. Pro-IL-1β and pro-IL-18 are cleaved into mature forms by caspase-1 following NLRP3 inflammasome activation. IL-1β and other cytokines were released to induce the aggregation of mononuclear/macrophages and Th cell differentiation. When administered with MNS, NLRP3 inflammasome activation was prevented and cytokine maturation release was reduced, thereby alleviating the inflammatory response.

model of DSS-induced colitis. Studies have shown that excessive IL-1β can lead to increased intestinal permeability, promote dendritic cell and macrophage activation, and facilitate the accumulation of IL-17A secreting cells (Al-Sadi et al., 2012; Harbour et al., 2015). Our study showed that MNS administration significantly relieved mouse colitis and decreased IL-1β secretion and macrophage infiltration. Meanwhile, other inflammatory factors, such as IL-12, were also decreased upon MNS treatment. Previous studies have shown that IL-1β and IL-12 can promote the differentiation of helper T cells (Mahida, 2000; Wang et al., 2021), and T helper 17 (Th17) cells are required for the development of IBD (Geremia et al., 2014; Harbour et al., 2015; Alexander et al., 2022). IFN-γ–deficient Th17 cells maintained their Th17 phenotype but failed to induce colitis in mouse models, and IL-17A$^+$IFN-γ$^+$CD4$^+$ T cells were considered to be more pathogenic (Harbour et al., 2015; Tian et al., 2021). During DSS-induced colitis, IL-17A$^+$IFN-γ$^+$CD4$^+$ T cell levels were significantly reduced after MNS treatment. In the development of colitis, macrophages secrete inflammatory cytokines such as IL-1β and IL-12, leading to inflammatory cell aggregation, increasing inflammatory cytokine secretion, and promoting Th cell differentiation, thereby exacerbating immune response [30] (**Figure 6**). From this point, inhibiting inflammatory cytokine secretion or IL-17A$^+$IFN-γ$^+$CD4$^+$ T cell differentiation may slow down or limit immune-mediated intestinal damage, which may provide a theoretical basis for IBD immunotherapy in the future.

There are still some limitations in our study. First, MNS is the NLRP3 inflammasome inhibitor, which has the same drug target as the classic inflammasome inhibitor MCC950. The effect of MNS can be further compared with that of MCC950; second, how MNS affects intestinal microflora and microenvironment changes needs to be further verified.

In conclusion, this is the first report showing that MNS reduced intestinal tissue damage, attenuated macrophage infiltration, and regulated IL-1β and IL-12 pro-inflammatory cytokine secretion in the mouse colon with DSS-induced colitis. It also impacted the contribution of IL-17A$^+$IFN-γ$^+$CD4$^+$ T cell differentiation. It is more efficient in inhibiting the secretion of interleukin-1β (IL-1β) than NLRP3-IN-2 and JC124. Therefore, MNS may serve as a potential treatment for inflammatory bowel disease in humans.

DATA AVAILABILITY STATEMENT

The original contributions presented in the study are included in the article/**Supplementary Material**; further inquiries can be directed to the corresponding authors.

ETHICS STATEMENT

The animal study was reviewed and approved by the Ethics Committee of Ruijin Hospital, Shanghai Jiao Tong University School of Medicine.

AUTHOR CONTRIBUTIONS

DX and JL contributed to the concept and designed the research work; JZ, ZJ, YS, SH, and YD performed the experiments, acquisition, analysis, and interpretation of the data; JZ, DX, and

JL drafted the article; DX, JL, ZJ, XY, YX, and ZM provided critical reagents and supervised the research. All authors have read and agreed to the published version of the manuscript.

FUNDING

This research was supported by the Excellent Youth Medical Talents Project of Qingdao (2019); funding from the Natural Science Foundation of Shandong Province (Grant No. ZR2016HM28); grants from the Youth Research Fund of Affiliated Hospital of Qingdao University (2019) to JL; Postdoctoral Project Qingdao (2016); and grants from the National Natural Science Foundation of China (NSFC) (81871274, 82071811, and 31670905).

SUPPLEMENTARY MATERIAL

The Supplementary Material for this article can be found online at: https://www.frontiersin.org/articles/10.3389/fphar.2022.866228/full#supplementary-material

REFERENCES

Agostini, L., Martinon, F., Burns, K., McDermott, M. F., Hawkins, P. N., and Tschopp, J. (2004). NALP3 Forms an IL-1beta-processing Inflammasome with Increased Activity in Muckle-Wells Autoinflammatory Disorder. *Immunity* 20 (3), 319–325. doi:10.1016/s1074-7613(04)00046-9

Al-Sadi, R., Guo, S., Dokladny, K., Smith, M. A., Ye, D., Kaza, A., et al. (2012). Mechanism of Interleukin-1β Induced-Increase in Mouse Intestinal Permeability *In Vivo*. *J. Interferon Cytokine Res.* 32 (10), 474–484. doi:10.1089/jir.2012.0031

Alexander, M., Ang, Q. Y., Nayak, R. R., Bustion, A. E., Sandy, M., Zhang, B., et al. (2022). Human Gut Bacterial Metabolism Drives Th17 Activation and Colitis. *Cell Host Microbe* 30 (1), 17–e9. doi:10.1016/j.chom.2021.11.001

Ambort, D., Johansson, M. E., Gustafsson, J. K., Nilsson, H. E., Ermund, A., Johansson, B. R., et al. (2012). Calcium and pH-dependent Packing and Release of the Gel-Forming MUC2 Mucin. *Proc. Natl. Acad. Sci. U. S. A.* 109 (15), 5645–5650. doi:10.1073/pnas.1120269109

Asquith, M., and Powrie, F. (2010). An Innately Dangerous Balancing Act: Intestinal Homeostasis, Inflammation, and Colitis-Associated Cancer. *J. Exp. Med.* 207 (8), 1573–1577. doi:10.1084/jem.20101330

Bauer, C., Duewell, P., Mayer, C., Lehr, H. A., Fitzgerald, K. A., Dauer, M., et al. (2010). Colitis Induced in Mice with Dextran Sulfate Sodium (DSS) Is Mediated by the NLRP3 Inflammasome. *Gut* 59 (9), 1192–1199. doi:10.1136/gut.2009.197822

Bernardo, D., Marin, A. C., Fernández-Tomé, S., Montalban-Arques, A., Carrasco, A., Tristán, E., et al. (2018). Human Intestinal Pro-inflammatory CD11chighCCR2+CX3CR1+ Macrophages, but Not Their Tolerogenic CD11c-CCR2-Cx3cr1- Counterparts, Are Expanded in Inflammatory Bowel Disease. *Mucosal Immunol.* 11 (4), 1114–1126. doi:10.1038/s41385-018-0030-7

Chen, T., Wang, R., Duan, Z., Yuan, X., Ding, Y., Feng, Z., et al. (2021). Akkermansia Muciniphila Protects against Psychological Disorder-Induced Gut Microbiota-Mediated Colonic Mucosal Barrier Damage and Aggravation of Colitis. *Front. Cell Infect. Microbiol.* 11, 723856. doi:10.3389/fcimb.2021.723856

Citalán-Madrid, A. F., Vargas-Robles, H., García-Ponce, A., Shibayama, M., Betanzos, A., Nava, P., et al. (2017). Cortactin Deficiency Causes Increased RhoA/ROCK1-dependent Actomyosin Contractility, Intestinal Epithelial Barrier Dysfunction, and Disproportionately Severe DSS-Induced Colitis. *Mucosal Immunol.* 10 (5), 1237–1247. doi:10.1038/mi.2016.136

Cohen, B. L., and Sachar, D. B. (2017). Update on Anti-tumor Necrosis Factor Agents and Other New Drugs for Inflammatory Bowel Disease. *Bmj* 357, j2505. doi:10.1136/bmj.j2505

Conforti-Andreoni, C., Spreafico, R., Qian, H. L., Riteau, N., Ryffel, B., Ricciardi-Castagnoli, P., et al. (2011). Uric Acid-Driven Th17 Differentiation Requires Inflammasome-Derived IL-1 and IL-18. *J. Immunol.* 187 (11), 5842–5850. doi:10.4049/jimmunol.1101408

Côté-Daigneault, J., Bouin, M., Lahaie, R., Colombel, J. F., and Poitras, P. (2015). Biologics in Inflammatory Bowel Disease: what Are the Data? *United Eur. Gastroenterol. J.* 3 (5), 419–428. doi:10.1177/2050640615590302

Dostert, C., Pétrilli, V., Van Bruggen, R., Steele, C., Mossman, B. T., and Tschopp, J. (2008). Innate Immune Activation through Nalp3 Inflammasome Sensing of Asbestos and Silica. *Science* 320 (5876), 674–677. doi:10.1126/science.1156995

Famularo, G., Trinchieri, V., and De Simone, C. (2002). Inflammatory Bowel Disease. *N. Engl. J. Med.* 347 (24), 1982–1984. doi:10.3748/wjg.v20.i1.91

Friedman, D. J., Künzli, B. M., A-Rahim, Y. I., Sevigny, J., Berberat, P. O., Enjyoji, K., et al. (2009). From the Cover: CD39 Deletion Exacerbates Experimental Murine Colitis and Human Polymorphisms Increase Susceptibility to Inflammatory Bowel Disease. *Proc. Natl. Acad. Sci. U. S. A.* 106 (39), 16788–16793. doi:10.1073/pnas.0902869106

Fulp, J., He, L., Toldo, S., Jiang, Y., Boice, A., Guo, C., et al. (2018). Structural Insights of Benzenesulfonamide Analogues as NLRP3 Inflammasome Inhibitors: Design, Synthesis, and Biological Characterization. *J. Med. Chem.* 61 (12), 5412–5423. doi:10.1021/acs.jmedchem.8b00733

Geremia, A., Biancheri, P., Allan, P., Corazza, G. R., and Di Sabatino, A. (2014). Innate and Adaptive Immunity in Inflammatory Bowel Disease. *Autoimmun. Rev.* 13 (1), 3–10. doi:10.1016/j.autrev.2013.06.004

Hara, H., Tsuchiya, K., Kawamura, I., Fang, R., Hernandez-Cuellar, E., Shen, Y., et al. (2013). Phosphorylation of the Adaptor ASC Acts as a Molecular Switch that Controls the Formation of Speck-like Aggregates and Inflammasome Activity. *Nat. Immunol.* 14 (12), 1247–1255. doi:10.1038/ni.2749

Harbour, S. N., Maynard, C. L., Zindl, C. L., Schoeb, T. R., and Weaver, C. T. (2015). Th17 Cells Give Rise to Th1 Cells that Are Required for the Pathogenesis of Colitis. *Proc. Natl. Acad. Sci. U. S. A.* 112 (22), 7061–7066. doi:10.1073/pnas.1415675112

Hayden, M. S., and Ghosh, S. (2008). Shared Principles in NF-kappaB Signaling. *Cell* 132 (3), 344–362. doi:10.1016/j.cell.2008.01.020

He, Y., Varadarajan, S., Muñoz-Planillo, R., Burberry, A., Nakamura, Y., and Núñez, G. (2014). 3,4-methylenedioxy-β-nitrostyrene Inhibits NLRP3 Inflammasome Activation by Blocking Assembly of the Inflammasome. *J. Biol. Chem.* 289 (2), 1142–1150. doi:10.1074/jbc.M113.515080

Huang, C. F., Chen, L., Li, Y. C., Wu, L., Yu, G. T., Zhang, W. F., et al. (2017). NLRP3 Inflammasome Activation Promotes Inflammation-Induced Carcinogenesis in Head and Neck Squamous Cell Carcinoma. *J. Exp. Clin. Cancer Res.* 36 (1), 116. doi:10.1186/s13046-017-0589-y

Juliana, C., Fernandes-Alnemri, T., Wu, J., Datta, P., Solorzano, L., Yu, J. W., et al. (2010). Anti-inflammatory Compounds Parthenolide and Bay 11-7082 Are Direct Inhibitors of the Inflammasome. *J. Biol. Chem.* 285 (13), 9792–9802. doi:10.1074/jbc.M109.082305

Kanneganti, T. D., Lamkanfi, M., and Núñez, G. (2007). Intracellular NOD-like Receptors in Host Defense and Disease. *Immunity* 27 (4), 549–559. doi:10.1016/j.immuni.2007.10.002

Kim, E. R., and Chang, D. K. (2014). Colorectal Cancer in Inflammatory Bowel Disease: the Risk, Pathogenesis, Prevention and Diagnosis. *World J. Gastroenterol.* 20 (29), 9872–9881. doi:10.3748/wjg.v20.i29.9872

Kuwar, R., Rolfe, A., Di, L., Xu, H., He, L., Jiang, Y., et al. (2019). A Novel Small Molecular NLRP3 Inflammasome Inhibitor Alleviates Neuroinflammatory Response Following Traumatic Brain Injury. *J. Neuroinflammation* 16 (1), 81. doi:10.1186/s12974-019-1471-y

Lazaridis, L. D., Pistiki, A., Giamarellos-Bourboulis, E. J., Georgitsi, M., Damoraki, G., Polymeros, D., et al. (2017). Activation of NLRP3 Inflammasome in Inflammatory Bowel Disease: Differences between Crohn's Disease and Ulcerative Colitis. *Dig. Dis. Sci.* 62 (9), 2348–2356. doi:10.1007/s10620-017-4609-8

Liu, T., Yamaguchi, Y., Shirasaki, Y., Shikada, K., Yamagishi, M., Hoshino, K., et al. (2014). Single-cell Imaging of Caspase-1 Dynamics Reveals an All-Or-None Inflammasome Signaling Response. *Cell Rep.* 8 (4), 974–982. doi:10.1016/j.celrep.2014.07.012

Ludwiczek, O., Vannier, E., Borggraefe, I., Kaser, A., Siegmund, B., Dinarello, C. A., et al. (2004). Imbalance between Interleukin-1 Agonists and Antagonists: Relationship to Severity of Inflammatory Bowel Disease. *Clin. Exp. Immunol.* 138 (2), 323–329. doi:10.1111/j.1365-2249.2004.02599.x

Mahida, Y. R. (2000). The Key Role of Macrophages in the Immunopathogenesis of Inflammatory Bowel Disease. *Inflamm. Bowel Dis.* 6 (1), 21–33. doi:10.1097/00054725-200002000-00004

Mahida, Y. R., Wu, K., and Jewell, D. P. (1989). Enhanced Production of Interleukin 1-beta by Mononuclear Cells Isolated from Mucosa with Active Ulcerative Colitis of Crohn's Disease. *Gut* 30 (6), 835–838. doi:10.1136/gut.30.6.835

Mangan, M. S. J., Olhava, E. J., Roush, W. R., Seidel, H. M., Glick, G. D., and Latz, E. (2018). Targeting the NLRP3 Inflammasome in Inflammatory Diseases. *Nat. Rev. Drug Discov.* 17 (9), 688. doi:10.1038/nrd.2018.149

Marchetti, C., Chojnacki, J., Toldo, S., Mezzaroma, E., Tranchida, N., Rose, S. W., et al. (2014). A Novel Pharmacologic Inhibitor of the NLRP3 Inflammasome Limits Myocardial Injury after Ischemia-Reperfusion in the Mouse. *J. Cardiovasc Pharmacol.* 63 (4), 316–322. doi:10.1097/FJC.0000000000000053

Mariathasan, S., Weiss, D. S., Newton, K., McBride, J., O'Rourke, K., Roose-Girma, M., et al. (2006). Cryopyrin Activates the Inflammasome in Response to Toxins and ATP. *Nature* 440 (7081), 228–232. doi:10.1038/nature04515

Martinon, F., Burns, K., and Tschopp, J. (2002). The Inflammasome: a Molecular Platform Triggering Activation of Inflammatory Caspases and Processing of proIL-Beta. *Mol. Cell* 10 (2), 417–426. doi:10.1016/s1097-2765(02)00599-3

Martinon, F., Pétrilli, V., Mayor, A., Tardivel, A., and Tschopp, J. (2006). Gout-associated Uric Acid Crystals Activate the NALP3 Inflammasome. *Nature* 440 (7081), 237–241. doi:10.1038/nature04516

McAlindon, M. E., Hawkey, C. J., and Mahida, Y. R. (1998). Expression of Interleukin 1β and Interleukin 1β Converting Enzyme by Intestinal Macrophages in Health and Inflammatory Bowel Disease. *Gut* 42 (2), 214–219. doi:10.1136/gut.42.2.214

Nannizzi-Alaimo, L., Alves, V. L., and Phillips, D. R. (2003). Inhibitory Effects of Glycoprotein IIb/IIIa Antagonists and Aspirin on the Release of Soluble CD40 Ligand during Platelet Stimulation. *Circulation* 107 (8), 1123–1128. doi:10.1161/01.cir.0000053559.46158.ad

Patel, D., Gaikwad, S., Challagundla, N., Nivsarkar, M., and Agrawal-Rajput, R. (2018). Spleen Tyrosine Kinase Inhibition Ameliorates Airway Inflammation through Modulation of NLRP3 Inflammosome and Th17/Treg axis. *Int. Immunopharmacol.* 54, 375–384. doi:10.1016/j.intimp.2017.11.026

Patel, D., Madani, S., Patel, S., and Guglani, L. (2016). Review of Pulmonary Adverse Effects of Infliximab Therapy in Crohn's Disease. *Expert Opin. Drug Saf.* 15 (6), 769–775. doi:10.1517/14740338.2016.1160053

Patel, S. H., Rachchh, M. A., and Jadav, P. D. (2012). Evaluation of Anti-inflammatory Effect of Anti-platelet Agent-Clopidogrel in Experimentally Induced Inflammatory Bowel Disease. *Indian J. Pharmacol.* 44 (6), 744–748. doi:10.4103/0253-7613.103278

Patil, S. B., Jackman, L. E., Francis, S. E., Judge, H. M., Nylander, S., and Storey, R. F. (2010). Ticagrelor Effectively and Reversibly Blocks Murine Platelet P2Y12-Mediated Thrombosis and Demonstrates a Requirement for Sustained P2Y12 Inhibition to Prevent Subsequent Neointima. *Arterioscler. Thromb. Vasc. Biol.* 30 (12), 2385–2391. doi:10.1161/atvbaha.110.210732

Petrovic, S. S., Vasiljevska, M. M., Obradovic, S. D., Tarabar, D. K., Doder, R. B., Majstorovic, I. J., et al. (2020). Antiplatelet Agents'-Ticagrelol and Eptifibatide-Safety in Experimental Colitis in Mice. *Turk J. Gastroenterol.* 31 (6), 451–458. doi:10.5152/tjg.2020.19454

Place, D. E., and Kanneganti, T. D. (2019). Cell Death-Mediated Cytokine Release and its Therapeutic Implications. *J. Exp. Med.* 216 (7), 1474–1486. doi:10.1084/jem.20181892

Qian, B., Wang, C., Zeng, Z., Ren, Y., Li, D., and Song, J. L. (2020). Ameliorative Effect of Sinapic Acid on Dextran Sodium Sulfate- (DSS-) Induced Ulcerative Colitis in Kunming (KM) Mice. *Oxid. Med. Cell Longev.* 2020, 8393504. doi:10.1155/2020/8393504

Rock, K. L., Latz, E., Ontiveros, F., and Kono, H. (2010). The Sterile Inflammatory Response. *Annu. Rev. Immunol.* 28, 321–342. doi:10.1146/annurev-immunol-030409-101311

Saadane, A., Masters, S., DiDonato, J., Li, J., and Berger, M. (2007). Parthenolide Inhibits IkappaB Kinase, NF-kappaB Activation, and Inflammatory Response in Cystic Fibrosis Cells and Mice. *Am. J. Respir. Cell Mol. Biol.* 36 (6), 728–736. doi:10.1165/rcmb.2006-0323OC

Subramanian, S., Ekbom, A., and Rhodes, J. M. (2017). Recent Advances in Clinical Practice: a Systematic Review of Isolated Colonic Crohn's Disease: the Third IBD? *Gut* 66 (2), 362–381. doi:10.1136/gutjnl-2016-312673

Tartey, S., and Kanneganti, T. D. (2020). Inflammasomes in the Pathophysiology of Autoinflammatory Syndromes. *J. Leukoc. Biol.* 107 (3), 379–391. doi:10.1002/jlb.3mir0919-191r

Tian, W. J., Wang, Q. N., Wang, X. F., and Dong, D. F. (2021). Clophosome Alleviate Dextran Sulphate Sodium-Induced Colitis by Regulating Gut Immune Responses and Maintaining Intestinal Integrity in Mice. *Clin. Exp. Pharmacol. Physiol.* 48 (6), 902–910. doi:10.1111/1440-1681.13468

Wang, J., Xu, Z., Wang, Z., Du, G., and Lun, L. (2021). TGF-beta Signaling in Cancer Radiotherapy. *Cytokine* 148, 155709. doi:10.1016/j.cyto.2021.155709

Wright, P. B., McDonald, E., Bravo-Blas, A., Baer, H. M., Heawood, A., Bain, C. C., et al. (2021). The Mannose Receptor (CD206) Identifies a Population of Colonic Macrophages in Health and Inflammatory Bowel Disease. *Sci. Rep.* 11 (1), 19616. doi:10.1038/s41598-021-98611-7

Wu, J., Wei, Z., Cheng, P., Qian, C., Xu, F., Yang, Y., et al. (2020). Rhein Modulates Host Purine Metabolism in Intestine through Gut Microbiota and Ameliorates Experimental Colitis. *Theranostics* 10 (23), 10665–10679. doi:10.7150/thno.43528

Xiao, M., Li, L., Li, C., Liu, L., Yu, Y., and Ma, L. (2016). 3,4-Methylenedioxy-β-Nitrostyrene Ameliorates Experimental Burn Wound Progression by Inhibiting the NLRP3 Inflammasome Activation. *Plast. Reconstr. Surg.* 137 (3), 566e–575e. doi:10.1097/01.prs.0000479972.06934.83

Zaki, M. H., Boyd, K. L., Vogel, P., Kastan, M. B., Lamkanfi, M., and Kanneganti, T. D. (2010). The NLRP3 Inflammasome Protects against Loss of Epithelial Integrity and Mortality during Experimental Colitis. *Immunity* 32 (3), 379–391. doi:10.1016/j.immuni.2010.03.003

Zhen, Y., and Zhang, H. (2019). NLRP3 Inflammasome and Inflammatory Bowel Disease. *Front. Immunol.* 10, 276. doi:10.3389/fimmu.2019.00276

Zhivaki, D., and Kagan, J. C. (2021). NLRP3 Inflammasomes that Induce Antitumor Immunity. *Trends Immunol.* 42 (7), 575–589. doi:10.1016/j.it.2021.05.001

Conflict of Interest: The authors declare that the research was conducted in the absence of any commercial or financial relationships that could be construed as a potential conflict of interest.

frontiers | Frontiers in Pharmacology

REVIEW
published: 12 July 2022
doi: 10.3389/fphar.2022.847702

Therapeutic Potential of Polyphenol and Nanoparticles Mediated Delivery in Periodontal Inflammation: A Review of Current Trends and Future Perspectives

Putri Ayu Jayusman[1], Nurrul Shaqinah Nasruddin[1], Nurul Inaas Mahamad Apandi[1], Norliwati Ibrahim[1] and Siti Balkis Budin[2]*

[1]Department of Craniofacial Diagnostics and Biosciences, Faculty of Dentistry, Universiti Kebangsaan Malaysia, Kuala Lumpur, Malaysia, [2]Centre for Diagnostic, Therapeutic and Investigative Studies, Universiti Kebangsaan Malaysia, Kuala Lumpur, Malaysia

Periodontitis is an oral inflammatory process involving the periodontium, which is mainly caused by the invasion of periodontopathogenic microorganisms that results in gingival connective tissue and alveolar bone destruction. Metabolic products of the oral pathogens and the associated host immune and inflammatory responses triggered are responsible for the local tissue destruction. Numerous studies in the past decades have demonstrated that natural polyphenols are capable of modulating the host inflammatory responses by targeting multiple inflammatory components. The proposed mechanism by which polyphenolic compounds exert their great potential is by regulating the immune cell, proinflammatory cytokines synthesis and gene expression. However, due to its low absorption and bioavailability, the beneficial effects of these substances are very limited and it hampers their use as a therapeutic agent. To address these limitations, targeted delivery systems by nanoencapsulation techniques have been explored in recent years. Nanoencapsulation of polyphenolic compounds with different carriers is an efficient and promising approach to boost their bioavailability, increase the efficiency and reduce the degradability of natural polyphenols. In this review, we focus on the effects of different polyphenolic substances in periodontal inflammation and to explore the pharmaceutical significance of polyphenol-loaded nanoparticles in controlling periodontitis, which may be useful for further enhancement of their efficacy as therapeutic agents for periodontal disease.

Keywords: periodonditis, inflammation, nanotechnolody, nanoencapsulation, polyphenol

OPEN ACCESS

Edited by:
Roberto Paganelli, Institute for Advanced Biologic Therapies, Italy

Reviewed by:
Francesca Diomede, University of Studies G d'Annunzio Chieti and Pescara, Italy
Evangelos Papathanasiou, Tufts University, United States

****Correspondence:***
Putri Ayu Jayusman
putriayu@ukm.edu.my

Specialty section:
This article was submitted to Inflammation Pharmacology, a section of the journal Frontiers in Pharmacology

Received: *03 January 2022*
Accepted: *21 June 2022*
Published: *12 July 2022*

Citation:
Jayusman PA, Nasruddin NS, Mahamad Apandi NI, Ibrahim N and Budin SB (2022) Therapeutic Potential of Polyphenol and Nanoparticles Mediated Delivery in Periodontal Inflammation: A Review of Current Trends and Future Perspectives. Front. Pharmacol. 13:847702. doi: 10.3389/fphar.2022.847702

INTRODUCTION

Periodontitis contributes to a significant public health problem globally due to its high prevalence, economic impact and health consequences (Dom et al., 2012; Marcenes et al., 2013). As a common complex inflammatory disease of the oral cavity, it has been estimated that severe periodontitis affects 11% of the world population in last decades (Kassebaum et al., 2014). Increasing burden of severe periodontitis is suggested to be partly due to an increase in life expectancy in the growing world population. In addition, recent study has reported that half of the adult population worldwide

have at least one tooth with apical periodontitis, which is usually asymptomatic and underestimated (Tibúrcio-Machado et al., 2021). Apart from the local effects on the dentition and tooth-supporting tissues, oral diseases may also have an impact on systemic health (Scannapieco and Cantos 2016).

Diseases of the periodontium such as gingivitis and periodontitis are preventable with the application of correct preventive strategies. Nonsurgical treatment modalities remain the gold standard for managing periodontal diseases. Dental cleaning, gingival scaling/root planing (SRP) and proper oral hygiene are among the periodontal treatments available that aim to reduce inflammation, pocket depth and clinical attachment gain (Plessas 2014). In scaling and root planning procedure, antibiotics have been used as adjunct microbial therapy in periodontal pockets through systemic or topical administration (Leszczyńska et al., 2011). According to literature, deep periodontal pockets pose a great challenge for nonsurgical periodontal treatment and in cases where surgical therapy cannot be undertaken, SRP alone may not be sufficient. Bacteria that penetrate the gingival tissue may not be eliminated by mechanical instrumentation hence local and systemic antibiotics are used as an adjunctive modality (Ahad et al., 2016).

The application of non-surgical or surgical periodontal therapy in certain cases as well as antimicrobial therapy however is not wholly successful. In addition to its unwanted side effects, the rise of antimicrobial resistance among patients with severe periodontitis necessitates new strategies in managing periodontal inflammation (Kwon et al., 2021). Based on a recent report in the management of periodontitis, the use of the highest dosage of antibiotic for the shortest duration of time should be considered by clinicians in order to reduce the risk of antibiotic resistance (McGowan et al., 2018). Other major disadvantages that are related to systemic administration are the availability of insufficient concentration of the drug in gingival crevicular fluid and disturbance of intestinal microflora related to the use of antibiotics. Recent studies have also suggested the use of antimicrobial photodynamic therapy (aPDT) as an adjunct to nonsurgical treatment of deep periodontal pockets, however controversial results were reported. Available evidence on aPDT is still scarce due to the low number of controlled studies and high heterogeneity in the study outcome (Salvi et al., 2020; Zhao et al., 2021).

Natural compounds with the capability to modulate host inflammatory response have gained considerable research attention (Palaska et al., 2013). Host modulation therapy (HMT) using anti-inflammatory and antioxidant agents has been investigated and explored as a non-invasive therapeutic approach for periodontitis (Preshaw 2018; Sulijaya et al., 2019). Plant-derived polyphenols have been known to possess antimicrobial, anti-inflammatory, immunomodulatory and antioxidant properties contributing to its benefits in human health. Such characteristics have been reported as the biological mechanisms involve in reducing the initiation and progression of periodontal inflammation. *In vitro* and *in vivo* studies demonstrated that polyphenol possesses an antimicrobial and immunomodulatory potential in treating and preventing periodontitis (Bunte et al., 2019). However, the use of systemic route administration in particular may yield limited results on account of poor pharmacokinetics and pharmacodynamics properties of polyphenol (Hoda et al., 2019). Despite its great potential, polyphenolic compounds have been associated with limited bioavailability mainly due to its low solubility, poor stability in the gastrointestinal tract (GIT) and low intestinal permeability as well as its extremely short plasma half-life (Lu et al., 2016).

Besides continuing the search for new agents that have anti-inflammatory or bone-regeneration properties, the development of slow-release agents is highly desirable to prevent this prevalent and costly disease. The economic burden of periodontitis is highly associated with its prevalence and cost of treatment and in fact is comparable with that of other chronic diseases (Mohd-Dom et al., 2014; Mohd Dom et al., 2016). One of the strategies to overcome the limitations related to polyphenol bioavailability and to enhance its therapeutic applications is by incorporating them into nanoparticles (Conte et al., 2016; Abdul Rahim et al., 2019). The therapeutic potential of polyphenol in managing periodontal inflammation from recently published studies is discussed and the effects of different polyphenol-loaded nanoparticles are highlighted in this present review.

HOST IMMUNE AND INFLAMMATORY RESPONSES IN PERIODONTAL INFLAMMATION

Gingivitis and periodontitis are the two most common gum diseases that affect periodontal tissues and the supporting structures of a tooth (Hasturk et al., 2012). Gingivitis is most commonly caused by bacterial plaque accumulation on the tooth surface resulting in gum inflammation. In gingivitis, the inflammatory condition is restricted to the soft-tissue area of the gingival epithelium and connective tissue without affecting the deeper compartments of the periodontium. Nonetheless, gingivitis may progress and develop into periodontitis, and therefore it is also considered as the prerequisite for the onset of periodontitis (Murukami et al., 2018). Periodontitis is a chronic multifactorial inflammatory disease characterized by progressive destruction of the periodontal supporting tissue including periodontal ligament and alveolar bone. It is indicated by gingival inflammation, clinical attachment loss, alveolar bone loss that could be assessed by radiography, presence of periodontal pocket and gingival bleeding (Papapanou et al., 2018).

Activation of Host Immune and Inflammatory Responses

Inflammation is an innate immune response of the body intended to eliminate the initial cause of tissue injury. Inflammatory responses play a major role in our body defence system against pathogens that also involve wound healing. Hence, inflammation is vital for our health and survival. The mouth provides a suitable environment for the growth of

microorganisms. Thus, bacteria are present constantly in the mouth and some of these bacteria can trigger inflammatory response and implicated in oral disease. Most of the cases in periodontal disease are originated from bacterial dental plaque or biofilm accumulated on the teeth that induce host periodontal tissues inflammatory response (Hajishengallis et al., 2020). Both chronic gingivitis and periodontitis are chronic lesions that display inflammation and attempts at healing (Hasan and Palmer 2014).

The earliest process of inflammation involves its response against the invading microorganisms. In a susceptible host, invasion of periodontal pathogens particularly a group of specific Gram-negative anaerobic species in subgingival dental biofilm including *Porphyromonas gingivalis, Tannerella forsythia*, and *Treponema denticola* may result in chronic inflammation. These complex bacteria are predominantly found in deep periodontal pockets of patients with periodontitis (Kwon et al., 2021). The major component of the most Gram-negative bacteria present in the oral biofilm particularly lipopolysachharide (LPS) along with other virulence factors cause stimulation of mast cells and the release of vasoactive amines that cause vasodilation of blood vessels. The release of preformed tumour necrosis factor α (TNF-α) causes a subsequent release of inflammatory mediators in the gingival tissue (Hasturk et al., 2012; Yucel-Lindberg & Båge 2013). The chemoattractant proteins (chemokines) generated at this stage results in the initiation of the first line of defence, which are neutrophils that move and migrate to the site of microbial invasion. This process leads to the release of lysosomal enzymes that may also contribute to tissue degradation (Ge et al., 2015). Neutrophil infiltration is then followed by the activation of macrophages. Macrophages activation play a critical role in the elimination of the invaded bacteria, recruitment of other cells to the site of infection, removal of neutrophils excess, production of cytokines and chemokines and activation of lymphocyte-mediated adaptive immunity (Hasturk et al., 2012).

As lymphocytes and macrophages further invade the tissue, collagen content in gingiva is degraded but the bone at the site of lesion may still be intact. At this point, the associated damage is still reversible as it is still possible for gingival tissues to undergo repair and remodelling. In complete resolution with healing, the outcome of the inflammatory process can be restricted or cleared by the role of neutrophils and macrophages. The destructive inflammatory lesion that results in loss of local collagen due to accumulation of polymicrobial biofilm at the gingiva of the teeth is reversible upon resolution of the inflammation (Van Dyke et al., 2020). At this stage, the process of fibrosis and scar tissue formation may limit the infection but failure to clear the infection might establish a chronic inflammatory lesion.

Progression From Gingivitis to Periodontitis

It is noted that gingivitis is a major risk factor for periodontitis and it may develop into periodontitis in disease-susceptible individuals in which the host response is ineffective and dysregulated (Yucel-Lindberg and Båge 2013; Hajishengallis 2015). The pathogenesis of periodontal disease can be generally categorized into four stages, based on histopathological examination of the development of periodontal inflammation due to plaque accumulation. These stages are called 1) the initial, 2) the early, 3) the established, and 4) the advanced lesions. The advanced lesion which is also known as the destructive phase is clinically recognised as periodontitis where the inflammation extends deeper, with the formation of periodontal pocket, clinical attachment loss, collagen and bone loss (Hasan and Palmer 2014). The "established lesion" can persist for many years and the progression to an "advanced lesion" marks the transition from chronic and successful defence mechanism to destructive immunopathological mechanism or periodontitis. Recently, a new periodontitis classification scheme has been adopted according to the staging and grading system. Classification of periodontitis based on stages is dependent upon the severity of disease at presentation and the complexity of disease management. Meanwhile, classification of periodontitis based on grades reflect biologic features of the disease including analysis of the rate of periodontitis progression, risk for further progression, possibility of poor treatment outcomes and assessment of the risk that the disease or its treatment could affect the systemic health of the patient (Papapanou et al., 2018).

The exact factors that are responsible for the progression of periodontal diseases are unknown but chronic periodontal diseases involve the interaction of several components, which are the bacterial product or the pathogenicity factor, various cell populations and inflammatory mediators (Yucel-Lindberg and Båge 2013). Interaction between the host and microflora with time may result in dysbiosis of microbiome and dysregulation of host inflammation (Hajishengallis 2015). Colonization of Gram-negative bacteria up to 80% in the gingival sulcus during the establishment of periodontal disease form subgingival plaque, leading to periodontal pockets formation and gum recession (Palaska et al., 2013). Among the major pathogens, *A. actinomycetemcomitants* are more commonly detected in high levels in patients with aggressive periodontitis (Teles et al., 2013). The growth of pathogenic microbes within the dental plaque produces substances that could exacerbate inflammation, which may then lead to tissue destruction and even tooth loss. The immune-inflammatory mechanism in periodontal diseases is in part controlled by an individual's susceptibility and interaction with environmental factors (Lamont et al., 2018).

The destruction of periodontal tissue and bone resorption are contributed by cellular activation, inflammatory mediators including cytokines, chemokines, prostaglandins and proteolytic enzymes particularly matrix metalloproteinases (MMP). The progression of periodontitis involves the release of prominent cytokines such as TNF-α, which is also involved at the early stage of inflammatory cascade, and IL-1 that are produced by the B-cell/plasma cell (Pan et al., 2019). These two cytokines may induce a number of inflammatory mediators such as IL-6, IL-8, MMP and prostaglandin E_2 (PGE_2), which is the most prominent prostaglandin implicated in the pathogenesis of periodontitis. IL-1 exerts different biologic effects on different cells and is an important biological mediator of autoimmune and inflammatory diseases. It plays a crucial role in both innate and adaptive immunity. Among first members of IL-1 identified include IL-1α and IL-1β (Dinarello 2018).

11 known members of IL-1 includes molecules with agonist activity such as IL-1α, IL-1β, IL-18, IL-33, IL-36α, IL-36β, and IL-36γ), receptor antagonists of IL-1Ra, IL-36Ra and two anti-inflammatory cytokines which are IL-37, and IL-38 (Dinarello 2018).

Dental biofilm dysbiosis will stimulate the release of IL-1 proinflammatory cytokines including IL-1α, IL-1β, IL-18, IL-36 from the oral junctional epithelium. These proinflammatory signals combined with bacterial products in the periodontal tissues in turn will stimulate both innate and adaptive immunity response. Hence, both complexes will promote release of inflammatory cell mediators into the periodontium (Papathanasiou et al., 2020). Virulence properties of periodontal pathogens such as lipopolysaccharides, stimulates the release of both IL-1α and IL-1β form oral epithelial cells hence resulting in periodontal destruction. Recently, it has been demonstrated that host defense peptides (HDPs) released from the gingival epithelium leading to accumulation of mast cells (MCs) that induces release of more pro-inflammatory cytokines. Therefore, enhancing further breakdown of periodontal tissue (Chompunud et al., 2020). IL-1β upregulates MMPs secretion hence contributing to augmented vasodilation, chemotaxis of inflammatory cells and degradation of collagen. In addition, osteoclastogenesis is also enhanced leading to elevated activity of bone resorption. A study reported that within gingival biopsies of active periodontal disease, there was reduced expression of inflammasome regulators while expression of messenger RNA (mRNA), NLRP3 and IL-1β were amplified (Aral et al., 2020).

Dendritic cells (DCs) release IL-18 that stimulates differentiation of T helper 1 cell (Th1) and T helper 17 cell (Th17) which in turn upregulates the release of IL-17, TNF-α, and IL-1β, hence contributing to further periodontal destruction. Elevated release of IL-1 proinflammatory has been associated with increased receptor activator of nuclear factor-κB ligand (RANKL) release, thus inducing osteoclasts progenitors responsible for alveolar bone resorption in periodontitis. However, IL-1 family members possessing anti-inflammatory properties play a defence role in periodontitis. Here, they will alleviate the magnitude of periodontal inflammation (Papathanasiou et al., 2020). The production of PGE_2 by the immune cells, fibroblasts and other resident gingival cells is associated with the formation of osteoclast via RANKL upregulation and osteoprotegerin (OPG) inhibition (Belibasakis & Guggenheim 2011).

Since the development of periodontitis is mediated by bacterial-induced inflammation that lead to an excessive host response, the use of conventional mechanical therapy and pharmacological adjuncts is therefore plausible to control the inflammation (Bartold and Van Dyke 2013). Evidence showed that, adjunctive antibiotics and other anti-inflammatory agents can be effective to inhibit or eliminate periodontopathogenic microorganisms and modulate the inflammatory response of the tissue (Da Rocha Júnior et al., 2015). The use of nonsurgical periodontal therapy with or without antimicrobials remains as standard of care that could mechanically removes dental biofilm but targeting only microbes does not equally favourable in all periodontal patients (Preshaw 2018). In addition, the use of adjunctive antibiotics is associated with the unwanted side effects and should only be recommended for progressive disease (Tilakaratne and Soory 2014). Some of the side effects associated with the most commonly used antibiotics in managing periodontal disease include nephritis, gastrointestinal problems, increased risk of allergy, allergic signs on the skin, disturbance in the nervous system and electrolytes imbalance (Heta and Robo 2018).

This is where other agents with similar properties and biological effects with fewer side effects can take its place in improving and managing periodontitis. In fact, One of the promising therapeutic approaches in managing periodontitis particularly in individuals with a higher risk for periodontitis is by modulation of host inflammatory mediators. The term 'host modulation therapy' was initially introduced by Golub et al., 30 years ago (Golub et al., 1998). In the last decades, the efficacy of HMT using anti-inflammatory and antioxidant agents in periodontitis was explored. The two major HMT categories accepted include firstly the modulation of the host's inflammatory response via inhibition or resolution and secondly modulation of host's pathologic collagenolytic response within the periodontal soft tissue along with alveolar bone (Van Dyke, 2017; Golub et al., 2018). The adjunctive use of host modulatory agents has been postulated to have a positive implication on the progression of periodontal disease particularly in susceptible patients and in individuals whom conventional therapeutic approach is ineffective (Balta et al., 2021). Recently, polyphenols have been documented to cause immunomodulatory effects by downregulating the proinflammatory cytokines, IL-1 and IFN-γ which could be beneficial to be used as adjunct therapeutic approaches in reducing the burden of various inflammatory diseases (Shakoor et al., 2021).

ROLE OF POLYPHENOLIC COMPOUNDS IN MANAGING PERIODONTAL INFLAMMATION

In recent years, polyphenolic compounds are among plant-derived phytochemicals that have gained remarkable attention due to their low toxicity, compared to allopathic drugs in the treatment of inflammatory diseases (Bellik et al., 2013). Polyphenols are secondary reactive metabolites, and they are abundant in plant-derived food, particularly fruits, seed and leaves. Polyphenols represent a wide variety of active compounds that are divided into several major categories based on the number of phenol rings and their structural elements (Belščak-Cvitanović et al., 2018). They are sub-categorized into phenolic acids (hydrobenzoic and hydroxycinnamic acid), flavonoids (flavones, flavonols, flavanols, isoflavones, flavanones, anthocyanins), stilbenes (resveratrol, piceatannol), lignans (sesamol, pinoresinol, sinol, enterodiol), and others including tannins (hydrolysable, non-hydrolysable, and condensed tannins), lignins, xanthones, chromones, anthraquinones (Singla et al., 2019).

Preservation and maintenance of periodontal health is an important component of oral and overall health (Baehni et al., 2010). A substantial number of studies have been done to ascertain the use of polyphenol as an adjunct to managing inflammatory conditions and hence support its role in the prevention and treatment of periodontal disease. Basically, these natural compounds regulate the inflammatory signalling by modifying the expression of several pro-inflammatory genes in addition to their antioxidative potential (Yahfoufi et al., 2018). *In vitro* and *in vivo* studies have demonstrated that the immune modulatory effect of polyphenols is particularly contributed by its potential in modulating immune cells populations, cytokines production and pro-inflammatory genes expression.

Apart from that, a number of studies supported the antimicrobial effect of polyphenols against a variety of pathogens including periodontal pathogens in complex biofilms. Ideally, prevention and treatment of periodontal diseases should also consist of strategies to eliminate or reduce these biofilms. Dietary polyphenols have been reported to have bacteriostatic/bactericidal activity against microbial species such as *P. gingivalis* (Basu et al., 2018). Since periodontal illnesses are inflammatory diseases of bacterial origin, anti-inflammatory and anti-microbial properties of polyphenols may anticipate various biological mechanisms for reducing the initiation and progression of periodontitis. In this review, we presented several polyphenolic compounds that have been reported to have remarkable anti-inflammatory properties particularly in an experimental model of periodontitis. Antibacterial properties of the selected polyphenolic compounds were also described in the current review.

Quercetin

Quercetin is categorized as a flavonol, one of the six subclasses of flavonoids compounds (Li et al., 2016). The antimicrobial and anti-inflammatory properties of quercetin have been found to be effective to restrict inflammatory reaction in periodontitis. During acute and chronic inflammation in periodontitis, high amount of TNF-α generated by activated macrophages may lead to periodontal tissues degeneration (Noh et al., 2013). A study by Xiong et al. (2019) has demonstrated that all three doses of quercetin (5, 10 and 20 μM) attenuated the production of inflammatory mediators including TNF-α, IL-1β, IL-6, and IL-8 in *Porphyromonas gingivalis* (*P. gingivalis*) LPS-treated human gingival fibroblast. In addition, quercetin has been found to suppress LPS-induced nuclear factor kappa-B (NF-κB) activation in a dose-dependent manner (Xiong et al., 2019). Suppression of these inflammatory mediators and its signalling pathway could restrict the initiation and progression of periodontal disease (Muniz et al., 2015).

In an earlier study, Cheng et al. (2010) investigated the effect of quercetin on experimental periodontitis induced by LPS injection and silk ligation (Cheng et al., 2010). The study has reported that 5 days of oral quercetin treatment at the dose of 75 mg/kg reduced LPS-induced osteoclast formation, ligature-enhanced periodontal inflammation and subsequent alveolar bone loss. Inflammation was induced in the quercetin-administered group but not severe enough to cause alveolar bone loss as evidenced from bone micro-computerized tomography (μ–CT) evaluation. Quercetin decreased the area of inflammatory cell infiltration in connective tissue and narrowed connective tissue attachment. However, the findings also reported a similar attachment loss in both ligation and the ligation-plus-quercetin groups. The results indicated that alveolar bone loss may be prevented in the experimental periodontitis but quercetin was unable to prevent attachment loss, which questioned the beneficial effects of quercetin. The author postulated that the study duration might not be sufficient to observe the effect of quercetin on long-term attachment loss in chronic periodontitis.

In another study, the anti-inflammatory properties of 100 mg/kg quercetin were evaluated using a mouse periodontitis model induced by inoculation of *A. actinomycetemcomitans* (Napimoga et al., 2013). Subcutaneous treatment with quercetin has been found to reduce gingival pro-inflammatory cytokines (IL-1, TNF-α, IL-17), and down-regulate adhesion molecule ICAM-1 and osteoclastogenic cytokine RANKL production in *A. actinomycetemcomitans*-induced alveolar bone loss. Alteration in cell-mediated and humoral levels of adaptive immune defence is thought to be involved in the development of experimental bacterial-immune inflammation in periodontal tissue. The potential of quercetin in reducing bone loss was also demonstrated in a study by Taskan and Gevrek (2020). Osteoblastic activity was increased while osteoclastic activity, apoptosis and inflammation were decreased in ligature-induced periodontitis rats treated with quercetin. A study by Demkovych et al. (2021) was carried out to investigate the effects of quercetin on adaptive immunity in relation to the development of experimental bacterial-immune periodontitis. Intramuscular injection of water-soluble quercetin at a dose of 100 mg/kg for 7 days was found to normalize the cellular adaptive immunity indices and reverse the inflammatory process in the periodontal complex.

It was suggested that the inhibition of periodontal pathogen virulent factor could hamper the progression of periodontitis, prevent and control periodontal inflammation. The effect of quercetin on *P. gingivalis* virulent pathogenicity was demonstrated in a study by He et al. (2020). The study found that quercetin inhibits virulence and physiological properties of *P. gingivalis* as indicated by gingipain, hemolytic and hemagglutination activity. Quercetin also could modulate cell surface hydrophobicity, aggregation, biofilm formation and virulence gene expression. These findings suggested that quercetin might be beneficial in the treatment of periodontitis as it could impair the pathogenicity of *P. gingivalis,* a keystone pathogen for periodontal disease. **Table 1** summarized the effects of quercetin in periodontal inflammation, *in vivo* and *in vitro*.

Resveratrol

Resveratrol (trans-3,4,5-trihydroxystilbene) is a common stilbene found in berries, grape skin and in other plants (Gambini et al., 2015). Resveratrol has attracted substantial attention, as it possesses remarkable biological properties and this could be due to its molecular structure that confers its ability to bind to many biomolecules. Based on its promising anti-inflammatory and antioxidant properties, resveratrol has been studied for its

TABLE 1 | The effects of quercetin in periodontal inflammation, *in vivo* and *in vitro*.

Researcher (year)	Type of study	Experimental method/type of induction	Dose/Delivery of polyphenol treatment	Study outcomes
Xiong et al. (2019)	*In vitro*	*P. gingivalis*-LPS-stimulated human gingival fibroblasts (HGFs)	5, 10 and 20 μM prior to LPS stimulation	• No cytotoxic effects on cell viability of HGF • Suppress IL-1β, IL-6, IL-8, and TNF-α • Suppress mRNA levels of IL-1β, IL-6, IL-8, TNF-α, p65, IκBα, TLR4 upregulation and PPAR-γ downregulation • Inhibit upregulation of TLR4 expression and the phosphorylation of p65 and IκBα • Up-regulate PPAR-γ expression
Cheng et al. (2010)	*In vivo*	Experimental periodontitis - daily LPS injection	Oral, 75 mg/kg, 5 days	• Reduced number of osteoclast • Apically located bone crests rebounded, more coronal alveolar crest bone levels, less inflammatory cell-infiltrated connective tissue areas and less connective tissue attachments
Napimoga et al. (2013)	*In vivo*	Experimental periodontitis - Oral inoculation of *A. actinomycetemcomitans*	Subcutaneous, 100 mg/kg, 15 days	• No effect on *A. actinomycetemcomitans* Colony-Forming Units (CFU) • Inhibit *A. actinomycetemcomitans*-induced bone loss • Inhibit IL-1β, TNF-α, and IL-17 production, ICAM-1 and RANKL expression
Taskan and Gevrek (2020)	*In vivo*	Experimental periodontitis - Silk ligation	75 and 150 mg/kg, 15 days	• Reduce alveolar bone loss • Decrease TRAP + osteoclast cells, increased osteoblast cells • Decrease iNOS, MMP-8, and caspase-3 levels • Increase TIMP-1 expression
Demkovych et al. (2021)	*In vivo*	Inoculation of microorganisms mixture diluted with egg protein with complete adjuvant of Freund	Intramuscular, 100 mg/kg, 7 days	• Increase in the blood of the T-helper cell content ($CD4^+$), common mature T-lymphocytes ($CD3^+$) $CD19^+$ and $CD16^+$ • Reduced level of $CD8^+$ and NK-cells content
He et al. (2020)	*In vitro*	*P. gingivalis* culture	50 and 100 μM	• Inhibit gingipains, hemolytic, hemagglutination activities and biofilm formation at sub-MIC concentrations • Sparce and thinner biofilm formation • Modulate cell surface hydrophobicity and bacterial aggregation • Down-regulate the expression of virulence genes

prophylaxis and therapeutic potential in controlling periodontal disease. Resveratrol was shown to have a favourable effect on vascular inflammation induced by periodontal pathogen, *P. gingivalis* as it was able to inhibit NF-κB-dependent cell adhesion molecules in monocyte adhesion to the endothelium (Park et al., 2009). Casati et al. (2013) studied the effect of resveratrol that was administered continually on the progression of experimental periodontitis. Findings of the study showed that bone-loss value in ligated molars and unligated teeth in the control group were higher than in the treatment group that was administered with 10 mg/kg resveratrol for 30 days (19 days before periodontitis induction and 11 days after ligature placement). Resveratrol treated group also showed lower concentration of IL-17 in the gingival tissue. Modulation of IL-17 levels in gingival tissue that presents ligature-induced experimental periodontitis suggests the possible biologic mechanism of resveratrol during periodontal inflammation.

It is known that periodontitis is a multicomponent disorder that affects the supporting structures of the teeth including periodontal ligament and the alveolar bone. Bone loss values were found insignificant between resveratrol, curcumin and the combined groups in a study of continuous curcumin and resveratrol administration against the progression of experimental periodontitis. When compared with the placebo group, the concentration of IL-1 was lower in the combined group as revealed by immune-enzymatic assays. However, resveratrol, curcumin and combined groups showed higher IL-4 levels when compared to placebo group. The reduction in IFN-γ level was only observed in the resveratrol group and the difference in TNF-α levels among groups were not significant. Whether agents were added singly or in combination, both poplyphenolic compounds were able to attenuate alveolar bone loss in the experimental model of periodontitis. Nonetheless, the effects were neither synergistic nor additive (Corrêa et al., 2017). In another study, resveratrol derivative-rich melinjo seed extract was found to have a potent impact on inflammation-induced bone loss in a murine model of established periodontitis as indicated by a reduction in osteoclast differentiation (Ikeda et al., 2018) The production of IL-1β in gingival tissue was reduced but no significant changes in IL-6, TNF-α, and IL-17 levels were observed.

The antibacterial effects of resveratrol against periodontal pathogens *P. gingivalis*, *T. forsythia* and *A. actinomycetemcomitans* were studied by Cirano et al. (2016) in experimental model of periodontitis. The study however found that resveratrol does not exert positive effects on microbiological

TABLE 2 | The effects of resveratrol in periodontal inflammation, *in vivo* and *in vitro*.

Researcher (year)	Type of study	Experimental method/type of induction	Dose/Delivery of polyphenol treatment	Study outcomes
Park et al. (2009)	*In vitro*	HMECs incubated with *P. gingivalis* LPS	1 μM or 10 μM	• Inhibit the leukocytes adhesion to endothelial cells and to the aortic endothelium by down-regulation of ICAM-1 and VCAM-1 • Suppress IκBα phosphorylation and nuclear translocation of the p65 subunit of NF-κB in HMECs • Suppress NF-κB expression
Casati et al. (2013)	*In vivo*	Experimental periodontitis—Cotton ligation	Gavage, 10 mg/kg, 30 days	• Lower alveolar bone loss in both ligated and unligated groups • Lower concentration of IL-17, no changes in in the IL-1b and IL-4 levels
Ikeda et al. (2018)	*In vivo*	Experimental periodontitis—Silk ligation	Intraperitoneal, 0.004% (w/w)	• Lower alveolar bone loss • Lower levels of IL-1β, no changes in f IL-6, TNF-α and IL17 levels • Inhibit M-CSF/RANKL mediated osteoclast formation and down-regulate osteoclast activity
Cirano et al. (2016)	*In vivo*	Experimental periodontitis—Cotton ligation	Gavage, 10 mg/kg, 30 days	• No difference in the concentration of periodontal pathogens *A. actinomycetemcomitans, P. gingivalis* and *T. forsythia* • No difference in the percentage of sites that were positive for periodontal bacteria after therapy
Kugaji et al. (2019)	*In vitro*	*P. gingivalis* culture	MIC and MBC concentration	• Prevent biofilm formation and reduce the expression of virulence factor genes fimbriae (type II and IV) and proteinases (kgp and rgpA)

outcomes suggesting other mechanisms could contribute to its promising effect in controlling periodontitis. Nevertheless, in a recent study, resveratrol has been found to prevent biofilm formation and inhibit the virulence properties of *P. gingivalis* by reducing the expression of virulence factor genes including fimbriae and proteinases (Kugaji et al., 2019). The effect of resveratrol in *in vivo* and *in vitro* model of periodontal inflammation has been summarized in **Table 2**.

Curcumin

Curcumin, a yellow-coloured compound with low molecular weight is the main polyphenols extracted from the rhizome of turmeric plant, *Curcuma longa* L., (family: *Zingiberaceae*) (Wilken et al., 2011). This natural polyphenol has attracted considerable attention due to its nontoxicity and it has been used to treat various inflammatory diseases since long ago. Curcumin (diferuloylmethane) makes up 2–5% of turmeric and no adverse effects were found when it is given even as high as 8 g/day (Bhatia et al., 2014). Therapeutic potential of curcumin was observed in controlling inflammation and bone resorption in periodontitis. The antioxidant, antimicrobial, anti-inflammatory and analgesic properties of curcumin make them a suitable candidate for the management of periodontal diseases (Forouzanfar et al., 2020).

The possible mechanisms of curcumin involved in the suppression of periodontal disease reported in the existing studies are mainly based on its antibacterial and anti-inflammatory properties. *In vitro* studies have shown that curcumin can inhibit various periodontal pathogens growth such as *A. actinomycetemcomitans, F. nucleatum*, and *P. gingivalis* and the formation of biofilms (Shahzad et al., 2015). Curcumin has been found to have anti-biofilm and high antibacterial activity against *P. gingivalis,* which is considered as the main pathogen and major colonizer in host tissues (Shahzad et al., 2015; Izui et al., 2021; Kumbar et al., 2021). On the other hand, curcumin has low antibacterial activity against *S. mitis*, which is a part of the normal flora in the oral cavity and exert no threat to oral health. This result suggested that curcumin may have selective antimicrobial properties. In gene expression studies done by Kumbar et al. (2021), the virulence of *P. gingivalis* was reduced by curcumin as indicated by a reduce expression of genes coding for major virulence factors including adhesions and proteinases.

The occurrence and development of periodontitis involve the production of a vast number of inflammatory mediators. A recent study carried out by Xiao et al. (2018) showed that the production of IL-β and TNF-α were attenuated in rat gingival fibroblasts supplemented with 10 and 20 μM curcumin. The ratio of OPG/RANKL and the activation of NF-κB induced by LPS *in vitro* were also inhibited. In the same study, an *in vivo* ligation-induced experimental periodontitis showed that curcumin at the dose of 30 and 100 μg/g could alleviate gingival inflammation and modulated collagen fibre and alveolar bone loss as observed in histological and micro-CT results. An earlier study by Zhou et al. (2013) reported that intra-gastric curcumin administration at the dose of 100 mg/kg for 30 days could reduce alveolar bone loss in ligature-induced experimental periodontitis through the suppression of RANKL/RANK/OPG expression and its inflammatory properties (Zhou et al., 2013). Moderate bone resorption and root exposure, and mild bone loss were observed microscopically in curcumin treated animals. The expression of TNF-α and IL-6 in the gingival tissues of experimental rats treated with curcumin was significantly lower than the experimental periodontitis animal. In line with this study, several other studies also reported that curcumin can modulate the inflammatory response, suppress the pro-inflammatory cytokines particularly TNF-α and IL-6 in ligature-induced experimental periodontitis rat model (Guimarães et al., 2011) and LPS-induced periodontitis rat model (Guimaraes et al., 2012). Though curcumin is effective in inhibiting cytokine gene expression at mRNA and protein levels, the inhibition of NF-κB in the gingival tissue was only

TABLE 3 | The effects of curcumin in periodontal inflammation, *in vivo* and *in vitro*.

Researcher (year)	Type of study	Experimental method/type of induction	Dose/Delivery of polyphenol treatment	Study outcomes
Shahzad et al. (2015)	*In vitro*	Inoculum suspension of *S. mitis* in artificial saliva	Planktonic minimum inhibitory concentration	• Inhibit adhesion of *S. mitis*, and biofilm formation and maturation
Izui et al. (2021)	*In vitro*	*P. gingivalis* outer membrane vesicles (OMV) induced cytotoxicity in HGE cells	0, 5, 10, 20 μg/ml	• Suppression of IL-6, IL-1β, and TNF-α gene expressions • Inhibit the cytotoxic effects of OMVs on cellular migration, adherence to and entry of cells, and cellular apoptotic death
Kumbar et al. (2021)	*In vitro*	*P. gingivalis* culture	MIC and MBC concentration (62.5 and 125 μg ml–1)	• Prevent bacterial adhesion and biofilm formation in a dose-dependent manner • Reduce the expression of genes coding for major virulence factors (Adhesions—fmA, hagA, and hagB. Proteinases - rgpA, rgpB, and kgp)
Xiao et al. (2018)	*In vitro*	LPS-induced gingival fibroblasts	10 and 20 μM	• Decrease IL-1β and TNF-α production, OPG/sRANKL ratio and NF-κB activation
	In vivo	Experimental periodontitis—silk ligation	30 and 100 μg/g	• Reduce alveolar bone loss, gingival inflammation and collagen fiber destruction
Zhou et al. (2013)	*In vivo*	Experimental periodontitis—nylon thread ligation	Oral gavage, 100 mg/kg, 30 days	• Lower bone resorption, RANKL, RANK, OPG, TNF-a and IL-6 expression
Guimarães et al. (2011)	*In vivo*	Experimental periodontitis—cotton ligation	Oral gavage, 30 and 100 mg/kg, 15 days	• No effect on bone resorption • Inhibit NF-κB activation but not p38 MAPK • Inhibit IL-6 and TNF-a gene expression
Guimarães et al. (2012)	*In vivo*	LPS injection in the gingival tissues	Oral gavage, 30 and 100 mg/kg, 15 days	• Inhibit NF-kB (lower dose), no effect on p38 MAPK • Reduce inflammatory infiltrate, increased collagen content and fibroblastic cell numbers

observed in the lower dose of curcumin (30 mg/kg), whereas p38 MAPK activation was not affected in both doses. Alveolar bone resorption was not prevented by daily dose of intragastric curcumin administration (30 and 50 mg/kg) for 15 days but its potential anti-inflammatory effect suggests their therapeutic potential in periodontal disease. **Table 3** summarized the effects of curcumin in periodontal inflammation, *in vivo* and *in vitro*.

Proanthocyanidins

Proanthocyanidins are condensed tannins that take the form if oligomers or polymers of monomeric flavan-3-ols produced as an end product of flavonoid biosynthesis pathway (Rauf et al., 2019). The flavan-3-ols are catechin, epicatechin or their substituted derivatives. It is termed as condensed tannins for its capability to form insoluble complexes with carbohydrates and proteins (Balalaie et al., 2018). Proanthocyanidins are highly hydroxylated structures that is categorized according to the number of hydroxyl substitutions in the B ring in which one hydroxyl substitution refers to propelargonidin, two hydroxyl substitution refers to procyanidin and three hydroxyl substitution refers to prodelphinidin. The therapeutic potential of proanthocyanidins emerges from their unique chemical structure (Luca et al., 2020).

The antibacterial activity of proanthocyanidins has been substantially reported in literature (Nawrot-Hadzik et al., 2021). A study by Savickiene et al. (2018) revealed that proanthocyanidins had a unique antibacterial property that could selectively targets the keystone periodontal pathogens viability such as *P. gingivalis* while preserving the beneficial oral commensal *S. salivarius*. Lagha et al. (2018) reported the antibacterial and anti-biofilm effects of proanthocyanidins against *A. actinomycetemcomitans*. The treatment with proanthocyanidins reduced the growth of *A. actinomycetemcomitans* and resulted in a loss of bacterial viability as indicated by the damage to the bacterial cell membrane. Proanthocyanidins also possessed an anti-biofilm activity against *P. aeruginosa* as reported by Ulrey et al. (2014) and its anti-virulence potential was further investigated in a study by Maisuria et al. (2016).

Apart from its ability to inhibit biofilm formation and adhesion of periodontopathogenic bacteria, the therapeutic effect of proanthocyanidins with regards to periodontal disease include its potential to inhibit cytokine production by immune and mucosal cells and its capability to inhibit MMP production (Bonifait and Grenier 2010). Their capability to inhibit MMP and dentin cross-linker activity have been reported as an additional notable benefit of proanthocyanidins (Balalalie et al., 2018). The anti-inflammatory properties of proanthocyanidins were revealed by the attenuation of pro-inflammatory cytokines secretion (IL-1β, TNF-α, IL-6) as well as MMP-3 and MMP-9 secretion by macrophages stimulated with *A. actinomycetemcomitans* (Lagha et al., 2018). In another recent study, Jekabsone et al. (2019) demonstrated a strong antibacterial, anti-inflammatory and gingival tissue protecting properties of proanthocyanidins in periodontitis mimicking condition. Proanthocyanidins fraction has been found to have a stronger efficiency in suppressing caspases as indicated by the level of caspase-3 and caspase-8, and preventing mediator release as indicated by IL-8 and PGE_2 secretion from gingival fibroblast, and IL-6 secretion from peripheral blood mononuclear cells. In an earlier study, proanthocyanidins-enriched cranberry fraction has been

TABLE 4 | The effects of proanthocyanidins in periodontal inflammation, *in vivo* and *in vitro*.

Researcher (year)	Type of study	Experimental method/type of induction	Dose/Delivery of polyphenol treatment	Study outcomes
Savickiene et al. (2018)	*In vitro*	*P. gingivalis* and *S. salivarius* culture	0.02–0.09 g/ml	• Strong antioxidant capacity • Reduce the viability of both *P. gingivalis* and *S. salivarius*
Lagha et al. (2018)	*In vitro*	*A. actinomycetemcomitans* culture	0–500 μg/ml	• Reduce the growth of *A. actinomycetemcomitans* and prevent biofilm formation • Loss of bacterial viability in preformed biofilms • Protect the oral keratinocytes barrier integrity from damage and macrophages from the deleterious effect of leukotoxin Ltx-A • Inhibit the secretion of IL-1β, IL-6, CXCL8, TNF-α, MMP-3, MMP-9, and sTREM-1 and activation of the NF-κB signaling pathway
Ulrey et al. (2014)	*In vitro*	*P. aeruginosa culture*	0–100 μg/ml	• Reduce *aeruginosa* swarming motility and inhibit biofilm formation • Up-regulate 12 proteins related to iron siderophores or cation transporters and proteins involved in amino acid synthesis • Down-regulate 2 proteins related to ATP synthesis and several proteins involved in DNA and RNA synthesis
Maisuria et al. (2016)	*In vivo*	*Drosophila melanogaster infected with P. aeruginosa*	200 μg/ml	• Reduce the production of N-acylhomoserine lactone (AHL)-mediated quorum sensing (QS)-regulated virulence determinants by reducing the level of AHLs produced by the bacteria • Inhibit the expression of AHL synthases LasI/RhlI and QS transcriptional regulators LasR/RhlR genes
Jekabsone et al. (2019)	*In vitro*	Rat Gingival Fibroblast Cell Culture	100 μg/ml	• Supress Staphylococcus and *Aggregatibacter* compared to *Escherichia* and prevent *A. actinomycetemcomitans* and LPS-induced death of fibroblasts • Decrease LPS-induced release of IL-8 and PGE2 from fibroblasts and IL-6 from leukocytes • Block IL-1β, iNOS, and surface presentation of CD80 and CD86 expression in LPS + IFNγ-treated macrophages, and IL-1β and COX-2 expression in LPS-treated leukocytes
Bodet et al. (2007)	*In vitro*	LPS-stimulated gingival fibroblasts	0, 10, 25 or 50 μg/ml in non-dialysable material	• Inhibit IL-6, IL-8, and PGE2 responses of gingival fibroblasts • Inhibit fibroblast intracellular signaling proteins, reduce cyclooxygenase 2 expression

shown to inhibit the production of MMP-3 and MMP-9 in LPS-induced gingival fibroblasts (Bodet et al., 2007). Gingival fibroblasts, the most abundant cells found in periodontal tissues are actively involved in the host inflammatory response to oral pathogens and is known to mediate local tissue destruction in periodontal disease. The productions of IL-6, IL-8 and PGE_2 by gingival fibroblast stimulated by LPS were inhibited with the treatment of proanthocyanidins-enriched cranberry fraction (Bodet et al., 2007). The effects of proanthocyanidins in *in vivo* and *in vitro* model of periodontal inflammation has been summarized in **Table 4**.

NANOPARTICLES AS POTENTIAL DELIVERY SYSTEM OF POLYPHENOL

Despite promising biological activities of natural polyphenol, several limitations have been addressed in relation to their bioavailability. The absorption of polyphenolic compounds is negatively affected by its molecular size and their pharmacokinetics is modified by pre-systemic metabolism and gastric environment, which is highly acidic (Neves et al., 2012). Polyphenols were metabolized extensively during their transport across the small intestine and liver causing remarkable alteration of the redox potential. Consequently, the small proportion of polyphenolic compounds that are available following oral administration limits the activity and beneficial health effects of polyphenols. For instance, only a trace amount of curcumin available in blood plasma even after high dose intake, and after rapid metabolization of orally administered curcumin, they form several reduced products in the intestine and is most excreted in the urine and faeces (Niu et al., 2012). Low solubility and stability, short biological half-life and rapid elimination of polyphenolic compounds hinder their clinical application and thus lead the way towards the establishment of systems that could deliver these substances effectively.

The potency of many species of medicinal plants is determined by the availability of the active compounds. Recent research has proposed to combine herbal medicine with nanotechnology because nanoencapsulated particles are expected to potentiate the action of the plant extracts, reduce the required dose and undesirable effects as well as improving its activity (Bonifácio et al., 2014). Nanomedicine is an on-going research area that applies nanotechnology to medical

intervention for prevention, diagnosis and treatment of diseases (Chang et al., 2015). Nanotechnology involved the production, processing, and application of particles with diameter ranging from 1 to 1,000 nm (Etheridge et al., 2013). Encapsulation is a process that incorporates an active compound or substances within a carrier material or another substance (Nedovic et al., 2011). The goal of encapsulation is to reduce the damage of sensitive and labile bioactive agents and to protect them from unwanted circumstances (Jafari 2017). Nanoencapsulation is then can be defined as a process of encapsulating a substance within another material at sizes on the nano-scale.

The incorporation with nanoparticles would basically protect the substances against chemical and enzymatic degradation (Muhamad et al., 2014). Nanoparticles have been used in advanced drug delivery systems as the size and surface characteristics of nanoparticles can be manipulated easily which prompt the use for passive and active drug targeting. In addition, nanoscale drug delivery systems could also enhance the solubility of hydrophobic compounds in aqueous medium. Since the biodistribution and clearance of substances from the body can be altered, the therapeutic efficacy can be increased and reduction in side effects can be achieved by the use of nanoparticles as carrier (Liang et al., 2017). Collectively, the nanoencapsulation process aims to enhance the properties of active compounds and to transport them to the target destinations more effectively (Esfanjani and Jafari 2016). Basically, the drug is made active in the targeted area at pre-determined release rate over a period of time (Harini & Kaarthikeyan 2014).

The process of encapsulating one compound to another involves several methods according to their chemical, physical and physiochemical properties (Conte et al., 2016). Chemical nanoencapsulation refers to polymerization of monomers through the addition of a cross-linker in the external phase while physical nanoencapsulation involves the interaction of the vector material with the encapsulated molecules when both are aerosolized or atomized (Wais et al., 2016). Physiochemical processes involve the formation of stable nanometre size drug nano-suspensions or nanoparticles through the reduction of particle size (Merisko-Liversidge & Liversidge 2011). Nanocarriers for phenolic compounds can be roughly divided into polysaccharide- and protein-based delivery systems (Milinčić et al., 2019). Substances such as cyclodectrins, polymeric nanoparticles, nanomicelles, food-protein nanoparticles, zein nanoparticles, gelatin nanoparticles and films, chitosan, lipid nanocarriers, or protein-polysaccharide complex nanoparticles are suitable to be used as carriers for nanoencapsulation of polyphenolic compounds. The interactions between polyphenol and nanocarrier can improve its bioavailability, prevent extensive degradation in the GIT, enhance its delivery to the targeted sites, or even provide stability during the storage or processing. Hence, the application of polyphenol-loaded nanoparticles is an interesting means to improve their overall activity.

NANOPARTICLES MEDIATED DELIVERY IN MANAGING PERIODONTAL INFLAMMATION

Nanoencapsulation of polyphenolic compounds could overcome the drawbacks related to its instability, limited bioavailability and short half-life *in vivo* and *in vitro* (Fang and Bhandari 2010). The most frequently encapsulated polyphenols reported are quercetin, catechins, epigallocatechin, epigallocatechin-gallate (ECGC), curcumin, eugenol and tea polyphenols (Milinčić et al., (2019). The incorporation of these polyphenols with nanoparticles could be one of the promising approaches to enhance their efficacy as therapeutic agents for managing periodontal diseases.

Rutin is a glycoside that comprise of flavonolic aglycone quercetin along disaccharide rutinose (Ganeshpurkar and Saluja 2017). Rutin or rutin glycoside of quercetin has been reported to have a number of pharmacological activities including anti-inflammatory and antioxidant properties (Wang et al., 2019). The mechanism in which it inhibits oxidative stress and inflammatory reactions in animal models is through the regulation of MAPK pathway (Ganeshpurkar and Saluja 2017). Xu et al. (2020) evaluated the therapeutic effect of local rutin application on gingiva of periodontitis rats. In the study, rutin was incorporated with poly-lactic-co-glycolic acid (PLGA) nanoparticles by chemical precipitation method to improve its bioavailability and to make it more targeted. PLGA is among the widely used biodegradable organic polymer as it has a good biocompatibility, non-toxic and has passed FDA certification. Findings of the study showed that local application of rutin-loaded PLGA nanospheres inhibit the inflammatory reaction in LPS-induced periodontitis that may be due to downstream target effect of rutin combined with prostaglandin endoperoxide synthase 2 and downregulation of NFκBIα.

In a recent study by Wang et al. (2019), the incorporation of quercetin onto nano-octahedral ceria by chemical bonding has been found to be efficient in reprogramming pro-inflammatory macrophages to the anti-inflammatory phenotype that eventually could alleviate inflammation. Post subgingival injection of quercetin-loaded nanoceria was also found efficient to decrease local periodontal inflammation in a rat model of periodontitis induced by *P. gingivalis* injection. This study discovered that quercetin and cerium oxide (CeO_2) nanoparticles (nanoceria) have synergistic and intense regulation on host immunity against periodontal disease. It is well documented that macrophage serves as the first line of host immune defense against periodontal pathogen infection as it is involved during the onset and resolution of inflammation (Yu et al., 2016). This nanocomposite was able to modulate the phenotypic switch of macrophages by inhibition of M1 (pro-inflammatory) polarization and also promotion of M2 (anti-inflammatory) polarization. Previously, quercetin has been proven to be able to modulate macrophage that eventually gives rise to efficient anti-inflammatory activity (Li et al., 2016; Hu et al., 2019). In the recent study, CeO_2 nanoparticles were shown to inhibit the polarization of M1

TABLE 5 | *In vivo* and *in vitro* effects of nanopolyphenols/nanoencapsulated polyphenols.

Researcher (year)	Type of study	Type of polyphenols	Experimental method/ type of induction	Dose/Delivery of polyphenol treatment	Study outcomes
Xu et al. (2020)	*In vivo*, Sprague-dawley rats	Rutin-loaded PLGA nanospheres	Experimental periodontitis—LPS injection on the gingiva	100 µL of 200 mg/ml Rutin added in 1 ml PLGA nanoparticles	• Decrease inflammatory response, expression of PTGS2 and NFBIα
Wang et al. (2019)	*In vitro*	Quercetin-Loaded Ceria Nanocomposite	*P. gingivalis* LPS stimulated RAW 264.7	50 µg/ml	• Decrease M1-related biomarkers (TNF-α, IL-6, and IL-1β) • Decrease in p65-positive cell counts and TNF-α-positive cell counts, ratio of IL-1β positive cells • Up-regulate all M2 biomarkers and inhibit inflammatory-related CD86 expression
	In vivo, Wistar rats	Quercetin-Loaded Ceria Nanocomposite	Experimental periodontitis—*P. gingivalis* injection	Local (subgingival injection), 50 µg/ml, 4 days	• Low relative fluorescence intensity at inflammatory sites • Lower number of inflammatory cells. Reduce collagen fibers degradation (high fraction of collagen volume) • Lower IL-1β positive cells but high amount of Arg-1 positive cells
Giménez-Siurana et al. (2020)	*In vivo*, Sprague-dawley rats	Silk fibroin nanoparticles loaded with resveratrol	Experimental periodontitis—silk ligation in diabetic rats	Oral gavage, 3 mg/ml, 4 weeks	• Reduce chemical inflammation mediator (IL-6 and TGF-β1) • Lower inflammation area, collagen compaction and vessel formation (angiogenesis), smaller thickness of the epithelium of the gum
Zambrono et al. (2018)	*In vivo*, Holtzman rats	Curcumin nanoparticles	Experimental periodontitis—LPS injection on the gingiva	Local (gingival tissue injection), 3 µL, 2x per week	• Inhibit inflammatory bone resorption • Decrease osteoclast counts and inflammatory infiltrate • Attenuate p38 MAPK and NF-kB activation
Tian et al. (2021)	*In vitro*	EGCG green tea derivative nanoparticles	Raw264.7 cells	20 and 40 µg/ml	• Down-regulate the expression of iNOS, IL-1β, IL-6 and TNF-α. Inhibition in mRNA expression of IL-6, TNF-α and iNOS markers than free EGCG group • Increase proportion of cells expressed CD206 (M2 phenotype specific markers) and reduce proportion of cells expressed CD80 (M1 phenotype specific marker)
	In vivo	EGCG green tea derivative nanoparticles	Experimental periodontitis—wire ligature	Local (subgingival injection), 50, 200 and 500 µg/ml, every 2 days for 3 weeks	• Reduce the cementoenamel junctions -alveolar bone crest (CEJ-ABC) distance and alveolar bone loss at both day 7 and 21, inhibit progression of bone resorption and alveolar bone loss • Reduce the expression of the IL-1β, IL-6 and TNF-α on day 7 and 21 • Lower total number of inflammatory cells and TRAP-positive osteoclast number. Lower number of osteoclast than in free EGCG group

macrophage by suppressing the inflammatory cytokines expression and arresting NF-κB signal pathway (Selvaraj et al., 2015). It has been reported that quercetin could also drive M2 phenotype macrophage polarization (Tan et al., 2020) and this is crucial as M2 macrophage activation could down-regulate gingival inflammation, prevent alveolar bone loss and more interestingly promote periodontal tissue regeneration. Incorporation of quercetin with cerium oxide nanoparticle may exhibit great potential in treating periodontitis.

Though resveratrol is well tolerated by humans, it is rapidly metabolized, leading to a short half-life and insubstantial effectiveness (Cottart et al., 2010). Researchers have mainly focused on increasing the absorption of resveratrol by increasing the residence time and lengthening its activity by incorporating it in biopolymers and lipids (Augustin et al., 2013; Sessa et al., 2014). A study by Giménez-Siurana et al. (2020) evaluated the therapeutic potential of silk fibroin nanoparticles loaded with resveratrol in diabetic-induced

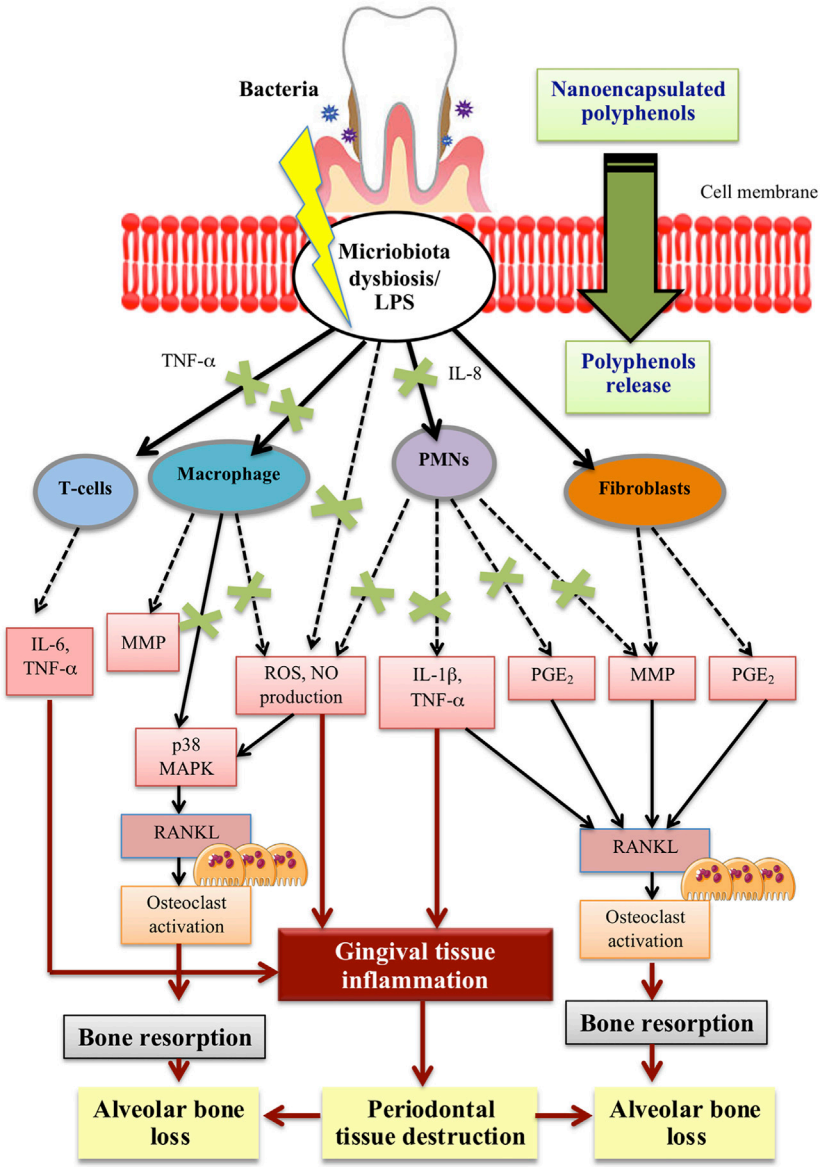

FIGURE 1 | Diagrammatic representation of the nanoencapsulated polyphenols effect on the main cellular pathways involve in periodontal inflammation.

periodontitis. The link between periodontitis and other systemic diseases such as diabetes has been widely reported. Proinflammatory factors specifically IL-6, IL-1β and TGF-1β are implicated in both diseases. In the recent study, the levels of IL-1β and IL-6 were significantly decreased with the administration of resveratrol-loaded silk fibroin nanoparticles in the experimental animal. The reduction of these two significant proinflammatory cytokines indicates the recovery from periodontitis (Corrêa et al., 2017). This effect is contributed not solely by silk fibroin nanoparticles but also due to the anti-inflammatory activity exhibited by polyphenol resveratrol that has undergone an encapsulation process (Giménez-Siurana et al., 2020).

The therapeutic potential of curcumin on pathologic bone resorption *in vivo* may be dependent on the dose, route of administration and the type of experimental model used (De Almeida Brandão et al., 2019). The heterogeneity of findings associated with the use of natural curcumin may also be contributed by other variables such as the source, type of vehicle and the pharmacokinetic-related issues including their short half-life and low absorption rate in the GIT. Different encapsulation techniques such as curcumin-based nanoparticles formula and curcumin structure modification are among the latest approaches that can be applied to increase the bioavailability of curcumin *in vivo* but studies are still scarce.

The use of alternative vehicles such as lipid-, chitosan- or hydrolysed corn protein associated nanoparticles formulation can be used to improve the pharmacodynamics and biological properties of curcumin (Shome et al., 2016; Wang et al., 2016). A study by Zambrono et al. (2018) reported the effect of curcumin-loaded nanoparticle in LPS-induced model of experimental periodontal disease but instead of using systemic route, this study investigates the local administration of polylactic acid and co-glycolic acid nanoencapsulated curcumin. These locally administered nanoparticles showed 15 times increase of curcumin half-life in the plasma of rats (Khalil et al., 2013). Apart from that, the application of nanoparticles also enables chemical modification that could specify its absorption in the given tissue or cell type and modify their absorption process to avoid macropinocytosis and liposome degradation or allow the tracking of its sub-cellular localization by the covalent binding with fluorescent molecules (Paka and Ramassamy 2017). Local application of nanocurcumin by direct injection into the gingival tissues twice a week in the LPS-induced model was shown to inhibit inflammatory bone resorption indicated by micro-CT analysis (Zambrano et al., 2018). This finding is explained by the reduction of osteoclast numbers, neutrophils (PMNs) and mononuclear cells numbers as indicated by histomorphometric analysis. The reduction of inflammatory cells infiltration suggests the anti-inflammatory effect of local nanocurcumin administration and this result is further supported by the attenuation of both signalling pathways in the gingival tissues, the p38 MAPK and NF-κB. In the earlier studies, systemic administration of curcumin in lipid vehicles was found to inhibit NF-κB activation but not p38 MAPK in LPS-induced experimental periodontitis (Guimarães et al., 2011; Guimaraes et al., 2012).

Tea is very rich in polyphenolic compounds mainly flavonoids including epicatechin (EC), epigallocatechin, epicatechin-3-gallate (ECG) and apigallocatechin-3-gallate (EGCG) (Kanwar et al., 2012). In dentistry, the use of catechin for the treatment of dental caries, periodontal and pulp diseases have been documented (Azmi et al., 2020). However, like other polyphenolic compounds, issues on its poor stability and low operational bioactivities lead to the unsatisfactory effect of tea polyphenol. Since previous methods of encapsulating tea polyphenol require tedious procedure, Tian et al. (2021) have developed a one-step polyphenolic condensation reaction that functionalized EGCG, the green tea derivative nanoparticles. The potent antioxidant capacity of EGCG-based nanoparticles was found to improve the chemical stability of epigallocatechin gallate. In addition, EGCG-based nanoparticles also provide more effective ROS scavenging activity and the expression of pro-inflammatory cytokines is down-regulated by reprogramming macrophages from pro-inflammatory M1 to anti-inflammatory M2 phenotype (Tian et al., 2021). *In vivo* findings showed that subgingival injection of EGCG nanoparticles could inhibit the alveolar bone loss and reduce osteoclastic activity in ligature-induced chronic periodontitis model in rats. EGCG nanoparticles have been found to remove ~50% ROS *in vivo* more efficiently and safely. Down-regulation of the inflammatory cytokines and stimulation of macrophages differentiation to anti-inflammatory phenotype eventually prevent alveolar bone loss. In light of these findings, the development of ECGC-based nanomaterial provides better biocompatibility and anticipates an effective antioxidant defence mechanism for the treatment of chronic periodontitis. **Table 5** summarizes recent studies on the effects of nanopolyphenols/ nanoencapsulated polyphenols in the application of periodontal inflammation. **Figure 1** illustrate the potential effect of polyphenol nanoencapsulation on the main cellular pathways involved in periodontal inflammation.

CONCLUSION

In the recent decades, phytochemicals, particularly polyphenols have been reported to have a remarkable therapeutic effect in preventing and/or treating inflammatory diseases. From the preclinical studies, polyphenol showed potential to modulate host immune and inflammatory profile in periodontal disease. However, poor water solubility, stability and bioavailability render the biological effects of polyphenol and limit their future clinical application. These drawbacks can be tackled by the application of nanosize delivery systems, which could increase the solubility and stability of phytochemicals and eventually improve their absorption. In addition, this delivery system could protect the substances from untimely enzymatic degradation or metabolism in the body and hence lengthen their circulation time. This review on the application of polyphenol-loaded nanoparticles may be useful for the enhancement of phytochemical efficacy as therapeutic agents in managing periodontal disease. A number of recent studies have investigated the pharmaceutical significance and therapeutic applicability of nanoparticles advance delivery system in improving and enhancing *in vitro* and *in vivo* performance of polyphenolic compounds, but much has yet to be explored. Comparative studies on advance delivery systems for the delivery of polyphenolic compounds and studies on safety/ toxicity profile of polyphenol-loaded nanoparticles are warranted to bring the anti-inflammatory phytochemicals closer to the clinical applications.

AUTHOR CONTRIBUTIONS

PJ and SB contributed toward conceptualization, planning and writing the paper. NN, NM, and NI contributed toward conceptualization and editing of the manuscript.

ACKNOWLEDGMENTS

We thank Ministry of Higher Education Malaysia for providing the Fundamental Research Grant Scheme (FRGS) for this study (FRGS/1/2019/STG03/UKM/01/3).

REFERENCES

A, D. S., Calarco, A., Napoletano, A., Valentino, A., Margarucci, S., Di Cristo, F., et al. (2016). Polyphenols Nanoencapsulation for Therapeutic Applications. *J. Biomol. Res. Ther.* 5, 2. doi:10.4172/2167-7956.1000139

Abdul Rahim, R., Jayusman, P. A., Muhammad, N., Ahmad, F., Mokhtar, N., Naina Mohamed, I., et al. (2019). Recent Advances in Nanoencapsulation Systems Using PLGA of Bioactive Phenolics for Protection against Chronic Diseases. *Int. J. Environ. Res. Public Health* 16 (24), 4962. doi:10.3390/ijerph16244962

Ahad, A., Lamba, A. K., Faraz, F., Tandon, S., Chawla, K., and Yadav, N. (2016). Effect of Antimicrobial Photodynamic Therapy as an Adjunct to Nonsurgical Treatment of Deep Periodontal Pockets: A Clinical Study. *J. Lasers Med. Sci.* 7 (4), 220–226. doi:10.15171/jlms.2016.39

Aral, K., Berdeli, E., Cooper, P. R., Milward, M. R., Kapila, Y., Karadede Ünal, B., et al. (2020). Differential Expression of Inflammasome Regulatory Transcripts in Periodontal Disease. *J. Periodontol.* 91 (5), 606–616. doi:10.1002/JPER.19-0222

Augustin, M. A., Sanguansri, L., and Lockett, T. (2013). Nano- and Micro-encapsulated Systems for Enhancing the Delivery of Resveratrol. *Ann. N. Y. Acad. Sci.* 1290 (1), 107–112. doi:10.1111/nyas.12130

Baehni, P., Tonetti, M. S., and Periodontology, G. O. T. E. W. O. (2010). Conclusions and Consensus Statements on Periodontal Health, Policy and Education in Europe: a Call for Action-Cconsensus View 1. Consensus Report of the 1st European Workshop on Periodontal Education. *Eur. J. Dent. Educ.* 14, 2–3. doi:10.1111/j.1600-0579.2010.00619.x

Balalaie, A., Rezvani, M. B., and Mohammadi Basir, M. (2018). Dual Function of Proanthocyanidins as Both MMP Inhibitor and Crosslinker in Dentin Biomodification: A Literature Review. *Dent. Mat. J.* 37 (2), 173–182. doi:10.4012/dmj.2017-062

Balta, M. G., Papathanasiou, E., Blix, I. J., and Van Dyke, T. E. (2021). Host Modulation and Treatment of Periodontal Disease. *J. Dent. Res.* 100 (8), 798–809. doi:10.1177/0022034521995157

Bartold, P. M., and Van Dyke, T. E. (2013). Periodontitis: a Host-Mediated Disruption of Microbial Homeostasis. Unlearning Learned Concepts. *Periodontol. 2000* 62 (1), 203–217. doi:10.1111/j.1600-0757.2012.00450.x

Basu, A., Masek, E., and Ebersole, J. L. (2018). Dietary Polyphenols and Periodontitis-A Mini-Review of Literature. *Molecules* 23 (7), 1786. doi:10.3390/molecules23071786

Belibasakis, G. N., and Guggenheim, B. (2011). Induction of Prostaglandin E(2) and Interleukin-6 in Gingival Fibroblasts by Oral Biofilms. *FEMS Immunol. Med. Microbiol.* 63 (3), 381–386. doi:10.1111/j.1574-695X.2011.00863.x

Bellik, Y., Boukraâ, L., Alzahrani, H. A., Bakhotmah, B. A., Abdellah, F., Hammoudi, S. M., et al. (2013). Molecular Mechanism Underlying Anti-inflammatory and Anti-allergic Activities of Phytochemicals: an Update. *Molecules* 18 (1), 322–353. doi:10.3390/molecules18010322

Belščak-Cvitanović, A., Durgo, K., Huđek, A., Bačun-Družina, V., and Komes, D. (2018). Overview of Polyphenols and Their Properties. *In Polyphenols Properties, Recovery, and Applications*. Elsevier, 3–44.

Ben Lagha, A., Lebel, G., and Grenier, D. (2018). Dual Action of Highbush Blueberry Proanthocyanidins on Aggregatibacter Actinomycetemcomitans and the Host Inflammatory Response. *BMC Complement. Altern. Med.* 18 (1), 10–14. doi:10.1186/s12906-017-2072-x

Bhatia, M., Urolagin, S. S., Pentyala, K. B., Urolagin, S. B., K B, M., and Bhoi, S. (2014). Novel Therapeutic Approach for the Treatment of Periodontitis by Curcumin. *J. Clin. Diagn. Res.* 8 (12), ZC65–9. doi:10.7860/jcdr/2014/8231.5343

Bodet, C., Chandad, F., and Grenier, D. (2007). Cranberry Components Inhibit Interleukin-6, Interleukin-8, and Prostaglandin E Production by Lipopolysaccharide-Activated Gingival Fibroblasts. *Eur. J. Oral Sci.* 115 (1), 64–70. doi:10.1111/j.1600-0722.2007.00415.x

Bonifait, L., and Grenier, D. (2010). Cranberry Polyphenols: Potential Benefits for Dental Caries and Periodontal Disease. *J. Can. Dent. Assoc.* 76, a130.

Bunte, O., Groote, J. F., Keiren, J. J. A., Laveaux, M., Neele, T., De Vink, E. P., et al. (2019). "The mCRL2 Toolset for Analysing Concurrent Systems," in 25th International Conference on Tools and Algorithms for the Construction and Analysis of Systems conference series, TACAS 2019 held as part of the 22nd European Joint Conferences on Theory and Practice of Software, (HW Den Haag, Netherlands: ETAPS), 21–39. doi:10.1007/978-3-030-17465-1_2

Casati, M. Z., Algayer, C., Cardoso da Cruz, G., Ribeiro, F. V., Casarin, R. C., Pimentel, S. P., et al. (2013). Resveratrol Decreases Periodontal Breakdown and Modulates Local Levels of Cytokines during Periodontitis in Rats. *J. Periodontol.* 84 (10), e58–64. doi:10.1902/jop.2013.120746

Cekici, A., Kantarci, A., Hasturk, H., and Van Dyke, T. E. (2014). Inflammatory and Immune Pathways in the Pathogenesis of Periodontal Disease. *Periodontol. 2000* 64 (1), 57–80. doi:10.1111/prd.12002

Chang, E. H., Harford, J. B., Eaton, M. A., Boisseau, P. M., Dube, A., Hayeshi, R., et al. (2015). Nanomedicine: Past, Present and Future - A Global Perspective. *Biochem. Biophys. Res. Commun.* 468 (3), 511–517. doi:10.1016/j.bbrc.2015.10.136

Cheng, W. C., Huang, R. Y., Chiang, C. Y., Chen, J. K., Liu, C. H., Chu, C. L., et al. (2010). Ameliorative Effect of Quercetin on the Destruction Caused by Experimental Periodontitis in Rats. *J. Periodontal Res.* 45 (6), 788–795. doi:10.1111/j.1600-0765.2010.01301.x

Chompunud Na Ayudhya, C., Roy, S., Thapaliya, M., Ali, H., and Ali, H. (2020). Roles of a Mast Cell-specific Receptor MRGPRX2 in Host Defense and Inflammation. *J. Dent. Res.* 99 (8), 882–890. doi:10.1177/0022034520919107

Cirano, F. R., Casarin, R. C., Ribeiro, F. V., Casati, M. Z., Pimentel, S. P., Taiete, T., et al. (2016). Effect of Resveratrol on Periodontal Pathogens during Experimental Periodontitis in Rats. *Braz. Oral Res.* 30 (1), e128–7. doi:10.1590/1807-3107BOR-2016.vol30.0128

Corrêa, M. G., Pires, P. R., Ribeiro, F. V., Pimentel, S. Z., Casarin, R. C., Cirano, F. R., et al. (2017). Systemic Treatment with Resveratrol And/or Curcumin Reduces the Progression of Experimental Periodontitis in Rats. *J. Periodontal Res.* 52 (2), 201–209. doi:10.1111/jre.12382

Cottart, C. H., Nivet-Antoine, V., Laguillier-Morizot, C., and Beaudeux, J. L. (2010). Resveratrol Bioavailability and Toxicity in Humans. *Mol. Nutr. Food Res.* 54 (1), 7–16. doi:10.1002/mnfr.200900437

Da Rocha, H. A., Silva, C. F., Santiago, F. L., Martins, L. G., Dias, P. C., and De Magalhães, D. (2015). Local Drug Delivery Systems in the Treatment of Periodontitis: a Literature Review. *J. Int. Acad. Periodontol.* 17 (3), 82–90.

de Almeida Brandão, D., Spolidorio, L. C., Johnson, F., Golub, L. M., Guimarães-Stabili, M. R., and Rossa, C. (2019). Dose-response Assessment of Chemically Modified Curcumin in Experimental Periodontitis. *J. Periodontol.* 90 (5), 535–545. doi:10.1002/JPER.18-0392

Demkovych, A., Bondarenko, Y., Shcherba, V., Luchynskyi, V., Vitkovskyy, V., and Machogan, V. (2021). Quercetin Effects on Adaptive Immune Response in Experimental Periodontitis of Bacterial-Immune Genesis. *Pharmacia* 68, 877. doi:10.3897/pharmacia.68.e70883

Dinarello, C. A. (2018). Overview of the IL-1 Family in Innate Inflammation and Acquired Immunity. *Immunol. Rev.* 281 (1), 8–27. doi:10.1111/imr.12621

Etheridge, M. L., Campbell, S. A., Erdman, A. G., Haynes, C. L., Wolf, S. M., and Mccullough, J. (2013). The Big Picture on Nanomedicine: the State of Investigational and Approved Nanomedicine Products. *Nanomedicine* 9 (1), 1–14. doi:10.1016/j.nano.2012.05.013

Fang, Z., and Bhandari, B. (2010). Encapsulation of Polyphenols - a Review. *Trends Food Sci. Technol.* 21 (10), 510–523. doi:10.1016/j.tifs.2010.08.003

Faridi Esfanjani, A., and Jafari, S. M. (2016). Biopolymer Nano-Particles and Natural Nano-Carriers for Nano-Encapsulation of Phenolic Compounds. *Colloids Surf. B Biointerfaces* 146, 532–543. doi:10.1016/j.colsurfb.2016.06.053

Forouzanfar, F., Forouzanfar, A., Sathyapalan, T., Orafai, H. M., and Sahebkar, A. (2020). Curcumin for the Management of Periodontal Diseases: a Review. *Curr. Pharm. Des.* 26 (34), 4277–4284. doi:10.2174/1381612826666200513112607

Gambini, J., Inglés, M., Olaso, G., Lopez-Grueso, R., Bonet-Costa, V., Gimeno-Mallench, L., et al. (2015). Properties of Resveratrol:In VitroandIn VivoStudies about Metabolism, Bioavailability, and Biological Effects in Animal Models and Humans. *Oxidative Med. Cell. Longev.* 2015, 1–13. doi:10.1155/2015/837042

Ganeshpurkar, A., and Saluja, A. K. (2017). The Pharmacological Potential of Rutin. *Saudi Pharm. J.* 25 (2), 149–164. doi:10.1016/j.jsps.2016.04.025

Ge, W., Li, D., Gao, Y., and Cao, X. (2015). The Roles of Lysosomes in Inflammation and Autoimmune Diseases. *Int. Rev. Immunol.* 34 (5), 415–431. doi:10.3109/08830185.2014.936587

Giménez-Siurana, A., Gómez García, F., Pagan Bernabeu, A., Lozano-Pérez, A. A., Aznar-Cervantes, S. D., Cenis, J. L., et al. (2020). Chemoprevention of Experimental Periodontitis in Diabetic Rats with Silk Fibroin Nanoparticles Loaded with Resveratrol. *Antioxidants* 9 (1), 85. doi:10.3390/antiox9010085

Golub, L. M., Lee, H. M., Ryan, M. E., Giannobile, W. V., Payne, J., and Sorsa, T. (1998). Tetracyclines Inhibit Connective Tissue Breakdown by Multiple Non-antimicrobial Mechanisms. *Adv. Dent. Res.* 12, 12–26. doi:10.1177/08959374980120010501

Golub, L. M., Gu, Y., Tenenbaum, H., Goldberg, M., and Sorsa, T. (2018). *A "Point by Point" Statement on Periodontal Host Modulation Therapy:SAFETY FIRST! Oral Health*, 1–8.

Guimarães, M. R., Coimbra, L. S., De Aquino, S. G., Spolidorio, L. C., Kirkwood, K. L., and Rossa, C. (2011). Potent Anti-inflammatory Effects of Systemically Administered Curcumin Modulate Periodontal Disease *In Vivo*. *J. Periodontal Res.* 46 (2), 269–279. doi:10.1111/j.1600-0765.2010.01342.x

Guimarães, M. R., De Aquino, S. G., Coimbra, L. S., Spolidorio, L. C., Kirkwood, K. L., and Rossa, C. (2012). Curcumin Modulates the Immune Response Associated with LPS-Induced Periodontal Disease in Rats. *Innate Immun.* 18 (1), 155–163. doi:10.1177/1753425910392935

Hajishengallis, G., Chavakis, T., and Lambris, J. D. (2020). Current Understanding of Periodontal Disease Pathogenesis and Targets for Host-Modulation Therapy. *Periodontol. 2000* 84 (1), 14–34. doi:10.1111/prd.12331

Hajishengallis, G. (2015). Periodontitis: from Microbial Immune Subversion to Systemic Inflammation. *Nat. Rev. Immunol.* 15 (1), 30–44. doi:10.1038/nri3785

Harini, G., Kaarthikeyan, G., and Kaarthikeyan, G. (2014). Advanced Drug Delivery Systems in Treating Periodontal Diseases-A Review. *Iosrjdms* 13 (1), 27–32. doi:10.9790/0853-13182732

Hasan, A., and Palmer, R. M. (2014). A Clinical Guide to Periodontology: Pathology of Periodontal Disease. *Br. Dent. J.* 216 (8), 457–461. doi:10.1038/sj.bdj.2014.299

Hasturk, H., Kantarci, A., and Van Dyke, T. E. (2012). Oral Inflammatory Diseases and Systemic Inflammation: Role of the Macrophage. *Front. Immunol.* 3, 118. doi:10.3389/fimmu.2012.00118

He, Z., Zhang, X., Song, Z., Li, L., Chang, H., Li, S., et al. (2020). Quercetin Inhibits Virulence Properties of Porphyromas Gingivalis in Periodontal Disease. *Sci. Rep.* 10 (1), 18313–13. doi:10.1038/s41598-020-74977-y

Heta, S., and Robo, I. (2018). The Side Effects of the Most Commonly Used Group of Antibiotics in Periodontal Treatments. *Med. Sci. (Basel)* 6 (1), 6. doi:10.3390/medsci6010006

Hoda, M., Hemaiswarya, S., and Doble, M. (2019). "Pharmacokinetics and Pharmacodynamics of Polyphenols," in *Role of Phenolic Phytochemicals in Diabetes Management* (Singapore: Springer), 159–173. doi:10.1007/978-981-13-8997-9_7

Hu, Y., Gui, Z., Zhou, Y., Xia, L., Lin, K., and Xu, Y. (2019). Quercetin Alleviates Rat Osteoarthritis by Inhibiting Inflammation and Apoptosis of Chondrocytes, Modulating Synovial Macrophages Polarization to M2 Macrophages. *Free Radic. Biol. Med.* 145, 146–160. doi:10.1016/j.freeradbiomed.2019.09.024

Ikeda, E., Ikeda, Y., Wang, Y., Fine, N., Sheikh, Z., Viniegra, A., et al. (2018). Resveratrol Derivative-Rich Melinjo Seed Extract Induces Healing in a Murine Model of Established Periodontitis. *J. Periodontol.* 89 (5), 586–595. doi:10.1002/JPER.17-0352

Izui, S., Sekine, S., Murai, H., Takeuchi, H., and Amano, A. (2021). Inhibitory Effects of Curcumin against Cytotoxicity of Porphyromonas Gingivalis Outer Membrane Vesicles. *Arch. Oral Biol.* 124, 105058. doi:10.1016/j.archoralbio.2021.105058

Jafari, S. M. (2017). "An Overview of Nanoencapsulation Techniques and Their Classification," in *Nanoencapsulation Technologies for the Food and Nutraceutical Industries* (Elsevier), 1–34. doi:10.1016/b978-0-12-809436-5.00001-x

Jekabsone, A., Sile, I., Cochis, A., Makrecka-Kuka, M., Laucaityte, G., Makarova, E., et al. (2019). Investigation of Antibacterial and Antiinflammatory Activities of Proanthocyanidins from pelargonium Sidoides DC Root Extract. *Nutrients* 11 (11), 2829. doi:10.3390/nu11112829

Kanwar, J., Taskeen, M., Mohammad, I., Huo, C., Chan, T. H., and Dou, Q. P. (2012). Recent Advances on Tea Polyphenols. *Front. Biosci. (Elite Ed.* 4, 111–131. doi:10.2741/363

Kassebaum, N. J., Bernabé, E., Dahiya, M., Bhandari, B., Murray, C. J., and Marcenes, W. (2014). Global Burden of Severe Periodontitis in 1990-2010: A Systematic Review and Meta-Regression. *J. Dent. Res.* 93 (11), 1045–1053. doi:10.1177/0022034514552491

Khalil, N. M., Do Nascimento, T. C., Casa, D. M., Dalmolin, L. F., De Mattos, A. C., Hoss, I., et al. (2013). Pharmacokinetics of Curcumin-Loaded PLGA and PLGA-PEG Blend Nanoparticles after Oral Administration in Rats. *Colloids Surf. B Biointerfaces* 101, 353–360. doi:10.1016/j.colsurfb.2012.06.024

Kugaji, M. S., Kumbar, V. M., Peram, M. R., Patil, S., Bhat, K. G., and Diwan, P. V. (2019). Effect of Resveratrol on Biofilm Formation and Virulence Factor Gene Expression of Porphyromonas Gingivalis in Periodontal Disease. *APMIS* 127 (4), 187–195. doi:10.1111/apm.12930

Kumbar, V. M., Peram, M. R., Kugaji, M. S., Shah, T., Patil, S. P., Muddapur, U. M., et al. (2021). Effect of Curcumin on Growth, Biofilm Formation and Virulence Factor Gene Expression of Porphyromonas Gingivalis. *Odontology* 109 (1), 18–28. doi:10.1007/s10266-020-00514-y

Kwon, T., Lamster, I. B., and Levin, L. (2021). Current Concepts in the Management of Periodontitis. *Int. Dent. J.* 71 (6), 462–476. doi:10.1111/idj.12630

Lamont, R. J., Koo, H., and Hajishengallis, G. (2018). The Oral Microbiota: Dynamic Communities and Host Interactions. *Nat. Rev. Microbiol.* 16 (12), 745–759. doi:10.1038/s41579-018-0089-x

Leszczyńska, A., Buczko, P., Buczko, W., and Pietruska, M. (2011). Periodontal Pharmacotherapy - an Updated Review. *Adv. Med. Sci.* 56 (2), 123–131. doi:10.2478/v10039-011-0044-9

Li, Y., Yao, J., Han, C., Yang, J., Chaudhry, M. T., Wang, S., et al. (2016). Quercetin, Inflammation and Immunity. *Nutrients* 8 (3), 167. doi:10.3390/nu8030167

Liang, J., Yan, H., Puligundla, P., Gao, X., Zhou, Y., and Wan, X. (2017). Applications of Chitosan Nanoparticles to Enhance Absorption and Bioavailability of Tea Polyphenols: A Review. *Food Hydrocoll.* 69, 286–292. doi:10.1016/j.foodhyd.2017.01.041

Lu, W., Kelly, A. L., and Miao, S. (2016). Emulsion-based Encapsulation and Delivery Systems for Polyphenols. *Trends Food Sci. Technol.* 47, 1–9. doi:10.1016/j.tifs.2015.10.015

Luca, S. V., Macovei, I., Bujor, A., Miron, A., Skalicka-Woźniak, K., Aprotosoaie, A. C., et al. (2020). Bioactivity of Dietary Polyphenols: The Role of Metabolites. *Crit. Rev. Food Sci. Nutr.* 60 (4), 626–659. doi:10.1080/10408398.2018.1546669

Maisuria, V. B., Los Santos, Y. L., Tufenkji, N., and Déziel, E. (2016). Cranberry-Derived Proanthocyanidins Impair Virulence and Inhibit Quorum Sensing of *Pseudomonas aeruginosa*. *Sci. Rep.* 6 (1), 1–12. doi:10.1038/srep30169

Marcenes, W., Kassebaum, N. J., Bernabé, E., Flaxman, A., Naghavi, M., Lopez, A., et al. (2013). Global Burden of Oral Conditions in 1990-2010: a Systematic Analysis. *J. Dent. Res.* 92 (7), 592–597. doi:10.1177/0022034513490168

McGowan, K., Mcgowan, T., and Ivanovski, S. (2018). Optimal Dose and Duration of Amoxicillin-Plus-Metronidazole as an Adjunct to Non-surgical Periodontal Therapy: A Systematic Review and Meta-Analysis of Randomized, Placebo-Controlled Trials. *J. Clin. Periodontol.* 45 (1), 56–67. doi:10.1111/jcpe.12830

Merisko-Liversidge, E., and Liversidge, G. G. (2011). Nanosizing for Oral and Parenteral Drug Delivery: a Perspective on Formulating Poorly-Water Soluble Compounds Using Wet Media Milling Technology. *Adv. Drug Deliv. Rev.* 63 (6), 427–440. doi:10.1016/j.addr.2010.12.007

Milinčić, D. D., Popović, D. A., Lević, S. M., Kostić, A. Ž., Tešić, Ž. L., Nedović, V. A., et al. (2019). Application of Polyphenol-Loaded Nanoparticles in Food Industry. *Nanomaterials* 9 (11), 1629. doi:10.1016/j.addr.2010.12.007

Mohd Azmi, F., Mp Sockalingam, S. N., Mohd Said, M., and Irfani Zakaria, A. S. (2020). Clinical Applications of Catechin in Dentistry: A Review. *J. Nat. Remedies* 20 (1), 2–15. doi:10.18311/jnr/2020/23941

Mohd Dom, T. N., Ayob, R., Abd Muttalib, K., and Aljunid, S. M. (2016). National Economic Burden Associated with Management of Periodontitis in Malaysia. *Int. J. Dent.* 2016, 1–6. doi:10.1155/2016/1891074

Mohd Dom, T. N., Mohd Said, S., Abdul Aziz, A. F., Abdul Manaf, M. R., and Aljunid, S. M. (2012). Periodontal Disease as an Indicator of Chronic Non-communicable Diseases: Evidence from Literatures. *BMC Public Health* 12 (2), 1. doi:10.1186/1471-2458-12-S2-A26

Mohd-Dom, T., Ayob, R., Mohd-Nur, A., Abdul-Manaf, M. R., Ishak, N., Abdul-Muttalib, K., et al. (2014). Cost Analysis of Periodontitis Management in Public Sector Specialist Dental Clinics. *BMC Oral Health* 14 (1), 56–10. doi:10.1186/1472-6831-14-56

Muhamad, I. I., Selvakumaran, S., and Lazim, N. a. M. (2014). Designing Polymeric Nanoparticles for Targeted Drug Delivery System. *Nanomed* 287, 287.

Muniz, F. W., Nogueira, S. B., Mendes, F. L., Rösing, C. K., Moreira, M. M., De Andrade, G. M., et al. (2015). The Impact of Antioxidant Agents

Complimentary to Periodontal Therapy on Oxidative Stress and Periodontal Outcomes: A Systematic Review. *Arch. Oral Biol.* 60 (9), 1203–1214. doi:10.1016/j.archoralbio.2015.05.007

Murakami, S., Mealey, B. L., Mariotti, A., and Chapple, I. L. C. (2018). Dental Plaque-Induced Gingival Conditions. *J. Periodontol.* 89, S17–S27. doi:10.1111/jcpe.12937

Napimoga, M. H., Clemente-Napimoga, J. T., Macedo, C. G., Freitas, F. F., Stipp, R. N., Pinho-Ribeiro, F. A., et al. (2013). Quercetin Inhibits Inflammatory Bone Resorption in a Mouse Periodontitis Model. *J. Nat. Prod.* 76 (12), 2316–2321. doi:10.1021/np400691n

Nawrot-Hadzik, I., Matkowski, A., Hadzik, J., Dobrowolska-Czopor, B., Olchowy, C., Dominiak, M., et al. (2021). Proanthocyanidins and Flavan-3-Ols in the Prevention and Treatment of Periodontitis-Antibacterial Effects. *Nutrients* 13 (1), 165. doi:10.3390/nu13010165

Nedovic, V., Kalusevic, A., Manojlovic, V., Levic, S., and Bugarski, B. (2011). An Overview of Encapsulation Technologies for Food Applications. *Procedia Food Sci.* 1, 1806–1815. doi:10.1016/j.profoo.2011.09.265

Neves, A. R., Lucio, M., Lima, J. L., and Reis, S. (2012). Resveratrol in Medicinal Chemistry: a Critical Review of its Pharmacokinetics, Drug-Delivery, and Membrane Interactions. *Curr. Med. Chem.* 19 (11), 1663–1681. doi:10.2174/092986712799945085

Niu, Y., Ke, D., Yang, Q., Wang, X., Chen, Z., An, X., et al. (2012). Temperature-dependent Stability and DPPH Scavenging Activity of Liposomal Curcumin at pH 7.0. *Food Chem.* 135 (3), 1377–1382. doi:10.1016/j.foodchem.2012.06.018

Noh, M. K., Jung, M., Kim, S. H., Lee, S. R., Park, K. H., Kim, D. H., et al. (2013). Assessment of IL-6, IL-8 and TNF-α Levels in the Gingival Tissue of Patients with Periodontitis. *Exp. Ther. Med.* 6 (3), 847–851. doi:10.3892/etm.2013.1222

Paka, G. D., and Ramassamy, C. (2017). Optimization of Curcumin-Loaded PEG-PLGA Nanoparticles by GSH Functionalization: Investigation of the Internalization Pathway in Neuronal Cells. *Mol. Pharm.* 14 (1), 93–106. doi:10.1021/acs.molpharmaceut.6b00738

Palaska, I., Papathanasiou, E., and Theoharides, T. C. (2013). Use of Polyphenols in Periodontal Inflammation. *Eur. J. Pharmacol.* 720 (1-3), 77–83. doi:10.1016/j.ejphar.2013.10.047

Pan, W., Wang, Q., and Chen, Q. (2019). The Cytokine Network Involved in the Host Immune Response to Periodontitis. *Int. J. Oral Sci.* 11 (3), 30–13. doi:10.1038/s41368-019-0064-z

Papapanou, P. N., Sanz, M., Buduneli, N., Dietrich, T., Feres, M., Fine, D. H., et al. (2018). Periodontitis: Consensus Report of Workgroup 2 of the 2017 World Workshop on the Classification of Periodontal and Peri-Implant Diseases and Conditions. *J. Clin. Periodontol.* 45, S162–S182. doi:10.1111/jcpe.12946

Papathanasiou, E., Conti, P., Carinci, F., Lauritano, D., and Theoharides, T. C. (2020). IL-1 Superfamily Members and Periodontal Diseases. *J. Dent. Res.* 99 (13), 1425–1434. doi:10.1177/0022034520945209

Park, H. J., Jeong, S. K., Kim, S. R., Bae, S. K., Kim, W. S., Jin, S. D., et al. (2009). Resveratrol Inhibits Porphyromonas Gingivalis Lipopolysaccharide-Induced Endothelial Adhesion Molecule Expression by Suppressing NF-kappaB Activation. *Arch. Pharm. Res.* 32 (4), 583–591. doi:10.1007/s12272-009-1415-7

Plessas, A. (2014). Nonsurgical Periodontal Treatment: Review of the Evidence. *Oral Health Dent. Manag.* 13 (1), 71–80.

Preshaw, P. M. (2018). Host Modulation Therapy with Anti-inflammatory Agents. *Periodontol. 2000* 76 (1), 131–149. doi:10.1111/prd.12148

Rauf, A., Imran, M., Abu-Izneid, T., Iahtisham-Ul-Haq, S., Patel, S., Pan, X., et al. (2019). Proanthocyanidins: A Comprehensive Review. *Biomed. Pharmacother.* 116, 108999. doi:10.1016/j.biopha.2019.108999

Salvi, G. E., Stähli, A., Schmidt, J. C., Ramseier, C. A., Sculean, A., and Walter, C. (2020). Adjunctive Laser or Antimicrobial Photodynamic Therapy to Non-surgical Mechanical Instrumentation in Patients with Untreated Periodontitis: A Systematic Review and Meta-Analysis. *J. Clin. Periodontol.* 47, 176–198. doi:10.1111/jcpe.13236

Savickiene, N., Jekabsone, A., Raudone, L., Abdelgeliel, A. S., Cochis, A., Rimondini, L., et al. (2018). Efficacy of Proanthocyanidins from Pelargonium Sidoides Root Extract in Reducing P. Gingivalis Viability while Preserving Oral Commensal S. Salivarius. *Mater. (Basel)* 11 (9), 1499. doi:10.3390/ma11091499

Scannapieco, F. A., and Cantos, A. (2016). Oral Inflammation and Infection, and Chronic Medical Diseases: Implications for the Elderly. *Periodontol. 2000* 72 (1), 153–175. doi:10.1111/prd.12129

Selvaraj, V., Manne, N. D., Arvapalli, R., Rice, K. M., Nandyala, G., Fankenhanel, E., et al. (2015). Effect of Cerium Oxide Nanoparticles on Sepsis Induced Mortality and NF-Kb Signaling in Cultured Macrophages. *Nanomedicine (Lond)* 10 (8), 1275–1288. doi:10.2217/nnm.14.205

Sessa, M., Balestrieri, M. L., Ferrari, G., Servillo, L., Castaldo, D., D'Onofrio, N., et al. (2014). Bioavailability of Encapsulated Resveratrol into Nanoemulsion-Based Delivery Systems. *Food Chem.* 147, 42–50. doi:10.1016/j.foodchem.2013.09.088

Shahzad, M., Millhouse, E., Culshaw, S., Edwards, C. A., Ramage, G., and Combet, E. (2015). Selected Dietary (Poly)phenols Inhibit Periodontal Pathogen Growth and Biofilm Formation. *Food Funct.* 6 (3), 719–729. doi:10.1039/C4FO01087F

Shakoor, H., Feehan, J., Apostolopoulos, V., Platat, C., Al Dhaheri, A. S., Ali, H. I., et al. (2021). Immunomodulatory Effects of Dietary Polyphenols. *Nutrients* 13 (3), 728. doi:10.3390/nu13030728

Shome, S., Talukdar, A. D., Choudhury, M. D., Bhattacharya, M. K., and Upadhyaya, H. (2016). Curcumin as Potential Therapeutic Natural Product: a Nanobiotechnological Perspective. *J. Pharm. Pharmacol.* 68 (12), 1481–1500. doi:10.1111/jphp.12611

Silva, P., Bonifácio, B., Ramos, M., Negri, K., Maria Bauab, T., and Chorilli, M. (2014). Nanotechnology-based Drug Delivery Systems and Herbal Medicines: a Review. *Ijn* 9, 1. doi:10.2147/IJN.S52634

Singla, R. K., Dubey, A. K., Garg, A., Sharma, R. K., Fiorino, M., Ameen, S. M., et al. (2019). Natural Polyphenols: Chemical Classification, Definition of Classes, Subcategories, and Structures. *J. AOAC Int.* 102, 1397–1400. doi:10.1093/jaoac/102.5.1397

Sulijaya, B., Takahashi, N., and Yamazaki, K. (2019). Host Modulation Therapy Using Anti-inflammatory and Antioxidant Agents in Periodontitis: A Review to a Clinical Translation. *Arch. Oral Biol.* 105, 72–80. doi:10.1016/j.archoralbio.2019.07.002

Tan, R. Z., Wang, C., Deng, C., Zhong, X., Yan, Y., Luo, Y., et al. (2020). Quercetin Protects against Cisplatin-Induced Acute Kidney Injury by Inhibiting Mincle/Syk/NF-Kb Signaling Maintained Macrophage Inflammation. *Phytother. Res.* 34 (1), 139–152. doi:10.1002/ptr.6507

Taskan, M. M., and Gevrek, F. (2020). Quercetin Decreased Alveolar Bone Loss and Apoptosis in Experimentally Induced Periodontitis Model in Wistar Rats. *Antiinflamm. Antiallergy Agents Med. Chem.* 19 (4), 436–448. doi:10.2174/1871523019666200124114503

Teles, R., Teles, F., Frias-Lopez, J., Paster, B., and Haffajee, A. (2013). Lessons Learned and Unlearned in Periodontal Microbiology. *Periodontol. 2000* 62 (1), 95–162. doi:10.1111/prd.12010

Tian, M., Chen, G., Xu, J., Lin, Y., Yi, Z., Chen, X., et al. (2022). Epigallocatechin Gallate-Based Nanoparticles with Reactive Oxygen Species Scavenging Property for Effective Chronic Periodontitis Treatment. *Chem. Eng. J.* 433, 132197. doi:10.1016/j.cej.2021.132197

Tibúrcio-Machado, C. S., Michelon, C., Zanatta, F. B., Gomes, M. S., Marin, J. A., and Bier, C. A. (2021). The Global Prevalence of Apical Periodontitis: a Systematic Review and Meta-Analysis. *Int. Endod. J.* 54 (5), 712–735. doi:10.1111/iej.13467

Tilakaratne, A., and Soory, M. (2014). Anti-inflammatory Actions of Adjunctive Tetracyclines and Other Agents in Periodontitis and Associated Comorbidities. *Open Dent. J.* 8, 109–124. doi:10.2174/1874210601408010109

Ulrey, R. K., Barksdale, S. M., Zhou, W., and Van Hoek, M. L. (2014). Cranberry Proanthocyanidins Have Anti-biofilm Properties against *Pseudomonas aeruginosa*. *BMC Complement. Altern. MedAltern. Med.* 14 (1), 1–12. doi:10.1186/1472-6882-14-499

Van Dyke, T. E., Bartold, P. M., and Reynolds, E. C. (2020). The Nexus between Periodontal Inflammation and Dysbiosis. *Front. Immunol.* 11, 511. doi:10.3389/fimmu.2020.00511

Van Dyke, T. E. (2017). Pro-resolving Mediators in the Regulation of Periodontal Disease. *Mol. Asp. Med.* 58, 21–36. doi:10.1016/j.mam.2017.04.006

Wais, U., Jackson, A. W., He, T., and Zhang, H. (2016). Nanoformulation and Encapsulation Approaches for Poorly Water-Soluble Drug Nanoparticles. *Nanoscale* 8 (4), 1746–1769. doi:10.1039/C5NR07161E

Wang, T., Ma, X., Lei, Y., and Luo, Y. (2016). Solid Lipid Nanoparticles Coated with Cross-Linked Polymeric Double Layer for Oral Delivery of Curcumin. *Colloids Surf. B Biointerfaces* 148, 1–11. doi:10.1016/j.colsurfb.2016.08.047

Wang, X., Zhao, W., Chen, Y., Shi, H., Wang, R., Zhong, W., et al. (2019). Preparation and Characterization of PEGylated Poly-L-Lysine-Hydroxycamptothecin Nanoparticles without and with Methotrexate. *Nanosci. Nanotechnol. Lett.* 11 (6), 795–803. doi:10.1166/nnl.2019.2942

Wilken, R., Veena, M. S., Wang, M. B., and Srivatsan, E. S. (2011). Curcumin: A Review of Anti-cancer Properties and Therapeutic Activity in Head and Neck Squamous Cell Carcinoma. *Mol. Cancer* 10 (1), 12–19. doi:10.1186/1476-4598-10-12

Xiao, C. J., Yu, X. J., Xie, J. L., Liu, S., and Li, S. (2018). Protective Effect and Related Mechanisms of Curcumin in Rat Experimental Periodontitis. *Head. Face Med.* 14 (1), 12–18. doi:10.1186/s13005-018-0169-1

Xiong, G., Ji, W., Wang, F., Zhang, F., Xue, P., Cheng, M., et al. (2019). Quercetin Inhibits Inflammatory Response Induced by LPS from Porphyromonas Gingivalis in Human Gingival Fibroblasts via Suppressing NF-Kb Signaling Pathway. *Biomed. Res. Int.* 2019, 6282635. doi:10.1155/2019/6282635

Xu, X., Li, C., Chen, Q., Sun, W., Xiao, F., Chen, Q., et al. (2020). Therapeutic Effect of Rutin-Loaded Poly Lactic-Co-Glycolic Acid Nanoparticles on Gingiva of Periodontitis Rats. *Mat. Express.* 10 (12), 2048–2055. doi:10.1166/mex.2020.1867

Yahfoufi, N., Alsadi, N., Jambi, M., and Matar, C. (2018). The Immunomodulatory and Anti-inflammatory Role of Polyphenols. *Nutrients* 10 (11), 1618. doi:10.3390/nu10111618

Yu, T., Zhao, L., Huang, X., Ma, C., Wang, Y., Zhang, J., et al. (2016). Enhanced Activity of the Macrophage M1/M2 Phenotypes and Phenotypic Switch to M1 in Periodontal Infection. *J. Periodontol.* 87 (9), 1092–1102. doi:10.1902/jop.2016.160081

Yucel-Lindberg, T., and Båge, T. (2013). Inflammatory Mediators in the Pathogenesis of Periodontitis. *Expert Rev. Mol. Med.* 15, e7. doi:10.1017/erm.2013.8

Zambrano, L. M. G., Brandao, D. A., Rocha, F. R. G., Marsiglio, R. P., Longo, I. B., Primo, F. L., et al. (2018). Local Administration of Curcumin-Loaded Nanoparticles Effectively Inhibits Inflammation and Bone Resorption Associated with Experimental Periodontal Disease. *Sci. Rep.* 8 (1), 1–11. doi:10.1038/s41598-018-24866-2

Zhao, Y., Pu, R., Qian, Y., Shi, J., and Si, M. (2021). Antimicrobial Photodynamic Therapy versus Antibiotics as an Adjunct in the Treatment of Periodontitis and Peri-Implantitis: A Systematic Review and Meta-Analysis. *Photodiagnosis Photodyn. Ther.* 34, 102231. doi:10.1016/j.pdpdt.2021.102231

Zhou, T., Chen, D., Li, Q., Sun, X., Song, Y., and Wang, C. (2013). Curcumin Inhibits Inflammatory Response and Bone Loss during Experimental Periodontitis in Rats. *Acta Odontol. Scand.* 71 (2), 349–356. doi:10.3109/00016357.2012.682092

Conflict of Interest: The authors declare that the research was conducted in the absence of any commercial or financial relationships that could be construed as a potential conflict of interest.

Publisher's Note: All claims expressed in this article are solely those of the authors and do not necessarily represent those of their affiliated organizations, or those of the publisher, the editors and the reviewers. Any product that may be evaluated in this article, or claim that may be made by its manufacturer, is not guaranteed or endorsed by the publisher.

frontiers | Frontiers in Pharmacology

TYPE Original Research
PUBLISHED 05 September 2022
DOI 10.3389/fphar.2022.849102

OPEN ACCESS

EDITED BY
Tharmarajan Ramprasath,
Georgia State University, United States

REVIEWED BY
Venkata Naga Lakshmi Ramarao Sure,
Tulane University, United States
Stalinraja Maruthamuthu,
University of California, San Francisco, United States
Nandakumar Natarajan,
The University of Texas Health Science Center at Tyler, United States

*CORRESPONDENCE
Lingan Huang,
huang_3469@163.com

SPECIALTY SECTION
This article was submitted to Inflammation Pharmacology, a section of the journal Frontiers in Pharmacology

RECEIVED 05 January 2022
ACCEPTED 05 August 2022
PUBLISHED 05 September 2022

CITATION
Zhao R, Wei X, Zhang C, Wu H, Xiang C, Li H, Duan W, Duan Z, Li C, Zhao Y and Huang L (2022), α2-macroglobulin-rich serum as a master inhibitor of inflammatory factors attenuates cartilage degeneration in a mini pig model of osteoarthritis induced by "idealized" anterior cruciate ligament reconstruction.
Front. Pharmacol. 13:849102.
doi: 10.3389/fphar.2022.849102

α2-macroglobulin-rich serum as a master inhibitor of inflammatory factors attenuates cartilage degeneration in a mini pig model of osteoarthritis induced by "idealized" anterior cruciate ligament reconstruction

Ruipeng Zhao[1], Xiaochun Wei[1], Chengming Zhang[1], Hongru Wu[2], Chuan Xiang[1], Haoqian Li[1], Wangping Duan[1], Zhiqing Duan[3], Chunjiang Li[1], Yu Zhao[1] and Lingan Huang[1,4]*

[1]Department of Orthopaedics, The Second Hospital of Shanxi Medical University. Shanxi Key Laboratory of Bone and Soft Tissue Injury Repair, Taiyuan, China, [2]Shanxi Institute of Sports Science, Taiyuan, China, [3]Department of Biochemistry and Molecular Biology, School of Basic Medical Sciences, Shanxi Medical University, Taiyuan, China, [4]Department of Pain Medicine, Sanya Central Hospital of Hainan Medical College, Sanya, China

Post-traumatic osteoarthritis is a special type of osteoarthritis and a common disease, with few effective treatments available. α2-Macroglobulin (α2M) is important to chondral protection in post-traumatic osteoarthritis. However, its injection into xenogeneic joint cavities involves safety hazards, limiting clinical applications. Exploring serum α2M-enriching strategies and the therapeutic effect and mechanism of α2M-rich serum (α2MRS) autologous joint injection to treat post-traumatic osteoarthritis has significant value. In the present study, a unique filtration process was used to obtain α2MRS from human and mini pig serum. We evaluated the potential of α2MRS in protecting against post-surgery cartilage degeneration. We identify the potential of α2MRS in reducing the expression of inflammatory cytokines and factors that hasten cartilage degeneration in post-operative conditions leading to post-traumatic osteoarthritis. The potential of α2MRS was analyzed in interleukin-1β induced human chondrocytes and mini pig models. In the chondrocyte model, α2MRS significantly promoted human chondrocyte proliferation and reduced apoptosis and chondrocyte catabolic cytokine gene transcription and secretion. The anterior cruciate ligament autograft reconstruction model of mini pigs was randomized into groups, operated on, and injected with α2MRS or saline. The results showed that α2MRS injection significantly suppressed the levels of inflammatory factors, improved gait, and showed significantly lower cartilage degeneration than the groups that did not receive α2MRS injections. This study highlights the chondroprotective effects of α2MRS, elucidated its potential applications against cartilage degeneration, and could provide a basis for the clinical translation of α2MRS.

KEYWORDS

osteoarthritis, α2M-rich serum, anterior cruciate ligament, articular cartilage, inflammation, mini pig

Introduction

Anterior cruciate ligament (ACL) rupture, one of the most common joint injuries in young people, is conventionally treated using surgical ACL reconstruction (ACL-R). However, even with the best surgical techniques available, these patients remain at a high risk for post-traumatic osteoarthritis (PTOA) (Barenius et al., 2014; Björnsson et al., 2016; Wang et al., 2020). Recently, researchers developed an "idealized" ACL autograft reconstruction (IACL-R) model (Bryan et al., 2011; Han et al., 2018). Notably, the authors found that cartilage degeneration still occurred despite this reconstruction and concluded that there was a significant correlation between the expression of inflammatory factors and cartilage injury. Moreover, other studies have indicated that catabolic proteases and cytokines reach their peak levels within 48 h after joint injury, initiating cell death and cartilage matrix degeneration (Lieberthal et al., 2015; Heard et al., 2016; Maerz et al., 2018). Thus, early intervention to reduce the expression of these catabolic proteases and cytokines is critical to prevent or delay cartilage degeneration.

α2-macroglobulin (α2M), a tetrameric macromolecular glycoprotein, is mainly synthesized and secreted into the body fluids by liver epithelial parenchymal cells (Rehman et al., 2013). To date, α2M has been shown to play an important role in the diagnosis of diseases, prediction of liver fibrosis staging (Ho et al., 2010), non-invasive diagnosis of type II diabetes (Chung et al., 2016), and the treatment of various diseases, including alleviating pain in subacromial bursitis, lateral epicondylitis, Achilles tendonitis, spinal intervertebral discogenic (Montesano and Cuellar, 2015; Cuellar et al., 2016), and jaw osteoradionecrosis (Li S. et al., 2019). Moreover, some studies have demonstrated that supplemental intra-articular α2M provides chondral protection in PTOA (Wang et al., 2014; Zhang et al., 2017; Li et al., 2019). However, α2M is expensive. More importantly, the long-term injection of α2M, a blood protein component, into the xenogeneic joint cavity involves safety hazards, such as immune rejection, which limits its clinical application. This study used ultrafiltration centrifugation to explore suitable centrifugation conditions, in an attempt to enrich α2M in serum, and finally prepare α2M-rich serum (α2MRS). The ultimate purpose of the α2MRS preparation is for clinical application and disease prevention and treatment. Therefore, its biological safety, efficacy, and specific mechanism of action need to be accurately evaluated and verified. We hypothesized that α2MRS could significantly reduce the expression of inflammatory factors in synovial fluid, promote early recovery of the gait, and effectively attenuate cartilage degeneration. This study will greatly promote the translation of α2MRS for clinical applications.

Materials and methods

Patient samples and experimental animals

All procedures in this study, including *in vitro* and *in vivo* experiments, were approved by the Ethics Committee of the Second Hospital of Shanxi Medical University (NO. SYDL2019001). Human chondrocytes used in this study were derived from the articular cartilage library of Shanxi Key Laboratory of Bone and Soft Tissue Injury Repair. All patients provided informed consent, and all procedures were approved by the Ethics Committee of the Second Hospital of Shanxi Medical University (NO. 2019YX260). Based on the purpose of this study, under the guidance of statistical experts, the number of samples numbersin this study was six. For the *in vitro* experiments, a sample size of six was used. For the *in vivo* experiments, the number of animals in each group was determined as six. Patient baseline characteristics were as follows: age, 64 ± 3.38 (years); sex, female (n = 4)/male (n = 2); height, 163 ± 3.53 (cm); weight: 65 ± 3.85 (kg). Mini pigs were purchased from the Beijing Shichuang Century Mini pig Breeding Base (Certificate number: SCXX (jing) 2013-0008). All animals were housed at the China Institute for Radiation Protection (Certificate number: SYXK (Jin) 2016-0002).

Reagents

The following antibodies were used in this study: collagen-2 (Col-2, ab34712, Abcam), matrix metalloproteinase -3 (MMP-3, bs-0413R, Bioss), MMP-9 (bs-4593R, Bioss), MMP-13 (K009743P, Solarbio), Col-10 (bs-0554R, Bioss), and Runt-related transcription factor 2 (Runx-2, ab76956, Abcam).

α2M concentrate from human serum

Whole blood (13 ml) was collected in a coagulation tube (BD Vacutainer SSTTM II,United States) and centrifuged at 2,000 × g for 20 min to obtain 6 ml of serum, which was then added to the upper filter of the ultrafiltration tube (Cytonics Corporation, West Palm Beach, Florida, United States). The upper concentrate was obtained under different conditions of centrifugal force (3,000, 4,000, and 5,000 × g) and time (20, 30, and 40 min). Finally, the best concentration conditions were determined based on the concentration of α2M in the upper concentrate.

Human chondrocyte isolation and primary culture

Human chondrocytes were isolated as previously described (Guo et al., 2019) and plated in 6-well culture plates at a density of 1×10^6 cells/plate. Chondrocytes culture medium was Dulbecco's Modified Eagle Medium/Nutrient Mixture F-12 (DMEM/F-12) containing 10% fetal bovine serum (Hyclone) At 90% confluence, the cells were cultured overnight under serum-free conditions and then treated with 10 ng/ml recombinant human interleukin (IL)-1β for 2 h before treatment with α2MRS. It was ensured that the concentration of α2M was 0.25 mg/ml in the culture medium. The culture medium and chondrocytes were collected and analyzed.

Elisa assays

α2M concentrations in the upper concentrate under different centrifugal conditions were determined using ELISA (EK1118, Boster Bio, China). The human chondrocyte culture medium was collected 24 h after α2MRS treatment and analyzed for the presence of MMP-13, tumor necrosis factor-α (TNF-α), and IL-6 using ELISA.

Human chondrocyte proliferation and apoptosis assays

Human chondrocyte proliferation was detected at 0, 24, 36, and 48 h using the Cell Counting Kit-8 (CCK-8) cell viability assay kit (Boster Biological Technology, China). Human chondrocytes were collected 24 h after α2MRS treatment and apoptosis was detected using a Terminal transferase dUTP end Labeling (TUNEL) assay kit (Key GEN Bio TECH, China). The percentage of positive cells was determined. The detailed procedure was in accordance with the manufacturer's protocol.

RNA isolation and real-time PCR assays

mRNA levels of *col-2, aggrecan, MMP-3*, and *MMP-13* in human chondrocyte samples and those plus *collagen-10 a1 (col-10 a1)* and *Runx-2* in minipig cartilage weight-bearing sites of the medial tibial plateau were measured by real-time PCR. Primer pairs are listed in Supplementary Table S1. Levels of gene expression were normalized to 18S rRNA expression. The data were analyzed using the comparison Ct ($2^{-\Delta\Delta Ct}$) method and expressed as the fold-change relative to the respective control. The detailed PCR procedure was described previously (Gu et al., 2019).

Idealized ACL autograft reconstruction surgery

Eighteen mature female mini pigs (age, 18 ± 1.55 months; weight, 43.3 ± 3.67 kg) were randomized into three groups based on animal ear numbers: sham ($n = 6$), IACL-R ($n = 6$), and IACL-R+α2MRS ($n = 6$). All surgeries were performed under anesthesia via an intramuscular injection of 25 mg/ml tiletamine and 25 mg/ml zolazepam (Zoletil 50, 1 ml/15 kg; Virbac Group, Carros, France). Unilateral surgery was performed on the right hind limbs of all mini pigs. Mini pigs in the IACL-R and IACL-R+α2MRS groups were subjected to surgery based on methods described previously (Figure 1; Bryan et al., 2011; Han et al., 2018). The minipigs in the sham group underwent arthrotomy, temporary patellar dislocation, and coring of one-third of the length of the lateral femoral condyle. Specific information on animal care can be found in the Supplementary Text S1.

Mini pig α2MRS reserve

With the help of a veterinarian, 120 ml of whole blood was collected from the anterior vena cava of each mini pig into coagulation tubes before IACL-R. According to the best concentration conditions (centrifugal force: 5,000 × *g*; time: 30 min), 12–15 ml of α2MRS was obtained per mini pig (marked according to the mini pig ear number), and these samples were frozen at −80°C.

Synovial fluid collection

Synovial fluid from the right hind limbs of all animals was collected preoperatively (day 0) and postoperatively on days 3, 6, 14, 29, and 90. The detailed procedure was described previously (Wei et al., 2010).

Intra-articular injections

Under general anesthesia, intra-articular injections were administered 2, 6, 14, and 29 days post-surgery using a sterile syringe. Under aseptic conditions, 2.5 ml autologous α2MRS was injected into the right hind limbs of mini pigs in the IACL-R+α2MRS group on the indicated days. Animals in the sham and IACL-R groups were administered an equivalent volume of saline.

Luminex assay

The Millipore Porcine Cytokine Magnetic Bead Panel (EMD Millipore, No. PCYTMAG-23K) was used to measure the levels

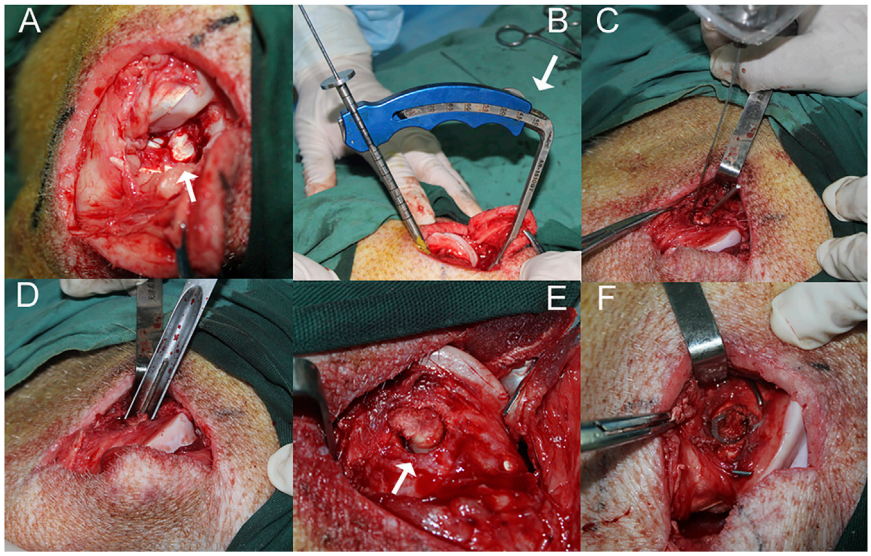

FIGURE 1
The surgical procedure performed on the right hind limb of a minipig in the IACL-R and IACL-R+α2MRS groups. **(A)** The stifle joint was open and the patella was dislocated to expose the ACL (arrow). **(B)** The ACL reconstruction guide was positioned at a 45° angle (arrow) to the longitudinal axis of the femur. **(C)** Before the hollow drill was about to penetrate the femoral tunnel, a Kirschner wire (diameter 1 mm) was drilled along outer edge of the tunnel to prevent the cartilage from splitting. **(D)** The tunnel was gently penetrated by the same diameter thin-walled ring osteotomy to completely severv tendon-bone segment **(E)** The tendon-bone segment was completely freed (arrow). **(F)** The tendon-bone segment was fixed *in situ* with two crossed Kirschner wires.

of IL-1α, IL-1β, IL-2, IL-6, IL-8, IL-18, TNF-α, and granulocyte-macrophage colony-stimulating factor (GM-CSF). Luminex assays were performed as previously described (Han et al., 2018).

Gait assessment

Six gait indicators related to biomechanics—maximum force, contact area, peak force, impulse, stance time, and swing time—were determined using the Tekscan Walkway system (Tekscan Inc., United States) (Rashid et al., 2013; Shah et al., 2020). To rule out individual differences in learning skills and walking states, each animal was subjected to over ten successful training sessions per day for ten consecutive days before the surgery, and all indicators were expressed as the ratio of the average values for the left hind limb divided by the average values for the right hind limb (Ruan et al., 2013). Gait data were collected preoperatively (day 0) and postoperatively on days 7, 15, 30, 45, 60, 75, and 90. All results obtained were the average of five successful repeated walkway trials performed at each time point for each animal.

Imaging assessment

Three months after the surgery, the mini pigs were euthanized with a pentobarbital overdose, and their right hind limbs were severed from the hip joint. Each right hind limb semi flexed was immediately subjected to X-ray examination, computed tomography (CT), three-dimensional CT reconstruction (3D CT), and magnetic resonance imaging (MRI). The specific imaging parameters are listed in Supplementary Text S2.

We determined the Kellgren-Lawrence grade of the right hind limb of each animal by examining the X-ray image (Kellgren and Lawrence, 1957; Misir et al., 2020). The CT values and thickness of the subchondral bone plate were determined (Hu et al., 2020). To avoid interference by metal artifacts, we obtained CT scans of only the middle sagittal plane from the medial femoral condyle and medial tibial plateau of the right hind limb. We also determined the whole-organ MRI score (WORMS) of the medial femoral condyle and medial tibial plateau of the right hind limb (Pozzi et al., 2015; Xue et al., 2021).

Macroscopic cartilage and osteophyte assessment

Macroscopic damage to the articular cartilage surfaces and osteophyte formation on the medial femoral condyle, medial tibial plateau, lateral femoral condyle, lateral tibial plateau, and trochlea were scored according to the Osteoarthritis Research Society International (OARSI) recommendations for sheep and goats (Little et al., 2010)

Histological assessment

Cartilage samples were obtained by drilling (φ8 mm; MOC Medizinische Geräte Gmbh, Fedderingen, Germany) the weight bearing site of the medial femoral condyle. The cartilage tissue sections (6 μm) were stained with safranin O and fast green as previously described and scored according to the recommendations of OARSI (Little et al., 2010). Furthermore, we collected synovium samples from inside the joint capsule. Synovium sections (4 μm) were stained with hematoxylin and eosin (H&E) as previously described and scored according to the OARSI recommendations (Little et al., 2010). Vertical meniscus slices from the middle region of the medial meniscus were processed and stained using H&E and scored according to the protocol detailed by Pauli et al. (2011).

Immunohistochemical assessment

Immunohistochemical analysis was conducted as reported previously (Li et al., 2020). Briefly, to detect the distribution of the target protein, 6-μm thick cartilage tissue sections from the medial femoral condyle were collected on positively-charged glass slides. Endogenous peroxidase was blocked by treating the sections with 3% hydrogen peroxide in methanol. The sections were incubated with specific antibodies against Col-2 (1:500), MMP-3 (1:200), MMP-9 (1:100), MMP-13 (1:100), Col-10 (1:50), and Runx-2 (1:50) at 4 °C overnight. Thereafter, the sections were treated sequentially with a biotinylated secondary antibody and streptavidin–peroxidase conjugate and then developed with 3,3′-diaminobenzidine chromogen. Quantitative immunohistochemical analysis was performed using an imaging analyzer.

Statistical analysis

The SPSS statistical software (version 13.0) was used to analyze the collected data. Differences in gaits and inflammatory factor levels between the preoperative (day 0) and postoperative time points in the same group were analyzed using multiple comparisons of repeated measurement data. Differences in human chondrocytes, minipig gait, inflammatory factor levels, CT values, thicknesses of the subchondral bone plate T2 values, and quantitative immunohistochemical analysis at the same time point among the different groups were estimated using one-way analysis of variance. Differences in macroscopic cartilage and osteophyte scores; microscopic cartilage, synovium, and meniscus scores; and WORMS were estimated using nonparametric tests (Wilcoxon rank-sum test). Differences in Kellgren-Lawrence grades were estimated using Fisher probabilities. Statistical significance was set at $p < 0.05$.

TABLE 1 Human α2M concentrations in the upper concentrate under different centrifugal conditions (mg/ml) (Mean ± SD, $n = 6$).

	3,000 × *g*	4,000 × *g*	5,000 × *g*
20min	4.82 ± 0.75	6.98 ± 1.15	8.23 ± 1.12
30min	6.46 ± 0.89	9.22 ± 1.08	11.13 ± 0.90
40min	7.39 ± 0.98	9.92 ± 1.17	11.93 ± 1.53

Results

All animals recovered from anesthesia and were fully awake within 3-5 h after the surgery. There were no instances of infection or immune rejections.

Concentration analysis of α2M in different concentrates from human and mini pig

As the centrifugal force increased and centrifugation time was prolonged, human α2M concentrations in the upper concentrate increased correspondingly (Table 1). Considering different factors, such as protein biological activity and concentrate volume, the concentration effect of α2M under the conditions of centrifugation at 5,000 *g* for 30 min was ideal. For human α2MRS, the concentration of α2M was 11.13 mg/ml, which was 4.88-fold higher than that in normal human serum. In mini pigs, the concentration of α2M was 12.32 mg/ml, which was 6.48-fold higher than that in normal pig serum (Figure 2A).

Human chondrocyte culture medium analysis

ELISA results demonstrated that exogenous α2MRS significantly inhibited the induction of MMP-13 ($p = 0.001$), TNF-α ($p = 0.005$), and IL-6 ($p < 0.001$) activity in IL-1β-induced human primary osteoarthritis chondrocytes (Figures 2B–D).

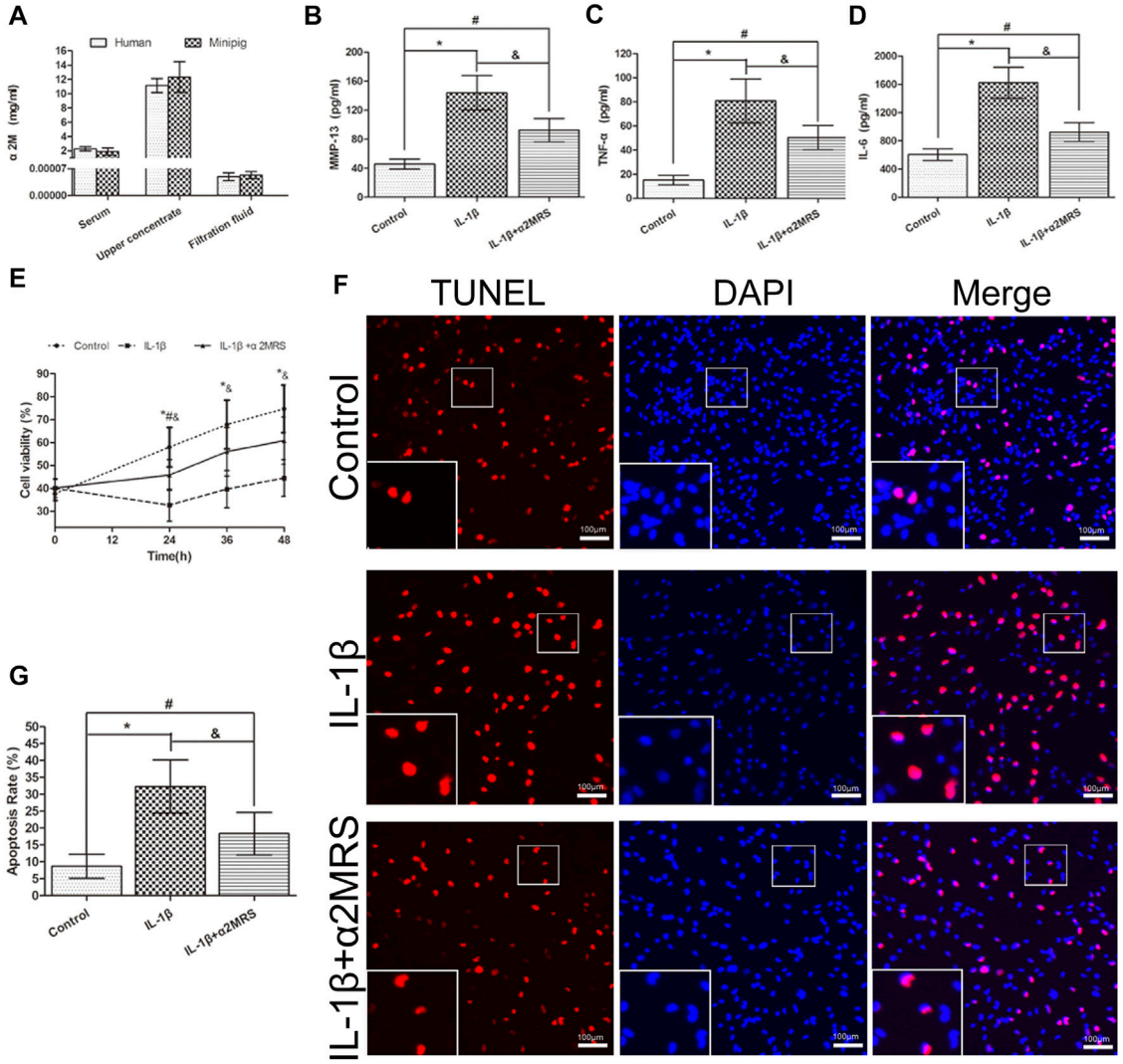

FIGURE 2
(A). Human and mini pig α2M concentrations after centrifugation at 5,000 *g* for 30 min. Human: serum: 2.28 ± 0.26 mg/ml; upper concentrate: 11.13 ± 0.90 mg/ml; filtration fluid: 0.000049 ± 0.00001 mg/ml; mini pigs: serum: 1.90 ± 0.46 mg/ml; upper concentrate: 12.32 ± 1.97 mg/ml; filtration fluid: 0.000053 ± 0.000008 mg/ml. **(B–D)**. α2MRS significantly inhibited the induction of MMP-13,TNF-α and IL-6 in IL-1β induced human primary osteoarthritic chondrocytes. **(E)** The CCK-8 assay results showed that the viability of chondrocytes was higher in IL-1β+α2MRS group relative to that in the IL-1β group, and the viability gradually increased with a longer treatment time. **(F)** TUNEL assay results showed that apoptosis (red) was reduced in the IL-1β+α2MRS group seem to that in the IL-1β group. The bottom panels are higher-magnification views of the boxed areas in the top panels **(G)** The percentage of TUNEL-positive cells was quantified, and the apoptosis rate of chondrocytes was significantly reduced in the IL-1β+α2MRS group relative to that in the IL-1β group. * = $p < 0.05$, control group versus IL-1β group; # = $p < 0.05$, control group versus IL-1β+α2MRS group; and = $p < 0.05$, IL-1β group versus IL-1β+α2MRS group. The bars show the mean ± SD ($n = 6$).

Human chondrocyte proliferation and apoptosis analysis

α2MRS promoted the proliferation and reduced the apoptosis of human chondrocytes *in vitro*. The results of the CCK-8 assay showed that the viability of chondrocytes was higher in the IL-1β+α2MRS group than in the IL-1β group ($p < 0.001$), and the viability gradually increased with treatment time (Figure 2E). The results of the TUNEL assay showed that apoptosis was significantly reduced in the IL-1β+α2MRS group (18.33% ± 5.71%) relative to that in the IL-1β group (32.33% ± 7.23%; $p < 0.001$; Figures 2F,G).

Real-time PCR analysis

Real-time PCR data indicated that supplementation with α2MRS reduced cartilage matrix catabolism and enhanced

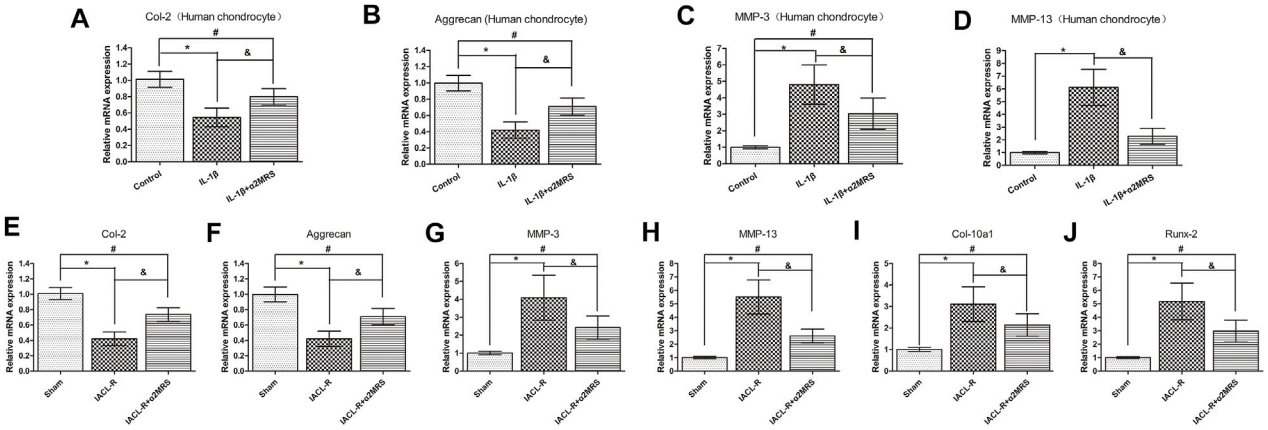

FIGURE 3
Real-time PCR data indicated that supplementation with α2MRS reduced cartilage matrix catabolism and enhanced anabolism *in-vitro* **(A–D)** and *in-vivo* **(E–J)**. mRNA levels of *MMP-3* ($p < 0.001$), *MMP-13* ($p < 0.001$), *Col-10* a1 ($p = 0.001$), and *Runx-2* ($p < 0.001$)were lower in IL-1β+α2MRS and IACL-R+α2MRS groups than in IL-1β and IACL-R groups respectively. In contrast, mRNA levels of *Col-2* ($p < 0.001$) and *aggrecan* ($p < 0.001$) followed the opposite pattern. Both were increased in IL-1β+α2MRS and IACL-R+α2MRS groups as compared to levels in IL-1β and IACL-R groups. * = $p < 0.05$, control group versus IL-1β group or sham group versus IACL-R group; # = $p < 0.05$, control group versus IL-1β+α2MRS group or sham group versus IACL-R+α2MRS group; and = $p < 0.05$, IL-1β group versus IL-1β+α2MRS group or IACL-R group versus IACL-R+α2MRS group. The bars show the mean ± SD ($n = 6$).

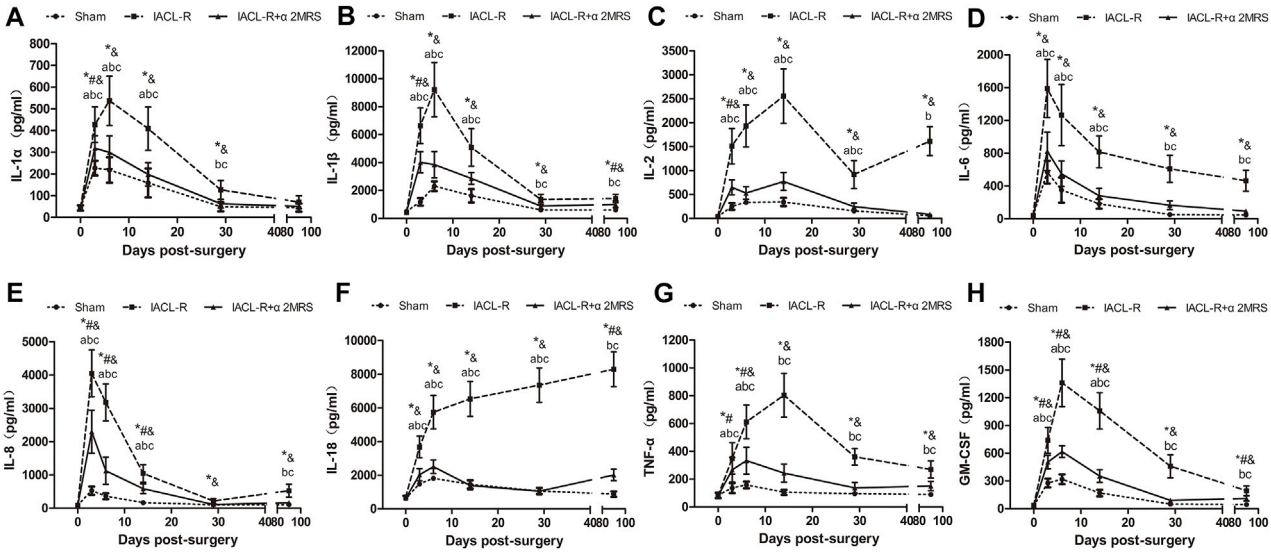

FIGURE 4
Line charts of inflammatory factors in synovial fluid. **(A)**: IL-1α; **(B)** IL-1β; **(C)** IL-2; **(D)** IL-6; **(E)** IL-8; **(F)** IL-18; **(G)** TNF-α; **(H)** GM-CSF. * = $p < 0.05$, sham group versus IACL-R group at the same time point; # = $p < 0.05$, sham group versus IACL-R+α2MRS group at the same time point; and = $p < 0.05$, IACL-R group versus IACL-R+α2MRS group at the same time point. a = $p < 0.05$, preoperative (day 0) versus postoperative (days 3, 6, 14, 29, and 90) in the sham group; b = $p < 0.05$, preoperative (day 0) versus postoperative (days 3, 6, 14, 29, and 90) in the IACL-R group; c = $p < 0.05$, preoperative (day 0) versus postoperative (days 3, 6, 14, 29, and 90) in the IACL-R+α2MRS group. The bars show the mean ± SD (n = 6)

anabolic metabolism *in vitro* (Figures 3A–D) and *in vivo* (Figures 3E–J). mRNA levels of *MMP-3* ($p < 0.001$), *MMP-13* ($p < 0.001$), *Col-10 a1* ($p = 0.001$), and *Runx-2* ($p < 0.001$) were lower in the IL-1β+α2MRS and IACL-R+α2MRS groups than in the IL-1β and IACL-R groups. In contrast, mRNA levels of *Col-2* ($p < 0.001$) and *aggrecan* ($p < 0.001$) showed the opposite pattern.

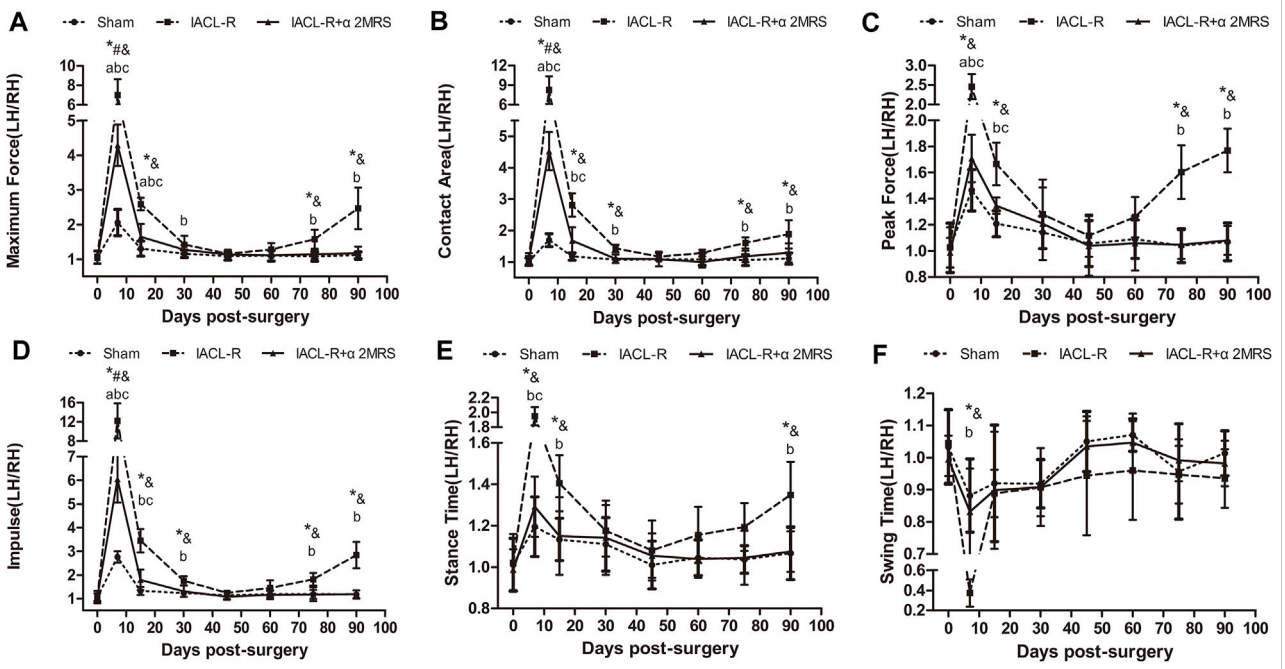

FIGURE 5
Line charts of gait analysis. **(A)**Maximum force; **(B)**Contact area; **(C)**Peak force; **(D)**Impulse; **(E)**Stance time; **(F)** Swing time. * = $p < 0.05$, sham group versus IACL-R group at the same time point; # = $p < 0.05$, sham group versus IACL-R+α2MRS group at the same time point; and = $p < 0.05$, IACL-R group versus IACL-R+α2MRS group at the same time point. a = $p < 0.05$, preoperative (day 0) versus postoperative (days 7, 15, 30, 45, 60, 75, and 90) in the sham group; b = $p < 0.05$, preoperative (day 0) versus postoperative (days 7, 15, 30, 45, 60, 75, and 90) in the IACL-R group; c = $p < 0.05$, preoperative (day 0) versus postoperative (days 7, 15, 30, 45, 60, 75, and 90) in the IACL-R+α2MRS group. The bars show the mean ± SD (n = 6)

Both were increased in the IL-1β+α2MRS and IACL-R+α2MRS groups as compared to the levels in the IL-1β and IACL-R groups, respectively.

Inflammatory factor analysis

Postoperatively, changes in the levels of inflammatory factors in different groups, except for IL-18 in the IACL-R group, showed similar trends; the levels markedly increased in the early stage and then decreased significantly. The IL-2 concentration in the IACL-R group subsequently showed an increasing trend from day 30 to day 90. The concentrations of inflammatory factors, including IL-1β, IL-6, IL-18, TNF-α, and GM-CSF, in the IACL-R and IACL-R+α2MRS groups after surgery were significantly higher than those before surgery ($p < 0.001$). The concentration of all tested inflammatory factors other than IL-1α after surgery was significantly lower in the IACL-R+α2MRS group than in the IACL-R group, and a significant difference in peak concentrations was observed in all factors ($p < 0.001$). Moreover, the peak concentrations of all detected inflammatory factors, other than IL-18 in the IACL-R group, appeared within 3–14 days after surgery (Figure 4).

Gait assessment

Across all groups, the ratios of all gait parameters of the left hind limb to those of the right hind limb initially showed an increasing trend, followed by a decreasing trend, except in the IACL-R group, which showed another increasing trend toward the end. In the IACL-R group, no gait parameters, from day 45 until day 75, differed significantly from those on day 0 ($p > 0.05$). In the IACL-R+α2MRS group, no gait parameters, from day 30 until euthanasia, differed significantly from those on day 0 ($p > 0.05$) (Figure 5).

The ratios of the left hind limb to the right hind limb of all gait parameters were similar and close to one for symmetry and did not differ significantly in all groups before surgery ($p > 0.05$). Meanwhile, the postoperative ratios of the left hind limb to the right hind limb of the gait parameters were significantly greater than one in all groups, and the values in the IACL-R group were significantly greater than those in the other two groups other than swing time, especially on days 7 and 15 ($p < 0.001$). The ratios of the left hind limb to the right hind limb of the gait parameters were close to one on days 45 and 60, indicating that there were no significant differences among the groups ($p > 0.05$). On day 75, this ratio increased only in the IACL-R group whereas it remained constant in the sham and IACL-R+α2MRS groups. On day 90, all gait parameters other than swing time ($p = 0.345$)

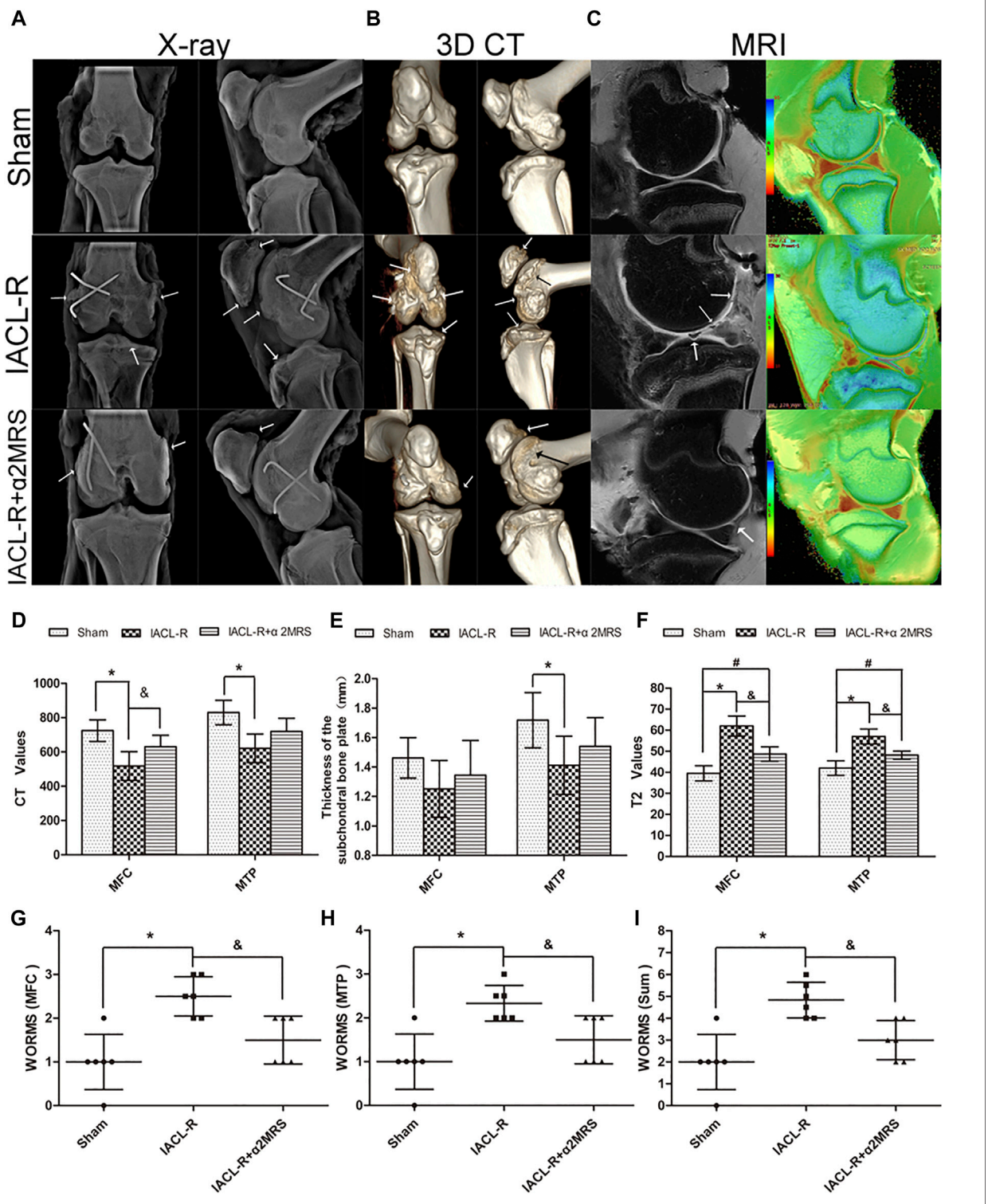

FIGURE 6
Imaging assessments **(A)**: X-ray examination;**(B)**: three-dimensional CT reconstruction;**(C)**: MRI examination (left: Osag fs PD; right: Osag T2MAP). **(D)**: The CT values of the subchondral bone plate. sham group (medial femoral condyle, 724.2 ± 62.95; medial tibial plateau, 830.3 ± 71.26); IACL-R group (medial femoral condyle, 517.7 ± 83.89; medial tibial plateau, 621.2 ± 83.57); IACL-R+α2MRS group (medial femoral condyle, 630 ± 66.9; medial tibial plateau, 719.2 ± 76.73). **(E)**: The thickness of the subchondral bone plate. sham group (medial femoral condyle, 1.46 ± 0.14; medial tibial plateau, 1.72 ± 0.19); IACL-R group (medial femoral condyle, 1.25 ± 0.19; medial tibial plateau, 1.41 ± 0.20); IACL-R+α2MRS group (medial femoral condyle, 1.35 ± 0.24; medial tibial plateau, 1.54 ± 0.19). **(F)**: Quantification of the T2 values obtained using MRI sag T2MAP.Sham
(*Continued*)

FIGURE 6
group (medial femoral condyle, 39.5 ± 3.62; medial tibial plateau, 42 ± 3.41); IACL-R group (medial femoral condyle, 62 ± 4.78; medial tibial plateau, 57 ± 3.58); IACL-R+α2MRS group (medial femoral condyle, 48.67 ± 3.45; medial tibial plateau, 48.17 ± 1.94). **(G–I)**: Quantification of the MRI OSag fs PD results using the WORMS guidelines. The white arrows indicate irregularities, osteophytes, and cartilage defects. * = $p < 0.05$, sham group versus IACL-R group; # = $p < 0.05$, sham group versus IACL-R+α2MRS group; and = $p < 0.05$, IACL-R group versus IACL-R+α2MRS group. The bars show the mean ± SD ($n = 6$).

TABLE 2 Kellgren-Lawrence grades on X-ray examination at 3 months ($n = 6$).

Group	Grade 0	Grade 1	Grade 2	Grade 3	Grade 4	P
sham	3	2	1	0	0	
IACL-R	0	1	3	2	0	>0.05
IACL-R+α2M	2	3	1	0	0	

significantly differed between the IACL-R group and the other two groups ($p < 0.001$; Figure 5).

Imaging assessment

The X-ray examinations showed that joint degeneration in the IACL-R group was relatively noticeable. The joints had a blurred border and mild osteophyte formation compared with those in the IACL-R+α2MRS group (Figure 6A). The Kellgren-Lawrence grades did not significantly differ among the three groups ($p > 0.05$; Table 2). Three-dimensional CT reconstruction showed that all joint surfaces were relatively smooth and flat in the IACL-R+α2MRS group compared to the IACL-R group. Osteophyte was seen on both sides of the patellofemoral joint in the IACL-R group (Figure 6B). Both the medial femoral condyle ($p < 0.001$) and medial tibial plateau ($p < 0.001$) showed significant differences in CT values in the subchondral bone plate between the sham and IACL-R groups. In addition, significant differences in CT values were found between the IACL-R+α2MRS and IACL-R groups in the medial femoral condyle ($p = 0.028$; Figure 6D). Significant differences in the thickness of the subchondral bone plate were found only between the sham and IACL-R groups in the medial tibial plateau ($p = 0.020$; Figure 6E). MRI OSag-fs PD showed that cartilage continuity was better without obvious local defects in the IACL-R+α2MRS group than in the IACL-R group (Figure 6C, left). WORMS of the medial femoral condyle ($p = 0.006$), medial tibial plateau ($p = 0.014$), and sum ($p = 0.004$) were significantly lower in the IACL-R+α2MRS group than in the IACL-R group (Figures 6G–I; Supplementary Table S2). Osag T2MAP showed that regular orange-red layers were more obvious in the IACL-R+α2MRS group than in the IACL-R group (Figure 6C, right). The T2 values of the medial femoral condyle ($p < 0.001$) and medial tibial plateau ($p < 0.001$) were significantly lower in the IACL-R+α2MRS group than in the IACL-R group (Figure 6F).

Macroscopic cartilage and osteophyte assessment

Compared to that in the IACL-R group, cartilage degeneration was relatively low and no obvious cartilage defects or large erosions were found in the IACL-R+α2MRS group (Figure 7A). OARSI scores of macroscopic cartilage were significantly lower in the IACL-R+α2MRS group than in the IACL-R group ($p = 0.031$; Figure 7B; Supplementary Figures S1A–E; Supplementary Table S2). Mild irregular protrusions were found only on sides of the trochlea in the IACL-R group (Figure 7A). No differences were found in the OARSI sum scores of the osteophyte among the three groups ($p = 0.438$; Figure 7C; Supplementary Figures S1F–J; Supplementary Table S2).

Histological assessment

Less decreases in safranin O staining and surface fibrillation were observed in the IACL-R+α2MRS group as compared to the IACLR-group (Figure 8A). The microscopic OARSI cartilage scores were lower in the IACL-R+α2MRS group than in the IACL-R group ($p = 0.015$; Figure 8B; Supplementary Figures 2A–E; Supplementary Table S2). Based on H&E staining of the synovium, we found mild intimal thickening, low inflammatory cell infiltration, and slight sub-intimal fibrosis and vascularity in the IACL-R+α2MRS group, relative to those in the IACL-R group (Figure 8C). Thus, the microscopic OARSI synovium scores, both total scores ($p = 0.002$) and single indicator scores, showed that synovial damage was lower in the IACL-R+α2MRS group than in the IACL-R group (Figure 8D; Supplementary Figures S2F–I; Supplementary Table S2). H&E staining of the meniscus also revealed mild surface fibrillation, normal cell distribution, and a normal collagen fiber organization (Figure 8E), and the meniscus score was lower in the IACL-

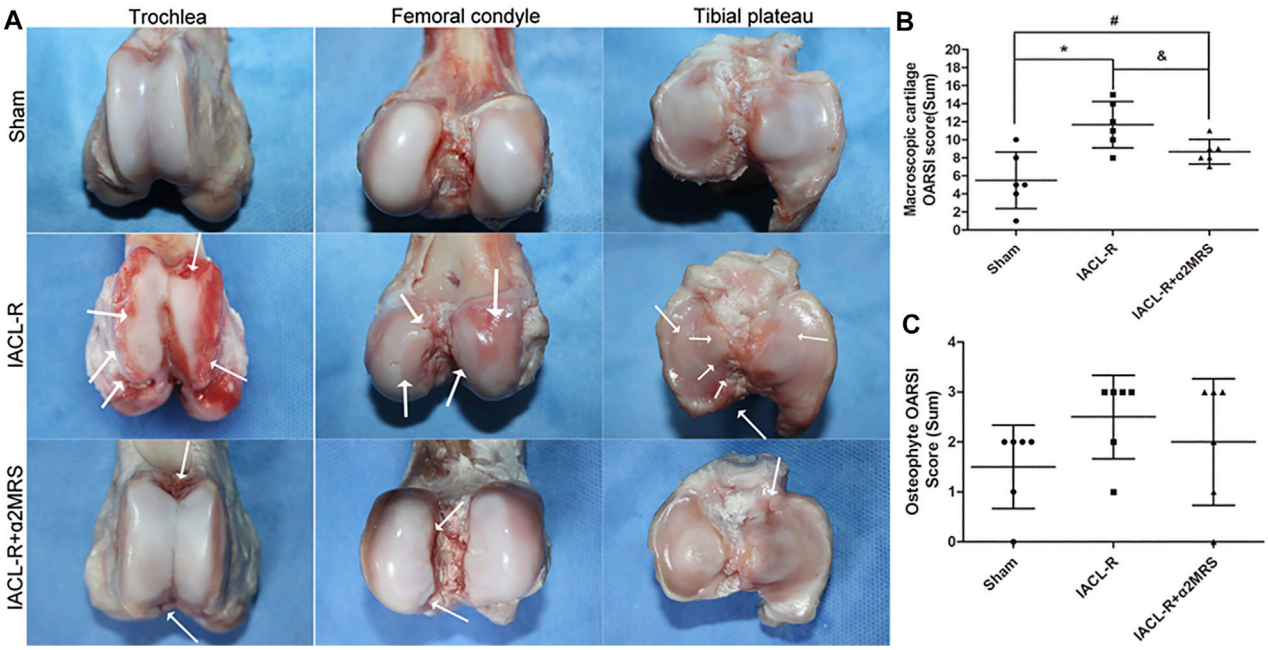

FIGURE 7
(A): Images of the trochlea, femoral condyle, and tibial plateau for the macroscopic cartilage and osteophyte assessment according to OARSI guidelines. The white arrows indicate cartilage damage, irregularities, and osteophytes. **(B)**: Macroscopic cartilage score were lower in the IACL-R+α2MRS group than in the IACL-R group ($p = 0.031$). **(C)**: Macroscopic osteophyte scores did not differ among the different groups ($p = 0.438$). * = $p < 0.05$, sham group versus IACL-R group; # = $p < 0.05$, sham group versus IACL-R+α2MRS group; and = $p < 0.05$, IACL-R group versus IACL-R+α2MRS group. The bars show the mean ± SD ($n = 6$).

R+α2MRS group than in the IACL-R group ($p < 0.001$; Figure 8F; Supplementary Figures 2J–L; Supplementary Table S2).

Immunohistochemical assessment

Both articular cartilage (Figures 9A,B) and synovium (Figures 9C,D) immunostaining showed that MMP-3 ($p < 0.001$), MMP-9 ($p < 0.001$), MMP-13 ($p < 0.001$), Col -10 ($p < 0.001$), and Runx-2 ($p = 0.001$) staining significantly increased in the IACL-R group compared with the IACL-R+α2MRS group. In contrast, Col-2 ($p < 0.001$) expression in articular cartilage was higher in the IACL-R+α2MRS group than in the IACL-R group.

Discussion

There are various conservative treatment methods for PTOA, including physical therapy, oral drugs, and intra-articular drug injection. Although physical therapy has the advantage of being non-invasive, it is mainly effective for patients with mild symptoms. Owing to the barrier function of the joint capsule, many oral drugs cannot enter the joint cavity to exert an effect. To date, intra-articular drug injection is the most effective method for the treatment of OA. α2M performs complex body functions, including the regulation of cytokine and hormone levels. It can bind several cytokines, including basic fibroblast growth factor, platelet-derived growth factor, nerve growth factor, IL-1β, and IL-6, and regulate the levels of hepcidin and leptin (Rehman et al., 2013). The specific mechanism of α2M has been previously reported by Sottrup-Jensen (Sottrup-Jensen 1989). Notably, recent studies showed that α2M can attenuate PTOA cartilage degeneration (Wang et al., 2014; Zhang et al., 2017; Li et al., 2019). However, α2M is not present in synovial fluid at sufficient levels due to its large molecular weight, which prevents its migration from the blood into the synovial fluid to counteract the increased concentrations of catabolic factors that appear after joint injury (Salvesen and Enghild, 1993). Thus, introducing supplemental α2M in the joint cavity might be a strategy to attenuate cartilage degeneration. However, considering the expense and potential safety concerns of biosynthetic α2M, α2MRS is a promising alternative for PTOA treatment. The results of our study demonstrate, for the first time, that α2MRS, as a master inhibitor of inflammatory factors, can attenuate cartilage degeneration *in vitro* and *in vivo*.

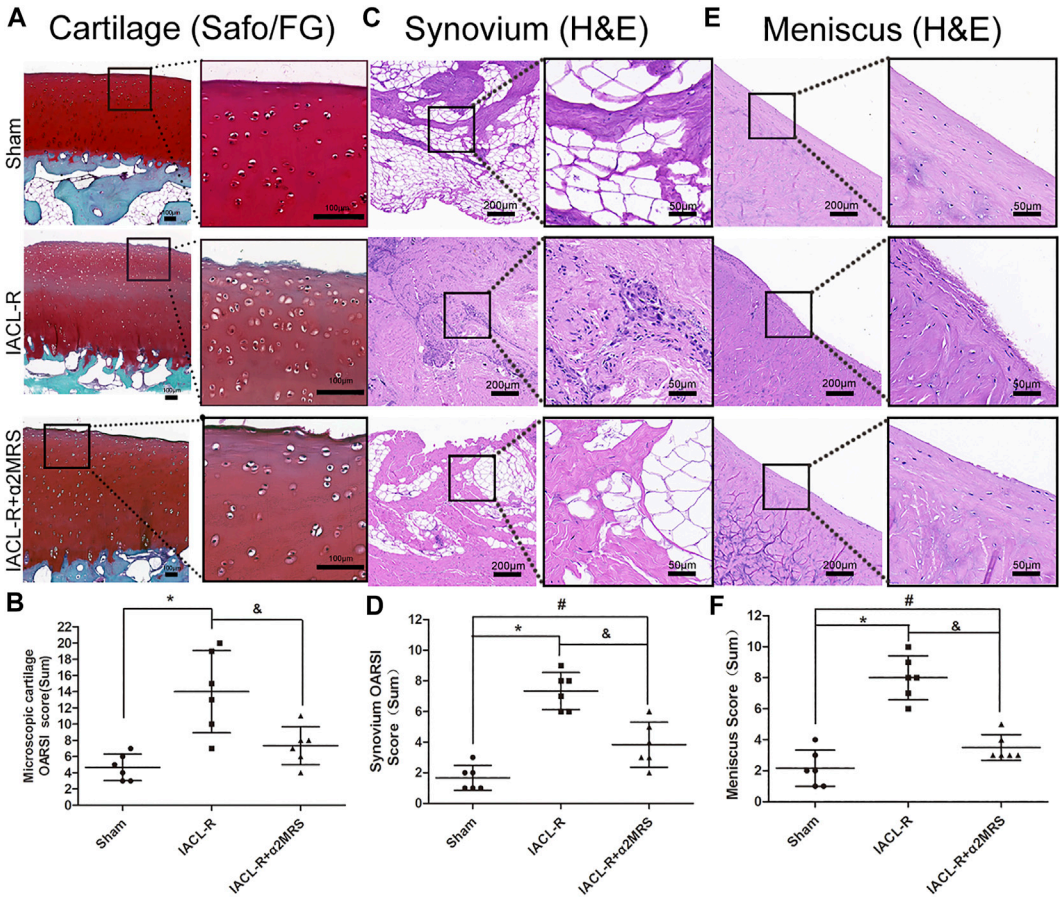

FIGURE 8
(A) Compared with the IACL-R group, less decrease in safranin O staining and surface fibrillation were observed in the IACL-R+α2MRS group. **(B)** Microscopic cartilage score were lower in the IACL-R+α2MRS group than in the IACL-R group ($p = 0.015$). **(C)** On H&E staining of the synovium, we found less degeneration in the IACL-R+α2MRS group than in the IACL-R group. **(D)** Microscopic synovium score were lower in the IACL-R+α2MRS group than in the IACL-R group ($p = 0.002$). **(E)** On H&E staining of the meniscus, we found less degeneration in the IACL-R+α2MRS group than in the IACL-R group **(F)** Microscopic meniscus score were lower in the IACL-R+α2MRS group than in the IACL-R group ($p < 0.001$). * = $p < 0.05$, sham group versus IACL-R group; # = $p < 0.05$, sham group versus IACL-R+α2MRS group; and = $p < 0.05$, IACL-R group versus IACL-R+α2MRS group. The bars show the mean ± SD ($n = 6$).

First, our *in vitro* data clearly demonstrated that human α2MRS promotes the proliferation of human chondrocyte, reduces the apoptosis of these, and decreases chondrocyte catabolic cytokine gene transcription and secretion, suggesting that α2MRS is a promising therapy. The ultimate goal of studying α2MRS is its clinical application. Thus, its biological safety and effectiveness need to be accurately evaluated and verified *in-vivo*.

Other studies have confirmed that significantly elevated inflammatory factors might be crucial for the pathogenesis of PTOA (Maerz et al., 2018; Zhao et al., 2021). There is a significant correlation between the expression of inflammatory factors, such as IL-1β, IL-6, and TNF-α, and cartilage injury (Han et al., 2018). Consistent with this, our findings demonstrated that different inflammatory factors exhibit different trends and could also play different pathogenic roles in the process of PTOA. Previous studies have demonstrated that the peak levels of cartilage catabolic enzymes could be detected on day 2 after joint injury (Zhao et al., 2021). Therefore, the mini pigs in the IACL-R+α2MRS group received the first α2MRS joint cavity injection 2 days after surgery, which inhibited the levels of various inflammatory factors. Luminex results revealed that not only the peak concentrations of inflammatory factors in synovial fluid were significantly reduced but that the speed of decline was also faster in the IACL-R+α2MRS group than in the IACL-R group, which demonstrated the early effect of α2MRS. In addition, gait analysis showed that the gait ratios of the left hind limb to the right hind limb of the IACL-R+α2MRS group were significantly greater than one at 7 days post-surgery, but it was significantly lower than that in the IACL-R group, which further proves the effectiveness of α2MRS. Other research results suggest

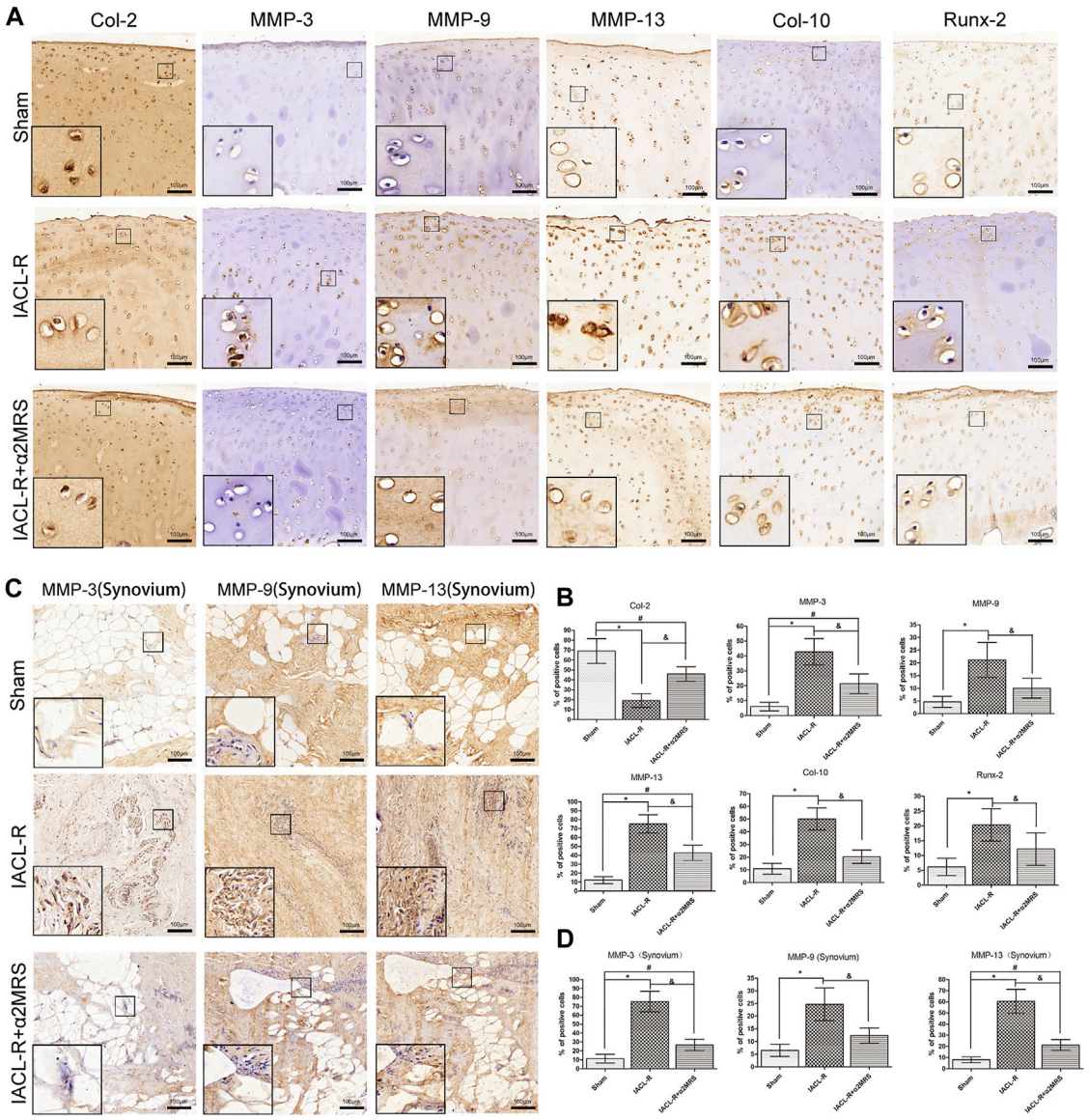

FIGURE 9
(A): Articular cartilage immunostaining showed that MMP-3, MMP-9, MMP-13, Runx-2, and Col -10 staining significantly increased in the IACL-R mini pig group but were lower in the IACL-R+α2MRS group. In contrast, Col-2 expression in articular cartilage was higher in the IACL-R+α2MRS group than in the IACL-R group. **(B)** Quantitative immunohistochemical analysis of articular cartilage. **(C)** synovium immunostaining showed that MMP-3, MMP-9 and MMP-13 staining significantly increased in the IACL-R mini pig group but were lower in the IACL-R+α2MRS group. **(D)** Quantitative immunohistochemical analysis of synovium. * = $p < 0.05$, sham group versus IACL-R group; # = $p < 0.05$, sham group versus IACL-R+α2MRS group; and = $p < 0.05$, IACL-R group versus IACL-R+α2MRS group. The bars show the mean ± SD ($n = 6$).

that the activity of some cartilage catabolic enzymes might have two peaks. The first phase appears after the initial trauma to the joint. The second peak is associated with progressive cartilage degeneration at weeks four and 6 after surgery. Therefore, we repeated α2MRS supplementation, which constantly exerts an inflammation-inhibitory effect, and the inflammatory storm or waterfall effect was interrupted in time (Pan et al., 2016). Therefore, in the later stage (days 30-90) of the experiment, the concentration of inflammatory factors in the synovial fluid in the IACL-R+α2MRS group was maintained at a low level, and no obvious rebound was observed. Gait analysis is a relatively sensitive test for abnormal biomechanics and pain in the knee joint (Muramatsu et al., 2014; Capin et al., 2018; Hughes-Oliver et al., 2018). Compared with preoperative parameters, the gait of the IACL-R group also returned to initial levels, showing no significant difference in the middle stage (days 30-60). We

conclude that the IACL-R model can restore the normal gait parameters of the knee joint and indirectly speculate that the ACL might have relatively stable biomechanical and consistent functions in different groups.

The mini pigs in the IACL-R+α2MRS group received α2MRS joint cavity injection four times starting from day 2 after surgery, which resulted in long-lasting inflammation suppression, significantly slowing the degeneration of articular cartilage. Therefore, the final imaging assessment, macroscopic cartilage assessment, and microscopic histological analysis confirmed that the articular cartilage in the IACL-R+α2MRS group was only slightly degenerated. Moreover, our biochemistry data demonstrated that supplemental α2MRS not only inhibited catabolic factors, including *MMP-3, MMP-13, Col-10,* and *Runx-2*, but also enhanced *Col-2* gene expression and protein synthesis. The increase in collagen suggests that α2MRS might have cartilage-repair functions. This finding is consistent with previous reports (Zhang et al., 2017). Moreover, the results of H&E staining of the synovium and meniscus proved that α2MRS injection into the joint cavity could significantly reduce inflammatory cell infiltration and vascularity, protecting the articular cartilage, synovium, and meniscus. Combining our results with those of other studies (Rehman, 2013), we speculate that α2MRS might act by binding cytokines, in addition to directly neutralizing enzyme activities, but the exact mechanism is not clear. The relative contributions of these mechanisms will be addressed in future studies.

Our study has a few limitations. First, the state of tension in the ACL or biomechanical changes in the knee joint post-surgery are crucial. To date, there is no technology or instrument that can accurately detect the smaller motions between the femur and tibia that are controlled by the ACL. The gait analysis used in this study can only roughly or indirectly assess the biomechanical stability of the knee joint. Second, although the concentration of α2M in α2MRS was 6.48-fold higher than that in normal mini pig serum, α2MRS is in fact a mixture containing extremely complex components. α2MRS was injected into the joint cavity, and proteins other than α2M might also play a role, but the exact mechanism is still unknown. Third, considering the side effects of the multiple anesthesia method used, we do not know the exact trend of inflammatory factor levels during the period from days 29–90 after surgery.

In summary, α2MRS is a promising bioinhibitor of catabolic proteases, and early and multiple injections in the joint cavity after IACL-R can significantly reduce the concentration of inflammatory factors in the joint synovial fluid of mini pigs and the degeneration of articular cartilage, exerting a chondroprotective effect.

Data availability statement

The original contributions presented in the study are included in the article/Supplementary Material further inquiries can be directed to the corresponding author.

Ethics statement

The studies involving human participants were reviewed and approved by the Ethics Committee of the Second Hospital of Shanxi Medical University. The patients/participants provided their written informed consent to participate in this study. The animal study was reviewed and approved by The Ethics Committee of the Second Hospital of Shanxi Medical University.

Author contributions

RZ and LH participated in the study design, wrote the manuscript, performed most of the experiments, and analyzed data. XW and LH conceived the study, revised the manuscript. CZ, HW, CX, WD, and ZD carried out imaging and histological assessment and helped to perform the statistical analysis. WD, HL, CL, and YZ performed the IACL-R of mini pigs and gait assessment. All authors read and approved the final manuscript.

Funding

The project was funded by the International Science and Technology Cooperation Program of China (Grant No. 2015DFA33050); Doctoral Fund Project of the Second Hospital of Shanxi Medical University (Grant No. 202001-8); Hainan Province Clinical Medical Center.

Acknowledgments

We would like to thank Yi Xu and Feipeng Song for providing assistance with the imaging examination, and Yipeng Xue, a veterinarian at the Sciences of ShanXi Agricultural Academy Institute of Animal Husbandry and Veterinary, for teaching us animal management. Moreover, we would like to thank Pengfei Han (Heping Hospital Affiliated to Changzhi Medical College), Xiaodong Gu (Bethune Hospital, Shanxi Medical University) and Pengcui Li (The Second Hospital of Shanxi Medical University) for providing assistance with the minipig model of IACL-R.

Conflict of interest

The authors declare that the research was conducted in the absence of any commercial or financial relationships that could be construed as a potential conflict of interest.

Publisher's note

All claims expressed in this article are solely those of the authors and do not necessarily represent those of their affiliated organizations, or those of the publisher, the editors and the reviewers. Any product that may be evaluated in this article, or claim that may be made by its manufacturer, is not guaranteed or endorsed by the publisher.

Supplementary material

The Supplementary Material for this article can be found online at: https://www.frontiersin.org/articles/10.3389/fphar.2022.849102/full#supplementary-material

References

Barenius, B., Sari, P., Adel, S., Robert, B., Louise, N., and Karl, E. (2014). Increased risk of osteoarthritis after anterior cruciate ligament reconstruction: A 14-year follow-up study of a randomized controlled trial. *Am. J. Sports Med.* 42 (5), 1049–1057. doi:10.1177/0363546514526139

Björnsson, H., Samuelsson, K., Sundemo, D., Desai, N., Sernert, N., Rostgård-Christensen, L., et al. (2016). A randomized controlled trial with mean 16-year follow-up comparing hamstring and patellar tendon autografts in anterior cruciate ligament reconstruction. *Am. J. Sports Med.* 44 (9), 2304–2313. doi:10.1177/0363546516646378

Bryan, J., Heard, Y. A., Chung, M., Nigel, G., Shrive, C. B., et al. (2011). Early joint tissue changes are highly correlated with a set of inflammatory and degradative synovial biomarkers after ACL autograft and its sham surgery in an ovine model. *J. Orthop. Res.* 29 (8), 1185–1192. doi:10.1002/jor.21404

Capin, J. J., Khandha, A., Zarzycki, R., Manal, K., Buchanan, T. S., and Snyder-Mackler, L. (2018). Gait mechanics after ACL reconstruction differ according to medial meniscal treatment. *J. Bone Jt. Surg. Am.* 100 (14), 1209–1216. doi:10.2106/JBJS.17.01014

Chung, T. J., Hsu, K. Y., Chen, J. H., Liu, J. S., Chang, H. W., Li, P. F., et al. (2016). Association of salivary alpha 2-macroglobulin levels and clinical characteristics in type 2 diabetes. *J. Diabetes Investig.* 7 (2), 190–196. doi:10.1111/jdi.12382

Cuellar, J. M., Cuellar, V. G., and Scuderi, G. J. (2016). α2-Macroglobulin: Autologous protease inhibition technology. *Phys. Med. Rehabil. Clin. N. Am.* 27 (4), 909–918. doi:10.1016/j.pmr.2016.06.008

Gu, X. D., Wei, L., Li, P. C., Che, X. D., Zhao, R. P., Han, P. F., et al. (2019). Adenovirus-mediated transduction with Histone Deacetylase 4 ameliorates disease progression in an osteoarthritis rat model. *Int. Immunopharmacol.* 75, 105752. doi:10.1016/j.intimp.2019.105752

Guo, L., Wei, X., Zhang, Z., Wang, X., Wang, C., Li, P., et al. (2019). Ipriflavone attenuates the degeneration of cartilage by blocking the Indian hedgehog pathway. *Arthritis Res. Ther.* 21 (1), 109. doi:10.1186/s13075-019-1895-x

Han, P. F., Wei, L., Duan, Z. Q., Zhang, Z. L., Chen, T. Y., Lu, J. G., et al. (2018). Contribution of IL-1β, 6 and TNF-α to the form of post-traumatic osteoarthritis induced by "idealized" anterior cruciate ligament reconstruction in a porcine model. *Int. Immunopharmacol.* 65, 212–220. doi:10.1016/j.intimp.2018.10.007

Heard, B. J., Solbak, N. M., Chung, M., Achari, Y., Shrive, N. G., Frank, C. B., et al. (2016). The infrapatellar fat pad is affected by injury induced inflammation in the rabbit knee: Use of dexamethasone to mitigate damage. *Inflamm. Res.* 65 (6), 459–470. doi:10.1007/s00011-016-0928-z

Ho, A. S., Cheng, C. C., Lee, S. C., Liu, M. L., Lee, J. Y., Wang, W. M., et al. (2010). Novel biomarkers predict liver fibrosis in hepatitis C patients: Alpha 2 macroglobulin, vitamin D binding protein and apolipoprotein AI. *J. Biomed. Sci.* 17 (1), 58. doi:10.1186/1423-0127-17-58

Hu, W., Chen, Y., Dou, C., and Dong, S. (2020). Microenvironment in subchondral bone: Predominant regulator for the treatment of osteoarthritis. *Ann. Rheum. Dis.* 80 (4), 413–422. doi:10.1136/annrheumdis-2020-218089

Hughes-Oliver, C. N., Srinivasan, D., Schmitt, D., and Queen, R. M. (2018). Gender and limb differences in temporal gait parameters and gait variability in ankle osteoarthritis. *Gait Posture* 65, 228–233. doi:10.1016/j.gaitpost.2018.07.180

Kellgren, J. H., and Lawrence, J. S. (1957). Radiological assessment of osteo-arthrosis. *Ann. Rheum. Dis.* 16 (4), 494–502. doi:10.1136/ard.16.4.494

Li, J., Kong, X. B., Chen, X. Y., Zhong, W. Z., Chen, J. Y., Liu, Y., et al. (2019). Protective role of α2-macroglobulin against jaw osteoradionecrosis in a preclinical rat model. *J. Oral Pathol. Med.* 48 (2), 166–173. doi:10.1111/jop.12809

Li, L., Wei, X., Wang, D., Lv, Z., Geng, X., Li, P., et al. (2020). Positive effects of a young systemic environment and high growth differentiation factor 11 levels on chondrocyte proliferation and cartilage matrix synthesis in old mice. *Arthritis Rheumatol.* 72 (7), 1123–1133. doi:10.1002/art.41230

Li, S., Xiang, C., Wei, X., Sun, X., Li, R., Li, P., et al. (2019). Early supplemental α2-macroglobulin attenuates cartilage and bone damage by inhibiting inflammation in collagen II-induced arthritis model. *Int. J. Rheum. Dis.* 22 (4), 654–665. doi:10.1111/1756-185X.13457

Lieberthal, J., Sambamurthy, N., and Scanzello, C. R. (2015). Inflammation in joint injury and post-traumatic osteoarthritis. *Osteoarthr. Cartil.* 23 (11), 1825–1834. doi:10.1016/j.joca.2015.08.015

Little, C. B., Smith, M. M., Cake, M. A., Read, R. A., Murphy, M. J., and Barry, F. P. (2010). The OARSI histopathology initiative - recommendations for histological assessments of osteoarthritis in sheep and goats. *Osteoarthr. Cartil.* 18, S80–S92. doi:10.1016/j.joca.2010.04.016

Maerz, T., Sherman, E., Newton, M., Yilmaz, A., Kumar, P., Graham, S. F., et al. (2018). Metabolomic serum profiling after ACL injury in rats: A pilot study implicating inflammation and immune dysregulation in post-traumatic osteoarthritis. *J. Orthop. Res.* 36 (7), 1969–1979. doi:10.1002/jor.23854

Misir, A., Yildiz, K. I., Kizkapan, T. B., and Incesoy, M. A. (2020). Kellgren-Lawrence grade of osteoarthritis is associated with change in certain morphological parameters. *Knee* 27 (3), 633–641. doi:10.1016/j.knee.2020.04.013

Montesano, G., and Cuellar, J. (2015). "Improving response to treatment for patients with DDD by the use of molecular markers," in 2015. 4th International Conference on Orthopedics & Rheumatology, Baltimore, Maryland, USA, October 26-28, 2015.

Muramatsu, Y., Sasho, T., Saito, M., Yamaguchi, S., Akagi, R., Mukoyama, S., et al. (2014). Preventive effects of hyaluronan from deterioration of gait parameters in surgically induced mice osteoarthritic knee model. *Osteoarthr. Cartil.* 22 (6), 831–835. doi:10.1016/j.joca.2014.03.016

Pan, L. P., Cao, Y. P., Wen, L. C., Chai, W. B., Jun-Bao, D. U., Jin, H. F., et al. (2016). Hydrogen sulfide in cartilage and its inhibitory effect on matrix metalloproteinase 13 expression in chondrocytes induced by interlukin-1β. *Beijing Da Xue Xue Bao Yi Xue Ban.* 48 (2), 194–202. PMID: 27080266

Pauli, C., Grogan, S. P., Patil, S., Otsuki, S., Hasegawa, A., Koziol, J., et al. (2011). Macroscopic and histopathologic analysis of human knee menisci in aging and osteoarthritis. *Osteoarthr. Cartil.* 19 (9), 1132–1141. doi:10.1016/j.joca.2011.05.008

Pozzi, F., Snyder-Mackler, L., and Zeni, J., Jr. (2015). Relationship between biomechanical asymmetries during a step up and over task and stair climbing after total knee arthroplasty. *Clin. Biomech.* 30 (1), 78–85. doi:10.1016/j.clinbiomech.2014.11.001

Rashid, M. H., Theberge, Y., Elmes, S. J., Perkins, M. N., and Mcintosh, F. (2013). Pharmacological validation of early and late phase of rat mono-iodoacetate model using the Tekscan system. *Eur. J. Pain* 17 (2), 210–222. doi:10.1002/j.1532-2149.2012.00176.x

Rehman, A. A., Ahsan, H., and Khan, F. H. (2013). α-2-Macroglobulin: A physiological guardian. *J. Cell. Physiol.* 228 (8), 1665–1675. doi:10.1002/jcp.24266

Ruan, M. Z. C., Patel, R. M., Dawson, B. C., Jiang, M. M., and Lee, B. H. L. (2013). Pain, motor and gait assessment of murine osteoarthritis in a cruciate ligament

transection model. *Osteoarthr. Cartil.* 21 (9), 1355–1364. doi:10.1016/j.joca.2013.06.016

Salvesen, G., and Enghild, J. J. (1993). alpha-Macroglobulins: detection and characterization. *Methods Enzymol.* 223, 121–141. doi:10.1016/0076-6879(93)23041-k

Shah, K. C., Linsley, C. S., and Wu, B. M. (2020). Evaluation of a shape memory implant abutment system: An up to 6-month pilot clinical study. *J. Prosthet. Dent.* 123 (2), 257–263. doi:10.1016/j.prosdent.2018.11.012

Sottrup-Jensen, L. (1989). Alpha-macroglobulins: Structure, shape, and mechanism of proteinase complex formation. *J. Biol. Chem.* 264 (20), 11539–11542.

Wang, L. J., Zeng, N., Yan, Z. P., Li, J. T., and Ni, G. X. (2020). Post-traumatic osteoarthritis following ACL injury. *Arthritis Res. Ther.* 24 (1), 57. doi:10.1186/s13075-020-02156-5

Wang, S., Wei, X., Zhou, J., Zhang, J., Li, K., Chen, Q., et al. (2014). Identification of α2-macroglobulin as a master inhibitor of cartilage-degrading factors that attenuates the progression of posttraumatic osteoarthritis. *Arthritis Rheumatol.* 66 (7), 1843–1853. doi:10.1002/art.38576

Wei, L., Fleming, B. C., Sun, X., Teeple, E., Wu, W., Jay, G. D., et al. (2010). Comparison of differential biomarkers of osteoarthritis with and without posttraumatic injury in the Hartley Guinea pig model. *J. Orthop. Res.* 28 (7), 900–906. doi:10.1002/jor.21093

Xue, Y., Chen, Y., Jiang, D., Wang, L., Wang, X., Li, M., et al. (2021). Self-reported weather sensitivity is associated with clinical symptoms and structural abnormalities in patients with knee osteoarthritis: A cross-sectional study. *Rheumatol. Ther.* 8 (3), 1405–1417. doi:10.1007/s40744-021-00340-w

Zhang, Y., Wei, X., Browning, S., Scuderi, G., Hanna, L. S., and Wei, L. (2017). Targeted designed variants of alpha-2-macroglobulin (A2M) attenuate cartilage degeneration in a rat model of osteoarthritis induced by anterior cruciate ligament transection. *Arthritis Res. Ther.* 19 (1), 175. doi:10.1186/s13075-017-1363-4

Zhao, R., Dong, Z., Wei, X., Gu, X., Han, P., Wu, H., et al. (2021). Inflammatory factors are crucial for the pathogenesis of post-traumatic osteoarthritis confirmed by a novel porcine model: "Idealized" anterior cruciate ligament reconstruction" and gait analysis. *Int. Immunopharmacol.* 99, 107905. doi:10.1016/j.intimp.2021.107905

Frontiers in Pharmacology

Explores the interactions between chemicals and living beings

The most cited journal in its field, which advances access to pharmacological discoveries to prevent and treat human disease.

Discover the latest Research Topics

See more →

Frontiers

Avenue du Tribunal-Fédéral 34
1005 Lausanne, Switzerland
frontiersin.org

Contact us

+41 (0)21 510 17 00
frontiersin.org/about/contact